UNIVERSIDAD COMPLUTENSE DE MADRID

FACULTAD DE CIENCIAS QUÍMICAS

Departamento de Química Orgánica

TESIS DOCTORAL

Nanopartículas poliméricas autoensambladas y bioactivas para el tratamiento del cáncer

MEMORIA PARA OPTAR AL GRADO DE DOCTOR

PRESENTADA POR

Raquel Palao Suay

Directores

Julio San Román del Barrio
María Rosa Aguilar de Armas

Madrid, 2017

NANOPARTÍCULAS POLIMÉRICAS AUTOENSAMBLADAS Y BIOACTIVAS PARA EL TRATAMIENTO DEL CÁNCER

RAQUEL PALAO SUAY

DIRECTORES:

Julio San Román del Barrio

María Rosa Aguilar de Armas

UNIVERSIDAD COMPLUTENSE DE MADRID

FACULTAD DE CIENCIAS QUÍMICAS

Departamento de Química Orgánica

INSTITUTO DE CIENCIA Y TECNOLOGÍA DE POLÍMEROS (ICTP-CSIC)

CSIC

CONSEJO SUPERIOR DE INVESTIGACIONES CIENTÍFICAS

Departamento de Nanomateriales Poliméricos y Biomateriales

Madrid, 2016

El presente trabajo de investigación, titulado: ***"Nanopartículas poliméricas autoensambladas y bioactivas para el tratamiento del cáncer"*** ha sido realizado en el Departamento de Nanomateriales poliméricos y Biomateriales del Instituto de Ciencia y Tecnología de Polímeros del CSIC, bajo la dirección de los doctores D. Julio San Román del Barrio y Dña. María Rosa Aguilar de Armas, para optar al grado de Doctor por la Universidad Complutense de Madrid.

AGRADECIMIENTOS

Por fin llega el momento de agradecer todo lo que he vivido estos años de tesis en los que he sido inmensamente feliz. Realmente, me siento una privilegiada por haber podido llevar a cabo mi tesis doctoral en el mejor sitio y con la mejor compañía posible.

En primer lugar me gustaría agradecer de corazón a mis directores de tesis, Julio y Curra. Julio, gracias por darme la oportunidad de realizar este trabajo tan apasionante, por confiar en mí, por tus fantásticas ideas y por tener siempre palabras de ánimo cuando más falta me han hecho. Curra, no tengo palabras para agradecerte el trabajo de todos estos años, día a día, confiando siempre en lo que tuviéramos entre manos, buscando en todo momento soluciones ante cualquier problema. He podido siempre contar contigo tanto en lo profesional como en lo personal. No he podido tener mejor compañera en este viaje. Sin vosotros nada de este proyecto hubiera sido posible.

También quiero agradecer a dos personas muy importantes para mí a lo largo de estos años, Blanca y Paco. Blanca ha sido un verdadero placer trabajar contigo codo con codo en todas las ocasiones, además siempre tuviste un consejo que darme y estuviste disponible para brindarme cualquier ayuda. Paquito me faltan páginas para expresar el agradecimiento por todo lo que me has enseñado de química en estos años, sin ti tampoco este trabajo hubiera tirado hacía delante en muchas ocasiones así que infinitas gracias.

No puedo olvidarme del Grupo de Biomateriales y de todos sus integrantes por hacerme sentir siempre en como en casa. Gracias a Gema, los Luises y sin olvidar a mis chicas de células Mar y Rosana. En especial, quiero

agradecer a Mar que tuvo la paciencia de enseñarme cómo trabajar en un laboratorio de células y a Rosana, siempre dispuesta a ayudarme. Chicas no voy a olvidar esos ratitos tan buenos que hemos pasado juntas. También agradecer a Mercedes por ser tan buena compañera, que bien lo pasamos en Dresden! A lo largo de este tiempo han pasado por el laboratorio muchos estudiantes que han dado vida al laboratorio y con los que he vivido momentos geniales. A todos ellos gracias, en especial a Alberto, Ángela, Angélica, Cecilia, Citlalli, Daniel, Daniela, Eduardo, Elvira, Fabiola, Giovanna, Hazel, Humberto, Ito, Laura Llopis, Leila, Noemí, Martina, Nancy y Sofía.

Una de las mejores cosas que me han pasado estos años ha sido conocer a personas en este grupo de trabajo que se han convertido en grandes amigos. Álvaro has sido mi gran compañero a lo largo de todo este tiempo, no olvidaré nunca todos tus consejos, esos desayunos con las fotos de tus peques que me alegraban las mañanas y un largo etcétera que seguiremos completando en el futuro. A mis chicas, Feli y Patri, no os podéis imaginar todo lo que os he echado de menos los últimos años en el laboratorio, sin vosotras nada era lo mismo. Patri por la tranquilidad que siempre me transmitías y Feli por tu alegría desbordante y esos ratos tan divertidos que siempre compartíamos a última hora. Sois las mejores y en un futuro recordaremos juntas esta etapa de nuestras vidas. Por último, Sergio ha sido un verdadero placer compartir los últimos meses contigo, mi compi de partículas; eres un crack y conseguirás todo lo que te propongas. Fuiste de los primeros en conocer mi secreto y en ayudarme en esos momentos que más lo necesité sin esperar nada a cambio, nunca lo olvidaré.

Agradecer también a Elma y Carlos por todos los fantásticos momentos que hemos compartido, que hubiera sido de nosotros sin esas sobremesas tan

apasionantes. Elma eres una persona increíble, los ratos en el parquecito me alegraban las tardes. Y Carlos, gracias por todos los momentos compartidos, en especial las visitas de tus peques.

No puedo olvidarme de los compañeros del máster con los que compartí muchos momentos inolvidables. En especial, dar infinitas gracias a Laura y Marta que fueron compañeras y ahora amigas. Lauri, te he echado mucho en falta desde que te fuiste del labo, gracias por todo tu apoyo y ya sabes que eres la próxima, estoy segura que presentarás una tesis espectacular. Marta, millones de gracias por todos esos momentos vividos de un lado al otro de nuestro pasillo. Tu apoyo y comprensión han sido imprescindibles para mí.

Me gustaría también dedicar unas palabras de agradecimiento a toda la gente y personal del instituto, en especial a todos los miembros del servicio de caracterización sin los cuales este trabajo no hubiera sido posible. A Carolina, gracias por tu ayuda con todos los equipos, a David por su paciencia infinita con mis nanos y a las chicas de reso. Tampoco puedo olvidarme de las limpiadoras del centro y en particular de Charo.

Debido al carácter multidisciplinar de este trabajo, he tenido el enorme placer de colaborar con distintos grupos de investigación. En primer lugar, quiero agradecer el trabajo realizado con la Unidad de Investigación del Hospital de Getafe. En especial, gracias a Carolina por enseñarme tantas cosas de células y a Laura y Juan por mejorar este trabajo desde otros puntos de vista. Por otra parte, no puedo olvidarme de la colaboración tan estrecha con la unidad de investigación del Hospital de La Paz. Gracias a Nuria, Pachi y Clara, siempre que estuve con vosotros me sentí como en casa, además de aprender muchísimas cosas nuevas. Finalmente, agradecer la ayuda y el excelente trabajo del Servicio de Experimentación Animal del Hospital del Vall d'Hebron, aunque

finalmente no pudo ser, infinitas gracias por la confianza y no perder nunca las ganas de seguir intentándolo.

A lo largo de estos años he tenido la oportunidad de trabajar fuera lo que me ha ayudado a mejorar tanto profesional como personalmente. Agradecer especialmente a Richard Hoogenboom y a Susan Thomas la oportunidad única que me dieron de formar parte de sus grupos de trabajo, considerándome como una más desde el primer día.

Por último y más importante, nada de esto hubiera sido posible sin el apoyo de toda mi familia. A mis padres nunca tendré palabras suficientes de agradecimiento por todo lo que me han dado, por la educación brindada y ser un ejemplo de superación. Sin su ayuda no hubiera podido terminar de escribir en los últimos meses, gracias por el gran esfuerzo que habéis hecho! A mi hermano Juanlu, que sé que nunca leerá estas líneas pero me gustaría que supiera que es el principal responsable de cómo soy, es un ejemplo en mi vida y lo mejor que me ha pasado. Tu sonrisa es lo que nos da fuerzas cada día. Tampoco puedo olvidarme de mis abuelos, los que me faltan que sé que estarían muy orgullosos de mí y a mi abuela Charo que siempre me pregunta si he inventado algo nuevo.

Finalmente, el gran apoyo y gran sufridor día a día a lo largo de estos años, Mario millones de gracias por aguantarme, quererme, apoyarme en todo momento y vivir juntos tantas experiencias inolvidables. No he podido tener mejor compañero de viaje y de vida, soy una auténtica privilegiada por tenerte a mi lado. Y sobre todo, gracias por formar nuestra familia con lo mejor que nos ha pasado. Clara, algún día te contaré que fuiste mi gran compañera cuando escribía la tesis lo que ha convertido esos momentos en únicos y que nunca podré olvidar. Eres tan especial que no existen palabras que puedan describir lo

que significas para nosotros. Como podíamos vivir sin ti!! Desde que te vi la cara supe lo que es la plena felicidad.

A todos, infinitas gracias

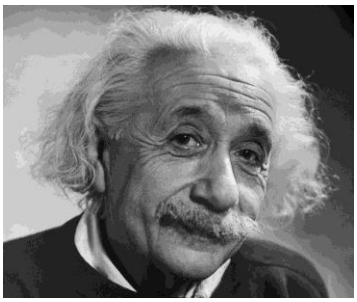

“Hay una fuerza motriz más poderosa que el vapor, la electricidad y la energía atómica: la voluntad.”

Albert Einstein

“Soy de las que piensan que la ciencia tiene una gran belleza. Un científico en su laboratorio no es sólo un técnico: es también un niño colocado ante fenómenos naturales que le impresionan como un cuento de hadas.”

Marie Curie

Índice de contenidos

ABREVIATURAS

AIBN: 2,2´-azo-bis-isobutironitrilo / 2,2´-azo-bis-isobutyronitrile

AFM: microscopía de fuerza atómica / atomic force microscopy

ANOVA: análisis de varianza / analysis of variance

ATP: adenosín trifosfato / adenosine triphosphate

ATR-FTIR: espectroscopía de infrarrojo con transformada de Fourier por reflectancia / attenuated total reflectance Fourier transform infrared spectroscopy

ATRP: polimerización radical por transferencia de átomo / atom transfer radical polymerization

BEC: índice bioenergético celular / bioenergetic signature

^{13}C: carbon / carbon

c6: cumarina 6 / coumarin 6

$CDCl_3$: cloroformo deuterado / deuteraded chloroform

CH_2Cl_2: diclorometano / dicholoromethane

CL: cardiolipina /cardiolipin

CLSM: microscopía confocal de barrido láser / confocal laser scanning microscopy

CMC: concentración micelar crítica / critical micelle concentration

CPT: cisplatino / cisplatin

CRP: polimerización radical controlada / controlled radical polymerization

CTA: agente de transferencia / chain transfer agent

Đ: polidispersidad / dispersity

DCC: *N, N'*-diciclohexilcarbodiimida */ N,N'*-dicyclohexylcarbodiimide

D_h: diámetro hidrodinámico aparente / apparent hydrodynamic diameter

DISC: complejo de señalización inductor de muerte / intracellular death-inducing signaling complex

DLS: dispersión de luz dinámica / dynamic light scattering

DMAP: 4-dimetilaminopiridina / 4-dimethylaminopyridine

DMEM: Dulbecco´s modified Eagle´s medium

DMF: dimetilformamida / dimethylformamide

DMSO: dimetilsulfóxido / dimethylsulfoxide

DMTMM: 4-(4,6-dimetoxi-1,3,5-triazin-2-il)-4-metilmorfolina / 4-(4,6-Dimethoxy-1,3,5-triazin-2-yl)-4-methylmorpholinium chloride

DOX: doxorrubicina / doxorubicin

DSC: calorimetría diferencial de barrido / differential scanning calorimetry

DTX: docetaxel

EDC: 1-etil-3-(3-dimetilaminopropil)carbodiimida / *N*-(3-dimethylaminopropyl)-*N*' ethylcarbodiimide hydrochloride

EE: eficiencia de encapsulación / encapsulation efficiency

EGF: factor de crecimiento epidérmico / epidermal growth factor

EGFR receptor del factor de crecimiento epidérmico / epidermal growth factor receptor

EPR: efecto de permeación y retención aumentada / enhanced permeability and retention effect

Et_3N: trietilamina / triethylamine

EtOH: etanol / ethanol

5-FU: 5-fluoroacilo / 5-fluoroacil

FaDu: células humanas de carcinoma escamoso de hipofaringe / hypopharynx carcinoma squamous cells

FBS: suero fetal bovino / fetal bovine serum

FDA: Agencia Reguladora del Medicamento / Food and Drug Administration

^1H: protón /proton

HEMA: metacrilato de 2-hidroxietilo / 2-hydroxyethyl methacrylate

HER2: receptor 2 del factor de crecimiento epidérmico humano / human epidermal growth factor receptor 2

HMEpC: células humanas epiteliales de mama / human breast epithelial cells

HPMA: poli(*N*-(2-hidroxipropil)metacrilamida) / poly (*N*- (2-hydroxypropyl) methacrylamide)

HRMS: espectroscopía de masas de alta resolución / high resolution mass spectroscopy

HUVEC: células endoteliales de la vena de cordón umbilical humano / human umbilical vein endothelial cells

IARC: Agencia Internacional de Investigación sobre el Cáncer / International Agency for Research on Cancer

IC_{50}: concentración inhibitoria del 50 % / average inhibitory concentration

IONs: nanopartículas de óxidos de hierro / iron oxide nanoparticles

LDE: electroforesis láser / laser doppler electrophoresis

LDH: lactatodeshidrogenasa / lactate dehydrogenase

M: concentración total de monómero / total monomer concentration

MCF-7: células humanas de adenocarcinoma de mama / human breast adenocarcinoma cells

MDA-MB-453: células de carcinoma metastático de mama / human breast metastatic carcinoma cells

MDR: resistentes a múltiples drogas / multidrug resistance

MEM: Eagle's Minimun Essential

MES: mono-2-(metacriloiloxi)etil succinato / mono-(2-(methacryloyloxy)ethyl) succinate

MG-63: células humanas de osteosarcoma / human osteosarcoma cells

MIR: resonancia magnética de imagen / magnetic resonance imagin

Mitocan: fármacos anticancerígenos dirigidos a la mitocondria / mitochondrial targeted anticancer drugs

M_n: peso molecular promedio en número / number average molecular weight

MPHY: derivado metacrílico del dihidrofitol / methacrylic derivative of dihydrophytol

MTOS: derivado metacrílico del α-TOS / methacrylic derivative of α-TOS

MTT: bromuro de 3-(4,5-dimetiltiazol-2-il)-2,5-difeniltetrazolio / 3-(4,5-dimethylthiazol-2-yl)-2,5-diphenyltetrazolium bromide

MVE: metacrilato de la vitamin E / vitamin E methacrylate

M_w: peso molecular promedio en peso / weight average molecular weight

NIR: fluorescencia de infrarrojo cercano / near infrared fluorescence

NMP: polimerización mediada por radicales estables nitróxidos / nitroxide mediated polymerization

NMR: resonancia magnética nuclear / nuclear magnetic resonance

NPs: nanopartículas / nanoparticles

OATPs: péptidos transportadores de aniones orgánicos / organic anion transporter peptides

OMM: membrana mitocondrial externa

PAA: poliaminoácidos / polyaminoacids

PAsp: ácido poliaspártico / polyaspartic acid

PBS: disolución de tampón fosfato / phosphate buffered saline solution

PC: fosfatidilcolina / phosphatidylcholine

PCL: policaprolactona / polycaprolactone

PDI: índice de polidispersidad / particle dispersion index

PDT: terapia fotodinámica / photodynamic therapy

PE: fosfatidiletanolamina / phosphatidyl ethanolamine

PEG: polietilenglicol / polyethylene glicol

PGA: ácido poliglutámico / polyglutamic acid

Pgp: glicoproteína / P-glycoprotein

PLA: ácido poliláctico / polylactic acid

PLGA: ácido poli(láctico-*co*-glicólico) / poly(lactic-*co*-glycolic acid)

POX: poli(2-oxazolinas) / poly(2-oxazolines)

PPO: óxido de polipropileno / polypropylene oxide

Ps: fotosensibilizador / photosensitizer

P/S: penicilina/estreptomicina / penicillin/streptomycin

PTT: terapia fototérmica / photothermal therapy

PTX: paclitaxel

QDs: quantum dots

r: relación de reactividad / reactivity ratios

RAFT: polimerización por adición, fragmentación y transferencia de cadena / reversible addition-fragmentation chain transfer polymerization

RES: sistema retículo endotelial / reticuloendothelial system

RNS: especias reactivas del nitrógeno / reactive nitrogen species

ROP: polimerización por apertura de anillo / ring-opening polymerization

ROS: especies reactivas al oxígeno / reactive oxygen species

SA: anhídrido succínico / succinic anhydride

SDH: succinato deshidrogenasa / succinate dehydrogenase

SEC: cromatografía de exclusión por tamaños / size exclusion chromatography

SEM: microscopía electrónica de barrido / scanning electron microscopy

SOD: superóxido dismutasa / superoxide dismutase

SORP: precipitación auto-organizada / self-organized precipitation

SPHY: derivado metacrílico del succinato de dihidrofitol / methacrylic derivative of dihydrophytol succinate

SPIONs: nanopartículas superparamagnéticas de óxidos de hierro / superparamagnetic iron oxide nanoparticles

$\boldsymbol{T_g}$: temperatura de transición vítrea / glass transition temperature

TEM: microscopía electrónica de transmisión / transmission electron microscopy

TGA: análisis termogravimétrico / thermogravimetric analysis

THF: tetrahidrofurano / tetrahydrofuran

TNF: factor de necrosis tumoral / tumor necrosis factor

TPGS: α-tocopheryl polyethylene glycol succinate / polietilenglicolsuccinato de α-tocoferilo

UbQ: ubiquinona / ubiquinone

UV/vis: ultravioleta/visible / ultravioleta/visible

VEGF: factor de crecimiento endotelial vascular /vascular endotelial growth factor

VEGFR: receptor del factor de crecimiento endotelial vascular /vascular endotelial growth factor receptor

VP: *N*-vinil-2-pirrolidona / *N*-vinyl-2-pyrrolidone

W_d: ancho de la distribución de tamaños de partícula /size distribution width

WiDr: células humanas de adenocarcinoma de colon / human colon adenocarcinoma cells

α-TOH: α-tocoferol / α-tocopherol

α-TOS: succinato del α-tocoferol/ α-tocopheryl succinate

ζ : potencial zeta / zeta potential

RESUMEN

Los tratamientos anticancerígenos que existen actualmente en el mercado se caracterizan por su elevada toxicidad debido a su escasa especificidad ya que afectan tanto a células tumorales como a células sanas. Por ello, la investigación en este campo se centra en el descubrimiento de nuevos fármacos que acaben selectivamente con las células cancerígenas. En este sentido, el succinato del α-tocoferol (α-TOS) es un mitocan (del inglés, *mitochondrial targeted anticancer drugs*) que ha demostrado inducir selectivamente la apoptosis vía mitocondrial de células tumorales sin afectar a células no patológicas. Esto le posiciona como un destacado candidato para el desarrollo de nuevos fármacos poliméricos que mejoren su solubilidad en medio fisiológico, facilitando su administración. Por eso, el principal objetivo de esta tesis doctoral ha sido el diseño, caracterización fisicoquímica y evaluación de la actividad biológica de diversos vehículos poliméricos nanoestructurados portadores del fármaco anticancerígeno α-TOS con el fin de lograr un tratamiento más eficaz, selectivo y menos tóxico contra el cáncer.

Para alcanzar este objetivo, en primer lugar se copolimerizaron con éxito derivados metacrílicos del α-TOS (MTOS), de la vitamina E (MVE) y del dihidrofitol (SPHY y MPHY) con la N-vinil-pirrolidona (VP) por polimerización radical convencional. Estos copolímeros fueron capaces de autoensamblarse en medio acuoso, debido a su naturaleza anfifílica y la mayor reactividad de los derivados metacrílicos frente a la VP. Las nanopartículas (NPs) obtenidas a partir de los copolímeros poli(VP-*co*-MVE) y poli(VP-*co*-MTOS) resultaron bioactivas, con una actividad intrínseca anticancerígena y antiangiogénica dependiente del contenido en monómero hidrofóbico (MVE y MTOS) y altamente selectiva, afectando en menor medida a células no patológicas y quiescentes. Además, la actividad antitumoral de estas NPs resultó estrechamente dependiente de la línea celular ensayada, siendo menos activas frente a células de carcinoma de hipofaringe FaDu. Por ello, las NPs basadas en los copolímeros poli(VP-*co*-MTOS) se emplearon eficazmente para la encapsulación de α-TOS en su núcleo hidrofóbico, mejorando su actividad anticancerígena *per se* frente a células FaDu. Además, se profundizó en el mecanismo de acción de las partículas vacías y cargadas, demostrando que producían la muerte celular por apoptosis intrínseca, vía complejo II de la cadena de transporte de electrones de las mitocondrias.

En segundo lugar, se preparó con éxito una segunda generación de NPs poliméricas mediante la polimerización radical controlada vía RAFT (del inglés, *reversible addition-fragmentation chain transfer polymerization*) del MTOS con polietilenglicol (PEG) de diferente peso molecular. Esto facilitó la obtención de NPs esféricas con control exhaustivo de su arquitectura macromolecular y una corona externa de PEG que les confería una alta estabilidad. El núcleo hidrofóbico de las NPs sirvió para encapsular eficazmente α-TOS y cumarina-6 cuya fluorescencia fue usada para confirmar la endocitosis de las NPs dentro de células tumorales de mama. Asimismo, los ensayos biológicos realizados pusieron de manifiesto que la actividad anticancerígena de estas NPs dependía del contenido en monómero activo (MTOS) así como de la longitud del bloque hidrofílico de PEG y de su peso molecular. Adicionalmente, la copolimerización del 2-hidroxietil metacrilato (HEMA) con el MTOS vía RAFT permitió sintetizar con éxito terpolímeros PEG-*b*-[poli(MTOS-*co*-HEMA)] donde las unidades de HEMA se distribuyeron al azar en el bloque hidrofóbico de MTOS. La incorporación del HEMA y la carga de α-TOS en el núcleo hidrofóbico de las NPs permitió una mejora sustancial de su actividad anticancerígena; debido probablemente a que las unidades de HEMA reducen la hidrofobicidad del núcleo de MTOS, mejorando la difusión de agua en su interior así como la liberación de la carga.

Finalmente, los copolímeros de bloque PEG-*b*-poliMTOS más activos se emplearon satisfactoriamente para la conjugación y encapsulación de la sonda fluorescente IR-780, aumentando la citotoxicidad *in vitro* del nanomaterial y dotándolo además de propiedades ópticas. Los resultados obtenidos tras la irradiación de las NPs confirmaron su capacidad fototérmica en disolución, alcanzando temperaturas efectivas para la hipertermia en el caso de los nanovehículos con más sonda encapsulada en su núcleo hidrofóbico. Por último, se comprobó que las partículas fluorescentes presentaban una fototoxicidad *in vitro.* Este comportamiento es probablemente debido a la existencia de un efecto fotodinámico dependiente exclusivamente de la presencia de la sonda IR-780, sin que se produzca una modificación permanente de la estructura polimérica de las partículas y que requiere de la irradiación NIR en un contexto donde el nanomaterial haya entrado en contacto previamente con las células.

SUMMARY

Actual cancer treatments are characterized by their high toxicity and low selectivity, affecting both tumor and nonmalignant cells. Therefore, the investigations in this field are focused on the development of new drugs that selectively target and kill cancer cells. In this sense, α-tocopherol succinate (α-TOS) is a mitocan (mitochondrial targeted anti-cancer drugs) that selectively induces apoptosis via complex II in the mitochondria of tumor cells, with little or no harm to nonmalignant cells. For that reason, this drug is an excellent candidate for the development of new polymeric drugs that improve its solubility in physiological media and facilitate its administration. Therefore, the main objective of this thesis has been the synthesis, physico-chemical characterization and biological evaluation of different polymeric nanovehicles based on α-TOS in order to achieve a more efficient, selective and less toxic anticancer treatment.

Firstly, methacrylic derivatives of vitamin E (MVE), α-TOS (MTOS) and dihydrophytol (SPHY and MPHY) were successfully copolymerized with *N*-vinylpyrrolidone (VP) by free radical polymerization. These copolymers were able to self-assemble in aqueous medium, due to their amphiphilic nature and the higher reactivity of methacrylic derivatives against VP. Self-assembled nanoparticles (NPs) obtained from poly(VP-*co*-MVE) and poly(VP-*co*-MTOS) were bioactive and presented anticancer and antiangiogenic activities as a function of the hydrophobic monomer content (MVE and MTOS) and high selectivity, with little or no harm to nonpathological and quiescent cells. Furthermore, the antitumor activity of these NPs was found to depend on the tested tumor cell lines, being less active against hypopharynx carcinoma FaDu cells than breast adenocarcinoma MCF7 cells. Therefore, NPs based on poly(VP-*co*-MTOS) copolymers were effectively used for the encapsulation of α-TOS in their hydrophobic core, improving their anticancer activity against FaDu cells. Furthermore, the mechanism of action of unloaded and α-TOS-loaded NPs was exhaustively studied, demonstrating that these nanoassemblies induce apoptosis by activating the mitochondria death pathway (via complex II of the electron transport chain).

Secondly, a second generation of NPs was successfully synthesized by radical controlled polymerization via RAFT (Reversible Addition-Fragmentation chain Transfer Polymerization) of MTOS with polyethylene glycol (PEG) of different molecular weight.

This methodology enabled to obtain spherical NPs with a precise control over their macromolecular architecture and core-shell morphology based on PEG hydrophilic shell that stabilized them. The hydrophobic core of these NPs was able to efficiently encapsulate α-TOS and coumarin-6 (c6). In fact, c6 was used as a fluorescent probe to trace the endocytosis of NPs within cancer cells. Moreover, the biological activity of the synthesized NPs was found to depend on the active monomer content (MTOS), the length of the hydrophilic block of PEG and its molecular weight. Additionally, 2-hydroxyethyl methacrylate (HEMA) was successfully copolymerized with MTOS via RAFT, obtaining PEG-*b*-[poly (HEMA-*co*-MTOS)] where HEMA monomeric units were randomly incorporated into the MTOS based hydrophobic block. The incorporation of HEMA and the load of additional α-TOS in the hydrophobic core of the NPs allowed to dramatically improve the anticancer activity of α-TOS-bearing NPs, probably by improving the water accessibility to the MTOS residues and favoring the hydrolysis and the release of the anticancer compound.

Finally, IR-780 fluorescent dye was successfully conjugated and encapsulated to most active PEG-*b*-polyMTOS block copolymers, obtaining NPs with improved *in vitro* cytotoxicity and interesting optical properties. NIR irradiation of NPs demonstrated their photothermal activity in solution, reaching effective temperatures for hyperthermia in the case of IR-780 loaded NPs. Finally, biological studies demonstrated that IR-780-bearing NPs presented *in vitro* phototoxicity, probably due to the appearance of a photodynamic effect where the NIR-dye behaves as a photosensitizer. This phototoxicity depends on the presence of intact IR-780 dye, discarding that NIR energy would produce a permanent change in the polymer structure, in a context where nanomaterial has previously been in contact with the cells.

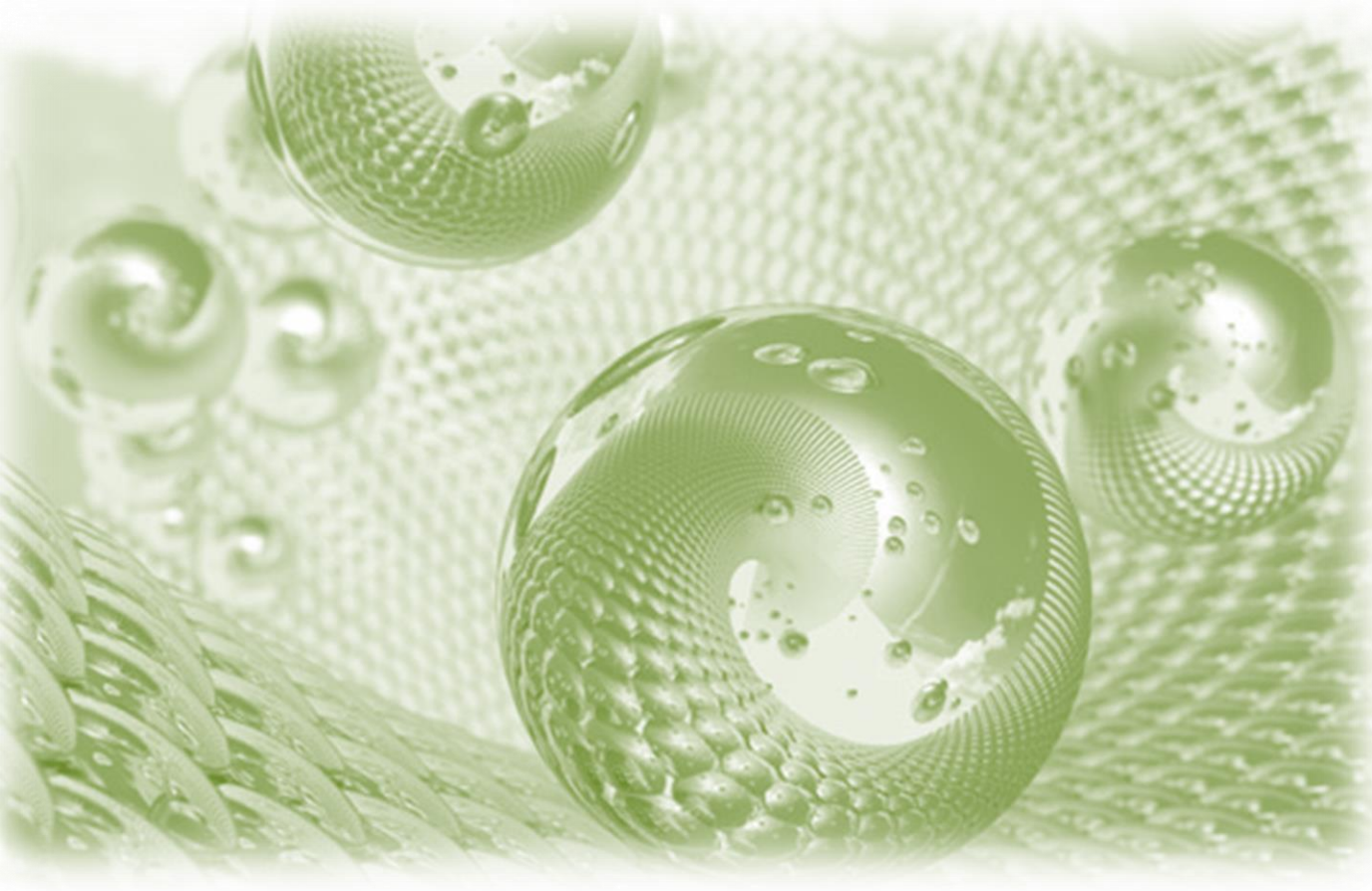

Capítulo I: Introducción

1.1. La problemática del cáncer

El término cáncer abarca un conjunto numeroso de enfermedades caracterizadas por el crecimiento de células anormales que proliferan y se propagan sin control por el organismo debido a su capacidad para invadir otros tejidos, penetrar en los vasos sanguíneos y linfáticos así como por su resistencia a la muerte celular (**figura 1A-B**). Hasta el momento se han identificado más de 100 tipos diferentes de cáncer que, por lo general, reciben el nombre de los órganos o tejidos en donde se forman[1-3].

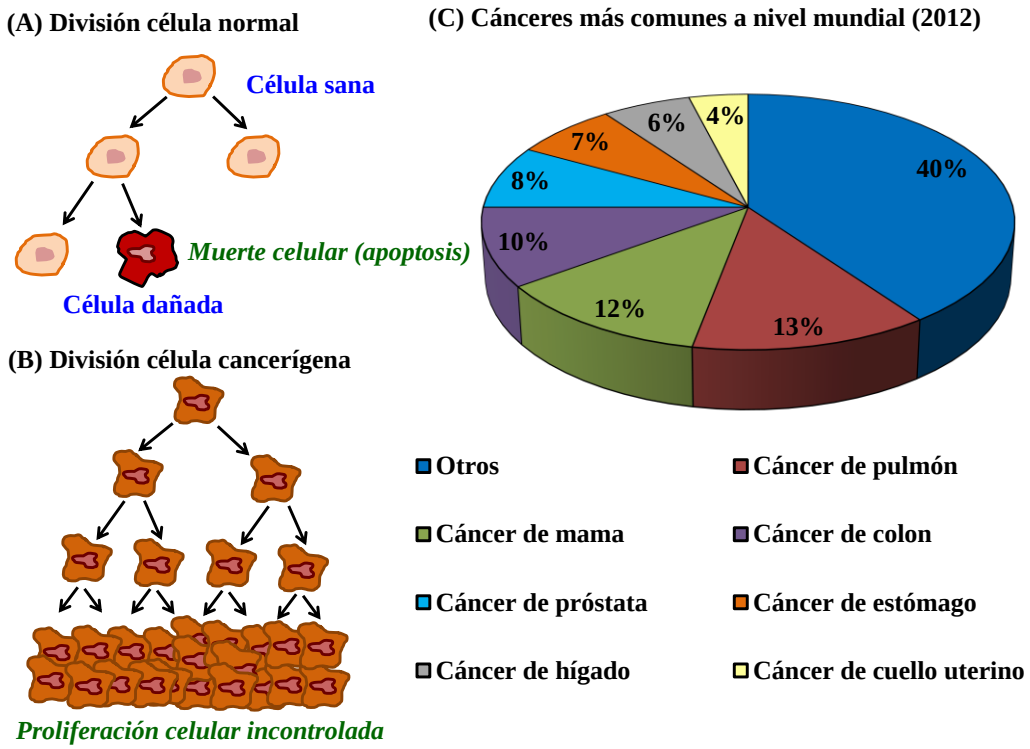

Figura 1: Diferencias en la proliferación de (A) células normales y (B) células cancerígenas. (C) Tipos de cáncer más comunes a nivel mundial en 2012. Fuente: GLOBOCAN 2012.

Los procesos cancerígenos se originan principalmente por cambios genéticos que afectan a proto-oncogenes, genes supresores de tumores y genes reparadores del ADN[4]. Las proteínas codificadas por estos genes regulan los procesos de proliferación, diferenciación y muerte celular, además de la reparación del ADN[5-7]. En este sentido, el avance en la investigación de mutaciones en los genes implicados en los procesos oncogénicos ha sido un paso fundamental en el estudio del cáncer. Sin embargo, muchas de las propiedades

adquiridas por las células tumorales no han podido explicarse en base únicamente a este tipo de mutaciones sino que hay otros muchos factores que juegan un papel fundamental en la progresión de esta enfermedad[8].

Actualmente, el cáncer es la segunda causa de muerte a nivel mundial, por detrás de las enfermedades cardiovasculares. Según los datos de la Agencia Internacional de Investigación sobre el cáncer (IARC, del inglés *International Agency for Research on Cancer*), más de 14 millones de nuevos casos de cáncer se diagnosticaron en el año 2012 con un total de más de 8 millones de muertes a nivel mundial. En particular, los cánceres de pulmón, mama y colón presentan las mayores tasas de incidencia en la población (**figura 1C**). Además, debido al crecimiento y envejecimiento de la población mundial, se estiman casi 22 millones de nuevos casos de cáncer en el año 2030[9]. Estas cifras revelan la importancia de esta enfermedad en nuestra sociedad así como la poca eficacia de los tratamientos actuales para combatirla.

La cirugía y radioterapia son dos de los tratamientos más habituales para tumores locales y no metastásicos. Sin embargo, estos tratamientos son realmente insuficientes cuando el cáncer ha metastatizado otros órganos. En estos casos, el uso de fármacos citotóxicos y antineoplásicos a través del torrente sanguíneo se hace fundamental en lo que se conoce como quimioterapia. En concreto, los quimioterápicos ejercen su acción inhibiendo el crecimiento descontrolado de las células cancerígenas[10]. El primer quimioterápico aprobado por la Agencia Reguladora del Medicamento (FDA, del inglés *Food and Drug Administration*) fue la mostaza nitrogenada (mecloretamina) que, tras su uso con fines militares en la Primera Guerra Mundial, se descubrió que disminuía los niveles de glóbulos blancos en los militares que estuvieron expuestos a este tipo de sustancia[11]. Desde ese momento hasta la actualidad, el desarrollo de fármacos citostáticos ha sido realmente espectacular con un gran número de posibilidades diferentes cuya elección depende del tipo de tumor, su localización, el estado general del paciente, etc. Cisplatino (CPT)[12], 5-fluoroacilo (5-FU)[13], doxorrubicina (DOX)[14] o paclitaxel (PTX)[15] son sólo algunos de los ejemplos más representativos de fármacos antineoplásicos utilizados hoy en día.

A pesar del gran avance en los tratamientos anticancerígenos que existen actualmente en el mercado, todos ellos se caracterizan por su elevada toxicidad afectando tanto a células tumorales como a células sanas, especialmente si se encuentran en división activa. Esto

conduce al debilitamiento del sistema inmune del paciente que habitualmente sufre importantes efectos secundarios. Además, la mayoría de los fármacos quimioterapéuticos no alcanzan el sitio de acción donde son requeridos en dosis eficaces, limitando significativamente el éxito del tratamiento. Por estas razones, la investigación en este campo se centra en el descubrimiento de nuevos medicamentos y tratamientos que ataquen selectivamente a las células cancerígenas sin afectar a las células sanas. En este contexto, a finales de la década de los 90 surgieron las terapias dirigidas que están diseñadas para bloquear de forma específica dianas moleculares que se encuentran sobre-expresadas en células cancerígenas favoreciendo su crecimiento incontrolado. De hecho, de los 19 nuevos fármacos anticancerígenos aprobados por la FDA entre 2012 y 2014, 18 de ellos se basan en terapias dirigidas[5]. El primer ejemplo de este tipo de tratamientos es el Rituximab que fue el primer anticuerpo monoclonal aprobado por la FDA en 1997 para el tratamiento de linfomas[16]. Posteriormente, se han desarrollado muchos otros tratamientos basados en anticuerpos monoclonales (Trastuzumab, Pertuzumab, Cetuximab, etc.)[17], inhibidores de la tirosina quinasa (Erlotinib, Gefitinib, Imanitib, etc.)[18], inhibidores de la formación de vasos sanguíneos (Bevacizumab), agentes inmunomoduladores (Mifamurtida, Ipilimumab) y nuevas terapias hormonales (Abiraterona o Enzalutamida). A pesar del gran avance que se ha llevado a cabo en los últimos años en estas terapias dirigidas, todavía queda mucho camino por recorrer para dominar la biología de la células tumorales con el objetivo de encontrar dianas terapéuticas más eficaces que eviten además las resistencias habituales que generan este tipo de tratamientos[19].

1.2. La mitocondria como diana terapéutica

Las mitocondrias son orgánulos extremadamente dinámicos que están presentes en la mayoría de las células eucarióticas. Se consideran el centro neurálgico de las células y sirven como la principal fuente de energía, sintetizando adenosín trifosfato (ATP, del inglés *adenosine triphosphate*) a expensas de glucosa, ácidos grasos y aminoácidos por medio de la fosforilación oxidativa[20]. Estructuralmente, la mitocondria consta de dos membranas que delimitan el espacio intermembrana y la matriz mitocondrial. Los canales aniónicos dependientes del voltaje están presentes en la membrana externa y se encargan de regular la entrada de metabolitos dentro de la mitocondria. Por el contrario, la membrana interna está formada por un gran número de pliegues denominados crestas y en ella se ubican las proteínas que llevan a cabo las reacciones de oxidación de la cadena respiratoria, el

complejo enzimático ATPasa que sintetiza el ATP así como otras proteínas específicas que regulan el paso de metabolitos a la matriz. Finalmente, la matriz mitocondrial alberga los ribosomas y las moléculas del ADN y ARN mitocondrial, siendo los únicos orgánulos que tienen su propio material genético. Además, en la matriz de las mitocondrias se encuentran las enzimas responsables de importantes rutas metabólicas como el ciclo de Krebs[21, 22].

Además de servir como fuente de energía primaria para las células, las mitocondrias están implicadas en la transducción de señales mediadas por calcio y especies reactivas al oxígeno (ROS, del inglés *reactive oxygen species*) y juegan un papel clave en la supervivencia y muerte celular[23, 24]. Todas estas características han convertido a las mitocondrias en un pilar fundamental para el correcto funcionamiento de la maquinaria celular de nuestro organismo y la desregulación de cualquiera de los procesos que en ella tienen lugar juega un papel fundamental en enfermedades como la diabetes, la obesidad, el Alzheimer y también el cáncer[25].

1.2.1. Efecto Warburg

Los primeros estudios sobre la alteración mitocondrial en las células cancerígenas fueron llevados a cabo por el científico alemán Otto Warburg a comienzos del siglo XX[26], descubriendo que la velocidad de glucólisis de las células tumorales era superior a la normal, probablemente debido al deterioro de la capacidad respiratoria de este tipo de células. Por este hallazgo, Otto Warburg recibió el Premio Nobel de Medicina en 1931 [27, 28]. En células normales, el 90% de la energía en forma de ATP proviene de la fosforilación oxidativa que tiene lugar en las mitocondrias. Por el contrario, las células tumorales obtienen esa energía a través de la glucólisis que tiene lugar previamente en el citosol de las células[29]. Este mecanismo de supervivencia de las células cancerígenas se conoce como efecto Warburg y es considerado como un mecanismo de respuesta de estas células a un ambiente de hipoxia que les permite continuar proliferando indiscriminadamente gracias a un metabolismo altamente glucolítico (**figura 2**)[30].

El descubrimiento del efecto Warburg puso de manifiesto la existencia de otras muchas diferencias en la estructura, composición y función de las células tumorales[31]. Éstas son menos numerosas, más pequeñas y con menor número de crestas. Además, la composición proteica y lipídica de la membrana interna también es diferente y se han demostrado diferencias en el potencial de membrana, la velocidad en el transporte de

electrones y aniones, la síntesis de proteínas y la producción de ROS[32]. Finalmente, importantes mutaciones y alteraciones en el ADN mitocondrial han sido detectadas en varios tipos de cáncer[33-35]. Por lo tanto, la mitocondria tiene un papel clave en la mayoría de las características distintivas del fenotipo de una célula tumoral que fueron descritas por D. Hanahan y R. Weinberg en 2011[36]. Estas señales de identidad fueron: potencial de replicación ilimitado, angiogénesis, evasión de la apoptosis, autosuficiencia de señales de crecimiento, insensibilidad a señales antiproliferativas así como una capacidad de invasión de tejidos y metástasis.

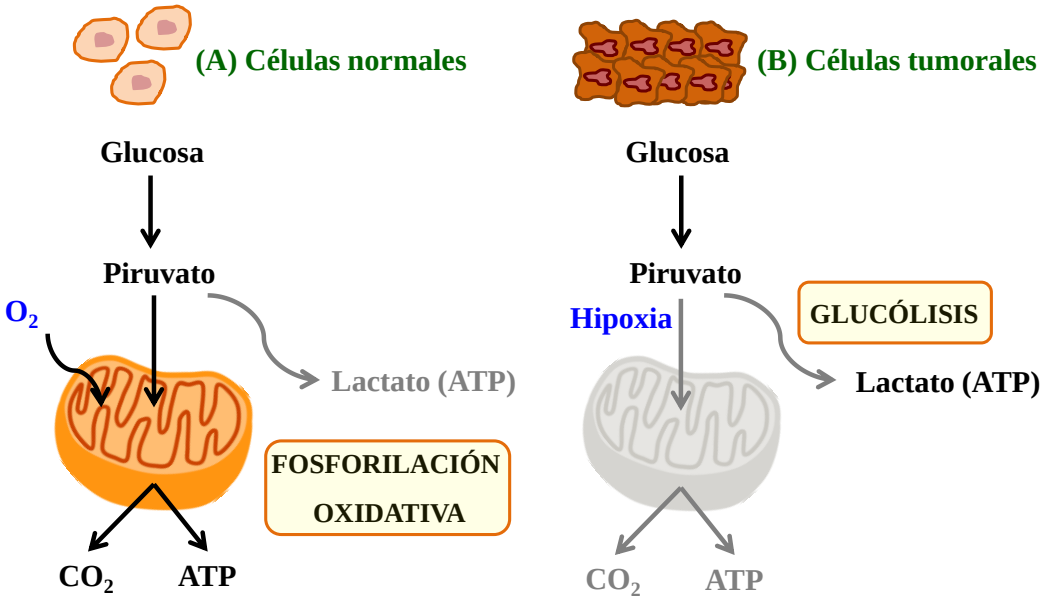

Figura 2: Efecto Warburg. Diferencias en el fenotipo metabólico de células normales (A) y tumorales (B).

A pesar de que estas disfunciones mitocondriales son habitualmente un patrón común en el desarrollo de la enfermedad del cáncer, es importante recalcar que tanto los cambios morfológicos como funcionales observados en las mitocondrias de las células cancerígenas dependen de un gran número de factores como son el tipo de cáncer, el tejido donde se forma originalmente, el estadio de la enfermedad y muchos otros. En este contexto, Cuezva et al. evaluaron el distinto grado de disfunción mitocondrial en numerosos tipos de líneas cancerígenas en un estudio denominado *la huella bioenergética del cáncer*. Para ello, estos autores utilizaron el Índice Bioenergético Celular (BEC) que relaciona el nivel de expresión de marcadores mitocondriales que regulan la biosíntesis de proteínas mitocondriales y que

controlan el metabolismo glucolítico de las células tumorales[37, 38]. Este índice fue calculado para 60 líneas celulares humanas derivadas de 9 tipos de tumores diferentes (mama, sistema nervioso central, colon, células de la sangre, pulmón, melanoma, ovario, próstata y riñón) que definieron el panel NCI-60 del Instituto Nacional del Cáncer a mediados de los años ochenta[39]. Los resultados de este estudio permitieron conocer que algunas de las líneas celulares analizadas presentaban niveles de disfunción mitocondrial especialmente llamativos como distintas células derivadas de cáncer de mama, colón o pulmón. Además, estos estudios han sido una herramienta de vital importancia para el desarrollo de nuevos fármacos y terapias contra el cáncer[40].

1.2.2. La mitocondria como regulador de la muerte celular

Las mitocondrias tienen un papel crucial en la correcta ejecución de la muerte celular programada o apoptosis[41, 42]. A diferencia de la necrosis que es un tipo de muerte celular incontrolada que supone la ruptura de la membrana celular y conlleva una respuesta inflamatoria, la apoptosis es la respuesta a diferentes estímulos: fisiológicos, que activan los receptores de la muerte en la vía extrínseca o bien, como respuesta al estrés, que involucran la cascada de señalización vía mitocondrial (vía intrínseca). Ambas rutas convergen en la liberación de caspasas[43].

La vía extrínseca se caracteriza por la participación de receptores de muerte como son la proteína Fas y el factor de necrosis tumoral (TNF, del inglés *tumor necrosis factor*)[44]. Estos receptores de muerte se unen específicamente a ligandos de muerte extrínsecos que provocan la oligomerización y cambios conformacionales en los receptores así como la formación del complejo de señalización de muerte (DISC, del inglés *death inducing signalling complex*), gracias a la activación de la caspasa 8[45]. Por el contrario, las mitocondrias regulan la vía intrínseca de apoptosis como respuesta al estrés celular. Esto conlleva la liberación de citocromo c al citosol de las células mediante la activación de proteínas pro-apoptóticas tales como Bax, Bak o miméticas BH3 que regulan específicamente la permeabilidad de la membrana mitocondrial externa. Además, estas proteínas se encargan de confiscar y bloquear la participación de proteínas anti-apoptóticas Bcl-2 y se unen creando un estructura porosa que permeabiliza la membrana mitocondrial externa, permitiendo la liberación del citocromo c así como la activación de la caspasa 9 (**figura 3**)[46].

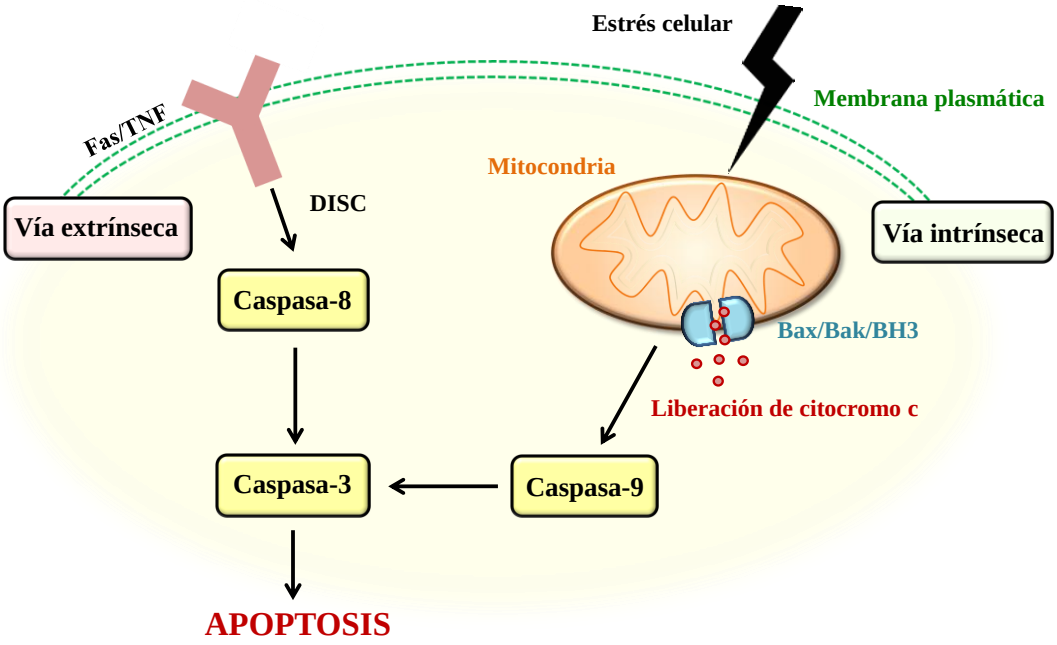

Figura 3: Representación esquemática de las posibles vías de la muerte celular programada o apoptosis: extrínseca (mediada por receptores de muerte) e intrínseca (mediada por la mitocondria en respuesta al estrés celular).

En células normales, las mitocondrias pueden ejercer su función en la regulación de la apoptosis desencadenando la muerte celular en respuesta a diferentes estímulos. Por el contrario, las células cancerígenas desarrollan numerosas estrategias para la evasión de la apoptosis lo que les permite proliferar indiscriminadamente[47]. Además, en las células tumorales con un metabolismo altamente glucolítico, la fosforilación oxidativa no funciona correctamente al igual que el transporte de electrones en la cadena respiratoria. Esto produce la generación de altas concentraciones de ROS, principalmente en los complejos I, II y III de esta cadena de transporte de electrones. La menor concentración de enzimas antioxidantes en las células tumorales (en comparación con las células no tumorales) conduce a la acumulación de estas especias reactivas, con consecuencias nefastas en la progresión de la proliferación celular y carcinogénesis, produciendo inestabilidad y mutaciones en el ADN mitocondrial o daño en distintos componentes celulares [48].

1.3. MITOCANES. Succinato de la vitamina E (α-TOS)

Las diferencias metabólicas, morfológicas y funcionales encontradas en las mitocondrias de células normales y tumorales han convertido a estos orgánulos celulares en

un diana terapéutica ideal para el desarrollo de tratamientos más eficaces y selectivos contra el cáncer[41, 49, 50]. Por ello, la investigación en este campo se centra cada vez más en atacar estas diferencias desarrollando nuevos fármacos que se conocen como mitocanes (del inglés, *mitochondrial targeted anticancer drugs*). Neuzil et al. han clasificado estos fármacos en 8 clases diferentes en función de su sitio de acción (**tabla 1**)[51, 52].

Tabla 1: Clasificación de las diferentes clases de mitocanes, incluyendo su sitio de acción en la mitocondria de células tumorales así como ejemplos de los fármacos más representativos en cada uno de los casos.

Clase	Mecanismo acción	Ejemplos	Refs
1 Inhibidores hexoquinasa	Regulación metabolismo energético Vía glucolítica	3-bromopiruvato (3BP) 2-dexosiglucosa (2DG)	53, 54
2 Miméticos BH3	Proteínas anti-apoptóticas Bcl-2, Bcl-xL	α-TOS, Gosipol, ABT-737	55, 56, 57
3 Inhibidores redox	Control estrés oxidativo Generación ROS	Isotiocianatos, As_2O_3	58, 59
4 Acción vía canal aniónico de voltaje	Permeabilidad membrana mitocondrial	Lonidamina, arsenito, CD437, bisfosfanatos	60, 61, 62
5 Cadena transporte electrones	Activación apoptosis Complejos I, II, III y IV	α-TOS, tamoxifen, resveratrol	63, 64
6 Membrana mitocondrial interna	Potencial de membrana	Rodamina 123, F16, MKT-077	65, 66
7 Ciclo de Krebs	Regulación metabolismo energético Respiración celular	3BP, Dicloroacetato	67, 68
8 ADN mitocondrial	Función, estabilidad y mutaciones ADN mitocondrial	Vitamina K3, fialuridina	69, 70, 71

Uno de los mitocanes más prometedores para el desarrollo de nuevas terapias contra el cáncer es el succinato de la vitamina E o α-tocoferol (α-TOS). Se trata de un mitocan que induce selectivamente la muerte celular programada o apoptosis de células tumorales (anticancerígeno)[72] o células endoteliales en proliferación (antiangiogénico)[73-75] vía mitocondrial[76]. Estructuralmente, el α-TOS es un derivado éster de la vitamina E, disponible comercialmente y en el que Neuzil et al. diferencian 3 dominios a nivel molecular: el dominio de funcionalización (grupo succinato), el dominio de señalización (grupo cromanol) y el dominio hidrofóbico (cadena alifática lateral). En particular, estos autores establecen que el dominio funcional es el principal responsable de su actividad mientras que el dominio hidrofóbico tiene un papel esencial como mediador en el acoplamiento en membranas lipídicas (**figura 4A**)[77, 78].

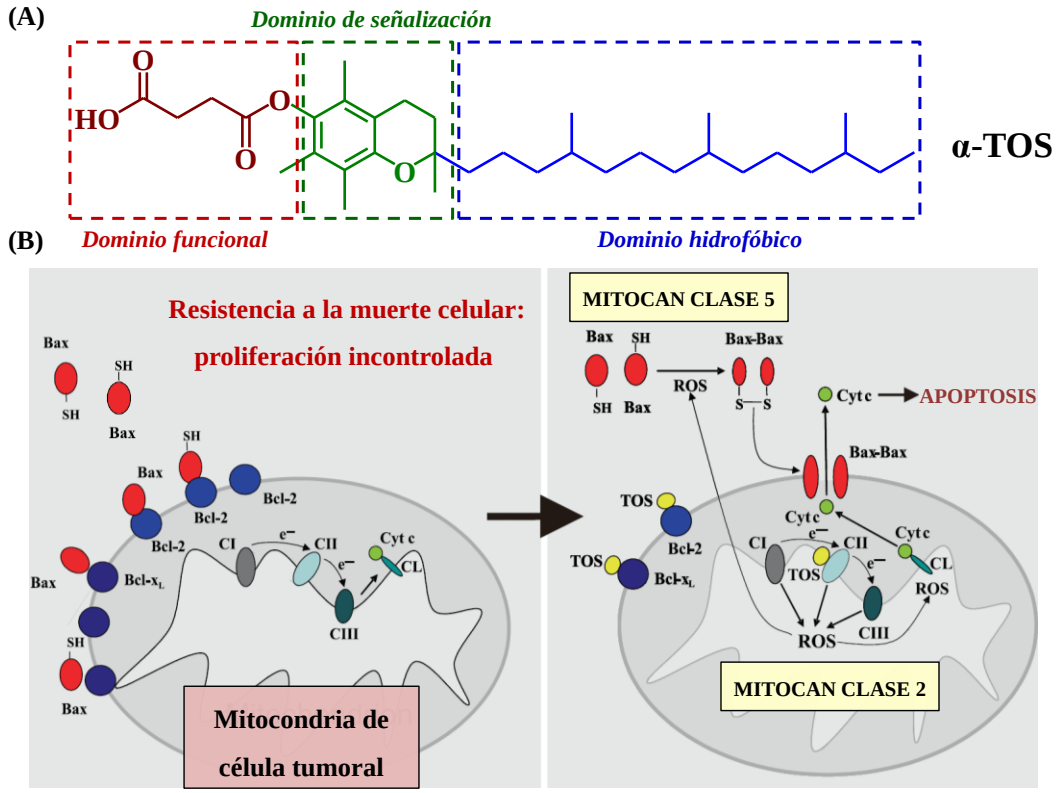

Figura 4: (A) Estructura y diferentes dominios del α-TOS. (B) Mecanismo de acción del α-TOS, actuando como un mitocan clase 2 y clase 5. (Modificada de *Mitochondria and Cancer* 2009, 211[79])

El α-TOS actúa, como un *mitocan clase 2*, en la cadena de transporte de electrones que se ubica en la membrana interna de las mitocondrias[80]. En particular, este fármaco

inhibe la actividad succinato deshidrogenasa del complejo II de la cadena respiratoria desplazando a la ubiquinona en las células cancerígenas[81, 82]. Como consecuencia, los electrones generados por la acción de este completo se recombinan con el oxígeno molecular produciendo altas concentraciones de ROS (especies superóxido, SOD). Estas especies reactivas generan un alto nivel de estrés celular que activa la familia de proteínas pro-apoptóticas Bax. Como resultado de esta activación, las proteínas Bax son capaces de dimerizarse y sufren cambios conformacionales que conducen a la formación de canales multiméricos en la membrana mitocondrial externa. Adicionalmente, los altos niveles de ROS producidos oxidan eficazmente el complejo de la cardiolipina (CL), liberándose el citocromo c que puede alcanzar fácilmente el citosol de las células a través del canal formado previamente en la membrana externa. Una vez que el citocromo c llega al citosol de las células tumorales se desencadena la cascada de eventos de la vía intrínseca de la apoptosis que comienza con la activación de la caspasa 9 y que finalmente termina con la muerte celular (**figura 4B**)[83, 84].

La actividad antitumoral del α-TOS no podría explicarse en base únicamente a este mecanismo de acción. Para que su actividad sea posible, es necesario que este fármaco anule la actividad de las proteínas anti-apoptóticas Bcl-2 que están presentes en las células tumorales. En este sentido, el α-TOS actúa como un *mitocan clase 5*, bloqueando la acción de estas proteínas a través de la su unión por los dominios miméticos tipo BH3 (**figura 4B**)[83, 85].

Una de las principales ventajas del uso del α-TOS es que su actividad contra las células tumorales o en proliferación es altamente selectiva, afectando en mucha menor medida a las células normales. Las razones de la selectividad en el mecanismo de acción de este fármaco no son del todo bien conocidas y hoy en día se continúa investigando en este sentido. Una de las principales teorías alude nuevamente a las diferencias existentes entre células cancerígenas y sanas, básicamente a los mecanismos de defensa que disponen unas y otras frente a situaciones de estrés celular. En concreto, las células normales son capaces de reaccionar ante la acumulación de ROS debido a la presencia de altas concentraciones de enzimas antioxidantes, como la MnSOD (del inglés, *manganese superoxide dismutase*) entre otras, que evitan su acumulación mediante su descomposición en agua oxigenada y oxígeno. En el caso de las células tumorales, los niveles de estas enzimas antioxidantes son muy inferiores por lo que las especies reactivas pueden acumularse fácilmente[73]. Además,

las células normales tienen altos niveles de enzimas hidrolíticas (esterasas) que pueden promover la pérdida de la actividad funcional del α-TOS por hidrólisis del enlace éster del grupo succinato. Esta hidrólisis está mucho más desfavorecida en células tumorales que presentan bajos niveles de esteras permitiendo la acción antitumoral del fármaco[48]. Otra de las diferencias más interesantes entre el tejido tumoral y sano es el pH de forma que se ha demostrado que está ligeramente acidificado (valores de pH entre 6,0 y 6,5) en una gran variedad de tumores sólidos. Esto puede favorecer la actividad anticancerígena del α-TOS que presenta una carga negativa debido a la presencia de su dominio funcional[77].

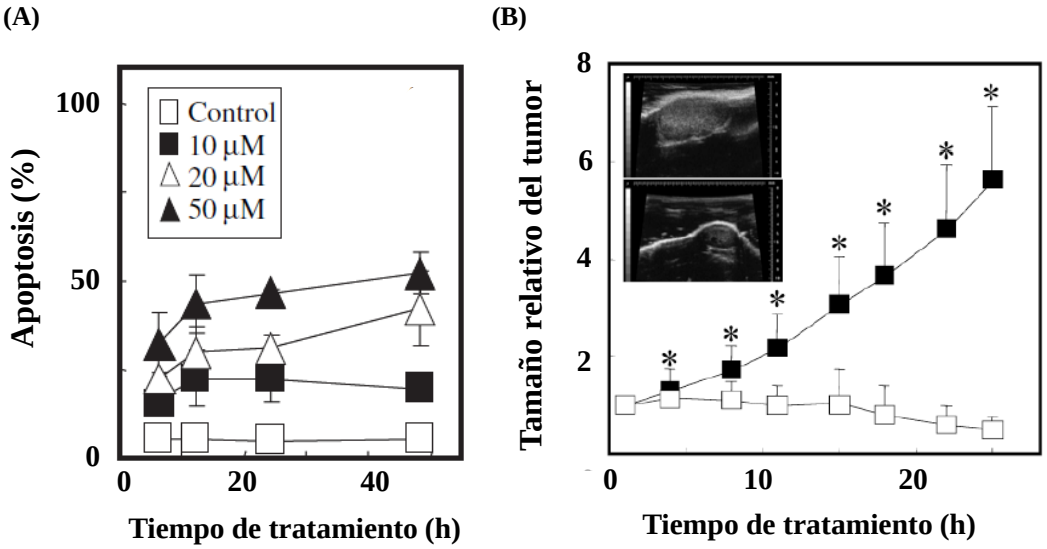

Figura 5: (A) Inducción de la apoptosis en células de neuroblastoma en función de la concentración de α-TOS y el tiempo de tratamiento (modificada de *Journal of Neurochemistry*, 2005, 94:1448 [86]). (B) Inhibición del crecimiento del tumor en un ratones inmunodeprimidos inoculados con células de cáncer de mama MCF-7. α-TOS administrado vía intraperitoneal, solubilizado en una mezcla de aceite de maíz con un 4% de etanol (modificada de *Oncogene*, 2008, 27: 4324 [81]).

La actividad apoptótica *in vitro* del α-TOS ha sido demostrada en más de 50 líneas celulares diferentes, incluyendo células de tumores especialmente agresivos o de mal pronóstico con los actuales tratamientos (mama, colón, pulmón, estomago, ovarios, próstata, neuroblastoma…) (**figura 5A**)[87, 88]. El efecto anticancerígeno de este fármaco depende de un gran número de factores como las características de las células, el tiempo y condiciones de incubación…[89, 90] Adicionalmente, el α-TOS ha sido probado en diferentes modelos *in vivo* en los que habitualmente es solubilizado en disolventes orgánicos como el

dimetilsulfóxido (DMSO)[91-93] o en emulsiones utilizando aceite de maíz o de sésamo[84, 94-96] debido a su alto carácter hidrofóbico (**figura 5B**). De esta forma, se ha demostrado que el α-TOS fue capaz de actuar eficazmente en modelos *in vivo* de cáncer de mama, colon, estómago y melanoma después de su inyección intraperitoneal en dosis adecuadas.

No obstante, la administración del α-TOS para su uso clínico es uno de los principales obstáculos para el avance en el desarrollo de terapias basadas en su mecanismo de acción selectivo. La solubilización en medios orgánicos o emulsiones no es la mejor alternativa para su inyección en el torrente sanguíneo, produciendo efectos negativos en algunos ratones inoculados como reacciones inflamatorias o procesos de embolización[97, 98]. Además, la naturaleza hidrofóbica del α-TOS disminuye su acción terapéutica con unos perfiles farmacocinéticos en plasma no apropiados. Por estas razones, queda mucho camino por recorrer con el fin de encontrar estrategias distintas y eficaces que permitan mejorar la administración de este medicamento.

1.4. La importancia de la nanomedicina

En la última década, la aplicación de la nanotecnología en el campo de la medicina ha emergido como un área de gran interés para la mejora del tratamiento del cáncer y otras enfermedades. Cuando la materia se encuentra confinada en dimensiones en el rango de los nanómetros aparecen nuevas y relevantes propiedades físico-químicas que no se observan a nivel macroscópico[99]. En concreto, la liberación controlada de fármacos es una de las aplicaciones más relevantes y con mayor proyección de la nanomedicina. La mayoría de los sistemas convencionales para la administración de fármacos están enormemente limitados por la solubilidad y toxicidad de los principios activos[100]. Así pues, el uso de vehículos de dimensiones nanométricas surge como una vía apropiada para la dosificación continua y sostenida de medicamentos durante un tiempo determinado en el sitio donde deben realizar su función[3, 101, 102].

En concreto, el uso de la nanomedicina para la administración de fármacos anticancerígenos tiene numerosas ventajas, entre las que destacan la disminución de la toxicidad y la mejora de la eficacia y especificidad de los fármacos utilizados, protegiéndolos a su vez de la degradación o excreción y mejorando los perfiles farmacocinéticos tras su administración[103]. Adicionalmente, otra de las principales ventajas del uso de nanovehículos es su capacidad para acumularse preferentemente en los tejidos

tumorales debido al Efecto de Permeación y Retención Aumentada (EPR) en lo que se conoce como *vectorización pasiva* [104]. Este fenómeno es consecuencia de la combinación de dos factores, la mayor permeabilidad de los vasos sanguíneos tumorales (permitiendo la extravasación del nanofármaco), y la falta de drenaje linfático en el tejido tumoral que provoca, consecuentemente, la retención de las macromoléculas (**figura 6**). La vectorización pasiva debido al efecto EPR depende de la concentración en plasma de las macromoléculas utilizadas y sólo es plausible cuando su peso molecular es superior a 30 kDa [105, 106].

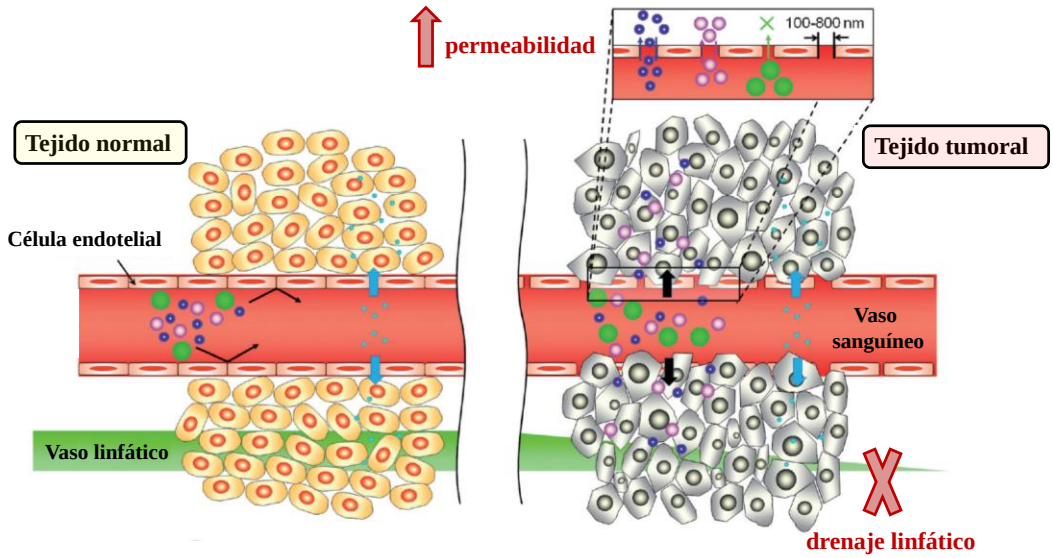

Figura 6: Vectorización pasiva debido al Efecto de Permeación y Retención Aumentada (efecto EPR). (Modificada de *Angewandte Chemie International Edition*, 2014, 53:12320 [107]).

En ocasiones, la vectorización pasiva no resulta lo suficientemente eficaz, especialmente para tumores que presentan un ambiente hipóxico con una baja vascularización y permeabilidad. Para estos casos, se pueden diseñar nanofármacos con *vectorización activa* [5] mediante la incorporación de ligandos que reconocen diferentes tipos de receptores que se encuentran sobre-expresados en las células tumorales como el receptor del factor de crecimiento endotelial vascular (VEGFR, del inglés *vascular endotelial growth factor receptor*)[108], los receptores de transferrina[109] o los receptores tirosina quinasa. Adicionalmente, los ligando utilizados pueden ser de muy diferentes naturaleza, destacando el uso de anticuerpos monoclonales[110], moléculas pequeñas como el ácido fólico[111], glicoproteínas y diferentes secuencias peptídicas, entre otros[112-114].

1.4.1. Tipos de nanovehículos

Actualmente, el tipo de nanovehículos disponibles es muy amplio, tal y como se ilustra en la **figura 7**. En su aplicación en la terapia contra el cáncer, destaca el gran avance en la investigación de nuevos y más sofisticados nanovehículos lipídicos, principalmente liposomas, conjugados poliméricos y nanovehículos basados en polímeros terapéuticos anfifílicos que pueden forman micelas o nanopartículas (NPs) poliméricas[103]. A continuación, se describen en líneas generales cada uno de estos tipos de nanovehículos, incluyendo ejemplos de los sistemas más representativos que actualmente se comercializan o se encuentran en ensayos clínicos para su futura aprobación en el tratamiento contra el cáncer.

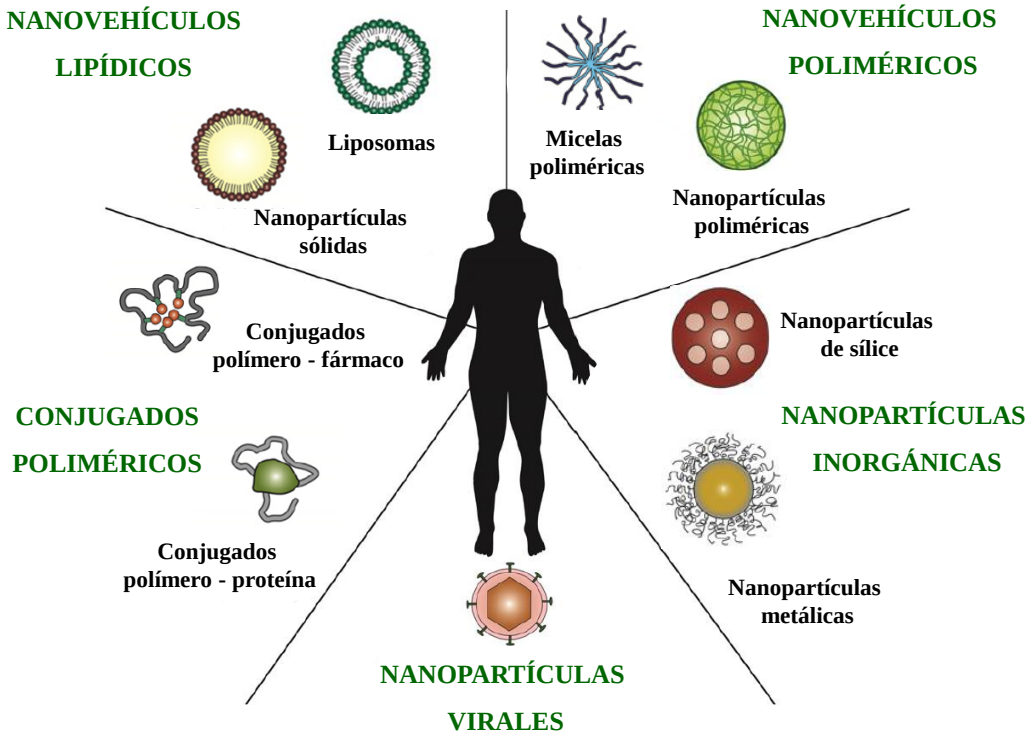

Figura 7: Tipos de nanovehículos utilizados para la liberación de fármacos y el desarrollo de tratamientos contra el cáncer. (Modificada de *Journal of Controlled Release*, 2015, 200:138 [103]).

- **Nanovehículos lipídicos: liposomas**

Los liposomas pueden definirse como vesículas esféricas formadas por bicapas lipídicas dispuestas concéntricamente y compuestas por distintos tipos de fosfolípidos como la lecitina o la fosfatidilcolina (PC, del inglés *phosphatidylcholine*), entre otros[115, 116]. De

esta forma, los liposomas pueden contener uno o más compartimentos acuosos en función de la metodología seguida para su preparación. Existen diferentes tecnologías para su obtención pero todas ellas se basan en la preparación de una suspensión de fosfolípidos en un medio hidrofóbico que se sustituye lentamente por una solución acuosa mediante procesos de dilución, evaporación o diálisis. Este cambio de disolvente provoca que los fosfolípidos se agrupen espontáneamente entre ellos[117].

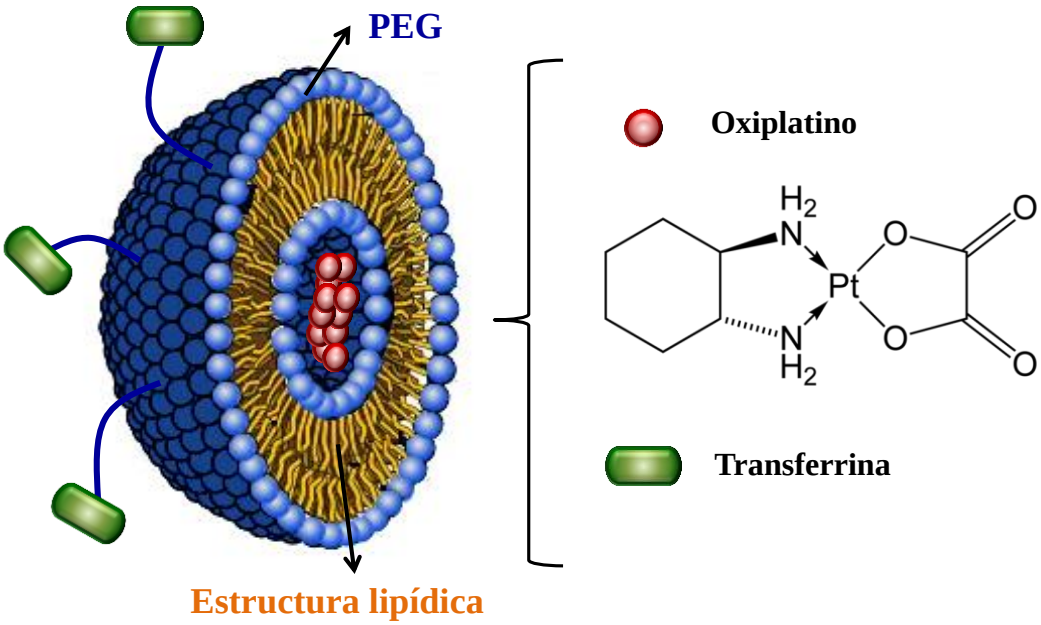

Figura 8: Representación esquemática de la estructura de los liposomas pegilados MBP-426, modificados con transferrina (vectorización activa) que se encuentran en la fase II de los ensayos clínicos.

Los liposomas fueron los primeros nanovehículos aprobados por la FDA para su uso en humanos en el tratamiento contra el cáncer; en concreto, el Doxil® en el año 1995. Estos liposomas se modificaron superficialmente con polietilenglicol (PEG) y encapsularon eficazmente la DOX para el tratamiento del cáncer de ovario y el sarcoma de Kaposi[118]. En años posteriores, sólo 5 formulaciones lipídicas más han sido aprobadas para el tratamiento del cáncer basadas en liposomas no modificados superficialmente con PEG (*pegilación*) para la encapsulación de DOX (DaunoXome®)[119], citarabina (DepoCyt®)[120], vincristina (Marqibo®)[121] y mifamurtida (Mepact®)[122]. Estos nanovehículos lipídicos se utilizan en el tratamiento del sarcoma de Kaposi, la leucemia o el osteosarcoma[103]. Todas estas formulaciones no incluyen ningún mecanismo de vectorización activa pero aun así han

logrado mejorar la toxicidad y los perfiles farmacocinéticos de los fármacos que administran. En la actualidad, se siguen investigando este tipo de formulaciones con más de 500 ensayos clínicos en Estados Unidos con distintos sistemas lipídicos[5]. En este contexto, uno de los ejemplos más prometedores es la formulación pegilada MBP-426 que se encuentra actualmente en la fase II de los ensayos clínicos, siendo una de las primeras en incorporar un elemento de vectorización activa. La superficie de los liposomas se modifica con transferrina que es una glicoproteína que transporta hierro hasta las células mediante su interacción con receptores celulares específicos que están sobre-expresados en células tumorales (**figura 8**). Estos liposomas encapsulan eficazmente oxiplatino para el tratamiento del cáncer de mama o hígado[123].

- **Conjugados poliméricos**

Los conjugados poliméricos se basan en la unión covalente de un fármaco a la estructura de un polímero y se distinguen principalmente dos tipos: conjugados polímero-fármaco y conjugados polímero-proteína. En 1970, Ringsdorf propuso un modelo ideal de sistema conjugado de forma que a la estructura del polímero se le añade un grupo solubilizador, que mejora la biodisponibilidad del sistema de transporte; un espaciador, cuya estabilidad química no debe modificarse durante su transporte, y por último, un ligando para alcanzar eficazmente el sitio de acción[124]. Tanto la elección del portador polimérico como la del enlace covalente son puntos clave en el diseño de este tipo de macromoléculas poliméricas. Por un lado, el polímero no debe ser ni tóxico, ni inmunogénico, y además, debe poseer una apropiada capacidad de carga. Por otra parte, el enlace covalente debe ser estable en plasma y capaz de biodegradarse a la velocidad adecuada cuando el conjugado llegue a la diana molecular establecida[125-127].

Hasta la fecha, no hay ningún conjugado polímero-fármaco aproado por la FDA para el tratamiento del cáncer[5]. Por el contrario, dos conjugados polímero-proteína están comercialmente disponibles. El PEG-L-asparaginasa (Oncaspar®) fue el primer conjugado anticancerígeno PEG-proteína en conseguir la aprobación de la FDA para el tratamiento de la leucemia[128]. Además, Maeda et al. desarrollaron el primer conjugado polímero-proteína que llegó al mercado, denominado SMANCS. Este sistema se basaba en la unión de la neocarzinostatina con el copolímero de ácido maleico y estireno para su administración local en pacientes con carcinoma hepatocelular[129].

A pesar de no llegar a comercializarse, el avance en el desarrollo de conjugados polímero-fármaco ha sido trepidante en los últimos años. Actualmente, hay más de 15 conjugados en diferentes fases de ensayos clínicos. La mayoría de estos sistemas utilizan polímeros sintéticos como el PEG[130], el poli(*N*-(2-hidroxipropil)metacrilamida) (HPMA)[131] y el ácido poliglutámico (PGA)[132] para la conjugación de diferentes fármacos como la DOX[133, 134], el PTX[135, 136] y la camptotecina[137, 138], entre otros. Un ejemplo relevante de estos conjugados es el NKTR-102 que actualmente se encuentra en la fase III de ensayos clínicos[139]. En este caso, el irinotecan, un derivado de la camptotecina, se ancla covalentemente al PEG para el tratamiento del cáncer de mama, ovario y colón.

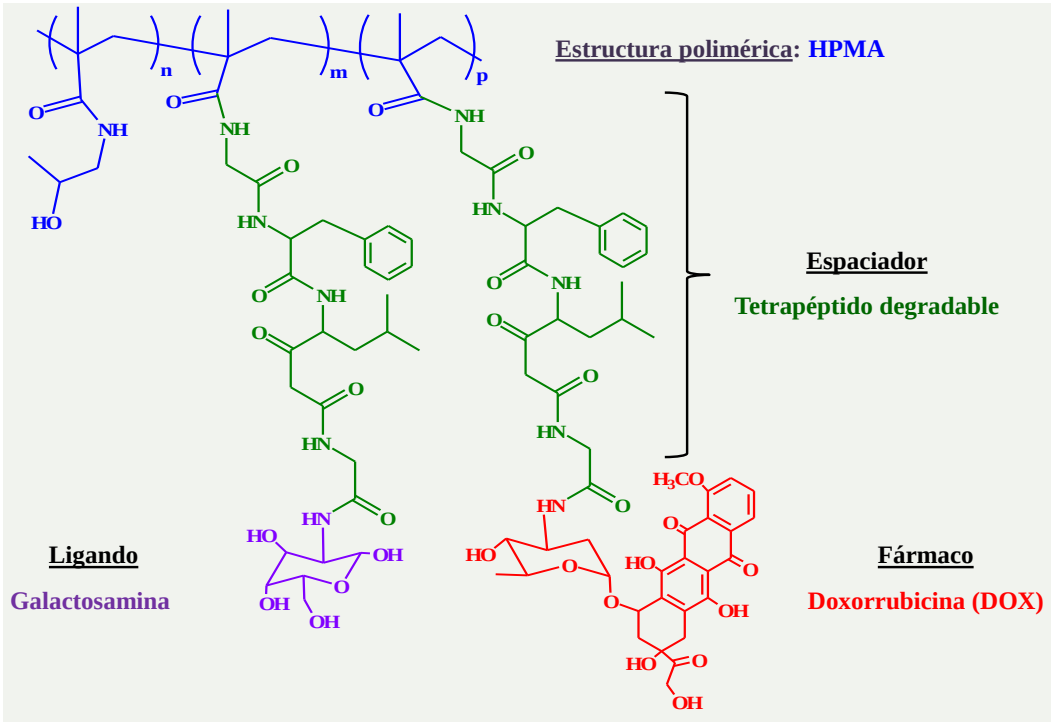

Figura 9: Estructura química y distintos componentes del primer conjugado polímero-fármaco (PK2) con vectorización activa que alcanza la evaluación clínica.

Actualmente, sólo un conjugado polímero – fármaco con elementos de vectorización activa se encuentra en evaluación clínica. Este es el caso del sistema polimérico PK2 en el que la DOX se ancla al HPMA, utilizando además la galactosamina como ligando con el fin de promover la vectorización hacia el receptor asialoglicoproteico para el tratamiento del cáncer hepatocelular o de hígado. Además, este conjugado incluye el tetrapéptido, Gly –

Phe – Leu – Gly, como espaciador de forma que permite la liberación del fármaco a través de su escisión por enzimas lisosomales presentes en las células tumorales (**figura 9**)[140].

- **Nanovehículos poliméricos autoensamblados**

Los sistemas poliméricos autoensamblados representan una de las alternativas más prometedoras para el desarrollo de nanofármacos, pudiendo formar parte en un futuro de tratamientos más eficaces y menos tóxicos contra el cáncer. El autoensamblado macromolecular es un proceso espontáneo basado en la organización de las moléculas en estructuras 3D supramoleculares con diferentes morfologías en un medio acuoso. Este proceso es posible debido a la naturaleza anfifílica de los sistemas poliméricos utilizados, conteniendo dominios hidrofílicos e hidrofóbicos en su composición[141, 142].

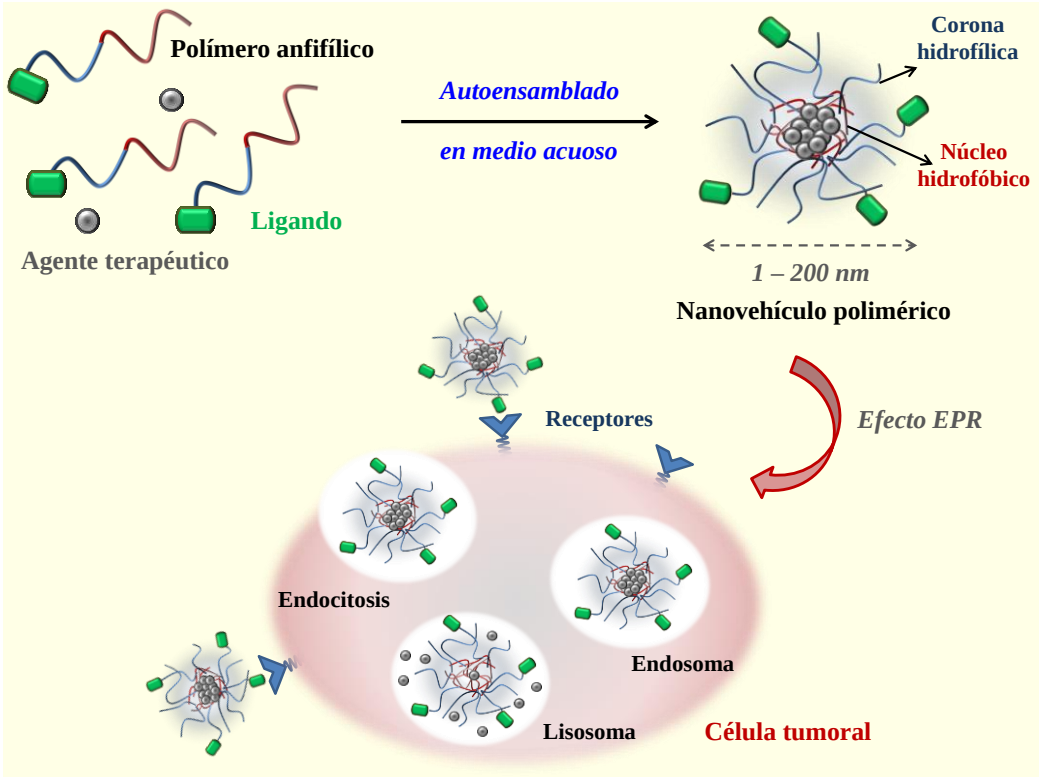

Figura 10: Representación esquemática del proceso espontáneo de formación de nanovehículos autoensamblados a partir de copolímeros anfifílicos y su acumulación preferencial en células tumorales debido al efecto EPR y la vectorización activa.

En el proceso de autoensamblado, los bloques hidrofóbicos constituyen el núcleo de los nanovehículos que a su vez están rodeados por una corona formada por los dominios

hidrofílicos del sistema polimérico. Adicionalmente, el núcleo hidrofóbico de estos nanovehículos puede utilizarse para encapsular fármacos anticancerígenos altamente tóxicos e hidrofóbicos, favoreciendo su liberación sostenida en el tumor debido al efecto EPR[143-145]. Por otra parte, la corona exterior de estos sistemas puede decorarse con diferentes ligandos potenciando la vectorización activa de los mismos (**figura 10**)[141]. En el **anexo II** se incluye una completa revisión bibliográfica acerca de la preparación y las aplicaciones más novedosas de sistemas poliméricos autoensamblados para el tratamiento del cáncer.

Tipos y métodos de preparación

Las características y propiedades de los sistemas poliméricos autoensamblados dependen de un gran número de factores, entre los que cabe destacar: su composición molecular, la secuencia de unidades monoméricas y su distribución a lo largo de las cadenas macromoleculares, el balance hidrofílico/hidrofóbico existente, etc.[141] Adicionalmente, estos nanovehículos pueden clasificarse en función de la estructura supramolecular que forman después del proceso de autoensamblado. En este sentido, se distingue entre micelas poliméricas[146] y distintos tipos de NPs[147], como nanocapsulas[148] o nanoesferas.

A pesar de que estos sistemas poliméricos pueden prepararse también a partir de polímeros naturales, como el ácido hialurónico[149] o el quitosano[150], los polímeros sintéticos forman parte del desarrollo de un gran número de nanovehículos que hay actualmente en evaluación clínica o que están todavía en fase de investigación. En particular, hay un amplio espectro de polímeros utilizados para este fin, entre los que cabe destacar: el PEG, los Plurónicos®, el poliHPMA, diferentes poliaminoácidos (PAA) así como poliésteres biodegradables[5, 151]. Adicionalmente, el uso de péptidos anfifílicos y poli(2-oxazolinas) (POX) está cobrando especial relevancia en los últimos años en este campo. En cualquiera de los casos, la preparación de estos nanovehículos poliméricos conlleva dos etapas: la síntesis de los polímeros anfifílicos y la posterior formación de las estructuras supramoleculares por diferentes metodologías[141, 152, 153].

Los polímeros anfifílicos se pueden preparan por diferentes métodos sintéticos como la polimerización por apertura de anillo (ROP), la polimerización radical convencional o controlada (CRP, del inglés *controlled radical polymerization*) así como por reacciones de química click. En primer lugar, la polimerización ROP es la técnica más empleada para la preparación poliésteres[154, 155], polipéptidos y POX[156]. Por otra parte, la polimerización por

radicales libres (o polimerización radical convencional) es un método de síntesis sencillo y económico que permite obtener polímeros de pseudo-bloque con una apropiada distribución de los monómeros a lo largo de sus cadenas macromoleculares. Esto es posible siempre y cuando se utilicen monómeros de muy diferente hidrofilia y reactividad. López-Donaire et al. copolimerizaron con éxito el metacrilato de oleil 2-acetamido-2-deoxi-α-D-glucopiranósido (OAG) con la *N*-vinil-2-pirrolidona (VP). La diferente reactividad de estos monómeros (r_{OAG} = 5,94 y r_{VP} = 0,01) favoreció la formación de dominios hidrofílicos e hidrofóbicos que se autoensamblaron formando micelas en agua [157]. Debido a la potente actividad antimitótica del OAG, estos autoensamblados redujeron selectivamente la viabilidad de células tumorales de glioblastoma. En la misma línea, García-Fernández et al. prepararon copolímeros utilizando un derivado metacrílico del ácido 5-amino-2-naftalensulfónico (MANSA) y el acrilato de butilo que demostraron una actividad antiangiogénica debido a la interacción del MANSA con factores de crecimiento específicos involucrados en la migración y proliferación celular[141, 158, 159].

En el campo del diseño y control de macromoléculas complejas, las técnicas de CRP representan la mejor alternativa para obtener polímeros con baja polidispersidad y un control exhaustivo de la microestructura y organización de los dominios anfifílicos en las cadenas poliméricas. Esto se consigue mediante la disminución de los procesos de terminación y de transferencia de cadena, aumentando el tiempo de vida media de los radicales en propagación. Para ello, se establece un equilibrio de activación y desactivación de cadenas en crecimiento entre especies activas (P·) y durmientes (P-X) (**figura 11**) [160].

Dentro de los métodos de CRP, la polimerización mediada por radicales estables nitróxidos (NMP, del inglés *nitroxide mediated polymerization*), la polimerización radical por transferencia de átomo (ATRP, del inglés *atom transfer radical polymerization*) y la polimerización por adición, fragmentación y transferencia de cadena reversible (RAFT, del inglés *reversible addition-fragmentation chain transfer polymerization*) son las que han sido más ampliamente utilizadas en la síntesis de polímeros anfifílicos[141]. Sin embargo, la poca versatilidad en cuanto a monómeros polimerizables de la polimerización NMP[161, 162] y la presencia de catalizadores metálicos en la polimerización ATRP[163, 164], han convertido la polimerización RAFT en la alternativa más versátil y ventajosa en el campo de la nanomedicina[165].

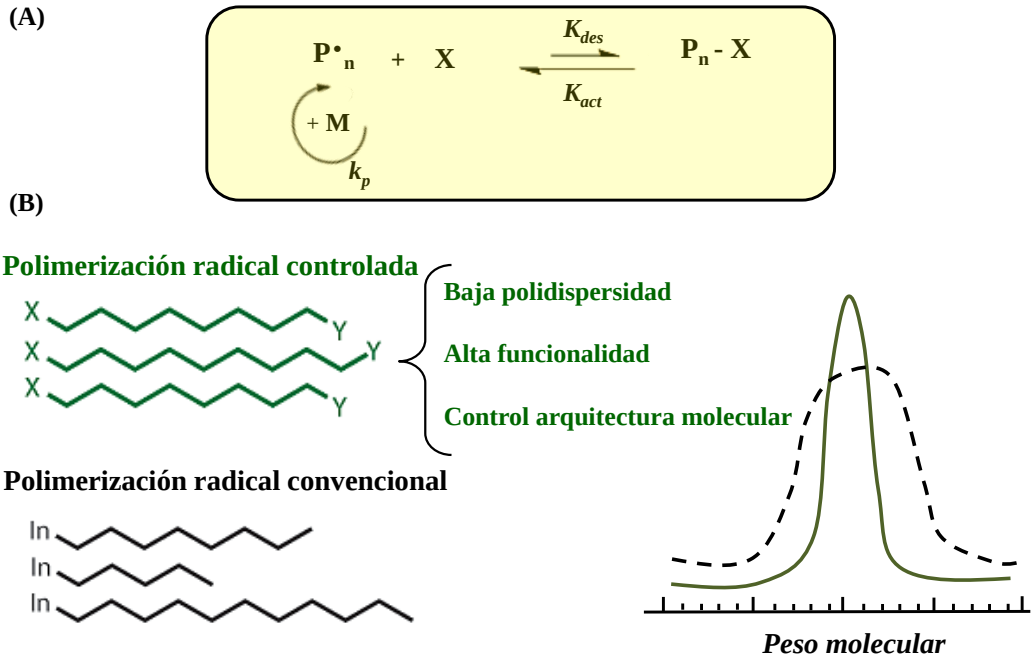

Figura 11: (A) Representación esquemática de la etapa de propagación en la polimerización radical controlada (CRP). (B) Ventajas de la CRP frente a la polimerización radical convencional.

La polimerización RAFT fue desarrollada por el grupo de Rizzardo, Moad y Thang en 1998 y en ella participan derivados de tioésteres (agentes de transferencia de cadena CTA, del inglés *chain transfer agents*) que controlan el crecimiento de las cadenas mediante un proceso de transferencia de cadena degenerativo. Inicialmente, el agente RAFT (1) se combina con la cadena propagante formándose una especie radicalaria intermedia (2) que puede fragmentarse dando lugar a una especie durmiente (3) y una nueva especie activa (R·). Esta nueva especie activa actúa como iniciador de nuevas cadenas por adición de monómero (**figura 12**).

Etapa de transferencia de cadena:

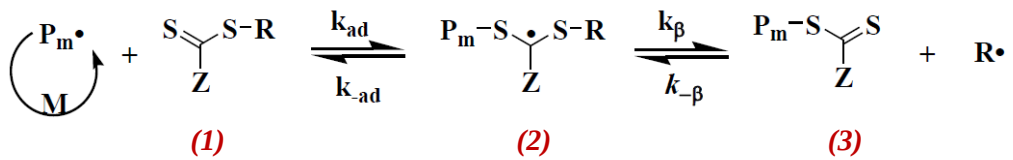

Figura 12: Representación de la etapa de transferencia de cadena característica de la polimerización RAFT.

Las ventajas de la polimerización RAFT en la preparación de polímeros anfifílicos son numerosas, destacando el gran número de monómeros polimerizables, en condiciones moderadas y dotando a los polímeros de una funcionalidad terminal proveniente del agente RAFT que puede utilizarse para la conjugación de otras moléculas o la transformación en otros grupos funcionales[166, 167]. A modo de ejemplo, Yang et al. sintetizaron copolímeros tribloque vía RAFT incluyendo una secuencia peptídica (GFLGKGLFG) en la cadena principal así como moléculas de DOX[168]. Adicionalmente, Priyadarsi et al. prepararon copolímeros de *N*-isopropilacrilamida (NIPAM) y *N*,*N*-dimetilacrilamida (DMA) que fueron capaces de autoensamblarse en medio acuoso[169].

Una vez sintetizados los polímeros anfifílicos, la obtención de los nanovehículos poliméricos puede llevarse a cabo por diferentes metodologías. Muchas de estas tecnologías se basan en la preparación de una suspensión de los polímeros en un disolvente orgánico y su posterior eliminación o sustitución por una fase acuosa. En este contexto, la nanoprecipitación o la diálisis son dos tecnologías habituales para la síntesis de nanoensamblados poliméricos. Otras metodologías muy utilizadas son el salting-out, el spray-drying, la polimerización en dispersión o la tecnología de fluidos supercríticos[141, 170].

Ejemplos representativos de nanovehículos poliméricos autoensamblados

A pesar del gran avance de la investigación en el campo de la nanomedicina y más en concreto en el desarrollo de nanofármacos, todavía ningún nanovehículo polimérico ha sido aprobado y comercializado para su uso en la terapia contra el cáncer[5]. Sin embargo, más de 10 sistemas autoensamblados se encuentran actualmente en distintas etapas de los ensayos clínicos necesarios para su aprobación y final uso en humanos. De entre todos los polímeros empleados en la síntesis de polímeros anfifílicos, destaca el PEG como el polímero más ampliamente utilizado. Se trata de un polímero soluble en agua, biocompatible y poco inmunogénico, aprobado por la FDA para su uso en aplicaciones farmacológicas. Su incorporación en nanovehículos (pegilación) cobra especial relevancia debido a que reduce su reconocimiento por el sistema retículo endotelial (RES, del inglés *reticuloendothelial system*), evitando su eliminación en el hígado, bazo o riñón. En efecto, la presencia de cadenas de PEG genera un impedimento estérico que bloquea la interacción con opsoninas que son las proteínas que reconocen los antígenos de los macrófagos característicos del sistema RES (**figura 13**) [171-173].

La mayor parte de los ensayos clínicos con sistemas autoensamblados con PEG utilizan polímeros de bloque que están formados también por PAA como el ácido poliaspártico (PAsp). Así pues, micelas formadas por copolímeros PEG-*b*-PAsp fueron utilizadas para encapsular PTX y evaluadas *in vitro* hasta en 12 líneas celulares tumorales diferentes. Actualmente, estas micelas, denominas NK105, se encuentran en la fase III de ensayos clínicos [174, 175]. En fase II se encuentran las micelas poliméricas NK911 en las que la DOX es conjugada químicamente al bloque hidrofóbico del copolímero PEG-*b*-PAsp [176]. Por otra parte, un derivado de la camptotecina (SN38) fue anclado químicamente al ácido poliglutámico (PGlu) que formaba el núcleo hidrofóbico de micelas con una corona exterior de PEG. Estos sistemas (denominados NK012) de un tamaño de aproximadamente 20 nm se encuentran actualmente en la fase II de ensayos clínicos para su futura aprobación y uso en humanos para el tratamiento de tumores sólidos de mama, estómago y pulmón, entre otros [177].

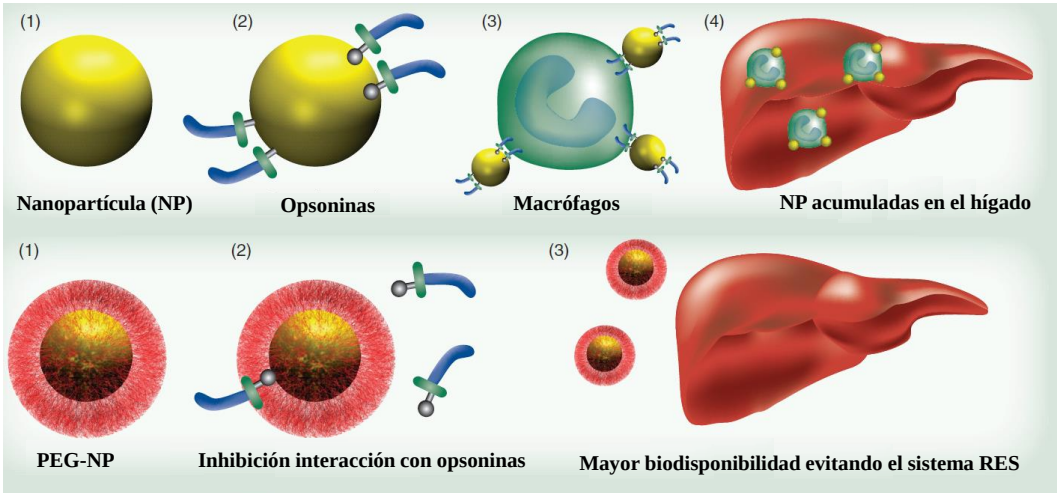

Figura 13: Efecto de la pegilación en nanovehículos poliméricos, reduciendo su interacción con las opsoninas y su eliminación por el sistema RES. (Modificada de *Nanomedicine*, 2011, 6:715 [178]).

Por otra parte, el PEG se ha combinado con éxito con otros polímeros hidrofóbicos como poliésteres. En efecto, el Genexol® es una micela polimérica basada en copolímeros de PEG-*b*-poli(ácido-D,L-láctico) (PEG-*b*-PDLA) que encapsula PTX para el tratamiento del cáncer de ovario, gástrico y de mama. Se encuentra en fase II de los ensayos clínicos, mostrando una eficacia mayor que el PTX libre y con menor número de efectos secundarios[179, 180]. Actualmente, sistemas más avanzados que incorporan ligandos como diferentes secuencias peptídicas[181-183] o moléculas específicas como el ácido fólico[184, 185] se

encuentran en fase de investigación con prometedores resultados *in vitro* e *in vivo* para el tratamiento de diversos tumores sólidos.

En la misma línea que el PEG, los Plurónicos® son una alternativa de interés para el desarrollo de nanovehículos poliméricos. Estos polímeros anfifílicos están compuestos por un bloque hidrofílico de poli(óxido de etileno) (PEO) y otro hidrofóbico de poli(óxido de propileno) (PPO), organizados en estructuras tribloque (PEO_x-*b*-PPO_y-*b*-PEO_x)[141]. Uno de estos sistemas, denominado SP1049C, ha alcanzado la evaluación clínica en fase III. En particular, se trata de micelas formadas por los Plurónicos® L61 y F127 que se emplean para la encapsulación de DOX con aplicación en un amplio rango de tumores sólidos, en especial, aquellos resistentes a múltiples drogas o multirresistentes (MDR, del inglés, *multidrug resistance*) debido a la inhibición de la glicoproteína P o Pgp (del inglés, *P-glycoprotein*) (**figura 14**)[186, 187].

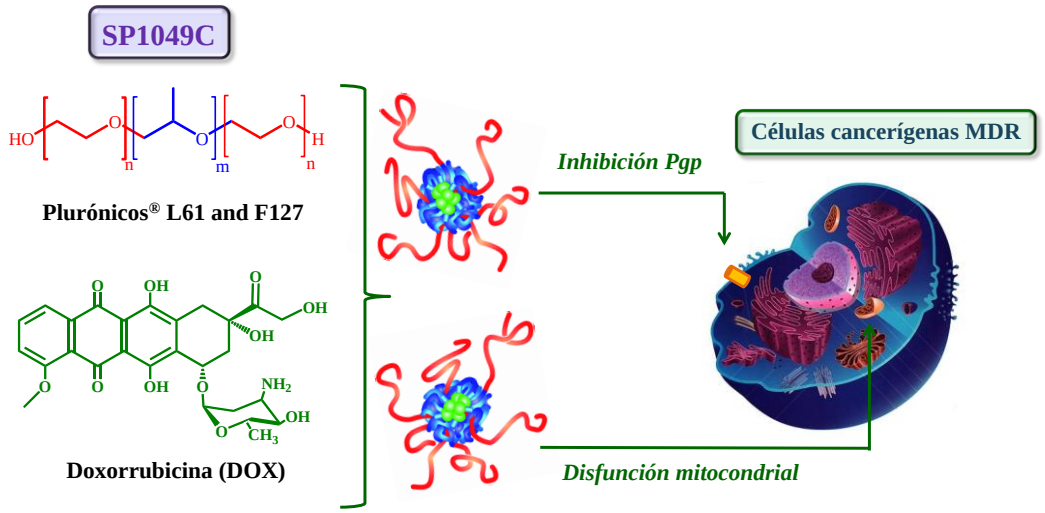

Figura 14: Representación esquemática del sistema conjugado SP1049C que se encuentra en la fase III de los ensayos clínicos para el tratamiento de tumores sólidos altamente resistentes.

A pesar de no alcanzar actualmente la comercialización y ni la fase clínica, muchos otros polímeros autoensamblados están siendo intensamente investigados para su uso como nanovehículos para el tratamiento del cáncer con resultados muy esperanzadores[141]. Un ejemplo es el HPMA que forma la corona hidrofílica de nanovehículos en los que se han conjugado distintos fármacos anticancerígenos mediante el uso de los grupos secundarios presentes en su estructura[188, 189]. En este contexto, Chytil et al. conjugaron la DOX usando diferente contenido de sustituyentes hidrofóbicos como el colesterol. Estos conjugados formaron estructuras supramoleculares de hasta 37 nm que mostraron una actividad

antitumoral en células de linfoma, acumulándose preferentemente en la zona tumoral debido al efecto EPR[190]. Por otra parte, Miller et al. utilizaron una estrategia similar para conjugar dos fármacos diferentes en la estructura polimérica del HPMA, el aminobisfosfonato alendronato y el PTX con prometedores resultados en células de carcinoma de próstata[191]. Un diseño más sofisticado fue propuesto por Jia et al. que copolimerizaron vía RAFT el HPMA con el 2-(2-piridildisulfuro)etilmetacrilato (PDSM). Además, la alta versatilidad de los grupos PDS permitió la conjugación de la DOX a través de enlaces hidrazona sensibles al pH. En un medio acuoso, estos polímeros se autoensamblaron, estabilizándose mediante puentes disulfuro. Gracias a la incorporación de enlaces sensibles al pH, la DOX se liberaba *in vitro* preferentemente a pH ácidos, característicos de tumores sólidos[192].

Otros ejemplos de sistemas autoensamblados muy investigados son los basados en poliésteres (como el ácido poliláctico (PLA)[193] o la policaprolactona (PCL)[194]) y más recientemente y de forma más novedosa, nanovehículos que utilizan péptidos anfifílicos[195-197] y POX[141, 198, 199].

1.5. Actuales nanovehículos para la administración de α-TOS

A pesar de su alto potencial terapéutico, el α-TOS es un fármaco muy hidrofóbico, no soluble en medio fisiológico y por tanto, muy difícil de administrar. Estas características han impedido su uso para el tratamiento selectivo del cáncer más allá de estudios de investigación *in vitro* e *in vivo*[89].

Actualmente, el gran avance de la nanomedicina puede suponer una estrategia eficaz para mejorar los problemas de administración del α-TOS[101, 200]. Una de las primeras estrategias utilizadas para aumentar la solubilidad del α-TOS ha sido la conjugación con PEG (1 kDa de peso molecular) a través del dominio funcional de este fármaco para formar el conjugado denominado TPGS (del inglés, *α-tocopheryl polyethylene glycol succinate*) (**figura 15A**). Esta molécula fue inventada por Eastman Kodak en 1950 y se ha demostrado que es capaz de autoensamblarse formando micelas de aproximadamente 13 nm con un concentración micelar crítica (CMC, del inglés *critical micelle concentration*) de 0,02 % w/w a 37 ºC[201, 202]. Sin embargo, no fue hasta años más tarde cuando Youk et al. demostraron su capacidad antitumoral. En efecto, este conjugado inhibió *in vivo* el crecimiento de células cancerígenas de pulmón de forma más efectiva que el propio α-TOS

debido a su mayor capacidad para generar radicales libres e inducir la apoptosis (**figura 15B**)[203].

El mecanismo por el que el TPGS produce la muerte celular mediada por apoptosis no es del todo conocido. Por una parte, la prolongación de un dominio hidrofílico en la molécula, manteniendo intacta su parte hidrofóbica, claramente mejora su solubilidad en un medio fisiológico. Además, esta modificación estructural tiene efectos positivos en la interacción del TPGS con membranas lipídicas, favoreciendo su capacidad para generar estrés mediado por ROS en las células tumorales. Por otra parte, diferentes autores han demostrado que el TPGS inhibe la función de la glicoproteína de membrana Pgp[204]. Esta proteína parece ser la responsable de una disminución en los niveles de distintos fármacos como la DOX o el PTX en el interior de las células tumorales mediante un mecanismo de transporte dependiente de ATP[205]. Por este motivo, algunos tipos de cáncer no responden eficazmente al tratamiento con fármacos antitumorales en lo que se conoce como "multirresistencia a fármacos" o MDR[206, 207].

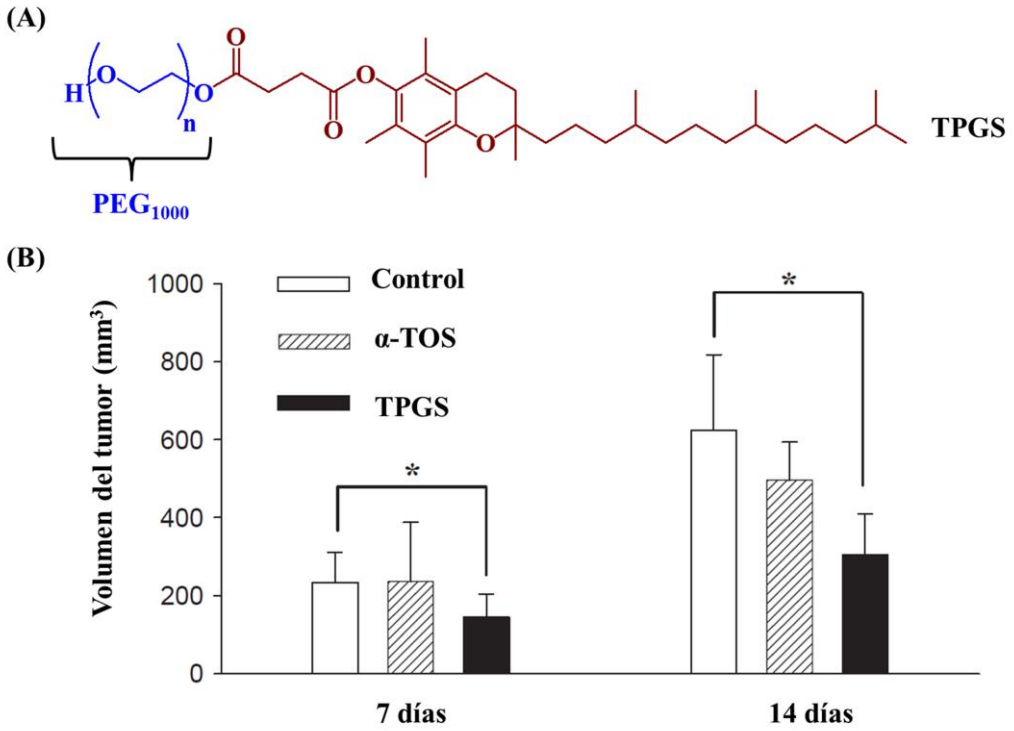

Figura 15: (A) Estructura química del TPGS, incluyendo la incorporación del PEG. (B) Comparación del crecimiento del tumor de células cancerígenas de pulmón inoculadas en ratones inmunodeprimidos, tras la administración de α-TOS y TPGS. (Modificada de *Journal of Controlled Release* 2005, 107:43 [203]).

Además de sus propiedades antitumorales, el TPGS es una molécula ampliamente utilizada como agente estabilizante y surfactante en sistemas de liberación controlada de fármacos[208]. De hecho, su uso con estos fines está aprobado por la FDA y ya en 2005 se incluyó en formulaciones en emulsión para la administración de PTX. Su poder emulsionante supera hasta en 77 veces el de otros emulsionantes tradicionales como el polialcohol vinílico (PVA)[209, 210]. Además, el TPGS es estable a valores de pH entre 4,5-7,5 y sufre una hidrólisis inferior al 10 % cuando se mantiene más de 3 meses en un medio acuoso neutro, quedando además demostrada la estabilidad del enlace éster entre la vitamina E y el grupo succinato[211].

1.5.1. Liposomas

La incorporación de α-TOS en nanovehículos lipídicos es una de las metodologías actuales para su mejorar su administración en medios fisiológicos. De acuerdo con su estructura, esta molécula interactúa con bicapas lipídicas de forma que su cadena alifática se extiende en el centro de la misma de forma paralela a las cadenas de fosfolípidos[212]. Adicionalmente, la estructura cromanol de la molécula se sitúa también dentro de la bicapa más superficialmente, quedando el grupo succinato en la interfase acuosa aumentado la carga superficial de la membrana lipídica[213]. Esto hace que la utilización de fosfolípidos con carga no sea necesaria a la hora de preparar las formulaciones lipídicas con α-TOS. En todos los casos, la composición de los liposomas, el ratio fármaco/lípido y la estabilidad de estas formulaciones son parámetros clave en el diseño de estos nanovehículos[97].

Uno de los fosfolípidos más empleados para la incorporación de α-TOS ha sido la PC [214]. Koudelka et al. prepararon liposomas con un ratio α-TOS/PC de 3:17 que además liofilizaron en presencia de sacarosa. Con esta metodología, se obtuvieron liposomas con tamaños entre 130-140 nm que fueron estables al menos 6 meses a temperaturas entre 2 y 8 ºC[215]. En la misma línea, Hamma et al. mejoraron la estabilidad de liposomas de α-TOS mediante la incorporación de PC de huevo (EPC, del inglés *egg phosphatidylcholine*). Además de obtener liposomas de 300 nm mucho más estables, la eficacia antitumoral *in vitro* fue 7 veces superior en células de melanoma B16-F1 en comparación con la formulación en ausencia de EPC (**figura 16**)[216].

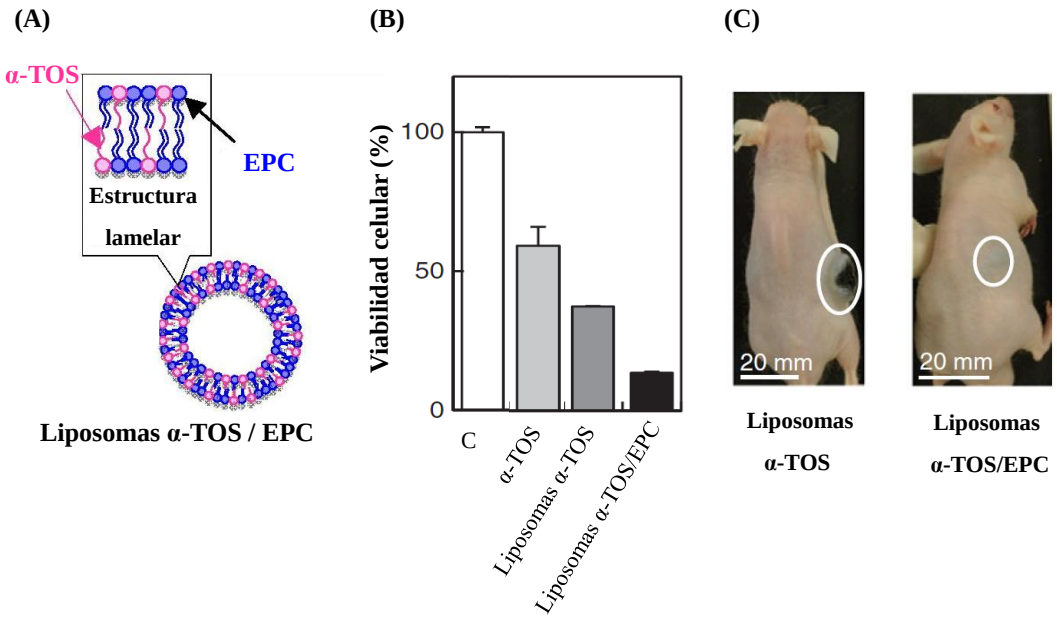

Figura 16: (A) Representación esquemática de liposomas formados por TPGS y EPC. Comparación de los resultados *in vitro* (B) e *in vivo* (C) de liposomas con y sin EPC en células de melanoma B16-F1. (Modificada de *Journal of Controlled Release* 2012, 161:843[216]).

Otro tipo de fosfolípidos como la fosfatidiletanolamina (PE, del inglés *phosphatidyl ethanolamine*) o la distearoil PE (DSPE, del inglés 1,*2-distearoyl-sn-glycero-3-phosphoethanolamine*) han sido empleados para la preparación de diferentes liposomas con α-TOS y TPGS[97, 217, 218].

1.5.2. Conjugados poliméricos

Tanto el α-TOS como el TPGS han sido utilizados para conjugar distintos fármacos antitumorales en su estructura. Cao y Feng anclaron químicamente la DOX al TPGS con el fin de evitar los problemas de resistencias asociados a este fármaco y potenciar además su actividad terapéutica. Este conjugado se internalizó mejor en las células tumorales de mama y glioma y demostró una eficacia antitumoral mayor en ambas líneas celulares en comparación con la DOX libre[219]. Adicionalmente, Anbharasi et al. mejoraron significativamente este sistema mediante la incorporación de ácido fólico que dotaba al sistema de una vectorización activa en células tumorales de mama. De hecho, este conjugado demostró una citotoxicidad 45 veces superior a la DOX libre en células MCF-7, mejorando además su biodistribución *in vivo*[220]. En la misma línea, Duhem et al. conjugaron este mismo fármaco pero en este caso a la estructura del α-TOS a través de su

dominio funcional mediante la formación de un enlace amida. Este conjugado fue capaz de formar nanoestructuras de aproximadamente 250 nm cuando el TPGS fue añadido como surfactante. En particular, el núcleo de estos agregados estaba formado por la DOX unida al α-TOS mientras que el PEG se situaba en la corona exterior de las mismas. Los experimentos biológicos realizados con estas micelas demostraron una alta actividad anticancerígena[221]. Finalmente, diferentes autores han conjugado otros fármacos como PTX[222] y cisplatino [223, 224] a la estructura del TPGS con prometedores resultados *in vitro* e *in vivo*.

1.5.3. Nanovehículos poliméricos

El desarrollo de nanovehículos poliméricos autoensamblados para potenciar la eficacia terapéutica del α-TOS se limita actualmente al uso del TPGS en distintas formulaciones. Sin embargo, esta molécula debe utilizarse en combinación con otros polímeros debido a que su alta CMC puede producir la disociación de sus micelas en plasma[89, 201]. Por esta razón, la estrategia más habitual ha sido la polimerización por apertura de anillo del TPGS con diferentes poliésteres biodegradables como el PLA o la PCL [154].

Zhang et al. copolimerizaron ya en 2006 el TPGS con varios ratios de láctico por ROP utilizando el octoato de estaño como catalizador[225]. Adicionalmente, la formación de NPs a partir de estos copolímeros resulta relativamente sencilla y se ha llevado a cabo por diferentes metodologías como la nanoprecipitación[226], diálisis[227] y emulsión[228]. En todos los casos, estas técnicas de obtención de las NPs han permitido la encapsulación eficaz de una gran variedad de fármacos anticancerígenos, entre los que cabe destacar el docetaxel (DTX)[229], la DOX[230], el PTX[227], la curcumina[231], entre otros. En la mayoría de los casos, la utilización de un vehículo con TPGS en su composición mejoró de forma significativa la internalización de las partículas en las células tumorales con perfiles óptimos de biodistribución y una actividad antitumoral superior *in vitro e in vivo* en comparación con la administración libre de los distintos fármacos. Estos nanovehículos poliméricos se han mejorado con éxito mediante la incorporación de distintos ligandos en su superficie como anticuerpos monoclonales[226, 232] o moléculas pequeñas como el ácido fólico[233] para potenciar su actividad y especialmente, mejorar su capacidad de acumularse en la zona del tumor reduciendo su toxicidad (**tabla 2).**

Tabla 2: Principales nanovehículos poliméricos que incorporan TPGS en su composición para el tratamiento del cáncer.

Tipo copolímero	Fármaco	Ligando	Método preparación	Tamaño (nm)	Resultados	Tipo cáncer	Refs
PLA-*b*-TPGS	DTX	-----	Emulsión simple	240-270	*In vitro*, biodistribución *in vivo*	Mama	228
PLA-*b*-TPGS	DTX	Transferrina	Nanoprecipitación	120	*In vitro*, biodistribución *ex vivo*	Glioblastoma	226
PLA-*b*-TPGS	DTX	Trastuzumab	Emulsión	----	*In vitro*, citotoxicidad e internalización	HER2-Mama	232
PLA-*b*-TPGS	PTX	---	Diálisis	360-475	*In vitro, in vivo*	----	227
PLA-*b*-TPGS	Curcumina	----	Nanoprecipitación	100-400	----	----	231
PCL-*b*-TPGS	Risperidona	----	Emulsión	1000	*In vitro*, liberación	----	234
PCL-*b*-PLA-*b*-TPGS	DTX	----	Emulsión	148-250	*In vitro*, citotoxicidad e internalización	Cuello uterino	229
PLGA-*b*-TPGS	DOX	Ácido fólico	Emulsión	350	*In vitro*, citotoxicidad e internalización	Mama	233
PLLA-b-TPGS	DOX	----	Nanoprecipitación	130-270	*In vitro*, citotoxicidad e internalización	Mama	230

1.6. Terapias avanzadas

En los últimos años, el avance en el campo de la nanomedicina ha sido realmente trepidante, posibilitando el desarrollo de nanovehículos para el tratamiento y diagnóstico simultáneo de la enfermedad del cáncer. Estos nanovehículos se denominan *teranósticos* y actualmente representan una de las terapias más avanzadas en fase de investigación para combatir de forma precoz el cáncer. Para cumplir eficazmente su función, los nanovehículos teranósticos conjugan o encapsulan agentes terapéuticos y de imagen en un mismo sistema. Además, se suelen incorporar ligandos en la superficie de estos vehículos para potenciar la vectorización activa de los mismos en la zona tumoral, favoreciendo su eficacia y disminuyendo su toxicidad (**figura 17**)[235, 236].

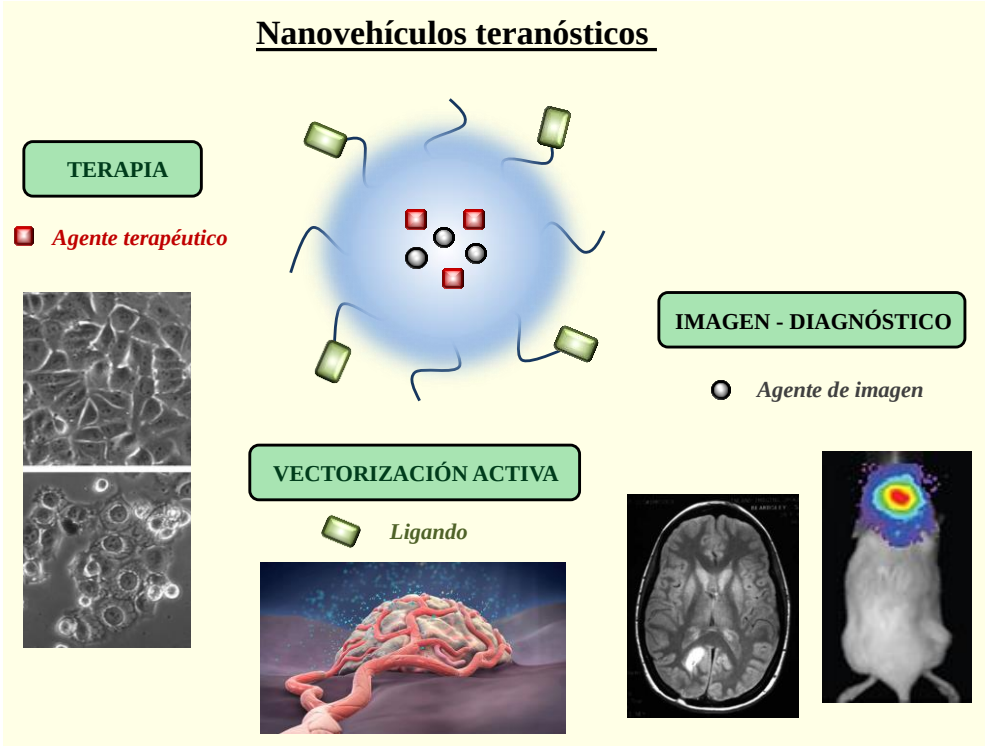

Figura 17: Nanovehículos teranósticos como una terapia avanzada contra el cáncer.

1.6.1. Resonancia magnética de imagen e hipertermia

Las aplicaciones de los nanovehículos teranósticos son muy variadas, incluyendo una gran variedad de modalidades de diagnóstico como los ultrasonidos, la tomografía por emisión de positrones, las imágenes ópticas…[237] Sin embargo, la resonancia magnética de imagen (MIR, del inglés *magnetic resonance imagin*) es la más utilizada debido a sus

ventajas, principalmente su alta resolución espacial evitando el uso de radiación ionizante. Adicionalmente, la exposición de los agentes de imagen más comúnmente utilizados a ondas electromagnéticas genera calor (temperaturas entre 42 y 45 ºC) en la zona donde se acumulan de forma que se puede producir la muerte celular. Este fenómeno se conoce como hipertermia y resulta de gran utilidad para la ablación térmica de tumores[238, 239].

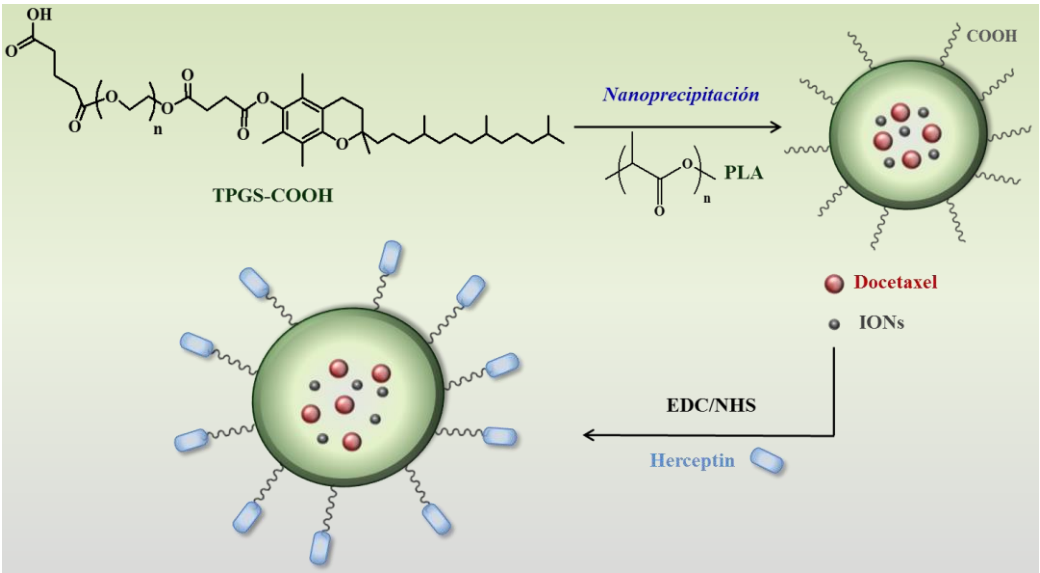

Figura 18: Representación esquemática de la obtención de NPs basadas en copolímeros PLA-*b*-TPGS capaces de encapsular efizcamente IONs y docetaxel (Modificada de *Progress in Polymer Science* 2016, 53:207 [141]).

Los agentes de imagen necesarios para esta aplicación se requieren en altas concentraciones para mejorar la sensibilidad del análisis. Esto puede provocar problemas debido a su alta toxicidad de forma que incorporarlos en un nanovehículo es una alternativa realmente interesante. El gadolinio, las nanopartículas de óxidos de hierro (IONs, del inglés *iron oxide nanoparticles*) y las nanopartículas superparamagnéticas de óxidos de hierro (SPIONs, del inglés *superparamagnetic iron oxide nanoparticles*)[240, 241] son los agentes magnéticos más empleados para la MRI (**tabla 3**). Zarabi et al. conjugaron con éxito el gadolinio y la DOX al HPMA para el tratamiento y diagnóstico precoz del cáncer de mama[242]. Adicionalmente, IONs fueron encapsulados dentro de nanovehículos lipídicos[243] y poliméricos basados en TPGS. Por otra parte, Mi y cols. modificaron copolímeros de bloque PLA-*b*-TPGS para la conjugación de Herceptin® a través del grupo carboxilo terminal del derivado pegilado de la vitamina E[244]. Estos copolímeros fueron capaces de

autoensamblarse formando NPs que encapsularon eficazmente DTX en su núcleo hidrofóbico. Además, estos autores incorporaron IONs para conseguir una terapia combinada de hipertemia y quimioterpaia (**figura 18**). Los resultados biológicos *in vitro* usando un modelo HER2 (receptor 2 de factor de crecimiento epidérmico humano) positivo de cáncer de mama demostraron una eficacia 2000 veces mayor de este nanovehículo en comparación con cada una de las terapias individualizadas[244].

1.6.2. Terapia fotodinámica

La terapia fotodinámica (PDT, del inglés *photodynamic therapy*) consiste en la administración tópica o sistémica de un compuesto con propiedades fotosensibilizadoras que se acumula preferentemente en tejidos tumorales. La posterior irradiación de estos tejidos con luz de una determinada longitud de onda ocasiona la formación de especies altamente reactivas de oxígeno que son las responsables de la destrucción selectiva del tumor. El fotosensibilizador (Ps, del inglés *photosensitizer*) puede dañar los vasos sanguíneos del tumor o activar el sistema inmunitario para la posterior muerte de las células cancerosas[245].

La PDT presenta varias ventajas respecto a otros tratamientos convencionales contra el cáncer como son su escasa toxicidad sistémica, debido a que el Ps sólo es activado en presencia de luz, así como su capacidad de destruir selectivamente tumores, con la consiguiente disminución de efectos secundarios sobre otros tejidos. Actualmente, la FDA ha aprobado el uso de más de 5 fotosensibilizadores y otros muchos se encuentran en fase clínica. Sin embargo, su incorporación en nanovehículos resulta de gran interés para mejorar su eficacia, selectividad y solubilidad[245]. En este sentido, Nakamura et al. anclaron químicamente la protoporfirina de Zn (ZnPP), que es un fotosensibilizador todavía en fase de investigación, al HPMA. Este conjugado formó espontáneamente micelas de 82 nm que permitieron la visualización y el tratamiento *in vivo* de sarcoma en un modelo animal[246] (**figura 19A-B**).

Actualmente, las limitaciones de la PDT son importantes. De hecho, los Ps disponibles en el mercado tienen una vida media corta dentro del tejido, son difíciles de sintetizar y poco estables[247]. Por estas razones, se ha investigado en los últimos años el empleo de agentes más eficaces, destacando el uso de NPs de oro[248] y quantum dots (QDs)[249].

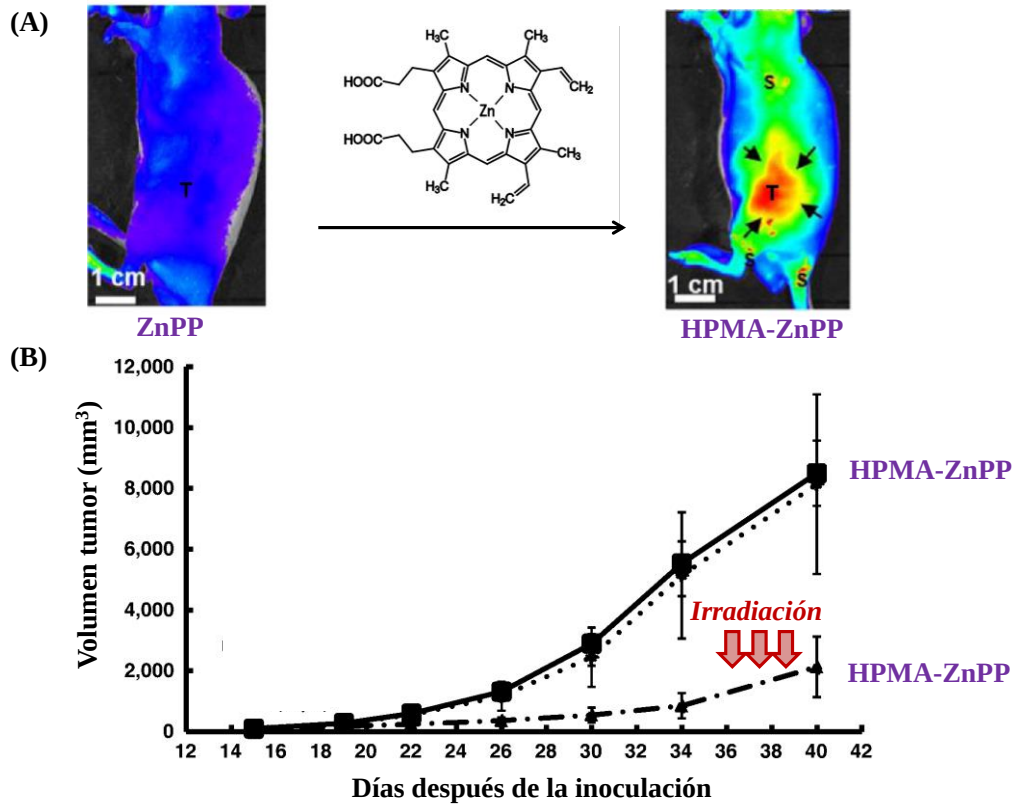

Figura 19: (A) Monitorización *in vivo* del tumor usando micelas basadas en el conjugado HPMA-ZnPP. (B) Reducción del tamaño del tumor tras la irradiación con luz a 400-800 nm. (Modificada de *Journal of Controlled Release* 2013, 165:191 [246]).

En concreto, los QDs fueron identificados en la década de 1980 y su síntesis se logró reproducir a principios de 1990. Sin embargo, no fue hasta 2004 cuando Bakalova et al. propusieron su uso para la PDT[250]. Estas partículas de pequeño tamaño (2-8 nm) están formadas por materiales semiconductores de forma que son capaces de emitir luz en amplio espectro de longitudes de onda en función de su tamaño y composición, con una alta estabilidad e intensidad[251]. Para mejorar su biocompatiblidad, los QDs han sido encapsulados junto con el DTX en liposomas[252] y nanovehículos poliméricos basados en TPGS. Estos nanovehículos fueron modificados superficialmente con ácido fólico, consiguiendo una mejora tanto *in vitro* como *in vivo* en el tratamiento del cáncer de mama[253] (**tabla 3**).

1.6.3. Terapia fototérmica por luz infrarroja

La terapia fototérmica (PTT, del inglés *photothermal therapy*) por luz infrarroja representa una de los sistemas teranósticos más pioneros en la actualidad. Se basa en el empleo de radiación infrarroja (700 – 1000 nm) que se caracteriza por su baja absorción y autofluorescencia en los tejidos, permitiendo mejorar la capacidad de penetración en los mismos con una alta sensibilidad y de forma no invasiva. Además, la absorción de la radiación infrarroja por parte de agentes fototérmicos produce un aumento de temperatura que es capaz de destruir las células tumorales, sin dañar al tejido sano circundante[254].

Los agentes fototérmicos utilizados para la PTT deben poseer una fuerte absorción, eficacia y fotoestabilidad en la región del infrarrojo cercano. Además, deben ser compuestos no tóxicos y con una apropiada selectividad para aminorar los efectos secundarios del tratamiento. En este contexto, se han utilizado agentes fototérmicos inorgánicos en estudios preclínicos utilizando diferentes metales (Au, Ag, Pt, etc.), nanoestructuras de carbono, IONs… Sin embargo, su naturaleza no biodegradable y su alta toxicidad han ralentizado su aplicación clínica. Por estas razones, el uso de agentes fototérmicos de naturaleza orgánica está avanzando de manera significativa en los últimos años, especialmente en el caso de las cianinas[255, 256].

Los colorantes de cianina son moléculas orgánicas pequeñas con dos heterociclos aromáticos que contienen nitrógeno y están unidos por un puente de polimentino. La extensión del número de carbonos del puente de unión entre los heterociclos aromáticos provoca un desplazamiento en la absorción de las moléculas de forma que pueden absorber incluso más allá de 1000 nm (cianina heptametina, Cy7). Estos colorantes son ampliamente utilizados en materiales semiconductores, materiales láser, pinturas…. De hecho, el verde de indocianina (ICG, del inglés *indocyanine green*) fue aprobado hace más de 50 años por la FDA para el análisis del flujo sanguíneo. No obstante, muchos de estos colorantes tienen problemas de fotoestabilidad, un bajo rendimiento cuántico y una muy baja especificidad hacia células tumorales lo que hace necesario su modificación química con ligandos específicos que mejoren su acumulación en la zona tumoral. Por todas estas razones y con el fin de superar estas limitaciones, la investigación en este campo se ha centrado en el desarrollo de colorantes con una multifuncionalidad intrínseca[254].

1.6.4. Sonda de imagen IR-780

Un ejemplo del gran avance en el desarrollo de colorantes para PDT y PTT es el yoduro de IR-780[257]. Se trata de un colorante lipófilo y multifuncional con un máximo de emisión a 780 nm. Su estructura química se caracteriza por la presencia de un anillo en su cadena principal que rigidiza la molécula y un átomo de cloro en el centro que proporciona mayor fotoestabilidad, disminuyendo el efecto de fotodegradación (**figura 20**). Adicionalmente, es estable en suero y tiene un peso molecular apropiado lo que lo convierte en una molécula ideal para el diagnóstico y seguimiento *in vivo* de tumores[258]. En efecto, puede ser utilizado para detectar lesiones muy pequeñas como el inicio de una metástasis o incluso células tumorales en circulación, siendo capaces de detectar hasta 10 células cancerígenas por milímetro en la sangre, lo que implica un gran avance clínico en la detección de tumores[254].

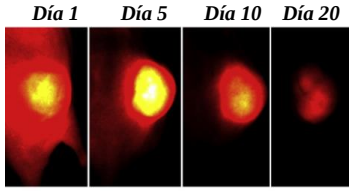

Diagnóstico – Monitorización *in vivo*

Ablación térmica del tumor – PDT y PTT

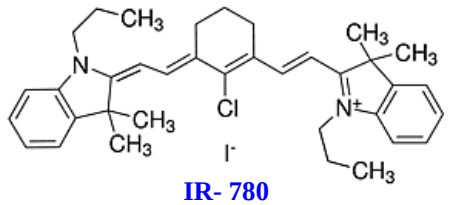

IR- 780

Vectorización: acumulación mitocondrias de células tumorales

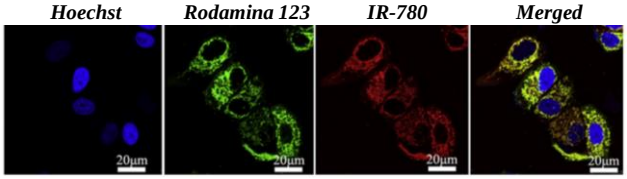

Figura 20: Estructura química y principales propiedades de la sonda IR-780 para PDT y PTT. (Modificada de *Biomaterials* 2014, 35:771 [259] y *Biomaterials* 2010, 31:6612 [258]).

Tabla 3: Resumen de los principales nanovehículos teranósticos poliméricos para el tratamiento avanzado de diferentes tipos de cáncer.

Tipo terapia	Nanovehículo	Agente imagen	Fármaco	Ligando	Tamaño (nm)	Tipo cáncer	Refs
MRI e hipertermia	Liposomas: PEG-DSPE	IONs	Mitoxantrona	Gonadorelina	124-136	Mama y ovario	243
	Conjugado polimérico: HPMA	Gadolinio	DOX	----	----	Mama	242
	Nanovehículo polimérico: PEG-*b*-PCL	SPIONs	Cisplatino	Ácido fólico	44	Hígado	240
	Nanovehículo polimérico: TPGS	SPIONs	----	----	146	Mama	241
	Nanovehículo polimérico: PLA-*b*-TPGS	IONs	DTX	Herceptin	80-155	Mama	244
PDT	Liposomas: TPGS -DSPE	QDs	DTX	Ácido fólico	210	Mama	252
	Conjugado polimérico: HPMA	ZnPP	----	----	82	Sarcoma	246
	Nanovehículo polimérico: PLGA-*b*-TPGS	QDs	DTX	Ácido fólico	250-260	Mama	253
	Nanovehículo polímero: POX-*b*-PLA	metatetrahidroxife-nilclorina (THPP)	----	Ácido fólico	100	Cérvico-uterino	260
PTT	Liposomas: DSPE-PEG	ICG	----	Ácido fólico	20	Mama	261
	Conjugado polimérico: PEG	IR780	---	---	50-150	Colon	262
	Conjugado polimérico: PEG	IR820	---	---	150	Ovario	263
	Nanovehículo polímero: PLGA-*b*-PEG	ICG	DOX	---	86 - 98	Mama	264

Una de las principales limitaciones del uso de la sonda IR-780 para PTT y PDT es su baja solubilidad y alta toxicidad en medio fisiológico[265]. Por esta razón, la investigación se centra actualmente en el desarrollo de nanovehículos que mejoren su administración. En este sentido, queda mucho camino por recorrer de forma que sólo se han descrito vehículos poliméricos sintéticos basados en conjugados con PEG[262, 263] (**tabla 3**).

1.7. Limitaciones de los nanovehículos actuales basados en α-TOS

A pesar del gran avance de la nanomedicina, los actuales nanovehículos que incorporan α-TOS en su composición presentan importantes limitaciones y no son capaces de explotar las principales características de este mitocan para lograr un tratamiento más eficaz, selectivo y menos tóxico contra el cáncer, dotando además a los pacientes de una mejor calidad de vida.

Como se ha descrito anteriormente, la mayor parte de los nanovehículos basados en α-TOS lo incorporan en forma de TPGS. Sin embargo, este conjugado con PEG sólo contiene una molécula de α-TOS en su estructura y además es altamente tóxico debido a sus propiedades como surfactante, afectando a la viabilidad tanto de células tumorales como de células sanas. Esto hace que se pierda una de los principales atractivos del α-TOS para el desarrollo de nuevos tratamientos contra el cáncer, su selectividad contra células tumorales[211].

Por otra parte, el PEG que forma la estructura del TPGS podría ser una ventaja debido a que su presencia en la superficie de estos nanovehículos podría evitar su eliminación en el sistema RES, manteniendo y alargado su tiempo de vida media en plasma. Sin embargo, el peso molecular del PEG utilizado para sintetizar el TPGS es muy reducido (1 kDa). En este sentido, se ha descrito que el impedimento estérico ofrecido por las cadenas de PEG en la superficie de nanovehículos sólo es efectivo cuando el peso molecular utilizado es superior a 3 kDa[172, 178].

Todas estas limitaciones indican que los vehículos actuales que incluyen α-TOS en su estructura representan más bien una prometedora opción como sistemas de liberación contralada de otros fármacos que se encapsulan en su núcleo hidrofóbico. En este sentido, no hay ningún nanovehículo descrito en la literatura que encapsule el α-TOS propiamente dicho para su liberación sostenida y vectorizada a la zona tumoral. Por estas razones, se puede concluir que existe una necesidad real de desarrollar un nanovehículo polimérico que contenga α-TOS en su estructura aunando sus características más ventajosas pero solventando al mismo tiempo sus limitaciones, basadas principalmente en su baja solubilidad.

En la presente tesis doctoral se han sintetizado distintos sistemas poliméricos que incorporan α-TOS en su estructura utilizando distintas técnicas de polimerización radical. Con el fin de dotarlos de propiedades anfifílicas, se han empleado diferentes monómeros hidrofílicos que al copolimerizarlos con un derivado metacrílico del α-TOS han sido capaces de autoensamblarse espontáneamente en medio acuoso formando nanopartículas de un tamaño óptimo para su aplicación en la terapia contra el cáncer. Estas nanopartículas se han utilizado además como vehículos para la encapsulación adicional de α-TOS en su estructura, estudiando su mecanismo de acción y toxicidad en diferentes líneas celulares. Finalmente, estas nanopartículas se han mejorado para lograr una vectorización activa eficaz con IR-780, un agente de imagen que permite un diagnóstico y monitorización simultaneo, propio de una terapia teranóstica avanzada.

1.8. Referencias

1. http://www.cancer.gov/espanol/cancer/que-es.
2. http://www.seom.org/es/informacion-sobre-el-cancer/que-es-el-cancer-y-como-se-desarrolla.
3. Estanqueiro, M.; Amaral, M. H.; Conceição, J.; Lobo, J. M. S., Nanotechnological carriers for cancer chemotherapy: The state of the art. *Colloids and Surfaces B: Biointerfaces* **2015,** 126, 631-648.
4. Croce, C. M., Oncogenes and cancer. *New England Journal of Medicine* **2008,** 358, (5), 502-511.
5. Pérez-Herrero, E.; Fernández-Medarde, A., Advanced targeted therapies in cancer: Drug nanocarriers, the future of chemotherapy. *European Journal of Pharmaceutics and Biopharmaceutics* **2015,** 93, 52-79.
6. Loeb, L. A., A mutator phenotype in cancer. *Cancer research* **2001,** 61, (8), 3230-3239.
7. Vogelstein, B.; Kinzler, K. W., Cancer genes and the pathways they control. *Nature medicine* **2004,** 10, (8), 789-799.
8. Aragó, M. S.; Cuezva, J. M., La mitocondria: un nuevo paradigma en oncología. *Monografías de la Real Academia Nacional de Farmacia* **2012**, 1-27.
9. GLOBOCAN 2012, Cancer Incidence and Mortality Worldwide. International Agency for Research on Cancer.
10. Chabner, B. A.; Roberts, T. G., Chemotherapy and the war on cancer. *Nature Reviews Cancer* **2005,** 5, (1), 65-72.
11. http://www.seom.org/es/informacion-sobre-el-cancer/guia-actualizada/que-es-como-funciona-y-tipos-de-quimioterapia.
12. Boulikas, T.; Pantos, A.; Bellis, E.; Christofis, P., Designing platinum compounds in cancer: structures and mechanisms. *Cancer Ther* **2007,** 5, 537-583.

13. Longley, D. B.; Harkin, D. P.; Johnston, P. G., 5-fluorouracil: mechanisms of action and clinical strategies. *Nature Reviews Cancer* **2003,** 3, (5), 330-338.
14. A'hern, R.; Gore, M., Impact of doxorubicin on survival in advanced ovarian cancer. *Journal of clinical oncology* **1995,** 13, (3), 726-732.
15. Miller, H. I., The story of taxol: Nature and politics in the pursuit of an anti-cancer drug. *Nature Medicine* **2001,** 7, (2), 148-148.
16. Scott, S. D., Rituximab: A New Therapeutic Monoclonal Antibody for Non-Hodgkin's Lymphoma. *Cancer practice* **1998,** 6, (3), 195-197.
17. Hudis, C. A., Trastuzumab—mechanism of action and use in clinical practice. *New England Journal of Medicine* **2007,** 357, (1), 39-51.
18. Capdeville, R.; Buchdunger, E.; Zimmermann, J.; Matter, A., Glivec (STI571, imatinib), a rationally developed, targeted anticancer drug. *Nature reviews Drug discovery* **2002,** 1, (7), 493-502.
19. http://www.seom.org/es/informacion-sobre-el-cancer/guia-actualizada/nuevos-tratamientos-biologicos-que-son-y-como-actuan?start=1#content.
20. Pathania, D.; Millard, M.; Neamati, N., Opportunities in discovery and delivery of anticancer drugs targeting mitochondria and cancer cell metabolism. *Advanced drug delivery reviews* **2009,** 61, (14), 1250-1275.
21. Milane, L.; Trivedi, M.; Singh, A.; Talekar, M.; Amiji, M., Mitochondrial biology, targets, and drug delivery. *Journal of Controlled Release* **2015,** 207, 40-58.
22. Sánchez, R.; Arboleda, G., Mitocondria y muerte celular. *NOVA* **2008,** 6, (10), 191-200.
23. Gutterman, D. D., Mitochondria and reactive oxygen species an evolution in function. *Circulation research* **2005,** 97, (4), 302-304.
24. Indran, I. R.; Tufo, G.; Pervaiz, S.; Brenner, C., Recent advances in apoptosis, mitochondria and drug resistance in cancer cells. *Biochimica et Biophysica Acta (BBA)-Bioenergetics* **2011,** 1807, (6), 735-745.
25. Wallace, D. C., A mitochondrial paradigm of metabolic and degenerative diseases, aging, and cancer: a dawn for evolutionary medicine. *Annual review of genetics* **2005,** 39, 359.
26. Warburg, O., On the origin of cancer cells. *Science* **1956,** 123, (3191), 309-314.
27. Ngo, H.; Tortorella, S. M.; Ververis, K.; Karagiannis, T. C., The Warburg effect: molecular aspects and therapeutic possibilities. *Molecular biology reports* **2015,** 42, (4), 825-834.
28. Lu, J.; Tan, M.; Cai, Q., The Warburg effect in tumor progression: Mitochondrial oxidative metabolism as an anti-metastasis mechanism. *Cancer letters* **2015,** 356, (2), 156-164.
29. Fulda, S.; Galluzzi, L.; Kroemer, G., Targeting mitochondria for cancer therapy. *Nature reviews Drug discovery* **2010,** 9, (6), 447-464.
30. Quir, R. E. M., El efecto Warburg: la mano derecha en el desarrollo del cáncer. *Revista de Especialidades Médico-Quirúrgicas* **2015,** 20, (2), 171-177.
31. Modica-Napolitano, J. S.; Singh, K. K., Mitochondrial dysfunction in cancer. *Mitochondrion* **2004,** 4, (5), 755-762.

32. Owens, K. M.; Modica-Napolitano, J.; Singh, K. K., Mitochondria and cancer. In *Mitochondria and Cancer*, Springer: 2009; pp 1-21.
33. Carew, J. S.; Huang, P., Mitochondrial defects in cancer. *Molecular cancer* **2002,** 1, (1), 1-12.
34. Lee, H.-C.; Wei, Y.-H., Mitochondrial DNA instability and metabolic shift in human cancers. *International journal of molecular sciences* **2009,** 10, (2), 674-701.
35. Chatterjee, A.; Dasgupta, S.; Sidransky, D., Mitochondrial subversion in cancer. *Cancer prevention research* **2011,** 4, (5), 638-654.
36. Hanahan, D.; Weinberg, R. A., Hallmarks of cancer: the next generation. *cell* **2011,** 144, (5), 646-674.
37. Cuezva, J. M.; Krajewska, M.; de Heredia, M. L.; Krajewski, S.; Santamaría, G.; Kim, H.; Zapata, J. M.; Marusawa, H.; Chamorro, M.; Reed, J. C., The bioenergetic signature of cancer a marker of tumor progression. *Cancer research* **2002,** 62, (22), 6674-6681.
38. Marcos, J. M. C., La huella metabólica del cáncer. *Monografías de la Real Academia Nacional de Farmacia* **2005**, 363-383.
39. Shoemaker, R. H., The NCI60 human tumour cell line anticancer drug screen. *Nature Reviews Cancer* **2006,** 6, (10), 813-823.
40. Isidoro, A.; Martínez, M.; Fernandez, P.; Ortega, A.; Santamaría, G.; Chamorro, M.; Reed, J.; Cuezva, J., Alteration of the bioenergetic phenotype of mitochondria is a hallmark of breast, gastric, lung and oesophageal cancer. *Biochem. J* **2004,** 378, 17-20.
41. Fulda, S., Exploiting mitochondrial apoptosis for the treatment of cancer. *Mitochondrion* **2010,** 10, (6), 598-603.
42. Gulbins, E.; Dreschers, S.; Bock, J., Role of mitochondria in apoptosis. *Experimental Physiology* **2003,** 88, (01), 85-90.
43. Pop, C.; Salvesen, G. S., Human caspases: activation, specificity, and regulation. *Journal of biological Chemistry* **2009,** 284, (33), 21777-21781.
44. Brenner, D.; Mak, T. W., Mitochondrial cell death effectors. *Current opinion in cell biology* **2009,** 21, (6), 871-877.
45. Creagh, E. M.; Conroy, H.; Martin, S. J., Caspase-activation pathways in apoptosis and immunity. *Immunological reviews* **2003,** 193, (1), 10-21.
46. McIlwain, D. R.; Berger, T.; Mak, T. W., Caspase functions in cell death and disease. *Cold Spring Harbor perspectives in biology* **2013,** 5, (4), 1-7.
47. Fulda, S.; Debatin, K., Extrinsic versus intrinsic apoptosis pathways in anticancer chemotherapy. *Oncogene* **2006,** 25, (34), 4798-4811.
48. Ralph, S. J.; Rodríguez-Enríquez, S.; Neuzil, J.; Saavedra, E.; Moreno-Sánchez, R., The causes of cancer revisited:"mitochondrial malignancy" and ROS-induced oncogenic transformation–why mitochondria are targets for cancer therapy. *Molecular aspects of medicine* **2010,** 31, (2), 145-170.
49. Wen, S.; Zhu, D.; Huang, P., Targeting cancer cell mitochondria as a therapeutic approach. *Future medicinal chemistry* **2013,** 5, (1), 53-67.
50. Biasutto, L.; Dong, L.-F.; Zoratti, M.; Neuzil, J., Mitochondrially targeted anti-cancer agents. *Mitochondrion* **2010,** 10, (6), 670-681.

51. Neuzil, J.; Dong, L.-F.; Rohlena, J.; Truksa, J.; Ralph, S. J., Classification of mitocans, anti-cancer drugs acting on mitochondria. *Mitochondrion* **2013,** 13, (3), 199-208.
52. Dong, L.-F.; Neuzil, J., Mitochondria in Cancer: Why Mitochondria Are a Good Target for Cancer Therapy. *Progress in molecular biology and translational science* **2014,** 127, 211.
53. Sahra, I. B.; Laurent, K.; Giuliano, S.; Larbret, F.; Ponzio, G.; Gounon, P.; Le Marchand-Brustel, Y.; Giorgetti-Peraldi, S.; Cormont, M.; Bertolotto, C., Targeting cancer cell metabolism: the combination of metformin and 2-deoxyglucose induces p53-dependent apoptosis in prostate cancer cells. *Cancer research* **2010,** 70, (6), 2465-2475.
54. Sun, Y.; Liu, Z.; Zou, X.; Lan, Y.; Sun, X.; Wang, X.; Zhao, S.; Jiang, C.; Liu, H., Mechanisms underlying 3-bromopyruvate-induced cell death in colon cancer. *Journal of Bioenergetics and Biomembranes* **2015,** 47, (4), 319-329.
55. Kang, M. H.; Reynolds, C. P., Bcl-2 inhibitors: targeting mitochondrial apoptotic pathways in cancer therapy. *Clinical cancer research* **2009,** 15, (4), 1126-1132.
56. Siddiqui, W. A.; Ahad, A.; Ahsan, H., The mystery of BCL2 family: Bcl-2 proteins and apoptosis: an update. *Archives of Toxicology* **2015,** 89, (3), 289-317.
57. Vela, L.; Marzo, I., Bcl-2 family of proteins as drug targets for cancer chemotherapy: the long way of BH3 mimetics from bench to bedside. *Current Opinion in Pharmacology* **2015,** 23, 74-81.
58. Trachootham, D.; Zhou, Y.; Zhang, H.; Demizu, Y.; Chen, Z.; Pelicano, H.; Chiao, P. J.; Achanta, G.; Arlinghaus, R. B.; Liu, J., Selective killing of oncogenically transformed cells through a ROS-mediated mechanism by β-phenylethyl isothiocyanate. *Cancer cell* **2006,** 10, (3), 241-252.
59. Trachootham, D.; Alexandre, J.; Huang, P., Targeting cancer cells by ROS-mediated mechanisms: a radical therapeutic approach? *Nature reviews Drug discovery* **2009,** 8, (7), 579-591.
60. Belzacq, A.-S.; El Hamel, C.; Vieira, H.; Cohen, I.; Haouzi, D.; Metivier, D.; Marchetti, P.; Brenner, C.; Kroemer, G., Adenine nucleotide translocator mediates the mitochondrial membrane permeabilization induced by lonidamine, arsenite and CD437. *Oncogene* **2001,** 20, (52), 7579-7587.
61. Oudard, S.; Carpentier, A.; Banu, E.; Fauchon, F.; Celerier, D.; Poupon, M. F.; Dutrillaux, B.; Andrieu, J. M.; Delattre, J. Y., Phase II study of lonidamine and diazepam in the treatment of recurrent glioblastoma multiforme. *Journal of neuro-oncology* **2003,** 63, (1), 81-86.
62. Liang, B.; Song, X.; Yuan, S.; Liu, Y., The function of AMPK activation on apoptosis induced by CD437 in cancer cell. *Cancer Research and Clinic* **2015,** 27, (4), 217-221.
63. Grimm, S., Respiratory chain complex II as general sensor for apoptosis. *Biochimica et Biophysica Acta (BBA)-Bioenergetics* **2013,** 1827, (5), 565-572.
64. Wang, B.; Liu, J.; Gong, Z., Resveratrol induces apoptosis in K562 cells via the regulation of mitochondrial signaling pathways. *International Journal of Clinical and Experimental Medicine* **2015,** 8, (9), 16926-16933.

65. Murphy, M. E., The HSP70 family and cancer. *Carcinogenesis* **2013,** 34, (6), 1181-1188.
66. Bonnet, S.; Archer, S. L.; Allalunis-Turner, J.; Haromy, A.; Beaulieu, C.; Thompson, R.; Lee, C. T.; Lopaschuk, G. D.; Puttagunta, L.; Bonnet, S., A mitochondria-K+ channel axis is suppressed in cancer and its normalization promotes apoptosis and inhibits cancer growth. *Cancer cell* **2007,** 11, (1), 37-51.
67. Bhat, T. A.; Kumar, S.; Chaudhary, A. K.; Yadav, N.; Chandra, D., Restoration of mitochondria function as a target for cancer therapy. *Drug discovery today* **2015,** 20, (5), 635-643.
68. Pereira Da Silva, A.; El-Bacha, T.; Kyaw, N.; Dos Santos, R.; Da-Silva, W.; Almeida, F.; Da Poian, A.; Galina, A., Inhibition of energy-producing pathways of HepG2 cells by 3-bromopyruvate1. *Biochem. J* **2009,** 417, 717-726.
69. Sasaki, R.; Suzuki, Y.; Yonezawa, Y.; Ota, Y.; Okamoto, Y.; Demizu, Y.; Huang, P.; Yoshida, H.; Sugimura, K.; Mizushina, Y., DNA polymerase γ inhibition by vitamin K3 induces mitochondria-mediated cytotoxicity in human cancer cells. *Cancer science* **2008,** 99, (5), 1040-1048.
70. Lewis, W.; Levine, E. S.; Griniuviene, B.; Tankersley, K. O.; Colacino, J. M.; Sommadossi, J.-P.; Watanabe, K. A.; Perrino, F. W., Fialuridine and its metabolites inhibit DNA polymerase gamma at sites of multiple adjacent analog incorporation, decrease mtDNA abundance, and cause mitochondrial structural defects in cultured hepatoblasts. *Proceedings of the National Academy of Sciences* **1996,** 93, (8), 3592-3597.
71. Kitano, T.; Yoda, H.; Tabata, K.; Miura, M.; Toriyama, M.; Motohashi, S.; Suzuki, T., Vitamin K3 analogs induce selective tumor cytotoxicity in neuroblastoma. *Biological and Pharmaceutical Bulletin* **2012,** 35, (4), 617-623.
72. Dong, Y.; Guo, Y.; Gu, X., Anticancer mechanisms of vitamin E succinate. *Chinese journal of cancer* **2009,** 28, (10), 1114-1118.
73. Dong, L.-F.; Swettenham, E.; Eliasson, J.; Wang, X.-F.; Gold, M.; Medunic, Y.; Stantic, M.; Low, P.; Prochazka, L.; Witting, P. K., Vitamin E analogues inhibit angiogenesis by selective induction of apoptosis in proliferating endothelial cells: the role of oxidative stress. *Cancer research* **2007,** 67, (24), 11906-11913.
74. Neuzil, J.; Swettenham, E.; Wang, X.-F.; Dong, L.-F.; Stapelberg, M., α-Tocopheryl succinate inhibits angiogenesis by disrupting paracrine FGF2 signalling. *FEBS letters* **2007,** 581, (24), 4611-4615.
75. Neuzil, J.; Rohlena, J.; Dong, L.; Kluckova, K.; Zobalova, R.; Goodwin, J.; Tilly, D.; Stursa, J.; Pecinova, A.; Philimonenko, A., Mitochondrially targeted-tocopheryl succinate is antiangiogenic: Potential benefit against tumor angiogenesis but caution against wound healing. *Antioxid Redox Signal* **2011**.
76. Dong, L.-F.; Neuzil, J., Vitamin E Analogues as Prototypic Mitochondria-Targeting Anti-cancer Agents. In *Mitochondria: The Anti-cancer Target for the Third Millennium*, Springer: 2014; pp 151-181.
77. Birringer, M.; EyTina, J.; Salvatore, B.; Neuzil, J., Vitamin E analogues as inducers of apoptosis: structure–function relation. *British journal of cancer* **2003,** 88, (12), 1948-1955.

78. Neuzil, J.; Tomasetti, M.; Zhao, Y.; Dong, L.-F.; Birringer, M.; Wang, X.-F.; Low, P.; Wu, K.; Salvatore, B. A.; Ralph, S. J., Vitamin E analogs, a novel group of "mitocans," as anticancer agents: the importance of being redox-silent. *Molecular pharmacology* **2007,** 71, (5), 1185-1199.
79. Ralph, S. J.; Neuzil, J., Mitochondria as targets for cancer therapy. In *Mitochondria and Cancer*, Springer: 2009; pp 211-249.
80. Neuzil, J.; Cerny, J.; Dyason, J. C.; Dong, L. F.; Ralph, S. J., Affinity of vitamin E analogues for the ubiquinone complex II site correlates with their toxicity to cancer cells. *Molecular nutrition & food research* **2011,** 55, (10), 1543-1551.
81. Dong, L.-F.; Low, P.; Dyason, J. C.; Wang, X.-F.; Prochazka, L.; Witting, P. K.; Freeman, R.; Swettenham, E.; Valis, K.; Liu, J., α-Tocopheryl succinate induces apoptosis by targeting ubiquinone-binding sites in mitochondrial respiratory complex II. *Oncogene* **2008,** 27, (31), 4324-4335.
82. Kluckova, K.; Bezawork-Geleta, A.; Rohlena, J.; Dong, L.; Neuzil, J., Mitochondrial complex II, a novel target for anti-cancer agents. *Biochimica et Biophysica Acta (BBA)-Bioenergetics* **2013,** 1827, (5), 552-564.
83. Neuzil, J.; Dyason, J. C.; Freeman, R.; Dong, L.-F.; Prochazka, L.; Wang, X.-F.; Scheffler, I.; Ralph, S. J., Mitocans as anti-cancer agents targeting mitochondria: lessons from studies with vitamin E analogues, inhibitors of complex II. *Journal of bioenergetics and biomembranes* **2007,** 39, (1), 65-72.
84. Dong, L.-F.; Freeman, R.; Liu, J.; Zobalova, R.; Marin-Hernandez, A.; Stantic, M.; Rohlena, J.; Valis, K.; Rodriguez-Enriquez, S.; Butcher, B., Suppression of tumor growth in vivo by the mitocan α-tocopheryl succinate requires respiratory complex II. *Clinical Cancer Research* **2009,** 15, (5), 1593-1600.
85. Neuzil, J.; Wang, X.-F.; Dong, L.-F.; Low, P.; Ralph, S. J., Molecular mechanism of 'mitocan'-induced apoptosis in cancer cells epitomizes the multiple roles of reactive oxygen species and Bcl-2 family proteins. *FEBS letters* **2006,** 580, (22), 5125-5129.
86. Swettenham, E.; Witting, P. K.; Salvatore, B. A.; Neuzil, J., α-Tocopheryl succinate selectively induces apoptosis in neuroblastoma cells: potential therapy of malignancies of the nervous system? *Journal of neurochemistry* **2005,** 94, (5), 1448-1456.
87. Neuzil, J.; Weber, T.; Gellert, N.; Weber, C., Selective cancer cell killing by α-tocopheryl succinate. *British journal of cancer* **2001,** 84, (1), 87.
88. Constantinou, C.; Papas, A.; Constantinou, A. I., Vitamin E and cancer: an insight into the anticancer activities of vitamin E isomers and analogs. *International journal of cancer* **2008,** 123, (4), 739-752.
89. Duhem, N.; Danhier, F.; Préat, V., Vitamin E-based nanomedicines for anti-cancer drug delivery. *Journal of Controlled Release* **2014,** 182, 33-44.
90. Zingg, J.-M., Modulation of signal transduction by vitamin E. *Molecular aspects of medicine* **2007,** 28, (5), 481-506.
91. Neuzil, J.; Weber, T.; Schröder, A.; Lu, M.; Ostermann, G.; Gellert, N.; Mayne, G.; Olejnicka, B.; Nègre-Salvayre, A.; Stícha, M., Induction of cancer cell apoptosis by α-tocopheryl succinate: molecular pathways and structural requirements. *The FASEB Journal* **2001,** 15, (2), 403-415.

92. Stapelberg, M.; Gellert, N.; Swettenham, E.; Tomasetti, M.; Witting, P. K.; Procopio, A.; Neuzil, J., α-Tocopheryl Succinate Inhibits Malignant Mesothelioma by Disrupting the Fibroblast Growth Factor Autocrine Loop *Journal of Biological Chemistry* **2005,** 280, (27), 25369-25376.
93. Barnett, K. T.; Fokum, F. D.; Malafa, M. P., Vitamin E succinate inhibits colon cancer liver metastases. *Journal of Surgical Research* **2002,** 106, (2), 292-298.
94. Malafa, M. P.; Fokum, F. D.; Smith, L.; Louis, A., Inhibition of angiogenesis and promotion of melanoma dormancy by vitamin E succinate. *Annals of surgical oncology* **2002,** 9, (10), 1023-1032.
95. Malafa, M. P.; Fokum, F. D.; Mowlavi, A.; Abusief, M.; King, M., Vitamin E inhibits melanoma growth in mice. *Surgery* **2002,** 131, (1), 85-91.
96. Malafa, M. P.; Neitzel, L. T., Vitamin E succinate promotes breast cancer tumor dormancy. *Journal of Surgical Research* **2000,** 93, (1), 163-170.
97. Koudelka, S.; Knotigova, P. T.; Masek, J.; Prochazka, L.; Lukac, R.; Miller, A. D.; Neuzil, J.; Turanek, J., Liposomal delivery systems for anti-cancer analogues of vitamin E. *Journal of Controlled Release* **2015,** 207, 59-69.
98. Ireland, D. J.; Kissick, H. T.; Beilharz, M. W., Alpha-Tocopheryl succinate: Toxicity and lack of anti-tumour activity in immuno-competent mice. *Food and chemical toxicology* **2008,** 46, (2), 508-512.
99. Nazir, S.; Hussain, T.; Ayub, A.; Rashid, U.; MacRobert, A. J., Nanomaterials in combating cancer: therapeutic applications and developments. *Nanomedicine: Nanotechnology, Biology and Medicine* **2014,** 10, (1), 19-34.
100. Williams, H. D.; Trevaskis, N. L.; Charman, S. A.; Shanker, R. M.; Charman, W. N.; Pouton, C. W.; Porter, C. J., Strategies to address low drug solubility in discovery and development. *Pharmacological reviews* **2013,** 65, (1), 315-499.
101. Bamrungsap, S.; Zhao, Z.; Chen, T.; Wang, L.; Li, C.; Fu, T.; Tan, W., Nanotechnology in therapeutics: a focus on nanoparticles as a drug delivery system. *Nanomedicine* **2012,** 7, (8), 1253-1271.
102. Uchegbu, I. F.; Siew, A., Nanomedicines and nanodiagnostics come of age. *Journal of pharmaceutical sciences* **2013,** 102, (2), 305-310.
103. Wicki, A.; Witzigmann, D.; Balasubramanian, V.; Huwyler, J., Nanomedicine in cancer therapy: challenges, opportunities, and clinical applications. *Journal of Controlled Release* **2015,** 200, 138-157.
104. Maeda, H., The enhanced permeability and retention (EPR) effect in tumor vasculature: the key role of tumor-selective macromolecular drug targeting. *Advances in enzyme regulation* **2001,** 41, (1), 189-207.
105. Maeda, H.; Nakamura, H.; Fang, J., The EPR effect for macromolecular drug delivery to solid tumors: Improvement of tumor uptake, lowering of systemic toxicity, and distinct tumor imaging in vivo. *Advanced drug delivery reviews* **2013,** 65, (1), 71-79.
106. Maeda, H.; Wu, J.; Sawa, T.; Matsumura, Y.; Hori, K., Tumor vascular permeability and the EPR effect in macromolecular therapeutics: a review. *Journal of controlled release* **2000,** 65, (1), 271-284.

107. Sun, T.; Zhang, Y. S.; Pang, B.; Hyun, D. C.; Yang, M.; Xia, Y., Engineered nanoparticles for drug delivery in cancer therapy. *Angewandte Chemie International Edition* **2014,** 53, (46), 12320-12364.
108. Neri, D.; Bicknell, R., Tumour vascular targeting. *Nature Reviews Cancer* **2005,** 5, (6), 436-446.
109. Li, H.; Qian, Z. M., Transferrin/transferrin receptor-mediated drug delivery. *Medicinal research reviews* **2002,** 22, (3), 225-250.
110. Acharya, S.; Dilnawaz, F.; Sahoo, S. K., Targeted epidermal growth factor receptor nanoparticle bioconjugates for breast cancer therapy. *Biomaterials* **2009,** 30, (29), 5737-5750.
111. Hilgenbrink, A. R.; Low, P. S., Folate receptor-mediated drug targeting: From therapeutics to diagnostics. *Journal of pharmaceutical sciences* **2005,** 94, (10), 2135-2146.
112. Bertrand, N.; Wu, J.; Xu, X.; Kamaly, N.; Farokhzad, O. C., Cancer nanotechnology: the impact of passive and active targeting in the era of modern cancer biology. *Advanced drug delivery reviews* **2014,** 66, 2-25.
113. Byrne, J. D.; Betancourt, T.; Brannon-Peppas, L., Active targeting schemes for nanoparticle systems in cancer therapeutics. *Advanced drug delivery reviews* **2008,** 60, (15), 1615-1626.
114. Brannon-Peppas, L.; Blanchette, J. O., Nanoparticle and targeted systems for cancer therapy. *Advanced drug delivery reviews* **2012,** 64, 206-212.
115. Malam, Y.; Loizidou, M.; Seifalian, A. M., Liposomes and nanoparticles: nanosized vehicles for drug delivery in cancer. *Trends in pharmacological sciences* **2009,** 30, (11), 592-599.
116. Allen, T. M.; Cullis, P. R., Liposomal drug delivery systems: from concept to clinical applications. *Advanced drug delivery reviews* **2013,** 65, (1), 36-48.
117. Mozafari, M. R., Liposomes: an overview of manufacturing techniques. *Cellular and Molecular Biology Letters* **2005,** 10, (4), 711.
118. Northfelt, D. W.; Dezube, B. J.; Thommes, J. A.; Miller, B. J.; Fischl, M. A.; Friedman-Kien, A.; Kaplan, L. D.; Du Mond, C.; Mamelok, R. D.; Henry, D. H., Pegylated-liposomal doxorubicin versus doxorubicin, bleomycin, and vincristine in the treatment of AIDS-related Kaposi's sarcoma: results of a randomized phase III clinical trial. *Journal of clinical oncology* **1998,** 16, (7), 2445-2451.
119. Rivera, E., Liposomal anthracyclines in metastatic breast cancer: clinical update. *The oncologist* **2003,** 8, (Supplement 2), 3-9.
120. Glantz, M. J.; Jaeckle, K. A.; Chamberlain, M. C.; Phuphanich, S.; Recht, L.; Swinnen, L. J.; Maria, B.; LaFollette, S.; Schumann, G. B.; Cole, B. F., A randomized controlled trial comparing intrathecal sustained-release cytarabine (DepoCyt) to intrathecal methotrexate in patients with neoplastic meningitis from solid tumors. *Clinical Cancer Research* **1999,** 5, (11), 3394-3402.
121. Rodriguez, M.; Pytlik, R.; Kozak, T.; Chhanabhai, M.; Gascoyne, R.; Lu, B.; Deitcher, S. R.; Winter, J. N., Vincristine sulfate liposomes injection (Marqibo) in heavily pretreated patients with refractory aggressive non-Hodgkin lymphoma. *Cancer* **2009,** 115, (15), 3475-3482.

122. Venkatakrishnan, K.; Liu, Y.; Noe, D.; Mertz, J.; Bargfrede, M.; Marbury, T.; Farbakhsh, K.; Oliva, C.; Milton, A., Pharmacokinetics and pharmacodynamics of liposomal mifamurtide in adult volunteers with mild or moderate hepatic impairment. *British journal of clinical pharmacology* **2014,** 77, (6), 998-1010.
123. Suzuki, R.; Takizawa, T.; Kuwata, Y.; Mutoh, M.; Ishiguro, N.; Utoguchi, N.; Shinohara, A.; Eriguchi, M.; Yanagie, H.; Maruyama, K., Effective anti-tumor activity of oxaliplatin encapsulated in transferrin–PEG-liposome. *International journal of pharmaceutics* **2008,** 346, (1), 143-150.
124. Ringsdorf, H. In *Structure and properties of pharmacologically active polymers*, Journal of Polymer Science: Polymer Symposia, 1975; Wiley Online Library: 1975; pp 135-153.
125. Greco, F.; Vicent, M. J., Combination therapy: opportunities and challenges for polymer–drug conjugates as anticancer nanomedicines. *Advanced Drug Delivery Reviews* **2009,** 61, (13), 1203-1213.
126. Li, C.; Wallace, S., Polymer-drug conjugates: recent development in clinical oncology. *Advanced drug delivery reviews* **2008,** 60, (8), 886-898.
127. Khandare, J.; Minko, T., Polymer–drug conjugates: progress in polymeric prodrugs. *Progress in Polymer Science* **2006,** 31, (4), 359-397.
128. Graham, M. L., Pegaspargase: a review of clinical studies. *Advanced drug delivery reviews* **2003,** 55, (10), 1293-1302.
129. Maeda, H., SMANCS and polymer-conjugated macromolecular drugs: advantages in cancer chemotherapy. *Advanced drug delivery reviews* **2001,** 46, (1), 169-185.
130. Pasut, G.; Veronese, F. M., PEG conjugates in clinical development or use as anticancer agents: an overview. *Advanced drug delivery reviews* **2009,** 61, (13), 1177-1188.
131. Duangjai, A.; Luo, K.; Zhou, Y.; Yang, J.; Kopeček, J., Combination cytotoxicity of backbone degradable HPMA copolymer gemcitabine and platinum conjugates toward human ovarian carcinoma cells. *European Journal of Pharmaceutics and Biopharmaceutics* **2014,** 87, (1), 187-196.
132. Ye, H.; Jin, L.; Hu, R.; Yi, Z.; Li, J.; Wu, Y.; Xi, X.; Wu, Z., Poly (γ, l-glutamic acid)–cisplatin conjugate effectively inhibits human breast tumor xenografted in nude mice. *Biomaterials* **2006,** 27, (35), 5958-5965.
133. Etrych, T.; Šubr, V.; Laga, R.; Říhová, B.; Ulbrich, K., Polymer conjugates of doxorubicin bound through an amide and hydrazone bond: Impact of the carrier structure onto synergistic action in the treatment of solid tumours. *European Journal of Pharmaceutical Sciences* **2014,** 58, 1-12.
134. Vasey, P. A.; Kaye, S. B.; Morrison, R.; Twelves, C.; Wilson, P.; Duncan, R.; Thomson, A. H.; Murray, L. S.; Hilditch, T. E.; Murray, T., Phase I clinical and pharmacokinetic study of PK1 [N-(2-hydroxypropyl) methacrylamide copolymer doxorubicin]: first member of a new class of chemotherapeutic agents—drug-polymer conjugates. *Clinical Cancer Research* **1999,** 5, (1), 83-94.
135. Terwogt, J. M. M.; ten Bokkel Huinink, W. W.; Schellens, J. H.; Schot, M.; Mandjes, I. A.; Zurlo, M. G.; Rocchetti, M.; Rosing, H.; Koopman, F. J.; Beijnen, J. H.,

Phase I clinical and pharmacokinetic study of PNU166945, a novel water-soluble polymer-conjugated prodrug of paclitaxel. *Anti-Cancer Drugs* **2001,** 12, (4), 315-323.
136. Bedikian, A.; DeConti, R.; Conry, R.; Agarwala, S.; Papadopoulos, N.; Kim, K.; Ernstoff, M., Phase 3 study of docosahexaenoic acid–paclitaxel versus dacarbazine in patients with metastatic malignant melanoma. *Annals of oncology* **2011,** 22, (4), 787-793.
137. Yurkovetskiy, A. V.; Fram, R. J., XMT-1001, a novel polymeric camptothecin pro-drug in clinical development for patients with advanced cancer. *Advanced drug delivery reviews* **2009,** 61, (13), 1193-1202.
138. Homsi, J.; Simon, G. R.; Garrett, C. R.; Springett, G.; De Conti, R.; Chiappori, A. A.; Munster, P. N.; Burton, M. K.; Stromatt, S.; Allievi, C., Phase I trial of poly-L-glutamate camptothecin (CT-2106) administered weekly in patients with advanced solid malignancies. *Clinical Cancer Research* **2007,** 13, (19), 5855-5861.
139. Awada, A.; Garcia, A. A.; Chan, S.; Jerusalem, G. H.; Coleman, R. E.; Huizing, M. T.; Mehdi, A.; O'Reilly, S. M.; Hamm, J. T.; Barrett-Lee, P. J., Two schedules of etirinotecan pegol (NKTR-102) in patients with previously treated metastatic breast cancer: a randomised phase 2 study. *The lancet oncology* **2013,** 14, (12), 1216-1225.
140. Seymour, L. W.; Ferry, D. R.; Anderson, D.; Hesslewood, S.; Julyan, P. J.; Poyner, R.; Doran, J.; Young, A. M.; Burtles, S.; Kerr, D. J., Hepatic drug targeting: phase I evaluation of polymer-bound doxorubicin. *Journal of clinical oncology* **2002,** 20, (6), 1668-1676.
141. Palao-Suay, R.; Gómez-Mascaraque, L.; Aguilar, M.; Vázquez-Lasa, B.; San Román, J., Self-assembling polymer systems for advanced treatment of cancer and inflammation. *Progress in Polymer Science* **2016,** 53,207-248.
142. Branco, M. C.; Schneider, J. P., Self-assembling materials for therapeutic delivery. *Acta biomaterialia* **2009,** 5, (3), 817-831.
143. Lu, Y.; Park, K., Polymeric micelles and alternative nanonized delivery vehicles for poorly soluble drugs. *International journal of pharmaceutics* **2013,** 453, (1), 198-214.
144. Oerlemans, C.; Bult, W.; Bos, M.; Storm, G.; Nijsen, J. F. W.; Hennink, W. E., Polymeric micelles in anticancer therapy: targeting, imaging and triggered release. *Pharmaceutical research* **2010,** 27, (12), 2569-2589.
145. Tyrrell, Z. L.; Shen, Y.; Radosz, M., Fabrication of micellar nanoparticles for drug delivery through the self-assembly of block copolymers. *Progress in Polymer Science* **2010,** 35, (9), 1128-1143.
146. Miyata, K.; Christie, R. J.; Kataoka, K., Polymeric micelles for nano-scale drug delivery. *Reactive and Functional Polymers* **2011,** 71, (3), 227-234.
147. Brigger, I.; Dubernet, C.; Couvreur, P., Nanoparticles in cancer therapy and diagnosis. *Advanced drug delivery reviews* **2002,** 54, (5), 631-651.
148. Mora-Huertas, C.; Fessi, H.; Elaissari, A., Polymer-based nanocapsules for drug delivery. *International journal of pharmaceutics* **2010,** 385, (1), 113-142.
149. Ossipov, D. A., Nanostructured hyaluronic acid-based materials for active delivery to cancer. *Expert opinion on drug delivery* **2010,** 7, (6), 681-703.

150. Park, J. H.; Saravanakumar, G.; Kim, K.; Kwon, I. C., Targeted delivery of low molecular drugs using chitosan and its derivatives. *Advanced drug delivery reviews* **2010,** 62, (1), 28-41.
151. Wang, X.; Wang, Y.; Chen, Z. G.; Shin, D. M., Advances of cancer therapy by nanotechnology. *Cancer research and treatment: official journal of Korean Cancer Association* **2009,** 41, (1), 1-11.
152. Drbohlavova, J.; Chomoucka, J.; Adam, V.; Ryvolova, M.; Eckschlager, T.; Hubalek, J.; Kizek, R., Nanocarriers for anticancer drugs-new trends in nanomedicine. *Current drug metabolism* **2013,** 14, (5), 547-564.
153. Stephanopoulos, N.; Ortony, J. H.; Stupp, S. I., Self-assembly for the synthesis of functional biomaterials. *Acta materialia* **2013,** 61, (3), 912-930.
154. Jérôme, C.; Lecomte, P., Recent advances in the synthesis of aliphatic polyesters by ring-opening polymerization. *Advanced Drug Delivery Reviews* **2008,** 60, (9), 1056-1076.
155. Bae, Y.; Kataoka, K., Intelligent polymeric micelles from functional poly (ethylene glycol)-poly (amino acid) block copolymers. *Advanced drug delivery reviews* **2009,** 61, (10), 768-784.
156. Hoogenboom, R., Poly (2-oxazoline) s: a polymer class with numerous potential applications. *Angewandte Chemie International Edition* **2009,** 48, (43), 7978-7994.
157. Donaire, M. L.; Parra-Cáceres, J.; Vázquez-Lasa, B.; García-Álvarez, I.; Fernández-Mayoralas, A.; López-Bravo, A.; San Román, J., Polymeric drugs based on bioactive glycosides for the treatment of brain tumours. *Biomaterials* **2009,** 30, (8), 1613-1626.
158. García-Fernández, L.; Aguilar, M.; Ochoa-Callejero, L.; Abradelo, C.; Martínez, A.; San Román, J., bFGF interaction and in vivo angiogenesis inhibition by self-assembling sulfonic acid-based copolymers. *Journal of Materials Science: Materials in Medicine* **2012,** 23, (1), 129-135.
159. Garcia-Fernandez, L.; Aguilar, M.; Fernandez, M.; Lozano, R.; Gimenez, G.; Valverde, S.; San Roman, J., Structure, morphology, and bioactivity of biocompatible systems derived from functionalized acrylic polymers based on 5-amino-2-naphthalene sulfonic acid. *Biomacromolecules* **2010,** 11, (7), 1763-1772.
160. Braunecker, W. A.; Matyjaszewski, K., Controlled/living radical polymerization: features, developments, and perspectives. *Progress in Polymer Science* **2007,** 32, (1), 93-146.
161. Sciannamea, V.; Jérôme, R.; Detrembleur, C., In-situ nitroxide-mediated radical polymerization (NMP) processes: their understanding and optimization. *Chemical reviews* **2008,** 108, (3), 1104-1126.
162. Grubbs, R. B., Nitroxide-mediated radical polymerization: limitations and versatility. *Polymer Reviews* **2011,** 51, (2), 104-137.
163. Wang, J.-S.; Matyjaszewski, K., Controlled/" living" radical polymerization. Atom transfer radical polymerization in the presence of transition-metal complexes. *Journal of the American Chemical Society* **1995,** 117, (20), 5614-5615.
164. Matyjaszewski, K.; Xia, J., Atom transfer radical polymerization. *Chemical reviews* **2001,** 101, (9), 2921-2990.

165. Chong, Y.; Le, T. P.; Moad, G.; Rizzardo, E.; Thang, S. H., A more versatile route to block copolymers and other polymers of complex architecture by living radical polymerization: the RAFT process. *Macromolecules* **1999,** 32, (6), 2071-2074.
166. York, A. W.; Kirkland, S. E.; McCormick, C. L., Advances in the synthesis of amphiphilic block copolymers via RAFT polymerization: stimuli-responsive drug and gene delivery. *Advanced drug delivery reviews* **2008,** 60, (9), 1018-1036.
167. Keddie, D. J., A guide to the synthesis of block copolymers using reversible-addition fragmentation chain transfer (RAFT) polymerization. *Chemical Society Reviews* **2014,** 43, (2), 496-505.
168. Yang, Y.; Pan, D.; Luo, K.; Li, L.; Gu, Z., Biodegradable and amphiphilic block copolymer–doxorubicin conjugate as polymeric nanoscale drug delivery vehicle for breast cancer therapy. *Biomaterials* **2013,** 34, (33), 8430-8443.
169. De, P.; Gondi, S. R.; Sumerlin, B. S., Folate-conjugated thermoresponsive block copolymers: highly efficient conjugation and solution self-assembly. *Biomacromolecules* **2008,** 9, (3), 1064-1070.
170. Soppimath, K. S.; Aminabhavi, T. M.; Kulkarni, A. R.; Rudzinski, W. E., Biodegradable polymeric nanoparticles as drug delivery devices. *Journal of controlled release* **2001,** 70, (1), 1-20.
171. Ikeda, Y.; Nagasaki, Y., PEGylation technology in nanomedicine. In *Advances in Polymer Science*, 2012; Vol. 247, pp 115-140.
172. Otsuka, H.; Nagasaki, Y.; Kataoka, K., PEGylated nanoparticles for biological and pharmaceutical applications. *Advanced drug delivery reviews* **2012,** 64, 246-255.
173. Ikeda, Y.; Nagasaki, Y., Impacts of PEGylation on the gene and oligonucleotide delivery system. *Journal of Applied Polymer Science* **2014,** 131, (9), 1-10.
174. Hamaguchi, T.; Matsumura, Y.; Suzuki, M.; Shimizu, K.; Goda, R.; Nakamura, I.; Nakatomi, I.; Yokoyama, M.; Kataoka, K.; Kakizoe, T., NK105, a paclitaxel-incorporating micellar nanoparticle formulation, can extend in vivo antitumour activity and reduce the neurotoxicity of paclitaxel. *British journal of cancer* **2005,** 92, (7), 1240-1246.
175. Negishi, T.; Koizumi, F.; Uchino, H.; Kuroda, J.; Kawaguchi, T.; Naito, S.; Matsumura, Y., NK105, a paclitaxel-incorporating micellar nanoparticle, is a more potent radiosensitising agent compared to free paclitaxel. *British journal of cancer* **2006,** 95, (5), 601-606.
176. Matsumura, Y.; Hamaguchi, T.; Ura, T.; Muro, K.; Yamada, Y.; Shimada, Y.; Shirao, K.; Okusaka, T.; Ueno, H.; Ikeda, M., Phase I clinical trial and pharmacokinetic evaluation of NK911, a micelle-encapsulated doxorubicin. *British journal of cancer* **2004,** 91, (10), 1775-1781.
177. Matsumura, Y., Preclinical and clinical studies of NK012, an SN-38-incorporating polymeric micelles, which is designed based on EPR effect. *Advanced drug delivery reviews* **2011,** 63, (3), 184-192.
178. Jokerst, J. V.; Lobovkina, T.; Zare, R. N.; Gambhir, S. S., Nanoparticle PEGylation for imaging and therapy. *Nanomedicine* **2011,** 6, (4), 715-728.

179. Lim, W.; Tan, E.; Toh, C.; Hee, S.; Leong, S.; Ang, P.; Wong, N.; Chowbay, B., Phase I pharmacokinetic study of a weekly liposomal paclitaxel formulation (Genexol®-PM) in patients with solid tumors. *Annals of oncology* **2010,** 21, (2), 382-388.
180. Lee, K. S.; Chung, H. C.; Im, S. A.; Park, Y. H.; Kim, C. S.; Kim, S.-B.; Rha, S. Y.; Lee, M. Y.; Ro, J., Multicenter phase II trial of Genexol-PM, a Cremophor-free, polymeric micelle formulation of paclitaxel, in patients with metastatic breast cancer. *Breast cancer research and treatment* **2008,** 108, (2), 241-250.
181. Wang, Y.; Liu, P.; Duan, Y.; Yin, X.; Wang, Q.; Liu, X.; Wang, X.; Zhou, J.; Wang, W.; Qiu, L., Specific cell targeting with APRPG conjugated PEG–PLGA nanoparticles for treating ovarian cancer. *Biomaterials* **2014,** 35, (3), 983-992.
182. Hu, Q.; Gao, X.; Kang, T.; Feng, X.; Jiang, D.; Tu, Y.; Song, Q.; Yao, L.; Jiang, X.; Chen, H., CGKRK-modified nanoparticles for dual-targeting drug delivery to tumor cells and angiogenic blood vessels. *Biomaterials* **2013,** 34, (37), 9496-9508.
183. Zhan, C.; Gu, B.; Xie, C.; Li, J.; Liu, Y.; Lu, W., Cyclic RGD conjugated poly (ethylene glycol)-co-poly (lactic acid) micelle enhances paclitaxel anti-glioblastoma effect. *Journal of Controlled Release* **2010,** 143, (1), 136-142.
184. Li, X.; Li, H.; Yi, W.; Chen, J.; Liang, B., Acid-triggered core cross-linked nanomicelles for targeted drug delivery and magnetic resonance imaging in liver cancer cells. *International journal of nanomedicine* **2013,** 8, 3019-3031.
185. Saxena, V.; Naguib, Y.; Hussain, M. D., Folate receptor targeted 17-allylamino-17-demethoxygeldanamycin (17-AAG) loaded polymeric nanoparticles for breast cancer. *Colloids and Surfaces B: Biointerfaces* **2012,** 94, 274-280.
186. Valle, J. W.; Armstrong, A.; Newman, C.; Alakhov, V.; Pietrzynski, G.; Brewer, J.; Campbell, S.; Corrie, P.; Rowinsky, E. K.; Ranson, M., A phase 2 study of SP1049C, doxorubicin in P-glycoprotein-targeting pluronics, in patients with advanced adenocarcinoma of the esophagus and gastroesophageal junction. *Investigational new drugs* **2011,** 29, (5), 1029-1037.
187. Alakhova, D. Y.; Zhao, Y.; Li, S.; Kabanov, A. V., Effect of doxorubicin/pluronic SP1049C on tumorigenicity, aggressiveness, DNA methylation and stem cell markers in murine leukemia. *PloS one* **2013,** 8, (8), 1-14.
188. Talelli, M.; Rijcken, C.; Van Nostrum, C.; Storm, G.; Hennink, W., Micelles based on HPMA copolymers. *Advanced drug delivery reviews* **2010,** 62, (2), 231-239.
189. Kopeček, J.; Kopečková, P., HPMA copolymers: origins, early developments, present, and future. *Advanced drug delivery reviews* **2010,** 62, (2), 122-149.
190. Chytil, P.; Etrych, T.; Koňák, Č.; Šírová, M.; Mrkvan, T.; Bouček, J.; Říhová, B.; Ulbrich, K., New HPMA copolymer-based drug carriers with covalently bound hydrophobic substituents for solid tumour targeting. *Journal of Controlled Release* **2008,** 127, (2), 121-130.
191. Miller, K.; Eldar-Boock, A.; Polyak, D.; Segal, E.; Benayoun, L.; Shaked, Y.; Satchi-Fainaro, R., Antiangiogenic antitumor activity of HPMA copolymer–paclitaxel–alendronate conjugate on breast cancer bone metastasis mouse model. *Molecular pharmaceutics* **2011,** 8, (4), 1052-1062.

192. Jia, Z.; Wong, L.; Davis, T. P.; Bulmus, V., One-pot conversion of RAFT-generated multifunctional block copolymers of HPMA to doxorubicin conjugated acid-and reductant-sensitive crosslinked micelles. *Biomacromolecules* **2008,** 9, (11), 3106-3113.
193. Jabbari, E.; Yang, X.; Moeinzadeh, S.; He, X., Drug release kinetics, cell uptake, and tumor toxicity of hybrid VVVVVVKK peptide-assembled polylactide nanoparticles. *European Journal of Pharmaceutics and Biopharmaceutics* **2013,** 84, (1), 49-62.
194. Huang, C.; Neoh, K. G.; Xu, L.; Kang, E. T.; Chiong, E., Polymeric nanoparticles with encapsulated superparamagnetic iron oxide and conjugated cisplatin for potential bladder cancer therapy. *Biomacromolecules* **2012,** 13, (8), 2513-2520.
195. McDaniel, J. R.; Bhattacharyya, J.; Vargo, K. B.; Hassouneh, W.; Hammer, D. A.; Chilkoti, A., Self-Assembly of Thermally Responsive Nanoparticles of a Genetically Encoded Peptide Polymer by Drug Conjugation. *Angewandte Chemie International Edition* **2013,** 52, (6), 1683-1687.
196. Cui, H.; Webber, M. J.; Stupp, S. I., Self-assembly of peptide amphiphiles: From molecules to nanostructures to biomaterials. *Peptide Science* **2010,** 94, (1), 1-18.
197. Aluri, S.; Janib, S. M.; Mackay, J. A., Environmentally responsive peptides as anticancer drug carriers. *Advanced drug delivery reviews* **2009,** 61, (11), 940-952.
198. Hoogenboom, R.; Schlaad, H., Bioinspired poly (2-oxazoline) s. *Polymers* **2011,** 3, (1), 467-488.
199. Schlaad, H.; Diehl, C.; Gress, A.; Meyer, M.; Demirel, A. L.; Nur, Y.; Bertin, A., Poly (2-oxazoline) s as Smart Bioinspired Polymers. *Macromolecular rapid communications* **2010,** 31, (6), 511-525.
200. Constantinides, P. P.; Han, J.; Davis, S. S., Advances in the use of tocols as drug delivery vehicles. *Pharmaceutical research* **2006,** 23, (2), 243-255.
201. Zhang, Z.; Tan, S.; Feng, S.-S., Vitamin E TPGS as a molecular biomaterial for drug delivery. *Biomaterials* **2012,** 33, (19), 4889-4906.
202. Wu, S.-W.; Hopkins, W. K., Characteristics of d-α-tocopheryl PEG 1000 succinate for applications as an absorption enhancer in drug delivery systems. *Pharmaceutical technology* **1999,** 23, (10), 52-68.
203. Youk, H.-J.; Lee, E.; Choi, M.-K.; Lee, Y.-J.; Chung, J. H.; Kim, S.-H.; Lee, C.-H.; Lim, S.-J., Enhanced anticancer efficacy of α-tocopheryl succinate by conjugation with polyethylene glycol. *Journal of controlled release* **2005,** 107, (1), 43-52.
204. Dintaman, J. M.; Silverman, J. A., Inhibition of P-glycoprotein by D-α-tocopheryl polyethylene glycol 1000 succinate (TPGS). *Pharmaceutical research* **1999,** 16, (10), 1550-1556.
205. Shieh, M.-J.; Hsu, C.-Y.; Huang, L.-Y.; Chen, H.-Y.; Huang, F.-H.; Lai, P.-S., Reversal of doxorubicin-resistance by multifunctional nanoparticles in MCF-7/ADR cells. *Journal of Controlled Release* **2011,** 152, (3), 418-425.
206. Collnot, E.-M.; Baldes, C.; Schaefer, U. F.; Edgar, K. J.; Wempe, M. F.; Lehr, C.-M., Vitamin E TPGS P-glycoprotein inhibition mechanism: influence on conformational flexibility, intracellular ATP levels, and role of time and site of access. *Molecular pharmaceutics* **2010,** 7, (3), 642-651.

207. Bansal, T.; Akhtar, N.; Jaggi, M.; Khar, R. K.; Talegaonkar, S., Novel formulation approaches for optimising delivery of anticancer drugs based on P-glycoprotein modulation. *Drug discovery today* **2009,** 14, (21), 1067-1074.
208. Bernabeu, E.; Chiappetta, D. A., Vitamin E TPGS Used as Emulsifier in the Preparation of Nanoparticulate Systems. *Journal of Biomaterials and Tissue Engineering* **2013,** 3, (1), 122-134.
209. Sadoqi, M.; Lau-Cam, C.; Wu, S., Investigation of the micellar properties of the tocopheryl polyethylene glycol succinate surfactants TPGS 400 and TPGS 1000 by steady state fluorometry. *Journal of colloid and interface science* **2009,** 333, (2), 585-589.
210. Feng, S.-S., New-concept chemotherapy by nanoparticles of biodegradable polymers: where are we now? **2006,** 1, 297-309.
211. Guo, Y.; Luo, J.; Tan, S.; Otieno, B. O.; Zhang, Z., The applications of Vitamin E TPGS in drug delivery. *European journal of pharmaceutical sciences* **2013,** 49, (2), 175-186.
212. Quinn, P., Is the distribution of α-tocopherol in membranes consistent with its putative functions? *Biochemistry (Moscow)* **2004,** 69, (1), 58-66.
213. Massey, J. B., Interfacial properties of phosphatidylcholine bilayers containing vitamin E derivatives. *Chemistry and physics of lipids* **2001,** 109, (2), 157-174.
214. Parmentier, J.; Hartmann, F. J.; Fricker, G., In vitro evaluation of liposomes containing bio-enhancers for the oral delivery of macromolecules. *European Journal of Pharmaceutics and Biopharmaceutics* **2010,** 76, (3), 394-403.
215. Koudelka, Š.; Mašek, J.; Neuzil, J.; Turánek, J., Lyophilised liposome-based formulations of α-tocopheryl succinate: Preparation and physico-chemical characterisation. *Journal of pharmaceutical sciences* **2010,** 99, (5), 2434-2443.
216. Hama, S.; Utsumi, S.; Fukuda, Y.; Nakayama, K.; Okamura, Y.; Tsuchiya, H.; Fukuzawa, K.; Harashima, H.; Kogure, K., Development of a novel drug delivery system consisting of an antitumor agent tocopheryl succinate. *Journal of Controlled Release* **2012,** 161, (3), 843-851.
217. Karanth, H.; Murthy, R., pH-sensitive liposomes-principle and application in cancer therapy. *Journal of pharmacy and pharmacology* **2007,** 59, (4), 469-483.
218. Gill, K. K.; Kaddoumi, A.; Nazzal, S., Mixed micelles of PEG 2000-DSPE and vitamin-E TPGS for concurrent delivery of paclitaxel and parthenolide: Enhanced chemosenstization and antitumor efficacy against non-small cell lung cancer (NSCLC) cell lines. *European Journal of Pharmaceutical Sciences* **2012,** 46, (1), 64-71.
219. Cao, N.; Feng, S.-S., Doxorubicin conjugated to d-α-tocopheryl polyethylene glycol 1000 succinate (TPGS): Conjugation chemistry, characterization, in vitro and in vivo evaluation. *Biomaterials* **2008,** 29, (28), 3856-3865.
220. Anbharasi, V.; Cao, N.; Feng, S. S., Doxorubicin conjugated to D-α-tocopheryl polyethylene glycol succinate and folic acid as a prodrug for targeted chemotherapy. *Journal of Biomedical Materials Research Part A* **2010,** 94, (3), 730-743.
221. Duhem, N.; Danhier, F.; Pourcelle, V.; Schumers, J.-M.; Bertrand, O.; LeDuff, C. c. S.; Hoeppener, S.; Schubert, U. S.; Gohy, J.-F. o.; Marchand-Brynaert, J., Self-assembling doxorubicin–tocopherol succinate prodrug as a new drug delivery system:

synthesis, characterization, and in vitro and in vivo anticancer activity. *Bioconjugate chemistry* **2013,** 25, (1), 72-81.
222. Lee, P.; Feng, S.-S., Vitamin E TPGS-modified paclitaxel: synthesis, characterizations, in vitro activities. *Cancer Research* **2005,** 65, (9 Supplement), 337-337.
223. Mi, Y.; Zhao, J.; Feng, S.-S., Targeted co-delivery of docetaxel, cisplatin and herceptin by vitamin E TPGS-cisplatin prodrug nanoparticles for multimodality treatment of cancer. *Journal of Controlled Release* **2013,** 169, (3), 185-192.
224. Mi, Y.; Zhao, J.; Feng, S.-S., Vitamin E TPGS prodrug micelles for hydrophilic drug delivery with neuroprotective effects. *International journal of pharmaceutics* **2012,** 438, (1), 98-106.
225. Zhang, Z.; Feng, S.-S., Nanoparticles of poly (lactide)/vitamin E TPGS copolymer for cancer chemotherapy: synthesis, formulation, characterization and in vitro drug release. *Biomaterials* **2006,** 27, (2), 262-270.
226. Gan, C. W.; Feng, S.-S., Transferrin-conjugated nanoparticles of poly (lactide)-D-α-tocopheryl polyethylene glycol succinate diblock copolymer for targeted drug delivery across the blood–brain barrier. *Biomaterials* **2010,** 31, (30), 7748-7757.
227. Zhang, Z.; Lee, S. H.; Gan, C. W.; Feng, S.-S., In vitro and in vivo investigation on PLA–TPGS nanoparticles for controlled and sustained small molecule chemotherapy. *Pharmaceutical research* **2008,** 25, (8), 1925-1935.
228. Wee Gan, C.; Chien, S.; Feng, S.-S., Nanomedicine: enhancement of chemotherapeutical efficacy of docetaxel by using a biodegradable nanoparticle formulation. *Current pharmaceutical design* **2010,** 16, (21), 2308-2320.
229. Ma, Y.; Huang, L.; Song, C.; Zeng, X.; Liu, G.; Mei, L., Nanoparticle formulation of poly (ε-caprolactone-co-lactide)-d-α-tocopheryl polyethylene glycol 1000 succinate random copolymer for cervical cancer treatment. *Polymer* **2010,** 51, (25), 5952-5959.
230. Li, P.-Y.; Lai, P.-S.; Hung, W.-C.; Syu, W.-J., Poly (L-lactide)-vitamin E TPGS nanoparticles enhanced the cytotoxicity of doxorubicin in drug-resistant MCF-7 breast cancer cells. *Biomacromolecules* **2010,** 11, (10), 2576-2582.
231. Ha, P. T.; Tran, T. M. N.; Pham, H. D.; Nguyen, Q. H.; Nguyen, X. P., The synthesis of poly (lactide)-vitamin E TPGS (PLA-TPGS) copolymer and its utilization to formulate a curcumin nanocarrier. *Advances in Natural Sciences: Nanoscience and Nanotechnology* **2010,** 1, (1), 1-7.
232. Sun, B.; Feng, S.-S., Trastuzumab-functionalized nanoparticles of biodegradable copolymers for targeted delivery of docetaxel. *Nanomedicine* **2009,** 4, (4), 431-445.
233. Zhang, Z.; Lee, S. H.; Feng, S.-S., Folate-decorated poly (lactide-co-glycolide)-vitamin E TPGS nanoparticles for targeted drug delivery. *Biomaterials* **2007,** 28, (10), 1889-1899.
234. Ren, F.; Jing, Q.; Cui, J.; Shen, Y., Synthesis and Characterization of D-α-Tocopheryl Polyethylene Glycol 1000 Succinate-Block-Poly (ε-caprolactone) Copolymer Used as Carriers for Microparticles. *Journal of Dispersion Science and Technology* **2009,** 30, (8), 1129-1134.

235. Muthu, M. S.; Leong, D. T.; Mei, L.; Feng, S.-S., Nanotheranostics- application and further development of nanomedicine strategies for advanced theranostics. *Theranostics* **2014,** 4, (6), 660-677.
236. Choi, K. Y.; Liu, G.; Lee, S.; Chen, X., Theranostic nanoplatforms for simultaneous cancer imaging and therapy: current approaches and future perspectives. *Nanoscale* **2012,** 4, (2), 330-342.
237. Janib, S. M.; Moses, A. S.; MacKay, J. A., Imaging and drug delivery using theranostic nanoparticles. *Advanced drug delivery reviews* **2010,** 62, (11), 1052-1063.
238. Luk, B. T.; Zhang, L., Current Advances in Polymer-Based Nanotheranostics for Cancer Treatment and Diagnosis. *ACS applied materials & interfaces* **2014,** 6, (24), 21859-21873.
239. Cole, A. J.; Yang, V. C.; David, A. E., Cancer theranostics: the rise of targeted magnetic nanoparticles. *Trends in biotechnology* **2011,** 29, (7), 323-332.
240. Hong, G. B.; Zhou, J. X.; Yuan, R. X., Folate-targeted polymeric micelles loaded with ultrasmall superparamagnetic iron oxide: Combined small size and high MRI sensitivity. *International Journal of Nanomedicine* **2012,** 7, 2863-2872.
241. Chandrasekharan, P.; Maity, D.; Yong, C. X.; Chuang, K.-H.; Ding, J.; Feng, S.-S., Vitamin E (d-alpha-tocopheryl-co-poly(ethylene glycol) 1000 succinate) micelles-superparamagnetic iron oxide nanoparticles for enhanced thermotherapy and MRI. *Biomaterials* **2011,** 32, (24), 5663-5672.
242. Zarabi, B.; Nan, A.; Zhuo, J.; Gullapalli, R.; Ghandehari, H., HPMA copolymer–doxorubicin–gadolinium conjugates: synthesis, characterization, and in vitro evaluation. *Macromolecular bioscience* **2008,** 8, (8), 741-748.
243. He, Y.; Zhang, L.; Zhu, D.; Song, C., Design of multifunctional magnetic iron oxide nanoparticles/mitoxantrone-loaded liposomes for both magnetic resonance imaging and targeted cancer therapy. *International Journal of Nanomedicine* **2014,** 9, (1), 4055-4066.
244. Mi, Y.; Liu, X.; Zhao, J.; Ding, J.; Feng, S.-S., Multimodality treatment of cancer with herceptin conjugated, thermomagnetic iron oxides and docetaxel loaded nanoparticles of biodegradable polymers. *Biomaterials* **2012,** 33, (30), 7519-7529.
245. Debele, T. A.; Peng, S.; Tsai, H.-C., Drug Carrier for Photodynamic Cancer Therapy. *International journal of molecular sciences* **2015,** 16, (9), 22094-22136.
246. Nakamura, H.; Liao, L.; Hitaka, Y.; Tsukigawa, K.; Subr, V.; Fang, J.; Ulbrich, K.; Maeda, H., Micelles of zinc protoporphyrin conjugated to N-(2-hydroxypropyl)methacrylamide (HPMA) copolymer for imaging and light-induced antitumor effects in vivo. *Journal of Controlled Release* **2013,** 165, (3), 191-198.
247. Allison, R. R.; Downie, G. H.; Cuenca, R.; Hu, X.-H.; Childs, C. J.; Sibata, C. H., Photosensitizers in clinical PDT. *Photodiagnosis and photodynamic therapy* **2004,** 1, (1), 27-42.
248. Arvizo, R.; Bhattacharya, R.; Mukherjee, P., Gold nanoparticles: opportunities and challenges in nanomedicine. *Expert opinion on drug delivery* **2010,** 7, (6), 753-763.
249. Mukerjee, A.; P Ranjan, A.; K Vishwanatha, J., Combinatorial nanoparticles for cancer diagnosis and therapy. *Current medicinal chemistry* **2012,** 19, (22), 3714-3721.

250. Bakalova, R.; Ohba, H.; Zhelev, Z.; Ishikawa, M.; Baba, Y., Quantum dots as photosensitizers? *Nature biotechnology* **2004,** 22, (11), 1360-1361.
251. Singh, S. P., Multifunctional magnetic quantum dots for cancer theranostics. *Journal of biomedical nanotechnology* **2011,** 7, (1), 95-97.
252. Muthu, M. S.; Kulkarni, S. A.; Raju, A.; Feng, S.-S., Theranostic liposomes of TPGS coating for targeted co-delivery of docetaxel and quantum dots. *Biomaterials* **2012,** 33, (12), 3494-3501.
253. Pan, J.; Liu, Y.; Feng, S.-S., Multifunctional nanoparticles of biodegradable copolymer blend for cancer diagnosis and treatment. *Nanomedicine* **2010,** 5, (3), 347-360.
254. Luo, S.; Zhang, E.; Su, Y.; Cheng, T.; Shi, C., A review of NIR dyes in cancer targeting and imaging. *Biomaterials* **2011,** 32, (29), 7127-7138.
255. Song, X.; Chen, Q.; Liu, Z., Recent advances in the development of organic photothermal nano-agents. *Nano Research* **2015,** 8, (2), 340-354.
256. Escobedo, J. O.; Rusin, O.; Lim, S.; Strongin, R. M., NIR dyes for bioimaging applications. *Current opinion in chemical biology* **2010,** 14, (1), 64-70.
257. Conceição, D. S.; Ferreira, D. P.; Ferreira, L. F. V., Photochemistry and Cytotoxicity Evaluation of Heptamethinecyanine Near Infrared (NIR) Dyes. *International journal of molecular sciences* **2013,** 14, (9), 18557-18571.
258. Zhang, C.; Liu, T.; Su, Y.; Luo, S.; Zhu, Y.; Tan, X.; Fan, S.; Zhang, L.; Zhou, Y.; Cheng, T., A near-infrared fluorescent heptamethine indocyanine dye with preferential tumor accumulation for in vivo imaging. *Biomaterials* **2010,** 31, (25), 6612-6617.
259. Zhang, E.; Luo, S.; Tan, X.; Shi, C., Mechanistic study of IR-780 dye as a potential tumor targeting and drug delivery agent. *Biomaterials* **2014,** 35, (2), 771-778.
260. Syu, W. J.; Yu, H. P.; Hsu, C. Y.; Rajan, Y. C.; Hsu, Y. H.; Chang, Y. C.; Hsieh, W. Y.; Wang, C. H.; Lai, P. S., Improved photodynamic cancer treatment by folate-conjugated polymeric micelles in a KB xenografted animal model. *Small* **2012,** 8, (13), 2060-2069.
261. Zheng, X.; Xing, D.; Zhou, F.; Wu, B.; Chen, W. R., Indocyanine green-containing nanostructure as near infrared dual-functional targeting probes for optical imaging and photothermal therapy. *Molecular Pharmaceutics* **2011,** 8, (2), 447-456.
262. Yuan, A.; Qiu, X.; Tang, X.; Liu, W.; Wu, J.; Hu, Y., Self-assembled PEG-IR-780-C13 micelle as a targeting, safe and highly-effective photothermal agent for in vivo imaging and cancer therapy. *Biomaterials* **2015,** 51, 184-193.
263. Fernandez-Fernandez, A.; Manchanda, R.; Carvajal, D. A.; Lei, T.; Srinivasan, S.; McGoron, A. J., Covalent IR820-PEG-diamine nanoconjugates for theranostic applications in cancer. *International journal of nanomedicine* **2014,** 9, 4631-4648.
264. Zheng, M.; Yue, C.; Ma, Y.; Gong, P.; Zhao, P.; Zheng, C.; Sheng, Z.; Zhang, P.; Wang, Z.; Cai, L., Single-step assembly of DOX/ICG loaded lipid–polymer nanoparticles for highly effective chemo-photothermal combination therapy. *Acs Nano* **2013,** 7, (3), 2056-2067.
265. Jiang, C.; Cheng, H.; Yuan, A.; Tang, X.; Wu, J.; Hu, Y., Hydrophobic IR780 encapsulated in biodegradable human serum albumin nanoparticles for photothermal and photodynamic therapy. *Acta biomaterialia* **2015,** 14, 61-69.

Capítulo II: Objetivos

II. Objetivos

Una de las patologías más importantes a las que tiene que hacer frente la sociedad actualmente es el cáncer. Los tratamientos más ampliamente utilizados han mejorado el tiempo y calidad de vida de los pacientes. Sin embargo, los efectos secundarios derivados de su uso, su falta de eficacia y la necesidad de un diagnóstico precoz evidencian la imperante necesidad de investigar nuevos fármacos anticancerígenos así como desarrollar tratamientos avanzados que permitan a su vez una monitorización a tiempo real de la enfermedad.

Las investigaciones en este campo se centran en atacar las diferencias encontradas en las mitocondrias de las células no patológicas y las células tumorales, convirtiendo a estos orgánulos en una diana terapéutica ideal para el desarrollo de tratamientos más selectivos contra el cáncer. En este contexto, surgen fármacos como el succinato de la vitamina E (α-TOS) que, sin embargo, al igual que ocurre con la mayoría de fármacos antitumorales, presenta una baja especificidad y solubilidad.

El objetivo de la presente tesis doctoral ha sido el diseño, caracterización fisicoquímica y evaluación de la actividad biológica de diversos vehículos poliméricos nanoestructurados portadores del fármaco anticancerígeno α-TOS con el fin de lograr un tratamiento más eficaz, selectivo y menos tóxico contra el cáncer.

Para alcanzar este objetivo global, se recogen 5 trabajos científicos que se agrupan en 3 capítulos diferentes con el fin de presentar los resultados con mayor claridad y de acuerdo con los objetivos más concretos que se desean alcanzar en cada uno de ellos y que se resumen a continuación:

1- En el capítulo 3 titulado "***Bioactive nanoparticles based on free radical copolymers of vitamin E derivatives***" se incluyen dos publicaciones científicas cuya principal objetivo es la preparación de vehículos poliméricos bioactivos portadores de derivados de la vitamina E y el estudio de la relación estructura-propiedades. Para ello, se lleva a cabo la síntesis y caracterización de cuatro familias de copolímeros preparados por polimerización radical convencional de derivados metacrílicos del α-TOS (MTOS), la vitamina E (MVE) y del dihidrofitol (MPHY y SPHY) con la *N*-vinil pirrolidona (VP). Además, se estudian las cinéticas de las reacciones de

copolimerización y la influencia de las propiedades microestructurales de los copolímeros preparados en la obtención de sistemas autoensamblados en forma de nanopartículas (NPs). La actividad biológica de estas NPs es evaluada en diversas líneas celulares, analizando la relación entre la actividad biológica obtenida y las características estructurales de los monómeros preparados. Finalmente, estas NPs se utilizan para encapsular eficazmente más α-TOS en su núcleo hidrofóbico, con el fin de mejorar su actividad y estudiar su mecanismo de acción a nivel celular.

2- El capítulo 4 titulado "***RAFT polymer-drugs derived from α-tocopheryl succinate***" recoge dos artículos que tienen como objetivo fundamental la obtención de NPs poliméricas bioactivas con una estructura y composición química bien definida y baja polidispersidad. Para ello, se emplea la polimerización controlada vía RAFT para la obtención de copolímeros de bloque formados por MTOS y polietilenglicol (PEG-*b*-poliMTOS). Asimismo, se analiza la influencia de las propiedades del PEG y del contenido de monómero activo (MTOS) en la capacidad de las NPs preparadas para internalizarse y afectar a la viabilidad de células tumorales. Finalmente, otro de los objetivos primordiales de este capítulo es el estudio de cómo afecta la modificación del bloque hidrófobo en la relación estructura-actividad de estas NPs mediante la preparación terpolímeros que incorporan 2-hidroxietil metacrilato (HEMA) en su estructura.

3- El capítulo 5 titulado "***Phototherapeutic nanoparticles***" pretende desarrollar nanopartículas fluorescentes basadas en los polímeros de bloque PEG-*b*-poliMTOS anteriormente descritos con el fin de mejorar su actividad antitumoral por fototerapia. Para ello, se recoge un trabajo científico en el que se optimiza la conjugación química y encapsulación física de la sonda fluorescente IR-780 en los polímeros de bloque más activos. Adicionalmente, se estudia la formación de NPs así como sus óptimas propiedades ópticas con el fin de obtener sistemas autoensamblados que puedan monitorizarse por fluorescencia, facilitando el tratamiento y diagnóstico simultáneo del cáncer. Por último, se evalúan las propiedades fototerapéuticas (fototérmicas y fotodinámicas) de estos sistemas nanoparticulados.

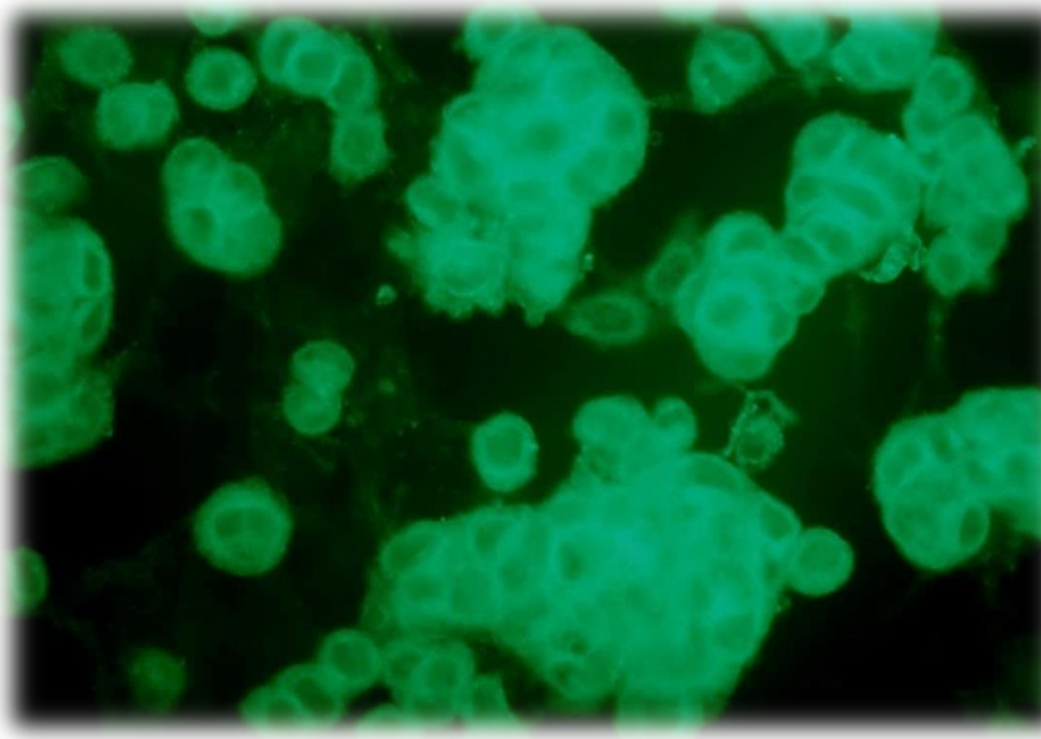

Chapter III: Bioactive nanoparticles based on free radical copolymers of vitamin E derivatives

3.1- Anticancer and Antiangiogenic Activity of Surfactant-Free Nanoparticles based on Self-assembled Polymeric Derivatives of Vitamin E: Structure-activity relationship

Biomacromolecules, **2015**

3.2- Mitochondrially targeted nanoparticles based on α-TOS for the selective cancer treatment.

Macromolecular Biosciences, **2015**

3.1. Anticancer and Antiangiogenic Activity of Surfactant-Free Nanoparticles based on Self-assembled Polymeric Derivatives of Vitamin E. Structure-activity relationship

Raquel Palao-Suay[1,2], María Rosa Aguilar[1,2], Francisco J. Parra-Ruiz[1], Mar Fernández-Gutiérrez[1,2], Juan Parra[2,3], Carolina Sánchez-Rodríguez[4], Ricardo Sanz-Fernández[4], Laura Rodrigáñez[4], Julio San Román[1,2]*

[1]Group of Biomaterials, Department of Polymeric Nanomaterials and Biomaterials, Institute of Polymer Science and Technology, CSIC, Madrid, Spain.

[2]Networking Biomedical Research Centre in Bioengineering, Biomaterials and Nanomedicine, CIBER-BBN, Spain.

[3]Clinical Research and Experimental Biopathology Unit, Healthcare Complex of Ávila, Ávila, Spain.

[4]Foundation for Biomedical Research, University Hospital of Getafe, Getafe (Madrid), Spain

**Corresponding author*: mraguilar@ictp.csic.es

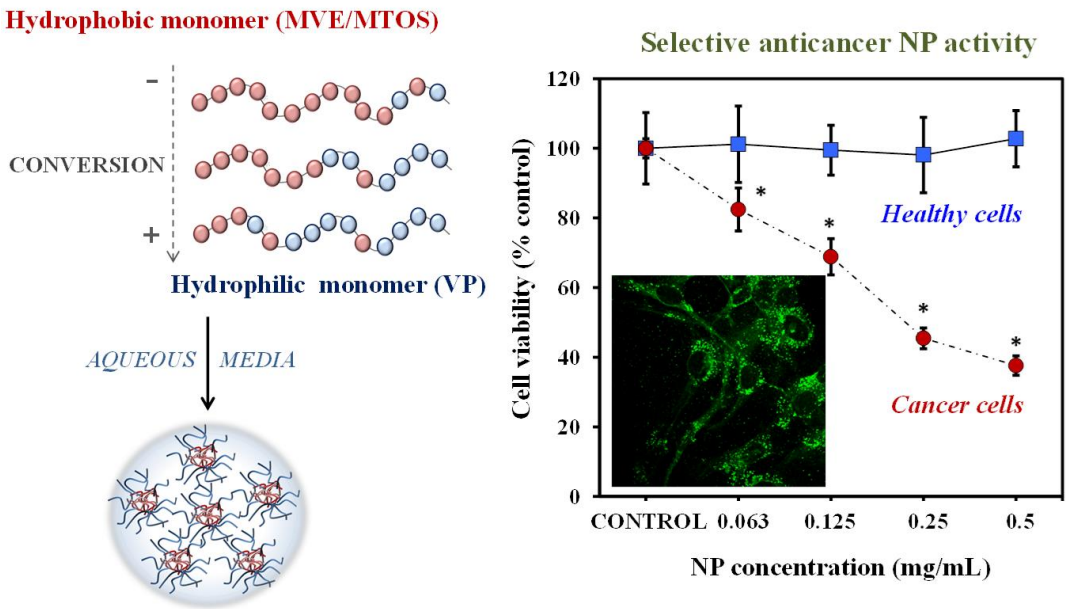

KEYWORDS: Vitamin E, α-tocopheryl succinate, polymer drug, anticancer, antiangiogenic, apoptosis.

3.1.1. Abstract

α-Tocopheryl succinate (α-TOS) is a well-known mitochondrially targeted anticancer compound, however it is highly hydrophobic and toxic. In order to improve its activity and reduce its toxicity, new surfactant-free biologically active nanoparticles (NPs) were synthesized. A methacrylic derivative of α-TOS (MTOS) was prepared and incorporated in amphiphilic pseudoblock copolymers when copolymerized with *N*-vinyl pyrrolidone (VP) by free radical polymerization (poly(VP-*co*-MTOS)). The selected poly(VP-*co*-MTOS) copolymers formed surfactant-free NPs by nanoprecipitation with sizes between 96 and 220 nm and narrow size distribution, and the *in vitro* biological activity was tested.

In order to understand the structure-activity relationship, three other methacrylic monomers were synthesized and characterized: MVE did not have the succinate group, SPHY did not have the chromanol ring, and MPHY did not have both the succinate group and the chromanol ring. The corresponding families of copolymers (poly(VP-*co*-MVE), poly(VP-*co*-SPHY) and poly(VP-*co*-MPHY)) were synthesised and characterized, and their biological activity was compared to poly(VP-*co*-MTOS). Both poly(VP-*co*-MTOS) and poly(VP-*co*-MVE) presented triple action: reduced cell viability of cancer cells with little or no harm to nonmalignant cells (anticancer), reduced viability of proliferating endothelial cells with little or no harm to quiescent endothelial cells (antiangiogenic), and efficiently encapsulated hydrophobic molecules (nanocarrier). The anticancer and antiangiogenic activity of the synthesized copolymers is demonstrated as the active compound (Vitamin E or α-tocopheryl succinate) do not need to be cleaved to trigger the biological action targeting ubiquinone binding sites of complex II. Poly(VP-*co*-SPHY) and poly(VP-*co*-MPHY) also formed surfactant-free NPs that were also endocyted by the assayed cells; however these NPs did not selectively reduce cell viability of cancer cells. Therefore, the chromanol ring of the vitamin E analogues has an important role in the biological activity of the copolymers. Moreover, when succinate moiety is substituted and vitamin E is directly linked to the macromolecular chain through an ester bond, the biological activity is maintained.

3.1.2. Introduction

α-Tocopheryl succinate (α-TOS) selectively induces apoptosis of cancer cells and acts as an angiogenesis regulator because it also induces apoptosis of proliferating endothelial cells with little or no harm to the quiescent endothelial cells. α-TOS presents mitochondrially targeted anticancer activity because it is a BH3 protein mimetic that blocks Bcl-2 or Bcl-xL antiapoptotic proteins (mitocan type II), and because it interferes with the electron transport chain; specifically, α-TOS displaces ubiquinone from binding to complex II inhibiting succinate deshydrogenase activity of complex II in the mitochondrial transport chain (mitocan type V)[1, 2]. As a result, the generated electrons recombine with molecular oxygen to produce high levels of reactive oxygen species (ROS) that activate the proteins that regulate mitochondrial permeabilization and trigger apoptosis[3, 4].

At a molecular level, Neuzil et al. described three different domains in α-TOS structure: the functional domain (succinate moiety), the signaling domain (chromanol ring moiety) and the hydrophobic domain (aliphatic chain moiety) and stated that the functional domain was the main responsible of the biological activity of α-TOS (**figure 1**)[5].

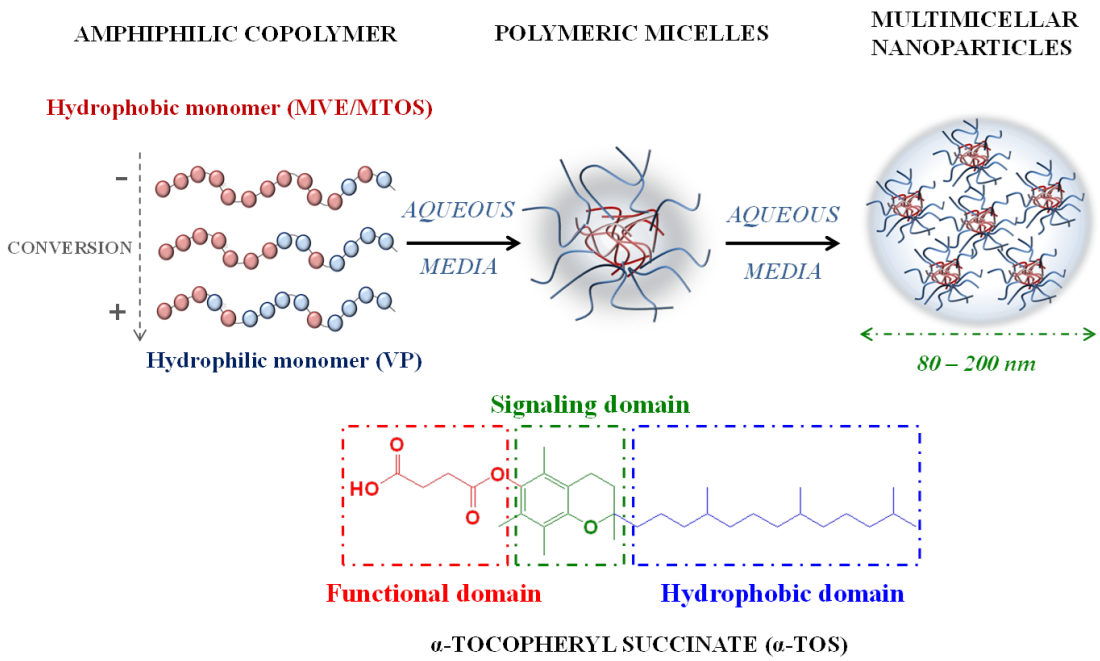

Figure 1: Formation of multimicellar NPs based on amphiphilic pseudoblock copolymer drugs.

α-TOS is a lipophilic molecule difficult to administrate in physiological media and therefore, several modifications have been performed in order to improve its hydrophilicity. One of the most common derivatives of α-TOS is the poly(ethylenglycol 1000)-α-TOS conjugate (TPGS)[6]. It is a nonionic surfactant that forms stable micelles in aqueous media at concentrations as low as 0.02 wt %. It was approved by the FDA as a safe pharmaceutic adjuvant and has been used in many drug delivery formulations. It presents similar anticancer activity as α-TOS; however it is highly toxic (IC_{50}: 33μM) mostly due to its surfactant nature[7].

Another strategy to improve α-TOS solubility is the incorporation of α-TOS in nanovehicles. Polymeric self-assembled nanovehicles (micelles, capsules, particles) present a hydrophilic shell and a hydrophobic core and therefore have been used for the controlled administration of hydrophobic drugs[8, 9]. They are obtained by self-assembling of amphiphilic macromolecules obtained by radical polymerization, controlled polymerization (ATRP, RAFT…) or modification of natural or synthetic polymers in order to obtain the appropriate hydrophilic/hydrophobic balance to form nanoparticles (NPs) in aqueous media. α-TOS could be encapsulated in the hydrophobic core or could be covalently attached to the macromolecular chain, which could present biological activity itself (polymer drug)[10, 11]. Moreover, the macromolecular nature of the polymeric systems will favor passive targeting of the systems by the accumulation and extravasation to the tumor area due to the so-called Enhanced Permeability and Retention (EPR) effect firstly described by Matsumura and Maeda in 1986[12]. This effect is due to the high permeability of the defective vasculature that irrigates the tumor and the lack of effective tumor lymphatic drainage that prevents clearance of penetrant macromolecules (M_w > 30 kDa) (**figure 1**)[13 14].

The aim of this work was the development of new α-TOS-based polymeric drugs with anticancer and antiangiogenic activity that form self-assembled polymeric micelles for controlled release of chemotherapeutic molecules. Therefore, the new polymers will present pharmacological activity, and will form NPs for the encapsulation and delivery of other hydrophobic drugs. For this purpose, a methacrylic derivative of α-TOS (MTOS) was synthesized in order to be polymerized with a hydrophilic monomer. MTOS presented all structural domains described by Neuzil, but the carboxylic group of the succinate was derived into a hydrolizable ester group to be attached to the polymerizable double bond.

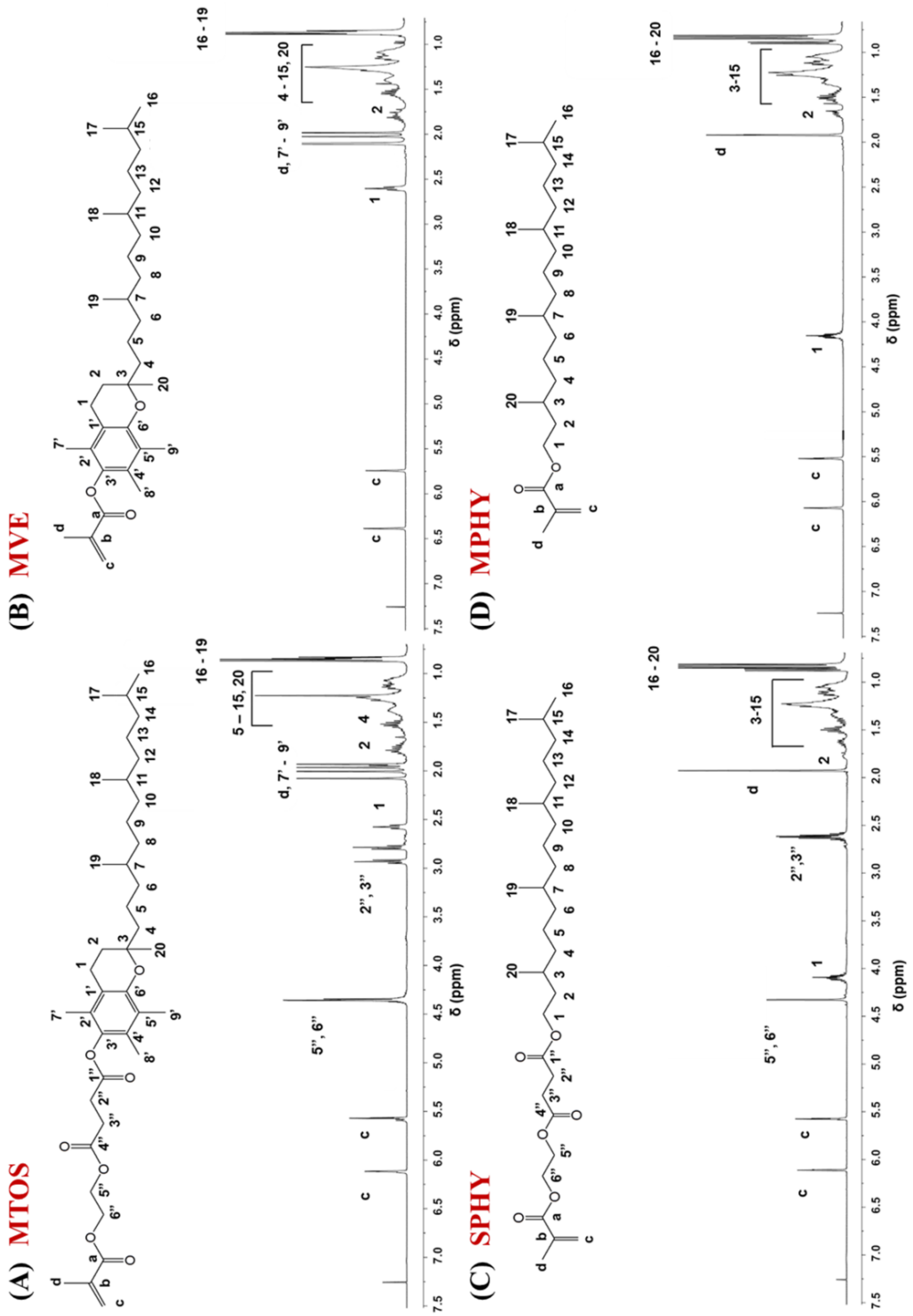

Figure 2: ^{1}H-NMR spectra of (A) MTOS, (B) MVE, (C) SPHY, and (D) MPHY.

In order to study the influence of the three domains of α-TOS in the biological activity of the polymeric drugs NPs, three other monomers were prepared (**figure 2**): MVE (the functional domain was eliminated), SPHY (the signaling domain was eliminated), and MPHY (both functional and signaling domains were eliminated). MTOS, SPHY and MPHY are described in this paper for the first time.

Four copolymeric families with *N*-vinyl pyrrolidone (VP) were obtained by free radical polymerization and were fully characterized. They were designed to present an appropriate hydrophilic/hydrophobic balance and an adequate distribution of the comonomers in the polymeric chains to form surfactant-free self-assembled NPs when nanoprecipitated in aqueous media. The hydrophobic core of the NPs allowed the encapsulation of other hydrophobic molecules. *In vitro* biological activity of the four families of NPs were compared in order to study structure-activity relationship and to understand the role of the three domains described by Neuzil for α-TOS in a macromolecular system.

Cell viability of human breast adenocarcinoma cells (MCF-7) and human breast epithelial cells (HMEpC) in the presence of the NPs was compared in order to evaluate the NP selectivity. Moreover, cell viability of proliferating and quiescent human umbilical vein endothelial cells (HUVEC) in the presence of the NPs was also evaluated in order to study the antiangiogenic effect of the new formulations. MTOS and MVE-bearing NPs could be administered in aqueous buffered solution, giving *in vitro* biological activity, higher selectivity, and much lower toxicity than α-TOS and TPGS.

3.1.3. Materials and methods

α-tocopherol (vitamin E, Sigma-Aldrich), phytol (Sigma-Aldrich), methacryloyl chloride (Fluka), triethylamine (Scharlau), 4-dimethylaminopyridine (DMAP, Sigma-Aldrich), tetrabutylammonium iodide (Sigma-Aldrich), Raney Nickel 2800 (Sigma-Aldrich), *N,N'*-dicyclohexylcarbodiimide (DCC, Sigma-Aldrich), dichloromethane (Sigma-Aldrich), hexane (Sigma-Aldrich), hydrochloric acid (HCl, VWR), sodium hydroxide (NaOH, Panreac) were used without further purification in the preparation of different monomers.

N-Vinyl pyrrolidone (VP, Sigma-Aldrich) and 1,4-dioxane (Panreac) were purified by distillation under reduced pressure and 2,2'-azobisisobutyronitrile (AIBN, Merck) was recrystallized from methanol (mp 104 ºC) for the preparation of amphiphilic copolymers. Deuteraded chloroform ($CDCl_3$, Sigma-Aldrich) and chromatographic grade tetrahydrofuran (THF, Sigma-Aldrich) were used without further purification to characterize polymeric systems. Additionally, phosphate buffered solution (PBS, pH 7.4, Sigma-Aldrich) and coumarin-6 (c6, Sigma-Aldrich) were used without further purification.

- **Characterization techniques**

^{1}H-NMR and ^{13}C-NMR were performed in a Mercury 400BB apparatus, operating at 400 and 100 MHz, respectively. The spectra were recorded by dissolving the corresponding sample in deuterated $CDCl_3$ at 25 ºC. Copolymer composition was calculated from ^{1}H-NMR spectra using MestreNova 9.0 software. High resolution mass spectroscopy (HRMS) was performed using an Agilent 5975 C spectrometer (perfluorokerosene (PKF) served as the internal reference). Fourier transform infrared attenuated total reflectance (ATR-FTIR) spectroscopy was performed in a Perkin Elmer Spectrum One FTIR spectrometer using 32 scans, and a resolution of 4 cm^{-1}.

Glass transition temperatures (T_g) were determined by differential scanning calorimetry with a Perkin Elmer DSC7 interfaced to a thermal analysis data system TAC 7/DX. The dry samples (7–10 mg) were placed in aluminium pans and heated from -30 to 160 or 200 ºC in the case of PVP at a constant rate of 20°C/min. T_g was taken as the midpoint of the heat capacity transition.

The average molecular weight (M_n and M_w) and dispersity ($Đ$) of all the polymers were determined by size exclusion chromatography (SEC), using a Perkin-Elmer Isocratic LC pump 250 coupled to a refraction index detector (Series 200). Three polystyrene-divinyl benzene columns (Polymer Laboratories) of average pore size of 10^3, 10^4 and 10^5 Å were used as solid phase, and degassed THF (1 mL/min) was used as eluent and temperature was fixed at 40 ºC. Monodisperse poly(methyl methacrylate) standards (Scharlab) with molecular weights (MWs) between 10.3 and 1.400 kDa were used to obtain the calibration curve. Data were analyzed using the Perkin-Elmer LC solution program.

- **Synthesis of monomers and copolymers**

Synthesis of the methacrylic derivative of the α-tocopheryl succinate (MTOS)

α-TOH (1 equiv) was dissolved in dichloromethane and introduced into a 250 mL round-bottom flask. Mono-(2-(methacryloyloxy)ethyl) succinate MES (1.4 equiv) and DMAP (0.1 equiv) were also added to the reaction mixture. DCC (1.5 equiv) was then added dropwise with constant stirring using an ice bath under nitrogen atmosphere. Afterward, the reaction mixture was stirred for 24 h at room temperature.

The reaction mixture was washed 3 times with NaOH (1N) and the solvent removed under reduced pressure. The resulting oil was resolved in hexane and washed with HCl (1N), dried over $MgSO_4$, and the solvent removed under reduced pressure. The yield of the reaction was 90 %. The chemical structure of the methacrylic derivative of α-TOS was elucidated by NMR spectroscopy.

^{1}H-NMR spectrum (400 MHz, $CDCl_3$): δ_H 6.12 (s, 1H), 5.57 (dq, J = 1.66, 3.17 Hz, 1H), 4.36-4.35 (m, 4 H), 2.94 (t, J = 6.34 Hz, 2 H), 2.79 (t, J = 6.92 Hz, 2 H), 2.58 (t, J = 6.53 Hz, 2 H), 2.08 (s, 3 H), 2.01 (s, 3 H), 1.97 (s, 3 H), 1.93 (s, 3 H), 1.89-1.67 (m, 4 H), 1.67-1.44 (m, 3 H), 1.44-1.17 (m+s, 13 H), 1.17-0.99 (m, 6 H), 0.92-0.79 ppm (4xd, J = 6.68 Hz, 12 H).

^{13}C-NMR spectrum (100 MHz, $CDCl_3$): δ_C 172.2, 171, 167.3, 149.6, 140.6, 136.0, 126.8, 126.3, 125.1, 123.2, 117.5, 75.3, 62.7, 62.5, 39.6, 37.6, 37.5, 33.0, 30.9, 29.6, 29.2, 29.0, 28.2, 26.4, 25.0, 24.9, 24.7, 22.9, 22.8, 21.2, 20.8, 20.0, 19.9, 19.8, 19.7, 18.5, 13.1, 12.3, 12.0 ppm.

ATR-FTIR spectrum (cm^{-1}): υ = 2928, 2866, 1744, 1722, 1456, 1377, 1297, 1142, 1109, 1065, 941, 814, 737, 704 cm.

HRMS (ESI): Calculated for $C_{40}H_{64}O_7$ $[M+H]^+$ 657.4725, found 657.4989.

Synthesis of the methacrylic derivative of α-Tocopherol (MVE)

Vitamin E methacrylate (MVE) was obtained as previously described[15].

Synthesis of the methacrylic derivative of dihydrophytol (MPHY)

Dihydrophytol was synthesized as previously described[16]. A methacrylic derivative of dihydrophytol (MPHY) was prepared by reaction of dihydrophytol with methacryloyl chloride using dichloromethane as solvent. Particularly, dihydrophytol (1 equiv), triethylamine (1.5 equiv), DMAP (0.1 equiv), and dichloromethane were incorporated to a 250 mL round bottom flask. Then, methacryloyl chloride (1.2 equiv) was added dropwise over the reaction mixture with constant stirring at room temperature under nitrogen atmosphere. Afterward, the reaction mixture was kept under magnetic stirring for 24 h at room temperature.

The reaction mixture was treated with NaOH (1N) and the organic phase evaporated under vacuum. The resulting oil was resolved in hexane, washed three times with HCl (1N), dried over $MgSO_4$, and the solvent removed under reduced pressure. The yield of this reaction was higher than 90 %. The chemical structure of MPHY was confirmed by NMR spectroscopy.

^{1}H-NMR spectrum (400 MHz, $CDCl_3$): δ_H 6.09 (dq, *J* = 1.02, 1.7 Hz, 1 H), 5.54 (dq, J = 1.61, 3.22, 1 H), 4.21-4.14 (m, 2H), 1.94 (m, 3 H), 1.76-1.63 (m, 1 H), 1.62-1.41 (m, 3 H), 1.41-0.98 (m, 20 H), 0.94-0.80 ppm (5xd, J = 6.5 Hz, 15 H).

^{13}C-NMR spectrum (100 MHz, $CDCl_3$): δ_C 167.7, 136.7, 125.4, 63.4, 39.6, 37.7, 37.6, 37.5, 35.7, 35.4, 33.0, 30.2, 28.2, 25.0, 24.7, 24.5, 23.0, 22.8, 20.0, 19.9, 19.8, 18.6 ppm.

ATR-FTIR spectrum (cm^{-1}): υ = 2955, 2927, 2890, 1721, 1678, 1639, 1463, 1378, 1321, 1296, 1164, 1111, 1040, 1012, 937, 814, 736, 698, 657.

HRMS (ESI): Calculated for $C_{24}H_{46}O_2$ $[M+H]^+$ 367.3571, found 367.3615.

Synthesis of the methacrylic derivative of dihydrophytol succinate (SPHY)

Dihydrophytol (1 equiv), MES (1.4 equiv) and DMAP (0.1 equiv) were dissolved in dichloromethane and added to a 250 mL round-bottom flask. Then, DCC (1.5 equiv) was added dropwise with constant stirring using an ice bath under nitrogen atmosphere. The reaction mixture was kept under magnetic stirring for 24 h at room temperature.

The reaction mixture was washed 3 times with NaOH (1N) and HCl (1N) solutions and the solvent was then evaporated under vacuum. The resulting oil was resolved in hexane and again purified by successive washed with NaOH (1N) and HCl (1N) solutions. After drying over $MgSO_4$, the residual solvent was removed under reduced pressure. The yield of this reaction was higher than 90 %. The chemical structure of SPHY was confirmed by NMR spectroscopy.

^{1}H-NMR spectrum (400 MHz, $CDCl_3$): δ_H 6.11 (bs, 1 H), 5.57 (dq, J = 1.51, 3.20, 12 H), 4.33 (s, 4 H), 4.15-4.05 (m, 2H), 2.69-2.56 (m, 2 H), 1.93 (t, *J* = 0.97 Hz, 3 H), 1.83-0.95 (m, 24 H), 0.91-0.76 ppm (5xd, J = 6.6 Hz, 15 H).

^{13}C-NMR spectrum (100 MHz, $CDCl_3$): δ_C 172.4, 172.3, 136.1, 126.3, 63.6, 62.5, 39.6, 37.7, 37.6, 37.5, 37.4, 35.7, 35.6, 33.0, 30.1, 29.3, 29.2, 28.2, 25.0, 24.7, 24.5, 22.9, 22.8, 20.0, 19.9, 19.8, 19.7, 19.6, 18.5 ppm.

ATR-FTIR spectrum (cm^{-1}): υ = 2955, 2927, 2869, 1737, 1638, 1521, 1461, 1378, 1319, 1297, 1151, 1052, 977, 941, 881, 814, 737, 658.

HRMS (ESI): Calculated for $C_{31}H_{56}O_6$ $[M+H]^+$ 525.4150, found 525.4158.

Synthesis of the homopolymers

VP and methacrylic monomers (MPHY, MTOS or SPHY) were polymerized in solution using 1,4-dioxane as solvent. The monomer solutions ([M] = 0. 25 mol/L) were deoxygenated with N_2 for 15 min. Afterward, the radical initiator AIBN ([I]=1.5 x 10^{-2} mol/L) was added to the solutions and the reaction medium transferred to an oven at 60 ºC. The reaction time was 24 h to obtain a high conversion polymer.

At the end of the reaction, homopolymers (PVP, PMTOS, PMPHY and PSPHY) were dialyzed (Spectrum Laboratories, 3.5K MW cut-off) against distilled water for 72 h. The resulted homopolymers were lyophilized to yield a white amorphous powder.

^{1}H-NMR spectrum (PMTOS, 400 MHz, $CDCl_3$): δ_H 4.44-4.88 (2xbs, 4 H), 3.02 (bs, 2 H), 2.83-2.63 (bs, 2 H), 2.61-2.43 (bs, 2 H), 2.14-1.85 (3xs, 9 H), 1.83-1.61 (m, 3 H), 1.62-1.44 (m, 5 H), 1.44-0.96 (m, 18 H), 0.92-0.64 ppm (m, 12 H).

^{13}C-NMR spectrum (PMTOS, 400 MHz, $CDCl_3$): δ_C 167.7, 136.7, 125.3, 63.5, 39.6, 37.7, 37.6, 37.5, 37.4, 35.7, 35.6, 33.0, 30.0, 28.2, 25.0, 24.7, 24.5, 22.9, 22.8, 20.0, 19.9, 19.8, 19.7, 18.6 ppm.

ATR-FTIR spectrum (PMTOS, cm^{-1}): 2952, 2924, 2869, 1736, 1661, 1580, 1524, 1457, 1413, 1376, 1351, 1314, 1245, 1142, 1111, 1063, 966, 919, 881, 864, 815, 748, 680.

Synthesis of the copolymeric systems

Copolymeric systems based on methacrylic derivatives of α-TOS and dihydrophytol were synthesized by free radical polymerization in solution using VP as comonomer and different feed molar ratios in order to obtain polymers with different hydrophilic – hydrophobic balance. Particularly, comonomers were dissolved in 1,4-dioxane at a total monomer concentration of 1 M (poly(VP-*co*-MVE)) or 0.25 M (poly(VP-*co*-MPHY), poly(VP-*co*-MTOS) and (poly(VP-*co*-SPHY)), and the mixture solutions were deoxygenated bubbling pure nitrogen during 15 minutes. Then, AIBN was added as free radical initiator to the solution ($[I]=1.5x10^{-2}$ M) and the reaction vessel was transferred to an oven at 60 ºC for 24 h with the aim to thermally induce the polymerization and obtain high conversion copolymers.

At the end of the polymerization reactions, copolymers (poly(VP-*co*-MVE), poly(VP-*co*-MTOS), poly(VP-*co*-MPHY) and poly(VP-*co*-SPHY)) were purified by dialysis (Spectrum Laboratories, 3.5K MW cut-off) against distilled water for 72 h in order to remove of residual unreacted monomers and low MW species. The resulting solutions were isolated by freeze-drying to yield white amorphous powders.

^{1}H-NMR spectrum (SPHY-24, 400 MHz, $CDCl_3$): δ_H 4.46-3.82 (m, 8 H), 3.81-3.54 (m, 1 H), 3.42-2.97 (m, 4 H), 2.85-2.53 (m, 6 H), 2.50-1.57 (m, 15 H), 1.57-0.96 (m, 28 H), 0.95-0.78 ppm (m, 15 H).

^{13}C-NMR spectrum (SPHY-24, 400 MHz, $CDCl_3$): δ_C 172.4, 172.3, 167.3, 136.1, 126.3, 63.6, 62.6, 62.5, 39.6, 37.6, 37.5, 37.4, 35.7, 35.6, 33.0, 30.1, 29.3, 29.2, 28.2, 25.0, 24.7, 24.5, 22.9, 22.8, 20.0, 19.9, 19.7, 19.6, 18.5 ppm.

ATR-FTIR spectrum (SPHY-24, cm^{-1}): 3438, 2955, 2926, 2866, 1733, 1659, 1494, 1461, 1423, 1377, 1317, 1287, 1272, 1231, 1159, 1076, 1053, 1020, 1000, 935, 893, 847, 735.

- **Reactivity ratios determination by 'in situ' ^{1}H-NMR**

Reactivity ratios of the synthesized copolymeric systems were determined by a method described in a previous publication using 'in situ' ^{1}H-NMR for the monitorization of the copolymerization reactions[17]. Copolymerization reactions were carried out inside a NMR tube in the same experimental conditions as described above but using 1,4-dioxane-d_8 as solvent. A solution of 1,4-dichlorobenzene (10 mg/mL) in DMSO-d_6 in a thin wall capillary tube introduced in the NMR tube was used as reference. Temperature was maintained at 60 ºC using the apparatus (Inova Mercury- 400 MHz) heat control system. Signals were integrated using MestreNova 9.0 software and the monomers concentrations were determined as follows:

$$[VP] = \frac{A1}{B1 + A1};\ [MMon] = \frac{B1}{B1 + A1}$$

where A1 corresponds to the integrated peak intensity of a vinylic proton assigned to VP (7.12 ppm), and *B*1 corresponds to the integrated peak intensity of an acrylic proton assigned to the methacrylic monomer (MMon: MTOS 6.12 ppm, MVE 6.37 ppm, MPHY 6.09 ppm and SPHY 6.13 ppm). The values were normalized using the initial feed compositions and the value of the reference peak.

- **NP formation by nanoprecipitation**

Self-assembled NPs were prepared by nanoprecipitation. For this purpose, copolymers were dissolved in 1,4-dioxane (10 mg/mL) and then added drop by drop over an aqueous phase (PBS, 0.01 M, pH 7.4) under constant magnetic stirring. The volume of the organic solution of copolymers was varied with the aim to obtain NP suspension at different concentration (2 – 0.05 mg/mL). After the nanoprecipitation, milky NP dispersions were dialyzed against PBS during 72 h in order to remove organic solvent. Afterward, each NP

suspension was sterilized by filtration through 0.22 µM poly(ether sulfone) membranes (PES, Millipore Express®, Millex GP) and stored at 4 ºC.

- **Coumarin-6 encapsulation**

c6-loaded NPs were also obtained by nanoprecipitation. c6 (1 % w/w respect to the polymer) and the corresponding polymer (10 mg/mL) were dissolved in dioxane and added dropwise to a PBS solution under magnetic stirring. The final polymer concentration was 2.0 mg/mL. The solution was dialyzed against PBS for 72 hours in order to eliminate the organic solvent and non-encapsulated c6.

- **Particle Size Distribution**

The particle size distribution of the NP suspensions was determined by dynamic light scattering (DLS) using a Malvern Nanosizer NanoZS Instrument equipped with a 4mW He-Ne laser (λ=633 nm) at a scattering angle of 173°. Measurements of NP dispersions were performed in square polystyrene cuvettes (SARSTEDT) and the temperature was kept constant at 25 ºC.

The autocorrelation function was converted in an intensity particle size distribution with ZetaSizer Software 7.10 version, to get the mean hydrodynamic diameter (D_h) and the particle dispersion index (PDI) between 0 (monodisperse particles) and 1 (polydisperse particles) based on the Stokes-Einstein equation, assuming the particle to be spherical. For each sample, the statistical average and standard deviation of data were calculated from 8 measurements of 20 runs each one.

- **Characterization morphology of NPs by scanning electron microscopy (SEM), transmission electron microscopy (TEM) and atomic force microscopy (AFM)**

The morphology of NPs was observed using scanning electron microscopy (SEM), transmission electron microscopy (TEM) and atomic force microscopy (AFM). SEM analysis was performed with a Hitachi SU8000 TED, cold-emission FE-SEM microscope working with an accelerating voltage between 15 and 25 kV. Samples were prepared by deposition of one drop of the corresponding NP suspension over small glass disks (12 mm diameter and 1 mm thickness), and evaporation at room temperature. Finally, the samples were coated with gold palladium alloy.

TEM analysis was done with Hitachi SU8000 TED, cold-emission FE-SEM microscope, operating at an acceleration voltage of 50 kV. A drop of NP suspension (0.02 mg/mL) was deposited over poly(vinyl formal)-coated copper TEM grid and evaporated overnight at room temperature. An additional drop of brilliant black dye (Sigma-Aldrich) was deposited on the grid, the excess was removed with filter paper, and the grid was allowed to dry before TEM observation.

For AFM examination, a drop of NP dispersion was deposited on a surface of small glass disks (14 mm of diameter) and allowed to dry overnight at room temperature. AFM was performed in tapping mode using a Multimode AFM (Veeco Instruments, Santa Barbara, CA, USA) with a Nanoscope IVa control system (software version 6.14r1), equipped with silicon tapping probes (RTESP, Veeco) with a spring constant of 42 N/m and a resonance frequency of 300 KHz and a scan rate of 0.5 Hz. Both the topography and the phase signal images were recorded with a resolution of 512x512 data points.

- **Cell culture**

Human mammary adenocarcinoma cells, MCF-7 (ECACC) cells were cultured in Dulbecco's modified Eagle's medium (DMEM), supplemented with 10% fetal bovine serum (FBS), 2% L-glutamine, 1% penicillin/streptomycin (P/S) and incubated at 37°C and 5% CO_2. Human mammary epithelial cells, HMEpC (obtained from the European Collection of Cell Cultures, ECACC) were cultured using mammary epithelial cell medium (Innoprot), supplemented with 10% FBS, 1% P/S as cultured medium at 37°C and 5% CO_2.

Human umbilical vein endothelial cells (HUVEC, kindly donated by the Institute of Pathology, Universitätsmedizin, Mainz, Germany) were isolated from umbilical cords and cultivated according to previously published methods[18] involving passages in gelatin-coated tissue culture flasks and the use of M199 medium (Sigma-Aldrich) supplemented with 20% FBS (Life Technologies), 1% P/S, 1% glutamax I (Life Technologies) 25µg/mL heparin (Sigma-Aldrich), and 25 µg/mL endothelial cell growth supplement (Becon Dickinson).

Human colon adenocarcinoma cells (WiDr, ECACC), and human osteosarcoma cells (MG-63, ECACC) were cultured in DMEM, supplemented with 10% FBS, 2% L-glutamine, 1% P/S and incubated at 37°C and 5% CO_2.

Hypopharynx carcinoma squamous cells (FaDu, ATCC) were cultured in Eagle's Minimun Essential (MEM), supplemented with 10% FBS, 1% P/S, and incubated at 37°C and 5% CO_2.

- **Uptake of coumarin-6 loaded NPs**

c6-loaded NPs obtained at 0.1 mg/mL were tested. HUVEC cells were seeded into 24 well assay plates at 90,000 cells/mL in complete medium. The cells were incubated overnight at 37 ºC. Afterward, the medium was replaced with the corresponding NPs dispersed in PBS (500 µL of the NP suspension and 500 µL of completed medium) and incubated for 5 h at 37 ºC. When this time was elapsed, the cells were washed 3 times with cold PBS and fixed by a paraformaldehyde solution in PBS (3.7 w/v %) for 15 min at room temperature. Afterward, the cells were washed with cold PBS observed by Nikon Eclipse TE 2000-S Inverted Microscope System and by Confocal Laser Scanning Microscopy (CLSM) (Leica TCS-SP5 RS AOBS).

- **MTT assay**

Cell viability in the presence of different concentrations of NPs or TPGS (Sigma-Aldrich; 1.00, 0.50, 0.25, 0.125, 0.062 mg/mL) was measured using MTT assay. Briefly, cells were seeded in 96-well plates at different densities: MCF-7 and WiDr at 60,000 cells/mL (6,000 cells/well), MG-63 at 50,000 cells/mL (5,000 cells/well), FaDu at 25,000 cells/mL (2,500 cells/well), and HMEpC at 100,000 cells/mL (10,000 cells/well). HUVEC were seeded at a density of 50,000 cells/mL (5,000 cells/well) in order to obtain 50% confluence or at 90,000 cells/mL (9,000 cells/well) to obtain cultures at 100% confluence.

After 24 h of incubation, MCF-7 cells were also pretreated for 1 h with 750 nM MitoQ (kindly donated by Dr. M.P. Murphy) in order to assess the capacity of MitoQ[19] to restore viability reduction produced by the most active NPs.

Afterward, the medium was replaced with the corresponding NPs or TPGS dispersed in PBS (50 µL of the NP suspension and 50 µL of completed medium). The plates were incubated at 37°C in a humidified air with 5% CO_2 for 24 h. A solution of 3-(4,5-dimethylthiazol-2-yl)-2,5-diphenyltetrazolium bromide (MTT) was prepared in warm PBS and filtered before use. MTT, 100 µL, was added to all wells to give a final concentration of 0.05 mg/mL, and the plates were incubated at 37°C, 5% CO_2 for 4 h. Excess medium and

MTT were removed, and 100 µL dimethyl sulfoxide (DMSO) was added to all wells in order to solubilize the MTT taken up by the cells. This was mixed for 10 min, and the absorbance was measured on a Biotek SYNERGY-HT plate reader, using a test wavelength of 570 nm and a reference wavelength of 630 nm. The results were normalized respect to the corresponding controls, and statistically tested with the analysis of variance (ANOVA) using $p < 0.05$ significance level.

3.1.4. Results and discussion

- **Monomers**

Four methacrylic monomers were successfully synthesized in mild conditions yielding pure products after their purification. ^{1}H-NMR spectra of these synthesized monomers are shown in **figure 2**. ^{1}H-NMR spectra confirmed esterification of the starting material due to the presence of resonance signals of the protons of the methacrylic group (CH_2-c and CH_3-d). Additionally, CH_2-5" and CH_2-6" that appeared at 4.33 ppm in the spectrum of MTOS and SPHY evidenced the presence of succinate group in the functional domain of these monomers. Finally, it is noteworthy that the signals of the methyl groups attached to the aromatic ring (CH_3-7', CH_3-8', CH_3-9' between 1.90 and 2.15 ppm) were not present in the SPHY and MPHY due to the absence of the chromanol ring.

- **Copolymers characterization**

The four methacrylic monomers (MTOS, SPHY, MVE and SHY) were successfully polymerized with VP by free radical polymerization in order to obtain macromolecules with different hydrophilic-hydrophobic balance. The chemical structures of the different types of copolymers are illustrated in **figure 3**. In this sense, a series of copolymers of each family were prepared with different feed compositions, and labelled indicating the copolymer molar composition. As an example, poly(VP-*co*-MTOS) (89:11; *i.e.* 0.11 MTOS molar fraction in the copolymer) will be labelled as MTOS-11. Polymerization of the comonomers was confirmed using NMR spectroscopy by the disappearing of the signals of vinyl protons (CH_2-c between 5.5 and 6.5 ppm), the appearance of the signals due to the methylene protons of the backbone chains (CH_2-c' and CH_2-f' between 1 and 1.88 ppm) and the broadening of the signals as a result of the macromolecular nature of the synthesized polymers (**figures S1 and S2**, see supporting information).

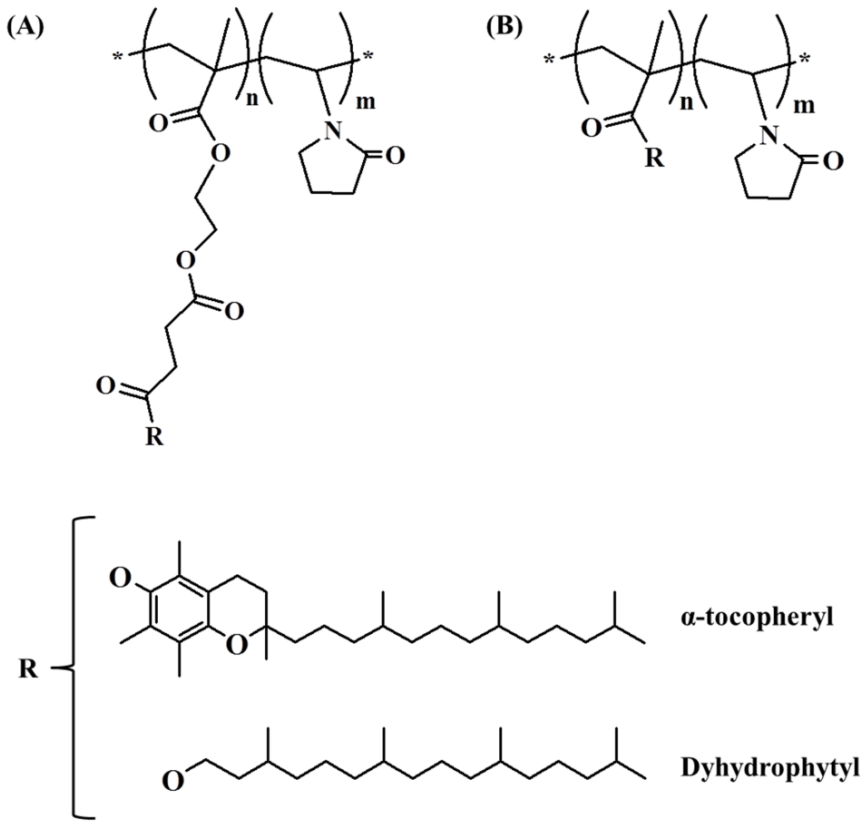

Figure 3: Chemical structure of (A) poly(VP-*co*-MTOS) and poly(VP-*co*-SPHY); (B) poly(VP-*co*-MVE) and poly(VP-*co*-SPHY).

Poly(VP-co-MTOS) vs poly(VP-co-SPHY)

Figure S1 (see supporting information) shows the ^{1}H-NMR spectra of MTOS-11 and SPHY-13. The average copolymer composition was quantitatively determined from their corresponding ^{1}H-NMR spectra by considering the signals between 3 and 4.5 ppm assigned to 3 protons of VP (CH-e', CH_2-4''') and 4 protons of MTOS (CH_2-5-6'') or 6 protons of SPHY (CH_2-1 and CH_2-5-6'') and the signal at 0.84 ppm , which is due to 12 protons of MTOS (CH_3-16-19) or 15 protons of SPHY (CH_3-16-20).

Average copolymer composition and reaction yields for both copolymeric systems are collected in **table 1**. Results of molecular weights (M_n and M_w), dispersity index ($Đ$) and glass transition temperatures (T_g) of these polymers are also summarized.

In both copolymeric systems, the polymerization successfully occurred in the whole range of compositions. However, copolymer MTOS molar composition greatly differs from

MTOS feed molar composition, mainly due to the big differences on chemical reactivity of the monomers (see next section), and also because total yield of the polymerization was not reached. Specifically, yields were lower than 85 % in all copolymerizations and this effect was more pronounced in those copolymers with the lowest and highest content on MTOS (yields were lower than 70 % for MTOS-5 and MTOS-88). Copolymers based on SPHY presented almost complete conversions and, although reactivity ratios were quite different, the difference between feed and copolymer SPHY molar composition was less pronounced than poly(VP-*co*-MTOS) formulations.

Average MW and dispersity of the copolymers increased with increasing content of MTOS and SPHY in the poly(VP-*co*-MTOS) and poly(VP-*co*-SPHY) systems, respectively. Additionally, MW of copolymers was higher than 30 kDa for all compositions that is a crucial requirement to enhance their accumulation and extravasation to the tumor area due to the EPR effect when NPs are disaggregated. Moreover, polydispersity indexes were typical of a conventional radical polymerization process.

All synthesized copolymers presented two glass transition temperatures confirming the microphase segregation and in good agreement with the different reactivities of the methacrylic monomers and VP. T_{g1} correspond to the T_g of the segments rich in MTOS, although the T_g of polyMTOS could not be determined using the described experimental conditions but might be around 60 ºC that is T_{g1} of MTOS-88, the copolymer with highest content on MTOS. T_{g2} correspond to the T_g of the segments rich in VP, as it is close to the polyVP T_g (172ºC). T_{g2} decreased as a function of MTOS concentration in the copolymer, adopting values between both homopolymers indicating an additive contribution of the monomers to the flexibility of the macromolecular chains, however T_{g1} varied randomly between 60 and 70 indicating an intermediate behavior between a plastifying effect of VP in the MTOS-rich segments and an additive contribution of the monomers to the flexibility of the macromolecular chains.

Poly(VP-*co*-SPHY) system presented also microphase segregation as confirmed by two T_g in the thermograms (T_{g1} due to SPHY-rich segments and T_{g2} due to VP-rich segments). T_{g1} and T_{g2} adopted values between the T_g of the homopolymers, that is, T_{g1} increased as a function of VP concentration and T_{g2} decreased as a function of SPHY concentration in the copolymer, indicating an additive contribution of the monomers to the flexibility of the macromolecular chains.

Poly(VP-co-MVE) vs poly(VP-co-MPHY)

^{1}H-NMR spectra of MVE-22 and MPHY-20 are shown in **figure S2** (see supporting information). The average copolymer molar fractions are collected in **table 2** and were quantitatively determined from their corresponding ^{1}H-NMR spectra by considering the signals between 3 and 4.8 ppm assigned to 3 protons of VP (CH-e', CH_2-4''') and 2 protons in the case of MPHY (CH_2-1) and the signal at 0.84 ppm, which is due to 12 protons of MVE (CH_3-16-19) or 15 protons of SPHY (CH_3-16-20). The corresponding reaction yields of the copolymerization reaction, molecular weights and T_g of these polymers were also described.

Copolymer molar composition was significantly enriched in the methacrylic monomer and copolymerization reaction yield decreased with the content on MVE. Particularly, reaction yield decreases to less than 60% when MVE concentration was higher than 15%. Furthermore, copolymers with MVE content higher than 20% were not successfully obtained using these experimental conditions. In fact, the homopolymerization of MVE was not feasible. Although the reactivity of MVE in free radical polymerization is much higher than VP, the moiety of vitamin E of the MVE offers noticeable antioxidant character with the deactivation of free radicals, in a similar way to strong transfer agents.

Poly(VP-*co*-MPHY) were effectively prepared in the whole range of compositions, including polyMPHY, and yields were higher in comparison to polymers based on MVE and, for that reason, feed and copolymer MPHY molar fractions were very similar.

Average molecular weight and dispersity of the poly(VP-*co*-MVE) copolymers decreased with increasing the MVE content. Furthermore, the polydispersity indexes were relatively low for free radical polymerization reactions and decreased with increasing content of MVE, reaching values close to the unity which is characteristic of the controlled free radical polymerization with specific transfer agents, such as, reversible addition-fragmentation chain transfer (RAFT) polymerization. However, poly(VP-*co*-MPHY) presented molecular weights and polydispersity indexes that increased with the MPHY content.

Table 1: Feed and copolymers molar fraction, yield of the copolymerization reaction, molecular weight, dispersity (*Đ*) and T_g of poly(VP-*co*-MTOS) and poly(VP-*co*-SPHY). Data obtained by ^{1}H-NMR, SEC and DSC, respectively.

Sample	**F(MTOS) feed**	**f(MTOS) copol**	**Yield (%)**	$M_w \cdot 10^{-3}$	$M_n \cdot 10^{-3}$	***Đ***	T_{g1} **(°C)**	T_{g2} **(°C)**
PVP	0	0	85	35.0	14.2	2.2	----	172.0
MTOS-5	0.05	0.05	69	55.6	30.5	1.8	70.0	134.7
MTOS-11	0.10	0.11	79	82.1	46.8	1.8	66.0	144.0
MTOS-28	0.15	0.28	79	89.3	46.9	1.9	63.4	144.6
MTOS-33	0.20	0.33	79	112.8	58.8	1.9	65.4	142.1
MTOS-41	0.30	0.41	83	106.0	58.2	1.8	67.2	132.7
MTOS-72	0.50	0.72	73	124.2	64.1	1.9	65.3	119.0
MTOS-78	0.70	0.78	75	123.8	48	2.5	61.1	108.8
MTOS-88	0.80	0.88	63	164.3	58.8	2.8	60.0	102.5
PMTOS	1	1	60	262.1	81.5	3.2	----	----
Sample	**F(SPHY) feed**	**f(SPHY) copol**	**Yield (%)**	$M_w \cdot 10^{-3}$	$M_n \cdot 10^{-3}$	***Đ***	T_{g1} **(°C)**	T_{g2} **(°C)**
PVP	0	0	85	35	14.2	2.2	---	172.0
SPHY-2	0.05	0.02	70	35.5	17.8	1.9	60.7	91.3
SPHY-13	0.10	0.13	91	82.2	40.2	2.0	61.3	88.4
SPHY-24	0.15	0.24	88	71.2	35.6	2.0	47.9	74.4
SPHY-21	0.20	0.21	78	85.0	37.0	2.2	43.6	72.8
SPHY-56	0.50	0.56	77	110.9	43.6	2.5	23.9	73.8
SPHY-84	0.80	0.84	80	195.5	69.6	2.8	12.9	68.9
PSPHY	1	1	89	306.6	85.2	1.8	---	---

Table 2: Feed and copolymers molar fraction, yield of the copolymerization reaction, molecular weights, dispersity (*Đ*), and T_g of poly(VP-*co*-MVE) and poly(VP-*co*-MPHY). Data obtained by ^{1}H-NMR, SEC and DSC, respectively.

Sample	**F(MVE) feed**	**f(MVE) copol**	**Yield (%)**	$M_w \cdot 10^{-3}$	$M_n \cdot 10^{-3}$	**Đ**	T_{g1} (°C)	T_{g2} (°C)
PVP	0	0	85	35	14.2	2.2	---	172.0
MVE-8	0.05	0.08	74	18.4	11.8	1.8	57.3	168.8
MVE-22	0.10	0.22	69	29.6	18.1	1.8	58.3	149.2
MVE-40	0.15	0.40	59	29.3	18	1.9	78.5	143.5
MVE-56	0.20	0.56	57	25.8	15.2	1.9	84.4	136.4
Sample	**F(MPHY) feed**	**f(MPHY) copol**	**Yield (%)**	$M_w \cdot 10^{-3}$	$M_n \cdot 10^{-3}$	**Đ**	T_{g1} (°C)	T_{g2} (°C)
PVP	0	0	85	35	14.2	2.2	---	172.0
MPHY-6	0.05	0.06	75	21.3	15.7	1.4	64.4	144.3
MPHY-14	0.10	0.14	69	26.3	16.3	1.6	67.7	111.3
MPHY-18	0.15	0.18	75	41.7	23.5	1.8	68.3	100.2
MPHY-20	0.20	0.20	78	30.3	17.2	1.8	72.7	96.8
MPHY-56	0.50	0.56	70	37.5	20.6	1.8	83.9	---
MPHY-92	0.80	0.92	72	51.7	21.1	2.4	---	---
PMPHY	1	1	52	46.2	21.1	2.2	---	---

These results support the idea that MVE partially deactivates or controls radical polymerization when is incorporated into the macromolecular chains, probably due to its inherent antioxidant character and delocalization of free radicals by conjugation of the methacrylic group with the high electron density of chromanol structure, as it was previously demonstrated[20]. Additionally, this effect could be enhanced by the steric hindrance due the presence of the chromanol moiety that is very bulky and is close to the reactive methacrylic group during the polymerization.

The inhibition of radical polymerization did not occur in the case of polymers based on derivatives of dihydrophytol due the absence of the chromanol moiety. Furthermore, the structure of poly(VP-*co*-MTOS) formulations was characterized by the presence of succinate moiety between the methacrylic and chromanol groups that probably avoids the radical stabilization.

As in the previously described systems, all synthesized copolymers presented two glass transition temperatures confirming the microphase segregation of incompatible domains. T_{g1} correspond to the T_g of the segments rich in MVE, and T_{g2} correspond to the T_g of the segments rich in VP as it is close to the polyVP T_g (172ºC). The presence of MVE units in the polyVP domains exerts a plastifying effect that increase its flexibility reducing T_{g2} as a function of MVE concentration. In a similar way, the presence of VP units in the polyMVE domains exerts a plastifying effect that increase its flexibility reducing T_{g1} as a function of VP concentration. These results are in good agreement with the big differences in reactivity ratios. Poly(VP-*co*-MPHY) system presented a similar behavior being T_{g1} the T_g of the MPHY-rich segments and T_{g2} the T_g of VP-rich segments. T_g of PMPHY could not be determined using the experimental conditions described in this paper.

- **Determination of reactivity ratios: *microstructural analysis***

Reactivity ratios (r_1 and r_2) are important kinetic parameters that provide information about average composition and monomer sequence distribution in statistical copolymer systems. These properties directly affect to the microstructure of polymeric systems and therefore, to their capacity to spontaneously self-assembly in aqueous environment.

Reactivity ratios were accurately determined by *in situ* ^{1}H-NMR monitorization of the copolymerization reaction of the corresponding monomers by the analysis of the instantaneous feed and instantaneous copolymer composition, as previously described by our group (**figure S3**, see supporting information)[17]. These data were fit to a solution of the differential copolymerization equation which defines the terminal model:

$$\frac{[M_2]}{[M_{20}]} = \left[\frac{[M_{20}][M_1]}{[M_{10}][M_2]}\right]^{r_2/1-r_2} \left[\frac{(r_1-1)([M_1]/[M_2]) - r_2 + 1}{(r_1-1)([M_{10}]/[M_{20}]) - r_2 - 1}\right]^{r_1 r_2 - 1/(1-r_1)(1-r_2)}$$

if $[M_1]/[M_2] = x$; $[M_{10}]/[M_{20}] = x_0$; $[M_2]=y$ and $[M_{20}]=y_0$

$$y = y_0 \left(\frac{x}{x_0}\right)^{r_2/1-r_2} \left(\frac{1-r_2+(r_1-1)x}{1-r_2+(r_1-1)x_0}\right)^{r_1 r_2 - 1/(1-r_1)(1-r_2)}$$

being M_i the molar concentration of monomer *i*, r_i the reactivity ration of monomer *i*, and M_{i0} the initial monomer concentration of monomer *i*.

Reactivity ratios of the four copolymeric systems (**figure 4**) were in good agreement with those described in the literature for similar systems that involved the reaction of a methacrylic monomer and VP[21, 22]. Although poly(VP-*co*-MVE) system has been previously synthesized and characterized, reactivity ratios were not reported due to technical difficulties[15]. *In situ* ^{1}H-NMR monitorization of the reaction allowed the accurate determination of r_{VP} = 0.03 and r_{MVE} = 2.20.

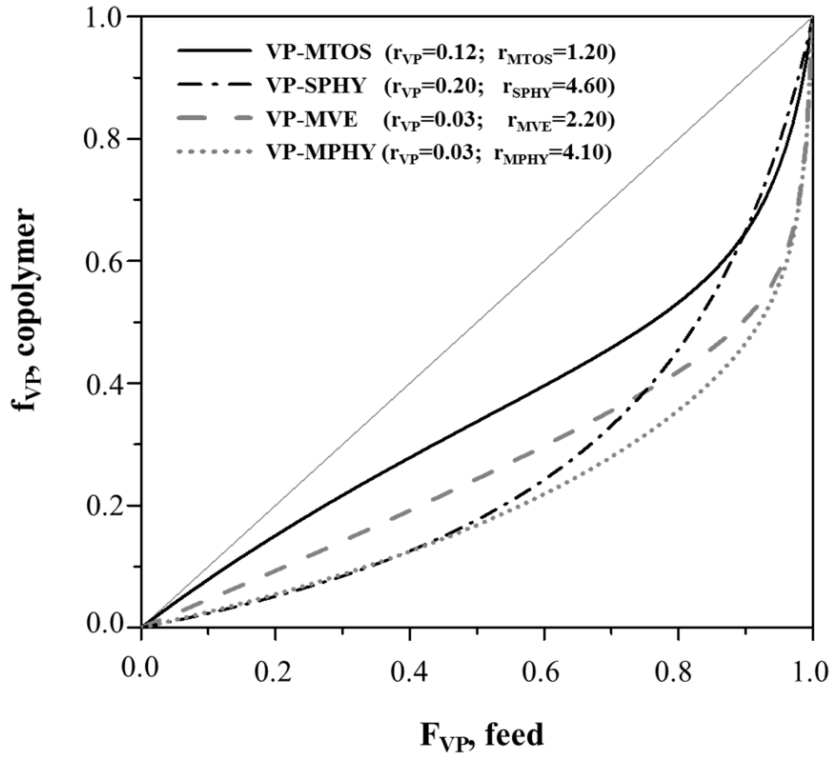

Figure 4: Composition diagrams of the four copolymeric systems.

In all copolymeric systems, propagating species preferably added methacrylic monomers that presented a much higher reactivity than VP and, consequently, they were firstly consumed and VP was second added at the end of the copolymerization reaction. However, both MPHY and SPHY presented higher reactivity ratios when copolymerized with VP than MVE and MTOS respectively. This effect was probably due to the radical

stabilization by conjugation or steric hindrance with the chromanol aromatic in the signalling domain of MVE. Furthermore, MVE is a methacrylic derivative of vitamin E which has been described as a potent antioxidant. In fact, properties of synthesized polymers based on MVE demonstrated this effect of free radical stabilization with reduced *Đ* and inhibition of polymerization when MVE content was higher than 20 %, as previously described.

In the case of MTOS, the chromanol group did not affect the properties of the polymers that exhibited typical characteristics of a free radical polymerization. On the one hand, the presence of a succinate group avoided the radical stabilization effect and, on the other hand, the steric hindrance due the presence of the chromanol moiety in its structure could reduce the reactivity of MTOS in comparison to SPHY during the copolymerization.

The chemical and physical properties of copolymeric systems are strongly influenced by the distribution of the comonomeric units along the macromolecular chains. In this sense, the big difference between the reactivity ratios in all systems allowed the formation of compositional gradient amphiphilic macromolecules. Specifically, long sequences of the hydrophobic units were formed at the beginning of the reaction and only few hydrophilic VP units were incorporated at the end of the macromolecule before the copolymerization reaction stopped. Even though the obtained macromolecules were not homogeneous but a mixture of macromolecules with a compositional gradient, the amphiphilic microstructure of these copolymers allowed the formation of surfactant-free NPs by spontaneous self-assembling in aqueous media, as will be demonstrated in the next section.

- **NP characterization**

Well-defined NPs were obtained in aqueous media by nanoprecipitation[23]. Polymeric micelles arranged by a self-assembling process where the rich hydrophobic segments of the macromolecule were organized in the core of the micelles stabilized through inter- and intramolecular hydrophobic interactions and the hydrophilic domains of the macromolecule (rich in VP) are exposed in the shell. Results of hydrodynamic diameter (D_h, by intensity) and polydispersity index (PDI) obtained by Dynamic Light Scattering are summarized in **table 3**. NPs were labelled as the copolymers that were used in their preparation.

Table 3: Hydrodynamic diameter (D_h) and polydispersity indexes (PDI) of NPs based on (A) poly(VP-*co*-MVE), poly(VP-*co*-MPHY) and (B) poly(VP-*co*-MTOS), poly(VP-*co*-SPHY), measured by Dynamic Light Scattering.

(A)

NP sample	D_h (nm)	PDI
MVE-8	96.9 ± 1.6	0.113 ± 0.048
MVE-22	138.2 ± 7.0	0.137 ± 0.020
MVE-40	154.1 ± 9.5	0.135 ± 0.014
MVE-56	197.7 ± 12.9	0.226 ± 0.017
MPHY-6	158.3 ± 14.2	0.189 ± 0.058
MPHY-14	145.4 ± 5.6	0.100 ± 0.014
MPHY-18	132.8 ± 7.6	0.203 ± 0.045
MPHY-20	113.5 ± 8.1	0.159 ± 0.023

(B)

NP sample	D_h (nm)	PDI
MTOS-5	106.6 ± 8.7	0.138 ± 0.022
MTOS-11	134.3 ± 9.2	0.128 ± 0.026
MTOS-28	136.2 ± 12.7	0.132 ± 0.058
MTOS-33	140.4 ± 5.1	0.126 ± 0.036
MTOS-41	164.9 ± 7.9	0.192 ± 0.058
MTOS-72	220 ± 17.5	0.208 ± 0.099
SPHY-2	80.4 ± 0.5	0.135 ± 0.013
SPHY-13	131.7 ± 6.5	0.159 ± 0.057
SPHY-24	133.9 ± 18.9	0.116 ± 0.024
SPHY-21	152.0 ± 5.4	0.112 ± 0.025

All distributions were unimodal and the hydrodynamic diameter of NPs ranged between 96 and 220 nm, which can be considered appropriate for their application as drug delivery systems for cancer treatment, because NPs with sizes lower than 100 nm can be easily eliminated by RES system with a short blood residence time and a low rate of extravasation into permeable tissues, and NPs with D_h higher than 200 nm have difficulties to be endocyted by the cells. Additionally, this range of sizes has been described as optimum to favor EPR effect[24-26]. Furthermore, PDI values were low in all cases, indicating a good stability in aqueous media.

The formation of stable NPs was only feasible in those formulations with VP content higher than 28 %. When the concentration of hydrophilic monomer was lower than this percentage, the polydispersity indexes increased significantly and the precipitation of copolymers was observed in the aqueous medium. This phenomenon is probably due the unsuitable hydrophilic – hydrophobic balance in the polymeric chains that avoids the spontaneous self-assembly in aqueous media.

Size and polydispersity indexes of nanoaggregates based on methacrylic derivatives of α-TOS and vitamin E (MTOS/MVE), increased with decreasing VP content (**figure S4**, see supporting information) indicating that the longer the hydrophilic segment that form the shell, the higher the stability of the NPs.

NP diameter varied also with other nanoprecipitation conditions, such as the concentration of copolymers in aqueous media. As an example, data from MTOS-bearing copolymers are shown in **table S1** (see supporting information). NP diameter increased not only with the content of MTOS in the polymeric chains, but also with the concentration of the copolymer in the organic phase. However, this effect was less significant in those formulations with lower MTOS content (MTOS-5 and MTOS-41) that presented a constant size over a critical concentration (around 0.10 mg/mL).

Therefore, size and morphology of the particles could be modulated by controlling the molar composition of the copolymers and the concentration of NPs in the aqueous media. This is especially relevant for the effective targeting and delivery into tumor tissues. Consequently, the biological properties and the therapeutic action of these polymeric systems are strongly affected by the size of the self-assembled nanoaggregates[27, 28].

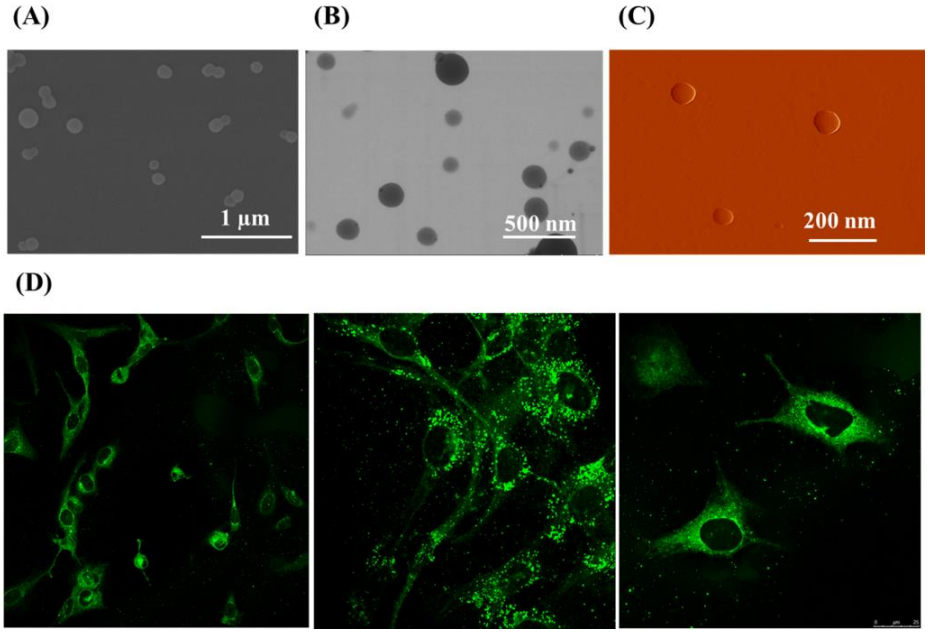

Figure 5: (A) SEM, (B) TEM and (C) AFM micrographs of MTOS-72 NP dried from aqueous solution at room temperature. (D) Fluorescence micrographs of endothelial cells (HUVEC) in culture where c6-loaded MTOS-33 NP were added. Images were registered after 5 hours.

SEM, TEM and AFM analysis were performed in order to characterize the NP morphology. As an example, **figure 5** displays the SEM (A), TEM (B), and AFM (C) micrographs of MTOS-72 NP after drying the aqueous suspension at room temperature. These copolymers with appropriate hydrophilic/hydrophobic balance formed stable and spherical NPs. According to the MW of the polymeric systems and the size of the micelles, NPs are probably based on multimicellar aggregates

- **Coumarin-6 encapsulation**

Nanospheres were able to encapsulate c6 that was simultaneously used as fluorescent probe and as a model of hydrophobic molecule. These fluorescent NPs were used to visualize the cellular uptake process when added to a HUVEC cell culture. NPs were observed under the confocal microscope, after 5 h of incubation. **Figure 5D** shows that green fluorescent c6-loaded NPs were located inside the cells around the nucleus. NPs were probably uptaken by endocytosis according to the size of these nanoaggregates. These results demonstrated that NPs were able to efficiently encapsulate hydrophobic molecules and could serve as nanovehicles for other hydrophobic chemotherapeutic drugs that are highly toxic and difficult to administer.

- **Biological activity**

Breast epithelial cells (HMEpC) vs. Human Breast Adenocarcinoma cells (MCF7)

In vitro biological activity of polymeric NPs was evaluated using human breast adenocarcinoma (MCF-7) and noncancerous human mammary epithelial cells (HMEpC) cells in order to determine if the therapeutic action of self-assembled NPs has an optimal selectivity towards cancer cells. Particularly, cell viability studies were assessed by MTT assay that measures the mitochondrial metabolic function of cells based on the ability of the mitochondrial enzyme succinate dehydrogenase to metabolize MTT into formazan, a reaction that takes place only in living cells[29-31].

Figure 6A shows that relative MCF7 viability decreased in a dose-dependent manner when MTOS-bearing NPs were added to the cell culture. Particularly, cell viability was reduced below 40 % in those formulations with relatively low MTOS content (MTOS-5 and MTOS-11 NP) at NP concentrations higher than 0.5 mg/ml. In fact, the cytotoxicity of these NPs was strongly influenced by the MTOS content in the copolymeric system. The

anticancer activity of these NPs was significantly reduced when the MTOS content in the copolymer was higher than 33%. These formulations probably are stabilized by the long hydrophobic sequences and subsequently the limited bioavailability, and the accessibility to the hydrophobic core are strongly hindered[32-34].

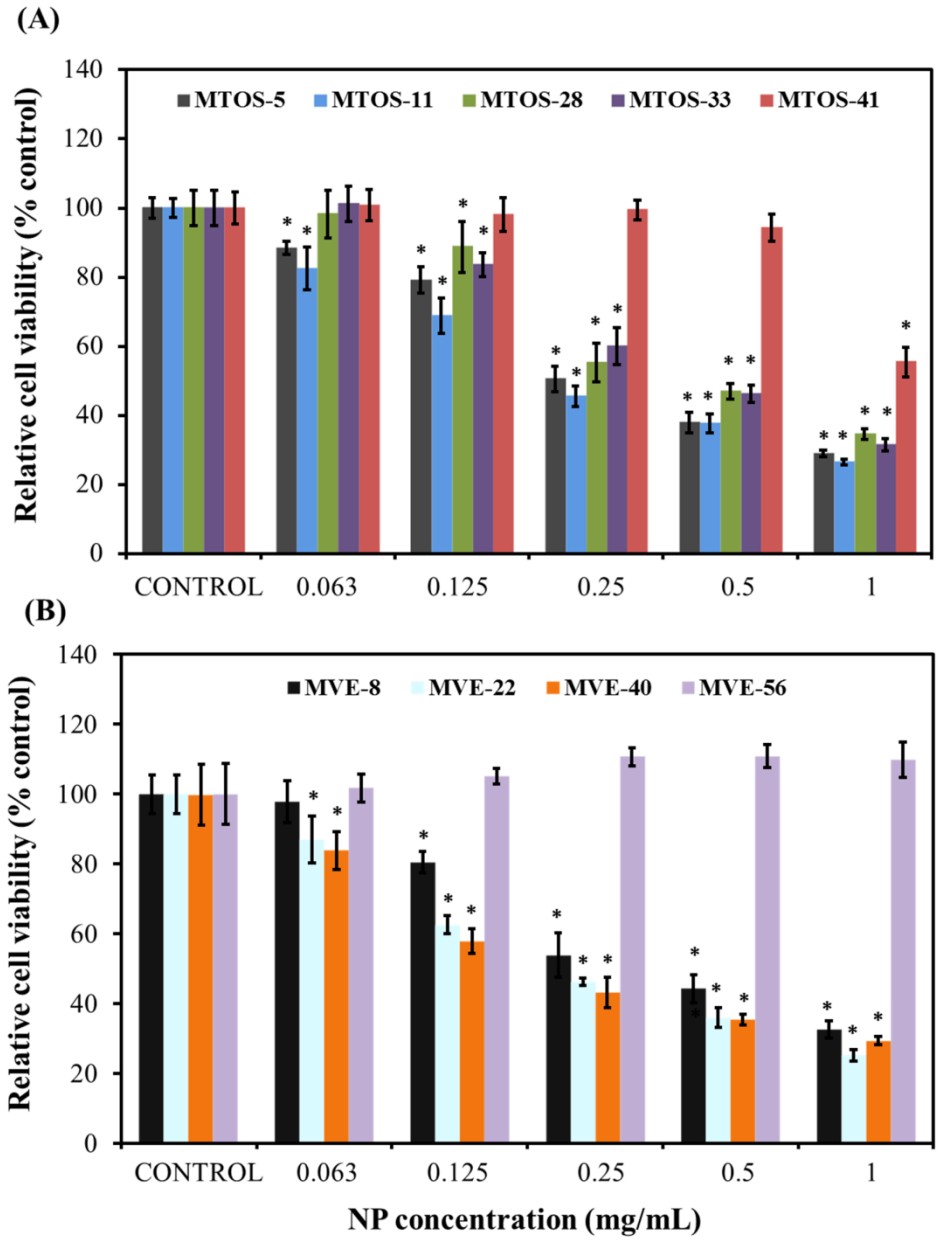

Figure 6: Relative cell viability of MCF7 as a function of (A) poly(VP-*co*-MTOS) and (B) poly(VP-*co*-MVE) NP concentration. The diagrams include the mean, the standard deviation (n=8) , and the ANOVA results at a significance level of *: $p < 0.05$.

Different research studies showed that the methylation of the free succinyl carboxyl group on α-TOS completely prevented its anticancer activity as proapoptotic agent[35]. However, the biological activity of MTOS-bearing NP evidence that the anticancer activity of this drug is maintained in spite of the esterification of the free carboxyl group on the succinyl moiety. Additionally, different researches have also modified this free carboxyl group by the conjugation of PEG, improving the solubility and apoptotic activity of α-TOS [36], or even other chemotherapeutic drugs, such as doxorubicin (DOX) through an amide bond[37] to form a water soluble prodrug. Youk et al. proposed that those modifications in the functional domain of α-TOS that increase its solubility in aqueous media may contribute positively to improve its therapeutic activity. However, modifications that enhanced the lipophilicity of α-TOS could have the opposite effect, reducing its apoptotic activity[36].

Cell viability in the presence of MVE-based NP also was studied in order to determine the effect of eliminating the succinate group (functional domain) from MTOS as shown in **figure 6B**. Unexpectedly, MVE-bearing NP were also active in a dose-dependent manner, in spite of the modification of the functional domain (succinate group of α-TOS is substituted by methacrylate residue, see **figures 2 and 3**). Moreover, these results indicate that the active molecule does not have to be released to induce its activity as free vitamin E (α-tocopherol) has not anticancer activity. Therefore, the esterification of the hydroxyl group in the functional moiety of vitamin E promotes the anticancer activity of NPs based on MVE. In fact, it is well known that vitamin E and its derivatives as tocotrienols are important antioxidants that do not exert apoptosis of tumor cells. However, their esterification made them proapoptotic. For that reason, most researchers have introduced different structural modifications within the functional moiety of vitamin E derivatives with the aim to evaluate their influence in the anticancer activity of these compounds. In fact, the nature of esterification is crucial in the therapeutic action of vitamin E derivatives[38]. For instance, the incorporation of esters with high number of carbons disfavored the biological activity of vitamin E, however, the esterification with unsaturated dicarboxylic acids enhanced their therapeutic activity with more proapoptoctic activity than even α-TOS[39]. Recent studies also have demonstrated the anticancer and antiangiogenic activities of tocotrienol esters[40].

Viability results of MVE bearing NPs could also indicate that the functional domain is not the main responsible of the anticancer and antiapoptotic activity of α-TOS-based polymeric drugs. The presence of the signalling domain (chromanol ring) in the structure of

MVE has an essential function in the anticancer activity of the self-assembled nanoaggregates. Neuzil et al. described different functions of this domain that specifically regulates certain signalling pathways, such as the protein phosphatase-2A (PP2A)/protein kinase C (PKC) pathway [39]. In fact, the inhibition of PKC by increasing the PP2A activity is directly related to the proapoptotic activity of vitamin E derivatives. Specifically, this inhibition has a direct effect at mitochondrial level because the function of antiapoptotic proteins bcl-2 is regulated by its phosphorylation via PKC/PP2A [41]. In summary, the signaling domain of MVE could be responsible for the inactivation of PKC which is crucial for the phosphorylation of bcl-2 proteins, resulting in the activation of caspases that causes cell death. Additionally, Neuzil et al. also demonstrated that structural modifications of signaling domains of vitamin E derivatives directly affected the anticancer activity of these compounds, specifically when the number and position of methyl substitutions on the aromatic ring were varied. For example, biological activity of β-, γ- and δ- tocopheryl succinate was compared and significant differences were found due to their different efficacy to inhibit PKC. Particularly, the less apoptotic compound was δ-tocopheryl succinate, although all of them exhibited apoptotic activity against cancer cells[39].

MTOS-11 and MVE-22 NP were chosen for further experiments because were the most active of all synthesized copolymers. In both cases, the hydrophilic and hydrophobic balance of macromolecular chains in the structure of these copolymers favored the formation of NPs with excellent physicochemical properties and anticancer activity. One of the most important disadvantages of actual cancer treatments is their nonselectivity against cancer cells that causes important side effects in patients [34, 42, 43]. Therefore, the evaluation of the cytotoxicity of these formulations against analogous breast nonmalignant cells (HMEpC) was performed (**figure 7A and 7B**).

Cell viability of nonmalignant cells was close to 100 % for all concentrations of polymeric NPs. According to the standard ISO 10993-5:2009, biocompatibility is only compromised when cell viability decreased by 30 % and, therefore, MTOS and MVE bearing-NPs significantly affect the mitochondrial activity of tumor cells, without compromising this activity in noncancerous cells. Particularly, the selectivity towards cancer cells improved with the increment of polymer concentration in aqueous media. In fact, the optimal range of concentrations to maximize this selectivity was in the range of 0.125 – 0.5 mg/mL.

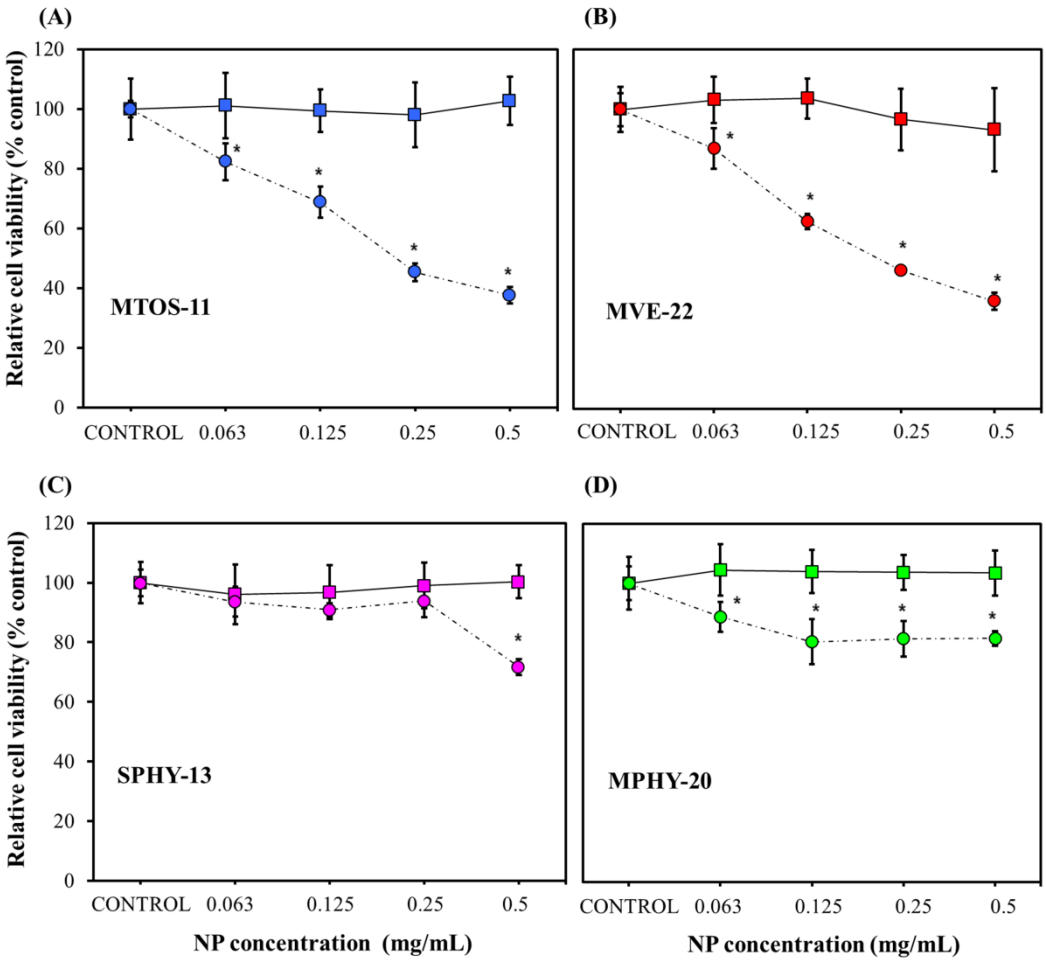

Figure 7: Comparison HMEpC (squares) and MCF7 (circles) cell viabilities of (A) MTOS-11 NP; (B) MVE-22 NP; (C) SPHY-13 NP and (D) MPHY-20 NP at different polymer concentrations with respect to control. The curves include the mean, the standard deviation (n=8), and the ANOVA results at a significance level of *: $p < 0.05$.

The mechanism of selectivity of polymeric formulations based on α-TOS towards cancer cells is not well-known nowadays. However, different authors have investigated diverse hypothesis to explain this behavior. Dong et al. stated that nonmalignant cells generate lower levels of ROS in response to α-TOS-treatment, mainly by differences in the cellular mechanisms that produce the generation of radicals[44]. Moreover, cancer cells express lower levels of antioxidant enzymes, such as manganese superoxide dismutase (MnSOD) than normal cells. These antioxidant enzymes prevent the accumulation of ROS species that are responsible for the activation of the proteins that regulate the mitochondrial permeabilization and trigger apoptosis.

Finally, the PKC activity has been associated with more proliferative and aggressive tumor cells in comparison to noncancerous cells, affecting not only in early carcinogenesis but also in cancer progression [45]. It is well-known that PKC is implicated in the regulation of a wide range of cellular functions such as proliferation, differentiation and apoptosis. Also, PKC activity has been associated with the enhancement of motility and invasion of cancer cells [46]. The enhancement of malignant phenotype of tumor could be associated with the activation of selective PKC isoenzymes in comparison to nonmalignant tissues. This behavior has been demonstrated in different cancer cell lines, including MCF-7[47]. Due to the importance of PKC in cancer formation and progression, various PKC inhibitors have been developed for the cancer treatment. As previously mentioned, the antiapoptotic activity of α-TOS has been related to the inhibition of PKC by increasing the PP2A activity that blocks the antiapoptotic actions of bcl-2 proteins[48].

The biological activity of self-assembled NPs based on dihydrophytol derivatives was also analyzed: SPHY that presented no signalling domain, and MPHY that is characterized by the absence of both, the functional and signalling domains. Breast epithelial and adenocarcinoma cell viabilities of SPHY (C) and MPHY (D)-bearing NPs are shown in **figure 7**. In both types of self-assembled nanoaggregates, HMEpC (nonmalignant cells) viabilities were very close to 100 % for all NP concentrations. Furthermore, the same experiments with MCF-7 (human breast adenocarcinoma) showed that cell viabilities were over 70 % for all compositions and NP concentrations. Therefore, it is possible to conclude that NPs based on methacrylic derivatives of dihydrophytol do not present anticancer activity, probably due to the absence of signalling group in the case of SPHY and also functional group for MPHY-bearing polymeric systems. Additionally, the absence of anticancer activity of NPs based on SPHY, which maintains the functional domain with no chromanol ring in their structure, confirms the importance of this signalling domain in the mechanism of action of these NP.

TPGS toxicity and selectivity

Selectivity of these NPs against tumor cells was significantly higher if compared to the effect of α-tocopheryl polyethylene glycol 1000 succinate ($TPGS_{1000}$), the most commonly used water soluble derivative of α-TOS [6, 7, 49-51]. **Figure S5** (see supporting information) shows that MTOS-11 NP did not affect the viability of noncancerous breast

epithelial cells in the range of the assayed concentrations; however, TPGS was intensively toxic for all tested concentrations.

Therefore, TPGS facilitates the administration of α-TOS, however this formulation is strongly toxic against nonmalignant cells, probably due to its surfactant properties. In fact, TPGS is commonly used as solubilizer, emulsifier and stabilizer of poorly soluble drugs, even in different commercial products because its use as a pharmaceutic adjuvant was approved by FDA. In conclusion, MVE and MTOS-bearing NPs are excellent candidates to develop selective anticancer nanomedicines because improve aqueous solubility and physiological administration of α-TOS, without compromising the viability of noncancerous cells.

Effect of MitoQ on cell viability

Cell viability of MitoQ pretreated or non-treated MCF-7 cells in the presence of different concentrations of NPs was studied in order to check the mechanism of action of the synthesized copolymeric NPs and to know if their anticancer activity is directly related to the accumulation of high levels of ROS and oxidative damage as α-TOS. Specifically, α-TOS has been reported as a competitive inhibitor of succinate dehydrogenase (SDH, complex II) by displacing ubiquinone (coenzyme Q) from binding to complex II in the cancer cell mitochondria. Electrons travelling through the electron transport chain accumulate and recombine with molecular oxygen producing high levels of ROS that trigger apoptosis[5, 52]. Murphy et al. developed MitoQ, a mitochondria targeted antioxidant that accumulate in this organelle and interact with complex II. It protects from oxidative damage by reducing ROS levels and therefore can be used to check if apoptosis was triggered by this mechanism[19]. In this sense, Dong et al. demonstrated that the pre-incubation of cells with MitoQ blocks the action of α-TOS in the complex II by targeting the UbQ-binding sites. This effect prevents the cellular death by apoptosis and restores the α-TOS cytotoxicity against cancer cells [53].

Figure 8 shows that cell viability of α-TOS treated cells was significantly reduced in the presence of MitoQ and cell viability of mitoQ pre-treated cells was significantly higher. In both types of NPs, cell viabilities were higher than 70 % after the treatment with mitoQ. However, mitoQ effect was not observed at concentrations of MTOS-11 NPs higher than 0.5 mg/mL due to its higher activity (**figure 8B**). These results strongly suggest that self-

assembled NPs with MTOS and MVE in their structure have a potent anticancer activity by interfering directly on the mitochondrial function of tumor cells and probably, targeting ubiquinone binding sites of complex II. In the case of NPs based on MTOS, the modification of succinate group of α-TOS did not prevent its anticancer activity, maintaining the same mechanism of action. In the same manner, the esterification of free hydroxyl group of vitamin E in MVE-bearing NPs could be responsible to their anticancer activity with the mechanism described by α-TOS. As it has been mentioned before, the active molecule is not released to induce cell death through this mechanism because vitamin E has not proapoptotic activity.

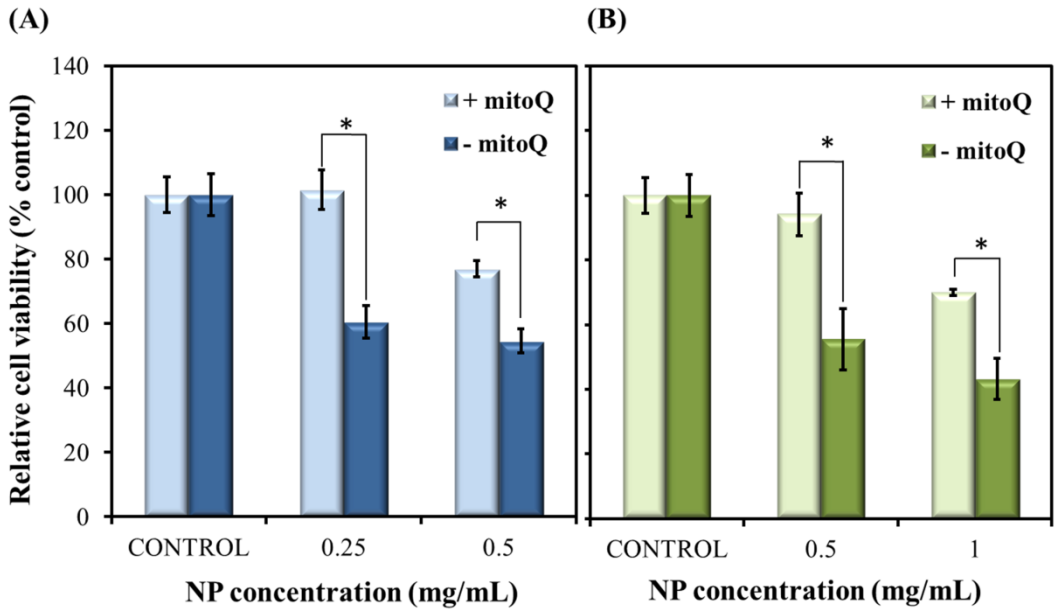

Figure 8: Influence of the mitoQ pretreatment in the breast cancer cell viability of most active MTOS (A) and MVE (B) bearing NPs. The diagrams include the mean, the standard deviation (*n*=8) , and the ANOVA results at a significance level of: *: $p < 0.05$.

Activity of MTOS-bearing nanoparticles against different tumor cell lines

The biological activity of most active MTOS-bearing NPs was also tested against different tumor cell lines. Particularly, hypopharynx squamous cell carcinoma (Fadu), colon adenocarcinoma cells (WirD), and osteosarcoma cells (MG63) were also considered in order to compare the efficacy of NPs based in MTOS, including the previous results against breast cancer cells. Results of different cancer cell viabilities after the treatment with MTOS-11 NP at 1mg/mL are shown in **figure 9**. NPs based on MTOS were active against

breast cancer cells (MCF), pharynx cancer cells (FaDu) and colon cancer cells (WirD) with little harm to osteosarcoma cells (MG63). Additionally, NPs activity was higher in breast cancer cells (cell viability was decreased below 26 %) in comparison to pharynx and colon cancer cells (viabilities were reduced to 56 and 69 %, respectively). These differences of NP activity against diverse tumor cells could be related with the energetic footprint of the cells [54-56].

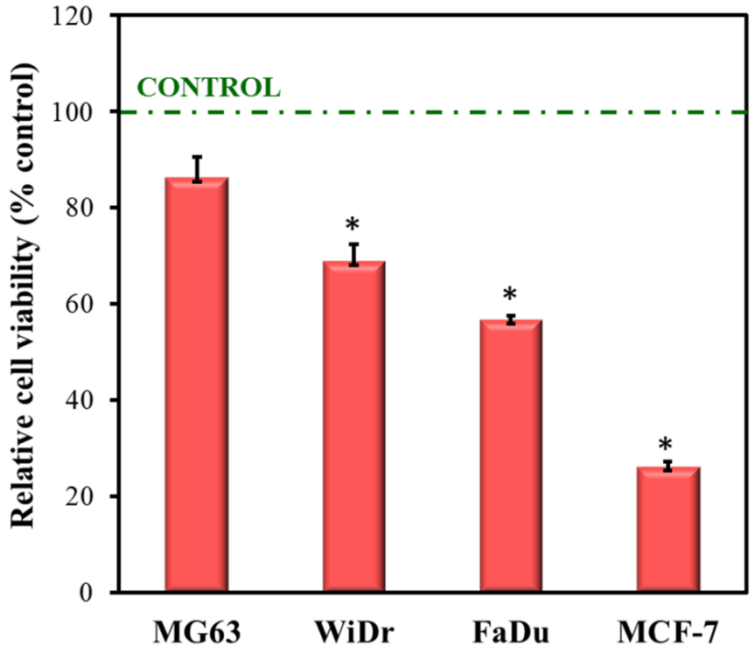

Figure 9: Relative cell viability of MTOS-11 NP against different tumor cell lines at 1 mg/mL in aqueous media. The curves include the mean, the standard deviation (n=8), and the ANOVA results at a significance level of *: $p < 0.05$.

Many cancers have something in common: their mitochondria are altered, and therefore, the energetic metabolism of cancer cells differs from that of normal cells. Specifically, Otto Warburg proposed the hypothesis that the mitochondrial alteration of cancer cells would result in the elevated rate of glycolysis that is a common characteristic of tumors. However, the grade of mitochondrial dysfunction significantly differs from one type of cancer to another. Particularly, the bioenergetic cellular index (BEC) is an effective tool that considers the expression level of a bioenergetic marker of mitochondria relative to a cellular glycolytic marker. This parameter has been calculated for a wide range of tumor cells[56, 57].

In fact, by mid 1980s, the National Cancer Institute selected 60 cell lines human derived from 9 different tumor types (breast, central nervous system, colon, blood cells, lung, melanoma, ovarian, prostate and kidney) that defined the panel NCI-60 cancer cells that have been used as very important tool to develop new drugs and therapies in cancer[58]. Cuezva et al. completely characterized the bioenergetic signature (BEC) of these different cell lines of the NCI-60 panel. According to this research, breast cancer cell lines, including MCF-7 cells, are characterized by the lowest levels of BEC index and the highest glycolytic metabolism in comparison to other cancer cell lines. These findings could explained the higher anticancer efficacy of MTOS-bearing NPs against MCF-7 cells and therefore, the existence of a relationship between the anticancer activity of vitamin E- based NPs and the energetic metabolism of cancer cells.

Proliferating Human Umbilical Vein Endothelial cells (HUVEC at 50% confluency) vs. quiescent HUVEC cells (100% confluency)

Angiogenesis is a key process in the development of solid tumors as a dense vasculature is required in order to supply nutrients to the cancerous tissue over 1-2 mm[3,59]. The inhibition of angiogenesis in tumors inhibited tumor growth, decreased tumor mass, and induced tumor regression. Therefore, a wide range of neoplastic pathologies can be controlled if angiogenic endothelial cell growth is inhibited. α-TOS has demonstrated anti-angiogenic activity as described by Dong et al. in preclinical breast cancer studies[44] and suggested that this effect could be due to a potential up-regulation of the antioxidant systems in the arrested endothelial cells that prevent the accumulation of ROS and the induction of apoptosis by the action of enzymes, such as manganese superoxide dismutase (MnSOD).

The antiangiogenic activity of the synthesized NPs was studied in quiescent (100% confluency, **figure 10**, squares) and proliferating endothelial cells (50% confluency, **figure 10**, triangles). Both MTOS and MVE-based polymers reduced cell viability of proliferating endothelial cells with little or no harm to quiescent endothelial cells. An effect of the copolymer composition (MTOS or MVE concentration in the copolymeric chains) on cell viability of endothelial cells cultured at a particular confluency was not observed. However, cell viability decreased drastically when NPs were added to proliferating endothelial cells (around 40% when NP concentration was 0.5 mg/mL).

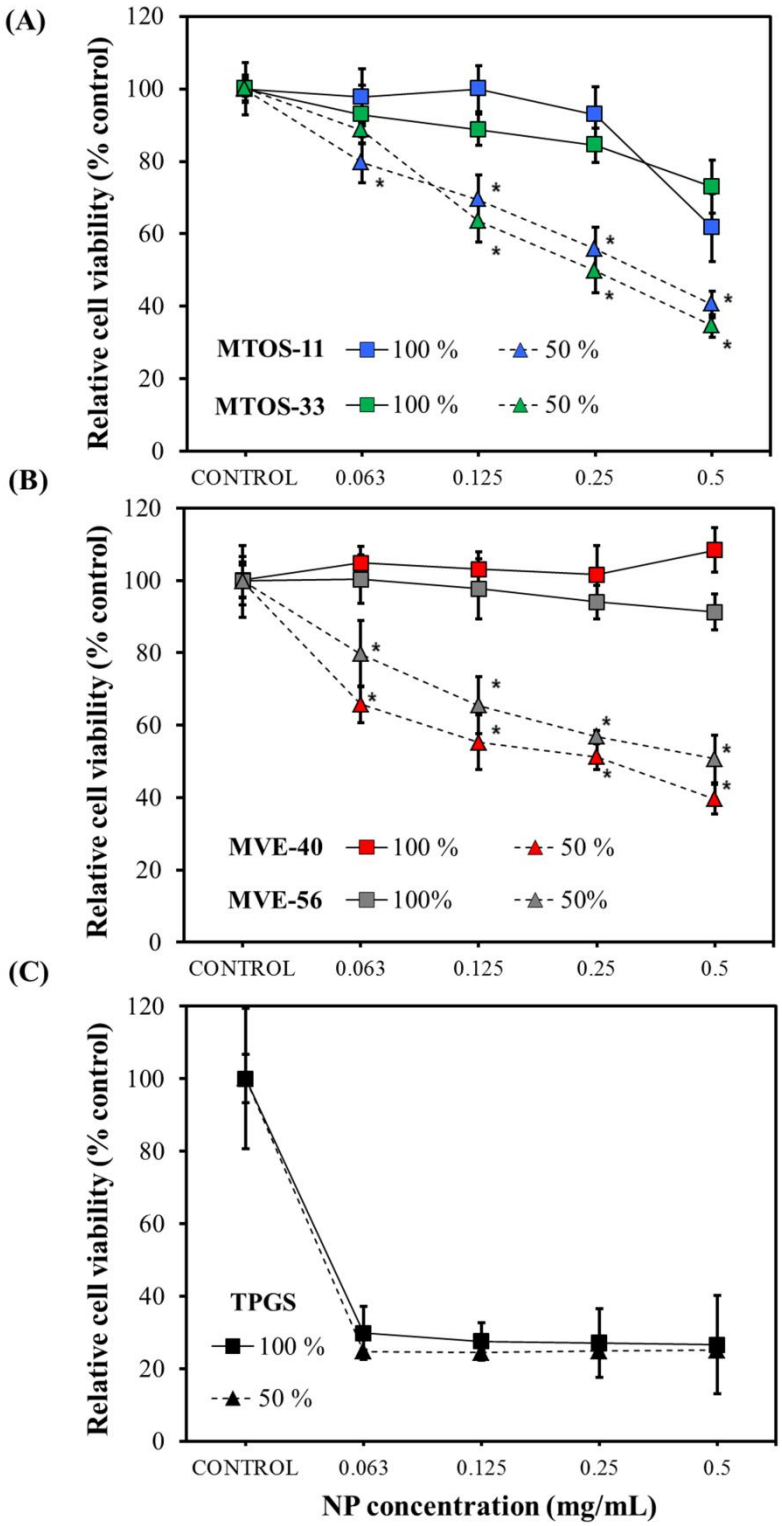

Figure 10: Relative cell viability of proliferating HUVEC at 50% confluency or quiescent HUVEC at 100% confluency in the presence of different concentrations of (A) MTOS-11 and MTOS-33 NP;

(B) MVE-40 and MVE-56 or (C) TPGS. The curves include the mean, the standard deviation (n=8), and the ANOVA results for each NP at a significance level of: *: $p < 0.05$.

TPGS did not present selective activity against proliferanting endothelial cells but resulted toxic for proliferating and quiescent endothelial cells in the whole range of assayed concentrations.

3.1.5. Conclusions

Four copolymeric systems have been synthesized and characterized in order to study the structure-activity relationship of MTOS-based amphiphilic copolymers. The big differences between the reactivity ratios in the free radical polymerization of the used comonomers (VP and a methacrylic monomer: MTOS, MVE, SPHY and MPHY) provided amphiphilic macromolecules that allowed the formation of self-assembling NPs with appropriate morphology to be internalized by cells. Not only MTOS-based NP, but also MVE-based NP presented a selective anticancer and antiangiogenic biological activity, as the NP reduced cell viability of cancer cells while nonmalignant cells tolerated the same dose of NPs, and NPs reduced cell viability of proliferating endothelial cells with little or no harm to quiescent endothelial cells. MTOS and MVE-based NP inhibit succinate deshydrogenase (complex II) by targeting UbQ-binding sites in the cancer mitochondria. Moreover, our experiments demonstrated that the active molecule (α-TOS or vitamin E) do not have to be released from the macromolecules to trigger the biological action, as vitamin E do not have pro-apoptotic activity, but the NPs do. The NPs were able to encapsulate coumarin-6 (fluorescent probe and hydrophobic molecule) and the resulting fluorescent NP were stable and endocyted by the cells. Therefore, the polymers can be considered polymeric drugs that self-assembled forming spherical NP with triple activity: anti-cancer, antiangiogenic and vehicle of other hydrophobic molecules.

3.1.6. Acknowledgements

Authors acknowledge Dr. Gema Rodríguez, Lautaro Biancotto, David Gómez, and Rosa Ana Ramírez for their help in AFM, SEM/TEM and cell culture experiments. Authors also thank Dr. M.P. Murphy for providing MitoQ for the experiments.

3.1.7. Supporting information

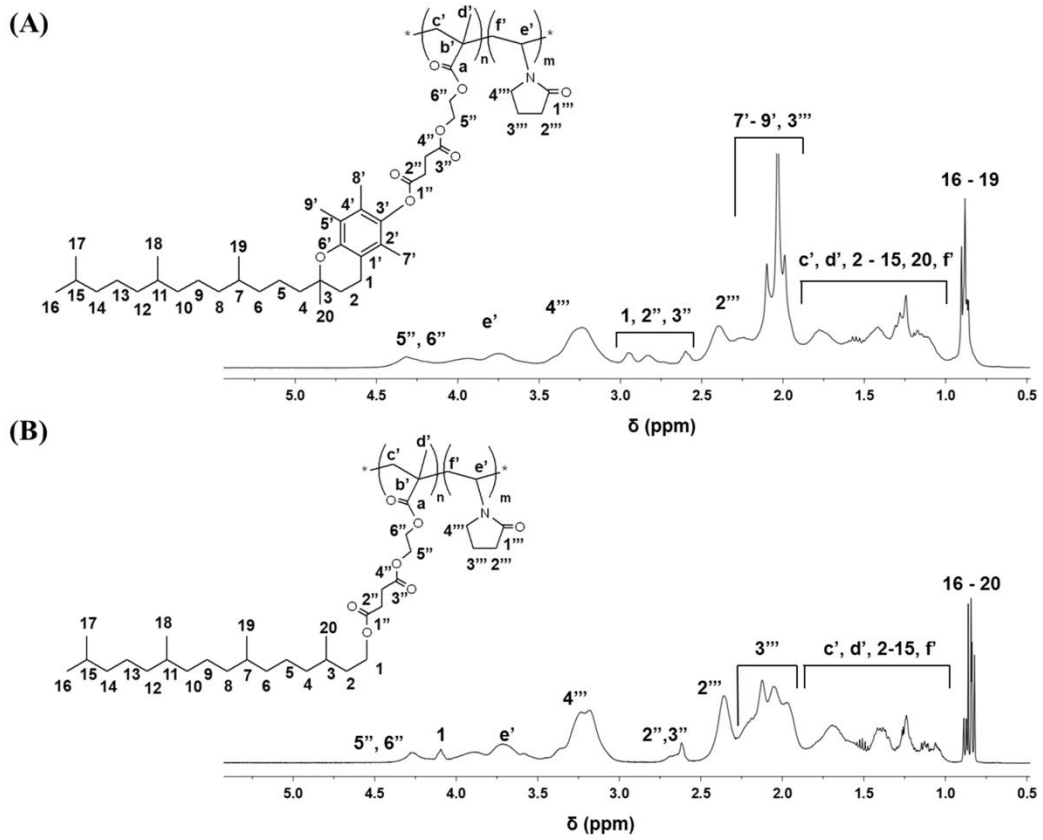

Figure S1: ^{1}H NMR spectra of (A) MTOS-11 and (B) SPHY-13

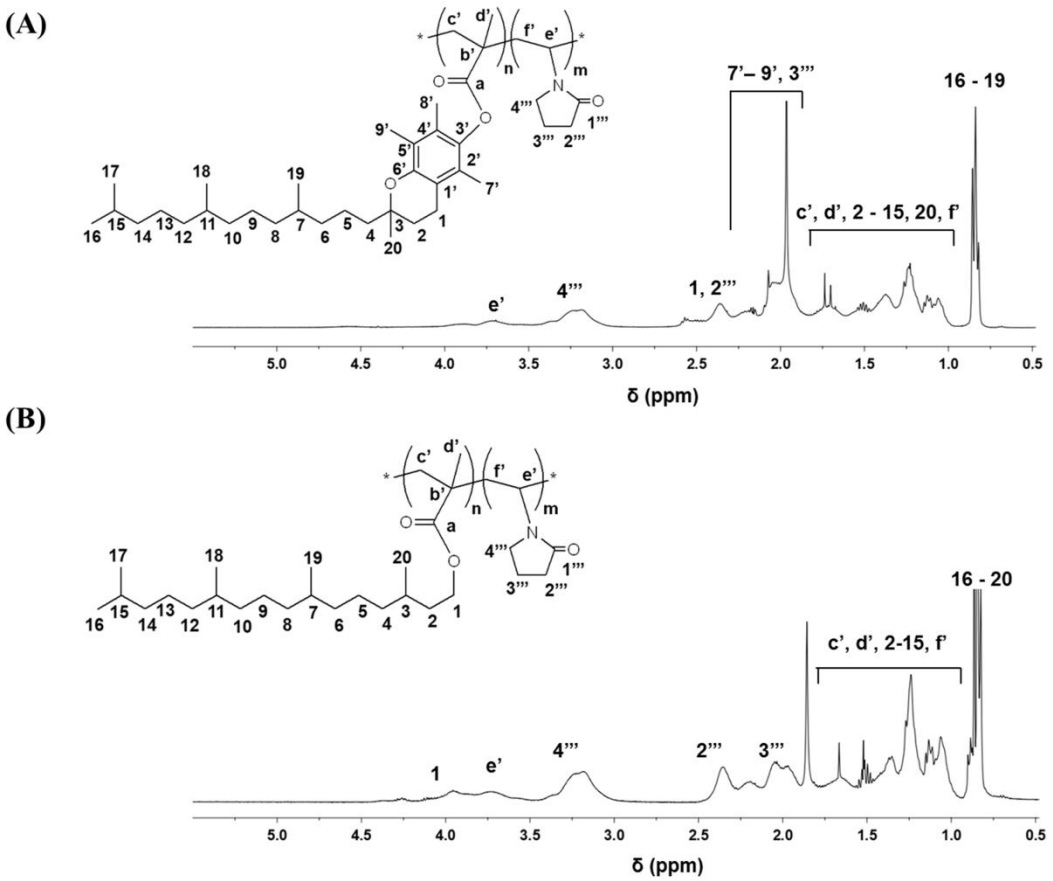

Figure S2: ^{1}H NMR spectra of (A) MVE-22 and (B) MPHY-20

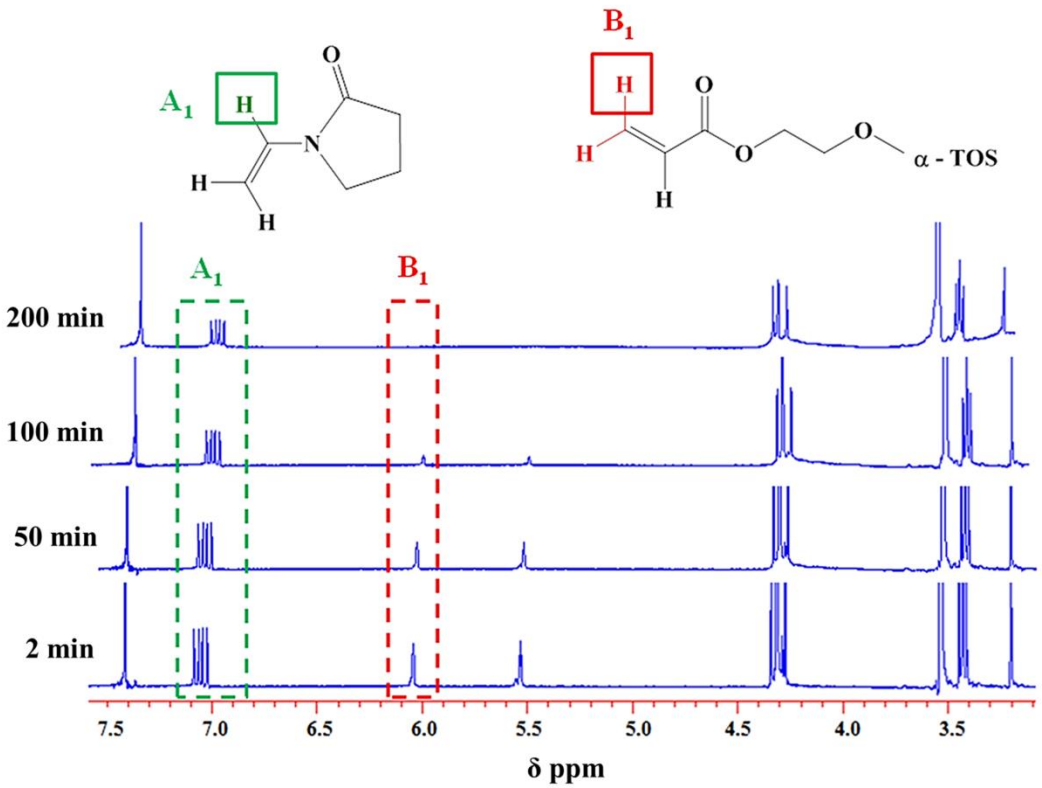

Figure S3: Acrylic region in the ^{1}H NMR spectra at different reaction times for the copolymerization reaction of MTOS-41

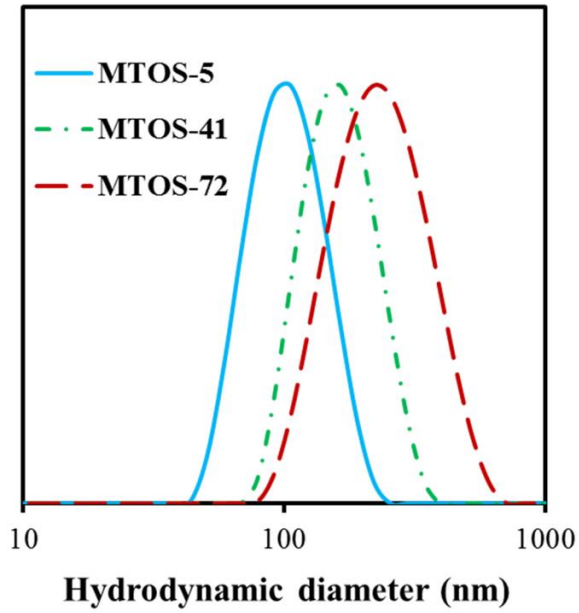

Figure S4: Effect of the molar composition of MTOS copolymers on the hydrodynamic diameter of self-assembled NPs. Blue: MTOS-5; Green: MTOS-41; Red: MTOS-72

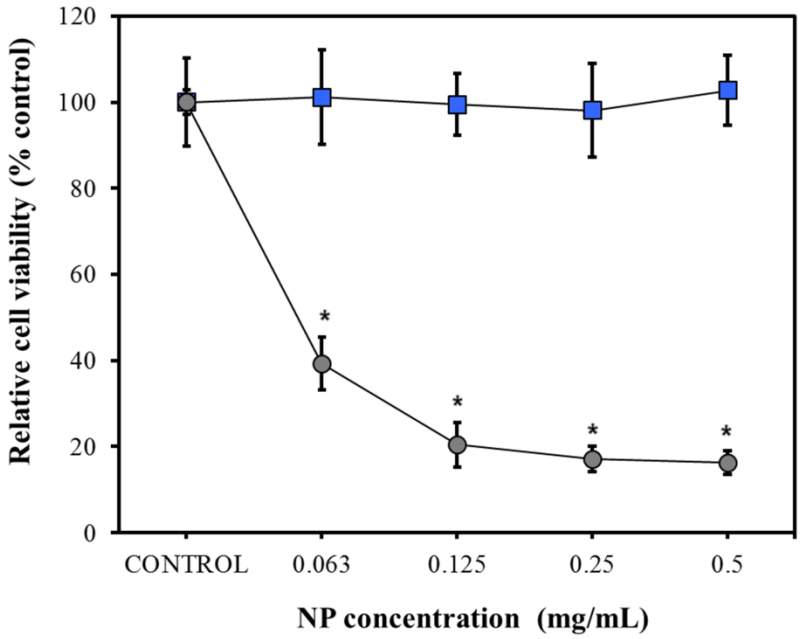

Figure S5: Relative cell viability of HMEpC as a function of TPGS (circles) or MTOS-11 (squares) NP at different concentrations in aqueous media. The curves include the mean, the standard deviation (n=8) and the ANOVA results for each preparation with respect to control at a significance level of *: $p < 0.05$.

Table S1: Effect of concentration of the NPs based on poly(VP-*co*-MTOS) on the hydrodynamic diameter (D_h) and polydispersity indexes (PDI), measured by Dynamic Light Scattering in milliQ water.

C (mg/mL)	MTOS-5		MTOS-41		MTOS-72	
	D_h (nm)	PDI	D_h (nm)	PDI	D_h (nm)	PDI
0.05	91.5 ± 0.9	0.107 ± 0.007	124.1 ± 1.5	0.062 ± 0.007	138.6 ± 2.3	0.107 ± 0.007
0.10	112.0 ± 7.8	0.112 ± 0.011	132.3 ± 4.7	0.071 ± 0.004	169.1 ± 13.7	0.112 ± 0.011
0.25	113.9 ± 2.1	0.109 ± 0.001	140.7 ± 2.0	0.068 ± 0.019	177.7 ± 7.1	0.109 ± 0.001
0.50	109.5 ± 6.5	0.136 ± 0.028	142.0 ± 3.3	0.076 ± 0.011	201.9 ± 2.2	0.136 ± 0.028
0.80	122.0 ± 5.7	0.122 ± 0.016	145.3 ± 10.0	0.067 ± 0.011	210.3 ± 2.8	0.122 ± 0.016

3.1.8. References

1. Neuzil, J.; Dong, L.-F.; Rohlena, J.; Truksa, J.; Ralph, S. J., Classification of mitocans, anti-cancer drugs acting on mitochondria. *Mitochondrion* **2013,** 13, (3), 199-208.

2. Kluckova, K.; Bezawork-Geleta, A.; Rohlena, J.; Dong, L.; Neuzil, J., Mitochondrial complex II, a novel target for anti-cancer agents. *Biochimica et Biophysica Acta (BBA)-Bioenergetics* **2013,** 1827, (5), 552-564.

3. Neuzil, S. J. R. a. J., Mitochondria and Cancer. In *Mitochondria and Cancer,* Singh, K. n., Leslie, Ed. Springer: New York, 2010; pp 1-21.

4. Fulda, S., Exploiting mitochondrial apoptosis for the treatment of cancer. *Mitochondrion* **2010,** 10, (6), 598-603.

5. Neuzil, J.; Cerny, J.; Dyason, J. C.; Dong, L. F.; Ralph, S. J., Affinity of vitamin E analogues for the ubiquinone complex II site correlates with their toxicity to cancer cells. *Molecular Nutrition and Food Research* **2011,** 55, (10), 1543-1551.

6. Guo, Y.; Luo, J.; Tan, S.; Otieno, B. O.; Zhang, Z., The applications of Vitamin E TPGS in drug delivery. *European journal of pharmaceutical sciences* **2013,** 49, (2), 175-186.

7. Duhem, N.; Danhier, F.; Préat, V., Vitamin E-based nanomedicines for anti-cancer drug delivery. *J. Controlled Release* **2014,** 182, 33-44.

8. Lu, Y.; Park, K., Polymeric micelles and alternative nanonized delivery vehicles for poorly soluble drugs. *Int. J. Pharm.* **2013,** 453, (1), 198-214.

9. Duncan, R., Polymer therapeutics as nanomedicines: new perspectives. *Curr. Opin. Biotechnol.* **2011,** 22, (4), 492-501.

10. Canal, F.; Sanchis, J.; Vicent, M. J., Polymer–drug conjugates as nano-sized medicines. *Curr. Opin. Biotechnol.* **2011,** 22, (6), 894-900.

11. Tao, Y.; Han, J.; Wang, X.; Dou, H., Nano-formulation of paclitaxel by vitamin E succinate functionalized pluronic micelles for enhanced encapsulation, stability and cytotoxicity. *Colloids and Surfaces B: Biointerfaces* **2013,** 102, 604-610.

12. Matsumura, Y.; Maeda, H., A new concept for macromolecular therapeutics in cancer chemotherapy: mechanism of tumoritropic accumulation of proteins and the antitumor agent smancs. *Cancer research* **1986,** 46, (12 Part 1), 6387-6392.

13. Maeda, H.; Bharate, G.; Daruwalla, J., Polymeric drugs for efficient tumor-targeted drug delivery based on EPR-effect. *European Journal of Pharmaceutics and Biopharmaceutics* **2009,** 71, (3), 409-419.

14. Torchilin, V., Tumor delivery of macromolecular drugs based on the EPR effect. *Advanced drug delivery reviews* **2011,** 63, (3), 131-135.

15. Ortiz, C.; Vázquez, B.; San Román, J., Synthesis, characterization and properties of polyacrylic systems derived from vitamin E. *Polymer* **1998,** 39, (17), 4107-4114.

16. Bendavid, A.; Burns, C. J.; Field, L. D.; Hashimoto, K.; Ridley, D. D.; Samankumara Sandanayake, K. R. A.; Wieczorek, L., Solution- and Solid-Phase Synthesis of Components for Tethered Bilayer Membranes. *The Journal of Organic Chemistry* **2001,** 66, (11), 3709-3716.

17. Aguilar, M. R.; Gallardo, A.; Fernández, M. d. M.; Román, J. S., In situ quantitative 1H NMR monitoring of monomer consumption: a simple and fast way of estimating reactivity ratios. *Macromolecules* **2002,** 35, (6), 2036-2041.

18. Jaffe, E. A.; Nachman, R. L.; Becker, C. G.; Minick, C. R., Culture of human endothelial cells derived from umbilical veins. Identification by morphologic and immunologic criteria. *Journal of Clinical Investigation* **1973,** 52, (11), 2745.

19. Kelso, G. F.; Porteous, C. M.; Coulter, C. V.; Hughes, G.; Porteous, W. K.; Ledgerwood, E. C.; Smith, R. A.; Murphy, M. P., Selective Targeting of a Redox-active Ubiquinone to Mitochondria within Cells antioxidant and antiapoptotic properties. *Journal of Biological Chemistry* **2001,** 276, (7), 4588-4596.

20. Méndez, J.; Aguilar, M. R.; Abraham, G. A.; Vázquez, B.; Dalby, M.; Di Silvio, L.; San Román, J., New acrylic bone cements conjugated to vitamin E: curing parameters, properties, and biocompatibility. *J. Biomed. Mater. Res. Part B* **2002,** 62, (2), 299-307.

21. Sánchez-Chaves, M.; Martínez, G.; López Madruga, E.; Fernández-Monreal, C., Synthesis of statistical glycidyl methacrylate-n-vinyl pyrrolidone copolymers and their reaction with naproxen. *J. Polym. Sci., Part A: Polym. Chem.* **2002,** 40, (8), 1192-1199.

22. Vazquez, B.; Ortiz, C.; San Roman, J.; Plasencia, M.; Lopez-Bravo, A., Hydrophilic polymers derived from vitamin E. *J. Biomater. Appl.* **2000,** 14, (4), 367-388.

23. Fessi, H.; Piusieux, F.; Devissaguet, J. P.; Ammoury, N.; Benita, S., Nanocapsule formation by interfacial polymer deposition following solvent displacement. *Int. J. Pharm.* **1989,** 55, (1), R1-R4.

24. Steichen, S. D.; Caldorera-Moore, M.; Peppas, N. A., A review of current nanoparticle and targeting moieties for the delivery of cancer therapeutics. *European Journal of Pharmaceutical Sciences* **2013,** 48, (3), 416-427.

25. Danhier, F.; Feron, O.; Préat, V., To exploit the tumor microenvironment: Passive and active tumor targeting of nanocarriers for anti-cancer drug delivery. *J. Controlled Release* **2010,** 148, (2), 135-146.

26. Jain, R. K.; Stylianopoulos, T., Delivering nanomedicine to solid tumors. *Nature reviews clinical oncology* **2010,** 7, (11), 653-664.

27. Alexis, F.; Pridgen, E.; Molnar, L. K.; Farokhzad, O. C., Factors affecting the clearance and biodistribution of polymeric nanoparticles. *Molecular pharmaceutics* **2008,** 5, (4), 505-515.

28. Yue, J.; Liu, S.; Xie, Z.; Xing, Y.; Jing, X., Size-dependent biodistribution and antitumor efficacy of polymer micelle drug delivery systems. *Journal of Materials Chemistry B* **2013,** 1, (34), 4273-4280.

29. Liu, Y.; Peterson, D. A.; Kimura, H.; Schubert, D., Mechanism of Cellular 3-(4,5-Dimethylthiazol-2-yl)-2,5-Diphenyltetrazolium Bromide (MTT) Reduction. *J. Neurochem.* **1997,** 69, (2), 581-593.

30. Berridge, M. V.; Herst, P. M.; Tan, A. S., Tetrazolium dyes as tools in cell biology: New insights into their cellular reduction. In *Biotechnology Annual Review*, El-Gewely, M. R., Ed. Elsevier: 2005; Vol. Volume 11, pp 127-152.

31. Berridge, M. V.; Tan, A. S., Characterization of the Cellular Reduction of 3-(4,5-dimethylthiazol-2-yl)-2,5-diphenyltetrazolium bromide (MTT): Subcellular Localization, Substrate Dependence, and Involvement of Mitochondrial Electron Transport in MTT Reduction. *Arch. Biochem. Biophys.* **1993,** 303, (2), 474-482.

32. Chen, H.; Khemtong, C.; Yang, X.; Chang, X.; Gao, J., Nanonization strategies for poorly water-soluble drugs. *Drug Discovery Today* **2011,** 16, (7), 354-360.

33. Fahr, A.; Liu, X., Drug delivery strategies for poorly water-soluble drugs. *Expert Opinion on Drug Delivery* **2007,** 4, 403-416

34. Cho, K.; Wang, X.; Nie, S.; Shin, D. M., Therapeutic nanoparticles for drug delivery in cancer. *Clinical cancer research* **2008,** 14, (5), 1310-1316.

35. Neuzil, J.; Tomasetti, M.; Zhao, Y.; Dong, L. F.; Birringer, M.; Wang, X. F.; Low, P.; Wu, K.; Salvatore, B. A.; Ralph, S. J., Vitamin E analogs, a novel group of "mitocans,"

as anticancer agents: The importance of being redox-silent. *Molecular Pharmacology* **2007,** 71, (5), 1185-1199.

36. Youk, H.-J.; Lee, E.; Choi, M.-K.; Lee, Y.-J.; Chung, J. H.; Kim, S.-H.; Lee, C.-H.; Lim, S.-J., Enhanced anticancer efficacy of α-tocopheryl succinate by conjugation with polyethylene glycol. *J. Controlled Release* **2005,** 107, (1), 43-52.

37. Duhem, N.; Danhier, F.; Pourcelle, V.; Schumers, J.-M.; Bertrand, O.; LeDuff, C. S.; Hoeppener, S.; Schubert, U. S.; Gohy, J.-F.; Marchand-Brynaert, J., Self-Assembling Doxorubicin–Tocopherol Succinate Prodrug as a New Drug Delivery System: Synthesis, Characterization, and in Vitro and in Vivo Anticancer Activity. *Bioconjugate chemistry* **2013,** 25, (1), 72-81.

38. Wang, X. F.; Dong, L.; Zhao, Y.; Tomasetti, M.; Wu, K.; Neuzil, J., Vitamin E analogues as anticancer agents: Lessons from studies with α-tocopheryl succinate. *Molecular nutrition & food research* **2006,** 50, (8), 675-685.

39. Birringer, M.; EyTina, J.; Salvatore, B.; Neuzil, J., Vitamin E analogues as inducers of apoptosis: structure–function relation. *British journal of cancer* **2003,** 88, (12), 1948-1955.

40. Behery, F. A.; Elnagar, A. Y.; Akl, M. R.; Wali, V. B.; Abuasal, B.; Kaddoumi, A.; Sylvester, P. W.; El Sayed, K. A., Redox-silent tocotrienol esters as breast cancer proliferation and migration inhibitors. *Bioorganic & medicinal chemistry* **2010,** 18, (22), 8066-8075.

41. Neuzil, J.; Weber, T.; Schröder, A.; Lu, M.; Ostermann, G.; Gelllert, N.; Mayne, G. C.; Olejnicka, B.; Nêgre-Salvayre, A.; Stícha, M., Induction of cancer cell apoptosis by α-tocopheryl succinate: molecular pathways and structural requirements. *The FASEB Journal* **2001,** 15, (2), 403-415.

42. Kedar, U.; Phutane, P.; Shidhaye, S.; Kadam, V., Advances in polymeric micelles for drug delivery and tumor targeting. *Nanomedicine: Nanotechnology, Biology and Medicine* **2010,** 6, (6), 714-729.

43. Blanco, E.; Hsiao, A.; Ruiz-Esparza, G. U.; Landry, M. G.; Meric-Bernstam, F.; Ferrari, M., Molecular-targeted nanotherapies in cancer: enabling treatment specificity. *Molecular oncology* **2011,** 5, (6), 492-503.

44. Dong, L.-F.; Swettenham, E.; Eliasson, J.; Wang, X.-F.; Gold, M.; Medunic, Y.; Stantic, M.; Low, P.; Prochazka, L.; Witting, P. K., Vitamin E analogues inhibit

angiogenesis by selective induction of apoptosis in proliferating endothelial cells: the role of oxidative stress. *Cancer research* **2007,** 67, (24), 11906-11913.

45. Neuzil, J.; Weber, T.; Gellert, N.; Weber, C., Selective cancer cell killing by alpha-tocopheryl succinate. *British Journal of Cancer* **2001,** 84, (1), 87-89.

46. Koivunen, J.; Aaltonen, V.; Peltonen, J., Protein kinase C (PKC) family in cancer progression. *Cancer letters* **2006,** 235, (1), 1-10.

47. Ways, D. K.; Kukoly, C. A., MCF-7 breast cancer cells transfected with protein kinase C-alpha exhibit altered expression of other protein kinase C isoforms and display a more aggressive neoplastic phenotype. *Journal of Clinical Investigation* **1995,** 95, (4), 1906.

48. Gopalakrishna, R.; Jaken, S., Protein kinase C signaling and oxidative stress. *Free Radical Biol. Med.* **2000,** 28, (9), 1349-1361.

49. Mi, Y.; Zhao, J.; Feng, S.-S., Vitamin E TPGS prodrug micelles for hydrophilic drug delivery with neuroprotective effects. *Int. J. Pharm.* **2012,** 438, (1), 98-106.

50. Li, P.-Y.; Lai, P.-S.; Hung, W.-C.; Syu, W.-J., Poly (l-lactide)-vitamin E TPGS nanoparticles enhanced the cytotoxicity of doxorubicin in drug-resistant MCF-7 breast cancer cells. *Biomacromolecules* **2010,** 11, (10), 2576-2582.

51. Zhang, Z.; Tan, S.; Feng, S.-S., Vitamin E TPGS as a molecular biomaterial for drug delivery. *Biomaterials* **2012,** 33, (19), 4889-4906.

52. Neuzil, S. J. R. a. J., Mitochondria as Targets for Cancer Therapy. In *Mitochondria and Cancer*, Singh, K. n., Leslie, Ed. Springer: New York, 2010; pp 211 - 247.

53. Dong, L.-F.; Low, P.; Dyason, J. C.; Wang, X.-F.; Prochazka, L.; Witting, P. K.; Freeman, R.; Swettenham, E.; Valis, K.; Liu, J., α-Tocopheryl succinate induces apoptosis by targeting ubiquinone-binding sites in mitochondrial respiratory complex II. *Oncogene* **2008,** 27, (31), 4324-4335.

54. Cuezva, J. M.; Ortega, Á. D.; Willers, I.; Sánchez-Cenizo, L.; Aldea, M.; Sánchez-Aragó, M., The tumor suppressor function of mitochondria: translation into the clinics. *Biochimica et Biophysica Acta (BBA)-Molecular Basis of Disease* **2009,** 1792, (12), 1145-1158.

55. Formentini, L.; Martínez-Reyes, I.; Cuezva, J. M., The mitochondrial bioenergetic capacity of carcinomas. *IUBMB life* **2010,** 62, (7).

56. Isidoro, A.; Martínez, M.; Fernandez, P.; Ortega, A.; Santamaría, G.; Chamorro, M.; Reed, J.; Cuezva, J., Alteration of the bioenergetic phenotype of mitochondria is a hallmark of breast, gastric, lung and oesophageal cancer. *Biochem. J* **2004,** 378, 17-20.

57. Cuezva, J. M.; Krajewska, M.; de Heredia, M. L.; Krajewski, S.; Santamaría, G.; Kim, H.; Zapata, J. M.; Marusawa, H.; Chamorro, M.; Reed, J. C., The bioenergetic signature of cancer a marker of tumor progression. *Cancer research* **2002,** 62, (22), 6674-6681.

58. Shoemaker, R. H., The NCI60 human tumour cell line anticancer drug screen. *Nature Reviews Cancer* **2006,** 6, (10), 813-823.

59. Zetter, P., Bruce R, Angiogenesis and tumor metastasis. *Annual review of medicine* **1998,** 49, (1), 407-424.

3.2. Mitochondrially targeted nanoparticles based on α-TOS for the selective cancer treatment.

Raquel Palao-Suay[1,2], Laura Rodrigáñez[3], María Rosa Aguilar[1,2], Carolina Sánchez-Rodríguez[3,4], Francisco Parra[1], Mar Fernández[1,2], Juan Parra[2,5], Juan Riestra-Ayora[3], Ricardo Sanz-Fernández[3,4], Julio San Román[1,2]*

[1]Group of Biomaterials, Department of Polymeric Nanomaterials and Biomaterials, Institute of Polymer Science and Technology, CSIC, Madrid, Spain.

[2]Networking Biomedical Research Centre in Bioengineering, Biomaterials and Nanomedicine, CIBER-BBN, Spain.

[3]Foundation for Biomedical Research, University Hospital of Getafe, Getafe (Madrid), Spain.

[4]European University of Madrid, C/ Tajo s/n. 28670, Villaviciosa de Odón (Madrid), Spain.

[5]Clinical Research and Experimental Biopathology Unit, Healthcare Complex of Ávila, Ávila, Spain.

**Corresponding author*: mraguilar@ictp.csic.es

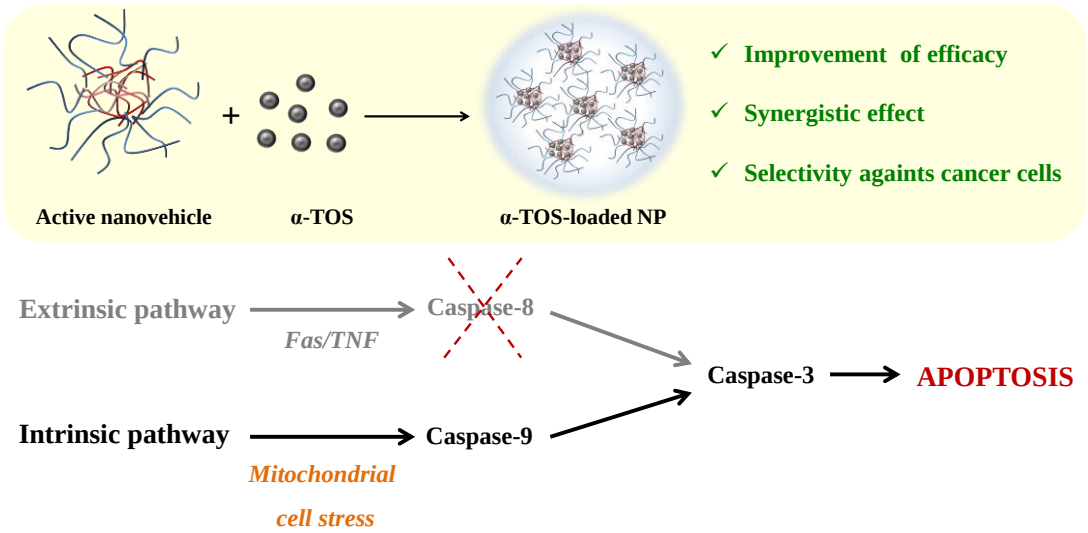

KEYWORDS: α-Tocopheryl succinate, nanovehicle, polymer drug, anticancer, apoptosis.

3.2.1. Abstract

The aim of this work is the preparation of an active nanovehicle for the effective administration of α-tocopheryl succinate (α-TOS). α-TOS is loaded in the core of nanoparticles (NPs) based on amphiphilic pseudoblock copolymers of *N*-vinyl pyrrolidone and a methacrylic derivative of α-TOS. These well-defined spherical NPs have sizes below 165 nm and high encapsulation efficiencies. *In vitro* activity of NPs is tested in hypopharynx squamous carcinoma (FaDu) cells and nonmalignant epithelial cells, demonstrating that the presence of additional α-TOS significantly enhances its anti-proliferative activity; however, a range of selective concentrations is observed. These NPs induce apoptosis of FaDu cells by activating the mitochondria death pathway (via caspase-9). Both loaded and unloaded NPs act via complex II and produce high levels of reactive oxygen species that trigger apoptosis. Additionally, these NPs effectively suppress the vascular endothelial growth factor (VEGF) expression of human umbilical vein endothelial cells (HUVECs).These results open the possibility to use this promising nanoformulation as an α-TOS delivery system for the effective cancer treatment, effectively resolving the current limitations of free α-TOS administration.

3.2.2. Introduction

Head and Neck Squamous Cell Carcinoma (HNSCC) is the sixth highest incidence worldwide cancer[1], constituting the 6.5% of all tumors[2] , with more than 600,000 new cases each year[3, 4]. Currently, the therapeutic approach of these tumors is the surgery when the tumor is resectable that is followed or combined with radiotherapy or chemoradiotherapy[5, 6]. However, the adverse effects of these therapies are multiple, including mucositis, dermatitis and dysphagia among others[6, 7].

In light of this data, the development of new treatments more effective, less toxic and aggressive has become a priority. An interesting strategy is the development of selective drug delivery systems that specifically target the tumor tissue[8, 9]. Nanocarriers based on polymer drugs have emerged as a good choice to enhance drug solubility, adjust drug pharmacokinetics and target organs, cells, or even organelles of a specific cell[10, 11]. Moreover, nanocarriers offer the possibility of loading multiple drugs which could present a synergistic effect. In addition, one of the main advantages of using macromolecular systems or nanoparticles (NPs) as drug delivery systems of anticancer compounds is that they present enhanced permeation and retention effect (EPR effect), that is responsible of the passive targeting of the tumor[12-14].

The aim of selective anticancer treatments is to effectively target the differences between cancer and nonmalignant cells[15, 16]. Normal cells metabolism is mostly based on the process of mitochondrial oxidative phosphorylation, while cancer cells metabolism/survival depends mostly on glycolysis. This altered energy dependency is known as the "Warburg effect" and is a hallmark of cancer cells [17-19].Therefore, drugs that directly act on the mitochondrial differences could represent the future of cancer treatments [16, 18, 20]. One of the most important advantages of these agents is that can exert their therapeutic action with independence of the upstream signalling cascades that potentially could acquire resistances using typical chemotherapeutics[21].

α-TOS is a "mitochondrially targeted anticancer compounds" or "mitocans" that acts as a competitive inhibitor of succinate dehydrogenase (SDH, complex II) by displacing ubiquinone (coenzyme Q) from binding to complex II in the cancer cell mitochondria[22-24]. As a result, accumulated electrons react with molecular oxygen and give rise to high concentrations of reactive oxygen species (ROS) that trigger apoptosis (mitocan type V)[25].

In this sense, complex II has been recently described as an important sensor for intrinsic apoptosis induction[26, 27]. Furthermore, α-TOS has also been described as a mitocan type II because it is considered a BH3 protein mimetic that blocks Bcl-2 or Bcl-xL antiapoptotic proteins [22, 28, 29]. This cell death mechanism has been demonstrated by different authors in a wide variety of cancer cells[30].

The main obstacle for the successful application of α-TOS-based clinical treatments is the hydrophobic nature of this drug that significantly reduces its bioavailability and therapeutic activity. In fact, the solubilization of α-TOS in an organic phase or oil emulsion, such as dimethyl sulfoxide (DMSO) or corn oil, is the most common methodology to perform *in vitro* and *in vivo* cancer studies. Particularly, this procedure can cause important side effects after the intravenous or intraperitoneal administration of α-TOS, such as the formation of aggregates as a result of drug mixing with blood plasma, inflammation and embolization processes[31]. In order to avoid these side effects, α-TOS has been PEGylated being α-TOS-PEG_{1000} (TPGS) the most common conjugate used in drug delivery as adjuvant due to its potent emulsification effect. However, the low concentration of the drug in the conjugate (only one molecule of α-TOS/PEG_{1000}), the lack of its selectivity against cancer cells due to its high toxicity, and its associated side effects prevent the tangible application of TPGS formulations[32, 33]. Additionally, Koudelka et at. have described the preparation of liposomal formulations of vitamin E analogues based on phosphatidylcholine or phosphatidylethanolamine with good results[31, 34]. Particularly, α-TOS formed stable nanovesicles with phosphatidylcholine that presented an improved *in vivo* activity due to its effective intratumoral distribution. Moreover, these nanovesicles were successfully used as siRNA delivery system[35].

However, the encapsulation of α-TOS into an appropriate polymeric nanovehicle has not been described in the literature, and therefore the aim of this work is to encapsulate α-TOS in self-assembled polymeric NPs based on a methacrylic derivative of α-TOS (MTOS) recently described by our group [36]. These surfactant-free polymeric NPs were obtained by self-assembling of amphiphilic copolymeric drugs. The hydrophilic segment of the copolymers was based on *N*-vinyl pyrrolidone (VP) and the hydrophobic segment incorporated MTOS (**figure 1**). NPs were uptaken by cells and selectively reduced cell viability of tumor (MCF-7, FaDu, WiDr) and proliferating endothelial cells with little or no harm to nonmalignant (HMEpC) or quiescent cells [37]. The copolymers were active

(polymer drugs), and the active principle (α-TOS) did not have to be released to exert its anticancer and antiangiogenic activity with higher selectivity than TPGS[36]. However, these NPs did not present a potent activity against FaDu cells (cell viability was reduced to 56% after 24 hours). For that reason, the aim of this work was to improve the biological activity of these NPs by the incorporation of additional α-TOS in their hydrophobic inner core. The chemical composition of the amphiphilic copolymers and the self-assembling organization will favored α-TOS encapsulation due to the structural similarity between α-TOS and MTOS. NPs were exhaustively characterized and the anticancer activity of these nanoassemblies was evaluated against hypopharyngeal adenocarcinoma cells (FaDu) cells, studying the mechanism of action of unloaded and α-TOS-loaded NPs and demonstrating the efficacy of this drug delivery system for the cancer treatment.

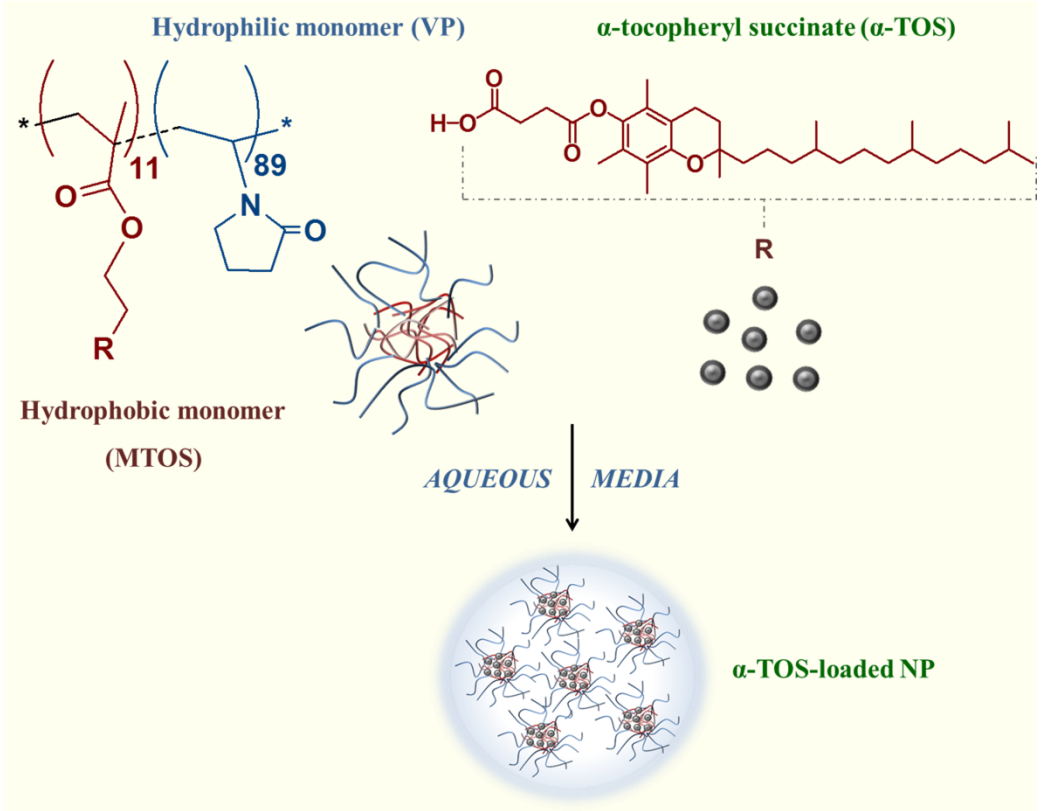

Figure 1: Scheme of the formation and the structure of surfactant-free NPs based on amphiphilic copolymeric drugs of VP and α-TOS.

3.2.3. Materials and methods

- **Synthesis of the copolymer**

The methacrylic derivative of α-TOS (MTOS) and poly(VP-*co*-MTOS) with a copolymer molar composition of VP:MTOS 89:11 (from now on MTOS-11) were synthesized as recently described by our group[36]. Briefly, the copolymer was obtained by free radical polymerization of both VP and MTOS in 1,4-dioxane (monomer concentration, 0.25 M), using AIBN (1.5×10^{-2} M) as radical initiator, at 60ºC for 24 hours. MTOS-11 was purified by dialysis against distilled water for 72 h, and isolated by freeze-drying.

- **Synthesis and characterization of NPs**

Self-assembled NPs were prepared by nanoprecipitation as previously described[36, 38]. Briefly, MTOS-11 was dissolved in 1,4-dioxane (10 mg/mL) and then added drop by drop over an aqueous phase (PBS, 0.01 M, pH 7.4) under constant magnetic stirring to obtain a final polymer concentration of 2 mg/mL. After the nanoprecipitation, milky NP dispersions were dialyzed against PBS during 72 h in order to remove organic solvent. Afterwards, each NP suspension was sterilized by filtration through 0.22 μM polyethersulfone membranes (PES, Millipore Express®, Millex GP) and stored at 4 ºC. In the next sections, unloaded NPs will be labelled as NP-0.

α-TOS or coumarin-6 encapsulation

α-TOS or coumarin-6 (c6) loaded NPs were also obtained by nanoprecipitation. α-TOS (10, 5 or 3 % w/w respect to the polymer) or c6 (1 % w/w respect to the polymer) and MTOS-11 (10 mg/mL) were dissolved in 1,4-dioxane and added dropwise to a PBS solution under magnetic stirring. The final polymer concentration was 2.0 mg/mL. The solution was dialyzed against PBS for 72 hours in order to eliminate the organic solvent and non-encapsulated α-TOS or c6.

In the following sections, α-TOS-based NPs will be labelled as a function of the feed percentage of α-TOS loading (NP-10, NP-5 and NP-3 for a 10, 5 or 3 % w/w with respect to the polymer, respectively).

Encapsulation efficiency (EE)

c6 and α-TOS loaded NPs were freeze dried in order to eliminate the aqueous phase. Amorphous powder was obtained in both types of NPs with a yield higher than 90 %. Afterwards, c6 entrapped in self-assembled NPs was measured by fluorescence spectroscopy. Particularly, c6 NPs (2 mg/mL) were dissolved in ethanol and their fluorescence was measured with an excitation wavelength of 485 nm and a maximum emission of 528 nm using a Biotek SYNERGY-HT plate reader, adjusting emission splits as required for the intensity measurements. The fluorescence intensity was correlated with c6 concentration using a calibration curve that was previously obtained using a range of c6 concentrations between 0.5 – 0.001 mg/mL in ethanol.

α-TOS entrapped in the NPs was quantified by absorbance spectroscopy. Specifically, α-TOS loaded NPs (5 mg/mL) were dissolved in ethanol and their absorbance was measured at 285 nm using a Perkin Elmer Lambda 35 UV/VIS spectrophotometer. The absorbance was correlated with α-TOS concentration using a calibration curve that was previously obtained using a range of α-TOS concentrations between 1 – 0.001 mg/mL in ethanol.

The encapsulation efficiency (EE) was defined as the ratio of calculated and original amount of c6 or α-TOS encapsulated in the NPs. The calculation equation is as follows:

$$Encapsulation\ efficiency\ (EE) = \frac{[loaded\ molecule]_i}{[loaded\ molecules]_0} \times 100 \qquad [1]$$

being $[\text{loaded molecule}]_i$ the concentration of the molecule (c6 or α-TOS) encapsulated in the core of the NPs and detected experimentally, and $[\text{loaded molecule}]_0$ the concentration of the molecule added in the nanoprecipitation process.

Particle Size Distribution and zeta potential measurements

The particle size distribution of the NP suspensions was determined by dymanic light scattering (DLS) using a Malvern Nanosizer NanoZS Instrument equipped with a 4mW He-Ne laser (λ=633 nm) at a scattering angle of 173°. Measurements of NP dispersions were performed in square polystyrene cuvettes (SARSTEDT), and the temperature was kept constant at 25 ºC. The autocorrelation function was converted in an intensity particle size distribution with ZetaSizer Software 7.10 version, to get the mean hydrodynamic diameter (D_h) and the particle dispersion index (PDI) between 0 (monodisperse particles) and 1

(polydisperse particles) based on the Stokes-Einstein equation, assuming the particle to be spherical. The zeta potential was determined for NP formulations at 0.2 mg/mL concentration containing 10 mM NaCl and using laser Dopper electrophoresis (LDE). The zeta potentials were automatically calculated from the electrophoretic mobility using the Smoluchowski´s approximation. For each sample, the statistical average and standard deviation of data were calculated from 8 measurements of 20 runs each one.

Characterization morphology of NPs

The morphology of NPs was observed using scanning electron microscopy (SEM), transmission electron microscopy (TEM) and atomic force microscopy (AFM). SEM analysis was performed with a Hitachi SU8000 TED, cold-emission FE-SEM microscope working with an accelerating voltage between 15 and 25 kV. Samples were prepared by deposition of one drop of the corresponding NPs suspension over small glass disks (12 mm diameter), and evaporation at room temperature. Finally, the samples were coated with gold palladium alloy (80:20).

TEM analysis was done with Hitachi SU8000 TED, cold-emission FE-SEM microscope, operating at an acceleration voltage of 50 kV. A drop of NPs suspension (0.02 mg/mL) was deposited over poly(vinyl formal)-coated copper TEM grid and evaporated overnight at room temperature. An additional drop of brilliant black dye (Sigma-Aldrich, 1 mg/mL) was deposited on the grid and the excess was removed with filter paper and the grid was allowed to dry before TEM observation.

For AFM examination, a drop of NPs dispersion was deposited on a surface of small glass disks (12 mm of diameter) and allowed to dry overnight at room temperature. AFM was performed in tapping mode using a Multimode AFM (Veeco Instruments, Santa Barbara, CA, USA) with a Nanoscope IVa control system (software version 6.14r1), equipped with silicon tapping probes (RTESP, Veeco) with a spring constant of 42 N/m and a resonance frequency of 300 KHz and a scan rate of 0.5 Hz. Both the topography and the phase signal images were recorded with a resolution of 512×512 data points.

- **Cell culture**

Hypopharynx carcinoma squamous cells (FaDu, ATCC) were cultured in Dulbecco's modified Eagle's Minimun Essential (DMEM), supplemented with 10% fetal bovine serum

(FBS), 1% penicillin/streptomycin (P/S), and incubated at 37°C and 5% CO_2. Human mammary epithelial cells, HMEpC (obtained from the European Collection of Cell Cultures, ECACC) were cultured using mammary epithelial cell medium (Innoprot), supplemented with 10% FBS, 1% P/S as cultured medium at 37°C and 5% CO_2. In the 3D experiments, FaDu cells were seeded on 2% Matrigel (BD Biosciences, 200 µL) precoated 24-well plates at a density of 90,000 cells/mL.

- **Uptake of coumarin-6 loaded NPs**

Endocytosis of c6 loaded NPs at 0.1 mg/mL was followed by fluorescence microscopy. FaDu cells in 2D and 3D cultures were seeded at 90,000 cells/mL and, in complete medium. The cells were incubated overnight at 37 ºC. Afterwards, the medium was replaced with the corresponding NPs dispersion in PBS (50 µL of the NPs suspension and 50 µL of completed medium) and incubated for 5 h at 37 ºC. When this time was elapsed, the cells were washed 3 times with cold PBS and fixed by a paraformaldehyde solution in PBS (3.7 w/v %) for 15 min at room temperature. Afterwards, the cells were rinsed with cold PBS and observed by Nikon Eclipse TE 2000-S Inverted Microscope System and by Confocal Laser Scanning Microscopy (CLSM) (Leica TCS-SP5 RS AOBS).

- **Cell viability assay**

Cell viability in the presence of different concentrations of NPs or TPGS (Sigma-Aldrich) (1.00, 0.50, 0.25, 0.125, 0.062 mg/mL) was measured using MTT assay. Briefly, cells were seeded in 96-well plates at different densities: FaDu at 25,000 cells/mL (2,500 cells/well) and HMEpC at 100,000 cells/mL (10,000 cells/well).

After 24 hours of incubation, the medium was replaced with the corresponding NPs dispersion or TPGS solution in PBS (50 µL of the NPs suspension and 50 µL of completed medium). The plates were incubated at 37°C in a humidified air with 5% CO_2 for 24 h. A solution of 3-(4,5-dimethylthiazol-2-yl)-2,5-diphenyltetrazolium bromide (MTT) was prepared in warm PBS and filtered before use. MTT, 100 µL, was added to all wells to give a final concentration of 0.05 mg/mL, and the plates were incubated at 37°C, 5% CO_2 for 4 h. Medium and MTT were removed, and 100 µL dimethyl sulfoxide (DMSO) was added to all wells in order to solubilize the formazan crystals formed in the cells, mixed for 10 min, and the absorbance was measured on a Biotek SYNERGY-HT plate reader, using a test wavelength of 570 nm and a reference wavelength of 630 nm.

Cell viability of FaDu cells was also determined after the pre-treatment of the cells with 900 nM MitoQ (kindly donated by Dr. M.P. Murphy) for 1 h in order to assess the capacity of MitoQ [39] to prevent the effect of the NPs.

- **Biochemical assays**

In order to perform the following biochemical assays, unloaded (NP-0) and α-TOS-loaded NP (NP-10) were selected at a polymer concentration of 1 and 0.25 mg/mL, respectively. In all cases, FaDu cells were treated with the NPs formulations during 24 h. For each sample, the statistical average and standard deviation of data were calculated from 4 measurements.

ELISA for Quantitation of EGF and VEGF

Supernatants from each experimental group were collected after 24 hours and used to measure the levels of epidermal growth factor (EGF) and vascular endothelial growth factor (VEGF). The enzyme immunoassay kits for specific cytokines were used (Quantikine, R&D systems, Minneapolis, MN, and Gen-Probe Diaclone SAS) according to the manufacturer's protocol. After development of the colorimetric reaction, the absorbance at 450 nm was quantitated by spectrophotometer (TECAN trading AG, Mänedorf, Swizerland), and the absorbance readings were converted to pg/ml based upon standard curves obtained with recombinant cytokine in each assay.

Lactate dehydrogenase release

Lactate dehydrogenase (LDH) activity was measured in the supernatant of FaDu cultures after being in contact with NP-0, NP-10, TPGS (100 µL each) or Triton X-100 (1% v/v). LDH was detected using the cytotoxicity LDH kit (Roche) following the instructions of the manufacturer. Basically, LDH reduces nicotinamide adenine dinucleotide (NAD^+/NADH) by the oxydation of lactate to pyruvate, and in a second enzymatic reaction the catalyst (diaphorase) transfers H/H^+ from NADH to the tetrazolium salt (2-p-iodophenyl-3-p-nitrophenyl-5-phenyl tetrazolium chloride, INT) and transforms it into a red formazan product that was detected colorimetrically (λ_{abs}=490 nm) using a GENios Plus plate reader (TECAN trading AG, Männedorf, Switzerland). The LDH activity of each sample was calculated from the standard LDH curve. Triton X-100 was used as a positive control and PBS as negative control.

Western blot and protein content

Extraction of protein homogenates and Western blot were performed in culture cells of FaDu, as we described previously[40], using a polyclonal antibodies against: EGFR (dilution 1:200), nitrotyrosine (dilution 1:100), active caspase-3, caspase-8 and caspase-9 (dilution 1:100) Abcam, Cambridge, UK). Followed by incubation with a rabbit peroxidase-conjugated secondary antibody (1:10000 dilution, Abcam, Cambridge, UK). Immunoreactive bands were detected using an enhanced chemiluminiscence detection kit Supersignal West Pico Chemiluminiscent substrate (Fisher Scientific) and quantified by densitometry using AlphaFaseFC (Fluor Chem) software (Alpha Innotech Corporation, San Leandro, CA, USA). Densitometry histograms are representative of the mean results from six independent experiments.

Caspase-9 activity

For the quantification of caspase-9 activity in FaDu cell lysates, a colorimetric assay selective for caspase-9, ApoTargetTM Caspase-9, was used according to the manufacturer's instructions (Life Technologies Corporation, Frederick, MD, USA). Color is proportional to the amount of caspase-9 activity present, and 10 µg/mL protein was utilized to normalize the results.

Indirect immunofluorescence for nitrotyrosine and Anexin-V detection

Cells were blocked and incubated overnight at 4 ºC with a polyclonal anti-nitrotyrosine antibody (dilution: 1:100, Millipore Corporation, Billerica, MA) or polyclonal anti-anexin-V antibody (dilution: 1:75, abcam, Cambridge, UK). Following washes with 0.1% Triton X-100 in PBS, cells were incubated with secondary Alexa Fluor 546-conjugated goat anti-rabbit antibody (dilution 1:250; Molecular Probes, Life Technologies, Alcobendas, Madrid) for 45 min at 37 ºC. Thereafter, cells were incubated with DAPI (300 nM) for 5 min at 37 ºC. Cells were then mounted and visualized using an Olympus BX51 inverted microscope (Japan). Specificity of the immunostaining was evaluated by omission of the primary antibody.

Superoxide anion detection

FaDu cells superoxide generation was determined by staining of cells with fluorescent-labeled dihydroethidium (DHE; Molecular Probes, Eugene, OR). Briefly, cells

were fixed with 4% paraformaldehyde and blocked in a PBS solution containing 4% goat serum and 0.1% Triton X-100. After, cells were incubated for 90 min at 37 ºC with the fluorescent probe dihydroethidium (DHE, 4 µmol/l; Calbiochem, Darmstadt, Germany). In the presence of superoxide anions, DHE is oxidized to ethidium, which intercalates with DNA, yielding bright red fluorescence.

Reactive species quantification (Total ROS/RNS)

Total ROS/RNS free radical activity was measured by the OxiSelect™ *In Vitro* ROS/RNS Assay Kit. The assay employs a dichlorodihydrofluorescin DiOxyQ (DCFH-DiOxyQ), which is a specific ROS/RNS probe. For this purpose, supernatants of FaDu cultures, after being in contact with PBS, NP-0, NP-10 (50 µL each), were added to the wells with 50 µL of a catalyst included in the kit (diluted in PBS at 1:250) in order to accelerate the oxidative reaction. After a brief incubation, 100 µL of the prepared DCFH probe was added to each well. The samples were measured fluorometrically against DCF standard and free radical content was determined by comparison with the predetermined DCF curve. Relative fluorescence was red with GENios Plus plate reader (TECAN trading AG, Männedorf, Switzerland) at 480 nm excitation / 530 nm emission.

- **Statistical analysis**

Results were expressed as mean ± standard deviation. Statistical significance (significance level of: *: $p < 0.05$) was evaluated using the analysis of variance (ANOVA, Tukey test) as required, by Origin 9. This study was approved by the Ethics Committee of the University Hospital of Getafe.

3.2.4. Results and discussion

- **Nanoparticle characterization: α-TOS or coumarin-6 encapsulation**

c6 was efficiently encapsulated in the core of the NPs (NP-c6) and was used as a model of hydrophobic molecule, and as a fluorescent probe for the *in vitro* experiments. The suspension of NP-c6 in water was green fluorescent. NP-c6 were uptaken by the FaDu cells in 2D and 3D cultures and accumulated around the nucleus in a similar manner as HMEpC (**figure S1**, see supporting information)[36]. α-TOS was also efficiently entrapped during the nanoprecipitation process. Particularly, EE was enhanced with the increasing of feed load of α-TOS (**table 1**). In the nanoprecipitation process, the direct hydrophobic interactions between free α-TOS and the nanodomains of methacrylic MTOS are the key factor for the increase of the encapsulation efficacy. The incorporation of free α-TOS molecules might increase the flexibility of PMTOS sequences, increasing the capacity of more interactions with the free drug.

Table 1: Characteristics of unloaded and loaded NPs: Hydrodynamic diameter (D_h), polydispersity indexes (PDI), zeta potential (ζ), and encapsulation efficiency (EE).

NP	Drug	Load (% w/w)	D_h (nm)	PDI	ζ (mV)	EE (%)
NP-0	-	-	134.3 ± 9.2	0.128 ± 0.022	− 3.0 ± 0.2	-
NP-3	α-TOS	3	123.7 ± 6.1	0.185 ± 0.039	− 8.5 ± 0.3	34
NP-5		5	139.7 ± 6.8	0.172 ± 0.056	− 8.8 ± 0.2	61
NP-10		10	164.3 ± 4.9	0.177 ± 0.042	− 18.2 ± 0.6	72
NP-c6	c6	1	172.5 ± 7.2	0.312 ± 0.054	− 4.4 ± 0.5	85

SEM, TEM and AFM micrographs demonstrate that α-TOS-loaded NPs obtained by nanoprecipitation were well-defined spherical (**figure 2**). All size distributions were unimodal with apparent hydrodynamic diameters (D_h, by intensity) between 123 and 164 nm, and low polydispersity indexes (PDI), which can be considered adequate for drug delivery NPs for cancer treatment (**table 1**).

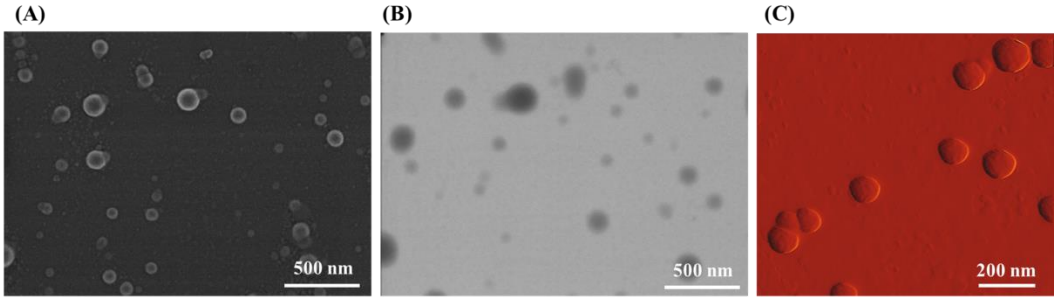

Figure 2: (A) SEM, (B) TEM and (C) AFM micrographs of NP-10 dried from aqueous solution at room temperature.

Particle size could be modulated as a function of the concentration and copolymer composition, as described in a previous publication[36]. The experimental conditions described in that article were used as starting point to adjust the particle size in the range of 100 to 200 nm as it is considered optimum to improve the EPR effect[12, 41]. Sizes smaller than 100 nm are rapidly eliminated by the reticuloendothelial system (RES), and cells have difficulties to endocyte NPs with sizes bigger than 200 nm[42-44].

Particle size increased as α-TOS encapsulation increased, however NP-3 presented smaller size than NP-0 probably due to a better organization of the hydrophobic core when small amounts of α-TOS were encapsulated. Particle size distributions of loaded NPs are shown in **figure S2** (see supporting information).

Zeta potential of all NPs was slightly negative, indicating an almost neutral charge of the surface. These values of zeta potential are typical of VP-based NPs, as described by Zhu et al. that prepared PVP-*b*-polycaprolactone (PVP-*b*-PCL) block NPs with zeta potential value about of – 4.4 mV[45]. Moreover, Gaucher et al. characterized nanoaggregates based on PVP-*b*-PDLLA that exhibited a zeta potential value around – 10 mV [46]. All these values indicate that these NPs exhibit a near neutral zeta potential owing to the VP external shell.

It is noticeable the increase of zeta potential value of NP-10 formulation (- 18.2 mV). This indicates that the molecules of free α-TOS, with a carboxylic end group, can be oriented at least partially with the long non-polar tail of the molecules inserted in the core domain of NPs whereas the polar carboxylic group oriented in the shell of the NPs (VP sequences). This effect contributes to increase the negative charge in the surface.

- **Biological activity**

Cell viability assay against cancer cells

α-TOS activity has been extensively studied by Neuzil et al. It is considered a mitocan as it selectively induces apoptosis of cancer cells by targeting the mitochondria. α-TOS mechanism of action only affects tumor and proliferating endothelial cells, with little or no harm to nonmalignant and quiescent endothelial cells. In fact, α-TOS was nontoxic to a wide range of normal cells, although the mechanism was not completely elucidated. Several hypotheses have been proposed to clarify this selective mechanism, being most of them based on the differences in the cellular metabolism and defense mechanisms (levels of esterases or antioxidant enzymes) between cancer and nonmalignant cells [30, 47, 48].

In the present work, α-TOS-loaded NPs (NP-3, NP-5 and NP-10) have been prepared in order to test if their biological activity increases. Therefore, cell viability of FaDu in the presence of different concentrations of these NPs was studied.

The biological activity of the NPs increased with NPs concentration and the loading charge as demonstrated in **figures 3 and 4**. **Figure 3** shows the effect of NP-0 and NP-3 after 24 (A and B) and 48 hours (C and D) and demonstrates that cell viability decreased as a function of the NP concentration, and was lower for NP-3. Additionally, **figure 4** shows the effect of NP-5 and NP-10 after 24 (A and B) and 48 hours (C and D) and demonstrates that the biological activity of these loaded NPs was much higher, being toxic (cell viability lower than 70%) for cancer cells but tolerated by nonmalignant cells (*e.g.*, concentrations of NP-10 higher than 0.5 mg/mL, and concentrations of NP-5 higher than 1.0 mg/mL were toxic for cancer cells).

Figure S3 (see supporting information) shows micrographs of FaDu culture treatment with NP-0 and NP-10 formulations with respect to negative control (PBS) after 24 hours. NPs treated cells were affected; especially in the case of NP-10 where it is possible to appreciate that cell morphology was not polygonal, but rounded if compared with the control. TPGS was also included in the study for comparative purposes, as it is the most common water-soluble derivative of α-TOS. Moreover, TPGS has been approved by the FDA as adjuvant in the synthesis of NPs[33]. However, its toxicity against cancer cells was confirmed, probably due to its surfactant properties.

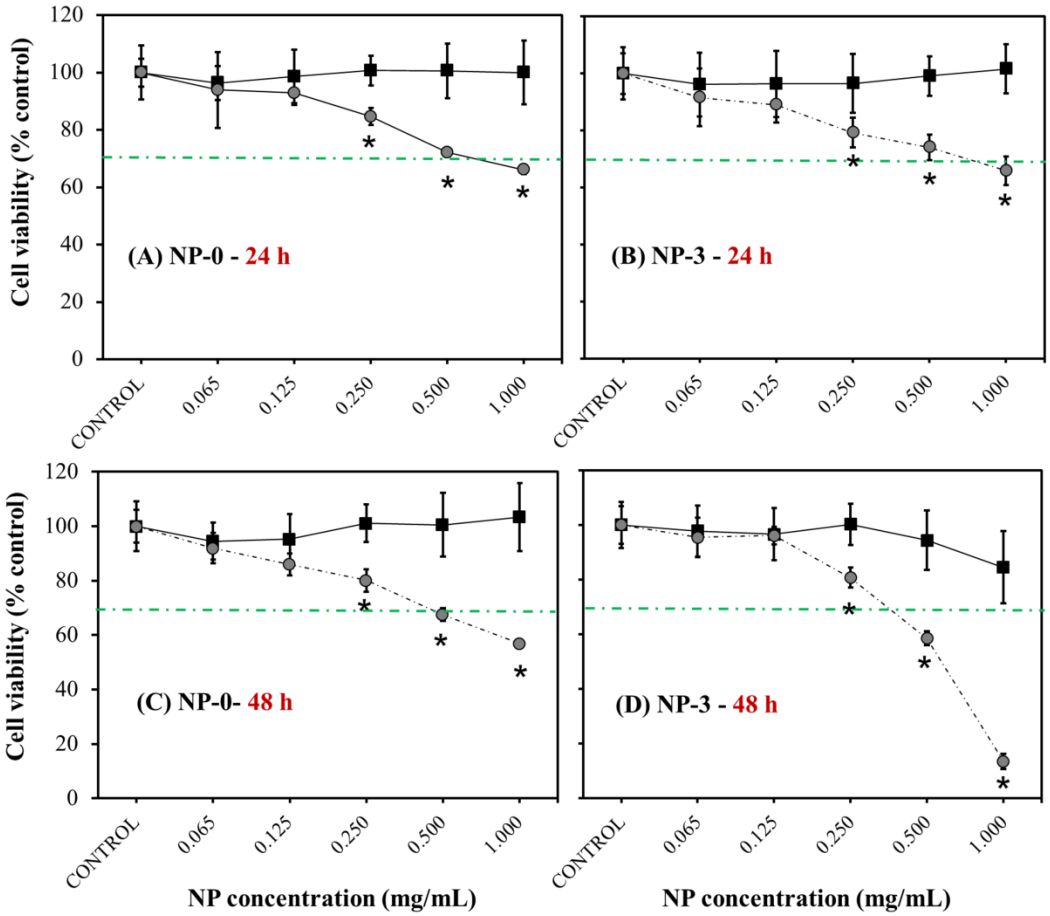

Figure 3: FaDu (●) and HMEpC (■) viability in the presence of different concentrations of NPs measured after 24 (A and B) and 48 hours (C and D). (A and C) NP-0, (B and D) NP-3. The diagrams include the mean, the standard deviation (n=8), and the ANOVA results from the comparison of cancer cells and nonmalignant cells (HMEpC), obtained at a significance level of: *: $p < 0.05$.

The effect of NP-0 was observed after 24 hours and this effect did not increase over time (no significant differences between data obtained after 24 and 48 hours were observed), however the activity of loaded NPs was significantly higher after 48 hours. This means that the NPs were uptaken by the cells at 24 hours but the release of α-TOS takes place not only during the first 24 hours but longer periods of time (48 hours). For instance, NP-3 at 1.0 mg/ml reduced cell viability of FaDu from 65.9 % at 24 hours to 13.5 % at 48 hours.

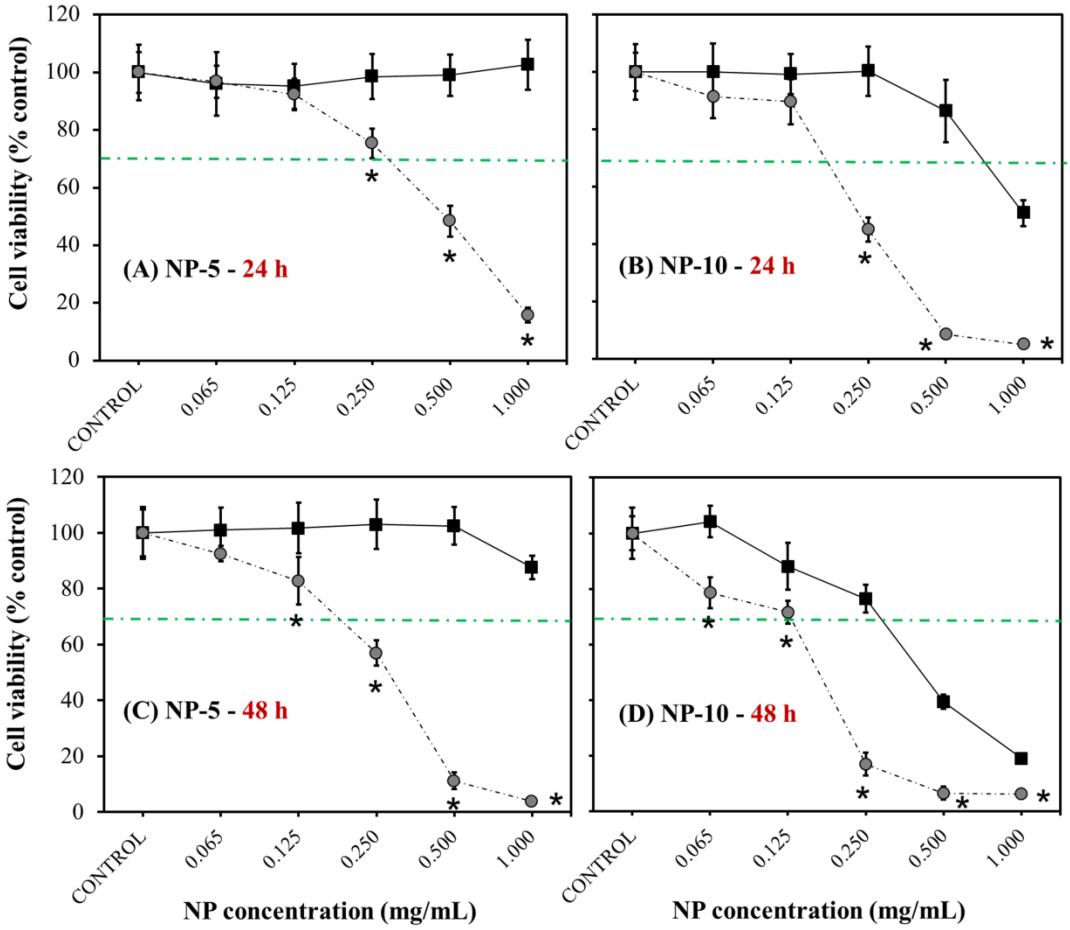

Figure 4: FaDu (●) and HMEpC (■) viability in the presence of different concentrations of NPs measured after 24 (A and B) and 48 hours (C and D). (A and C) NP-5, (B and D) NP-10. The diagrams include the mean, the standard deviation (n=8), and the ANOVA results from the comparison of cancer cells (FaDu and MDA-MB-231) and nonmalignant cells (HMEpC), obtained at a significance level of: *: $p < 0.05$.

Selectivity assay: Breast epithelial cells (HMEpC) vs. Human pharynx squamous carcinoma cells (FaDu)

FaDu cancer cells were more sensitive to the presence of the NPs than HMEpC. Furthermore, loaded NPs were more active than unloaded NPs, and this activity increased overtime. In fact, unloaded NPs reduced cell viability of FaDu cells in a dose-dependent manner, being toxic (cell viability below 70%) at high concentrations (0.5 and 1.0 mg/mL). However, HMEpC viability was not affected by the presence of unloaded NPs (**figure 3**).

Loaded NPs reduced cell viability of cancer and nonmalignant cells in a dose-dependent manner. However, nonmalignant epithelial cells were less sensitive to the presence of these NPs existing selective concentrations of NPs that induce the apoptosis of cancer cells (see also the apoptosis section) with little or no harm to nonmalignant cells. The selective intervals of unloaded and loaded NPs in cancer cells are summarized in the **table S1** (see supporting information). For example, 0.25 mg/mL of NP-10 reduced cell viability of FaDu cells (45% after 24 hours and 17% after 48 hours) whilst cell viability of nonmalignant cells was maintained over 70% (100% after 24 hours and 76% after 48 hours).

- **Biochemical assays**

NP-10 at a concentration of 0.25 mg/mL was used in the following experiments as this concentration was the highest concentration of the NPs loaded with the highest concentration of α-TOS that presented selectivity against FaDu cells. Moreover, NP-0 at the highest concentration of 1 mg/mL was also considered in order to analyze the effect of the intrinsic biological activity of the polymeric nanovehicle (MTOS-11).

Epidermal growth factor and its receptor

Epidermal growth factor receptor (EGFR) is a member of the ErbB/HER family of receptors. Its stimulation by different ligands, such as EGF or transforming growth factor-alpha (TGF-α), leads the activation of intracellular tyrosine kinase that controls gene transcription, cell proliferation, invasion, angiogenesis and metastasis. For that reason, EGFR plays an important role in human carcinogenesis and it is correlated with poor prognosis, more resistance behavior and an increased risk of metastasis in a wide variety of cancers, including head and neck, breast, bladder, ovarian, renal, and colon[49, 50].

Particularly, up to 80% of HNSCC overexpress high level of EGFR and consequently, the survival rate of patients significantly decreases. Currently, the EGFR represents the most relevant target for new anticancer therapy in HNSCC. Advances in the understanding of the EGFR signaling pathways have led the development therapeutic strategies to inhibit the stimulation of this receptor, based on the use of monoclonal antibodies (Cetuximab) and small-molecule tyrosine kinase inhibitors (Gefitinib, Erlotinib) [51-53]. However, the majority of tumors develop acquired resistance to EGFR inhibition. In

this sense, nanotechnology may provide a new tool for the development of improvement therapeutic treatments[54-56].

EGFR and its ligand (EGF) levels were measured by Western Blot and Elisa quantification, respectively, after the treatment with unloaded (NP-0) and loaded (NP-10) NPs during 24 h. As it is shown in **figure 5**, EGFR and EGF levels significantly decreased using both types of NPs with respect to control. Particularly, the reduction of EGFR was remarkable in the case of NP-10 group (EGFR expression was downregulated 22 and 84 % with respect to the control by NP-0 and NP-10, respectively). These results suggest that NPs based on α-TOS could regulate tumor progression by inhibition of EGFR and this effect is enhanced by the load of additional drug in the core of these amphiphilic NPs.

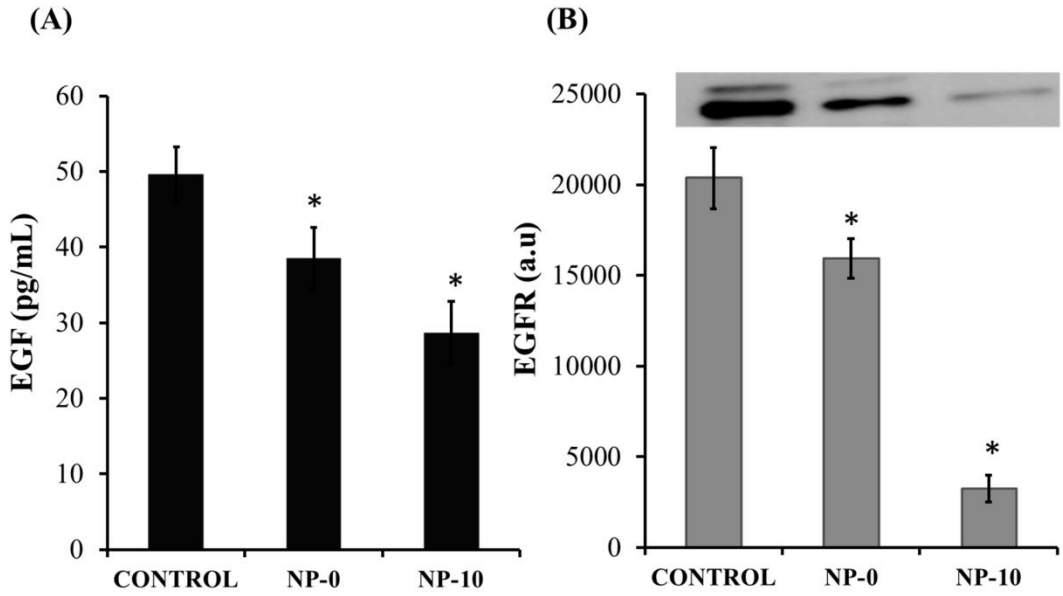

Figure 5: Levels of EGF (A) and EGFR (B) after the treatment with NP-0 and NP-10 in FaDu cells. The diagrams include the mean, the standard deviation (n=4), and the ANOVA results from the comparison of NPs formulations with respect to control, obtained at a significance level of: *: $p < 0.05$.

α-TOS has been also considered as an angiogenic regulator, decreasing the viability of proliferating endothelial cells, with little or no harm to quiescent cells[47, 57]. In fact, our group recently reported the selective antiangiogenic activity of MTOS11-based NPs (NP-0) against human umbilical vein endothelial cells (HUVECs). Mainly, NP-0 formulation

decreased the viability to 40% when NP concentration was 0.5 mg/mL, maintaining the viability of quiescent cells above 80 %[36].

Dual anticancer and antiangiogenic therapies are an interesting goal to achieve effective cancer treatments. The inhibition of angiogenesis in tumors inhibited tumor growth, decreased tumor mass, and induced tumor regression[58, 59]. Downregulation of the most active proangiogenic factors (such as vascular endothelial growth factor, VEGF) has become a promising target for the development of anti-angiogenic therapies.

VEGF levels were determined by Elisa quantification after the NP-0 and NP-10 treatments. Results show that VEGF levels in FaDu cells were significantly lower in the case of NP-0 and NP-10 if compared with the control (**figure 6**). The reduction of VEGF expression was higher than 15 and 43 % after the treatment with unloaded and loaded NPs, respectively. These results suggest that α-TOS entrapped into NPs might enhance the antiangiogenic activity of MTOS-11-based nanovehicle.

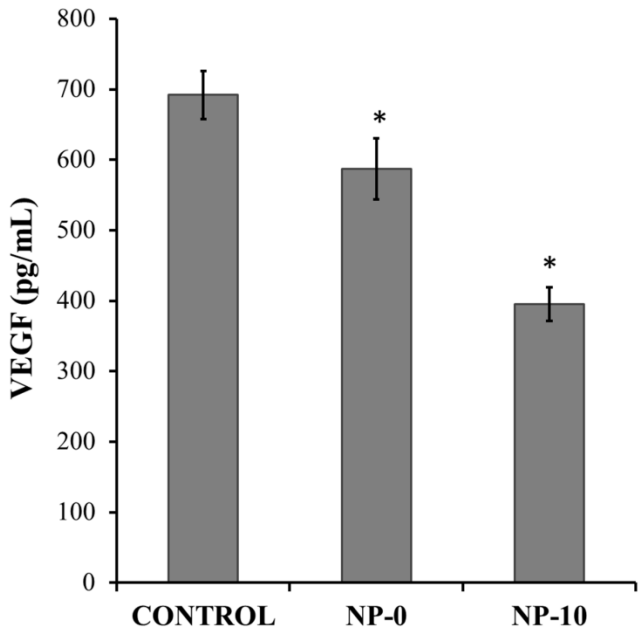

Figure 6: Levels of VEGF after the treatment with NP-0 and NP-10 in FaDu cells. The diagrams include the mean, the standard deviation (n=4), and the ANOVA results from the comparison of NPs formulations with respect to control, obtained at a significance level of: *: $p < 0.05$

Type of cell death: necrosis vs apoptosis

In order to determine the type of cell death that takes place during the reduction of cell viability, necrosis and apoptosis assays were performed. Necrosis is an uncontrolled cell death which causes vacuolation, rupture of the plasma membrane, extensive DNA hydrolysis, and finally cell lysis. This process produces the release of factors from death cells that activate the immune system, resulting in an inflammatory response[60, 61].

Necrosis was indirectly evaluated by the quantification of lactate dehydrogenase (LDH) activity in the supernatant of FaDu cultures[62]. Specifically, LDH is a cytoplasmatic enzyme that is released into the extracellular space when plasma membrane is damaged. **Figure 7A** shows that LDH percentages of FaDu culture after the treatment with NP-0 and NP-10 were lower than 42 %. In fact, the increment of LDH activity was only significant in the case of NP-10 group.

Additionally, TPGS treatment increased LDH levels (higher than 80 % at 1.25 mg/ml of TPGS) that were very close to positive control based on Triton X-100. Therefore, TPGS is much toxic than the NPs at this concentration probably due to its surfactant character. Youk et al. demonstrated that TPGS at a lower concentration (in the range of 10 and 50 μM) induced apoptosis and ROS generation[63]. In spite of the presence of α-TOS in the structure of TPGS, the mechanism by which TPGS triggers apoptosis is not well known. Researches are needed to elucidate the underlying mechanism of TPGS anticancer properties using different cancer cell lines[33]. The first data suggest that the anticancer effect of TPGS is mediated by an alternative pathway in comparison to α-TOS. In this sense, TPGS has been shown to inhibit the function of P-glycoprotein (P-gp) and to rigidify lipid bilayers of cell membrane. Different authors have proposed that P-gp inhibition could be influenced by its effect on the conformational flexibility and ATPase activity, probably mediated via an alteration in mitochondrial membrane fluidity and membrane potential[64-66].

In contrast to necrosis, apoptosis is a programmed death in response to cellular stress [67]. This genetically regulated process is characterized by different perturbations to the cellular architecture such as nuclear and chromosomal DNA fragmentation, chromatin condensation, exteriorization of phosphatidylserine (PS), cell shrinkage and blebbing …[61] All these morphologic features of apoptosis require energy in the form of ATP and the

activation of caspases by either the regulation of death receptors (extrinsic pathway) or the release of apoptotic mediators from the mitochondria (intrinsic pathway), as will be explained in the following sections. Currently, numerous novel therapies are being developed to target specific apoptotic regulators due to its importance as a pathogenic mechanism with a contributing role for many diseases such as cancer and inflammation processes[68]. In the case of cancer, apoptosis is implicated in the therapeutically induced tumor regression by elimination of malignant cells[18].

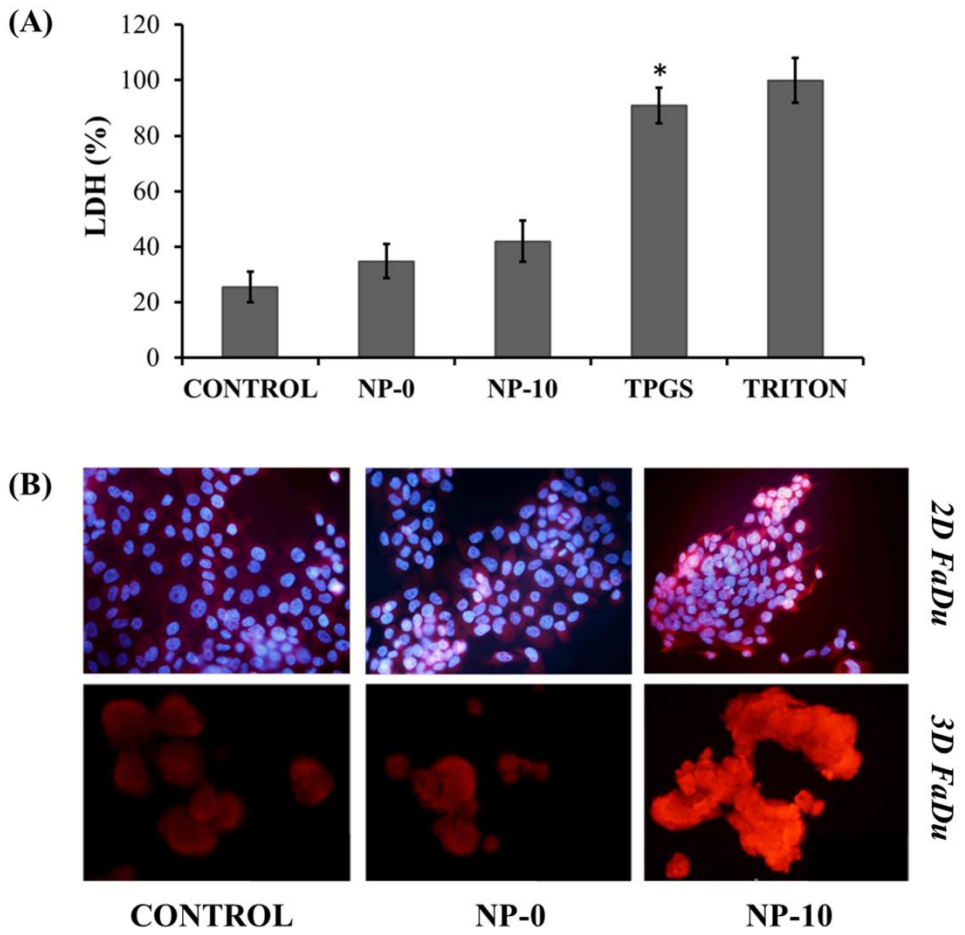

Figure 7: (A) LDH quantification after the treatment with NP-0 and NP-10 in FaDu cells. The diagrams include the mean, the standard deviation (n=4), and the ANOVA results from the comparison of NPs formulations with respect to negative control (PBS), obtained at a significance level of: *: $p < 0.05$. (B) Fluorescence photographs of 2D and 3D Fadu cultures treated with NP-0 and NP-10 formulation using Annexin V- Alexa Fluor 546 conjugate (red fluorescence).

Low levels of LDH activity after the NPs treatment indicate that the cell death could be mediated by apoptotic processes. For that reason, this programmed cell death was qualitatively evaluated by immunofluorescence using Annexin V- Alexa Fluor 546 conjugate as apoptotic marker. Particularly, Annexin V is a Ca^{2+} dependent phospholipid-binding protein with high affinity for PS that is translocated from the inner side of the plasma membrane to the outer layer in the early stages of apoptosis[69, 70].

Figure 7B includes the fluorescence photographs of 2D and 3D FaDu culture after the addition of NP-0 and NP-10. In both types of cultures, red fluorescence increased in the group with NP-10 in comparison to control and unloaded NPs. The enhancement of fluorescence was qualitatively more evident in the case of 3D culture. These qualitative results allow to conclude that α-TOS loaded NPs affect the cell viability of FaDu through a cell-programmed death.

Activation of caspases

A typical feature of apoptosis is the functional activation of caspases that plays a central role in the execution phase of cell programmed death. Specifically, caspases are a family of cysteine proteases that can be activated by two different signaling routes: extrinsic death receptor pathway and the intrinsic mitochondrial pathway[71, 72].

Extrinsic pathway is characterized by the participation of transmembrane death receptors that are members of the tumor necrosis factor (TNF) receptor gene superfamily. Death receptors specifically bind to extrinsic death ligands (such as Fas ligand (FasL) and TNF-related apoptosis-inducing ligand (TRAIL)). As a result, oligomerization and conformational changes are produced in these receptors. These modifications involve the formation of intracellular death-inducing signaling complex (DISC) through the enrollment of the adapter molecules such as the Fas-associated death domain protein (FADD). These specific proteins recruit and acummulate molecules of caspase-8, promoting its activation. In conclusion, this route of apoptosis is mediated by the activation of caspase-8 and bypasses the mitochondria in most cells[73, 74].

In contrast, mitochondria are only involved in the *intrinsic mechanism* of apoptosis that mainly depends on the induction of cellular stress and consequently the release of cytochrome c from these organelles into the cytosol. Pro-apoptotic proteins such as Bax, Bak, and BH3-only proteins specifically regulate the permeability of the outer

mitochondrial membrane (OMM) and thereby the release of cytochrome c. The involvement of these proapoptotic proteins is the vital importance to overcome the inhibitory effect of Bcl-2 antiapoptotic proteins. In fact, BH3-only proteins confiscate anti-apoptotic Bcl-2-family members and promote the assembly of Bak–Bax oligomers within mitochondrial outer membranes. On release from mitochondria, cytochrome c associates with apoptosis protease-activating factor-1 (Apaf-1) and selectively activates *caspase-9* to form the apoptosome[73-75].

Both apoptotic routes are interconnected by the activation of executioner caspases such as caspase-*3*, caspase-6 and caspase-7[76]. Regardless of the caspase activation route, the major effector caspases are activated cleaving selected target proteins. Consequently, the proteolysis is executed as one of the most important feature of the demolition phase of apoptosis.

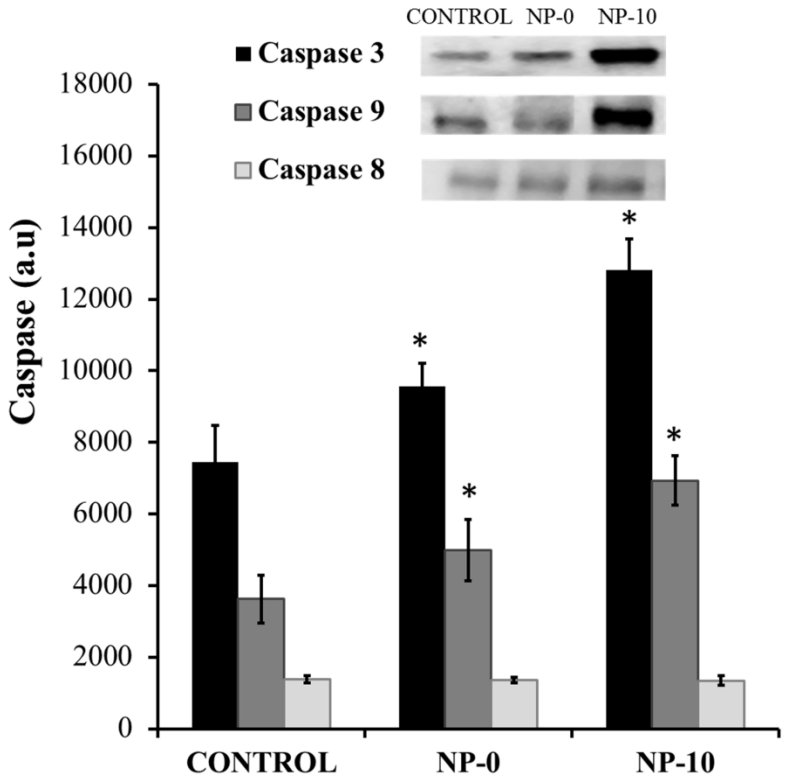

Figure 8: Quantification of caspase-3, 8 and 9 by Western Blot after the treatment of FaDu culture with NP-0 and NP-10 formulations. The diagrams include the mean, the standard deviation (n=4), and the ANOVA results from the comparison of NPs formulations with respect to negative control (PBS), obtained at a significance level of: *: $p < 0.05$.

In order to identify the route of caspases activation that is involved in the induction of apoptosis by α-TOS-based NPs, levels of active caspase-3 (caspase-mediated programmed apoptosis), active caspase-8 (caspase-mediated extrinsic pathway) and active caspase-9 (caspase-mediated intrinsic pathway *via mitochondria*) were measured by Western Blot Analysis in protein extracts from FaDu cell cultures lysates after 24 hours of incubation with unloaded and loaded NPs.

Results of different levels of caspases after the NPs treatments are summarized in **figure 8**. Particularly, caspase-8 levels were similar to the control and no significant differences were observed after the incubation with both types of NPs. Consequently, these NPs did not induce the apoptotic processes by extrinsic pathway. However, levels of both caspase 3 and caspase 9 significantly increased in the case of NP-0 and NP-10 formulations. Specifically, NP treatments produced an upregulation in the expression of caspase-3 of 29 and 72 % with respect to control using NP-0 and NP-10 formulations, respectively.

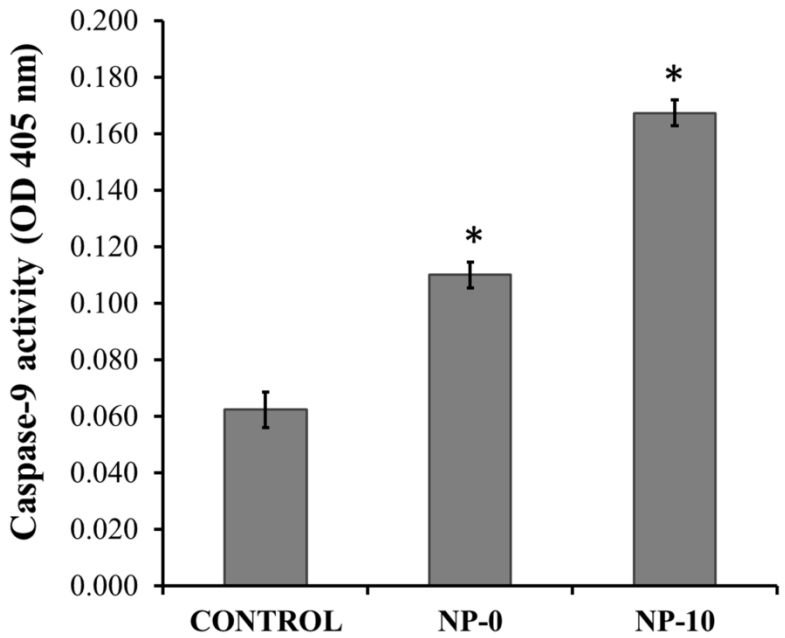

Figure 9: Caspase-9 activity by Elisa quantification after the treatment of FaDu culture with NP-0 and NP-10 formulations. The diagrams include the mean, the standard deviation (n=4), and the ANOVA results from the comparison of NPs formulations with respect to negative control (PBS), obtained at a significance level of: *: $p < 0.05$.

Furthermore, the high caspase-9 levels after the addition of different NPs (the level of caspase 9 increased above to 37 % and 90 % with NP-0 and NP-10 groups, respectively) allow to conclude that intrinsic pathway mediated apoptosis is the mainly mechanism that regulate the FaDu viability reduction through the active involvement of mitochondria of these cancer cells. In the same manner, caspase-9 activity was also measured by Elisa quantification with the aim to confirm the previous data. Activity of caspase-9 was also enhanced after the treatment with unloaded and loaded NPs (**figure 9**).

Mitochondrial action via complex II

α-TOS-loaded NPs formulations selectively induced apoptosis of FaDu cells, as it was previously demonstrated. In order to elucidate if MTOS-11-based NPs act via complex II of cancer mitochondria, in the same manner as α-TOS, cell viability and caspase 3 levels of Mito-Q pretreated or nontreated FaDu cells in the presence of NP-0 and NP-10 were measured. These experiments have also the aim to evaluate if α-TOS loaded in the core of nanoassemblies have a synergistic effect on the induction of complex II-mediated apoptosis in comparison with the unloaded NPs.

MitoQ is a mitochondria-targeted antioxidant[77]. Murphy et al. developed this antioxidant with a chemical structure that can be divided in two different parts[39]. On the one hand, MitoQ incorporates a lipophilic cation based on the triphenylphosphonium structure that can preferentially accumulate within the negative mitochondrial matrix[78, 79]. On the other hand, the antioxidant part of mitoQ is an ubiquinone moiety that allows the conversion of mitoQ to the active ubiquinol, by the action of the enzyme complex II[80]. This conversion avoids the accumulation of ROS that are responsible to activate the intrinsic pathway of apoptosis. For that reason, the pretreatment of cells with MitoQ could protect them from oxidative damage by reducing ROS levels and therefore can be used to check if apoptosis was triggered by this mechanism[81].

Figure 10A shows that cell viability of MitoQ pre-treated cells was significantly higher in comparison to untreatment FaDu cultures. In both types of NPs formulations, viabilities were higher than 70 % after the treatment with MitoQ (cell viabilities of 86 and 75 % were obtained for NP-0 and NP-10, respectively). Therefore, the addition of MitoQ alleviated the action of the NPs and therefore prevented the reduction of cell viability.

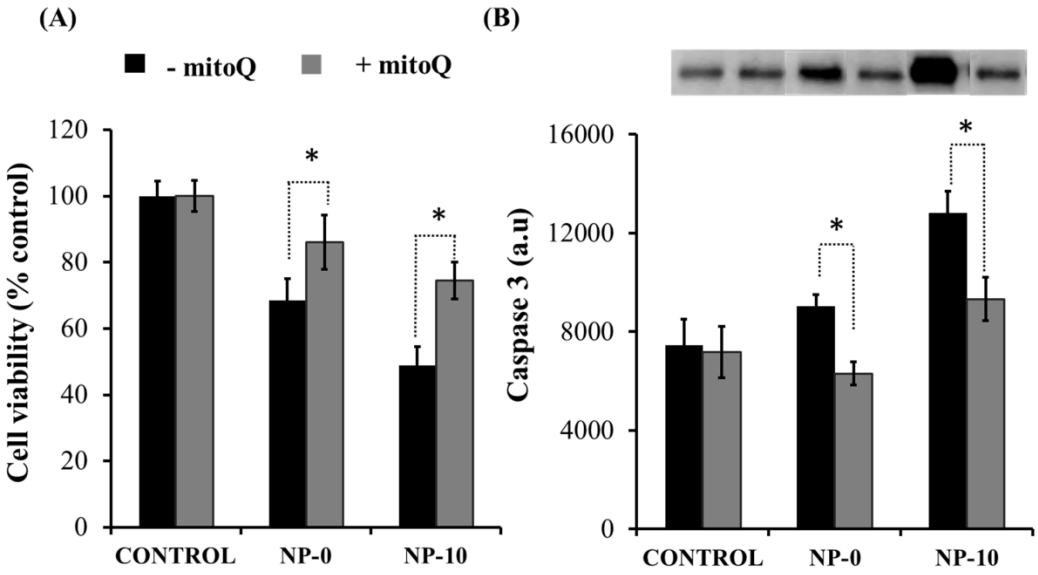

Figure 10: Influence of MitoQ pretreatment in the FaDu viability (A) and the caspase-3 levels (B) after the treatment of FaDu culture with NP-0 and NP-10 formulations. The diagrams include the mean, the standard deviation (n=4), and the ANOVA results from the comparison of NPs formulations with respect to untreated cells, obtained at a significance level of: *: $p < 0.05$.

The influence of MitoQ pretreatment was also confirmed by the visualization of the cell morphology after 24 h of NPs incubation. **Figure S4** (see supporting information) includes optical micrographs of MitoQ-pretreated and nontreated FaDu culture. Cells that were not pretreated with MitoQ were affected, especially those treated with NP-10. Additionally, the number of cells was reduced after NP-10 treatment and they were not so extended in comparison to control. However, morphology of MitoQ-pretreated cultures was not so affected if compared with non-pretreated cultures.

Caspase-3 levels were also reduced when the cells were pretreated using MitoQ (**figure 10B**). The incorporation of this antioxidant allowed the downregulation of the caspase-3 after the treatment with NP-0 and NP-10. These results strongly suggest that α-TOS-based nanoparticles directly interfere on the mitochondrial function of tumor cells, via complex II [82]. This mechanism of action is significantly enhanced by the addition of more α-TOS in the core of the NP, maintaining the selectivity against cancer cells.

Quantification of cellular stress: oxidative and nitrosive stress

ROS have an important role in the metabolic functions of cells at normal cellular concentrations. However, high levels of ROS have negative consequences in a variety of

pathological diseases such as the progression of carcinogenesis, angiogenesis, cell proliferation, aging, etc. Mitochondria are one of the most important sources of cellular stress based on ROS formed by one-electron reduction of oxygen. This side reaction occurs through metabolic processes in the respiratory chain of the mitochondria. The most relevant sources of these species are complex I and III that essentially produce superoxide. Complex II can also produce ROS when the cells are damaged or in hypoxia conditions[48, 83].

In normal cells, ROS are inactivated to hydrogen peroxide (H_2O_2) and oxygen by superoxide dismutases; mainly, MnSOD and CuZnSOD that are present in the mitochondrial matrix and in the intramembrane space, respectively. However, cancer cells have an altered mitochondrial electron transport chains that make them more effective to accumulate ROS with respect to normal cells. The high accumulation of ROS (relative to nonmalignant cells) induced a cascade of different events such as mtDNA mutations, DNA instability, damage of cellular components, etc.[48, 83].

The metabolic differences between normal and cancer cells regarding ROS production have converted the targeting of ROS production in the new paradigm of cancer therapies. Currently, researches are focused on the development of new drugs that enhance ROS production at unsuitable levels by the cell mitochondria (*ROS regulators*) to undergo apoptosis[21, 84]. A wide range of ROS regulators has been described in the literature. Particularly, α-TOS has been included as important ROS regulator that rapidly increases ROS production in only 30 – 60 min[48]. The low levels of antioxidant enzymes in cancer cells can enable the development of selective cancer treatments using α-TOS-based formulations.

Total reactive species were quantified after the treatment of FaDu with NP-0 and NP-10 formulations using a dichlorodihydrofluorescin probe. This probe allows the detection of total reactive species, including ROS and reactive nitrogen species (RNS). RNS are also reactive species that are typically produced after stress processes in cells, as it will be explained later. Additionally, cells were pre-treated 1 h with MitoQ (900 nM) in order to test if these species were produced in the mitochondria.

After both types of NPs treatments, total ROS/RNS significantly increased above 71 % and 177 % in comparison to control with unloaded and loaded NPs, respectively **(figure 11A**). Furthermore, the ROS production was significantly inhibited when cells were

pretreated with MitoQ. Effectively, ROS generation induced by NP-0 and NP-10 in the presence of MitoQ was downregulated 29 and 38 % with respect to control, respectively.

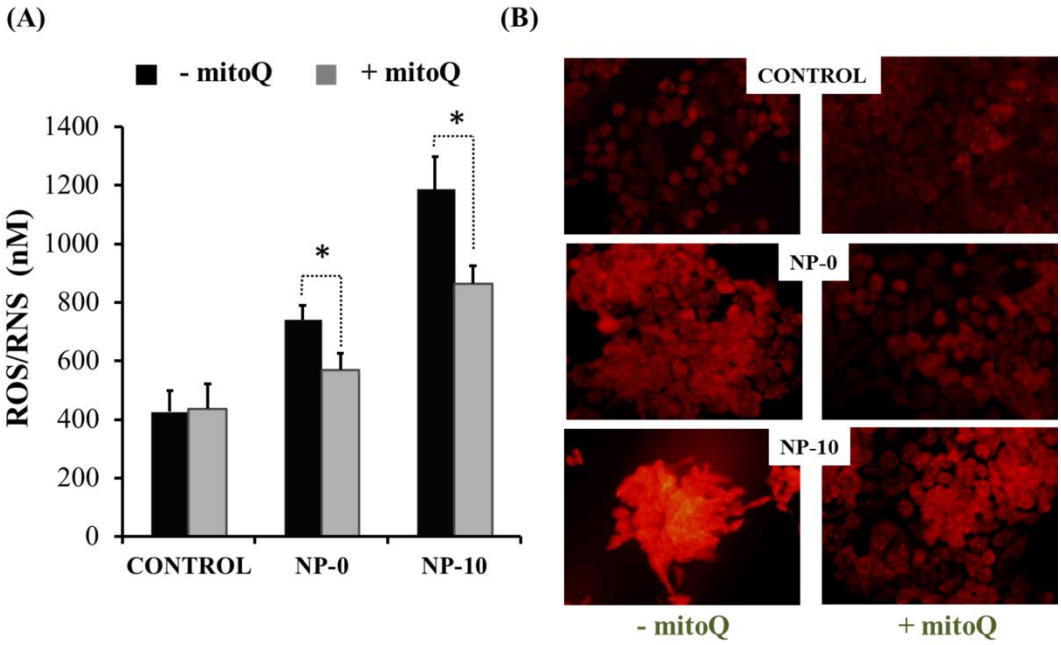

Figure 11: (A) Total ROS/RNS quantification by Elisa after the treatment with NP-0 and NP-10 in FaDu cells. The diagrams include the mean, the standard deviation (n=4), and the ANOVA results from the comparison of NPs formulations with respect to untreated cells, obtained at a significance level of: *: $p < 0.05$. (B) Fluorescence photographs of 2D FaDu cultures treated with NP-0 and NP-10 formulation using dihydroethidium (DHE, red fluorescence).

These results were supported with FaDu cells micrographs that were stained with fluorescent-labeled dihydroethidium after NPs treatment. This red fluorescent probe is useful for the detection of superoxide anion detection (**Figure 11B**). In fact, red fluorescence intensity of un-pretreated cells increased after the treatment with NP-0 and NP-10 groups. However, the red fluorescence was very close to control when mitoQ was added to the cells.

Other important source of reactive species is based on nitric oxide ($NO^{\cdot}$) that plays an important function in cancer progression [85]. Particularly, RNS are synthesized by nitric oxide synthases on the amino acid arginine and they can react with different oxygen species to produce peroxynitrite, nitrogen dioxide or dinitrogen trioxide. These different nitrogen species are potent molecules that induce cellular stress and trigger apoptosis[86, 87].

Researches have demonstrated that RNS are overexpressed in a wide range of malignant tumors at higher concentration than normal tissues, including breast, ovary, lung [86] and head and neck squamous carcinoma[88, 89].

RNS production was indirectly measured by nitrotyrosine quantification. Specifically, nitrotyrosine is a marker of cell damage that is produce in the tyrosine nitration mediated by RNS such as peroxynitrite anion and nitrogen dioxide . Results of nitrotyrosine levels after NPs treatments are summarized in **figure 12A**. An increment of 50 % nitrotyrosine levels was observed with respect to control after the treatment with NP-10. 2D and 3D FaDu cultures were used to test nitrosative stress. Red fluorescence intensity increased in both types of cultures when NP-10 group was considered (**figure 12B**).

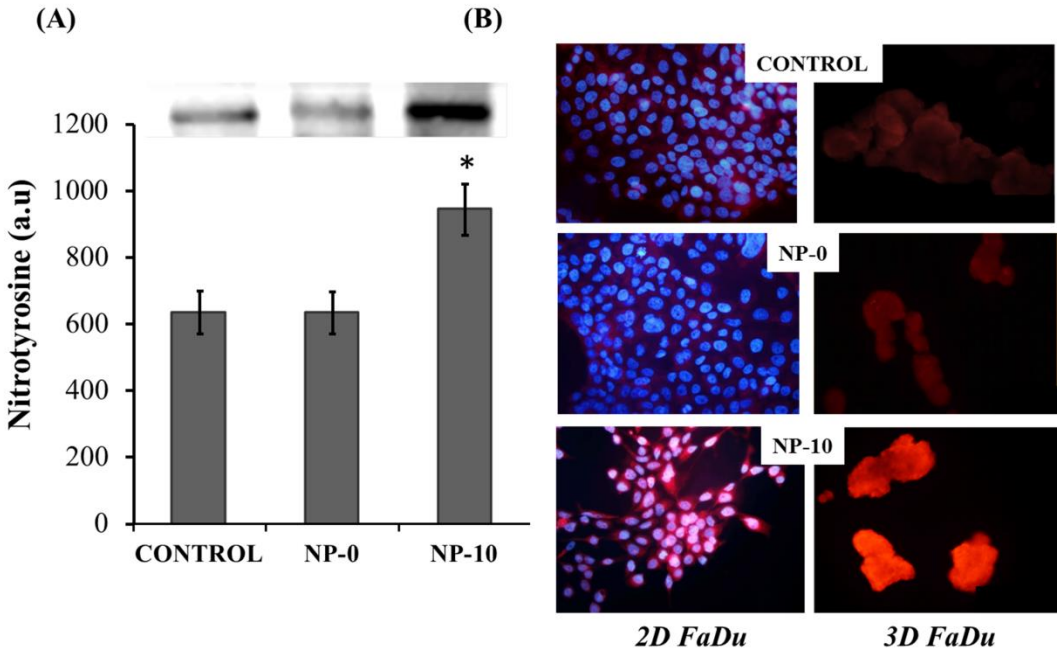

Figure 12: (A) Nitrotyrosine levels after the treatment with NP-0 and NP-10 in FaDu cells. The diagrams include the mean, the standard deviation (n=4), and the ANOVA results from the comparison of NPs formulations with respect to control (PBS), obtained at a significance level of: *: $p < 0.05$. (B) Fluorescence photographs of 2D and 3D FaDu cultures treated with NP-0 and NP-10 formulation using a polyclonal antibody anti-nitrotyrosine and ALEXAFLUOR-546-conjugated goat anti-rabbit antibody.

In conclusion, MTOS-11 based formulations increased the production of reactive species that induce a cellular stress in the cancer cells and finally trigger intrinsic apoptosis.

In the case of ROS, cellular stress produced after NPs treatment is mediated via complex II in the mitochondria due to the suppression of ROS production after the pretreatment with MitoQ. Levels of both ROS and RNS were significantly upregulated when α-TOS-loaded NPs (NP-10) were added to the cell culture.

3.2.5. Conclusions

Surfactant-free α-TOS loaded NPs were obtained using amphiphilic pseudoblock copolymers based on VP and MTOS. Unloaded and loaded NPs were active through the same action mechanism, however, loaded NPs presented higher activity than unloaded NPs against cancer cells, and this activity increased in a dose-dependent manner, and overtime. Loaded NPs presented a range of selective concentrations, inducing apoptosis of cancer cells with little or no harm to nonmalignant cells. Both unloaded and loaded NPs activated the intrinsic route of apoptosis via caspase-9 while the extrinsic route (caspase-8) was not induced in the presence of the NPs. Apoptosis was related with the accumulation of reactive species, both ROS and RNS. α-TOS acted via complex II, and electrons that were transported through the electron transport chain leaked and reacted with molecular oxygen to form high concentrations of ROS. This phenomenon did not occur in the presence of MitoQ, a mitochondria-targeted antioxidant, that avoided the accumulation of ROS and the induction of apoptosis.

Therefore, the employed amphiphilic pseudoblock copolymers could be used to efficiently encapsulate α-TOS and other hydrophobic drugs and could be used in combinatorial treatments when the different drugs present a synergistic effect on cancer treatment.

3.2.6. Acknowledgements

Authors would like to thank financial support from the Spanish Ministry of Economy and Competitiveness (MAT2010-18155), CIBER BBN-ECO Foundation project, and the European University of Madrid. Authors also acknowledge Dr. Pilar Posadas, David Gómez, and Rosa Ana Ramírez for their help in AFM, SEM/TEM and cell culture experiments, respectively. Authors also thank Dr. M.P. Murphy for providing MitoQ for the experiments.

3.2.7. Supporting information

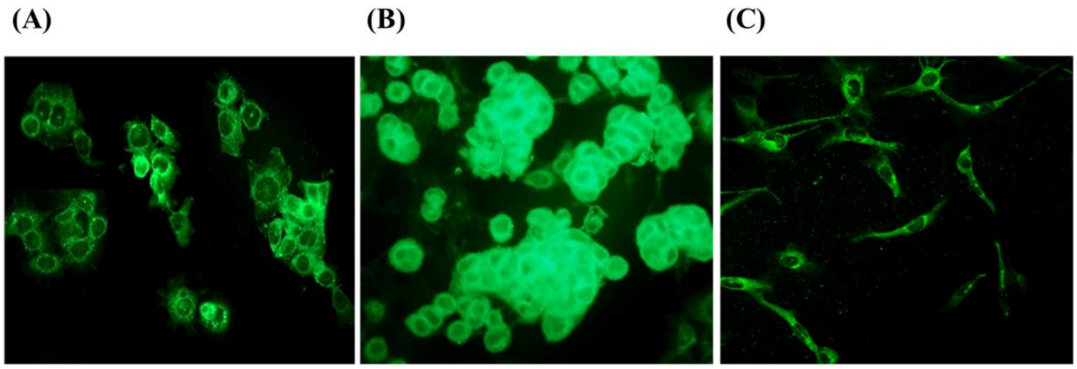

Figure S1: Fluorescent micrographs of FaDu in 2D culture (A), 3D culture (B), and HMEpC in 2D culture (C) after 5 hours in contact with coumarin-6 loaded NPs.

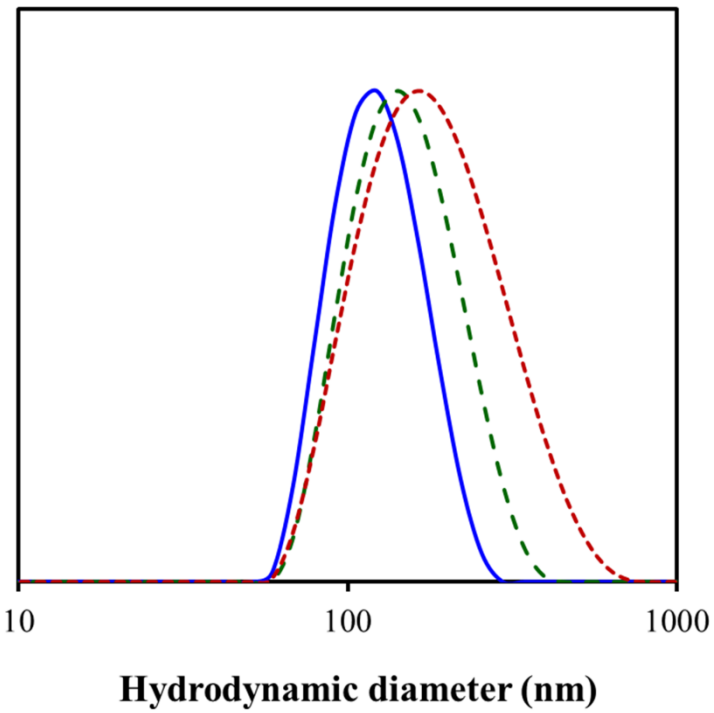

Figure S2: Particle size distributions (D_h, by intensity) of α-TOS-loaded NPs, measured by Dynamic Light Scattering. Blue: NP-3; Green: NP-5; Red: NP-10.

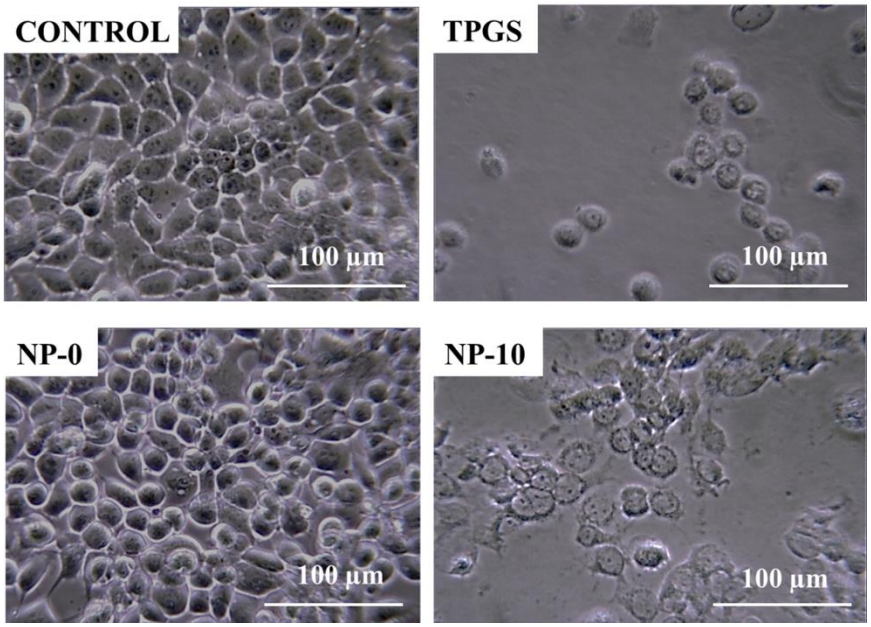

Figure S3: Optical micrographs of FaDu cells after 24 hours in contact with TPGS, NP-0 or NP-10. Control: PBS. Bar=100µm.

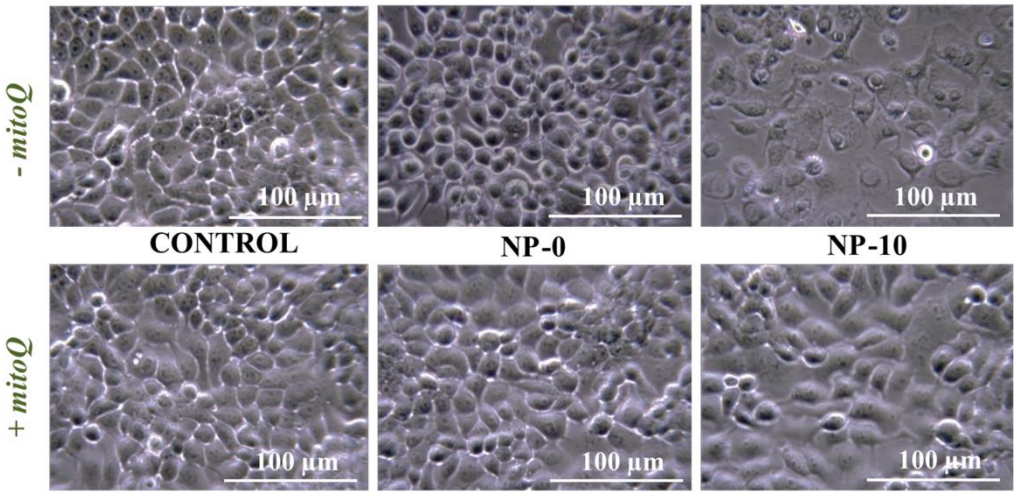

Figure S4: Optical micrographs of untreated and MitoQ (900 nM, 1 h) pretreated FaDu cells after 24 hours in contact with NP-0 or NP-10. Control: PBS. Bar=100µm.

Table S1: Selectivity intervals of unloaded and loaded NPs in FaDu cancer cells.

NP	Time (h)	Selectivity interval (mg/mL)	
NP-0	24	1.000	
	48	0.500	1.000
NP-3	24	1.000	
	48	0.500	1.000
NP-5	24	0.500	1.000
	48	0.250	1.000
NP-10	24	0.250	0.500
	48	0.250	

3.2.8. References

[1] D. L. B. de Souza, M. M. B. Pérez, M. P. Curado, *Cancer epidemiology* **2011**, *35*, 510.

[2] J. S. Cooper, K. Porter, K. Mallin, H. T. Hoffman, R. S. Weber, K. K. Ang, E. G. Gay, C. J. Langer, *Head & Neck* **2009**, *31*, 748.

[3] F. Kamangar, G. M. Dores, W. F. Anderson, *Journal of clinical oncology* **2006**, *24*, 2137.

[4] S. Marur, A. A. Forastiere, "Head and neck cancer: changing epidemiology, diagnosis, and treatment", in *Mayo Clinic Proceedings*, Elsevier, 2008, p. 83/489.

[5] J. Bernier, J. S. Cooper, *The Oncologist* **2005**, *10*, 215.

[6] J. Bernier, C. Domenge, M. Ozsahin, K. Matuszewska, J.-L. Lefèbvre, R. H. Greiner, J. Giralt, P. Maingon, F. Rolland, M. Bolla, *New England Journal of Medicine* **2004**, *350*, 1945.

[7] J. S. Cooper, T. F. Pajak, A. A. Forastiere, J. Jacobs, B. H. Campbell, S. B. Saxman, J. A. Kish, H. E. Kim, A. J. Cmelak, M. Rotman, *New England Journal of Medicine* **2004**, *350*, 1937.

[8] L. Brannon-Peppas, J. O. Blanchette, *Advanced drug delivery reviews* **2012**, *64*, 206.

[9] Y. Lu, K. Park, *International journal of pharmaceutics* **2013**, *453*, 198.

[10] R. Duncan, *Current opinion in biotechnology* **2011**, *22*, 492.

[11] K. Cho, X. Wang, S. Nie, D. M. Shin, *Clinical cancer research* **2008**, *14*, 1310.

[12] H. Maeda, G. Bharate, J. Daruwalla, *European Journal of Pharmaceutics and Biopharmaceutics* **2009**, *71*, 409.

[13] H. Maeda, *Bioconjugate chemistry* **2010**, *21*, 797.

[14] V. Torchilin, *Advanced drug delivery reviews* **2011**, *63*, 131.

[15] J. S. Modica-Napolitano, K. K. Singh, *Mitochondrion* **2004**, *4*, 755.

[16] A. Olszewska, A. Szewczyk, *IUBMB life* **2013**, *65*, 273.

[17] O. Warburg, *Science* **1956**, *123*, 309.

[18] V. Gogvadze, *Current pharmaceutical design* **2011**, *17*, 4034.

[19] D. C. Wallace, *Nat Rev Cancer* **2012**, *12*, 685.

[20] L.-F. Dong, J. Neuzil, *Progress in molecular biology and translational science* **2014**, *127*, 211.

[21] S. Fulda, *Mitochondrion* **2010**, *10*, 598.

[22] J. Neuzil, X.-F. Wang, L.-F. Dong, P. Low, S. J. Ralph, *FEBS letters* **2006**, *580*, 5125.

[23] J. Neuzil, J. C. Dyason, R. Freeman, L.-F. Dong, L. Prochazka, X.-F. Wang, I. Scheffler, S. J. Ralph, *Journal of bioenergetics and biomembranes* **2007**, *39*, 65.

[24] J. Neuzil, L.-F. Dong, L. Ramanathapuram, T. Hahn, M. Chladova, X.-F. Wang, R. Zobalova, L. Prochazka, M. Gold, R. Freeman, *Molecular aspects of medicine* **2007**, *28*, 607.

[25] J. Neuzil, J. Cerny, J. C. Dyason, L. F. Dong, S. J. Ralph, *Molecular nutrition & food research* **2011**, *55*, 1543.

[26] S. Grimm, *Biochimica et Biophysica Acta (BBA)-Bioenergetics* **2013**, *1827*, 565.

[27] K. Kluckova, A. Bezawork-Geleta, J. Rohlena, L. Dong, J. Neuzil, *Biochimica et Biophysica Acta (BBA)-Bioenergetics* **2013**, *1827*, 552.

[28] Y.-H. Dong, Y. Guo, X. Gu, *Chinese journal of cancer* **2009**, *28*, 1114.

[29] K. N. Prasad, B. Kumar, X.-D. Yan, A. J. Hanson, W. C. Cole, *Journal of the American College of Nutrition* **2003**, *22*, 108.

[30] J. Neuzil, T. Weber, N. Gellert, C. Weber, *British journal of cancer* **2001**, *84*, 87.

[31] S. Koudelka, P. T. Knotigova, J. Masek, L. Prochazka, R. Lukac, A. D. Miller, J. Neuzil, J. Turanek, *Journal of Controlled Release* **2015**, *207*, 59.

[32] E. Bernabeu, D. A. Chiappetta, *Journal of Biomaterials and Tissue Engineering* **2013**, *3*, 122.

[33] N. Duhem, F. Danhier, V. Préat, *Journal of Controlled Release* **2014**, *182*, 33.

[34] Š. Koudelka, J. Mašek, J. Neuzil, J. Turánek, *Journal of pharmaceutical sciences* **2010**, *99*, 2434.

[35] S. Hama, S. Utsumi, Y. Fukuda, K. Nakayama, Y. Okamura, H. Tsuchiya, K. Fukuzawa, H. Harashima, K. Kogure, *Journal of Controlled Release* **2012**, *161*, 843.

[36] R. Palao-Suay, M. R. Aguilar, F. J. Parra-Ruiz, M. Fernández-Gutiérrez, J. Parra, C. Sánchez-Rodríguez, R. Sanz-Fernández, L. Rodrigáñez, J. S. Román, *Biomacromolecules* **2015**, *16*, 1566.

[37] J. M. Cuezva, M. Krajewska, M. L. de Heredia, S. Krajewski, G. Santamaría, H. Kim, J. M. Zapata, H. Marusawa, M. Chamorro, J. C. Reed, *Cancer research* **2002**, *62*, 6674.

[38] H. Fessi, F. Puisieux, J. P. Devissaguet, N. Ammoury, S. Benita, *International journal of pharmaceutics* **1989**, *55*, R1.

[39] G. F. Kelso, C. M. Porteous, C. V. Coulter, G. Hughes, W. K. Porteous, E. C. Ledgerwood, R. A. Smith, M. P. Murphy, *Journal of Biological Chemistry* **2001**, *276*, 4588.

[40] C. Peiró, N. Lafuente, N. Matesanz, E. Cercas, J. L. Llergo, S. Vallejo, L. Rodríguez-Mañas, C. F. Sánchez-Ferrer, *British journal of pharmacology* **2001**, *133*, 967.

[41] R. K. Jain, T. Stylianopoulos, *Nature Reviews Clinical Oncology* **2010**, *7*, 653.

[42] S. D. Steichen, M. Caldorera-Moore, N. A. Peppas, *European Journal of Pharmaceutical Sciences* **2013**, *48*, 416.

[43] F. Alexis, E. Pridgen, L. K. Molnar, O. C. Farokhzad, *Molecular pharmaceutics* **2008**, *5*, 505.

[44] J. Yue, S. Liu, Z. Xie, Y. Xing, X. Jing, *Journal of Materials Chemistry B* **2013**, *1*, 4273.

[45] Z. Zhu, Y. Li, X. Li, R. Li, Z. Jia, B. Liu, W. Guo, W. Wu, X. Jiang, *Journal of Controlled Release* **2010**, *142*, 438.

[46] G. Gaucher, M. Poreba, F. Ravenelle, J.-C. Leroux, *Journal of Pharmaceutical Sciences* **2007**, *96*, 1763.

[47] L.-F. Dong, E. Swettenham, J. Eliasson, X.-F. Wang, M. Gold, Y. Medunic, M. Stantic, P. Low, L. Prochazka, P. K. Witting, *Cancer research* **2007**, *67*, 11906.

[48] S. J. Ralph, S. Rodríguez-Enríquez, J. Neuzil, E. Saavedra, R. Moreno-Sánchez, *Molecular aspects of medicine* **2010**, *31*, 145.

[49] C. Yewale, D. Baradia, I. Vhora, S. Patil, A. Misra, *Biomaterials* **2013**, *34*, 8690.

[50] A. Tomas, C. E. Futter, E. R. Eden, *Trends in Cell Biology* **2014**, *24*, 26.

[51] S. Schmitz, K. K. Ang, J. Vermorken, R. Haddad, C. Suarez, G. T. Wolf, M. Hamoir, J.-P. Machiels, *Cancer Treatment Reviews* **2014**, *40*, 390.

[52] R. B. Cohen, *Cancer treatment reviews* **2014**, *40*, 567.

[53] D. C. Gaffney, H. P. Soyer, F. Simpson, *Australasian Journal of Dermatology* **2014**, *55*, 24.

[54] A. Master, A. Malamas, R. Solanki, D. M. Clausen, J. L. Eiseman, A. Sen Gupta, *Molecular pharmaceutics* **2013**, *10*, 1988.

[55] C. Liao, Q. Sun, B. Liang, J. Shen, X. Shuai, *European journal of radiology* **2011**, *80*, 699.

[56] I. H. El-Sayed, *Current oncology reports* **2010**, *12*, 121.

[57] J. Neuzil, E. Swettenham, X.-F. Wang, L.-F. Dong, M. Stapelberg, *FEBS letters* **2007**, *581*, 4611.

[58] P. Zetter, Bruce R, *Annual review of medicine* **1998**, *49*, 407.

[59] J. Folkman, "Role of angiogenesis in tumor growth and metastasis", in *Seminars in oncology*, Elsevier, 2002, p. 29/15.

[60] N. Festjens, T. V. Berghe, P. Vandenabeele, *Biochimica et Biophysica Acta (BBA)-Bioenergetics* **2006**, *1757*, 1371.

[61] A. L. Edinger, C. B. Thompson, *Current opinion in cell biology* **2004**, *16*, 663.

[62] F. K.-M. Chan, K. Moriwaki, M. J. De Rosa, "Detection of necrosis by release of lactate dehydrogenase activity", in *Immune Homeostasis*, Springer, 2013, p. 65.

[63] H. J. Youk, E. Lee, M. K. Choi, Y. J. Lee, J. H. Chung, S. H. Kim, C. H. Lee, S. J. Lim, *Journal of controlled release : official journal of the Controlled Release Society* **2005**, *107*, 43.

[64] E.-M. Collnot, C. Baldes, M. F. Wempe, R. Kappl, J. Hüttermann, J. A. Hyatt, K. J. Edgar, U. F. Schaefer, C.-M. Lehr, *Molecular pharmaceutics* **2007**, *4*, 465.

[65] E.-M. Collnot, C. Baldes, U. F. Schaefer, K. J. Edgar, M. F. Wempe, C.-M. Lehr, *Molecular pharmaceutics* **2010**, *7*, 642.

[66] X. X. Zhou, S. S. Song, D. K. Wang, *Chinese Journal of New Drugs* **2012**, *21*, 2758.

[67] R. C. Taylor, S. P. Cullen, S. J. Martin, *Nature reviews Molecular cell biology* **2008**, *9*, 231.

[68] U. Fischer, K. Schulze-Osthoff, *Pharmacological reviews* **2005**, *57*, 187.

[69] V. A. Fadok, D. L. Bratton, D. M. Rose, A. Pearson, R. A. B. Ezekewitz, P. M. Henson, *Nature* **2000**, *405*, 85.

[70] S. Orrenius, B. Zhivotovsky, P. Nicotera, *Nature reviews Molecular cell biology* **2003**, *4*, 552.

[71] C. Pop, G. S. Salvesen, *Journal of biological Chemistry* **2009**, *284*, 21777.

[72] G. Nuñez, M. A. Benedict, Y. Hu, N. Inohara, *Oncogene* **1998**, *17*, 3237.

[73] E. M. Creagh, H. Conroy, S. J. Martin, *Immunological reviews* **2003**, *193*, 10.

[74] D. Brenner, T. W. Mak, *Current opinion in cell biology* **2009**, *21*, 871.

[75] J.-E. Ricci, R. A. Gottlieb, D. R. Green, *The Journal of cell biology* **2003**, *160*, 65.

[76] D. R. McIlwain, T. Berger, T. W. Mak, *Cold Spring Harbor perspectives in biology* **2013**, *5*, a008656.

[77] M. P. Murphy, R. A. Smith, *Annu. Rev. Pharmacol. Toxicol.* **2007**, *47*, 629.

[78] M. Ross, G. Kelso, F. Blaikie, A. James, H. Cocheme, A. Filipovska, T. Da Ros, T. Hurd, R. Smith, M. Murphy, *Biochemistry (Moscow)* **2005**, *70*, 222.

[79] M. Ross, T. Prime, I. Abakumova, A. James, C. Porteous, R. Smith, M. Murphy, *Biochem. J* **2008**, *411*, 633.

[80] A. M. James, H. M. Cochemé, R. A. Smith, M. P. Murphy, *Journal of Biological Chemistry* **2005**, *280*, 21295.

[81] L.-F. Dong, P. Low, J. C. Dyason, X.-F. Wang, L. Prochazka, P. K. Witting, R. Freeman, E. Swettenham, K. Valis, J. Liu, *Oncogene* **2008**, *27*, 4324.

[82] K. Kluckova, M. Sticha, J. Cerny, T. Mracek, L. Dong, Z. Drahota, E. Gottlieb, J. Neuzil, J. Rohlena, *Cell death & disease* **2015**, *6*, e1749.

[83] G. Bartosz, *Biochemical pharmacology* **2009**, *77*, 1303.

[84] L. Biasutto, L.-F. Dong, M. Zoratti, J. Neuzil, *Mitochondrion* **2010**, *10*, 670.

[85] D. Fukumura, S. Kashiwagi, R. K. Jain, *Nat Rev Cancer* **2006**, *6*, 521.

[86] D. G. Hirst, T. Robson, *Front Biosci* **2007**, *12*, 3406.

[87] D. G. Hirst, T. Robson, *Current pharmaceutical design* **2010**, *16*, 45.

[88] J. E. Bradburn, P. Pei, L. A. Kresty, J. C. Lang, A. J. Yates, A. P. McCormick, S. R. Mallery, *Anticancer research* **2007**, *27*, 3819.

[89] M. H. Rasheed, S. S. Beevi, A. Geetha, *Oral Oncology* **2007**, *43*, 333.

Chapter IV: RAFT polymer-drugs derived from α-tocopheryl succinate

4.1- α-TOS-based RAFT block copolymers and their NPs for the treatment of cancer.

Polymer Chemistry, **2016**

4.2- Enhanced bioactivity of α-tocopheryl succinate based block copolymer nanoparticles by reduced hydrophobicity.

Macromolecular Bioscience, **submitted**

4.1. α-TOS-based RAFT block copolymers and their NPs for the treatment of cancer.

Raquel Palao-Suay[1,2], María Rosa Aguilar[1,2], Francisco J. Parra-Ruiz[1], Samarendra Maji[3], Richard Hoogenboom[3], N.A.Rohner[4], Susan N. Thomas[4] and Julio San Román[1,2]*

[1]Group of Biomaterials, Department of Polymeric Nanomaterials and Biomaterials, Institute of Polymer Science and Technology, CSIC, Madrid, Spain.

[2]Networking Biomedical Research Centre in Bioengineering, Biomaterials and Nanomedicine, CIBER-BBN, Spain.

[3]Supramolecular Chemistry Group. Department of Organic and Macromolecular Chemistry. Ghent University, Ghent, Belgium.

[4]George W. Woodruff School of Mechanical Engineering and Parker H. Petit Institute of Bioengineering and Bioscience, Georgia Institute of Technology, Atlanta, Georgia, USA.

**Corresponding author*: mraguilar@ictp.csic.es

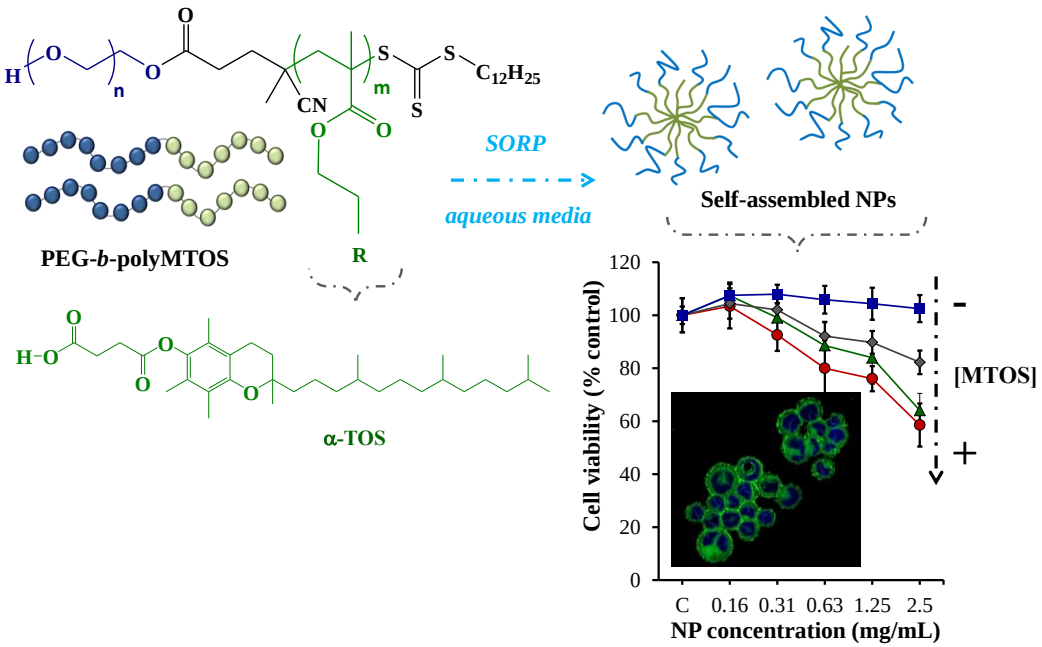

KEYWORDS: α-tocopheryl succinate, poly(ethylene glycol), RAFT polymerization, self-organized precipitation**,** self-assembled nanoparticle.

4.1.1. Abstract

α-Tocopheryl succinate (α-TOS) is a well-known mitochondrially targeted anticancer compound. However, a major factor limiting the use of α-TOS is its low solubility in physiological media. To overcome this problem, the aim of this work is the preparation of new polymeric and active α-TOS-based nanovehicle with a precise control over its macromolecular architecture. Reversible addition-fragmentation chain transfer polymerization (RAFT) is used to synthesize an α-TOS amphiphilic block copolymer with highly homogeneous molecular weight and relatively narrow dispersity. Macro-chain transfer agents (macro-CTA) based on poly(ethylene glycol) (PEG) of different molecular weights (MW, ranging from 4.6 to 20 kDa) are used to obtain block copolymers with different hydrophilic/hydrophobic ratios with PEG being the hydrophilic block and a methacrylic derivative of α-tocopheryl succinate (MTOS) being the monomer that formed the hydrophobic block. PEG-*b*-polyMTOS form spherical nanoparticles (NPs) by self-organized precipitation (SORP) or solvent exchange in aqueous media enabling to encapsulate and deliver hydrophobic molecules in their core. The resulting NPs are rapidly endocytosed by cancer cells. The biological activity of the synthesized NPs are found to depend on the MW of PEG, with NP comprised of the higher MW copolymer resulting in a lower bioactivity due to PEG shielding, inhibiting cellular uptake by endocytosis. Moreover, the biological activity also depends on the MTOS content, as the biological activity increases as a function of MTOS concentration.

4.1.2. Introduction

The rapid growth of nanomedicine has opened the possibility to create sophisticated strategies against cancer and other diseases at a nanoscale where the properties of materials often differ from those of the corresponding bulk materials[1, 2]. As such, a wide range of materials based on natural or synthetic polymers are available to design self-assembled nanostructures[3-5]. Macromolecular self-assembly represents a spontaneous process that involves the organization of amphiphilic macromolecules in an aqueous environment, forming different supramolecular structures[6, 7]. One interesting example of this variety of supramolecular assemblies is nanoparticles (NPs) that exhibit a core-shell morphology based on the use of amphiphilic polymers with hydrophobic and hydrophilic domains[8-10].

The preparation of advanced nanoassemblies using amphiphilic copolymeric systems requires optimal control over the chemical composition and distribution of monomeric units into the macromolecular chains. In this sense, amphiphilic polymers can be obtained by different synthetic methodologies, such as free radical or controlled radical polymerization (CRP). Both techniques proceed *via* the analogous radical mechanism. However, conventional free radical polymerization does not allow the complete control of the molecular weight (MW) and therefore, heterogeneous mixtures of macromolecular chains are obtained. Thus, CRP methods have emerged as potent tools for the synthesis of macromolecular architectures that exhibit a narrow dispersity and controlled MW[11]. Among them, Reversible Addition-Fragmentation Chain Transfer (RAFT) polymerization is one of the most versatile polymerization technique because it can be applied to a great variety of functional monomers using mild reactions conditions and avoiding the use of metal catalysts[12, 13].

α-Tocopheryl succinate (α-TOS) is a well-known vitamin E derivative that has been described as a mitochondrially targeted anticancer compound (mitocan) with anticancer and antiangiogenic properties[14-16]. In fact, this molecule selectively induces apoptosis of cancer and proliferating cells by the displacement of ubiquinone by binding to complex II and by the disablement of Bcl-2 or Bcl-xL antiapoptotic proteins in the mitochondria electron transport chain[17-19]. The combination of these complementary actions produces high levels of reactive oxygen species (ROS) that activate the intrinsic apoptosis cascade and therefore induce cell death after exposure[20].

Despite the potential and attractive activity of α-TOS, its hydrophobic nature significantly limits its successful use in cancer therapy as it causes high toxicity and reduced bioavailability. For this reason, the development of α-TOS based delivery systems is desirable[21]. Specifically, one strategy to increase the bioavailability and stability of α-TOS has been the conjugation of poly(ethylene glycol) (PEG), obtaining PEG_{1000}-α-TOS conjugate (TPGS)[22, 23]. In fact, this macromolecule has been approved by the FDA as an adjuvant at concentrations lower than 0.02 wt %, and it presents an emulsification effect 67 times higher than other surfactants such as PVA[24]. For this reason, this molecule has been incorporated in the formulation of biodegradable NPs based on poly(lactic-*co*-glycolic acid) (PLGA)[25-27], polylactic acid (PLA)[28-30] and poly(*ε*-caprolactone) (PCL)[31, 32]. In spite of enhancements in solubility, permeability and stability, TPGS-based nanoassemblies have important disadvantages for their use as anticancer agents. Particularly, these NPs exhibit cytotoxicity against nonmalignant cells without optimal selectivity toward tumour tissues or cancerous cells. Additionally, TPGS-based nanoformulations incorporate a limited amount of α-TOS into the macromolecular system and the MWs of PEG chains are not enough to avoid the opsonization by the reticuloendothelial system (RES)[33]. These limitations could be surmounted, however, through the development of an effective α-TOS delivery system.

Our group has extensively experience in the preparation of drug delivery systems of hydrophobic drugs[34-37]. In fact, we recently described the preparation of amphiphilic copolymers of *N*-vinyl pyrrolidone (VP) and a methacrylate derivative of α-TOS (MTOS) by free radical polymerization [38]. However, the development of self-assembling systems based on α-TOS with precise control over the macromolecular architecture has not been achieved. For this reason, the goal of this work was the preparation of new amphiphilic nanoassemblies as drug delivery systems of α-TOS using PEG as a hydrophilic domain, PMTOS as hydrophobic block, and using RAFT as a polymerization method enabling the preparation of defined block copolymers (**figure 1**).

The selection of PEG as hydrophilic macromolecule was based on its biocompatibility and non-toxicity and its capacity to create a hydrophilic shell that can improve the accumulation of NPs into the tumor tissues by the enhanced permeation and retention effect. This effect is only feasible with the use of an appropriate MW of PEG, higher than 3 kDa that enhances the stealth character of NPs, avoiding the RES system[33, 39].

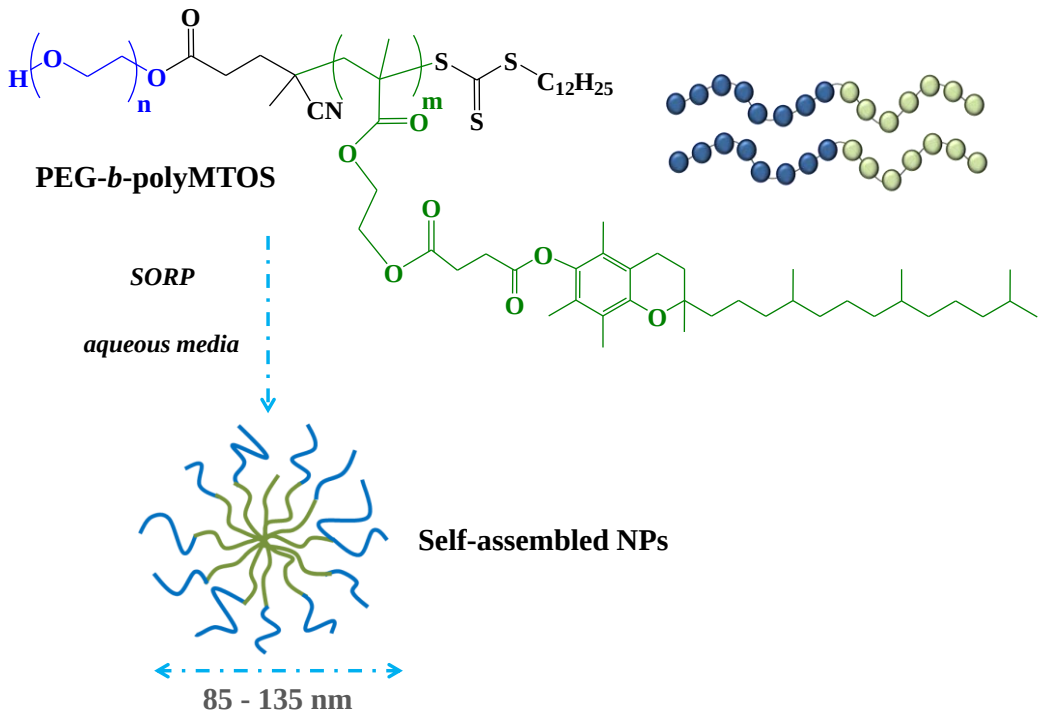

Figure 1: Chemical structure of PEG-*b*-polyMTOS. Scheme of the self-assembled NPs formation based on these block copolymers, prepared by SORP or solvent exchange.

In this sense, the effect of PEG block length was studied by the preparation of PEG based chain transfer agents (PEG macro-CTA agents) with different MWs (between 4.6 and 20 kDa). The RAFT polymerization of MTOS with these different PEG macro-CTA agents allowed the incorporation of a controlled number of units of its active drug into the macromolecular chains. The formation of self-assembled NPs by self-organized precipitation (SORP) was also investigated with the complete characterization of their physico-chemical properties. The anticancer activity of MTOS based NPs were examined against breast cancer cells (**figure 1**).

4.1.3. Materials and methods

- **Materials**

Poly(ethylene glycol) (PEG, number average MW (M_n) between 4.6 and 20 kDa, Sigma-Aldrich), 4-cyano-4-[(dodecylsulfanylthiocarbonyl)sulfanyl]pentanoic acid (CTA, Sigma-Aldrich), *N*-(3-dimethylaminopropyl)-*N'*-ethylcarbodiimide hydrochloride (EDC, Sigma-Aldrich), 4-dimethylaminopyridine (DMAP, Sigma-Aldrich), $MgSO_4$ anhydrous (Qemical), dichloromethane (CH_2Cl_2, Sigma-Aldrich), hexane (SDS) and diethylether (SDS) were used without further purification in the preparation of different macro-chain transfer agent (CTA). 2,2'-Azobisisobutyronitrile (AIBN, Merck) was recrystallized from methanol (m.p. 104 ºC) before use. Deuterated chloroform ($CDCl_3$, Sigma-Aldrich) and chromatographic grade tetrahydrofuran (THF, Sigma-Aldrich) were used without further purification to characterize polymeric systems. Additionally, sodium chloride (NaCl, Panreac) and coumarin-6 (c6, Sigma-Aldrich) were used without further purification.

- **Characterization techniques**

^{1}H-NMR and ^{13}C-NMR spectroscopy was performed on a Mercury 400BB apparatus, operating at 400 and 100 MHz, respectively. The spectra were recorded by dissolving the corresponding sample in $CDCl_3$ at 25 ºC. Fourier transform infrared attenuated total reflectance (ATR-FTIR) spectroscopy was performed on a Perkin Elmer Spectrum One FTIR spectrometer using 32 scans, and a resolution of 4 cm^{-1}.Thermogravimetric analysis was performed using a TGA Q500 apparatus (TA instruments), under dynamic nitrogen atmosphere at a heating rate of 10 ºC/min in a range of 25–600 ºC with the aim to study the thermal stability of the polymeric systems. The number and weight average MW (M_n and M_w) and dispersity ($Đ$) of all the polymers were determined by size exclusion chromatography (SEC) using a Perkin-Elmer Isocratic LC pump 250 coupled to a refraction index detector (Series 200). Three polystyrene-divinyl benzene columns (PLgel, Varian, Polymer Laboratories) of average pore size of 10^3, 10^4 and 10^5 Å were used as the solid phase, and degassed THF (1 mL/min) was used as the eluent at 40ºC. Monodisperse poly(methyl methacrylate) (PMMA) standards (Scharlab) with MWs between 10.3 and 1,400 kDa were used to obtain the calibration curve. Data were analyzed using the Perkin-Elmer LC solution program.

- **Preparation of block copolymers by RAFT polymerization**

Synthesis of the methacrylic derivative of the α-tocopheryl succinate (MTOS)

MTOS was obtained as previously described[38]. *N,N'*-dicyclohexylcarbodiimide (DCC,1.5 equivalent) in CH_2Cl_2 was added dropwise to a solution of α-tocopherol (α-TOH, 1 equivalent), mono-(2-(methacryloyloxy)ethyl) succinate (MES, 1.4 equivalent) and DMAP (0.1 equivalent) in CH_2Cl_2. The reaction was stirred for 24 h under nitrogen atmosphere at room temperature. The reaction mixture was washed with NaOH (1N) and HCl (1N), dried over $MgSO_4$ and the solvent was removed under reduced pressure.

Synthesis of PEG macro-CTA agents

The modification of the commercial 4-cyano-4-[(dodecylsulfanylthiocarbonyl)sulfanyl]pentanoic acid CTA was performed by EDC coupling in order to incorporate PEG of different MWs between 4.6 and 20 kDa. For this purpose, diverse PEG (1 eq) and CTA (1.2 eq) were dissolved in CH_2Cl_2 and introduced into a 250 mL round-bottom flask. Additionally, EDC (1.5 eq) and DMAP (0.12 eq) in CH_2Cl_2 were then added dropwise with constant stirring using an ice bath under a nitrogen atmosphere. Afterwards, the reaction mixture was stirred for 24 h at room temperature.

The reaction mixture was washed with MilliQ water and the solvent was removed under reduced pressure. The resulting product was resolved in the minimal volume of CH_2Cl_2 and precipitated in a cold mixture of hexane and diethylether (50:50 v:v). After drying over $MgSO_4$, the residual solvent was removed under reduced pressure until constant weight. The yield of the reaction was 90%. The chemical structure of the different PEG macro-CTA agents was elucidated by NMR spectroscopy.

^{1}H-NMR spectrum (400 MHz, $CDCl_3$): δ_H 4.25 (t, *J* = 4.8 Hz, 2H), 3.72 (t, *J* = 4.8 Hz, 2H), 3.64 (s, 749H), 3.32 (t, *J* = 7.5 Hz, 2H), 2.65 (m, 2H), 2.52 (m, 1H), 2.37 (m, 1H), 1.87 (s, 3H), 1.68 (quint, *J* = 7 Hz, 2H), 1.39 ((quint, *J* = 7.6 Hz, 2H), 1.33-1.21 (m, 16H), 0.87 (t, *J* = 7 Hz, 3H) ppm.

^{13}C-NMR spectrum (100 MHz, $CDCl_3$): δ_C 171.6, 119.2, 77.5, 72.7, 71.9, 70.7, 70.5, 70.3, 69.6, 69.1, 46.5, 37.2, 34.0, 32.1, 29.9, 29.8, 29.7, 29.6, 29.2, 29.1, 27.9, 25.0, 22.9, 14.3 ppm.

ATR-FTIR spectrum (cm^{-1}): υ = 2950, 2884, 2803, 2744, 2695, 2167, 1973, 1740, 1467, 1414, 1360, 1342, 1279, 1242, 1146, 1101, 1060, 961, 952, 842 cm^{-1}.

RAFT polymerization

Block copolymers based on MTOS and different PEG-macro CTA agents were synthesized by RAFT polymerization. Particularly, PEG-macro CTA agent, MTOS, AIBN and anhydrous 1,4-dioxane were sealed in a 25 mL Schlenk tube. The reaction mixture was degassed by three freeze-pump-thaw cycles and heated in an oil bath at 70 ^{o}C under magnetic stirring. The total monomer concentration [M], the reaction time and the feed molar ratio [MTOS]:[CTA]:[AIBN] were varied as a function of the PEG-macro CTA used for the copolymerization of MTOS (**table S1,** see supporting information). For the kinetic investigations, samples (250 µL) were taken from the polymerization mixture after different reaction times (30, 60, 90, 120, 180, 300 and 360 min). These samples were cooled and characterized using SEC and ^{1}H-NMR spectroscopy.

When the reaction time had elapsed, block copolymers were purified by dialysis (Spectrum Laboratories, 25 kDa MW cut-off) against a mixture of THF and water (50:50 v:v) that was gradually replaced by distilled water over three days in order to remove the residual unreacted monomers and low MW species. The resulting solutions were isolated by freeze-drying to yield white amorphous powders. The conversion and chemical structure of block copolymers were elucidated by NMR spectroscopy using MestreNova 9.0 software.

^{1}H-NMR spectrum (400 MHz, $CDCl_3$): δ_H 4.46-3.88 (2xbs, 4H), 3.64 (s, 753 H) 2.89 (bs, 2H), 2.83-2.63 (bs, 2H), 2.54 (bs, sH), 2.10-1.90(3xs, 9H), 1.84-1.62 (m, 3H), 1.62-0.97 (m, 23H), 0.95-0.78 ppm (m, 12H).

^{13}C-NMR spectrum (100 MHz, $CDCl_3$): δ_C 172.1, 171.2, 171.1, 149.6, 140.7, 136.1, 126.9, 126.3, 125.2, 123.2, 123.1, 117.6, 117.5, 77.5, 75.2, 70.8, 62.5, 45.1, 39.6, 37.6, 37.5, 33.0, 32.9, 31.3, 29.0, 28.2, 25.0, 24.7, 23.0, 22.9, 21.3, 20.8, 20.0, 19.9, 13.1, 12.3, 12.0 ppm.

ATR-FTIR spectrum (cm^{-1}): υ = 2954, 2927, 2899, 2871, 1737, 1666, 1581, 1521, 1461, 1411, 1379, 1364, 1344, 1313, 1280, 1247, 1203, 1145, 1109, 1062, 996, 964, 944, 922, 863, 845, 818, 749, 681 cm^{-1}.

- **NP formation by SORP**

Surfactant-free NPs were prepared by SORP[40] or solvent exchange. Specifically, block copolymers were dissolved in 1,4-dioxane at 10 mg/mL. Additionally, an aqueous solution of NaCl (100 mM) was incorporated drop by drop over the organic phase under constant magnetic stirring to obtain a final polymer concentration of 5 mg/mL. c6 (1% w/w respect to the polymer) was also added to the organic phase in order to prepare NPs that entrapped this hydrophobic molecule in their inner core. After the precipitation, milky NP dispersions were dialyzed against NaCl for 72 h in order to remove organic solvents and unloaded c6. Afterwards, each NP suspension was sterilized by filtration through 0.22 μM polyethersulfone membranes (PES, Millipore Express®, Millex GP) and stored at 4 ºC.

The encapsulation efficiency (EE) of c6 was measured by fluorescence spectroscopy. For this purpose, NPs were freeze dried and dissolved in ethanol (2 mg/mL) and their fluorescence was measured ($\lambda_{excitation}$ = 485 nm and $\lambda_{emission}$ = 528 nm) using a Biotek SYNERGY-HT plate reader. The fluorescence intensity was correlated with c6 concentration using a calibration curve at c6 concentrations between 0.5 and 0.001 mg/mL in ethanol.

Morphology, particle size distribution and zeta potential

The morphology of NPs was analyzed by scanning electron microscopy (SEM) using a Hitachi SU8000 TED, cold-emission FE-SEM microscope working with an accelerating voltage between 25 and 50 kV. Samples were prepared by deposition of one drop of the corresponding NP suspension (0.05 mg/mL) over small glass disks. The aqueous phase was evaporated at room temperature for 24 h. The samples were coated with gold palladium alloy (80:20) prior to examination by SEM.

For AFM examination, a drop of NP dispersion was deposited on the surface of small glass disks and dried overnight at room temperature. AFM was performed in tapping mode using a Multimode AFM (Veeco Instruments, Santa Barbara, CA, USA) with a Nanoscope IVa control system (software version 6.14r1), equipped with silicon tapping probes (RTESP, Veeco) with a spring constant of 42 N/m and a resonance frequency of 300 KHz and a scan rate of 0.5 Hz.

The particle size distribution of the self-assembled NPs was determined by dynamic light scattering (DLS) using a Malvern Nanosizer NanoZS Instrument equipped with a

4mW He-Ne laser (λ=633 nm) at a scattering angle of 173°. Measurements of NP dispersions were performed in square polystyrene cuvettes (SARSTEDT) at 25 ºC. The autocorrelation function was converted into an intensity particle size distribution with ZetaSizer Software 7.10 version, to get the mean hydrodynamic diameter (D_h, by intensity) and the polydispersity index (PDI) between 0 (monodisperse particles) and 1 (polydisperse particles) based on the Stokes-Einstein equation. The zeta potential was determined for NP formulations at 0.5 mg/mL concentration containing 10 mM NaCl using laser Dopper electrophoresis (LDE). The zeta potentials were automatically calculated from the electrophoretic mobility using the Smoluchowski´s approximation. For each sample, the statistical average and standard deviation of data were calculated from 8 measurements of 20 runs each one.

- **Biological experiments**

Cell culture

Human metastatic carcinoma cells, MDA-MB-453 cells (ATCC), were cultured in Dulbecco's modified Eagle's medium (DMEM), supplemented with 10% fetal bovine serum (FBS), 1% penicillin/streptomycin (P/S) and incubated at 37°C and 5% CO_2.

Cellular uptake study: monitoring of coumarin-6 loaded NPs

MDA-MB-453 cells were seeded into 6-well plate at 200,000 cells/mL in complete medium and incubated at 37 ºC for 48 h. Afterwards, the monolayer was washed with culture medium and subsequently incubated with the corresponding c6 entrapped NPs dispersed in NaCl (1000 µL of the NP suspension and 1000 µL of completed medium) at 37 ºC. At different time points (30 min, 1, 2, 4, 6 and 8 h) , NPs were removed and cells were washed four times with PBS in order to efficiently remove non-endocytosed NPs by cells. Then, the cells were trypsinized (0.5 mL of Trysin-EDTA per well), centrifuged (10 min, 1500 rpm) and lysed with 0.4 mL of ethanol at room temperature. The c6 concentration in the cell lysate was quantified by using a fluorescence plate reader ($\lambda_{excitation}$ = 485 nm and $\lambda_{emission}$ = 528 nm). The cellular uptake was normalized to the total amount of cells for each sample.

The endocytosis of NPs was also visualized using a fluorescent EVOS® FL microscopy at the different experimental points. Particularly, the cells were fixed by a

paraformaldehyde solution in PBS (3.7 w/v %) for 15 min at room temperature. In the same manner, cells were observed by Confocal Laser Scanning Microscopy (CLSM, LSM 710, Zeiss) after 4 h of NP treatment.

In vitro cytotoxicity assay

Cell viability in the presence of different concentrations of NPs (2.5, 1.25, 0.63, 0.31 and 0.16 mg/mL) was measured using Alamar Blue assay (Sigma-Aldrich) [41]. Briefly, MDA-MB-453 cells were seeded at 35,000 cells/mL (17,500 cells/well) in 24-well plates. After 24 h of incubation, the medium was replaced with the corresponding NPs dispersed in NaCl (50:50 v/v of the NP suspension and completed medium). The plates were incubated at 37°C under humidified air with 5% CO_2 for 24 h. Afterwards, 100 µL of Alamar Blue solution (10 % Alamar Blue solution in phenol red free DMEM medium) was added to all wells. After 4 h of incubation, the fluorescence was measured on a Biotek SYNERGY-HT plate reader ($\lambda_{excitation}$ = 530 nm and $\lambda_{emission}$ = 590 nm).

Statistical analysis

Results were expressed as mean ± standard deviation. Statistical significance (significance level of: *: $p < 0.05$) was evaluated using the analysis of variance (ANOVA, Tukey test) as required, by Origin 9.

4.1.4. Results and discussion

- **PEG macro-CTA agents**

RAFT polymerization is one of the most attractive and effective technique to synthesize well-defined polymers and therefore to prepare amphiphilic block copolymers with a precise control of their macromolecular nature[13]. This type of radical polymerization involves a chain transfer agent (CTA) that is commonly formed by a thiocarbonylthio moiety in order to exhaustively control the uniform chain growth, the generated MWs of macromolecular chains and their dispersity. In fact, the selection of the most appropriate chain transfer agent is the key to reach an excellent control during the polymerization[12, 13, 42]. In particular, 4-cyano-4-[(dodecylsulfanylthiocarbonyl)sulfanyl]pentanoic acid was selected for the polymerization of MTOS due to the presence of a carboxylic end group that facilitates the conjugation of PEG to obtain a hydrophilic macro-CTA agent and its suitability to control the polymerization of methacrylic monomers[43].

PEG was selected as the hydrophilic block because it is a water soluble, hydrophilic and biocompatible polymer that can reduce the adhesion of opsonins, avoiding the NP recognition by the RES and increasing the blood circulation half-life of polymeric NPs. Furthermore, PEG can be easily functionalized with different ligands for targeted drug delivery[44, 45]. Five different PEG macro-CTA agents were successfully synthesized under mild conditions by EDC coupling of PEG to the CTA, obtaining pure products after their purification. In fact, the synthesis of similar PEG based macro-CTA agents was previously reported in the literature[46, 47]. Particularly, EDC is one of the most widely used coupling agents to conjugate a carboxylic acid to an alcohol, using DMAP as a catalyst. Specifically, the esterification involves the activation of carboxylic acid by EDC which forms an O-acylisourea intermediate. The most important advantage of EDC over other coupling agents like DCC is that the urea sub-product is readily soluble in water and can easily be removed by extraction, facilitating the purification of the final product[48-50].

The MW of PEG was varied between 4.6 and 20 kDa in order to change the length of this hydrophilic block and to analyse its influence on the physico-chemical properties of the polymeric systems and to change the hydrophilic/hydrophobic balance of the block copolymers. The MWs of the PEG blocks were lower than 30 kDa, and therefore they can be cleared from the body through renal filtration[51]. Moreover, the MW is a critical factor to

control the stealth properties of self-assembled systems, as will be described in the next sections. In this sense, the capacity to create a high-density of PEG chains on the surface of the NPs is diminished when its MW is lower than 3 kDa.

The esterification of the commercial RAFT agent was confirmed using ^{1}H-NMR spectroscopy by the appearance of the methylene protons of the PEG chains (CH_2-a at 4.2 ppm and CH_2-b-d between 3.35 and 3.85 ppm) (**figure S1,** see supporting information). The synthesized PEG macro-CTA agents were labelled as CTA-PEG and their MWs (kDa) were determined by ^{1}H-NMR spectroscopy.

Results of number average MW (M_n), dispersity (***Đ)*** and the number of PEG units (nPEG) are summarized in **table S2** (see supporting information). nPEG was quantitatively calculated by ^{1}H-NMR spectra by considering the signals between 3.30-3.85 ppm assigned to 4 protons of PEG backbone chains (CH_2-a, CH_2-b) and the signal at 0.81 ppm which is due to 3 protons of CTA (CH_3-19). In all PEG macro-CTA agents, *Đ* values were less than 1.20 and SEC traces evidenced that the esterification allowed us to obtain monomodal and narrow MW distributions of the hydrophilic macro-CTA agents. All traces were shifted to lower elution times in comparison to the commercial PEG after their esterification. Additionally, SEC traces of different PEG macro-CTA agents showed tailing peaks at lower MW areas that are attributed to the original PEG (**figure S2**, see supporting information).

Thermal degradation curves of different PEG macro-CTA agents showed a single weight loss step at temperatures ranging from 320 to 440 ºC. The thermal decomposition rate presented a maximum around 400ºC that slightly increased with the MW of PEG block (**figure S3**, see Supporting Information).

- **Synthesis of block copolymers PEG-*b*-polyMTOS**

The RAFT polymerization of MTOS was successfully performed with the synthesized PEG macro-CTA agents and AIBN as the radical initiator, using the conditions that were previously summarized in **table S1** (see supporting information). All copolymerizations were performed at 70ºC in anhydrous dioxane. The total molar concentration (M), ratio [MTOS]:[CTA]:[AIBN], and copolymerization time were optimized in order to control the polymerization reaction and avoid undesired termination reactions during the chain growth[52].

In order to prevent the gelation of the reaction product due to significant increase of the reaction medium viscosity, the total MTOS concentration was reduced as the MW of the PEG macro-CTA increased (0.5 M for CTA-PEG_5, CTA-PEG_8, CTA-PEG_{10} and 0.25 M for CTA-PEG_{12} and CTA-PEG_{22}). Additionally, the concentration of AIBN was increased for the polymerizations of the highest PEG MW (CTA-PEG_{12} and CTA-PEG_{22}) in order to counteract the effect of the reduction of the total MTOS concentration, avoiding prolonged reaction times. Finally, the copolymerizations were stopped at the reaction time that allowed to maintain a linear kinetic of the reaction with an optimal *Đ*, as will be demonstrated in the following sections.

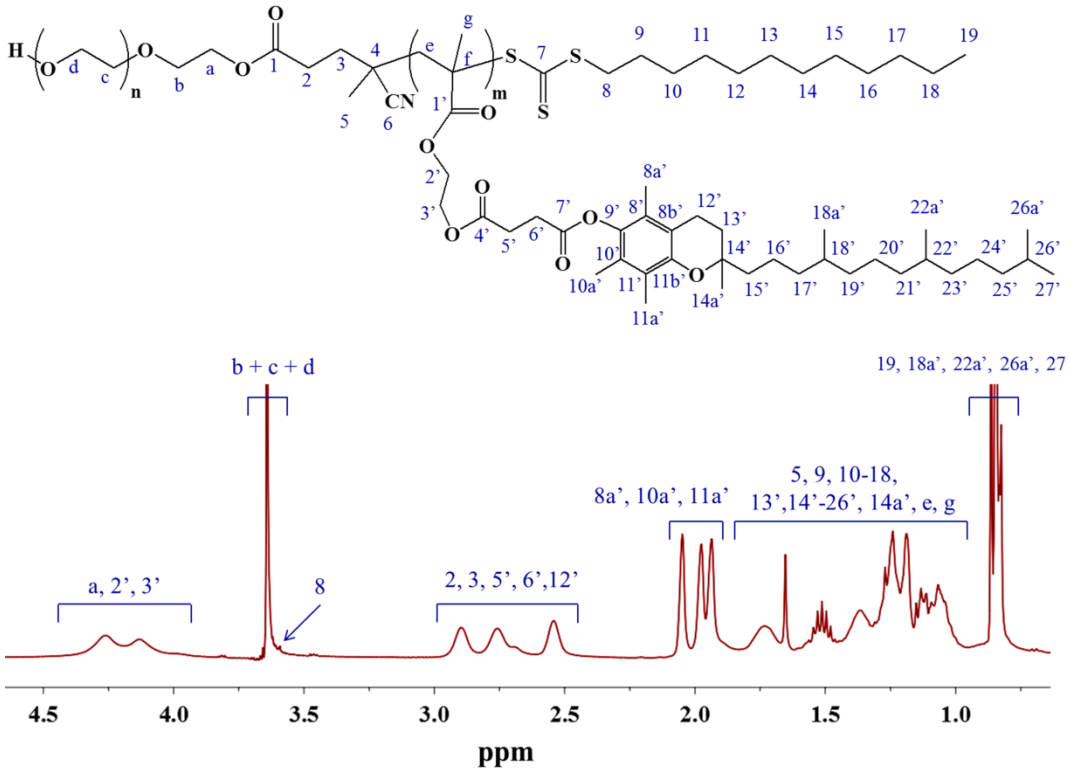

Figure 2: ^{1}H-NMR spectrum of PEG-71.

Polymerization of the MTOS was confirmed using ^{1}H-NMR spectroscopy by the disappearance of the vinyl protons of MTOS between 5.5 and 6.5 ppm and the broadening of the signals as a result of the macromolecular nature of the synthesized block polymers (**figure 2**). Additionally, other characteristic proton signals of MTOS could be appropriately assigned, confirming the presence of its chemical structure in the backbone of the copolymeric systems.

Kinetics of RAFT polymerizations

The polymerization kinetics of MTOS with PEG macro-CTAs were investigated by analyzing the aliquots withdrawn from the polymerization mixture at different reaction times. Specifically, samples were analyzed by SEC and ^{1}H-NMR spectroscopy in order to quantify the MW and the *Đ* and to determine MTOS monomer conversion, respectively. Specifically, the conversion of MTOS was calculated by considering the vinyl proton signal at 6.1 ppm that disappeared over reaction time and the signal at 0.8 ppm corresponding to 12 protons of MTOS that did not change during the polymerization reaction (**figure S4**, see supporting information).

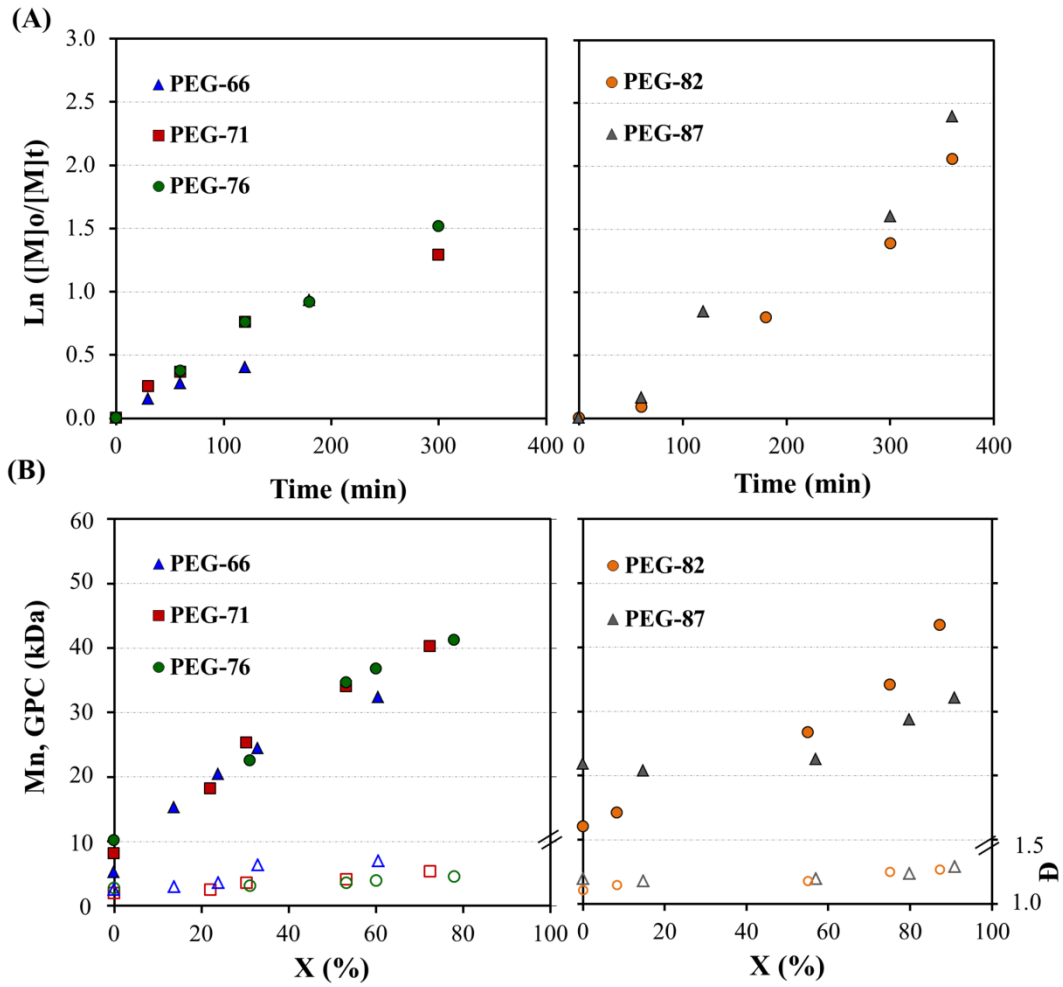

Figure 3: Kinetics of polymerization of PEG-*b*-polyMTOS copolymers. (A) Ln($[M]_o/[M]_t$) plotted against reaction time and (B) M_n and *Đ* values as a function of MTOS conversion for PEG-66 (blue), PEG-71 (red), PEG-76 (green), PEG-82 (orange) and PEG-87 (grey) amphiphilic block copolymers.

Figure 3 shows the polymerization kinetics of all synthesized block copolymers. In all cases, the evolution of Ln($[M]_0/[M]_t$) as the function of time revealed a linear first order kinetic dependence, indicating a constant free radical concentration and, thus, the absence of significant termination reactions. Additionally, the linear increase of M_n with conversion demonstrated an appropriate control over the polymerization of MTOS[12].

In the case of the MTOS polymerization with CTA-PEG_{5-10}, the ratio [MTOS]:[CTA]:[AIBN] was maintained constant and, therefore, the concentration of radicals was not varied. Polymerization rates did not correlate with the PEG MW and depended on the concentration of free radicals as expected.

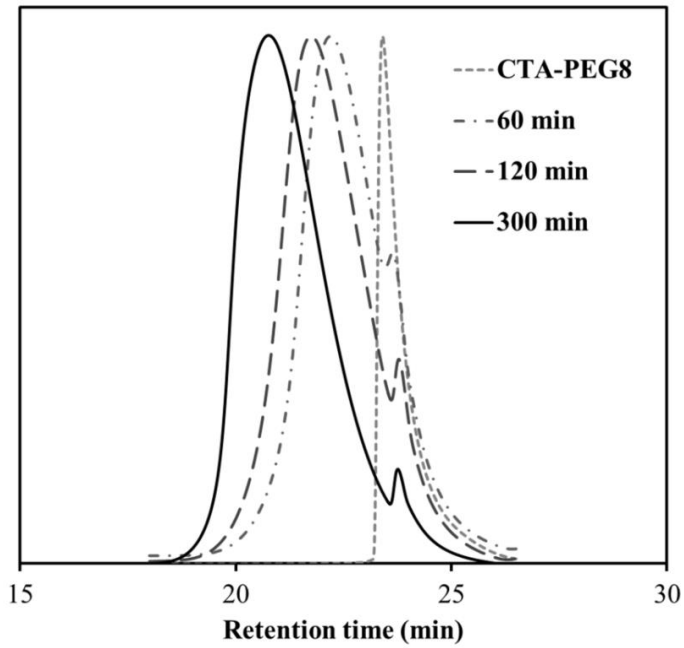

Figure 4: SEC traces as a function of a time polymerization of MTOS using CTA-PEG_8.

The monomer concentration (*M*) was reduced when using macro-CTA agents with the highest MW of PEG (CTA-PEG_{12-22}). The polymerization should not be affected by changing this monomer concentration. However, the polymerization volume significantly increased and thus, the radical concentration decreased, leading to a reduction in polymerization rate. For this reason, the ratio [MTOS]:[CTA]:[AIBN] was changed, increasing the concentration of AIBN. This modification enhanced the polymerization rate in spite of the reduction of monomer concentration, avoiding the gelation of reaction product.

An example of the evolution of SEC traces during the RAFT polymerization is included in **figure 4**. The traces were clearly shifted at lower elution times in comparison to the PEG macro-CTA agent as a function of the progression of the MTOS polymerization. Additionally, the SEC curves were bimodal indicating the presence of a minor fraction of unreacted PEG macro-CTA. This behavior is commonly observed for this type of polymerization, indicating that the efficiency of macro CTA agents was not complete[53, 54]. Finally, it is noteworthy that no high MW species were observed at low retention times, confirming the absence of chain coupling reactions and the appropriate control over the RAFT polymerization. The MW distributions were narrow as demonstrated by the relatively low dispersity ($Đ < 1.35$).

Characterization of block copolymers

Block copolymers were exhaustively characterized after their purification by dialysis, that effectively eliminated the unreacted MTOS as a result of the non-full conversion reached and the majority of low MW chains of the unreacted PEG macro-CTA agents. **Table 1** summarizes the most relevant characteristics of the prepared copolymers.

The composition of the different block copolymers was calculated based on ^{1}H-NMR spectroscopy, using the integrals of the signals between 3.55 and 3.75 ppm assigned to 4 protons of PEG (CH-e', CH_2-4''') and the signal between 1.84 and 2.2 ppm (CH_3-8a', CH_3-10a', CH_3-11a') corresponding to 9 protons of MTOS (**figure S4**, see supporting information).

The MTOS molar composition significantly decreased with increasing PEG MW, varying between 13 and 34 %-mol. This variable will be crucial to explain the amphiphilic properties of polymeric systems and their capacity to self-assembly in aqueous media, as will be described in the following sections. Additionally, the MWs of block copolymers (calculated based on ^{1}H-NMR spectroscopy) were slightly lower in comparison to the theoretical values, being more pronounced with the increment of PEG MW of the macro CTA agents. This difference can be explained based on the reduction of the efficiency of macro RAFT agents as a function of PEG MW. In fact, the SEC traces of different copolymerization reactions before their purification revealed that the narrow peak at a high retention time, associated with the PEG macro-CTA, significantly increased with the number of PEG units in the macro RAFT agents (**figure S5**, see supporting information). In

the case of PEG-82, this peak overlaps with the peak of the block copolymer due to its high MW. After the purification of block copolymers, unreacted PEG macro-CTA concentrations are very low and their incorporation in the self-assembling process of amphiphilic macromolecules will be not favored.

Table 1: Summary of the most relevant structural characteristics of PEG-*b*-polyMTOS amphiphilic copolymers.

Sample	**CTA-PEG**	**[a] M_n x 10^{-3}**	**[b] $M_{n\ theo}$ x 10^{-3}**	**[c] $M_{n\ SEC}$ x 10^{-3}**	**[c] $Đ$**	**[a] n_{PEG}**	**[a] m_{MTOS}**	**f_{PEG}-f_{MTOS} (mol %)**	**[d] T_{max} (ºC)**
PEG-66	CTA-PEG_5	42.9	44.4	38.8	1.35	111	58	66-34	381
PEG-71	CTA-PEG_8	54.3	54.4	48.4	1.27	177	73	71-29	394
PEG-76	CTA-PEG_{10}	55.6	60.3	51.8	1.23	223	71	76-24	392
PEG-82	CTA-PEG_{12}	59.5	67.9	50.5	1.27	266	56	82-18	404
PEG-87	CTA-PEG_{22}	68.5	80.2	37.7	1.29	487	73	87-13	403

a) Determinated using ^{1}H-NMR spectroscopy.

b) Calculated applying the equation $M_{ntheo} = ([MTOS]/[CTA]*X_{MTOS}*100*MW_{MTOS}) + MW_{CTA}$.

c) Determinated by SEC (THF) using PMMA standards.

d) Measured by TGA under nitrogen atmosphere.

Results of M_n and $Đ$ calculated by SEC are also shown in **table 1**. It is noteworthy that these values were significantly lower than those obtained theoretically or by ^{1}H NMR spectroscopy. In this case, this deviation is most likely due to the PMMA calibration curve that was used to quantify the SEC measurements. Furthermore, $Đ$ values were lower than 1.35, confirming the good control of the polymerization, obtaining well-defined amphiphilic block copolymers.

The thermal stabilities of block copolymers were investigated by TGA under a nitrogen atmosphere. The TGA curves of different block copolymers are compared in **figure S6** (see supporting information). The weight-loss rate of all block copolymers presented a maximum between 380 and 403 ºC that increased with the content of PEG in the copolymers. Moreover, these values were lower in comparison to the maximum degradation temperatures of PEG macro RAFT agents due to the incorporation of MTOS.

In fact, TGA curves presented a shoulder at the temperature range from 300 to 350 ^{o}C that significantly increased with the MTOS content.

- **Characterization of self-assembled NPs**

Amphiphilic block copolymers are excellent candidates for the preparation of micellar drug nanocarriers. Particularly, PEG-*b*-poly(MTOS) family presented a precise architecture with two well-defined hydrophilic and hydrophobic blocks. The appropriate hydrophilic/hydrophobic balance of these macromolecules will give rise to the self-organization of these polymer chains in aqueous media[7, 55, 56]. In the following sections, self-assembled NPs will be appointed as a function of the PEG molar composition in the polymeric systems. As an example, NPs prepared from PEG-71 will be labelled as NP-71.

Surfactant-free NPs were prepared by SORP or solvent exchange. This procedure has advantages in comparison to other alternatives, such as the conventional nanoprecipitation. SORP can be used for a wide type of polymeric materials, such as block copolymers, in order to obtain particles from nanometers to a micrometer scale. This simple methodology allows the progressive organization of amphiphilic chains due to the slow addition of aqueous phase drop to drop, avoiding the use of surfactants or protective colloids[40, 57, 58].

The morphology of self-assembled NPs was confirmed by SEM and AFM. Representative micrographs of NP-71 are shown in **figure 5**. These images confirmed the spherical morphology of NPs. The amphiphilic NPs had a typical core-shell morphology with a MTOS hydrophobic core that was stabilized by a hydrophilic shell based on PEG chains.

Results of the most relevant characteristic of unloaded NPs are summarized in **table 2**. The preparation of stable NPs could not be achieved using the PEG-66 polymeric system, due to an unsuitable hydrophobic/ hydrophilic balance.

In the other copolymeric systems, the particle size varied between 88 and 135 nm with optimal values of PDI, below 0.1. Additionally, particle size distributions were narrow and unimodal with a width less than 50 nm for all compositions (**figure 5C**). These results confirmed that the controlled polymerization of MTOS with a PEG-based hydrophilic block favoured the self-assembly of the macromolecular chains in aqueous media, obtaining defined NP sizes that are suitable for their application in cancer treatments, improving their

endocytosis and accumulation in tumor tissues by the Enhanced Permeability and Retention Effect (EPR)[59, 60].

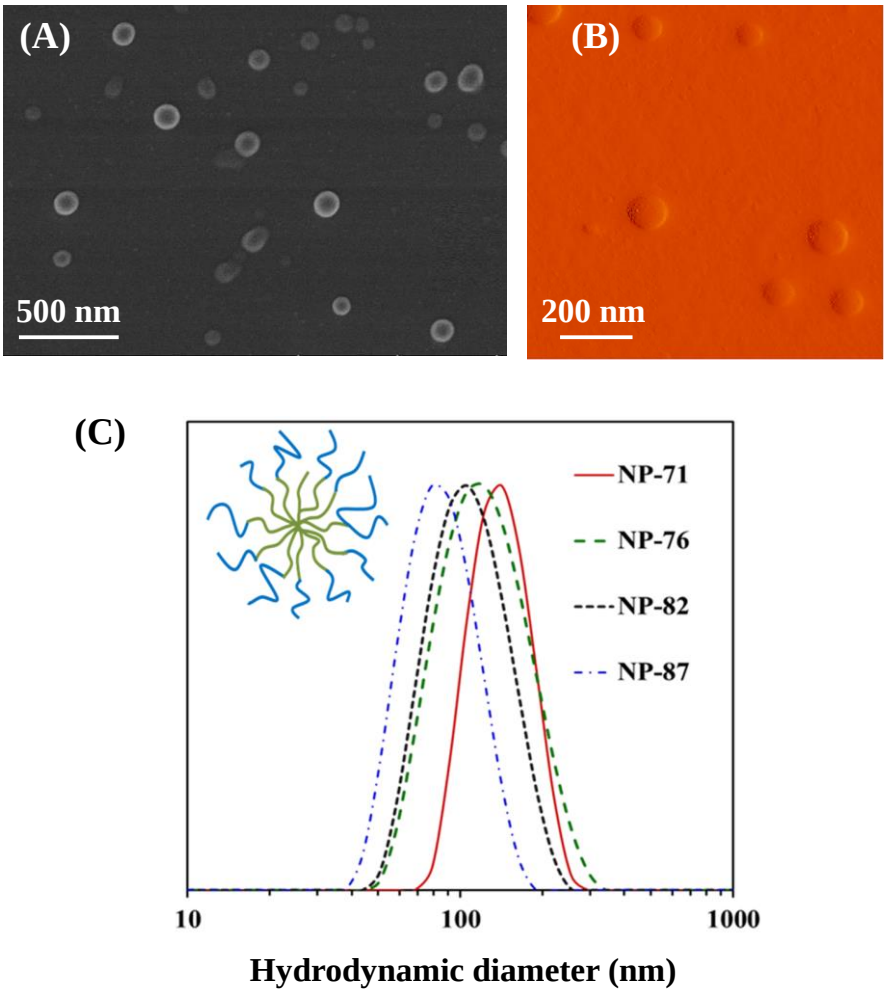

Figure 5: SEM (A) and AFM (B) micrographs of NP-71 polymeric systems dried from aqueous solution at room temperature. (C) Particle size distributions (D_h, by intensity) of unloaded NP, measured by DLS. Red: NP-71; green: NP-76; black: NP-82; blue: NP-87.

It is noteworthy that the hydrodynamic diameter of NPs decreased with increasing PEG content in the copolymeric systems. This trend could be explained due to the presence of PEG in the external shell of NP that could stabilize them through inter- and intramolecular interactions[61, 62]. In fact, it is well-known that PEG can also form hydrogen bonds in the aqueous environment and its presence also has multiple advantages such as the effective protection of NPs against hydrolysis or enzymatic degradation and the prevention of their recognition by RES[63, 64].

Table 2: Most relevant characteristics of unloaded and c6 loaded NPs: Hydrodynamic diameter (D_h, by intensity), size distribution width (W_d), polydispersity index (PDI); and zeta potential values (ζ), measured by DLS and LDE respectively.

NP Sample	EE (%)	D_h (nm)	*W*d (nm)	PDI	ζ (mV)
NP-71	---	134.9 ± 6.5	31	0.079 ± 0.012	-2.38
NP-76	---	110.2 ± 4.3	47	0.101 ± 0.014	-1.08
NP-82	---	100.8 ± 5.8	31	0.087 ± 0.011	-0.68
NP-87	---	87.9 ± 2.6	27	0.079 ± 0.009	-0.16
NP-71 + c6	92.4	159.8 ± 8.8	43	0.079 ± 0.009	-0.68
NP-76 + c6	91.2	156.8 ± 3.3	55	0.056 ± 0.008	-0.60
NP-82 + c6	91.0	133.7 ± 4.4	62	0.044 ± 0.013	-0.51
NP-87 + c6	90.3	90.2 ± 5.7	49	0.080 ± 0.010	-0.44

Additionally, the characteristic of NPs can be regulated as a function of the chemical composition, MW and the block lengths of the amphiphilic copolymers. In this sense, their synthesis by RAFT polymerization facilitates the easy and controlled modification of these different variables. These changes would not be possible if other polymerization techniques had been used, such as conventional radical polymerization. Recently, our group described the preparation of amphiphilic NPs based on MTOS that were copolymerized with VP by free radical polymerization (poly(VP-*co*-MTOS))[38]. In this case, control over the microstructure was only possible due to the different reactivities of the amphiphilic monomers. As a result, NPs presented PDI values higher than 0.1 and higher distribution width in comparison to these block copolymers[38].

The organization of amphiphilic macromolecular chains into nanoassemblies affected the properties of the copolymeric systems. As an example, an interesting comparison of the thermal degradation of PEG-71 and PEG-76 and their corresponding NPs is illustrated in **figure 6**. The normalized curves of the derivative weight loss of both NP systems showed three defined peaks in comparison to the polymeric systems. On the one hand, the degradation peaks corresponding to MTOS and PEG were more defined in the NP systems. On the other hand, a new degradation peak appeared at an intermediate temperature. This

new degradation stage could be due to the interface of these NPs with a core-shell morphology, the formation of inter- and intramolecular interactions that facilitated the stabilization of surfactant-free NP and finally the segregation of PEG and MTOS based domains.

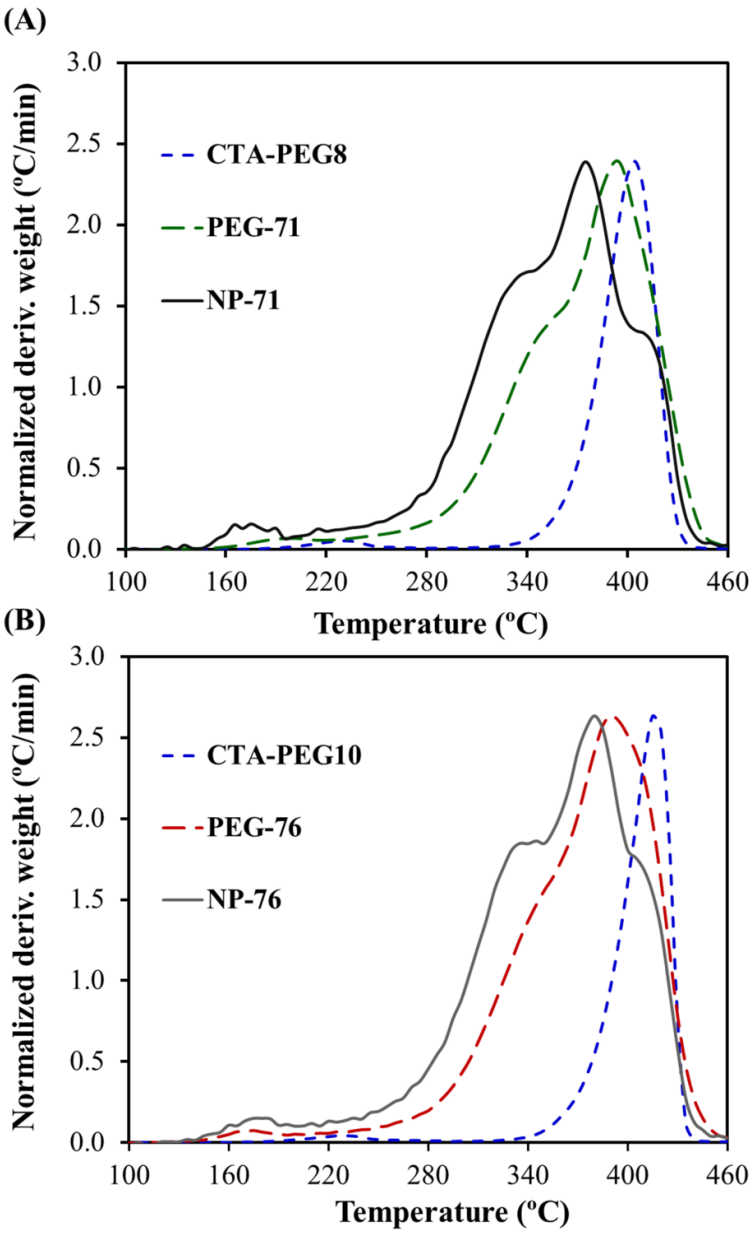

Figure 6: Overlay of normalized curves of derivative weight loss of (A) PEG-71 and (B) PEG-76 polymeric systems and their corresponding self-assembled NPs.

Finally, all NPs had a nearly neutral charge on their surface, exhibiting slightly negative zeta potential values similar to the zeta potential values in the same magnitude order described for other PEG nanoassemblies[65]. Such neutral charge of PEG-based NPs is based on the absence of the charged groups in its structure. Additionally, the neutral charge of NP slightly increased with the increasing of PEG number units into the NP surface.

- **Coumarin-6 monitoring**

The first step towards examining the therapeutic action of self-assembled NPs is characterizing the ability of polymeric systems to cross the cellular membrane of cancer cells in order to exert their biological activity. In this way, c6 was efficiently encapsulated in the core of the NPs (EE higher than 90%) and, thus, was used as a fluorescent probe to trace the NP within cancer cells.

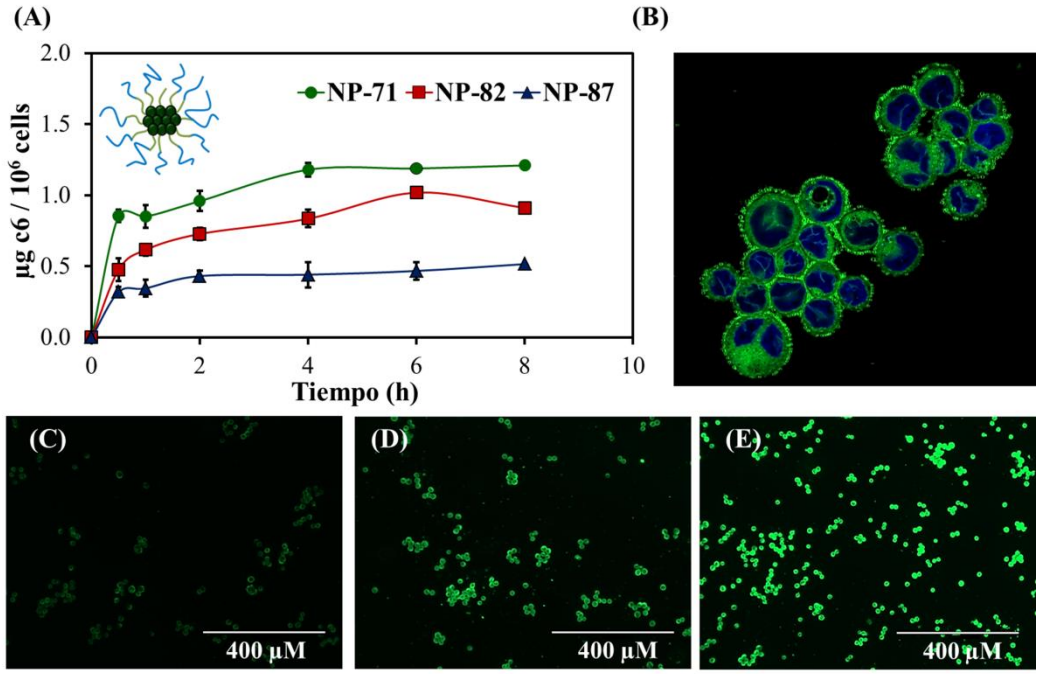

Figure 7: (A) Accumulated uptake of c6 loaded NPs in MDA-MB-453 cells along 8 h after the NP incubation. Green: NP-71; red: NP-82 and blue: NP-87. (B) Confocal micrographs of MDA-MB-453 cells after 5 hours in contact with c6-NP-71. Fluorescent micrographs of MDA-MB-453 cells in 2D culture after 30 min (C), 4 (D) and 8 hours (E) in contact with c6-NP-71.

The green fluorescence of c6 entrapped NPs was quantified in a MDA-MB-453 cell culture for 8 h after the NP incubation, also studying the effect to vary the PEG length into the polymeric NPs. As shown in **figure 7A**, the accumulation of c6 in MDA cells was gradually enhanced over time in all cases. This effect can be appreciated in the increment of fluorescence of the micrographs of cancer cells that were obtained after 30 min, 4 and 8 h in contact with c6-NP-71 using fluorescence microscopy (**figure 7C-E**). Additionally, these fluorescence results demonstrated that the cellular uptake was significantly diminished as a function of PEG composition into the NPs. In fact, the longer the PEG segment the slower the cellular uptake of NPs. This phenomenon is known in the literature as the "PEG dilemma" that significantly decreases the interaction between polymeric NPs and the cell surface membrane and therefore, their therapeutic action, as will be demonstrated in the next section[66, 67]

After 5 h, c6-NP-71 were observed under a confocal microscopy revealing that self-assembled nanoparticles were located inside the cytoplasm of cancer cells around the nucleus, probably by an endocytosis mechanism[68]. Specifically, confocal micrographs (**figure 7B**) allowed us to observe that the cellular membrane of MDA cells was clearly affected as a result of NP treatment.

- **Anticancer activity**

Human epidermal growth factor receptor 2 (HER2) overexpressing breast tumors constitute an aggressive disease subtype that results in poor prognosis[69-71]. HER2 has therefore emerged as a viable molecular target for disease treatment[72, 73]. Resistance to HER2-targeted therapies such as Trastuzumab that has emerged in the recent years[74], however, warrants the development of alternative therapeutic strategies to treat HER2-positive breast cancer.

In vitro biological activity of block copolymer NPs was therefore evaluated against HER2 positive human adenocarcinoma MDA-MB-453 cells. Cell viability was assessed using Alamar Blue. **Figure 8** shows the MDA-MB-453 cell viability after the treatment with different concentrations (between 2.50 and 0.16 mg/mL) of the NPs for 24 h.

In fact, cell viability decreased in a dose-dependent manner as a function of the NP concentration. Particularly, cell viability was reduced to around 60% in those formulations with the highest MTOS content (NP-71 and NP-76 with 29 and 24 mol- % of MTOS in the

block copolymer, respectively) at 2.5 mg/mL. This cytotoxicity was only maintained at this highest NP concentration. Therefore, NP-71 and NP-76 formulations demonstrated anticancer activity in spite of the esterification of terminal carboxylic group of α-TOS that was performed in order to obtain a polymerizable methacrylic monomer. Neuzil et al. previously examined the mechanism of action of this mitocan and found its succinate group to be the functional domain that resulted in cell apoptosis due to increases in ROS within the mitochondria of exposed cells[16].

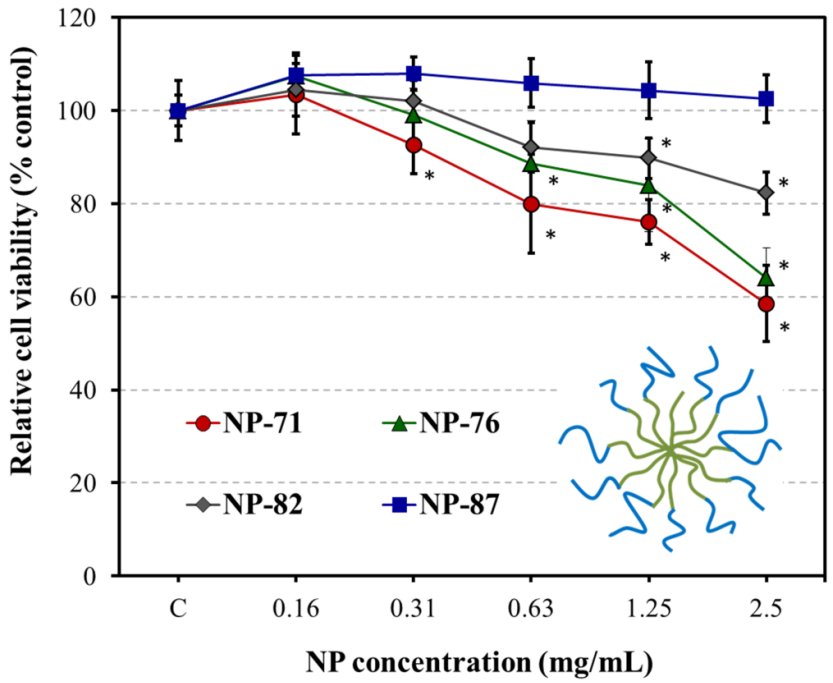

Figure 8: MDA-MB-453 viability in the presence of different NP concentrations, measured after 24 h with respect to the control. The diagrams include the mean, the standard deviation (*n*=8), and the ANOVA results at a significance level of *: $p < 0.05$.

In contrast, NP-82 and NP-87 formulations were not cytotoxic with viabilities higher than 80% for all NP concentrations, in spite of their lower particle size when compared with NP-71 and NP-76. Our group recently described the anticancer activity of MTOS-based NP based on poly(VP-*co*-MTOS) pseudoblock copolymer[38]. The most active NP from this family of copolymer only presented 11 mol% of MTOS in its structure and therefore it was remarkable that PEG-*b*-PMTOS copolymers with higher content on MTOS were less active[38].

As it was previously mentioned, PEG was selected as the hydrophilic block due to its well-known stealth properties that increase the circulation time in blood and its ability to minimize opsonization and resulting immune response. MW, surface chain density and conformation of PEG macromolecules are critical parameters to regulate their stealth properties. Particularly, MWs higher than 2000 are desired to guarantee the flexibility of PEG chains. The surface density directly affects the configuration of PEG chains and their mobility. At a high surface coverage, PEG chains have a brush configuration that completely covers the surface of NPs and in contrast, reduces their mobility. The PEG chains adopt a mushroom configuration at a low surface coverage that can facilitate the presence of gaps where opsonins can bind to the surface[33].

On the other hand, the incorporation of too much PEG prevented cellular uptake by endocytosis due to the PEG dilemma. In this sense, the loss of anticancer activity of synthesized NPs with high PEG MWs (NP-82 and NP-87 formulations) not only depended on the MTOS content, but also on the PEG segment length. These results suggest the importance of an appropriate balance between the escape from the RES system and the controlled cellular uptake of PEGylated NPs, adjusting the MW of PEG chain and the hydrophobic and hydrophilic balance of macromolecular chains into the NPs.

4.1.5. Conclusions

RAFT polymerization was used for the synthesis of amphiphilic block copolymers with controlled molecular weight and relatively low dispersity ($Đ$ < 1.35) using PEG macro-CTAs of different molecular weights to control the radical polymerization of MTOS. Block copolymers PEG-*b*-polyMTOS were obtained after the controlled polymerization of MTOS with appropriate hydrophobic/hydrophilic balances to self-assemble in aqueous media by SORP. Bioactive NPs with unimodal size distributions and sizes between 88 and 135 nm were obtained. These NPs were stable and were endocytosed by cancer cells as demonstrated by the experiments carried out with coumarin-6-loaded NPs. Biological experiments revealed that the anticancer activity of self-assembled NPs significantly enhanced with an increase in MTOS content in the macromolecular chains and the reduction of PEG MW that inhibited the endocytosis of nanoassemblies. Finally, these NPs could encapsulate and deliver hydrophobic drug enabling combined therapy. When decorated with targeting moieties, these therapeutic NP formulations have the potential to exhibit superior cytotoxicity and selective activity in eliminating cancer cells.

4.1.6. Acknowledgements

Authors would like to thank financial support from the Spanish Ministry of Economy and Competitiveness (MAT2010-18155), CIBER BBN-ECO Foundation project, and the National Institutes of Health Cell and Tissue Engineering Training Grant T32 GM008433. Authors also acknowledge, David Gómez, and Rosa Ana Ramírez and Mar Fernández for their help in SEM, and cell culture experiments, respectively. Samarendra Maji gratefully acknowledges FWO for the Pegasus Marie Curie Fellowship.

4.1.7. Supporting information

Table S1: Summary of experimental conditions for the synthesis of block copolymers by RAFT.

M_n PEG (kDa)	Reaction time (min)	M	[MTOS]:[CTA]:[AIBN] (mol. %)
4.6	180	0.5	[100]:[1]:[0.3]
8	300	0.5	[100]:[1]:[0.3]
10	300	0.5	[100]:[1]:[0.3]
14	360	0.25	[100]:[1]:[0.5]
20	360	0.25	[100]:[1]:[0.5]

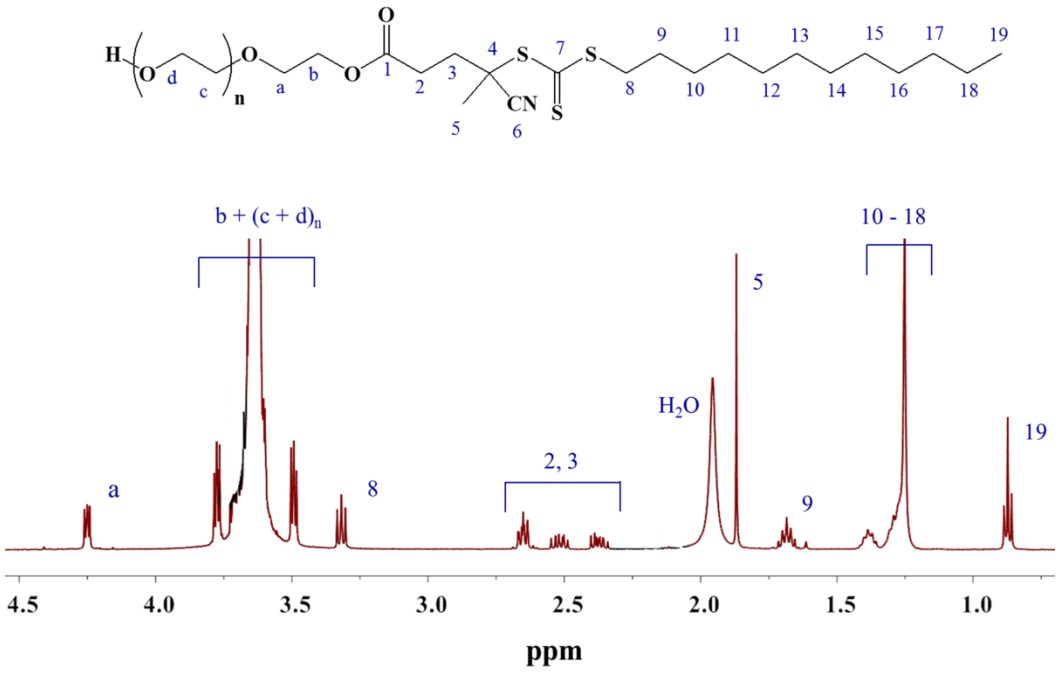

Figure S1: ^{1}H-NMR spectra of CTA-PEG$_8$.

Table S2: Molecular weight (M_n) measured by ^{1}H-NMR and SEC, dispersity ($Đ$), PEG units (n) and T_{max} of synthesized PEG macro-CTA agents.

Sample	$M_n \times 10^{-3}$	**nPEG**	$M_n \times 10^{-3}$	$Đ$	T_{max} (°C)
	^{1}H-NMR		SEC (THF, PMMA standards)		TGA
CTA-PEG$_5$	5.2	111	5.8	1.13	397
CTA-PEG$_8$	8.2	177	9.8	1.10	402
CTA-PEG$_{10}$	10.2	223	11.1	1.14	404
CTA-PEG$_{12}$	12.1	266	12.5	1.11	415
CTA-PEG$_{22}$	21.8	487	16.8	1.20	418

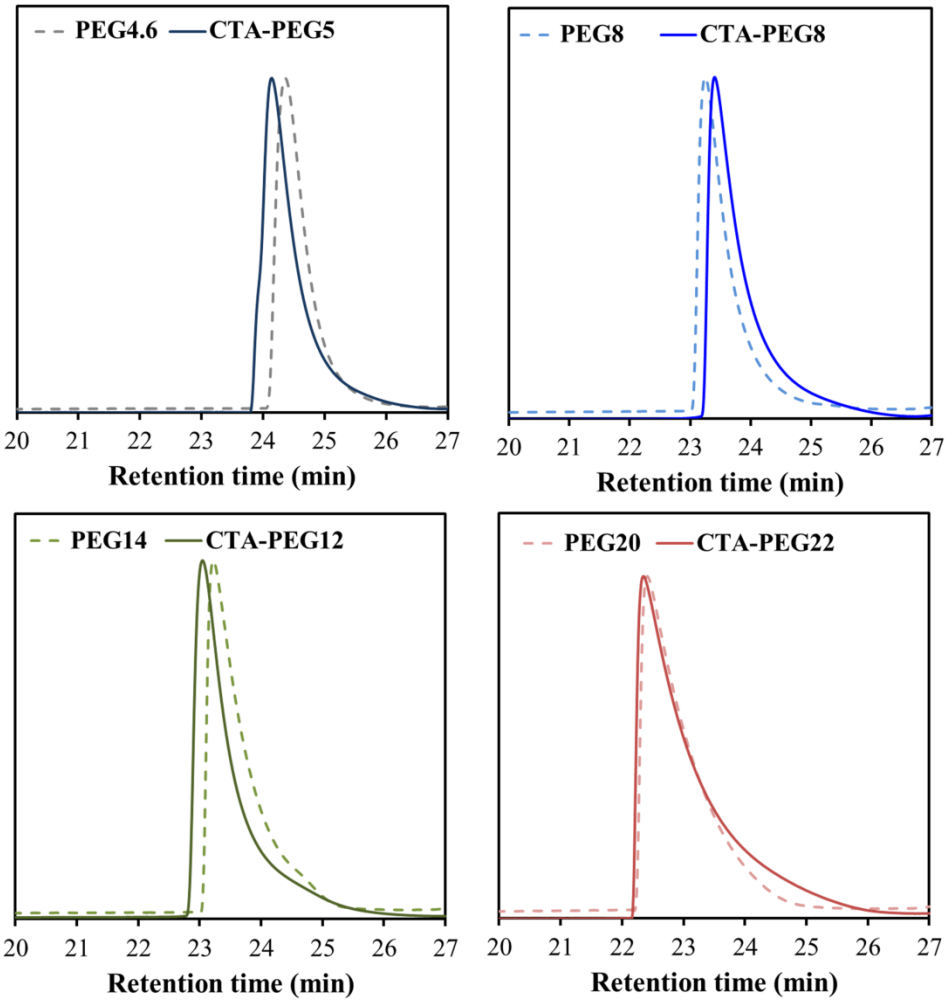

Figure S2: Normalized SEC traces of the PEG macro-CTA agents and their corresponding PEG. Black: CTA-PEG_5; Blue: CTA-PEG_8; Green: CTA-PEG_{12} and Red: CTA-PEG_{22}.

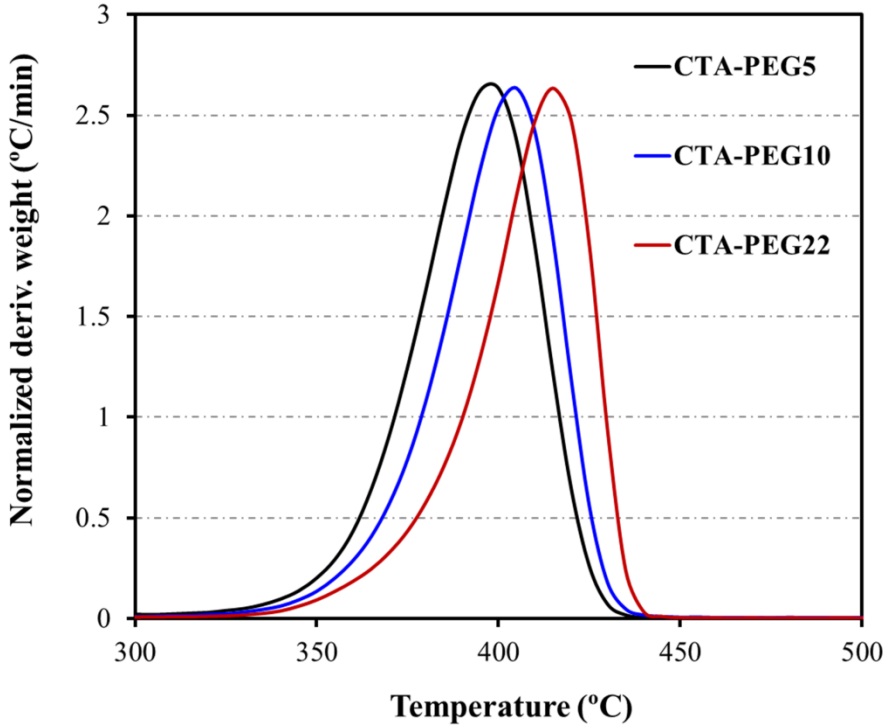

Figure S3: Normalized derivate weight loss of PEG macro-CTA agents. Black: CTA-PEG_5; Blue: CTA-PEG_{10} and Red: CTA-PEG_{22}.

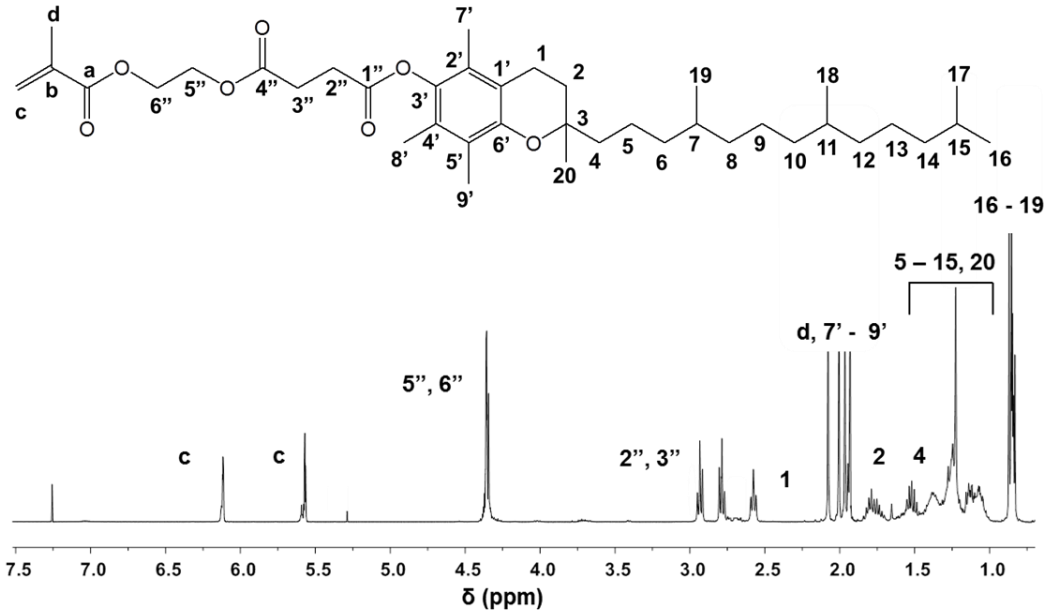

Figure S4: ^{1}H-NMR spectra of MTOS.

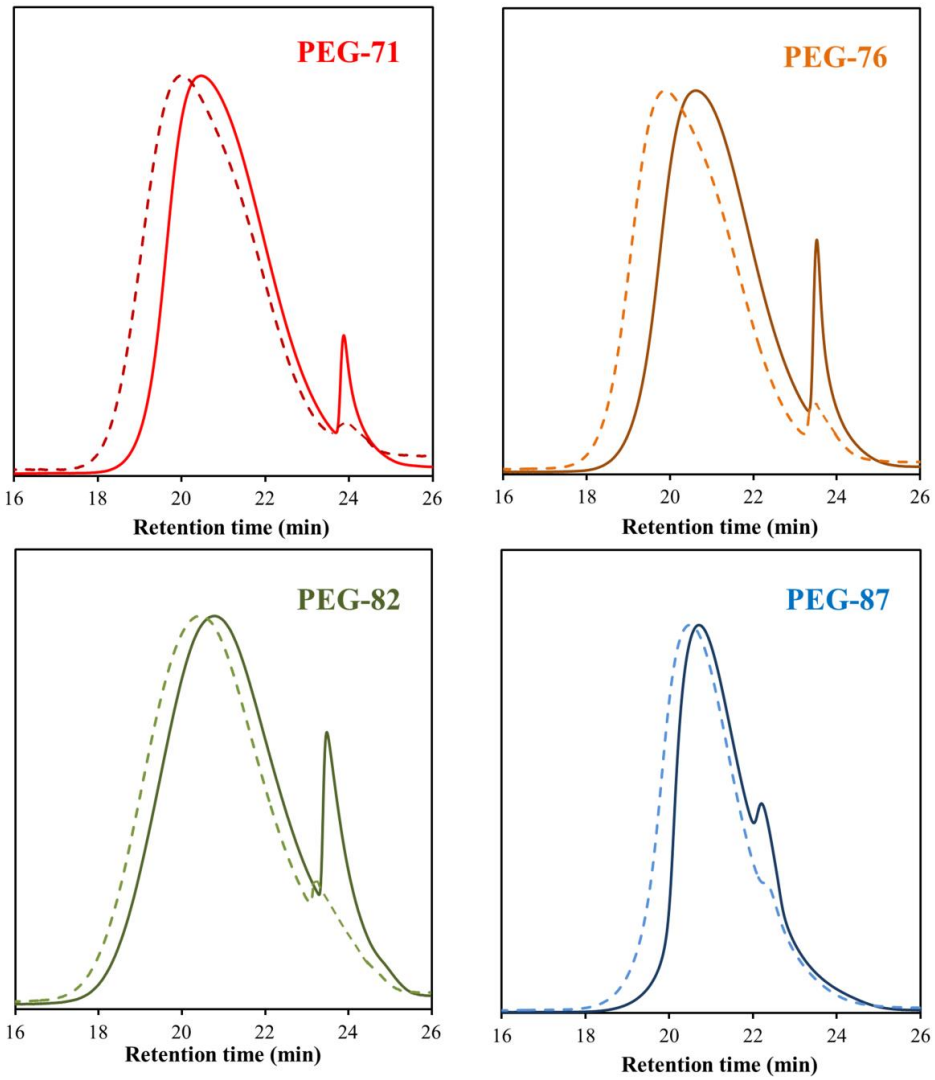

Figure S5: SEC traces of PEG-71 (Red), PEG-76 (orange), PEG-82 (Green) and PEG-87 (Blue) at the end of the RAFT copolymerization. Solid line: before purification by dialysis and dashed line: after purification by dialysis

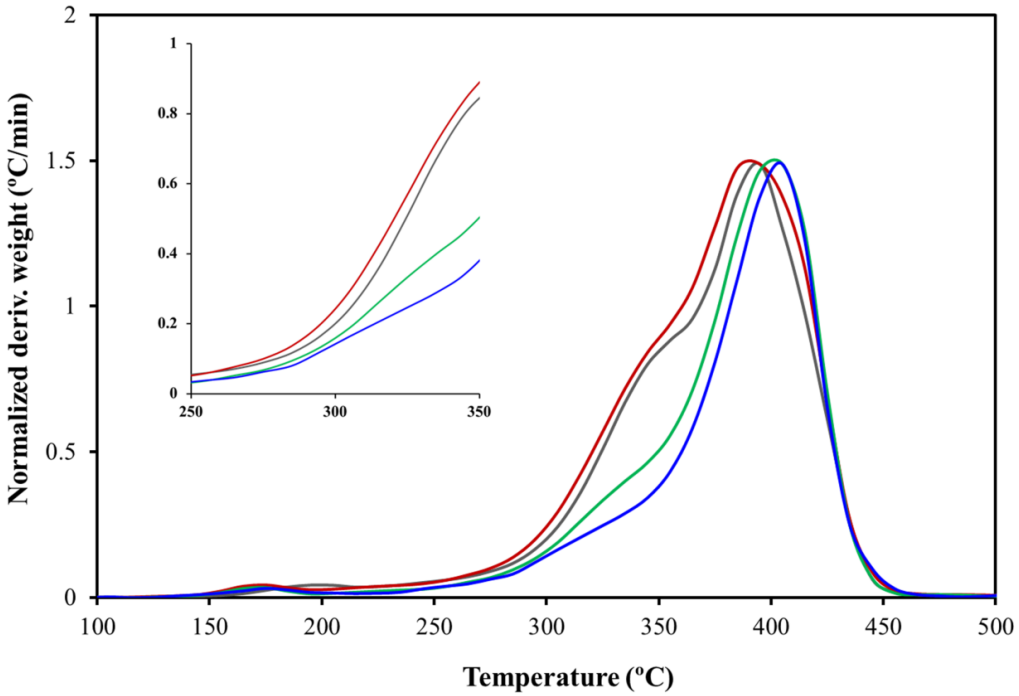

Figure S6: Comparative of normalized curves of derivative weight loss of PEG-71 (Red), PEG-76 (Grey), PEG-82 (Green) and PEG-87 (Blue) polymeric systems, measured by TGA under a nitrogen atmosphere.

4.1.8. References

1. I. F. Uchegbu and A. Siew, *Journal of pharmaceutical sciences*, 2013, **102**, 305-310.
2. R. Wang, P. S. Billone and W. M. Mullett, *Journal of Nanomaterials*, 2013, **2013**, 1-12.
3. X. Xu, W. Ho, X. Zhang, N. Bertrand and O. Farokhzad, *Trends in molecular medicine*, 2015, **21**, 223-232.
4. L. Y. Rizzo, B. Theek, G. Storm, F. Kiessling and T. Lammers, *Current opinion in biotechnology*, 2013, **24**, 1159-1166.
5. J. H. Park, S. Lee, J.-H. Kim, K. Park, K. Kim and I. C. Kwon, *Progress in Polymer Science*, 2008, **33**, 113-137.
6. M. C. Branco and J. P. Schneider, *Acta biomaterialia*, 2009, **5**, 817-831.
7. A. Rösler, G. W. Vandermeulen and H.-A. Klok, *Advanced drug delivery reviews*, 2012, **64**, 270-279.
8. S. Parveen, R. Misra and S. K. Sahoo, *Nanomedicine: Nanotechnology, Biology and Medicine*, 2012, **8**, 147-166.
9. U. Kedar, P. Phutane, S. Shidhaye and V. Kadam, *Nanomedicine: Nanotechnology, Biology and Medicine*, 2010, **6**, 714-729.
10. B. Louage, Q. Zhang, N. Vanparijs, L. Voorhaar, S. Vande Casteele, Y. Shi, W. E. Hennink, J. Van Bocxlaer, R. Hoogenboom and B. G. De Geest, *Biomacromolecules*, 2015, **16**, 336-350.
11. W. A. Braunecker and K. Matyjaszewski, *Progress in Polymer Science*, 2007, **32**, 93-146.
12. D. J. Keddie, *Chemical Society Reviews*, 2014, **43**, 496-505.
13. A. W. York, S. E. Kirkland and C. L. McCormick, *Advanced drug delivery reviews*, 2008, **60**, 1018-1036.
14. J. Neuzil, L.-F. Dong, J. Rohlena, J. Truksa and S. J. Ralph, *Mitochondrion*, 2013, **13**, 199-208.
15. J. Neuzil, T. Weber, N. Gellert and C. Weber, *British journal of cancer*, 2001, **84**, 87-89.

16. J. Neuzil, L.-F. Dong, L. Ramanathapuram, T. Hahn, M. Chladova, X.-F. Wang, R. Zobalova, L. Prochazka, M. Gold and R. Freeman, *Molecular aspects of medicine*, 2007, **28**, 607-645.
17. K. Kluckova, A. Bezawork-Geleta, J. Rohlena, L. Dong and J. Neuzil, *Biochimica et Biophysica Acta (BBA)-Bioenergetics*, 2013, **1827**, 552-564.
18. J. Neuzil, J. Cerny, J. C. Dyason, L. F. Dong and S. J. Ralph, *Molecular nutrition & food research*, 2011, **55**, 1543-1551.
19. J. Neuzil, J. C. Dyason, R. Freeman, L.-F. Dong, L. Prochazka, X.-F. Wang, I. Scheffler and S. J. Ralph, *Journal of bioenergetics and biomembranes*, 2007, **39**, 65-72.
20. N. Duhem, F. Danhier and V. Préat, *Journal of Controlled Release*, 2014, **182**, 33-44.
21. N. Duhem, F. Danhier, V. Pourcelle, J.-M. Schumers, O. Bertrand, C. c. S. LeDuff, S. Hoeppener, U. S. Schubert, J.-F. o. Gohy and J. Marchand-Brynaert, *Bioconjugate chemistry*, 2013, **25**, 72-81.
22. H. J. Youk, E. Lee, M. K. Choi, Y. J. Lee, J. H. Chung, S. H. Kim, C. H. Lee and S. J. Lim, *Journal of controlled release : official journal of the Controlled Release Society*, 2005, **107**, 43-52.
23. Z. Zhang, L. Mei and S.-S. Feng, *Nanomedicine*, 2012, **7**, 1645-1647.
24. E. Bernabeu and D. A. Chiappetta, *Journal of Biomaterials and Tissue Engineering*, 2013, **3**, 122-134.
25. Z. Zhang, S. H. Lee and S.-S. Feng, *Biomaterials*, 2007, **28**, 1889-1899.
26. H. Chen, Y. Zheng, G. Tian, Y. Tian, X. Zeng, G. Liu, K. Liu, L. Li, Z. Li and L. Mei, *Nanoscale Res Lett*, 2011, **6**, 1-10.
27. W. Tao, X. Zeng, T. Liu, Z. Wang, Q. Xiong, C. Ouyang, L. Huang and L. Mei, *Acta biomaterialia*, 2013, **9**, 8910-8920.
28. H. N. Nguyen, T. M. N. Hoang, T. T. T. Mai, T. Q. T. Nguyen, H. D. Do, T. H. Pham, T. L. Nguyen and P. T. Ha, *Advances in Natural Sciences: Nanoscience and Nanotechnology*, 2015, **6**, 1-8.
29. J. Pan and S.-S. Feng, *Biomaterials*, 2008, **29**, 2663-2672.
30. P.-Y. Li, P.-S. Lai, W.-C. Hung and W.-J. Syu, *Biomacromolecules*, 2010, **11**, 2576-2582.

31. E. Bernabeu, G. Helguera, M. J. Legaspi, L. Gonzalez, C. Hocht, C. Taira and D. A. Chiappetta, *Colloids and Surfaces B: Biointerfaces*, 2014, **113**, 43-50.
32. L. Jiang, X. Li, L. Liu and Q. Zhang, *Nanoscale research letters*, 2013, **8**, 1-11.
33. J. V. Jokerst, T. Lobovkina, R. N. Zare and S. S. Gambhir, *Nanomedicine*, 2011, **6**, 715-728.
34. P. Suárez, L. Rojo, Á. González-Gómez and J. S. Román, *Macromolecular bioscience*, 2013, **13**, 1174-1184.
35. L. García-Fernández, S. Halstenberg, R. E. Unger, M. R. Aguilar, C. J. Kirkpatrick and J. San Román, *Biomaterials*, 2010, **31**, 7863-7872.
36. F. Reyes-Ortega, G. Rodríguez, M. R. Aguilar, M. Lord, J. Whitelock, M. H. Stenzel and J. San Román, *Journal of Materials Chemistry B*, 2013, **1**, 850-860.
37. M. L. Donaire, J. Parra-Cáceres, B. Vázquez-Lasa, I. García-Álvarez, A. Fernández-Mayoralas, A. López-Bravo and J. San Román, *Biomaterials*, 2009, **30**, 1613-1626.
38. R. Palao-Suay, M. R. Aguilar, F. J. Parra-Ruiz, M. Fernández-Gutiérrez, J. Parra, C. Sánchez-Rodríguez, R. Sanz-Fernández, L. Rodrigáñez and J. S. Román, *Biomacromolecules*, 2015, **16**, 1566-1581.
39. H. Otsuka, Y. Nagasaki and K. Kataoka, *Advanced drug delivery reviews*, 2012, **64**, 246-255.
40. H. Yabu, *Bulletin of the Chemical Society of Japan*, 2012, **85**, 265-274.
41. B. Page, M. Page and C. Noel, *International journal of oncology*, 1993, **3**, 473-476.
42. Y. Chong, T. P. Le, G. Moad, E. Rizzardo and S. H. Thang, *Macromolecules*, 1999, **32**, 2071-2074.
43. D. J. Keddie, G. Moad, E. Rizzardo and S. H. Thang, *Macromolecules*, 2012, **45**, 5321-5342.
44. Y. Ikeda and Y. Nagasaki, *Journal*, 2012, **247**, 115-140.
45. H. Otsuka, Y. Nagasaki and K. Kataoka, *Advanced Drug Delivery Reviews*, 2012, **64**, 246-255.
46. E. Velasquez, J. Rieger, F. Stoffelbach, B. Charleux, F. D'Agosto, M. Lansalot, P.-E. Dufils and J. Vinas, *Polymer*, 2013, **54**, 6547-6554.
47. J. Rieger, G. Osterwinter, C. Bui, F. o. Stoffelbach and B. Charleux, *Macromolecules*, 2009, **42**, 5518-5525.
48. N. Nakajima and Y. Ikada, *Bioconjugate chemistry*, 1995, **6**, 123-130.

49. C. A. G. N. Montalbetti and V. Falque, *Tetrahedron*, 2005, **61**, 10827-10852.
50. S.-Y. Han and Y.-A. Kim, *Tetrahedron*, 2004, **60**, 2447-2467.
51. F. M. Veronese and G. Pasut, *Drug Discovery Today*, 2005, **10**, 1451-1458.
52. A. Favier and M. T. Charreyre, *Macromolecular Rapid Communications*, 2006, **27**, 653-692.
53. M. Müllner, A. Schallon, A. Walther, R. Freitag and A. H. Müller, *Biomacromolecules*, 2009, **11**, 390-396.
54. S. Kumar, R. Acharya, U. Chatterji and P. De, *Langmuir*, 2013, **29**, 15375-15385.
55. Y. Mai and A. Eisenberg, *Chemical Society Reviews*, 2012, **41**, 5969-5985.
56. G. Gaucher, M.-H. Dufresne, V. P. Sant, N. Kang, D. Maysinger and J.-C. Leroux, *Journal of Controlled Release*, 2005, **109**, 169-188.
57. H. Yabu and S. Sato, *Colloid and Polymer Science*, 2013, **291**, 181-186.
58. H. Yabu, *Polymer journal*, 2013, **45**, 261-268.
59. H. Maeda, *Bioconjugate chemistry*, 2010, **21**, 797-802.
60. V. Torchilin, *Advanced drug delivery reviews*, 2011, **63**, 131-135.
61. D. Pozzi, V. Colapicchioni, G. Caracciolo, S. Piovesana, A. L. Capriotti, S. Palchetti, S. De Grossi, A. Riccioli, H. Amenitsch and A. Laganà, *Nanoscale*, 2014, **6**, 2782-2792.
62. G. Cai and H. Jiang, *Journal of Materials Science: Materials in Medicine*, 2009, **20**, 1315-1320.
63. H. Otsuka, Y. Nagasaki and K. Kataoka, *Advanced Drug Delivery Reviews*, 2012, **64, Supplement**, 246-255.
64. Y. Ikeda and Y. Nagasaki, *Journal of Applied Polymer Science*, 2014, **131**, 1-10.
65. Y. Hu, J. Xie, Y. W. Tong and C.-H. Wang, *Journal of Controlled Release*, 2007, **118**, 7-17.
66. H. Hatakeyama, H. Akita and H. Harashima, *Advanced Drug Delivery Reviews*, 2011, **63**, 152-160.
67. H. Hatakeyama, H. Akita and H. Harashima, *Biological and Pharmaceutical Bulletin*, 2013, **36**, 892-899.
68. T.-G. Iversen, T. Skotland and K. Sandvig, *Nano Today*, 2011, **6**, 176-185.
69. M. A. Owens, B. C. Horten and M. M. Da Silva, *Clinical breast cancer*, 2004, **5**, 63-69.

70. S. Sjögren, M. Inganäs, A. Lindgren, L. Holmberg and J. Bergh, *Journal of Clinical Oncology*, 1998, **16**, 462-469.

71. D. J. Slamon, G. M. Clark, S. G. Wong, W. J. Levin, A. Ullrich and W. L. McGuire, *Science*, 1987, **235**, 177-182.

72. S. Vrbic, I. Pejcic, S. Filipovic, B. Kocic and M. Vrbic, *J buon*, 2013, **18**, 4-16.

73. D. L. Holliday and V. Speirs, *Breast Cancer Res*, 2011, **13**, 215.

74. G. Valabrega, F. Montemurro and M. Aglietta, *Annals of oncology*, 2007, **18**, 977-984.

4.2. Enhanced bioactivity of α-tocopheryl succinate based block copolymer nanoparticles by reduced hydrophobicity

Raquel Palao-Suay[1,2], María Rosa Aguilar[1,2], Francisco J. Parra-Ruiz[1], Samarendra Maji[3], Richard Hoogenboom[3], N.A.Rohner[4], Susan N. Thomas[4] and Julio San Román[1,2]*

[1]Group of Biomaterials, Department of Polymeric Nanomaterials and Biomaterials, Institute of Polymer Science and Technology, CSIC, Madrid, Spain.

[2]Networking Biomedical Research Centre in Bioengineering, Biomaterials and Nanomedicine, CIBER-BBN, Spain.

[3]Supramolecular Chemistry Group. Department of Organic and Macromolecular Chemistry. Ghent University, Ghent, Belgium.

[4]George W. Woodruff School of Mechanical Engineering and Parker H. Petit Institute of Bioengineering and Bioscience, Georgia Institute of Technology, Atlanta, Georgia, USA.

**Corresponding author*: mraguilar@ictp.csic.es

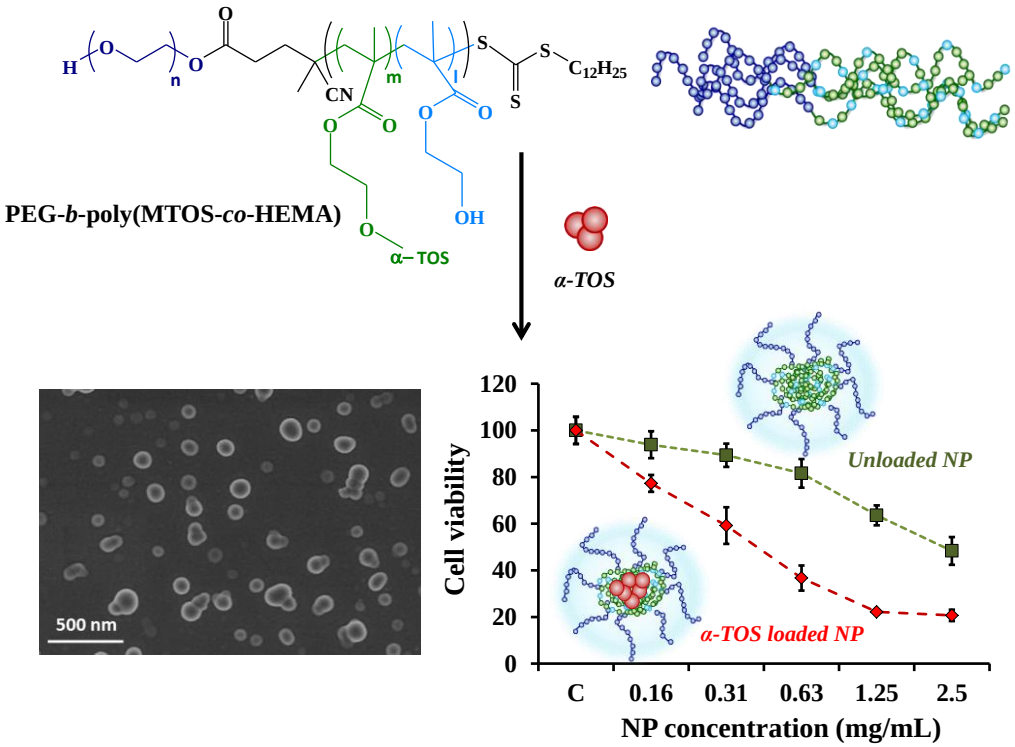

KEYWORDS: α-tocopheryl succinate, RAFT polymerization, amphiphilic polymer**,** HEMA, terpolymers, anticancer nanoparticles

4.2.1. Abstract

Well-structured amphiphilic copolymers are necessary to obtain self-assembled nanoparticles (NPs) based on synthetic polymers. Highly homogeneous and monodispersed macromolecules obtained by controlled polymerization have successfully been used for this purpose. However, disaggregation of the organized macromolecules is desired when a bioactive element, such as α-tocopheryl succinate (α-TOS), is introduced in self-assembled NPs and this element must be exposed or released to exert its action.

The aim of this work is to demonstrate that the bioactivity of synthetic NPs based on defined RAFT copolymers can be enhanced by the introduction of hydrophilic comonomers in the hydrophobic segment. The amphiphilic terpolymers are based on poly(ethylene glycol) (PEG) as hydrophilic block, and a hydrophobic block based on a methacrylic derivative of α-TOS (MTOS) and small amounts of 2-hydroxyethyl methacrylate (HEMA) (PEG-*b*-poly(MTOS-*co*-HEMA)). The introduction of HEMA reduces hydrophobicity and introduces 'disorder' both in the homogeneous blocks and the compact core of the corresponding NPs. These NPs are able to encapsulate additional α-TOS with high efficiency and their biological activity is much higher than that described for the unmodified copolymers, proposedly due to more efficient macromolecular disaggregation and release of α-TOS, demonstrating the importance of the hydrophilic-hydrophobic balance.

4.2.2. Introduction

Current available cancer therapies based on chemotherapeutic drugs suffer from their inability to differentiate between cancerous versus nonmalignant cells as well as their inappropriate pharmacokinetics and nonspecific biodistribution[1, 2]. Significant deleterious side effects and drug resistances are also becoming more frequent[3]. Nanotechnology, and more specifically surfactant free polymeric nanoparticles (NPs), have emerged as a potent new class of anticancer drug delivery vehicles with higher activities, selectivity and lower toxicities than many existing drugs[4, 5]. Such nanovehicle-based platforms have multiple advantages that can overcome the current limitations of conventional anticancer treatments, for example by smartly responding to the heterogeneous and complex environment inside the tumors [3, 6, 7].

NPs based on well-structured amphiphilic polymers have been obtained by self-assembly process via phase-inversion. This process is governed by a delicate balance between hydrophobic and hydrophilic interactions and it is especially relevant when the amphiphilic polymer includes bioactive elements (*e.g.* drugs) covalently attached to its structure (polymer drug) to avoid premature leaching and release of the drug[8, 9]. If the drug is hydrophobic and forms part of a hydrophobic block, it will be concentrated in the core of the NPs when suspended in water, and the disaggregation of the organized macromolecules will be necessary to expose or release the active principle and exert its action[10]. The hydrophobic interactions between hydrophobic blocks lead to the chain organization in polymeric particles, and the hydrophilic repulsion contributes to the stabilization of the particles and to facilitate water diffusion to the interior of the NPs, that may play a critical role in chain disaggregation resulting hydrolysis of cleavable linkers and drug delivery[11, 12].

There are numerous reports in the literature describing the synthesis and characterization of amphiphilic polymeric nanocarriers for the treatment of cancer[12-14]. However, there are not so many examples describing how the structure modification of one segment affects the bioactivity of the particle. In this sense, Zhang et al. prepared NPs of poly(styrene-*b*-ethylene-*co*-butylene-*b*-styrene) by microphase inversion and studied the effect of different concentrations of carboxylic groups in the styrene residues. They observed that the NPs gradually changed from a uniform and compact globule to a hyperbranched and loose cluster as the extension of the carboxylation increased. Moreover,

the cluster was broken by simple dilution of the suspension[15]. Additionally, Akiyoshi et al. described how amphiphilic cholesteryl group-bearing pullulans formed nanogels in dilute conditions due to the hydrophobic interactions between cholesteryl groups[16]. Later, these authors introduced cationic groups in the cholesteryl group-bearing pullulans (cCHP) to efficiently deliver proteins to myeloma cells and primary $CD4^+$ T lymphocytes by induction of macropinocytosis. The complex of the nanogel-protein dissociated and the protein was released inside the cell[17].

Our group described the "progressive accessibility model" to explain the zero-order release of hydrophobic drugs from copolymer drugs based on a hydrophobic monomer (a methacrylic derivative of Triflusal, THEMA) and an ionic hydrophilic comonomer (2-acrylamido-2-methylpropano sulfonic acid, AMPS) randomly distributed and obtained by free radical copolymerization (poly(THEMA-*co*-AMPS))[18]. The article emphasized the importance of the presence of the hydrophilic monomer (AMPS) in the Trifusal release process. AMPS warranted the water accessibility to the THEMA residues and favored its hydrolysis and the release of the anti-thrombogenic compound.

Moreover, our group also described the formation of oriented micelles by an amphiphilic copolymeric system based on butylacrylate (BA) and 5-methacrylamide-2-naphthalenesulfonic acid (MANSA) (poly(BA-*co*-MANSA)), and stablished that its antiangiogenic activity was related with the self-assembled micellar morphology of the NPs, which placed the sulfonic groups in an adequate position to interact and inhibit fibroblast growth factor[19].

The aim of this paper is to demonstrate that small changes in the delicate hydrophilic-hydrophobic balance of amphiphilic polymer drugs (by the introduction of small amounts of a hydrophilic comonomer in the hydrophobic block) are important not only in the self-assembly process of the NPs, but also in the control of the bioactivity of the polymer drug and the correspondent NP. For this purpose, we obtained reversible addition-fragmentation chain transfer polymerization (RAFT) block copolymers based on poly(ethylene glycol) (PEG) as hydrophilic block, and a hydrophobic block based on a methacrylic derivative of α-tocopheryl succinate (MTOS) and small amounts of 2-hydroxyethyl methacrylate (HEMA) randomly copolymerized (**figure 1**).

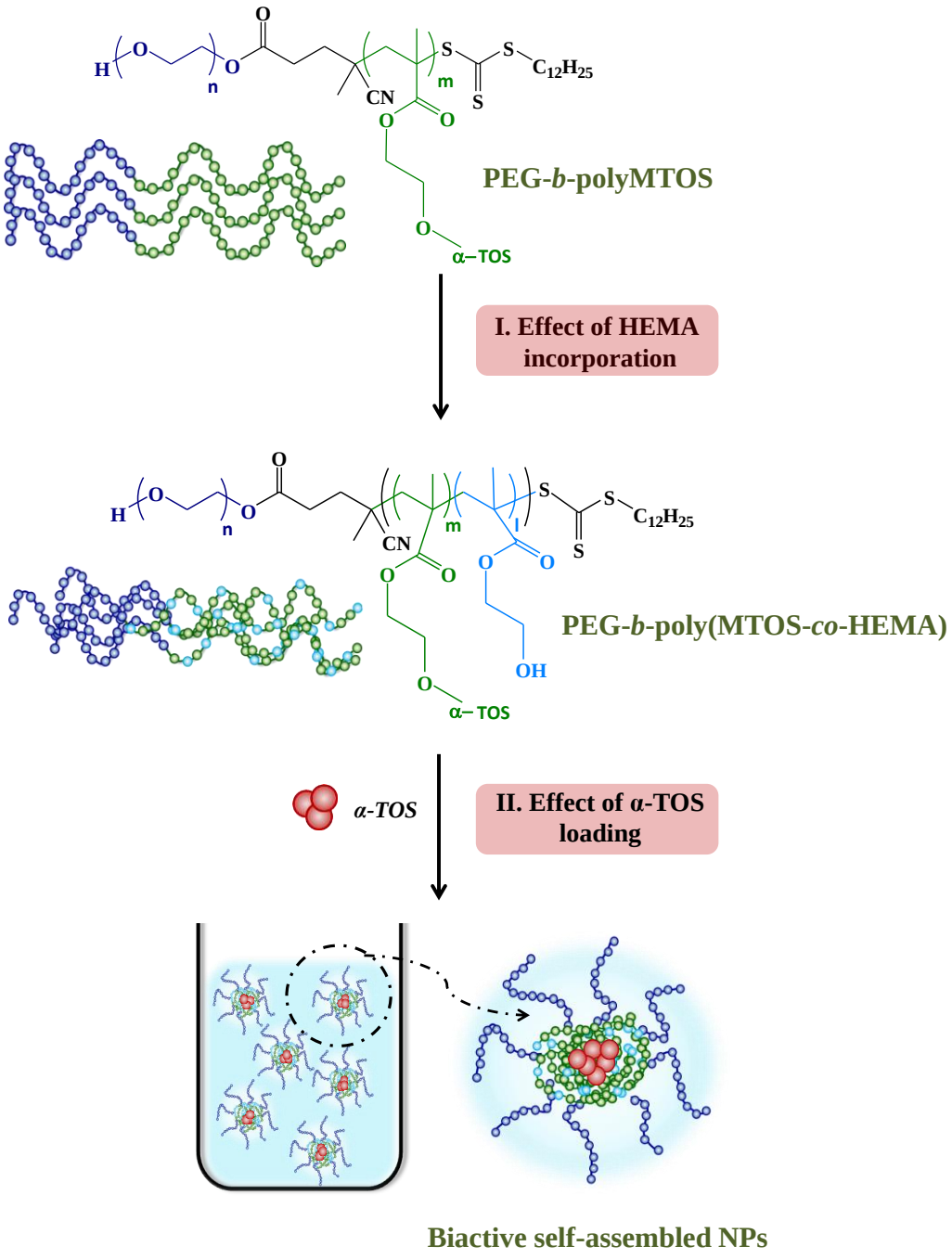

Figure 1: Scheme of PEG-*b*-polyMTOS, PEG-*b*-poly(MTOS-*co*-HEMA) and α-TOS-loaded NPs based on PEG-*b*-poly(MTOS-*co*-HEMA) in aqueous solution.

α-Tocopheryl succinate (α-TOS) is a mitochondrially targeted anticancer compound (mitocan)[20] that selectively induces apoptosis of cancer cells and regulates angiogenesis by inducing apoptosis of proliferating endothelial cells with no harm to quiescent endothelial cells[21-23]. However, the hydrophobicity of this drug significantly limits its real application in cancer treatments and therefore, the design of optimal and efficient drug delivery systems of α-TOS are an important goal to achieve[24, 25].

Our group has recently described new bioactive self-assembled NPs based on amphiphilic copolymers bearing α-TOS with antiproliferative and antiangiogenic properties, and able to encapsulate hydrophobic molecules in the core. These copolymers were obtained by free radical polymerization of monomers with different hydrophilicity and reactivity[26] or by RAFT [27]. In this sense, RAFT is considered one of the most versatile living/controlled radical polymerization as it allows the design and synthesis of functional polymers with a well-defined architecture and controlled molecular weight (MW) with relatively low dispersity (*Đ*) [28, 29]. The structural homogeneity and the amphiphilic nature of the obtained macromolecules allows the self-assembly in aqueous media to form 3D supramolecular structures when the adequate hydrophilic/hydrophobic balance is reached.

Although the RAFT-based block copolymers PEG-*b*-polyMTOS presented higher content of α-TOS than the free radical polymerized copolymers (poly(*N*-vinyl pyrrolidone-co-MTOS))[26], their biological activity was significantly lower, probably due to the so called 'PEG dilemma'[30] [31] and the high stability of the NPs obtained by these highly homogeneous block copolymers resulting from too strong hydrophobic interactions making the core impermeable for water. Therefore, the new synthetic terpolymers described in this paper were designed in order to reduce the hydrophobicity of the hydrophobic block by introducing the hydrophilic comonomer HEMA (**figure 1**) to favor water diffusion in the core of the NPs, the disaggregation of the macromolecules forming the NPs, and the release of the loaded cargo.

4.2.3. Materials and methods

- **Materials**

2-Hydroxyethyl methacrylate (HEMA, Sigma-Aldrich) was purified according to the literature[32]. 2,2'-Azobisisobutyronitrile (AIBN, Merck) was recrystallized from methanol (m.p. 104 ºC). Anhydrous 1,4-dioxane (Sigma-Aldrich), deuterated chloroform ($CDCl_3$, Sigma-Aldrich) and chromatographic grade tetrahydrofuran (THF, Sigma-Aldrich) were used without further purification to synthesis and characterize polymeric systems. Additionally, sodium chloride (NaCl, Panreac), α-tocopherol succinate (α-TOS, Sigma-Aldrich) and coumarin-6 (c6, Sigma-Aldrich) were used without further purification to prepare self-assembled NPs.

- **Characterization techniques**

^{1}H-NMR was performed in a Mercury 400BB apparatus, operating at 400 MHz and dissolving the corresponding sample in $CDCl_3$ at 25 ºC. Fourier transform infrared attenuated total reflectance (ATR-FTIR) spectroscopy was obtained in a Perkin Elmer Spectrum One FTIR spectrometer using 32 scans, and a resolution of 4 cm^{-1}. Thermogravimetric analysis were performed using a TGA Q500 apparatus (TA instruments), under dynamic nitrogen atmosphere between 25–600 ºC at a heating rate of 10 ºC/min in order to analyze the thermal degradation of the polymeric systems.

The number and weight average molecular weight (M_n and M_w) and dispersity ($Đ$) of the polymers were determined by size exclusion chromatography (SEC), using a Perkin-Elmer Isocratic LC pump 250 coupled to a refraction index detector (Series 200). Three polystyrene-divinyl benzene columns (PLgel, Varian, Polymer Laboratories) of average pore size of 10^3, 10^4 and 10^5 Å were used as solid phase, and degassed THF (1 mL/min) was used as eluent at 40ºC. Monodisperse poly(methyl methacrylate) (PMMA) standards (Scharlab) with molecular weights between 10.300 and 1.400.000 Da were used to obtain the calibration curve. Data were analyzed using the Perkin-Elmer LC solution program.

- **Preparation of terpolymers PEG-*b*-[poly(MTOS-*co*-HEMA)**

The methacrylic derivative of α-TOS (MTOS), the PEG macro-CTA agents (4-cyano-4-[(dodecylsulfanylthiocarbonyl)sulfanyl]pentanoic acid was conjugated to PEG

with M_n between 8 and 22 kDa) and PEG-*b*-polyMTOS were obtained as previously described [26, 27].

PEG-*b*-[poly(MTOS-*co*-HEMA)] were obtained by RAFT polymerization using PEG-macro CTA of 8 kDa MW (CTA-PEG_8). Two different feed molar ratios of methacrylic monomers were used, particularly 10 or 20 mol. % HEMA with respect to MTOS. In this way, CTA-PEG_8, MTOS, HEMA, AIBN and anhydrous 1,4-dioxane were sealed in a 25 mL Schlenk tube. The reaction mixture was degassed by three freeze-pump-thaw cycles and heated in an oil bath under magnetic stirring at 70 ºC. The total monomer concentration ([M]), the reaction time and the feed molar ratio [MTOS]:[CTA]:[AIBN] were 0.5 M, 300 min, and [100]:[1]:[0.3], respectively.

Samples (250 μL) were taken from the polymerization after different reaction times (30, 60, 120 and 300 min) in order to analyse the polymerization kinetics. These samples were cooled and characterized by SEC to determine the molecular weight and ^{1}H-NMR spectroscopy to calculate the composition of copolymer chains and conversion of the reaction. At the end of the polymerization reactions, terpolymers were purified by dialysis (Spectrum Laboratories, 25KDa MW cut-off) against a mixture of THF and water (50:50 v:v) that was progressively replaced by water during three days with the aim to remove the residual unreacted monomers and low molecular weight species. The resulting solutions were isolated by freeze-drying to yield white amorphous powders.

- **Self-assembled NPs by self-organized precipitation (SORP)**

Unloaded NPs were prepared by SORP or solvent exchange as described before [27, 33]. Briefly, an aqueous solution of NaCl (100 mM, 2 mL) was added dropwise to the organic solution of the polymer (10 mg/mL in dioxane, 2 mL) under constant magnetic stirring. The final polymer concentration was 5 mg/mL. Furthermore, the preparation of loaded NPs was optimized by the addition of the appropriate amount of α-TOS (10 % w/w respect to the polymer) or c6 (1 % w/w respect to the polymer) to the organic phase.

Milky NPs dispersions were dialyzed against NaCl during 72 h in order to remove organic solvent and unloaded α-TOS or c6. Each NP suspension was then sterilized by filtration through 0.22 μM polyethersulfone membranes (PES, Millipore Express®, Millex GP) and stored at 4 ºC.

Encapsulation efficiency (EE)

NPs were freeze dried (yield higher than 80%) in order to calculate the EE of α-TOS or c6, that can be defined as the ratio of calculated and theoretical amount of the drug entrapped in the NPs. The calculation equation is as follows:

$$Encapsulation\ efficiency\ (EE) = \frac{[loaded\ molecule]_i}{[loaded\ molecules]_0} \times 100 \qquad [1]$$

being $[\text{loaded molecule}]_i$ the concentration of the α-TOS or c6 encapsulated in the inner core of the NPs and detected experimentally, and $[\text{loaded molecule}]_0$ the concentration of the molecule added in the nanoprecipitation process.

In both cases, loaded NPs were dissolved in ethanol. The EE of α-TOS was quantified by absorbance spectroscopy (λ = 285 nm) using a Perkin Elmer Lambda 35 UV/VIS spectrophotometer (calibration curve using α-TOS concentrations between 1 – 0.001 mg/mL in ethanol). Additionally, c6 entrapped in the NPs was quantified by fluorescence spectroscopy ($\lambda_{excitation}$ = 485 nm and $\lambda_{emission}$ = 528 nm) using a Biotek SYNERGY-HT plate reader, adjusting emission splits as required for the intensity measurements (calibration curve was obtained using c6 concentrations between 0.5 – 0.001 mg/mL in ethanol).

NP Characterization

The morphology of NPs was investigated by scanning electron microscopy (SEM) using a Hitachi SU8000 TED, cold-emission FE-SEM microscope working with an accelerating voltage between 25 and 50 kV. Samples were prepared by deposition of one drop of the NP suspension (0.05 mg/mL) over small glass disks (12 mm diameter). After the evaporation of the aqueous phase overnight, the samples were coated with a gold palladium alloy (80:20) prior to examination by SEM.

The hydrodynamic diameter (D_h, by intensity) and polydispersity index (PDI) of unloaded and α-TOS entrapped NPs was determined by dynamic light scattering (DLS) using a Malvern Nanosizer NanoZS Instrument equipped with a 4mW He-Ne laser (λ=633 nm) at a scattering angle of 173°. Different samples were measured in square polystyrene cuvettes (SARSTEDT) at 25 ºC. The autocorrelation function was converted in an intensity particle size distribution with ZetaSizer Software 7.10 version, based on the Stokes-Einstein equation. The zeta potential was quantified by laser Dopper electrophoresis (LDE) using

NPs formulation at 0.5 mg/mL in 10 mM NaCl. The zeta potentials were automatically calculated from the electrophoretic mobility using the Smoluchowski´s approximation. For each sample, the statistical average and standard deviation of data were calculated from 8 measurements of 20 runs each one.

- **Biological activity**

Cell culture

Human mammary adenocarcinoma cells, MCF-7 cells (ECACC), were cultured in Dulbecco's modified Eagle's medium (DMEM), supplemented with 10% fetal bovine serum (FBS), 2% L-glutamine, 1% penicillin/streptomycin (P/S) and incubated at 37°C and 5% CO_2. Additionally, human metastatic carcinoma cells, MDA-MB-453 cells (ATCC), were cultured in DMEM, supplemented with 10% FBS, 1% PS and incubated at 37°C and 5% CO_2. Finally, human mammary epithelial cells, HMEpiC cells (obtained from Innoprot, P10891), were cultured using mammary epithelial cell medium (MepiCM, Innoprot), at 37°C and 5% CO_2.

Uptake and intracellular location of c6 loaded NPs

Endocytosis of c6 loaded NPs was followed by Confocal Laser Scanning Microscopy (CLSM) (Leica TCS-SP5 RS AOBS). For this propose, MDA-MB-453 cells were seeded into 24 well plates at 100,000 cells/mL, in complete medium. The cells were incubated for 48 h at 37 ºC. Afterwards, the medium was replaced with the corresponding NPs dispersion in NaCl (500 µL of the NPs suspension and 500 µL of completed medium) and incubated at 37 ºC. At different time points (30 min, 2 and 6 h), the cells were washed 3 times with cold PBS and fixed by a paraformaldehyde solution in PBS (3.7 w/v %) for 15 min at room temperature. Then, the cells were rinsed with cold PBS and observed by CLSM. The fluorescence intensity was measured using the quantification analysis tool that is available in the Leica software (*Leica LAS-AF Software*).

To track the intracellular location of NPs, MDA-MB-453 cell monolayer was incubated with c6 loaded NPs for 6 h. Cells were washed 3 times with PBS and mitochondria were stained with MitoTracker® Red CMXRos (Life Technologies) for 30 min at 50 nM, and then washed 3 times with PBS. Cells were fixed using a paraformaldehyde solution in PBS (3.7 w/v %) for 15 min and observed by CLSM. This

work has been performed by the Confocal Microscopy Service of the Universidad de Alcalá de Henares (UAH) and the Biomedical Networking Center (CIBER-BBN), located at the facilities of the Cell Culture Unit.

In vitro cytotoxicity assay

The cytoxicity of diverse concentrations of NPs (2.5, 1.25, 0.63, 0.31 and 0.16 mg/mL) was analyzed by Alamar Blue assay (Sigma-Aldrich) [34]. For this propose, cells were seeded at different densities: MCF-7 at 30,000 cells/mL (15,000 cells/well), MDA-MB-453 at 35,000 cells/mL (20,500 cells/well) in 24-well plates and HMEpiC at 80,000 cells/mL (40,000 cells/well) in 48-well plates.

After 24 h of incubation, the medium was replaced with the NPs dispersed in NaCl (50:50 v/v of the NPs suspension and completed medium). The plates were incubated at 37°C in a humidified air with 5% CO_2 for 24 h. Then, 100 µL of Alamar Blue solution (10 % Alamar Blue solution in phenol red free DMEM medium) was added to all wells and the fluorescence was measured on a Biotek SYNERGY-HT plate reader ($\lambda_{excitation}$ = 530 nm and $\lambda_{emission}$ = 590 nm) after 4 h of incubation.

Statistical analysis

Results were expressed as mean ± standard deviation. Statistical significance (significance level of: *: $p < 0.05$) was evaluated using the analysis of variance (ANOVA, Tukey test) as required, by Origin 9.

4.2.4. Results and discussion

- **RAFT polymerization: characterization of PEG-*b*-[poly(MTOS-*co*-HEMA)]**

PEG-*b*-polyMTOS block copolymers with a molar composition of PEG:MTOS 66:34, 71:29, 76:24, 82:18 and 87:13 were previously reported and labelled as PEG-66, PEG-71, PEG-76, PEG-82 and PEG-87, being PEG-71 the best in terms of self-assembling, hydrodynamic characteristics and bioactivity[27]. In order to change the structural homogeneity of these block copolymers and analyze the resulting effect on the biological activity, HEMA was copolymerized with MTOS (10 and 20 mol. % with respect to MTOS) using the PEG-CTA_8 (MW of 8 kDa) at 0.5 M and 70 ºC during 5 h. Other experimental conditions are collected in **table 1**.

Table 1: Experimental conditions and the most relevant structural characteristics of PEG-*b*-poly(MTOS-*co*-HEMA) terpolymers.

Sample	[MTOS]:[HEMA]:[CTA]:[AIBN] (mol. %)	a) M_n x 10^{-3}	a) $Đ$	b) n_{PEG}	b) m_{MTOS}	f_{PEG}-f_{MA} (mol %)	c) T_{max} (ºC)
PEG-10H	[90]:[10]:[1]:[0.3]	51.6	1.26	177	51	76-24	405
PEG-20H	[80]:[20]:[1]:[0.3]	47.8	1.25	177	35	80-20	407

a) Determinated by SEC (THF) using PMMA standards

b) Determinated using ^{1}H-NMR spectroscopy

c) Measured by TGA under nitrogen atmosphere

The macro CTA, PEG-CTA_8, was selected due to its high compatibility towards methacrylic monomers and its optimal molar mass, avoiding their elimination by the reticuloendothelial (RES) system while still allowing clearance by renal filtration (MW cut-off for glomerular filtration is around 30 kDa)[35-37]. HEMA was added to the terpolymers due to its excellent biocompatibility and hydrophilicity of the resulting polymer polyHEMA. Additionally, polyHEMA has been approved by the FDA for biomedical and pharmaceutical applications[38-41]. The methacrylic group of HEMA is linked to a hydroxyl ethyl moiety that is also present in the MTOS monomer. Therefore, the similar chemical structure in the proximity of the double-bond is expected to provide similar reactivity to both monomers, and a statistical copolymer will be formed with close to a random

distribution of HEMA in the MTOS hydrophobic block. Moreover, the HEMA monomer was also chosen because it is the chemical residue that will result from the hydrolysis of MTOS by esterases from body fluids and the release of α-TOS. The complete hydrolysis of PEG-*b*-polyMTOS will thus give rise to the hydrophilic block copolymer PEG-*b*-polyHEMA[42]. The terpolymers were labelled PEG-YH where Y indicates the feed molar composition of HEMA and their characteristics are shown in **table 1.**

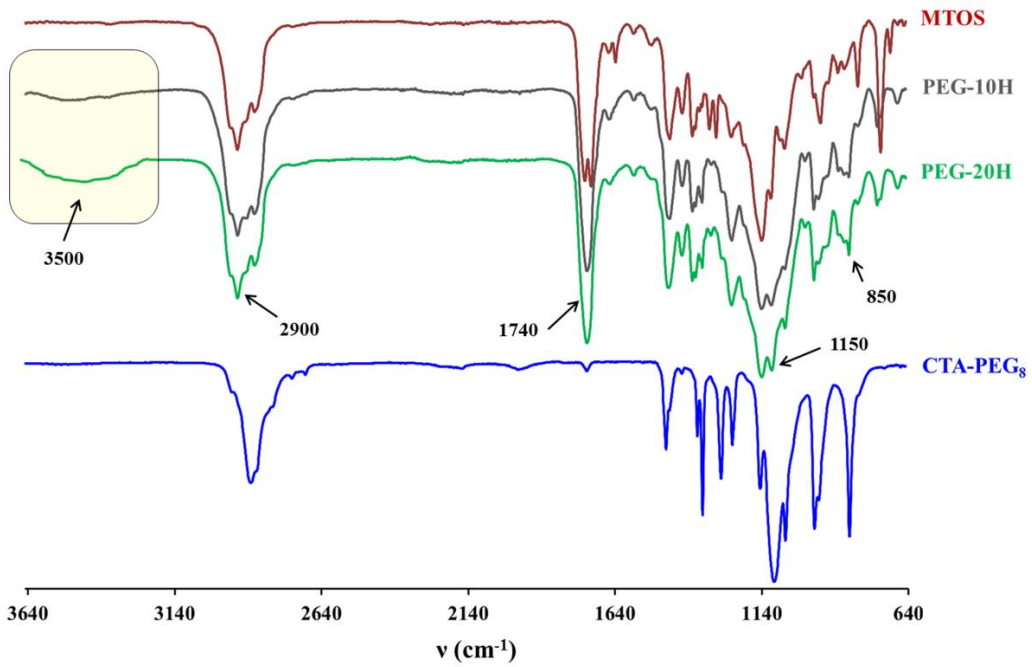

Figure 2: Comparison of ATR-FTIR spectra of MTOS (Red), CTA-PEG8 (Blue), PEG-10H (Grey) and PEG-20H (Green).

The HEMA copolymerization was confirmed by ^{1}H-NMR by the disappearance of the signals of vinyl protons corresponding to its methacrylate group at 5.58 ppm and comparison with that of MTOS protons at 5.55 ppm. The MTOS units into the macromolecular chains were elucidated by ^{1}H-NMR[27] and the HEMA units by considering that 100% of the conversion was reached as the signal at 5.58 ppm disappears during the polymerization reaction. As a result, terpolymers with molar composition PEG:MA (MA is MTOS+HEMA) of 76:24 and 80:20 were obtained. ATR-FTIR spectra of PEG-10H and PEG- 20H showed a characteristic O-H stretching vibration band of HEMA at 3500 cm^{-1} (**figure 2**), also confirming the successful incorporation of HEMA units into the macromolecular chains.

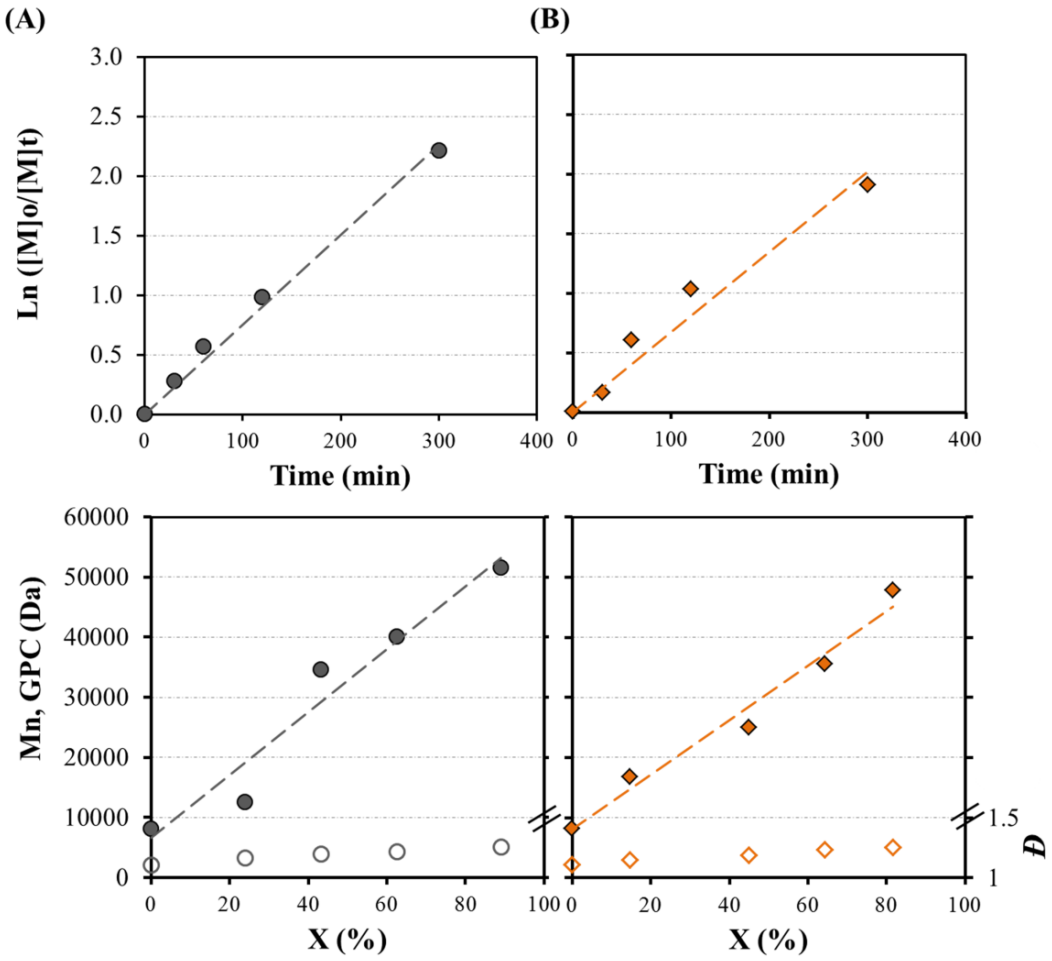

Figure 3: Kinetics of polymerization of (A) PEG-10H and (B) PEG-20H, including the variation of $Ln([M]_o/[M]_t)$ and M_n values as a function of reaction time and MTOS conversion.

SEC characterization revealed that both terpolymers had a relatively narrow MW distribution with $Đ < 1.26$. The terpolymerization kinetics are summarized in **figure 3**, showing the evolution of $Ln([M]_o/[M]_t)$ and M_n values as a function of reaction time and MTOS conversion, respectively. In both cases, linear first order kinetic plots were obtained that is an indicative a constant free radical concentration and, thus, demonstrates the absence of significant termination reactions while the linear increase of M_n with conversion confirms fast initiation and absence of significant irreversible transfer reactions. Additionally, SEC traces at different polymerization times are compared in **figure 4**. As expected, the traces were clearly shifted to lower elution times, indicating an increase in the molecular weight, with increasing reaction time[43]. It is noteworthy that traces were

bimodal, due to the presence of a minor fraction of unreacted macro-CTA. This behavior is commonly observed for this type of polymerizations, indicating that the efficiency of macro CTA agents was not complete[44,45]. The purification of copolymers by dialysis effectively eliminated the majority of low MW chains of the unreacted PEG macro-CTA agents (**figure S1**, see supporting information).

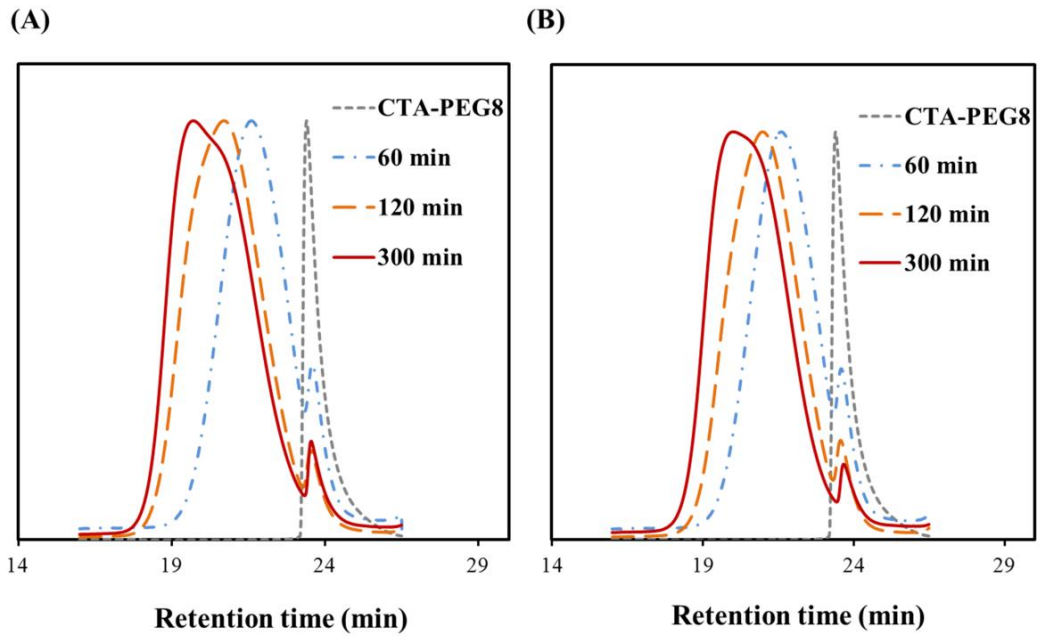

Figure 4: Normalized SEC traces during the polymerization of (A) PEG-10H and (B) PEG-20H.

These results confirmed that the copolymerization with HEMA allowed to maintain the control of the polymerization. The HEMA monomeric units were presumably incorporated randomly into the MTOS based hydrophobic block polymers due to a similar reactivity of both methacrylic monomers, as previously commented. These structural modifications affected the self-assembly behavior of the copolymers and their therapeutic action, as will be demonstrated in the next sections.

- **Characterization of self-assembled NPs**

The incorporation of low concentrations of HEMA into the hydrophobic block of PEG-*b*-poly(MTOS-*co*-HEMA) allowed to obtain spherical NPs by SORP or solvent exchange as indicated by the very low PDI values resulting from DLS [33, 46]. These NPs

were labelled as NP-YH where Y indicates the feed molar composition of HEMA and their characteristics are shown in **table 2**.

Table 2: Most relevant characteristics of unloaded based on PEG-10H and PEG-20H and loaded NPs: Hydrodynamic diameter (D_h, by intensity), size distribution width (W_d), polydispersity index (PDI); and zeta potential values (ζ), measured by DLS and LDE respectively.

NP Sample	EE (%)	D_h (nm)	W_d (nm)	PDI	ζ (mV)
NP-0	---	134.9 ± 6.5	31	0.079 ± 0.012	-2.38
NP-10H	---	104.2 ± 10.3	24	0.061 ± 0.002	-2.36
NP-20H	---	144.0 ± 8.2	35	0.057 ± 0.010	-1.60
NP-10H + c6	89.8	115.8 ± 6.5	52	0.098 ± 0.018	- 1.86
NP-20H + c6	90.1	160.3 ± 7.7	46	0.106 ± 0.021	-0.98
NP-10H + α-TOS	75.1	123.6 ± 9.2	45	0.114 ± 0.059	-2.01
NP-20H + α-TOS	88.4	155.2 ± 8.3	47	0.086 ± 0.019	-1.94
NP-71 + α-TOS	88.5	153.6 ± 7.6	39	0.122 ± 0.034	-2.26
NP-76 + α-TOS	94.9	140.3 ± 6.6	60	0.127 ± 0.013	-1.84
NP-82 + α-TOS	98.6	145.1 ± 5.2	44	0.075 ± 0.010	-1.29
NP-87 + α-TOS	95.8	95.9 ± 2.3	21	0.096 ± 0.010	-1.01

Figure 5A shows the size distributions of NP-10H and NP-20H. Both distributions were narrow and unimodal, as revealed by PDI values lower than 0.06. D_h of 104 and 144 nm were obtained from NP-10H and NP-20H, respectively. NP-10H presented a lower size in comparison to NP-20H. This effect could be due to a balance between the formation of hydrogen bonds through hydroxyl groups of HEMA and the alteration of the well-defined structure of the block copolymers.

This behavior was also observed by Zhang et al. for carboxylated poly(styrene -*b*-ethylene-*co*-butylene-*b*- styrene)[15]. D_h decreased with low concentrations of carboxylic groups and

then increased when the concentration of carboxylic groups raised[15]. These sizes are quite appropriate for their application as drug delivery system for cancer treatment, avoiding the RES system and improving the uptake by cells. Slightly negative zeta potentials were obtained for all NPs, indicating a nearly neutral charge of the surface. This behavior has also been observed in other PEG nanoassemblies[47]. Additionally, SEM micrographs (**figure 5B**) confirmed the spherical morphology of these nanoassemblies.

Encapsulation efficiency: α-TOS-loaded NP

The described block copolymers are excellent candidates to encapsulate hydrophobic molecules in their inner core. α-TOS-loaded NPs (10 % w/w respect to the polymer) were successfully prepared and characterized and the results are summarized in **table 2**. Particularly, EE was higher than 75% in all copolymeric systems. The EE was especially improved for the NPs with a high PEG content (EE higher than 94%), probably as a result of the protection and stabilization of the hydrophobic core by the PEG shell[36].

All size distributions were unimodal with low PDI values. Furthermore, the hydrodynamic diameters were lower than 155 nm. NP-10H+α-TOS were significantly smaller than those based on NP-20H+α-TOS (**figure 5C**). α-TOS-loaded NPs presented slightly higher D_h and PDI values in comparison to analogous unloaded NPs. Moreover, no appreciable differences in the zeta potentials of unloaded versus α-TOS-loaded NPs were found. Additionally, the size of α-TOS-loaded NPs based on block copolymers PEG-*b*-polyMTOS decreased as a function of PEG content into macromolecular chains. As an example, size distributions of loaded NPs based on PEG-71 and PEG-87 are compared in **figure 5E**. It is noteworthy that the distribution curves were narrow, unimodal and were clearly shifted to lower D_h as a result of the stabilization of PEG chain into the shell of the nanoassemblies. SEM micrograph of loaded NPs from NP-87+α-TOS (**figure 5F**) revealed the well-defined spherical morphology of the NPs. No aggregation was observed at room temperature.

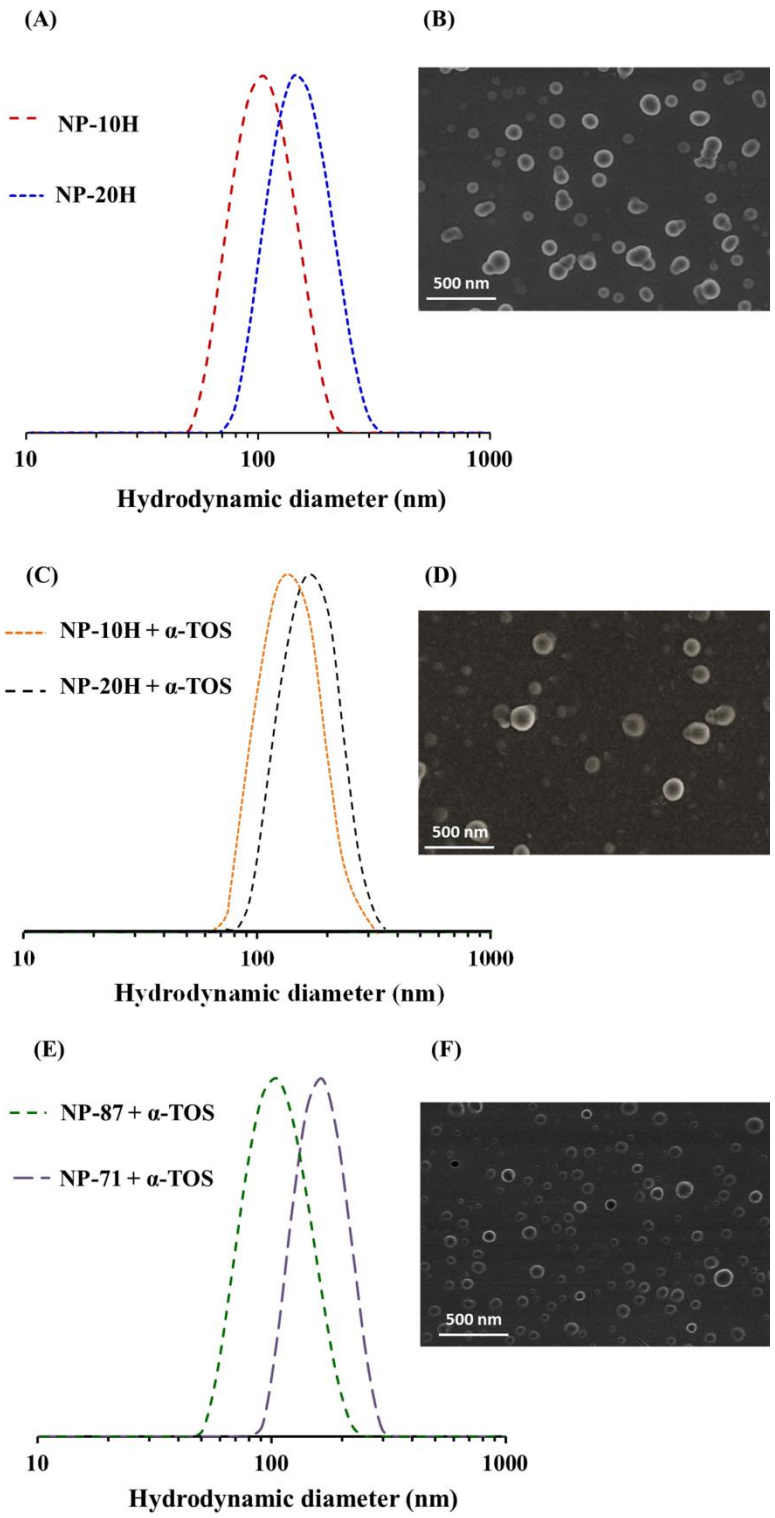

Figure 5: (A) Particle size distributions (D_h, by intensity) of unloaded NP, measured by DLS. Red: NP-10H; Blue: NP-20H. (B) SEM micrographs of NP-10H polymeric system dried from aqueous

solution at room temperature. (C) and (E) Particle size distributions of α-TOS entrapped NPs. Orange: NP-10H + α-TOS; Black: NP-20H + α-TOS; Green: NP-87 + α-TOS and Purple: NP-71 + α-TOS;. SEM micrographs of (D) NP-10H + α-TOS and (F) NP-87 + α-TOS dried from aqueous solution at room temperature.

- **Uptake and co-localization of c6-loaded NP**

c6 as a fluorescent probe was efficiently entrapped in the core of the NPs (EE higher than 89 %), obtaining NP sizes between 115 and 160 nm and a nearly neutral charge on their surface (**table 2**). These fluorescent NPs were used to trace their cellular uptake by MDA-MB-453 cells. **Figure 6A** shows the evolution of green fluorescence intensity in cancer cells, including confocal micrographs after 0.5, 2 and 6 h of incubation with NP-10H+c6. These results demonstrated that c6-loaded NPs were able to cross the cellular membrane of cancer cells in only 30 min. However, the intensity of fluorescence increased progressively after 2 and 6 h of NP treatment. Additionally, confocal images proven that the NPs were located inside the cytoplasm of cells, around the nucleus. According to the particle size of c6-loaded NPs, the endocytosis could be the most probable mechanism of NP uptake within cancer cells[48].

After 6 h, mitochondria of cancer cells were stained with MitoTracker® Red CMXRos in order to examine the ability of c6-loaded NPs to accumulate inside these organelles. Confocal micrographs of the co-localization study using NP-10H+c6 and NP-20H+c6 are shown in **figure 6B and C**, respectively. Bright orange fluorescence was observed as a result of the composition of green and red fluorescent images, confirming the co-localization of c6-loaded NPs into the mitochondria of cancer cells. According to the morphology of the NPs, the surface is essentially hydrophilic and constituted by PEG chains. c6 is incorporated in the hydrophobic core formed by copolymer segments of MTOS and low amounts of HEMA. It is possible that the diffusion of the fluorescent c6 should be partially produced in the interval of the endocytosis, but from an experimental point of view, the MitoTracker® assay represented in **figure 6B and C** demonstrates that there is an evident accumulation of the core-shell NPs in the mitochondria. Further experiments are being carried out with specific targeting components to investigate the interaction of the functionalized nanoparticles with the mitochondria.

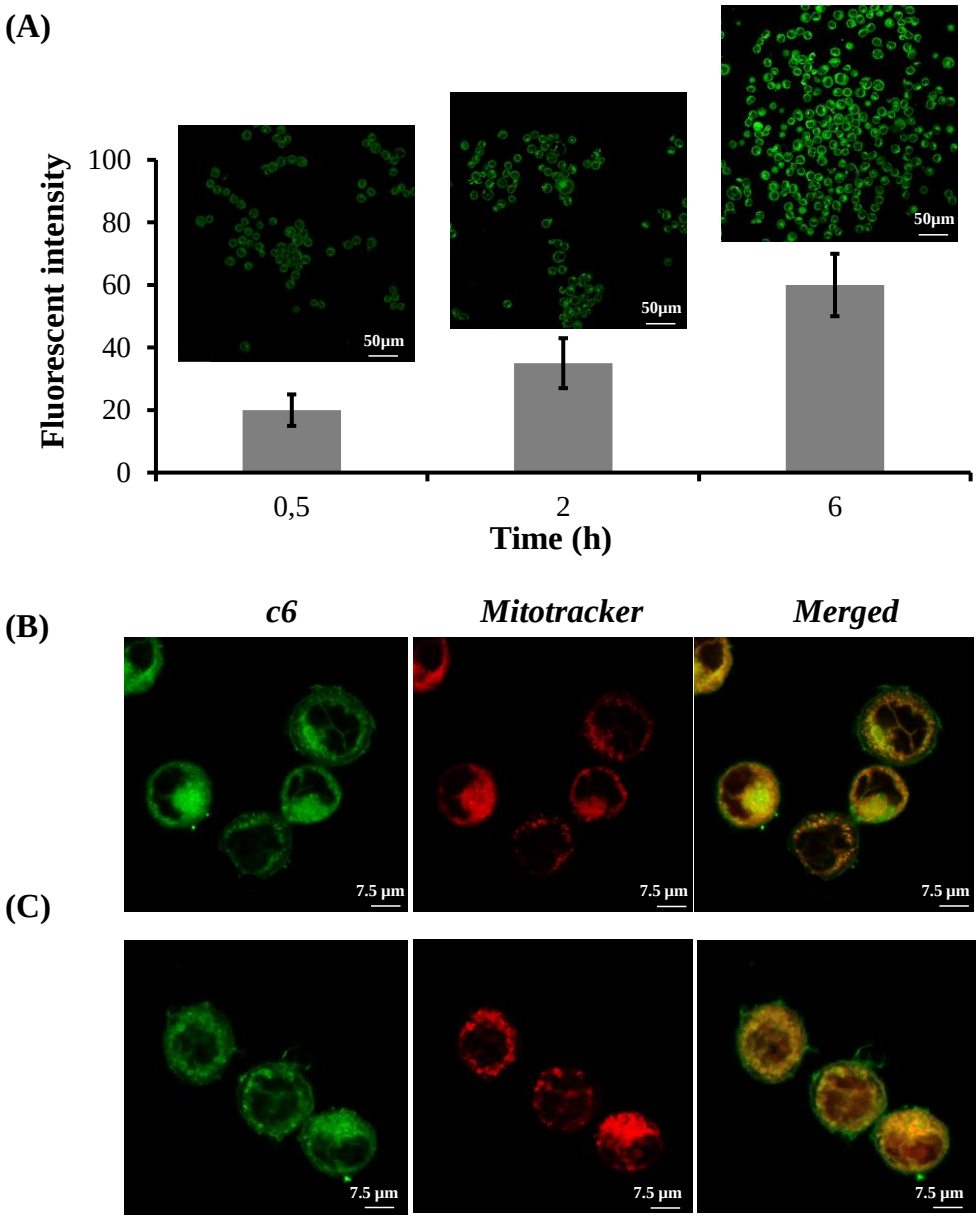

Figure 6: (A) Monitoring of endocytosis of c6 loaded NP-10H, including confocal micrographs of MDA-MB-453 cells after 0.5, 2 and 6 h of NPs incubation. Co-localization of c6 loaded NP-10H (B) and NP-20H (C) into the mitochondria of MDA-MB-453 cells by confocal microscopy.

α-TOS acts as a competitive inhibitor of succinate dehydrogenase (SDH, complex II) by displacing ubiquinone (coenzyme Q) from binding to complex II in the cancer cell mitochondria[49, 50]. Therefore, the localization of the synthesized NPs inside this organelle could enhance their biological activity.

- **Biological activity**

The therapeutic activity of all NPs was tested by Alamar Blue assay using two different breast cancer cells: luminal A human metastatic carcinoma (MCF-7) and HER2 positive human breast adenocarcinoma (MDA-MB-453) cells[51].

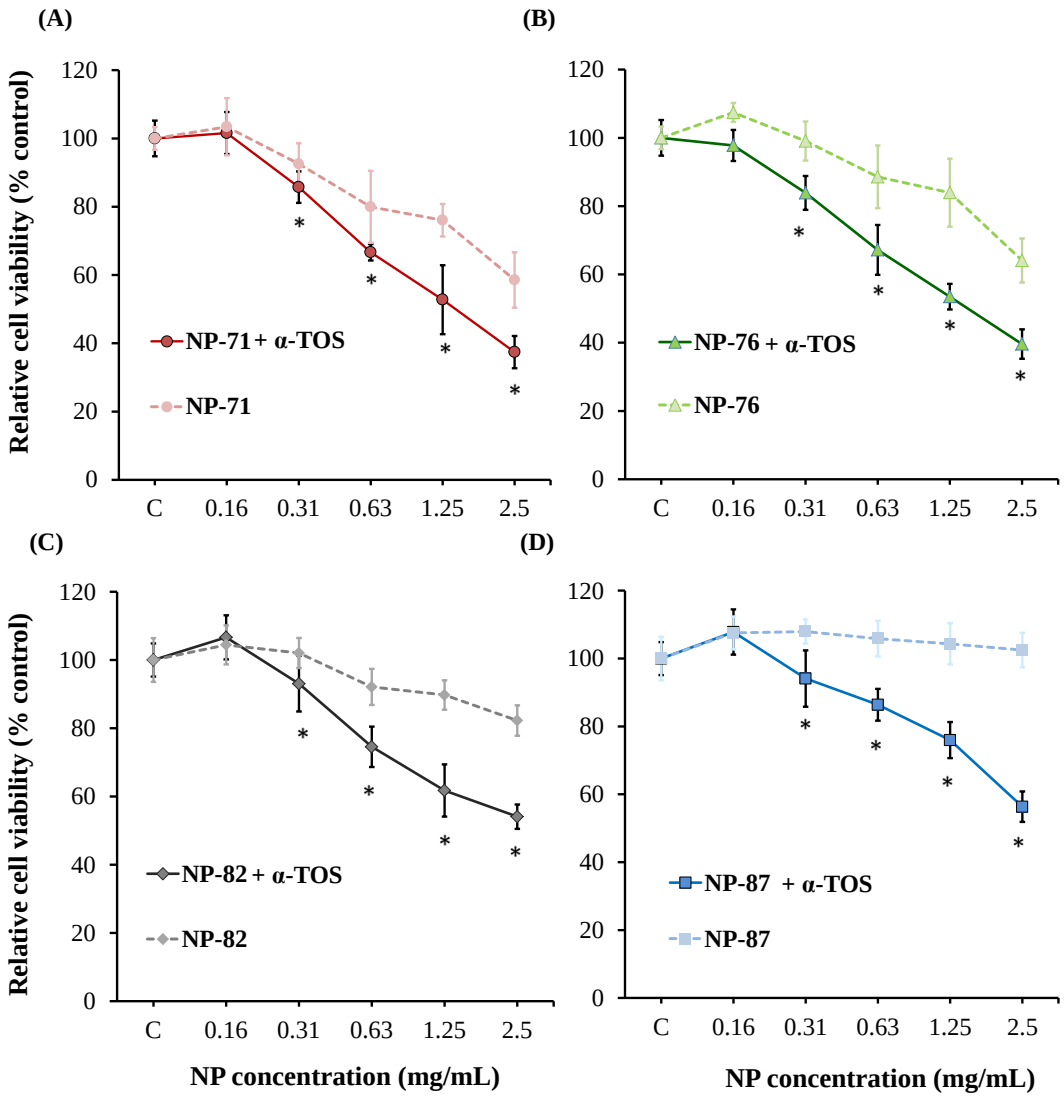

Figure 7: MDA-MB-453 viability in the presence of different α-TOS entrapped NP concentrations, measured after 24 h with respect to the control. Cell viability of unloaded NPs is also compared for all copolymeric systems. (A) Red: NP-71 ± α-TOS, (B) Green: NP-76 ± α-TOS, (C) Grey: NP-82 ± α-TOS and (D) Blue: NP-87 ± α-TOS. The diagrams include the mean, the standard deviation (n=8), and the ANOVA results at a significance level of *: $p < 0.05$

It should be noted that physical mixtures of block copolymer NPs with free α-TOS could not be utilized as control due to insolubility of α-TOS in PBS buffer. Moreover, the NPs loaded with α-TOS were prepared with 10 % w/w with respect to polymer and the drug loading of the HEMA containing copolymers will also be slightly lower compared to the pure PEG-*b*-polyMTOS block copolymers. However, these changes are less than 10% in drug loading and, therefore, we have chosen to discuss the biological activity based on NP concentration rather than amount of α-TOS in the following.

α-TOS-loaded NPs based on PEG-*b*-polyMTOS were significantly more active than unloaded NPs (**figure 7**). The biological activity of loaded NPs significantly increased as a function of the NP concentration and MTOS content of the block copolymers. All NP formulations reduced the viability below 70% at the highest NP concentration. In fact, cell viability was lower than 40% for NP-71 and NP-76, and 60% for NP-82 and NP-87. Additionally, the significant cytotoxicity of the different NP formulations was observed at lower concentrations until 0.63 mg/mL in comparison to unloaded NPs. The improvement of the antiproliferative activity of MTOS-based NPs was more significant in the case of NP-82 and NP-87 with a high PEG content.

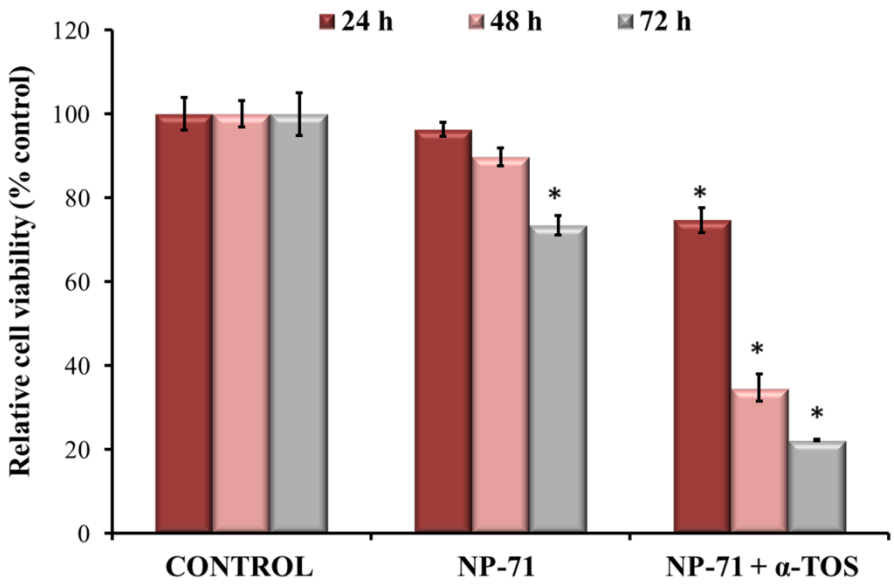

Figure 8: MCF-7 viability in the presence of unloaded and α-TOS-loaded NP-71 at 2.5 mg/ml measured overtime until 72 hours. The diagram includes the mean, the standard deviation (n=8), and the ANOVA results with respect to control at a significance level of: *: $p < 0.05$.

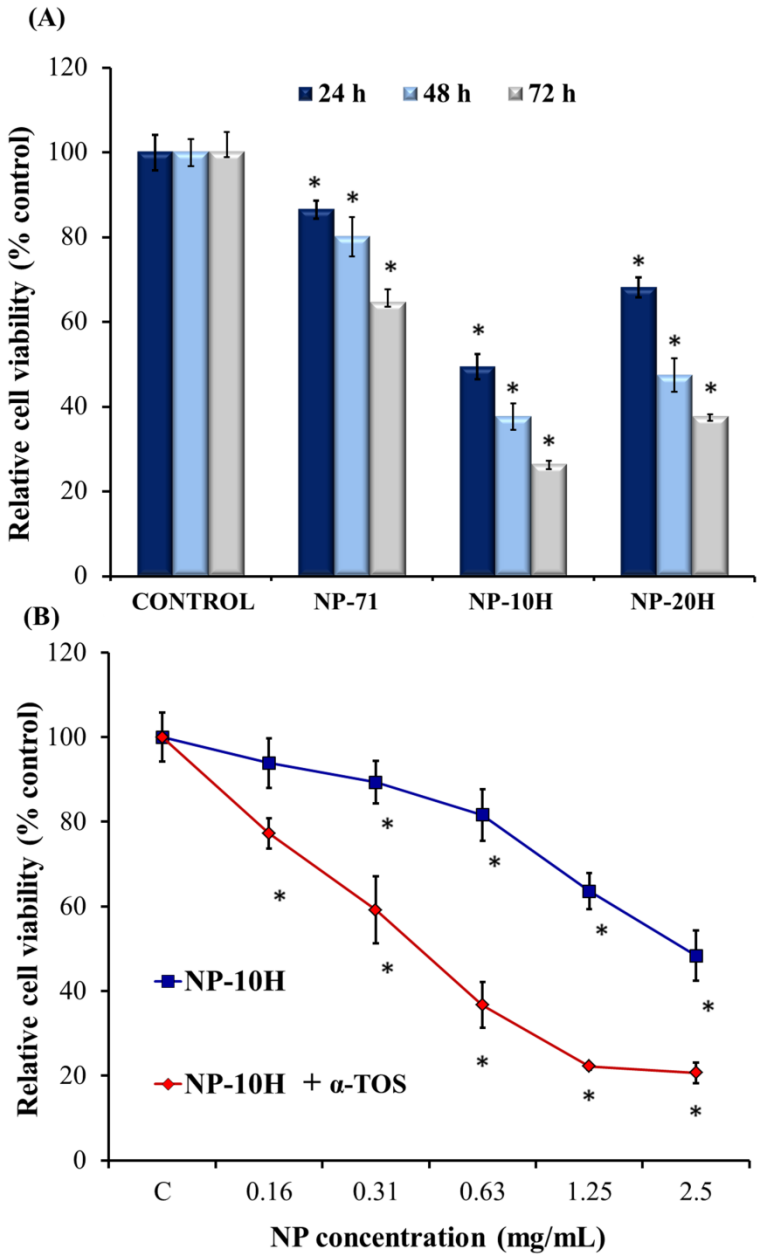

Figure 9: (A) Comparison of MCF-7 viability in the presence of NP-71, NP-10H and NP-20H formulations at 2.5 mg/ml, measured overtime until 72 hours. (B) Comparison of MDA-MB-453 viability in the presence of different concentrations of unloaded and α-TOS loaded NP-10H, measured after 24 h. The diagram includes the mean, the standard deviation (n=8), and the ANOVA results with respect to control at a significance level of: *: $p < 0.05$.

The most active loaded NPs (NP-71+α-TOS) was selected to analyze its effect on MCF-7 viability over 72 h. In fact, the presence of additional α-TOS enhanced the

cytotoxicity of NP-71 formulation and this effect was more pronounced after 48 and 72 hours (**figure 8**). In particular, the viability of unloaded NPs was not reduced below 70% within the timeframe of experimentation and a slight decrease in cell viability was only observed between 48 and 72 hours. In contrast, the effect of α-TOS loaded NPs was significantly higher after 48 hours, as the viability was reduced from 75% at 24 hours to 35% at 48 hours, probably due to the release of the drug into the cancer cells during this period of time. It is noteworthy that MCF-7 cells were less sensitive than MDA-MB-453 to the presence of NPs. This difference could be probably attributed to the metabolic characteristics of MDA-MB-453 and MCF-7, regarding to the alteration of their mitochondria and the relative importance of glycolic metabolism for each cell line[52, 53].

The effect of the incorporation of HEMA into the hydrophobic polyMTOS block on the anticancer activity of polymeric formulations was evaluated on MCF-7. **Figure 9A** shows that the therapeutic action of these NPs greatly increased with the incorporation of HEMA monomeric units. The viability of MCF-7 cells decreased to 49 and 68% after 24 hours for NP-10H and NP-20H, respectively. Furthermore, this effect was more evident at longer periods of time, reaching viabilities lower than 40% after 72 hours.

The enhancement of therapeutic action of polymeric systems as a result of HEMA incorporation can be explained by considering the modification of hydrophobicity of MTOS based-core of NPs. In absence of HEMA, the precise control of the macromolecular architecture gave rise to well-organized stable nanoassemblies. However, the increase of the hydrophilicity of hydrophobic block, favored the therapeutic action of NPs[54, 18], probably due to the enhancement of the water diffusion and the hydrolysis rate that represent crucial factors for the release of α-TOS from NPs by hydrolysis as we recently demonstrated for related acid-degradable thermoresponsive polymers[55].

Unexpectedly, NP-20H (with higher content of HEMA) had a lower effect on cell viability than NP-10H, possibly due to a decrease in MTOS units into the hydrophobic block copolymers. For that reason, it maybe speculated that NP-10 had a better balance between the number of active MTOS and HEMA units that were randomly distributed in the hydrophobic block.

The most active NPs based on PEG-10H were also evaluated against MDA-MB-453 and the effect of loading of α-TOS in the core of the NPs was also studied. **Figure 9B** shows the MDA-MB-453 cell viability after the treatment of different concentrations of

unloaded and loaded NP-10H. The loading of additional α-TOS into the core of NPs based on PEG-10H significantly improved their anticancer activity. In fact, cell viability was reduced to 20% at 2.5 and 1.25 mg/mL after 24 h. Additionally, the NPs were found to be cytotoxic down to concentrations of 0.31 mg/mL

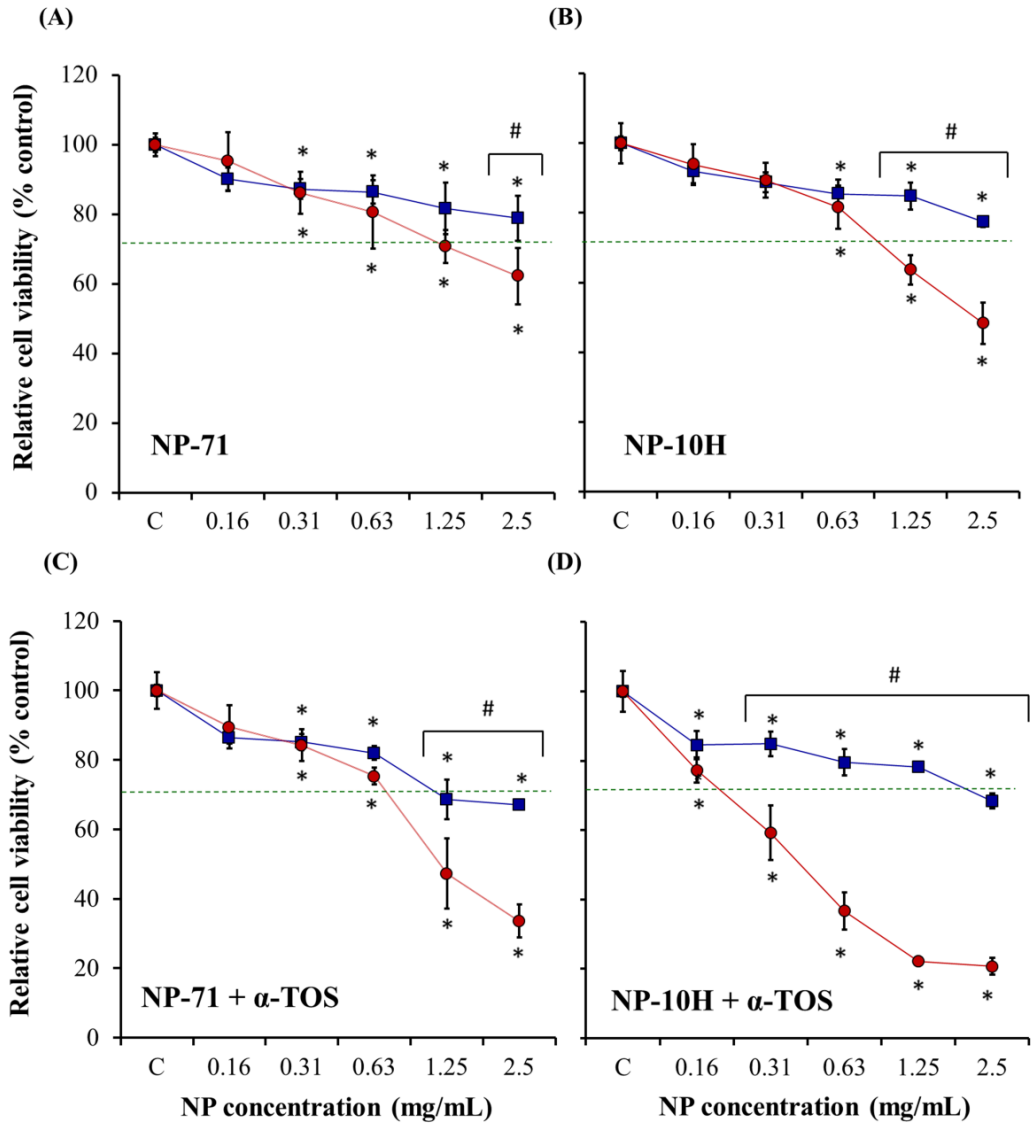

Figure 10: HMEpiC (Blue line) and MDA-MB-453 (Red line) cell viability in the presence of different concentrations of NPs measured after 24. (A) NP-71, (B) NP-10H, (C) NP-71 + α-TOS and (D) NP-10H + α-TOS. The diagrams include the mean, the standard deviation (n=8), and the ANOVA results from the comparison of cancer cells and healthy cells, obtained at a significance level of: $^{\#}$, *: $p < 0.05$.

α-TOS has demonstrated selectivity against cancer cells. However, the mechanisms involved in this selectivity are not well understood at the present. The most commonly accepted theory to explain this behavior is based on the difference of cellular metabolism between cancer and healthy cells, which is related to the levels of esterase and antioxidants enzymes and the mechanism to produce ROS[56, 57]. In particular, the levels of these enzymes are diminished in cancer cells, allowing the accumulation of ROS species that stimulate the release of cytochrome C and therefore trigger apoptosis[58, 59]. Furthermore, the negative charge of α-TOS at neutral pH could also be correlated with its selective anticancer activity due to the acidic pH of most solid tumors (around 6.0 – 6.5), whilst pH is neutral in the case of the healthy tissues[57]. For that reasons, the biological activity of NP-71 and NP-10H was also measured against nontumoral HMEpiC cells in order to know if these nanoassemblies preserve α-TOS selectivity towards breast cancer cells.

Nontumoral HMEpiC cells were significantly less sensitive to the presence of the NPs. In fact, viability of HMEpiC cells was higher than 70% in the presence of unloaded NPs (**figure 10A and B**). In the case of loaded NPs, the viability of HMEpiC only decreased below 70% at high NP concentrations. However, NP-10H + α-TOS reduced MDA-MB-453 cancer cell viability to 20% at 2.5 mg/mL after 24 hours, whilst the HMEpiC cell viability was maintained very close to 70%. This formulation presented a high activity and a selective interval from 0.31 till 2.50 mg/mL (**figure 10C and D**).

4.2.5. Conclusions

The chemical incorporation of small amounts of HEMA in the hydrophobic block of PEG-*b*-polyMTOS (obtained by RAFT polymerization), to give rise to PEG-*b*-(poly(MTOS-*co*-HEMA) terpolymers, significantly increased the bioactivity of the correspondent NPs (NP-10H). HEMA reduced the hydrophobicity of the polyMTOS block without jeopardizing NP self-assembly as the hydrodynamic diameter and polydispersity were maintained or even improved if compared with the NPs obtained with no HEMA (PEG-*b*-polyMTOS). The terpolymers were also able to encapsulate additional α-TOS (NP-10H + α-TOS) with high efficiency and the resulting NPs presented the highest bioactivity with the highest selectivity. These results indicate that the strategy followed in this work increased dramatically the biological activity of α-TOS based NPs, probably by improving

the water accessibility to the MTOS residues and favoring its hydrolysis and the release of the anticancer compound.

4.2.6. Acknowledgements

Authors would like to thank David Gómez, Rosa Ana Ramírez and Mar Fernández, and María Isabel Trabado for their help in SEM, cell culture and CLSM experiments, respectively.

4.2.7. Supporting information

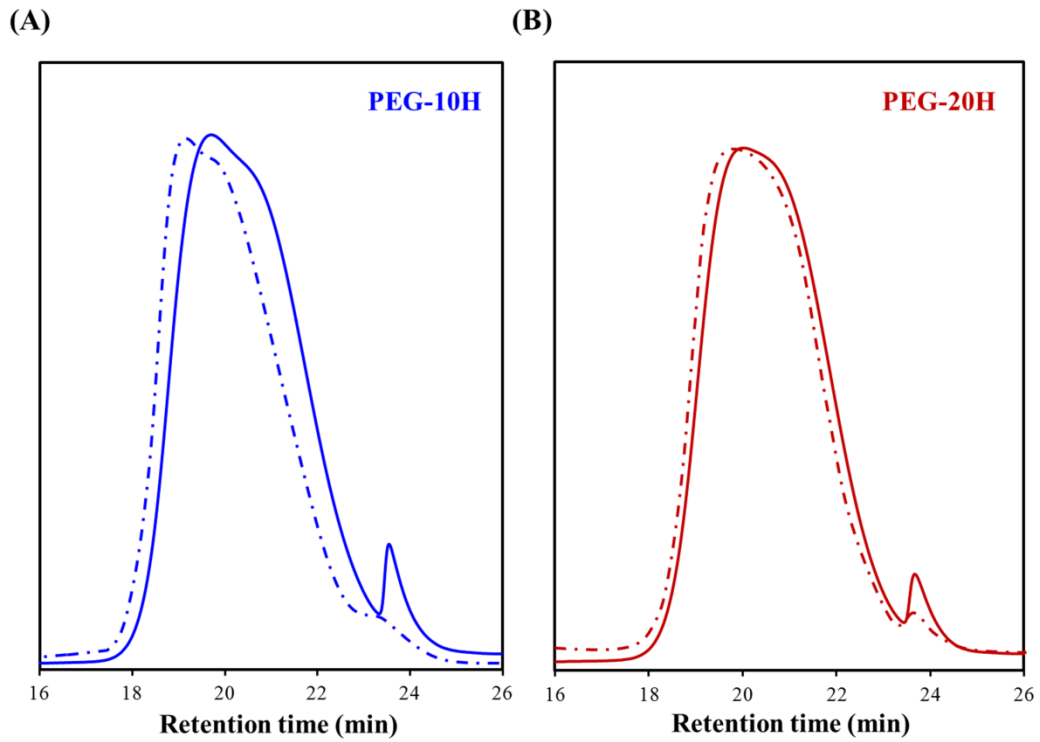

Figure S1: SEC traces of (A) PEG-10H (Blue) and (B) PEG-20H (Red) at the end of the RAFT copolymerization. Solid line: before purification by dialysis and dashed line: after purification by dialysis

4.2.8. References

[1] S. Sandhiya, S. A. Dkhar, A. Surendiran, *Fundamental & clinical pharmacology* **2009**, *23*, 263.

[2] M. Estanqueiro, M. H. Amaral, J. Conceição, J. M. S. Lobo, *Colloids and Surfaces B: Biointerfaces* **2015**, *126*, 631.

[3] A. Wicki, D. Witzigmann, V. Balasubramanian, J. Huwyler, *Journal of Controlled Release* **2015**, *200*, 138.

[4] N. Ponnappan, A. Chugh, *Pharmaceutical Medicine* **2015**, 1.

[5] D. J. Bharali, S. A. Mousa, *Pharmacology & therapeutics* **2010**, *128*, 324.

[6] K. H. Bae, H. J. Chung, T. G. Park, *Molecules and cells* **2011**, *31*, 295.

[7] S. P. Egusquiaguirre, M. Igartua, R. M. Hernández, J. L. Pedraz, *Clinical and Translational Oncology* **2012**, *14*, 83.

[8] F. Greco, M. J. Vicent, *Advanced Drug Delivery Reviews* **2009**, *61*, 1203.

[9] Z. L. Tyrrell, Y. Shen, M. Radosz, *Progress in Polymer Science* **2010**, *35*, 1128.

[10] M. C. Branco, J. P. Schneider, *Acta biomaterialia* **2009**, *5*, 817.

[11] S. Bamrungsap, Z. Zhao, T. Chen, L. Wang, C. Li, T. Fu, W. Tan, *Nanomedicine* **2012**, *7*, 1253.

[12] R. Palao-Suay, L. Gómez-Mascaraque, M. Aguilar, B. Vázquez-Lasa, J. San Román, *Progress in Polymer Science* **2016**, *53*, 207.

[13] U. Kedar, P. Phutane, S. Shidhaye, V. Kadam, *Nanomedicine: Nanotechnology, Biology and Medicine* **2010**, *6*, 714.

[14] A. Rösler, G. W. Vandermeulen, H.-A. Klok, *Advanced drug delivery reviews* **2012**, *64*, 270.

[15] G. Zhang, L. Liu, Y. Zhao, F. Ning, M. Jiang, C. Wu, *Macromolecules* **2000**, *33*, 6340.

[16] K. Kuroda, K. Fujimoto, J. Sunamoto, K. Akiyoshi, *Langmuir* **2002**, *18*, 3780.

[17] K. Watanabe, Y. Tsuchiya, Y. Kawaguchi, S.-i. Sawada, H. Ayame, K. Akiyoshi, T. Tsubata, *Biomaterials* **2011**, *32*, 5900.

[18] A. Gallardo, G. Rodríguez, M. R. Aguilar, M. Fernández, J. San Román, *Macromolecules* **2003**, *36*, 8876.

[19] L. Garcia-Fernandez, M. Aguilar, M. Fernandez, R. Lozano, G. Gimenez, S. Valverde, J. San Roman, *Biomacromolecules* **2010**, *11*, 1763.

[20] J. Neuzil, L.-F. Dong, J. Rohlena, J. Truksa, S. J. Ralph, *Mitochondrion* **2013**, *13*, 199.

[21] J. Neuzil, J. C. Dyason, R. Freeman, L.-F. Dong, L. Prochazka, X.-F. Wang, I. Scheffler, S. J. Ralph, *Journal of bioenergetics and biomembranes* **2007**, *39*, 65.

[22] J. Neuzil, L.-F. Dong, L. Ramanathapuram, T. Hahn, M. Chladova, X.-F. Wang, R. Zobalova, L. Prochazka, M. Gold, R. Freeman, *Molecular aspects of medicine* **2007**, *28*, 607.

[23] K. N. Prasad, B. Kumar, X.-D. Yan, A. J. Hanson, W. C. Cole, *Journal of the American College of Nutrition* **2003**, *22*, 108.

[24] N. Duhem, F. Danhier, V. Préat, *Journal of Controlled Release* **2014**, *182*, 33.

[25] S. Koudelka, P. T. Knotigova, J. Masek, L. Prochazka, R. Lukac, A. D. Miller, J. Neuzil, J. Turanek, *Journal of Controlled Release* **2015**, *207*, 59.

[26] R. Palao-Suay, M. R. Aguilar, F. J. Parra-Ruiz, M. Fernández-Gutiérrez, J. Parra, C. Sánchez-Rodríguez, R. Sanz-Fernández, L. Rodrigáñez, J. S. Román, *Biomacromolecules* **2015**, *16*, 1566.

[27] R. Palao-Suay, M. R. Aguilar, F. J. Parra-Ruiz, S. Maji, R. Hoogenboom, N. Rohner, S. N. Thomas, J. San Román, *Polymer Chemistry* **2016**, *7*, 838.

[28] Y. Chong, T. P. Le, G. Moad, E. Rizzardo, S. H. Thang, *Macromolecules* **1999**, *32*, 2071.

[29] G. Moad, E. Rizzardo, S. H. Thang, *Australian journal of chemistry* **2005**, *58*, 379.

[30] H. Hatakeyama, H. Akita, H. Harashima, *Biological and Pharmaceutical Bulletin* **2013**, *36*, 892.

[31] H. Hatakeyama, H. Akita, H. Harashima, *Advanced Drug Delivery Reviews* **2011**, *63*, 152.

[32] P. Suárez, L. Rojo, Á. González-Gómez, J. S. Román, *Macromolecular bioscience* **2013**, *13*, 1174.

[33] H. Yabu, *Bulletin of the Chemical Society of Japan* **2012**, *85*, 265.

[34] B. Page, M. Page, C. Noel, *International journal of oncology* **1993**, *3*, 473.

[35] Y. Ikeda, Y. Nagasaki, "PEGylation technology in nanomedicine", in *Advances in Polymer Science*, 2012, p. 247/115.

[36] J. V. Jokerst, T. Lobovkina, R. N. Zare, S. S. Gambhir, *Nanomedicine* **2011**, *6*, 715.

[37] F. M. Veronese, G. Pasut, *Drug Discovery Today* **2005**, *10*, 1451.

[38] J.-P. Montheard, M. Chatzopoulos, D. Chappard, *Journal of Macromolecular Science, Part C: Polymer Reviews* **1992**, *32*, 1.

[39] S. L. Tomić, M. M. Mićić, S. N. Dobić, J. M. Filipović, E. H. Suljovrujić, *Radiation Physics and Chemistry* **2010**, *79*, 643.

[40] H. Yavuz, G. Bayramoğlu, Y. Kaçar, A. Denizli, M. Yakup Arica, *Biochemical Engineering Journal* **2002**, *10*, 1.

[41] J. Křížová, A. Španová, B. Rittich, D. Horák, *Journal of Chromatography A* **2005**, *1064*, 247.

[42] J. Weaver, I. Bannister, K. Robinson, X. Bories-Azeau, S. Armes, M. Smallridge, P. McKenna, *Macromolecules* **2004**, *37*, 2395.

[43] D. J. Keddie, *Chemical Society Reviews* **2014**, *43*, 496.

[44] M. Müllner, A. Schallon, A. Walther, R. Freitag, A. H. Müller, *Biomacromolecules* **2009**, *11*, 390.

[45] S. Kumar, R. Acharya, U. Chatterji, P. De, *Langmuir 2013*, *29*, 15375.

[46] H. Yabu, *Polymer journal* **2013**, *45*, 261.

[47] Y. Hu, J. Xie, Y. W. Tong, C.-H. Wang, *Journal of Controlled Release* **2007**, *118*, 7.

[48] T.-G. Iversen, T. Skotland, K. Sandvig, *Nano Today* **2011**, *6*, 176.

[49] L.-F. Dong, P. Low, J. C. Dyason, X.-F. Wang, L. Prochazka, P. K. Witting, R. Freeman, E. Swettenham, K. Valis, J. Liu, *Oncogene* **2008**, *27*, 4324.

[50] L. F. Dong, V. J. A. Jameson, D. Tilly, J. Cerny, E. Mahdavian, A. Marín-Hernández, L. Hernández-Esquivel, S. Rodríguez-Enríquez, J. Stursa, P. K. Witting, B. Stantic, J. Rohlena, J. Truksa, K. Kluckova, J. C. Dyason, M. Ledvina, B. A. Salvatore, R. Moreno-Sánchez, M. J. Coster, S. J. Ralph, R. A. J. Smith, J. Neuzil, *Journal of Biological Chemistry* **2011**, *286*, 3717.

[51] D. L. Holliday, V. Speirs, *Breast Cancer Res* **2011**, *13*, 1.

[52] J. M. Cuezva, M. Krajewska, M. L. de Heredia, S. Krajewski, G. Santamaría, H. Kim, J. M. Zapata, H. Marusawa, M. Chamorro, J. C. Reed, *Cancer research* **2002**, *62*, 6674.

[53] A. Isidoro, M. Martínez, P. Fernandez, A. Ortega, G. Santamaría, M. Chamorro, J. Reed, J. Cuezva, *Biochem. J* **2004**, *378*, 17.

[54] M. R. Aguilar, G. Rodríguez, M. Fernández, A. Gallardo, J. San Román, *Journal of Materials Science: Materials in Medicine* **2002**, *13*, 1099.

[55] Q. Zhang, Z. Hou, B. Louage, D. Zhou, N. Vanparijs, B. G. De Geest, R. Hoogenboom, *Angewandte Chemie* **2015**, *127*, 11029.

[56] S. J. Ralph, S. Rodríguez-Enríquez, J. Neuzil, E. Saavedra, R. Moreno-Sánchez, *Molecular aspects of medicine* **2010**, *31*, 145.

[57] R. Allen, A. K. Balin, *Experimental cell research* **2003**, *289*, 307.

[58] L.-F. Dong, E. Swettenham, J. Eliasson, X.-F. Wang, M. Gold, Y. Medunic, M. Stantic, P. Low, L. Prochazka, P. K. Witting, *Cancer research* **2007**, *67*, 11906.

[59] J. Neuzil, T. Weber, N. Gellert, C. Weber, *British journal of cancer* **2001**, *84*, 87.

[60] M. Birringer, J. EyTina, B. Salvatore, J. Neuzil, *British journal of cancer* **2003**, *88*, 1948.

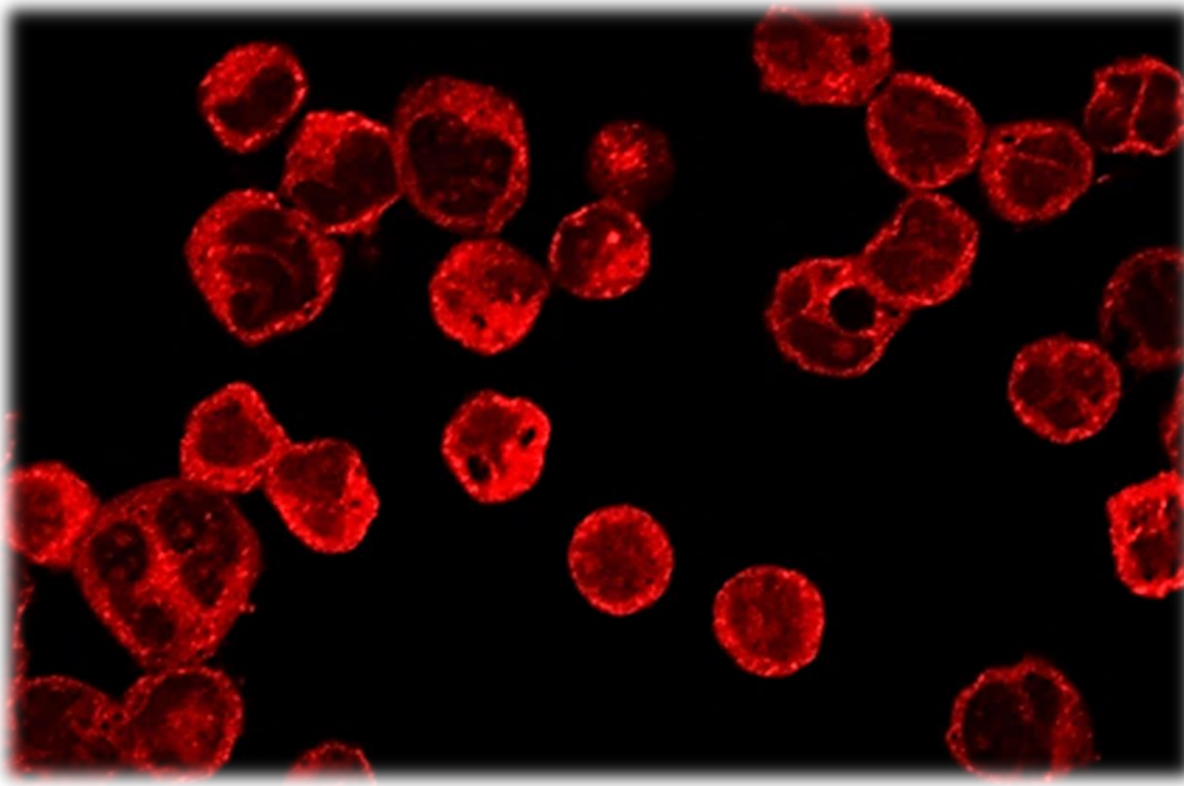

Chapter V: Phototherapeutic nanoparticles

5.1- Phototherapeutic effect of polymeric nanoparticles based on α-TOS-RAFT block copolymers conjugated to IR-780.

5.1. Phototherapeutic effect of polymeric nanoparticles based on α-TOS-RAFT block copolymers conjugated to IR-780.

Raquel Palao-Suay[1,2], María Rosa Aguilar[1,2], Sergio Martín-Saldaña[3], Francisco M. Martin-Saavedra[4,2], Clara Escudero Duch, Francisco J. Parra-Ruiz[1], N.A.Rohner[5], Susan N. Thomas[5], Nuria Vilaboa[4,2] and Julio San Román[1,.2]*

[1]Group of Biomaterials, Department of Polymeric Nanomaterials and Biomaterials, Institute of Polymer Science and Technology, CSIC, Madrid, Spain

[2]Networking Biomedical Research Centre in Bioengineering, Biomaterials and Nanomedicine, CIBER-BBN, Spain.

[3]Department of Otorhinolaryngology, Puerta de Hierro University Hospital, Majadahonda, Spain

[4]La Paz University Hospital-IdiPAZ, Madrid, Spain.

[5]George W. Woodruff School of Mechanical Engineering and Parker H. Petit Institute of Bioengineering and Bioscience, Georgia Institute of Technology, Atlanta, Georgia, USA.

**Corresponding author*: mraguilar@ictp.csic.es

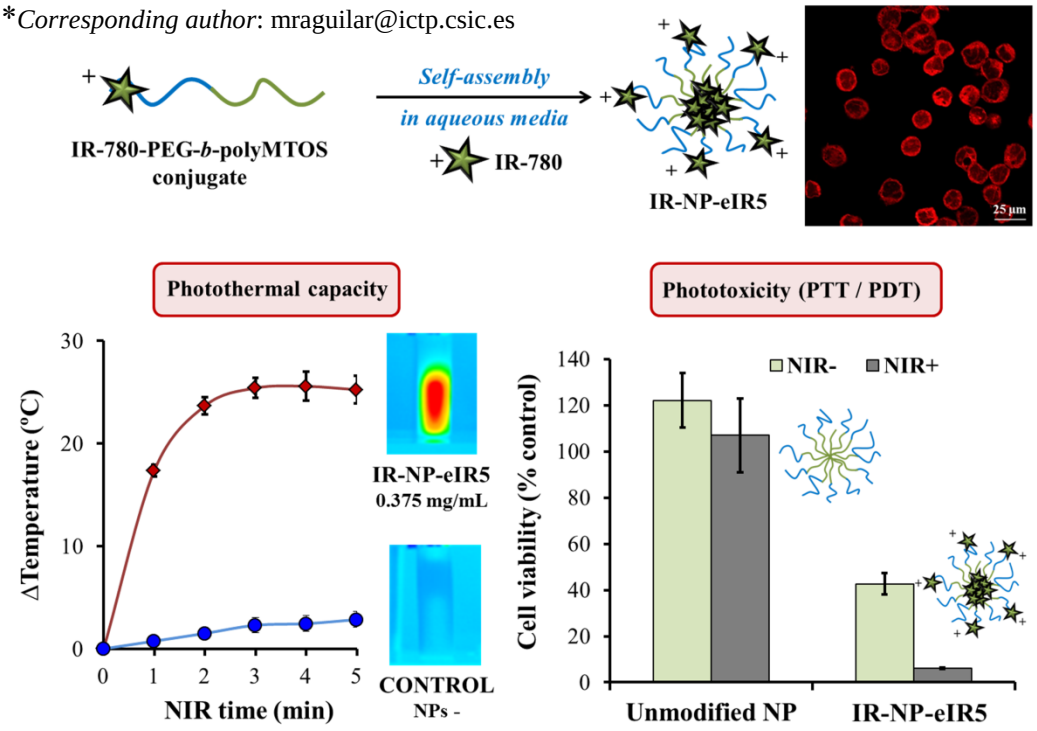

KEYWORDS: IR-780, nanoparticles, α-tocopheryl succinate, phototherapeutic nanomaterials, RAFT polymerization.

5.1.1. Abstract

The aim of this work was the generation of a multifunctional polymeric theranostic system that incorporate IR-780 dye, a near-infrared (NIR) imaging probe that exhibits photothermal and photodynamic properties; and a derivate of α-tocopheryl succinate (α-TOS), a mitochondria-targeted anticancer compound (mitocan) with antiangiogenic activity.

IR-780 was conjugated to the hydrophilic segment of RAFT block copolymer PEG-*b*-polyMTOS to generate IR-NP, self-assembled nanoparticles (NPs) in aqueous media which exhibit a hydrophilic shell and a hydrophobic core. During assembly, the hydrophobic core of IR-NP could encapsulate additional IR-780 to give rise to derived subspecies which differed in the amount of encapsulated probe (IR-NP-eIR).

Characterization and evaluation of photo-inducible properties in theranostic NPs synthesized were thoroughly assessed *in vitro*. The obtained NPs exhibited emitted NIR fluorescence under NIR light excitation, however IR-780 encapsulated within IR-NP-eIR resulted in a severe quench of the fluorescence exhibited by the RAFT copolymer conjugated to IR-780. Excitation by a laser emitting at 808 nm showed that IR-NP-eIR exhibit greater photothermal efficiency than that conducted by IR-NP. Cytotoxic activity exerted by IR-NP or IR-NP-eIR in MDA-MB-453 cells increased significantly after treatment with the NIR laser due to the photothermal and photodynamic effect of IR-780. However, in the case of IR-NP, phototoxic activity observed in tumor cells could not be attributed to the generation of lethal hyperthermia as occurs at nanomaterial concentrations which did not produce a net increase in temperature after NIR irradiation.

5.1.2. Introduction

The future of oncology relies on the development of multifunctional theranostic nanosystems which combine diagnostics tests with targeted therapies and real-time monitoring to the therapies in a single platform[1-3]. Nanoparticles (NPs), due to their unique physical and chemical properties, have been exhaustively explored as platforms to deliver imaging and therapeutic agents to the target site. Particularly, a wide number of nanosized delivery vehicles have been applied for theranostic applications, including quantum dots, superparamagnetic iron oxides NPs, gold NPs, liposomes, or niosomes[4, 5]. Polymer-based NPs are expected to play a significant role in the dawning era of nanotheranostics for personalized medicine[4]. Polymeric NPs improve the efficacy and selectivity of entrapped or conjugated agents via the enhanced permeability and retention (EPR) effect or through active targeting with a prolonged circulation half-life and sustained drug release[1, 6].

Near infrared (NIR) fluorescence is used for imaging purposes *in vivo* due to extremely low absorption and autofluorescence from organic tissues in the wavelength range from 700 to 1000 nm. This characteristic significantly improves the image sensitivity (minimizing background interference) and tissue depth penetration. Particularly, NIR dyes absorb light of NIR wavelengths to reach an excited singlet state. Part of the energy of the excited singlet state would be dissipated in the form of fluorescence. Some energy of the excited singlet state can be transited through vibronic relaxation or other non-radiative transitions pathways, which will be converted into heat. If the rate of heat production exceeds that of heat dissipation within a tissue, the temperature would increase gradually promoting cellular cytotoxicity[7]. Alternatively, the excited singlet state can move to a lower-energy excited triplet state via intersystem crossing. Under this condition, the triplet state can undergo two different reactions: it can react with a substrate through electron or hydrogen atom transfer reactions, producing free radicals and other reactive oxygen species (ROS) (type I reaction); or it can transfer its energy directly to ground-state triplet oxygen to form excited state single oxygen (type II reaction)[8, 9]. These products induce oxidation reaction with nearby biomacromolecules and destruct organic tissue effectively. Therefore, NIR dyes can effectively be used as promising agents for photophotothermal (PTT) and photodynamic (PDT) therapy[10-12].

To ascertain biosafety, it is crucial to evaluate the potential health impact of any nanomaterial introduced into the body. Most typical nanoabsorbers of NIR energy are

inorganic compounds with a non-degradable nature, nonspecific biodistribution and poorly characterized bioretention, leading to an undetermined long-term toxicity that hinders clinical translation[13, 14]. Organic NIR dyes such cyanine compounds are efficient NIR-absorbers that have high molar absorptivity, good photostability and the ability to generate strong fluorescence emission at the NIR range, simultaneously serving as a fluorescent imaging probes as well as phototherapeutic agents. With small molecular weights, NIR dyes usually could be excreted shortly after injection, without rendering much long-term toxicity concern[13, 14]. Particularly, IR-780 iodide is a lipophilic cation heptamethine dye with specific absorption peak at 780 nm. As result of the presence of a rigid cyclohexenyl ring in the heptamethine chain with a central chlorine atom, the photostability and quantum yield are increased in comparison to other inorganic NIR nanoabsorbers based in noble metals (e.g. Au, Ag, Pt), metal oxides or carbon[15].

The most important drawbacks for the clinical use of IR-780 iodide are poor solubility in physiological medium[16] and a low tolerance *in vivo* experimental animals (e.g.,1.5 mg/kg is the maximal tolerance dose in mice)[17]. In order to overcome these limitations, IR-780 dye has been successfully encapsulated into polymeric multifunctional micelles labeled with rhenium-188[18], silica NPs[19] or liposomes[20]. However, these vehicles were complicated to synthesize and non-biodegradable, exhibiting photothermal properties that were inefficient for PTT. Recently, Yue et al. encapsulated IR-780 iodide in the inner core of the heparin-folic acid conjugate through ultrasonic sound method[21]. Jiang et al. used human serum albumin to effectively load IR-780 iodide, forming NPs by protein self-assembly. These NPs were able to increase the aqueous solubility of the dye 1000-fold while the toxicity was reduced (from 2.5 mg/kg to 25 mg/kg)[17].

Nevertheless, the use of synthetic polymer-based nanovehicles has not been fully explored to effectively administer IR-780 iodide. In this sense, Yuan et al. modified the IR-780 iodide structure using the central chlorine atom in order to conjugate a hydrophilic PEG_{2000}, forming micelles that improved its water solubility[22]. The appropriate size of theses micelles (~100 nm) favored its preferential accumulation into tumor area due to the EPR effect[23], avoiding the opsonization of the nanomaterial by the reticuloendothelial system (RES)[24] and the clearance from the body by renal filtration[25]. Nevertheless, these authors did not investigate the use of these PEG-based micelles as a drug delivery system to encapsulate hydrophobic molecules in their inner core.

One of the most attractive possibilities of nanoassembly designing based on polymeric and synthetic macromolecules, is the use of amphiphilic block copolymers that are typically obtained by controlled polymerization techniques[26]. In particular, our group has recently synthesized RAFT block copolymers based on PEG_{8000} and MTOS, a methacrylic derivative of α-tocopheryl succinate (α-TOS), forming bioactive self-assembled NPs for anticancer therapy[27]. The presence of a PEG-block and an appropriate molecular weight (MW) of the block copolymer favored the cytotoxic activity of α-TOS, a mitocan that selectively induces the apoptosis of malignant cells by targeting the mitochondria while exerting minimal toxicity towards normal cells and tissues[28]. Relatively slow uptake of α-TOS by malignant cells, which relies on passive diffusion, is a limiting point in efficient delivery of this anticancer drug[29, 30]. NPs derived from MTOS could be employed to entrap additional α-TOS in their inner core to significantly increase the amount of drug that reaches the cell interior and thereby improving its cytotoxic potential[31].

The incorporation of IR-780 iodide on the surface of the polymeric NPs derived from MTOS could increase the selectivity of these nanosystems for cancer cells. The lipophilic cationic nature of IR-780 dye facilitates the penetration through the mitochondrial membrane which is known to have a zeta potential between -120 and -160 mV[32, 33]. Cancer cells typically show a more hyperpolarized mitochondrial membrane potential than nonmalignant cells[34, 35]. A recent work showed that IR-780 iodide has a preferential accumulation into the mitochondria of tumor cells[36]. Moreover, these and other authors discovered that IR-780 showed a high affinity for the organic anion transporter peptides (OATPs) that are frequently overexpressed in several tumor cell lines[36, 37].

The aim of this work was the preparation of NPs based in block copolymers of PEG_{8000} and MTOS that incorporate IR-780 in order to enhance their anticancer activity by phototherapy and enabling real-time monitoring of target tissue by NIR fluorescence. Specifically, IR-780 was successfully conjugated to amphiphilic block copolymers COOH-PEG-*b*-polyMTOS. Additionally, the formation of spherical NPs entrapping free IR-780 iodide by self-organized precipitation (SORP) was investigated with the complete characterization of their physico-chemical properties. The photothermal properties of obtained nanoassemblies incorporating IR-780 were examined in detail. Finally, the endocytosis, anticancer and phototherapeutic activities of these theranostic NPs were evaluated *in vitro* using breast carcinoma cells (**figure 1**).

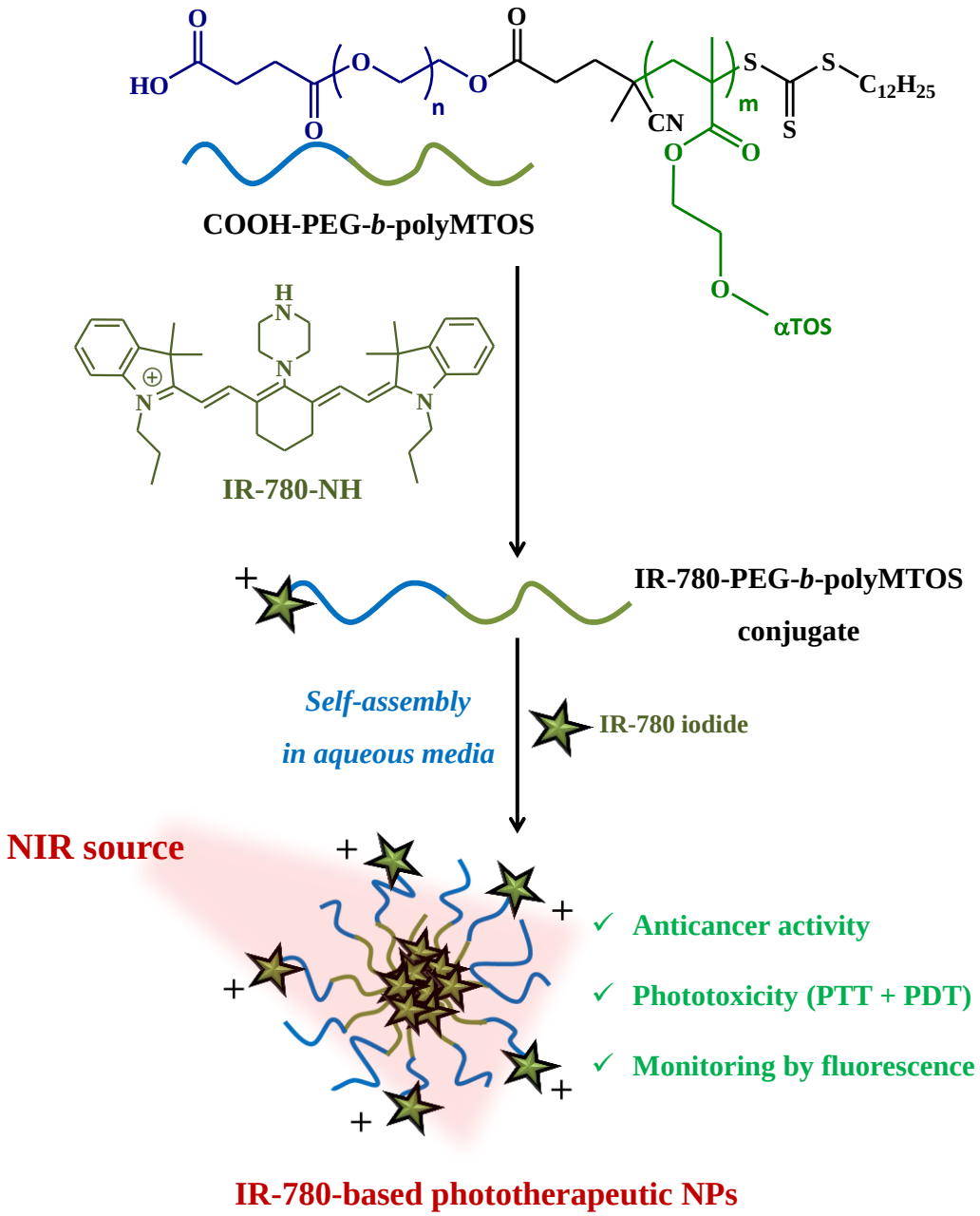

Figure 1: Scheme of preparation of IR-780-based NPs

5.1.3. Materials and methods

- **Materials**

MTOS and CTA-PEG_8 were obtained as previously described[27, 38]. 4-dimethylaminopyridine (DMAP, Sigma-Aldrich), triethylamine (Et_3N, Scharlau) and succinic anhydride (SA, Sigma- Aldrich) were used without further purification in the modification of PEG macro-CTA agent. 1,4-dioxane anhydrous (Sigma-Aldrich) were used without further purification and 2,2'Azobisisobutyronitrile (AIBN, Merck) was recrystallized from methanol (m.p. 104 ºC) for the RAFT polymerization. 2-[2-[2-Chloro-3-[(1,3-dihydro-3,3-dimethyl-1-propyl-2H-indol-2-ylidene)ethylidene]-1-cyclohexen-1-yl]ethenyl]-3,3-dimethyl-1-propylindolium iodide (IR-780 iodide, Sigma-Aldrich), 4-(4,6-Dimethoxy-1,3,5-triazin-2-yl)-4-methylmorpholinium chloride (DMTMM, Sigma-Aldrich), tetrahydrofuran anhydrous (THF, Sigma-Aldrich), dimethylformamide anhydrous (DMF, Sigma-Aldrich) and ethanol (EtOH, Merck) were used without further purification in the preparation of IR-780 based polymer conjugate. Deuteraded chloroform ($CDCl_3$, Sigma-Aldrich) and chromatographic grade tetrahydrofuran (THF, Sigma-Aldrich) were used without further purification to characterize the polymeric conjugate. Additionally, sodium chloride (NaCl, Panreac) was used without further purification for the preparation of self-assembled NPs.

- **Synthesis of COOH-PEG-*b*-polyMTOS**

CTA-PEG_8 (1 equiv), SA (5 equiv) and DMAP (0.1 equiv) were dissolved in DMF anhydrous and added to a 50 mL round-bottom flask. Then, Et_3N (10 equiv) was added dropwise with constant stirring using an ice bath under nitrogen atmosphere. The reaction mixture was kept under magnetic stirring for 24 h at room temperature. At the end of the reaction, CTA-PEG-COOH were dialyzed (Spectrum Laboratories, 3.5 kDa MW cut-off) against distilled water for 72 h. The resulting solution was isolated by freeze-drying to yield white amorphous powders.

COOH-PEG-*b*-polyMTOS was successfully synthesized by RAFT polymerization. In particular, CTA-PEG_8-COOH, MTOS and AIBN were dissolved in anhydrous 1,4-dioxane and sealed in a 25 mL Schlenk tube. The total monomer concentration (M) and the feed molar ratio [MTOS]:[CTA]:[AIBN] were 0.5 M and [100]:[1]:[0.3], respectively. The reaction mixture was then degassed by three freeze-pump-thaw cycles and heated in an oil

bath under magnetic stirring at 70 ºC for 5 h. At the end of the polymerization, block copolymer was purified by dialysis (Spectrum Laboratories, 25 kDa MW cut-off) against a mixture of THF and EtOH (75:25 v:v) that was progressively replaced by water during three days.

- **Synthesis of IR-780-PEG-*b*-polyMTOS conjugate**

IR-780-NH was obtained as previously described[39]. Briefly, IR-780 iodide (1 equiv) and piperazine (5 equiv) were dissolved in 15 mL of dry DMF. The reaction mixture was then stirred and refluxed for 4 h at 80 ºC. Afterwards, the solvent was removed under reduced pressure and the resulting product was purified by silica gel column chromatography using CH_2Cl_2/ EtOH (10:0.5, v/v) as eluent.

COOH-PEG-*b*-polyMTOS (1 equiv) was dissolved in THF anhydrous using a 50 mL round-bottom flask. IR-780-NH (5 equiv) and DMTMM (10 equiv) in DMF anhydrous were then added to a copolymer solution with constant stirring using an ice bath under nitrogen atmosphere. The reaction was stirred for 24 h under nitrogen atmosphere at room temperature. When the reaction time had elapsed, IR-780-PEG-*b*-polyMTOS conjugate were purified by dialysis (Spectrum Laboratories, 3.5 kDa MW cut-off) against a mixture of THF and EtOH (75:25 v:v) that was gradually replaced by distilled water over three days. The resulting solution was isolated by freeze-drying to yield green amorphous powder.

The chemical structure of the block copolymer and IR-780-based polymer conjugate was elucidated by ^{1}H-NMR spectroscopy in a Mercury 400BB apparatus, operating at 400 MHz. Additionally, the number and weight average molecular weight (M_n and M_w) and dispersity ($Đ$) of the block polymer were determined by size exclusion chromatography (SEC) using a Perkin-Elmer Isocratic LC pump 250 coupled to a refraction index detector (Series 200). Three polystyrene-divinyl benzene columns (Polymer Laboratories) of average pore size of 10^3, 10^4 and 10^5 Å were used as solid phase, and degassed THF (1 mL/min) was used as eluent at 40ºC. Monodisperse poly(methyl methacrylate) (PMMA) standards (Scharlab) with MWs between 10.3 and 1400 kDa were used to obtain the calibration curve. Data were analyzed using the Perkin-Elmer LC solution program.

- **Preparation of IR-780-based NPs**

Theranostic NPs were prepared by solvent exchange or SORP method. Specifically, 2 mL of NaCl at 100 mM was incorporated dropwise over an organic dissolution (2mL of

THF:MeOH or THF:EtOH 50:50 v:v) of IR-780-PEG-*b*-polyMTOS conjugate at 6 mg/mL under constant magnetic stirring. The final polymer concentration was 3 mg/mL. Additionally, IR-780 iodide (3, 5 and 10 % w/w with respect to polymer conjugate) was also incorporated to the organic phase with the aim to obtain NPs that entrapped this hydrophobic dye in their inner core. NP dispersions were dialyzed against an excess amount of NaCl solution for 72 h, followed by filtering through a 0.22 µM polyethersulfone membranes (PES, Millipore Express®, Millex GP).

- **Characterization of IR-780-based NPs**

The particle size distribution and polydispersity (PDI) of NPs were determined by dynamic light scattering (DLS) using a Malvern Nanosizer NanoZS Instrument equipped with a 4mW He-Ne laser (λ=633 nm) at a scattering angle of 173°. All measurements were performed in square polystyrene cuvettes (SARSTEDT) at 25 ºC. Additionally, zeta potential values were determined at 0.3 mg/mL NP concentration containing 10 mM NaCl, using laser Dopper electrophoresis (LDE) and the Smoluchowski´s approximation. For each sample, the statistical average and standard deviation of data were calculated from 8 measurements of 20 runs each one.

The morphology of NPs was analyzed by scanning electron microscopy (SEM) using a Hitachi SU8000 TED, cold-emission FE-SEM microscope working with an accelerating voltage between 25 and 50 kV. Samples were prepared by deposition of one drop of the corresponding NP suspension (0.03 mg/mL) over small glass disks. The aqueous phase was evaporated at room temperature for 24 h. The samples were coated with gold palladium alloy (80:20) prior to examination by SEM.

The absorption and fluorescence properties of self-assembled NPs were measured on a Bioteck SYNERGY-H4 microplate reader. Particularly, the absorption spectra were obtained from 400-900 nm. Moreover, the emission spectra were recorded from 790 nm to 850 nm after excitation at 770 nm.

- **Biological experiments**

Cell culture

Human mammary gland/breast carcinoma cells, MDA-MB-453 cells (ATCC), derived from metastatic site, were cultured in Dulbecco's modified Eagle's medium

(DMEM), supplemented with 10% fetal bovine serum (FBS), 1% penicillin/streptomycin (PS) and incubated at 37°C in a humidified air with 5% CO_2 (37ºC-5%CO_2). Furthermore, human mammary epithelial cells, HMEpiC cells (obtained from Innoprot, P10891), were cultured using mammary epithelial cell medium (MepiCM, Innoprot), at 37ºC-5%CO_2.

Cellular imaging studies

Endocytosis of IR-780-NPs was followed by fluorescence microscopy (EVOS® FL microscope). Particularly, MDA-MB-453 cells were seeded into 24 well plates at 100,000 cells/mL and incubated for 48 h at 37ºC-5%CO_2. The complete medium was then replaced with the corresponding NP dispersions in NaCl (500 µL of the NPs suspension and 500 µL of completed medium) and incubated at 37ºC-5%CO_2. At different time points (0.5, 1, 2, 5, 6.5 and 8 h), the cells were washed with cold PBS and fixed by a paraformaldehyde solution in PBS (3.7 w/v %) for 15 min at room temperature. Finally, the cells were rinsed with cold PBS and visualized by fluorescence microscopy (EVOS® FL microscope, Cy7 lightcube filter at $\lambda_{excitation}$ = 731 nm and $\lambda_{emission}$ = 825 nm). In the same manner, cells were observed by Confocal Laser Scanning Microscopy (CLSM, Leica TCS-SP5 RS AOBS, $\lambda_{excitation}$ = 633 nm and emission spectrum between 700 and 800 nm) after 5 h of NP treatment. This work has been performed by the Confocal Microscopy Service of the Universidad de Alcalá de Henares (UAH) and the Biomedical Networking Center (CIBER-BBN), located at the facilities of the Cell Culture Unit.

In vitro cytotoxicity assay

Cell viability in the presence of different concentrations of NPs (1.5, 0.75, 0.375, 0.188 and 0.094 mg/mL) was measured using alamarBlue assay (Sigma-Aldrich)[40]. Briefly, MDA-MB-453 cells were seeded at 60,000 cells/mL (6,000 cells/well) in 96-well plates. After 48 h of incubation, the medium was replaced with the corresponding NP dispersed in NaCl (50:50 v/v of the NP suspension and completed medium). The plates were incubated at 37ºC-5%CO_2 for 24 h. Afterwards, 100 µL of Alamar Blue solution (10 % Alamar Blue solution in phenol red free DMEM medium) was added to all wells. After 4 h of incubation, the fluorescence was measured on a Biotek SYNERGY-HT plate reader ($\lambda_{excitation}$ = 530 nm and $\lambda_{emission}$ = 590 nm).

- **Determination of phototherapeutic effect of IR-780-based NPs**

Photothermal properties in solution

Different concentrations of IR-780-NP suspensions (0.375, 0.188 and 0.094 mg/mL) were incorporated to polystyrene cuvettes and exposed to 808 nm wavelength laser irradiation using and experimental setup described elsewhere[41]. NIR-irradiation of cell cultures was performed inside a thermostatically-controlled chamber (Model Stuart SI60D, Fisher Scientific Afora, Madrid, Spain) to establish the environmental temperature at 37 ºC. Temperature changes in the NPs suspension were monitored by IR thermography using a Testo 875-2i thermal imaging camera (Instrumentos Testo S.A, Madrid, Spain).

Phototherapeutic effect in vitro of IR-780 NPs

MDA-MB-453 cells were seeded into a 48 well plate at a density of 100,000 cells/ml per well and incubated for 24 h at 37ºC-5%CO_2 . Then, cells were cultured with the medium containing different concentrations of NPs (0.375, 0.188 and 0.094 mg/mL). After 24 h of incubation, cells were washed with PBS and cultured with fresh culture medium. To quantify the photo-therapeutic efficacy of these NPs, cells were irradiated with a 44 mW/mm^2 808 nm laser for 10 min. The cells without NPs and NIR irradiation were taken as the negative control. Finally, viability of cells was investigated using the alamarBlue assay. After washing with PBS, samples were incubated inDMEM-10% FBS containing 10% (v/v) alamarBlue dye for 2 h at 37ºC-5%CO_2. After excitation at 530 nm, emitted fluorescence at 590 nm was quantified using a Synergy4 spectrofluorimeter.

Statistical analysis

Results were expressed as mean ± standard deviation. Statistical significance (significance level of: *: $p < 0.05$) was evaluated using the analysis of variance (ANOVA, Tukey test) as required, by Origin 9.

5.1.4. Results and discussion

To overcome the low solubility of α-TOS in physiological media, PEG-*b*-polyMTOS with different PEG:MTOS ratios were successfully synthesized by RAFT polymerization, as recently described by our group[27]. These bioactive block copolymers presented the ability to self-assemble in aqueous media forming micellar nanoaggregates with a hydrophilic shell and a hydrophobic core that were able to encapsulate and transport other hydrophobic molecules. The synthesized NPs presented anticancer and antiangiogenic properties. PEG-*b*-polyMTOS (71:29) exhibited the highest cytotoxicity as a result of its highest MTOS content and the appropriate chain length of PEG macromolecules that facilitated the escape from the RES system, without significantly affecting the cellular uptake into cancer cells[27]. This balance is well-known in the literature as PEG dilemma[42]. Therefore, PEG-*b*-polyMTOS (71:29) is an excellent candidate to incorporate therapeutic agents in its structure with the aim to achieve superior cytotoxicity and provide them with new exciting features such as optical properties for diagnosis and photo-therapeutic activity.

- **Synthesis and characterization of IR-780-PEG-*b*-polyMTOS**

PEG-*b*-polyMTOS are quite attractive to incorporate therapeutic agents that increase their biological activity due to the presence of hydroxyl endo group of PEG that can be easily functionalized. In this way, CTA-PEG_8 was firstly modified to introduce carboxyl groups, yielding pure product after its purification. The chemical structure of CTA-PEG_8-COOH was confirmed using ^{1}H-NMR spectroscopy by the appearance of the methylene protons CH_2-f at 4.25 ppm and CH_2-h or CH_2-i protons within range between 2.30 and 2.70 ppm (**figure 2**). Other relevant characteristics of this macro-CTA are shown in the **table 1**. In particular, SEC characterization of this CTA confirmed that the incorporation of carboxyl groups maintained its narrow MW distribution with a *Đ* value of 1.12.

CTA-PEG_8-COOH was successfully used to polymerize MTOS by RAFT at 70ºC in anhydrous dioxane. ^{1}H-NMR spectra of the synthesized polymeric system COOH-PEG-*b*-polyMTOS is shown in **figure 3**. Polymerization of the MTOS was confirmed by the disappearance of the vinyl protons of MTOS between 5.5 and 6.5 ppm, the appearance of its characteristics proton signals and the broadening of the signals as a result of the macromolecular nature of the synthesized block polymers.

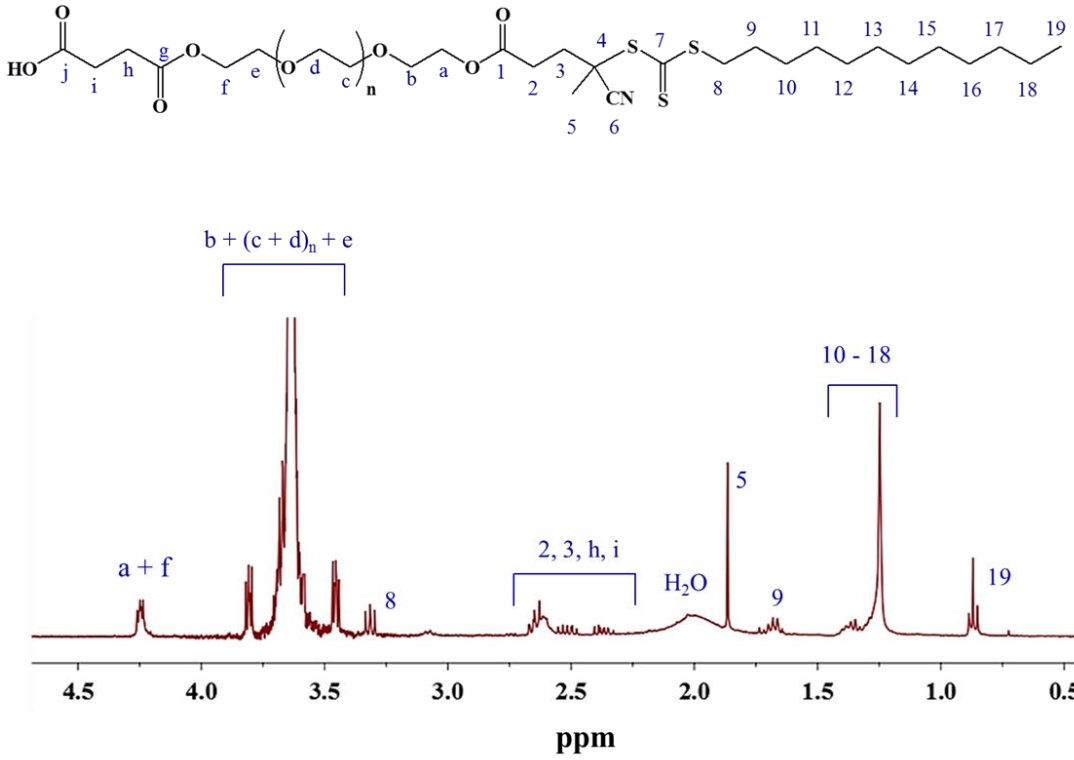

Figure 2: ^{1}H-NMR spectra of CTA-PEG$_8$-COOH

After their purification by dialysis, the synthesized block copolymer was characterized, obtaining the results that are collected in **table 1**. The composition of the different block copolymers was elucidated by ^{1}H-NMR spectroscopy, using the same methodology that was previously described by our group (**figure 3**)[27]. According to this procedure, COOH-PEG-*b*-polyMTOS with a molar composition of PEG:MTOS 70:30 was obtained. Additionally, SEC characterization indicated that polymeric system presented a MW higher than 65 kDa with a relatively low *Đ* as a result of the control over the polymerization.

Finally, IR-780-NH was successfully conjugated to the synthesized block copolymer by forming an amide bond between the amine group of the dye and the carboxyl group of PEG chains using DMTMM as coupling reagent. This was selected due to its several advantages in comparison to other reagents as EDC. In particular, DMTMM is a triazine derivative that facilitates an efficient one-step condensation of polymers and other small molecules with a high yield, easy removal of subproducts and a wide range of reaction

conditions regarding to the use of solvents or pH range [43-45]. In fact, the successful conjugation of the dye was confirmed by ^{1}H-NMR spectroscopy. As it is shown in **figure 4**, the conjugate spectrum contained peaks contributed by IR-780 dye and the polymeric system based in PEG.

Table 1: Summary of most relevant structural characteristics of CTA-PEG$_8$-COOH and COOH-PEG-*b*-polyMTOS block copolymer.

Sample	[a] M_n x 10^{-3}	[b] $M_{n\ SEC}$ x 10^{-3}	[b] $Đ$	[a] n_{PEG}	[a] m_{MTOS}	f_{PEG}-f_{MTOS} (mol %)
CTA-PEG$_8$-COOH	8.2	9.9	1.12	177	---	---
COOH-PEG-*b*-PMTOS	68.3	66.6	1.40	177	75	70-30

a) Determinated using ^{1}H-NMR spectroscopy

b) Determinated by SEC (THF) using PMMA standards

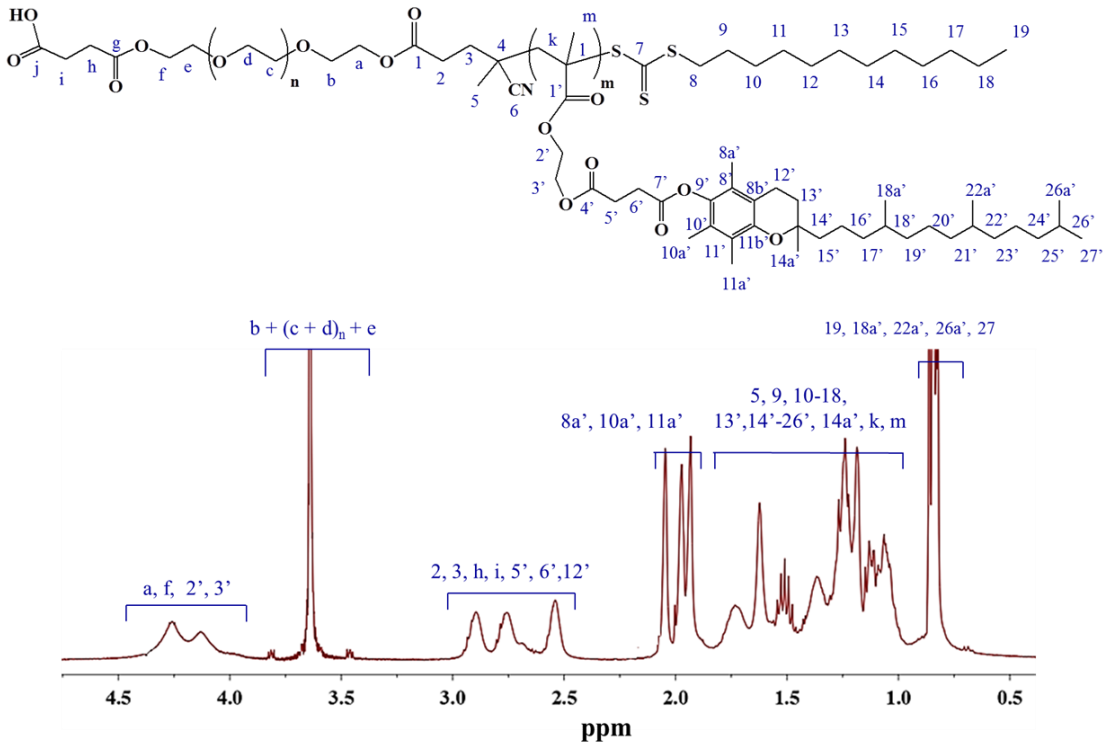

Figure 3: ^{1}H-NMR spectrum of COOH-PEG-*b*-polyMTOS

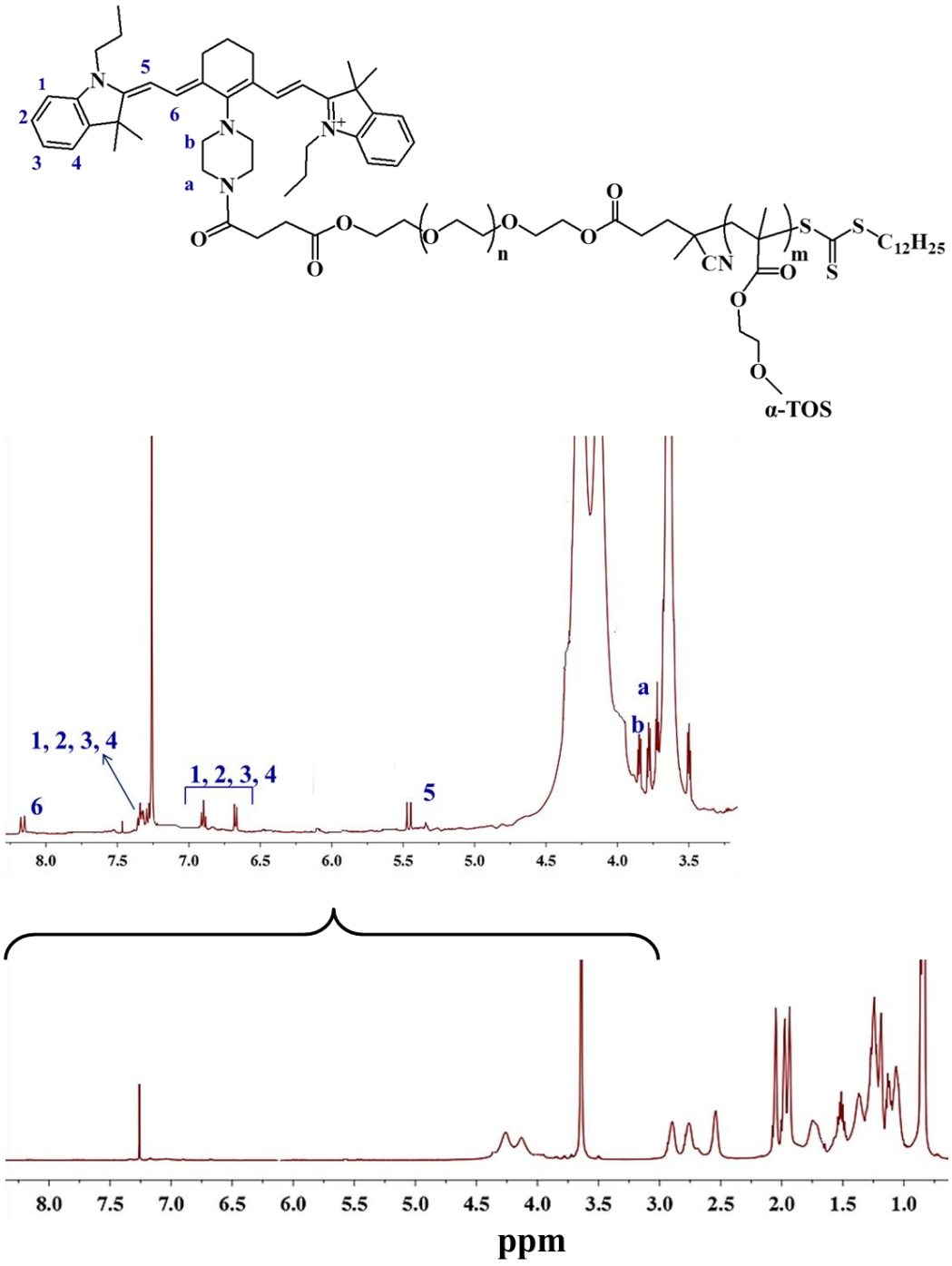

Figure 4: ^{1}H-NMR spectrum of the polymeric conjugate IR-780-PEG-*b*-polyMTOS

- **Characterization of NPs based on the IR-780-PEG-*b*-polyMTOS conjugate**

IR-780-PEG-*b*-polyMTOS conjugate was able to form spherical NPs by a spontaneous self-assembly process where PEG hydrophilic chains were distributed in the external shell, stabilizing the MTOS-based hydrophobic core through inter- and intramolecular interactions. The most relevant characteristics of the NPs obtained from PEG-*b*-polyMTOS and IR-780-PEG-*b*-polyMTOS conjugate (labelled as unmodified-NP and IR-NP, respectively) are summarized in **table 2**.

Table 2: Most relevant characteristics of unloaded and IR-780 iodide entrapped NPs, including hydrodynamic diameter (D_h, by intensity), polydispersity index (PDI); and zeta potential values (ζ), measured by DLS and LDE respectively.

NP sample	Organic phase	% Load	D_h (nm)	PDI	ζ (mV)
Unmodified-NP	Dioxane	---	134.9 ± 6.5	0.079 ± 0.012	-2.4
IR-NP	THF:MeOH (50:50 v:v)	---	178.4 ± 11.8	0.187 ± 0.020	3.1
IR-NP	THF:EtOH (50:50 v:v)	---	88.8 ± 6.7	0.058 ± 0.022	2.9
IR-NP-eIR3	THF:EtOH (50:50 v:v)	3	110.2 ± 6.4	0.160 ± 0.017	9.2
IR-NP-eIR5		5	134.6 ± 5.8	0.150 ± 0.012	12.6
IR-NP-eIR10		10	167.2 ± 8.3	0.253 ± 0.023	15.7

IR-NP exhibited an average hydrodynamic diameter of 178.4 ± 11.8 nm when a mixture of THF:MeOH (50:50 v:v) was used during the precipitation by solvent exchange. However, the replacement of MeOH by EtOH allowed obtaining IR-NP of reduced size and PDI, probably due to the improved solubility of the polymeric conjugate incorporating IR-780 (**figure 5A**). Additionally, IR-NP dispersions had zeta potential values around +3 mV, demonstrating the presence of the IR-780 lipophilic cation in the external shell of the NPs. The positive charge of NPs incorporating IR-780 dye has been described for other authors. In this sense, Yuan et al. conjugated IR-780 iodide to the chemical structure of PEG_{2000},

obtaining micelles with a zeta potential around +8 mV[22]. Finally, the SEM micrograph of IR-NP confirmed their spherical shape with an optimal monodispersity (**figure 5B**).

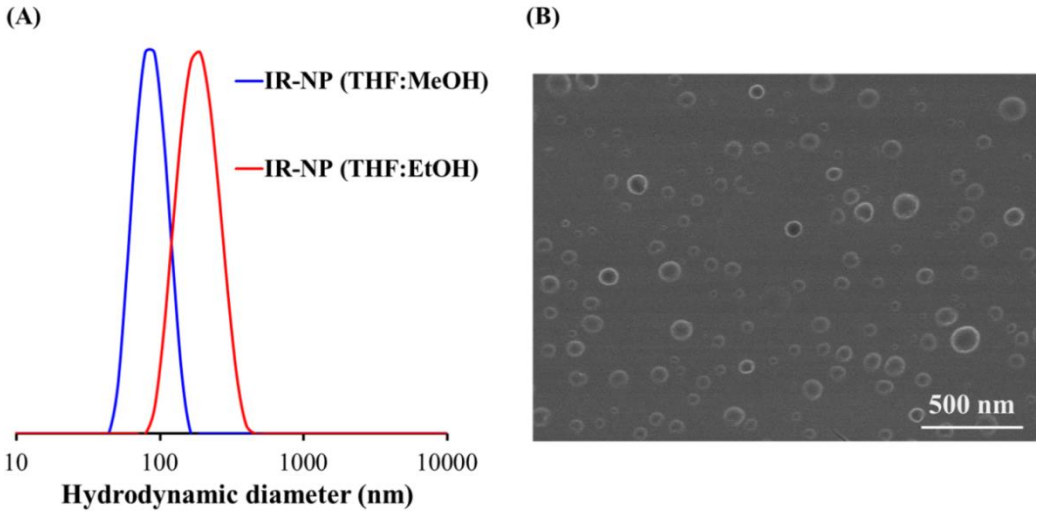

Figure 5: (A) Particle size distributions (D_h, by intensity) of IR-NP as a function of the organic phase used during the SORP method using NaCl as aqueous phase in both cases, measured by Dynamic Light Scattering. Blue: THF:MeOH; Red: THF:EtOH. (B) SEM micrograph of IR-NP dried from aqueous solution at room temperature. Scale bar: 500 nm.

Self-assembled IR-NP with additional load of IR-780 iodide in their inner core were successfully synthesized in order to combine the chemical conjugation and the physical entrapment of the NIR-dye in a single nanotheranostics platform. These NP derived from IR-NP were appointed as a function of the feed percentage of IR-780 iodide entrapped: IR-NP-eIR3, IR-NP-eIR5 and IR-NP-eIR10 for a 3, 5 or 10 % w/w with respect to polymer conjugate, respectively. As it is shown in **table 2**, particle size and zeta potential values increased with the amount of IR-780 iodide loaded. However, the average particle size remained below 170 nm, encouraging their use for cancer therapy.

- **Optical properties of NPs based on IR-780-PEG-*b*-polyMTOS conjugate**

The formation of self-assembling NPs significantly affected the optical properties of the NIR dye conjugated to COOH-PEG-*b*-polyMTOS. In particular, this polymeric conjugate exhibited a maximum emission peak at 810 nm (**figure 6A**). However, the emission intensity significantly decreased after the incorporation of aqueous media by

SORP and the purification of NPs by dialysis, probably due to the hydrophilic media significantly screened off the fluorescence of the dye. However, photostability of IR-NP in aqueous media at 37 ºC was optimal, being stable during 1 week **(figure 6B)**, what is interesting for biomedical imaging.

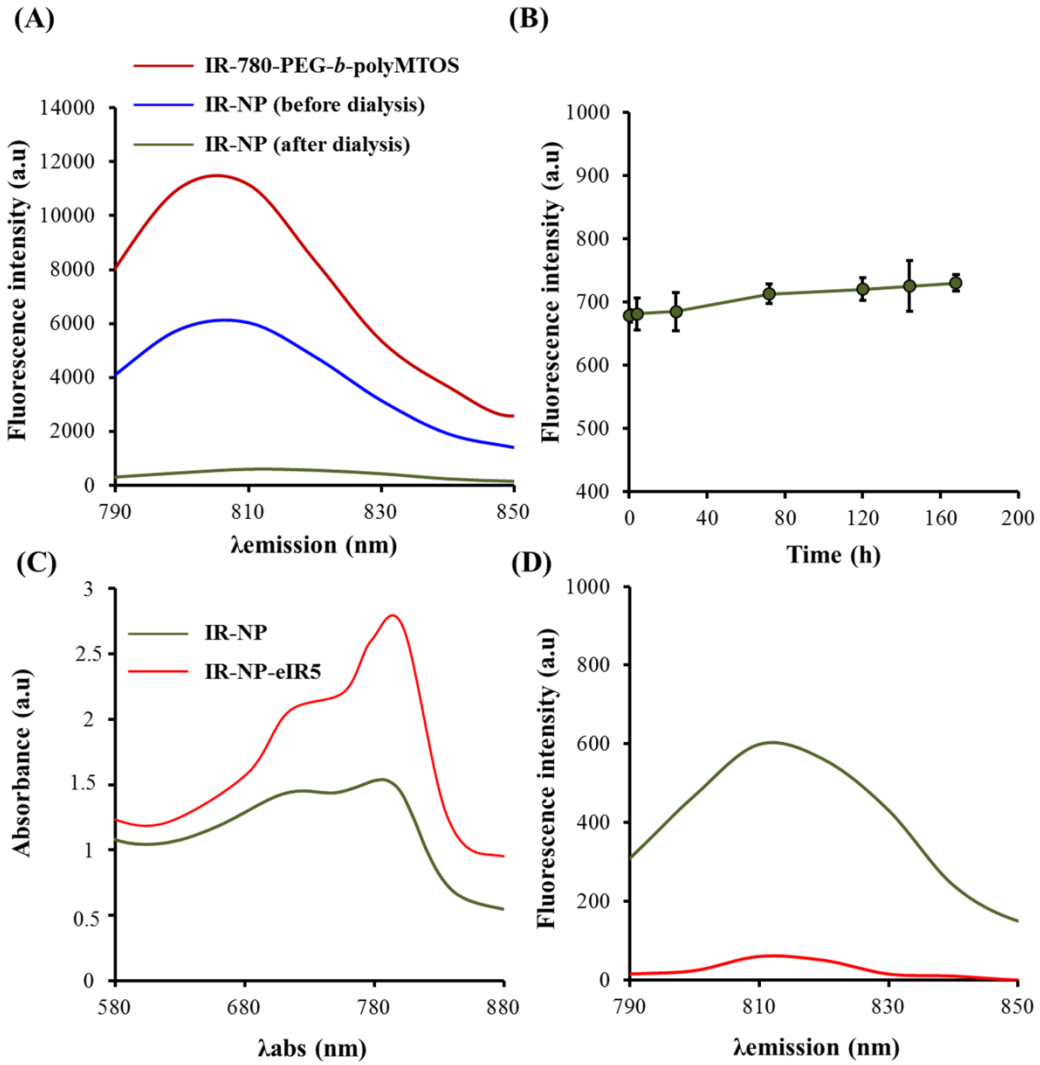

Figure 6: (A) Fluorescence spectra of IR-780-PEG-*b*-polyMTOS conjugate and IR-NP before and after their purification by dialysis. (B) Photostability of IR-NP at 37 ºC. Comparison of absorbance (C) and fluorescence spectra (D) of IR-780 bearing NPs. Green: IR-NP and red: IR-NP-eIR5.

The encapsulation of additional IR-780 iodide in the inner core of IR-NP significantly modified their optical properties. As an example, the absorption and emission spectra of IR-NP and IR-NP-eIR5 are compared in **figure 6C-D**. The maximum absorbance

of IR-NP-eIR5 was higher in comparison to IR-NP; however, the emission intensity was severely quenched by the self-aggregation of the dye that led to a significant energy transfer between the dye molecules. In fact, Shimizu *et al.* successfully entrapped the cyanine dye IC7-1, which has florescence signals in the NIR region, in the core of amphiphilic lactosomes based on poly(sarcosine)-*b*-poly(L-lactate). These authors demonstrated that the IC7-1 fluorescence was quenched with increasing concentrations of the NIR-dye entrapped into lactosomes[20].

- **Cellular imaging studies**

The endocytic fate of IR-NP in tumor cells was studied exploiting the NIR-fluorescence properties of the IR-780 dye. MDA-MB-453 cells were exposed to IR-NP and excited with NIR-light at different time points along 8 h of incubation at 37ºC (**figure 7A**). Fluorescence measurements in the NIR range demonstrated that fluorescence intensity detected in the cell culture increased gradually with time of exposure to IR-NP. CLSM images of cells treated with IR-NP for 5 h showed that IR-780 dye was uniformly distributed in the cytoplasm but excluded from the cell nucleus (**figure 7B**). These results demonstrated that IR-NP were rapidly incorporated in cancer cells, allowing sustained real-time monitoring by imaging techniques.

According to the literature, the majority of NPs with sizes between 100 and 200 nm enter into cells via endocytosis pathways and accumulate within intracellular vesicles[46]. This process is strongly influenced by the surface change of the nanovehicle, among others. As previously mentioned, IR-NP and IR-NP-eIR had positive surface charge as a result of the lipophilicity of the dye. For this reason, the uptake of these NPs and their access to the interior of the mitochondria could be favored in tumor cells due to the hyperpolarization of cell and mitochondria membranes[32, 47-51]. Furthermore, other cellular mechanisms could be related to the uptake of NPs incorporating IR-780. In this way, Zhang et al. have exhaustively investigated the influence of organic anion transporter peptides (OATPs) that are overexpressed in various human cancer tissues as well as in cancer cell lines. These authors demonstrated that the uptake of the NIR-dye could be mediated by these peptides because of its internalization was offset by the addition of OATPs inhibitors such as bromosulfophthalein (BSP)[52].

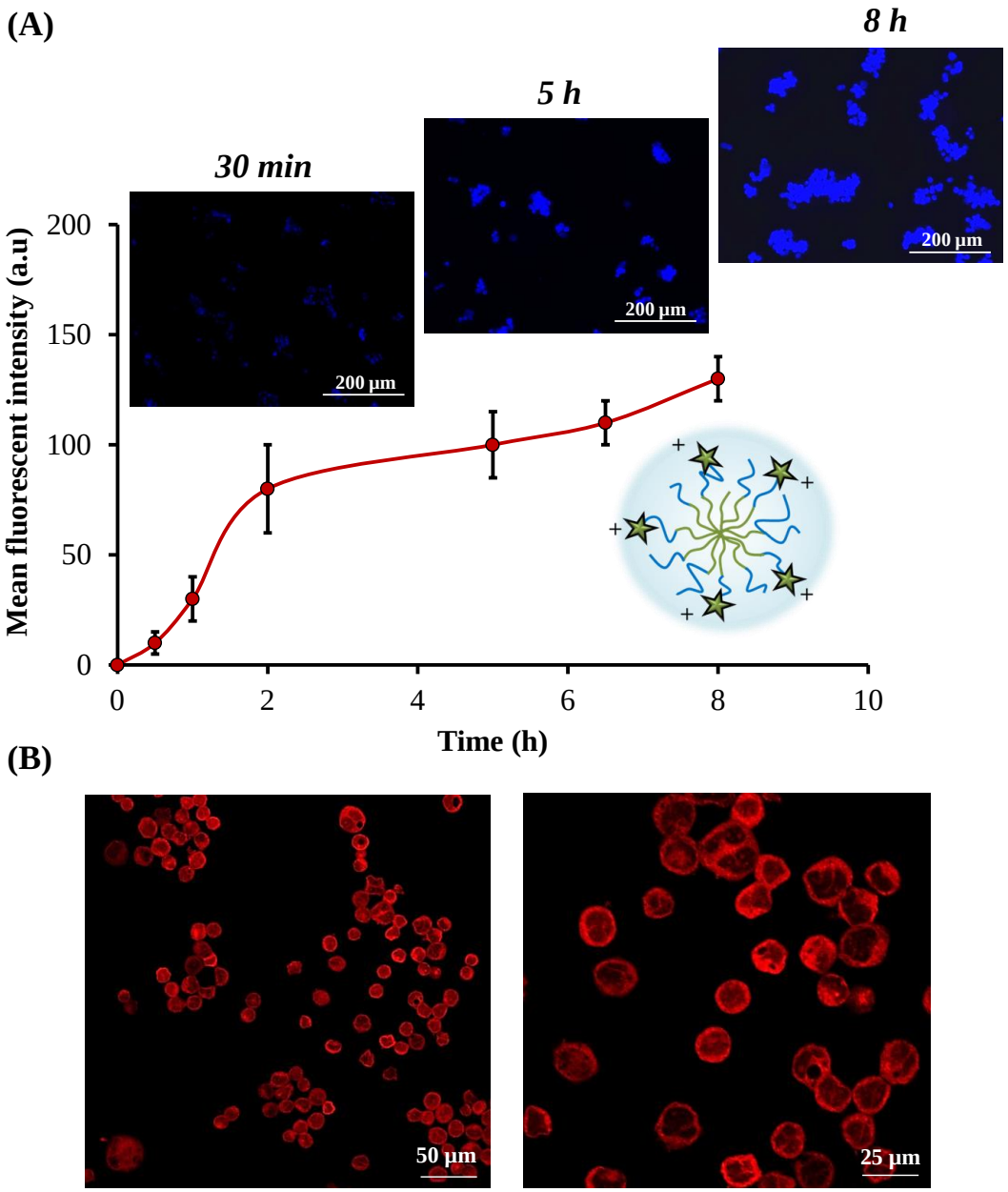

Figure 7: (A) NIR epifluorescence micrographs of MDA-MB-453 cells after 0.5, 5 and 8 h of incubation with IR-NP. (B) CLSM micrographs of MDA-MB-453 cells after 5 h of incubation with IR-NP.

- ***In vitro* cytotoxicity**

To study the cytotoxic effects of IR-NP or IR-NP-eIR in cancer cells, we used alamarBlue assay with MDA-MB-453 cells exposed to the nanoassemblies. For this purpose, IR-NP-eIR5 formulation was selected due to their optimal balance between the IR-780 iodide entrapped in their inner core and the particle characteristics regarding to their size, surface charge, and concentration of NIR dye.

As shown in **figure 8**, 2.5 mg/mL of unmodified-NP reduced by 35 % the metabolic activity of cell culture after 24 h. However, 0.188 mg/mL of IR-NP or IR-NP-eIR5 was sufficient to reduce cell viability to levels below 70% after the same period of incubation. It is noteworthy that the encapsulation of additional IR-780 iodide in the core of IR-NP increased significantly the cytotoxicity of the nanomaterial when used at concentrations ≥ 0.375 mg/mL.

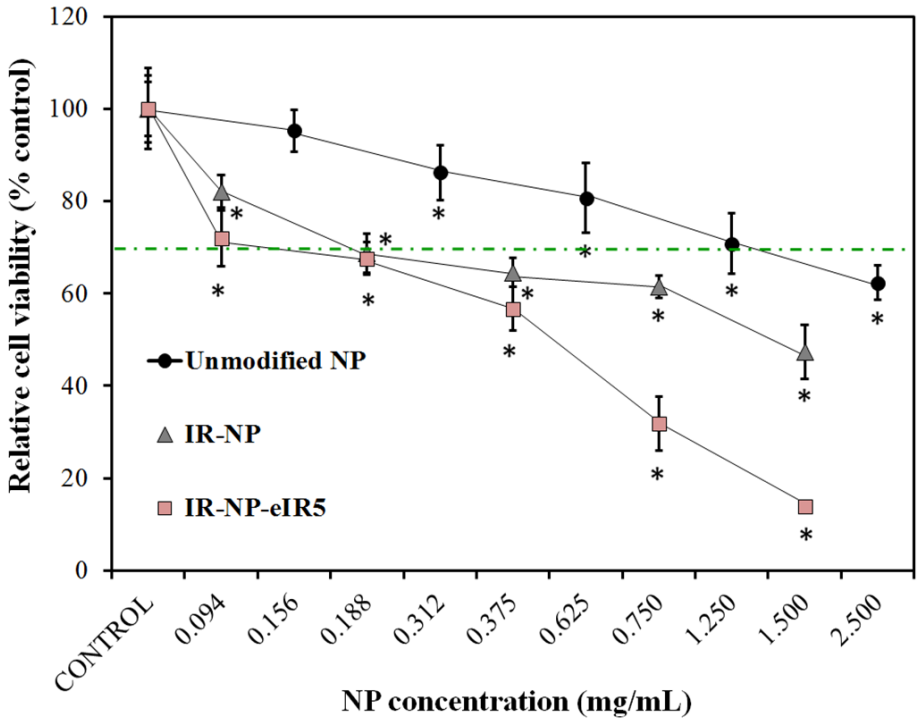

Figure 8: Viability of MDA-MB-453 cells incubated with indicated concentrations of unmodified-NP, IR-NP and IR-NP-5 for 24 h. The data shown are mean ± S.D. (error bars) relative to the metabolic activity detected in untreated cells. Statistical significance level was established at a p-value < 0.05 (*).

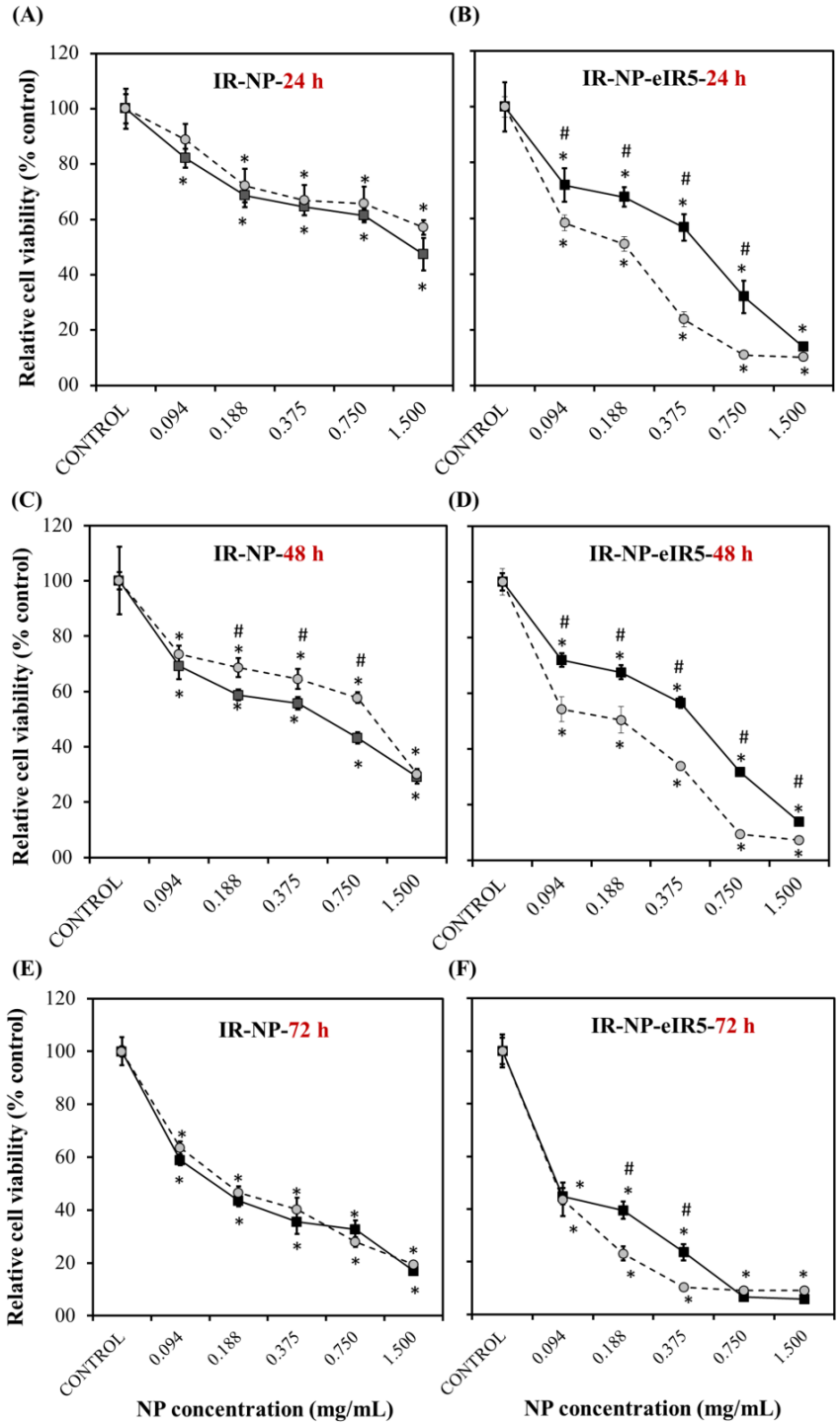

Figure 9: Viability of HMEpiC (●) and MDA-MB-453 (■) cells exposed to the indicated concentrations of IR-NP and IR-NP-eIR5 for 24 (A and B), 48 hours (C and D) and 72 h (E and F). The data shown are mean ± S.D. (error bars) relative to the metabolic activity detected in untreated cells (*). The diagrams include the ANOVA results for each NP formulation with respect to control

(*) and from the comparison of viability of cancer and nonmalignant cells (#) at a statistical significance level of $p < 0.05$.

Figure 9 shows metabolic activity of MDA-MB-453 and nonmalignant HMEpiC cells incubated with IR-NP or IR-NP-eIR5 for 72 h. The cytotoxicity of both NP formulations was higher with increasing dose of nanomaterial and the incubation time. HMEpiC cells were also sensitive to the cytotoxic activity of NPs incorporating IR-780. However, HMEpiC cells were more sensitive to the presence of IR-NP-eIR5 in the growth medium than MDA-MB-453 cells. These results indicated that encapsulation of additional amounts IR-780 dye in the structure of NPs based in IR-780-PEG-*b*-PMTOS conjugate hinders its cytotoxic selectivity toward tumor cells[27].

- **Photothermal properties of NPs based on IR-780-PEG-*b*-polyMTOS conjugate**

To investigate the photothermal properties of NPs based on IR-780-PEG-*b*-polyMTOS conjugate, aqueous solutions of IR-NP and IR-NP-eIR5, containing concentrations of nanomaterial lower than the IC50 values obtained for MDA-MB-453 cells, were irradiated using a NIR laser emitting at 808 nm. As control, unmodified-NP diluted in aqueous solution at 0.375-0.094 mg/mL were subjected to the same NIR treatment. Analysis of infrared thermal images revealed that the presence of 0.375 mg/mL of IR-NP increased the temperature of the medium by 2.15 ºC after 5 min of NIR irradiation (**figure 10B**). This temperature rise, that slightly exceeded the heating level occurring in the sample by the laser scattering and minimum NIR energy absorption in the aqueous media, could not be detected in solutions containing 0.375 mg/mL of unmodified NPs (**figure 10A**) or lower concentrations of IR-NP. It is well known that the confinement of NIR dyes within NAs can significantly enhance the efficiency of PTT[12].

As it is shown in **figure 10C**, thermal curves obtained by IR thermography of IR-NP-eIR5 dispersions showed a rapid increase in the temperature of the samples during the first 2 min of NIR-irradiation that gradually reached a steady level. NIR irradiation of IR-NP-eIR5 samples in the range of concentration tested produced a temperature rise significantly higher than that detected in the IR-NP counterparts. For example, NIR irradiation of solution containing 0.375 mg/mL of IR-NP-eIR5 induced an average net increase of 21.2ºC in the temperature of the sample while, as described above, the same

concentration of IR-NP could only raise the temperature of the solution 2.15 ºC above the unspecific sample heating.

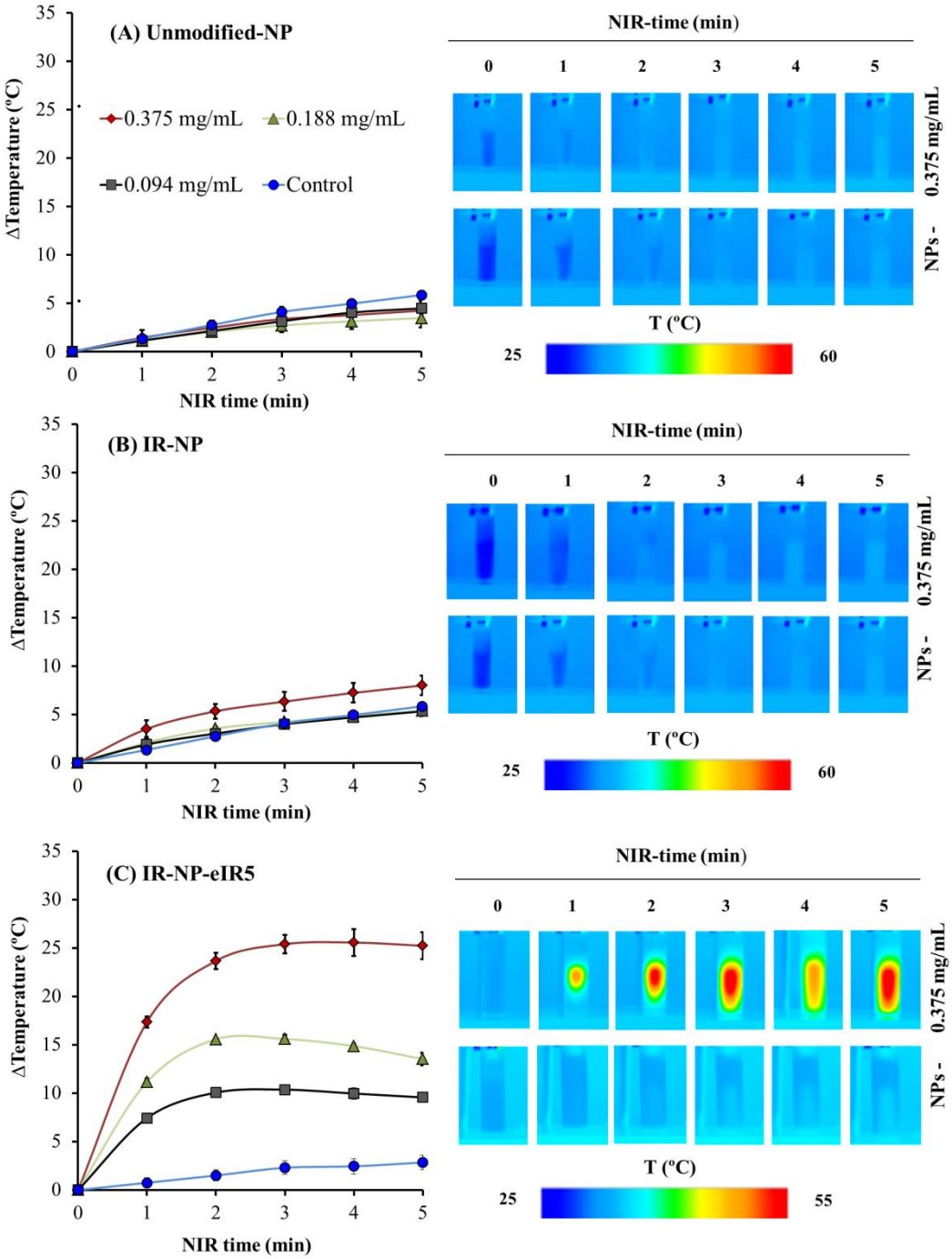

Figure 10: Photothermal properties of NPs based in the IR-780-PEG-*b*-polyMTOS conjugate. Aqueous solutions containing the indicated dose of unmodified-NPs (A), IR-NP (B) or IR-NP-eIR5

(C) were exposed to NIR-laser emitting at 44 mW/mm^2 for 5 minutes and monitored by IR-thermography at the indicated time points. The graph shows the maximum temperature rise detected in the sample during laser treatment. Images show the IR thermography of solutions containing (+) or not (-) 0.375 mg/mL of NPs during NIR-treatment for the indicated times. Data are expressed as mean ± S.D.

- **Phototoxicity of NPs based on IR-780-PEG-*b*-polyMTOS conjugate**

In order to investigate the phototherapeutic properties of NPs formulations based on IR-780-PEG-*b*-polyMTOS conjugate, MDA-MB-453 cells were incubated with IR-NP or IR-NP-eIR5 for 24 h and then irradiated with 808 nm NIR laser for 10 minutes. Metabolic activity measurements in MDA-MB-453 cells after 24 h of the NIR treatment are summarized in **figure 11**.

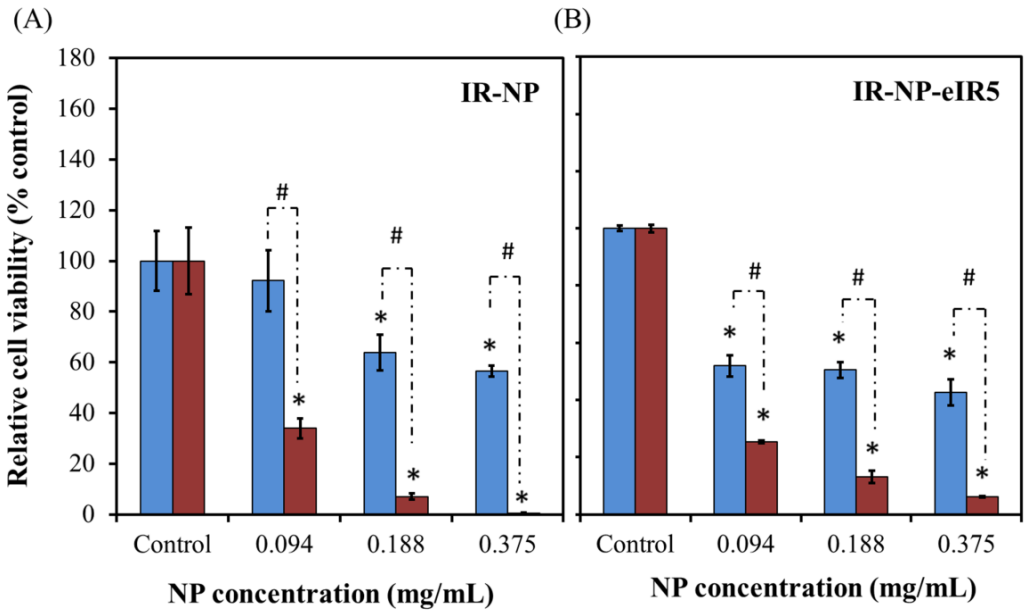

Figure 11: Metabolic activity of MDA-MB-453 cells incubated for 24 h with IR-NP (A) or IR-NP-eIR5 (B), then exposed (red) or not (blue) to NIR-laser irradiation at 44 mW/mm^2 for 10 min and further incubated at 37ºC-5%CO_2 for 18 h in the absence of NPs. The data shown are mean ± S.D. (error bars) relative to the metabolic activity detected in untreated cells not exposed to NIR laser. The diagrams include the ANOVA results for each NP formulation with respect to control (*) and from the comparison of the metabolic activity of nonirradiated and irradiated cells (#) at a statistical significance level of $p < 0.05$.

Laser treatment of cells preincubated with NP suspensions drastically reduced their metabolic activity in a dose-dependent manner. The dose of 0.094 mg/mL of IR-NP was sufficient to reduce by more than 60% the viability of the cell culture treated with NIR (**figure 11A**), while 0.375 mg/mL of NPs produced a negligible metabolic activity (< 0.6%) relative to unirradiated control. MDA-MB-453 cells, preincubated with an equivalent concentration range of IR-NP-eIR5, showed a marked decline in viability which was reinforced by the NIR-laser treatment to achieve metabolic activity levels similar to those found in cells exposed to IR-NP and NIR-light (**figure 11B**).

As described above, photothermal behavior of synthesized NPs species derived from IR-780-PEG-*b*-polyMTOS was quite different. For the range of tested doses, IR-NP-eIR5 was very efficient at transducing NIR-energy into heat, most likely due the spatial confinement of high amounts of NIR-probe inside the nanoassembly [12]. By contrast, aqueous solutions of IR-NP showed a very poor ability to dissipate heat to the environment after the exposure to incident NIR-light. Hence, other mechanism different to hyperthermia may be responsible of the cytotoxicity enhancement observed after NIR-laser irradiation of cells incorporating IR-NP (**figure 11**).

We hypothesized that NIR irradiation of IR-NP results in byproducts which have a superior cytotoxic activity in tumor cells. To test this hypothesis, unmodified-NPs or IR-NP suspensions were irradiated with the NIR laser for 10 min and then immediately added to cultures of MBA-MD-453 cells. Metabolic activity measurements obtained after 18 h of incubation at 37ºC showed that NIR irradiation of unmodified-NPs did not significantly altered their biological activity (**figure 12A**). However, laser treatment of IR-NP significantly reduced the cytotoxic potential observed *in vitro* for the range of concentration tested (**figure 12B**). This finding, as opposed to the hypothesis initially raised, could be closely related to the photobleaching experienced by IR-NP preparations exposed to the 808 nm laser, and indicated that cytotoxic activity of low concentrations of IR-NP depends largely on the persistence of intact IR-780 dye **(figure 12C).**

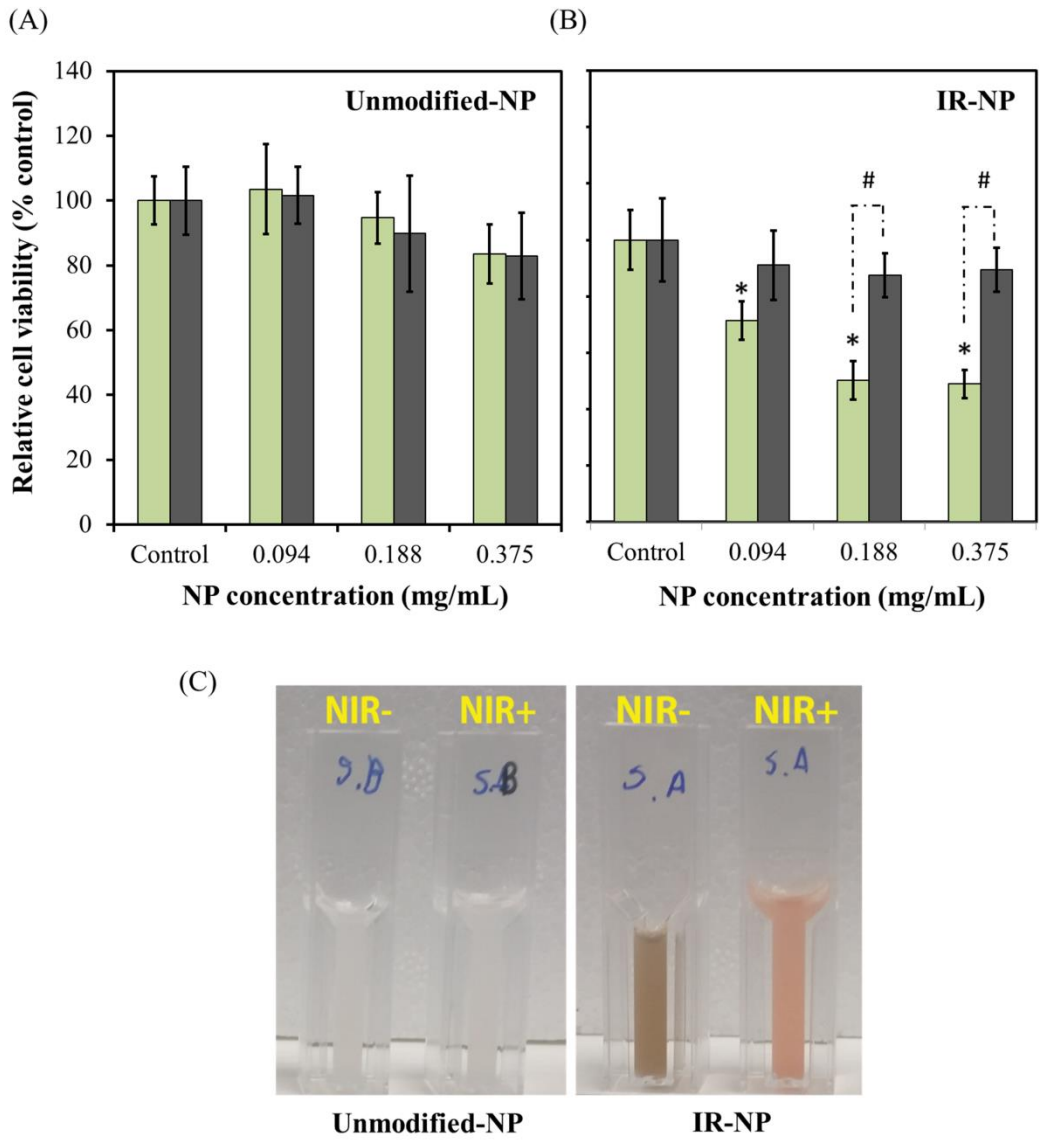

Figure 12: Metabolic activity of MDA-MB-453 cells incubated with solutions of unmodified-NP (A) or IR-NP (B) previously irradiated (grey) or not (green) with NIR-laser emitting at 44 mW/mm^2 for 10 min. (C) Photograph shows NPs solutions of 0.375 mg/mL, subjected (+) or not (-) to the NIR-laser treatment. The data shown are mean ± S.D. (error bars) relative to the metabolic activity detected in untreated cells. The diagrams include the ANOVA results for each NP formulation with respect to control (*) and from the comparison of the metabolic activity of nonirradiated and irradiated cells (#) at a statistical significance level of $p < 0.05$.

Figure 13 compares the metabolic activity detected in MDA-MB-453 cells that were incubated with unmodified-NP or IR-NP for 24 h, subjected to NIR-laser treatment for 10 min and further incubated 18h at 37ºC in the absence of NPs. Cell viability measurements show that increasing concentration of unmodified-NP did not altered significantly the metabolic activity after NIR irradiation, which was similar to that detected in cell cultures not exposed to NPs. Taken all together, these results suggest that cytoxicity exerted by low concentrations of IR-NP depends on the presence of intact IR-780 dye, discarding that NIR energy would produce a permanent change in the polymer structure that resulted in an increase of its anticancer potential.

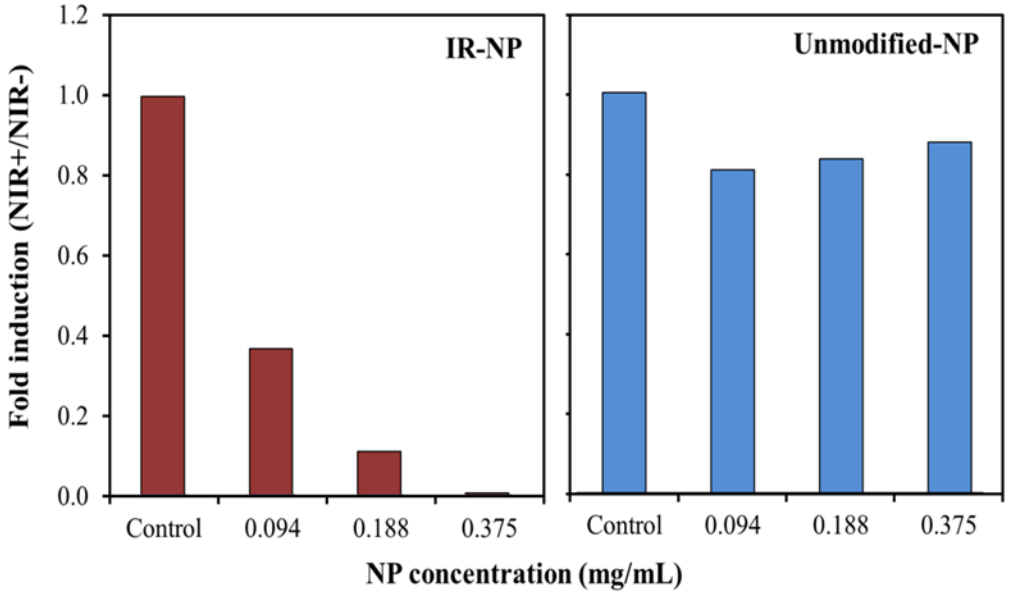

Figure 13: Metabolic activity of MDA-MB-453 cells incubated for 24 h with IR-NP (left) or unmodified-NP (right), then exposed to NIR-laser irradiation at 44 mW/mm^2 for 10 min and further incubated at 37ºC-5%CO_2 for 18 h in the absence of NPs. The data are expressed as the ratio of metabolic activity detected in NIR-irradiated to nonirradiated samples.

A plausible justification for the phototoxicity exhibited by IR-NP formulation, which did not depend on hyperthermia, is the appearance of a photodynamic effect where the NIR-dye behaves as a photosensitizer (Ps). Thereby, the photochemical reactions triggered by this photoactivated dye may involve the generation of ROS with a short lifetime that immediately reacts with vital biomolecules and causes the damage of tumor cells[11, 53, 54]. In this sense, Jiang *et al.* investigated the phototherapeutic effect of IR-780 encapsulated in the

core of biodegradable human serum albumin NPs (HSA-NP). These authors demonstrated that IR-780-HAS-NP simultaneously produced hyperthermia and a photodynamic effect mediated by the generation of a high amount of ROS species[17]. On the other hand, Weber et al., demonstrated in a previous study that the high sensitivity of malignant cells to α-TOS effects is based on its ability to efficiently induce the mitochondrial signal transmissions mechanisms, including ROS generation, which trigger apoptosis[55]. The propensity for cells to accumulate ROS in a prerequisite before they can be killed by α-TOS[56] and is at least one of the reasons for the selectivity of vitamin E analogues for cancer cells[57], which commonly express lower levels of anti-oxidant enzymes such as the manganese superoxide dismutase (MnSOD) than normal cells[58]. Normal cells are well protected against α-TOS toxicity through mechanisms of resistance including higher expression of the anti-apoptotic Bcl-2 family proteins and decreased accumulation of ROS[57].

Future experiments will focus on elucidating the existence of a synergistic relationship between the cytotoxic activities exerted by the methacrylic derivative of α-TOS and the photosensitization of IR-780 in the context of cancer cells that internalized nanoassemblies based in the IR-780-PEG-*b*-polyMTOS conjugate.

5.1.5. Conclusions

IR-780 dye was conjugated to PEG-*b*-polyMTOS copolymer to obtain NIR-fluorescent NPs by SORP occurring in aqueous medium. These NPs were efficiently internalized by MDA-MB-453 cells inhibiting the viability of the cell culture. The conjugation of IR-780 to the surface of PEG-*b*-polyMTOS copolymer reduced the specificity for tumor cells exhibited by unmodified-NP. During the self-assembly of IR-NP, physical encapsulation of additional IR-780 was possible by the hydrophobic core resulting in the generation of IR-NP-eIR with a modulable content in NIR-probe. NIR-fluorescence exhibited by IR-NP-eIR was severely quenched by their cargo, however, they showed a higher capacity to transduce into heat electromagnetic energy delivered by a NIR laser emitting at 808 nm than IR-NP, which showed very poor photothermal efficiency. However, IR-NP severely reduced the metabolic activity of tumor cells that incorporated them and were treated with NIR-laser. This phototoxic activity, independent of the induction of lethal hyperthermia or the generation of toxic photodegradation byproducts, could be related to photodynamic events conducted by IR-780 after NIR-irradiation. Finally, we hypothesize the establishment of a synergistic interaction

between the IR-780 and the methacrylic derivative of α-TOS during NIR irradiation, which enhances their cytotoxic potential.

5.1.6. Acknowledgements

Authors would like to thank financial support from the Spanish Ministry of Economy and Competitiveness (MAT2014-51918-C2-1-R), CIBER BBN-ECO Foundation project, and the National Institutes of Health Cell and Tissue Engineering Training Grant T32 GM008433. Authors also acknowledge, David Gómez, Rosa Ana Ramírez and Mar Fernández and María Isabel Trabado for their help in SEM, cell culture and CLSM experiments, respectively

5.1.7. References

1. Muthu, M. S.; Leong, D. T.; Mei, L.; Feng, S.-S., Nanotheranostics- application and further development of nanomedicine strategies for advanced theranostics. *Theranostics* **2014,** 4, (6), 660-667.

2. Thakor, A. S.; Gambhir, S. S., Nanooncology: the future of cancer diagnosis and therapy. *CA Cancer J. Clin.* **2013,** 63, (6), 395-418.

3. Ahmed, N.; Fessi, H.; Elaissari, A., Theranostic applications of nanoparticles in cancer. *Drug Discov. Today* **2012,** 17, (17), 928-934.

4. Mukerjee, A.; P Ranjan, A.; K Vishwanatha, J., Combinatorial nanoparticles for cancer diagnosis and therapy. *Curr. Med. Chem.* **2012,** 19, (22), 3714-3721.

5. Barlas, F. B.; Demir, B.; Guler, E.; Senisik, A. M.; Arican, H. A.; Unak, P.; Timur, S., Multimodal theranostic assemblies: double encapsulation of protoporphyrine-IX/Gd 3+ in niosomes. *RSC Advances* **2016,** 6, (36), 30217-30225.

6. Xie, J.; Lee, S.; Chen, X., Nanoparticle-based theranostic agents. *Adv. Drug Del. Rev.* **2010,** 62, (11), 1064-1079.

7. Issels, R. D., Hyperthermia adds to chemotherapy. *Eur. J. Cancer* **2008,** 44, (17), 2546-2554.

8. Mroz, P.; Yaroslavsky, A.; Kharkwal, G. B.; Hamblin, M. R., Cell death pathways in photodynamic therapy of cancer. *Cancers (Basel)* **2011,** 3, (2), 2516-2539.

9. Dolmans, D. E.; Fukumura, D.; Jain, R. K., Photodynamic therapy for cancer. *Nature reviews cancer* **2003,** 3, (5), 380-387.

10. Tan, X.; Luo, S.; Wang, D.; Su, Y.; Cheng, T.; Shi, C., A NIR heptamethine dye with intrinsic cancer targeting, imaging and photosensitizing properties. *Biomaterials* **2012,** 33, (7), 2230-2239.

11. Shibu, E. S.; Hamada, M.; Murase, N.; Biju, V., Nanomaterials formulations for photothermal and photodynamic therapy of cancer. *Journal of Photochemistry and Photobiology C: Photochemistry Reviews* **2013,** 15, (1), 53-72.

12. Yuan, A.; Wu, J.; Tang, X.; Zhao, L.; Xu, F.; Hu, Y., Application of near-infrared dyes for tumor imaging, photothermal, and photodynamic therapies. *J. Pharm. Sci.* **2013,** 102, (1), 6-28.

13. Song, X.; Chen, Q.; Liu, Z., Recent advances in the development of organic photothermal nano-agents. *Nano Research* **2015,** 8, (2), 340-354.

14. Luo, S.; Zhang, E.; Su, Y.; Cheng, T.; Shi, C., A review of NIR dyes in cancer targeting and imaging. *Biomaterials* **2011,** 32, (29), 7127-7138.

15. Resch-Genger, U.; Grabolle, M.; Cavaliere-Jaricot, S.; Nitschke, R.; Nann, T., Quantum dots versus organic dyes as fluorescent labels. *Nat. Methods* **2008,** 5, (9), 763-775.

16. Conceição, D. S.; Ferreira, D. P.; Ferreira, L. F. V., Photochemistry and Cytotoxicity Evaluation of Heptamethinecyanine Near Infrared (NIR) Dyes. *Int. J. Mol. Sci.* **2013,** 14, (9), 18557-18571.

17. Jiang, C.; Cheng, H.; Yuan, A.; Tang, X.; Wu, J.; Hu, Y., Hydrophobic IR780 encapsulated in biodegradable human serum albumin nanoparticles for photothermal and photodynamic therapy. *Acta Biomater.* **2015,** 14, (1), 61-69.

18. Peng, C.-L.; Shih, Y.-H.; Lee, P.-C.; Hsieh, T. M.-H.; Luo, T.-Y.; Shieh, M.-J., Multimodal image-guided photothermal therapy mediated by 188Re-labeled micelles containing a cyanine-type photosensitizer. *ACS nano* **2011,** 5, (7), 5594-5607.

19. Singh, A. K.; Hahn, M. A.; Gutwein, L. G.; Rule, M. C.; Knapik, J. A.; Moudgil, B. M.; Grobmyer, S. R.; Brown, S. C., Multi-dye theranostic nanoparticle platform for bioimaging and cancer therapy. *International journal of nanomedicine* **2012,** 7, (2), 2739.

20. Shimizu, Y.; Temma, T.; Hara, I.; Makino, A.; Yamahara, R.; Ozeki, E.-i.; Ono, M.; Saji, H., Micelle-based activatable probe for in vivo near-infrared optical imaging of cancer biomolecules. *Nanomed. Nanotechnol. Biol. Med.* **2014,** 10, (1), 187-195.

21. Yue, C.; Liu, P.; Zheng, M.; Zhao, P.; Wang, Y.; Ma, Y.; Cai, L., IR-780 dye loaded tumor targeting theranostic nanoparticles for NIR imaging and photothermal therapy. *Biomaterials* **2013,** 34, (28), 6853-6861.

22. Yuan, A.; Qiu, X.; Tang, X.; Liu, W.; Wu, J.; Hu, Y., Self-assembled PEG-IR-780-C13 micelle as a targeting, safe and highly-effective photothermal agent for in vivo imaging and cancer therapy. *Biomaterials* **2015,** 51, (1), 184-193.

23. Maeda, H.; Nakamura, H.; Fang, J., The EPR effect for macromolecular drug delivery to solid tumors: Improvement of tumor uptake, lowering of systemic toxicity, and distinct tumor imaging in vivo. *Adv. Drug Del. Rev.* **2013,** 65, (1), 71-79.

24. Veronese, F. M.; Pasut, G., PEGylation, successful approach to drug delivery. *Drug Discov. Today* **2005,** 10, (21), 1451-1458.

25. Jokerst, J. V.; Lobovkina, T.; Zare, R. N.; Gambhir, S. S., Nanoparticle PEGylation for imaging and therapy. *Nanomedicine* **2011,** 6, (4), 715-728.

26. York, A. W.; Kirkland, S. E.; McCormick, C. L., Advances in the synthesis of amphiphilic block copolymers via RAFT polymerization: stimuli-responsive drug and gene delivery. *Adv. Drug Del. Rev.* **2008,** 60, (9), 1018-1036.

27. Palao-Suay, R.; Aguilar, M. R.; Parra-Ruiz, F. J.; Maji, S.; Hoogenboom, R.; Rohner, N.; Thomas, S. N.; San Román, J., α-TOS-based RAFT block copolymers and their NPs for the treatment of cancer. *Polymer Chemistry* **2016,** 7, (4), 838-850.

28. Dong, L.-F.; Neuzil, J., Mitochondria in Cancer: Why Mitochondria Are a Good Target for Cancer Therapy. *Prog. Mol. Biol. Transl. Sci.* **2014,** 127, 211-227.

29. Dong, L.-F.; Jameson, V. J.; Tilly, D.; Cerny, J.; Mahdavian, E.; Marín-Hernández, A.; Hernández-Esquivel, L.; Rodríguez-Enríquez, S.; Stursa, J.; Witting, P. K., Mitochondrial targeting of vitamin E succinate enhances its pro-apoptotic and anti-cancer activity via mitochondrial complex II. *J. Biol. Chem.* **2011,** 286, (5), 3717-3728.

30. Wang, X.-F.; Birringer, M.; Dong, L.-F.; Veprek, P.; Low, P.; Swettenham, E.; Stantic, M.; Yuan, L.-H.; Zobalova, R.; Wu, K., A peptide conjugate of vitamin E succinate targets breast cancer cells with high ErbB2 expression. *Cancer Res.* **2007,** 67, (7), 3337-3344.

31. Palao-Suay, R.; Rodrigáñez, L.; Aguilar, M. R.; Sánchez-Rodríguez, C.; Parra, F.; Fernández, M.; Parra, J.; Riestra-Ayora, J.; Sanz-Fernández, R.; Román, J. S., Mitochondrially Targeted Nanoparticles Based on α-TOS for the Selective Cancer Treatment. *Macromol. Biosci.* **2015,** 16, (3), 395-411.

32. Murphy, M. P., Targeting lipophilic cations to mitochondria. *Biochimica et Biophysica Acta (BBA)-Bioenergetics* **2008,** 1777, (7), 1028-1031.

33. Fulda, S., Exploiting mitochondrial apoptosis for the treatment of cancer. *Mitochondrion* **2010,** 10, (6), 598-603.

34. Davis, S.; Weiss, M.; Wong, J.; Lampidis, T. J.; Chen, L. B., Mitochondrial and plasma membrane potentials cause unusual accumulation and retention of rhodamine 123 by human breast adenocarcinoma-derived MCF-7 cells. *J. Biol. Chem.* **1985,** 260, (25), 13844-13850.

35. Chen, L. B., Mitochondrial membrane potential in living cells. *Annu. Rev. Cell Biol.* **1988,** 4, (1), 155-181.

36. Zhang, E.; Luo, S.; Tan, X.; Shi, C., Mechanistic study of IR-780 dye as a potential tumor targeting and drug delivery agent. *Biomaterials* **2014,** 35, (2), 771-778.

37. Wang, Y.; Liu, T.; Zhang, E.; Luo, S.; Tan, X.; Shi, C., Preferential accumulation of the near infrared heptamethine dye IR-780 in the mitochondria of drug-resistant lung cancer cells. *Biomaterials* **2014,** 35, (13), 4116-4124.

38. Palao-Suay, R.; Aguilar, M. R.; Parra-Ruiz, F. J.; Fernández-Gutiérrez, M.; Parra, J.; Sánchez-Rodríguez, C.; Sanz-Fernández, R.; Rodrigáñez, L.; Román, J. S., Anticancer and Antiangiogenic Activity of Surfactant-Free Nanoparticles Based on Self-Assembled Polymeric Derivatives of Vitamin E: Structure–Activity Relationship. *Biomacromolecules* **2015,** 16, (5), 1566-1581.

39. Li, C.-Y.; Kong, X.-F.; Li, Y.-F.; Zou, C.-X.; Liu, D.; Zhu, W.-G., Ratiometric and colorimetric fluorescent chemosensor for Ag+ based on tricarbocyanine. *Dyes and Pigments* **2013,** 99, (3), 903-907.

40. Page, B.; Page, M.; Noel, C., A new fluorometric assay for cytotoxicity measurements in-vitro. *International journal of oncology* **1993,** 3, (3), 473-476.

41. Cebrián, V.; Martín-Saavedra, F.; Gómez, L.; Arruebo, M.; Santamaria, J.; Vilaboa, N., Enhancing of plasmonic photothermal therapy through heat-inducible transgene activity. *Nanomed. Nanotechnol. Biol. Med.* **2013,** 9, (5), 646-656.

42. Hatakeyama, H.; Akita, H.; Harashima, H., The polyethyleneglycol dilemma: advantage and disadvantage of PEGylation of liposomes for systemic genes and nucleic acids delivery to tumors. *Biol. Pharm. Bull.* **2013,** 36, (6), 892-899.

43. Pelet, J. M.; Putnam, D., An in-depth analysis of polymer-analogous conjugation using DMTMM. *Bioconj. Chem.* **2011,** 22, (3), 329-337.

44. Kunishima, M.; Kawachi, C.; Monta, J.; Terao, K.; Iwasaki, F.; Tani, S., 4-(4, 6-dimethoxy-1, 3, 5-triazin-2-yl)-4-methyl-morpholinium chloride: an efficient condensing agent leading to the formation of amides and esters. *Tetrahedron* **1999,** 55, (46), 13159-13170.

45. Montalbetti, C. A.; Falque, V., Amide bond formation and peptide coupling. *Tetrahedron* **2005,** 61, (46), 10827-10852.

46. Yameen, B.; Choi, W. I.; Vilos, C.; Swami, A.; Shi, J.; Farokhzad, O. C., Insight into nanoparticle cellular uptake and intracellular targeting. *J. Controlled Release* **2014,** 190, 485-499.

47. Marquez, M.; Nilsson, S.; Lennartsson, L.; Liu, Z.; Tammela, T.; Raitanen, M.; Holmberg, A., Charge-dependent targeting: results in six tumor cell lines. *Anticancer Res.* **2004,** 24, (3A), 1347-1352.

48. Ross, M. F.; Da Ros, T.; Blaikie, F. H.; Prime, T. A.; Porteous, C. M.; Severina, I. I.; Skulachev, V. P.; Kjaergaard, H. G.; Smith, R. A.; Murphy, M. P., Accumulation of lipophilic dications by mitochondria and cells. *Biochem. J.* **2006,** 400, (1), 199-208.

49. Rin Jean, S.; Tulumello, D. V.; Wisnovsky, S. P.; Lei, E. K.; Pereira, M. P.; Kelley, S. O., Molecular vehicles for mitochondrial chemical biology and drug delivery. *ACS Chem. Biol.* **2014,** 9, (2), 323-333.

50. Smith, R. A.; Porteous, C. M.; Gane, A. M.; Murphy, M. P., Delivery of bioactive molecules to mitochondria in vivo. *Proceedings of the National Academy of Sciences* **2003,** 100, (9), 5407-5412.

51. Dolowy, K., Bioelectrochemistry of cell surfaces. *Prog. Surf. Sci.* **1984,** 15, (3), 245-368.

52. Yang, X.; Shi, C.; Tong, R.; Qian, W.; Zhau, H. E.; Wang, R.; Zhu, G.; Cheng, J.; Yang, V. W.; Cheng, T., Near IR heptamethine cyanine dye–mediated cancer imaging. *Clin. Cancer. Res.* **2010,** 16, (10), 2833-2844.

53. Lucky, S. S.; Soo, K. C.; Zhang, Y., Nanoparticles in photodynamic therapy. *Chem. Rev.* **2015,** 115, (4), 1990-2042.

54. Nguyen, K. T.; Menon, J. U.; Jadeja, P. V.; Tambe, P. P.; Vu, K.; Yuan, B., Nanomaterials for photo-based diagnostic and therapeutic applications. *Theranostics* **2013,** 3, (3), 152-166.

55. Weber, T.; Dalen, H.; Andera, L.; Nègre-Salvayre, A.; Augé, N.; Sticha, M.; Lloret, A.; Terman, A.; Witting, P. K.; Higuchi, M.; Plasilova, M.; Zivny, J.; Gellert, N.; Weber,

C.; Neuzil, J., Mitochondria play a central role in apoptosis induced by α-tocopheryl succinate, an agent with antineoplastic activity: Comparison with receptor-mediated pro-apoptotic signaling. *Biochemistry* **2003,** 42, (14), 4277-4291.

56. Kogure, K.; Hama, S.; Manabe, S.; Tokumura, A.; Fukuzawa, K., High cytotoxicity of α-tocopheryl hemisuccinate to cancer cells is due to failure of their antioxidative defense systems. *Cancer Lett.* **2002,** 186, (2), 151-156.

57. Neuzil, J.; Tomasetti, M.; Mellick, A. S.; Alleva, R.; Salvatore, B. A.; Birringer, M.; Fariss, M. W., Vitamin E analogues: A new class of inducers of apoptosis with selective anti-cancer effects. *Curr. Cancer Drug Targets* **2004,** 4, (4), 355-372.

58. Borrello, S.; De Leo, M.; Galeotti, T., Defective gene expression of MnSOD in cancer cells. *Mol. Aspects Med.* **1993,** 14, (3), 253-258.

Capítulo VI: Resultados y aportaciones

VI. Resultados y aportaciones

Fruto del trabajo experimental desarrollado en la presente tesis doctoral, se han elaborado los trabajos científicos recogidos en los capítulos anteriores y que tienen como finalidad global la preparación y completa caracterización de nanovehículos poliméricos portadores del fármaco anticancerígeno succinato de α-tocoferilo o succinato de la vitamina E (α-TOS) para el tratamiento selectivo del cáncer. A continuación, se resumen los resultados y aportaciones más relevantes recogidos en los diferentes trabajos científicos, haciendo especial hincapié en la estrecha relación existente entre ellos así como en su conjunto, encaminados a lograr con éxito el propósito final de la presente tesis doctoral.

CAPÍTULO III: Bioactive nanoparticles based on free radical copolymers of vitamin E derivatives

- **Capítulo 3.1- Anticancer and antiangiogenic activity of surfactant-free nanoparticles based on self-assembled polymeric derivatives of vitamin E: structure – activity relationship.**

La falta de efectividad y la alta toxicidad de los actuales tratamientos contra el cáncer han posibilitado el desarrollo de nuevos fármacos anticancerígenos que basan su acción en las diferencias metabólicas encontradas entre células tumorales y células no patológicas. Un ejemplo de este tipo de moléculas bioactivas es el α-TOS que ha sido descrito como un mitocan (del inglés, *mitochondrial targeted anticancer drugs*) que induce selectivamente la muerte celular programada o apoptosis en un gran número de células tumorales y células endoteliales en proliferación, vía mitocondrial. Neuzil et al. han dividido su estructura en 3 dominios: el dominio de funcionalización (grupo succinato) que consideran el principal responsable de su actividad, el dominio de señalización (grupo cromanol) y el dominio hidrofóbico (cadena alifática lateral). Sin embargo, la alta hidrofobicidad y, por tanto, la baja solubilidad en medio acuoso de esta molécula limita drásticamente su aplicación real para la terapia contra el cáncer, sin superar a día de hoy estudios de investigación *in vivo*. En este sentido, el avance de la nanomedicina y en concreto de los sistemas nanoestructurados en forma de nanopartículas (NPs) puede representar una solución atractiva a los problemas de administración de este fármaco, aún por resolver de forma efectiva. Por ello, el objetivo de este primer trabajo científico fue la preparación de un

nanovehículo polímero que incorporase α-TOS en su estructura para el tratamiento selectivo y eficaz del cáncer.

En esta publicación, se abordó en primer lugar la síntesis del derivado metacrílico del α-TOS (MTOS) que se obtuvo con éxito con un rendimiento del 90%. Para establecer posteriormente una relación entre la estructura de este monómero y su actividad biológica, se prepararon además otros tres derivados metacrílicos más: MVE caracterizado por la ausencia del grupo funcional succinato, SPHY que no disponía del grupo cromanol o de señalización y el MPHY que carecía de ambos grupos en su estructura química.

Para la preparación de los sistemas nanoestructurados basados en conjugados polímero-fármaco, el primer paso fue la correcta elección de un comonómero que permitiera modular el marcado carácter hidrofóbico de los monómeros metacrílicos previamente sintetizados. Tras un exhaustivo estudio, se decidió utilizar la *N*-vinil-pirrolidona (VP) por sus óptimas propiedades físico-químicas, excelente biocompatibilidad una vez polimerizado y su naturaleza hidrofílica que dotaría a los conjugados poliméricos de la naturaleza anfifílica necesaria para la posterior formación de las NPs. Así pues, se prepararon satisfactoriamente las diferentes familias de copolímeros (poli(VP-*co*-MTOS), poli(VP-*co*-MVE), poli(VP-*co*-SPHY) y poli(VP-*co*-MPHY)) por polimerización radical convencional en disolución.

Las familias de copolímeros fueron exhaustivamente caracterizadas de forma que su estructura química se confirmó por resonancia magnética nuclear (NMR, del inglés *nuclear magnetic resonance*). Esta misma técnica experimental permitió conocer con exactitud la composición de los diferentes copolímeros preparados. De esta forma, resultó especialmente llamativo cómo el contenido en MVE en los copolímeros poli(VP-*co*-MVE) era significativamente superior con respecto a la alimentación. Además, a diferencia del resto de las familias poliméricas sintetizadas, no se obtuvieron polímeros en todo en rango de composiciones de forma que el rendimiento de la polimerización disminuía drásticamente con el contenido en MVE en los polímeros (rendimiento inferior al 60 % cuando la concentración molar de MVE en la alimentación era superior al 15 %). La caracterización por cromatografía de exclusión de tamaños (SEC, del inglés *size exclusion chromatography*) reveló como el peso molecular (MW, del inglés *molecular weight*) y la polidispersidad (*Đ*) de estos copolímeros disminuía además con el aumento de MVE en su composición. Estos resultados indican que la vitamina E presente en la estructura del

monómero MVE posee un marcado carácter antioxidante, desactivando los radicales libres que guían cualquier proceso de polimerización convencional. Además, es probable la existencia de un fenómeno de deslocalización de radicales por la conjugación de los dobles enlaces del grupo metacrílico con el anillo aromático del MVE. En el resto de familias poliméricas obtenidas, los MWs y la *Đ* aumentaban con el contenido de monómero metacrílico, dando lugar en la mayor parte de los casos a polímeros con un MW superior a 30 kDa, necesario para su acumulación y extravasación a la zona del tumor por el efecto efecto de Permeación y Retención Aumentada (EPR). Finalmente, la caracterización de las propiedades térmicas por calorimetría diferencial de barrido de estos sistemas poliméricos relevó la presencia en todos los casos de dos temperaturas de transición vítreas, características de un fenómeno de segregación fases.

Las relaciones de reactividad de los monómeros (r_{VP} = 0,12, r_{MTOS} = 1,20; r_{VP} = 0,20, r_{SPHY} = 4,60; r_{VP} = 0,03, r_{MVE} = 2,20; r_{VP} = 0,03, r_{MPHY} = 4,10) determinadas mediante un método de resonancia magnética nuclear "in situ" y aplicando la ecuación integral de copolimerización que describe el modelo terminal, evidenciaron una mayor reactividad de los monómeros metacrílicos frente a la VP. Además, tanto MPHY como SPHY presentaron mayor reactividad al copolimerizar con la VP que sus análogos MVE y MTOS. Esto es debido nuevamente al efecto de estabilización de radicales en el caso del MVE y probablemente al impedimento estérico del grupo cromanol presente en la estructura MTOS que podría reducir su reactividad. En todos los casos, los valores tan diferentes de las reactividades entre los monómeros metacrílicos y la VP indican que la cinética de la reacción de polimerización es especialmente sensible al grado de conversión de forma que la distribución de secuencias monoméricas en las cadenas macromoleculares cambia notablemente en función de la composición en la alimentación y del grado de conversión. Como es de esperar, primero se consumen, en gran parte, los monómeros metacrílicos más reactivos, y a continuación, la VP reacciona formando cadenas ricas en este monómero en los últimos estadios de la reacción.

La peculiar microestructura de los copolímeros preparados y su naturaleza anfifílica posibilitó la obtención de NPs autoensambladas de morfología esférica mediante el método de nanoprecipitación desarrollado por Fessi et al. En concreto, la formación de partículas estables sólo fue posible en aquellas formulaciones poliméricas con un contenido en VP superior al 28%, indicando la importancia de la existencia de un óptimo balance hidrofóbico

– hidrofílico en las cadenas poliméricas que favorezca el proceso de autoensamblado en agua.

El diámetro hidrodinámico aparente (D_h) de estas NPs, determinado en función de la intensidad, se encontró en el rango comprendido entre 96 y 220 nm y su distribución de tamaños fue unimodal con unos índices de polidispersidad (PDI) típicos de distribuciones estrechas. Estos tamaños favorecen a priori su acumulación preferencial en la zona tumoral, evitando su eliminación por el sistema retículo endotelial (RES, del inglés *reticuloendothelial system*) y mejorando su internalización en las células tumorales. Además, su D_h aumentó con el incremento de la concentración de NPs en medio acuoso y la disminución del contenido en VP en el copolímero, indicando su efecto estabilizador al formar parte de la corona externa de estas partículas.

El núcleo hidrofóbico de las partículas preparadas fue utilizado satisfactoriamente para encapsular cumarina-6 (c6) cuya fluorescencia permitió conocer como las NPs eran capaces de penetrar en el citoplasma de células endoteliales (HUVEC, del inglés *human vein endothelial cells*) después de 5 h de incubación, acumulándose alrededor del núcleo. Para evaluar su actividad biológica, se llevaron a cabo ensayos de citotoxicidad MTT en cultivos de células tumorales de adenocarcinoma de mama (MCF-7) y células epiteliales no patológicas (HMEpC).

Los estudios celulares realizados revelaron que las NPs basadas en los polímeros poli(VP-*co*-MTOS) y poli(VP-*co*-MVE) reducían significativamente la viabilidad de las células tumorales MCF-7 de una forma dosis dependiente. Estos resultaron demuestran que la esterificación del grupo succinato del MTOS no supone la pérdida de la actividad del fármaco. Además, la ausencia de este grupo funcional en el MVE evidencia que no es el principal responsable de la actividad de este fármaco. Por tanto, la esterificación del grupo hidroxilo de la vitamina E y la presencia del grupo de señalización juegan un papel fundamental en la actividad anticancerígena de las partículas basadas en los copolímeros poli(VP-*co*-MVE). Adicionalmente, la actividad de estas partículas disminuía drásticamente cuando el contenido en monómero metacrílico superaba una concentración límite (contenido molar en MTOS y MVE superior al 33 y 40 %, respectivamente). Esto puede deberse principalmente a un efecto de estabilización ante la presencia de largas secuencias hidrofóbicas que limitan la biodisponibilidad y accesibilidad al núcleo hidrofóbico activo de las partículas.

Las NPs más activas (con un contenido molar en MTOS y MVE del 11 y 22 %, denominadas como MTOS-11 y MVE-22 respectivamente) fueron seleccionadas para estudiar su citotoxicidad en células no patológicas de forma que se demostró su óptima biocompatibilidad, posibilitando la existencia de un rango de concentración de NPs con una adecuada selectividad hacía células tumorales. Esta selectividad es especialmente atractiva teniendo en cuenta que el único derivado soluble del α-TOS disponible en el mercado (TPGS) mostró una toxicidad acusada en ambas líneas celulares en el mismo rango de concentraciones. Además, la actividad de estas partículas fue comparada con sus análogas basadas en derivados del dihidrofitol, en concreto con las formulaciones SPHY-13 y MPHY-20 (con un contenido molar en SPHY y MPHY del 13 y 20 %, respectivamente). En este caso, estas formulaciones poliméricas no resultaron citotóxicas. Esto permite concluir que las NPs basadas en los polímeros poli(VP-*co*-SPHY) y poli(VP-*co*-MPHY) no poseen actividad anticancerígena, fundamentalmente por la ausencia del grupo funcional succinato en el SPHY y también del grupo de señalización en el MPHY.

Finalmente, se comprobó que la actividad de las partículas más activas dependía en gran medida de la línea celular utilizada de forma que su toxicidad fue progresivamente menor al emplear células tumorales de carcinoma de hipofaringe (FaDu), de adenocarcinoma de colón (WiDr) y de osteosarcoma (MG63). Este fenómeno puede estar estrechamente relacionado con las diferencias existentes en su metabolismo energético y disfunción mitocondrial. Además, debido a la estrecha relación existente entre el crecimiento tumoral y los procesos de vascularización y angiogénesis, la actividad de estas partículas se estudió utilizando células endoteliales en proliferación y quiescentes. Así pues, la viabilidad celular tras el tratamiento con las NPs disminuyó significativamente en cultivos de células en proliferación, afectando en mucha menor medida a células quiescentes.

- **Capítulo 3.2- Mitochondrially targeted nanoparticles based on α-TOS for the selective cancer treatment.**

En el anterior trabajo experimental se demuestra que las NPs autoensambladas preparadas a partir de copolímeros de VP y derivados metacrílicos del α-TOS (MTOS) y la vitamina E (MVE) son excelentes nanovehículos con una actividad intrínseca anticancerígena y antiangiogénica. De hecho, estas partículas mostraron una alta toxicidad hacía células tumorales de mama MCF-7 que, sin embargo, fue más moderada al utilizar

cultivos de células de carcinoma de hipofaringe FaDu. Por tanto, el objetivo de este trabajo científico fue mejorar su eficacia en el tratamiento del cáncer escamoso de cabeza y cuello mediante la encapsulación de α-TOS en su núcleo hidrofóbico, profundizando además en su mecanismo de acción. De esta forma, es la primera vez que se encapsula con éxito esta molécula dentro de un vehículo polimérico sintético que además contiene el propio fármaco anclado químicamente a su estructura.

Para lograr el objetivo de este trabajo, se escogió el copolímero poli(VP-*co*-MTOS) más activo con una composición molar en MTOS del 11% (MTOS-11). La principal razón para seleccionar esta familia de copolímeros fue la similitud estructural entre MTOS y α-TOS que favoreció su encapsulación efectiva dentro del núcleo de las NPs autoensambladas. De hecho, se prepararon con éxito NPs cargadas con un 3, 5 y 10 % w/w de α-TOS con respecto al polímero por el método de nanoprecipitación y que se designaron como NP-3, NP-5 y NP-10, respectivamente. La eficacia de encapsulación (EE) aumentó significativamente con el porcentaje de carga del fármaco, variando desde el 34 % para la formulación NP-3 hasta el 72 % para los autoensamblados NP-10. Este comportamiento puede explicarse teniendo en cuenta las interacciones entre el α-TOS libre y los dominios hidrofóbicos del MTOS que podrían incrementar su flexibilidad y por tanto la capacidad de carga efectiva de las micelas.

El D_h de las partículas cargadas se incrementó significativamente con el porcentaje de α-TOS encapsulado, variando entre 123 y 164 nm y obteniéndose en todos los casos distribuciones de tamaño estrechas y unimodales. Por otra parte, el potencial zeta de las NPs preparadas presentó valores ligeramente negativos, debido a la presencia de VP en la corona externa de las mismas. Sin embargo, este potencial se hizo más negativo en las partículas con mayor carga de α-TOS, alcanzando el valor de -18 mV para la formulación NP-10. Este fenómeno podría deberse a la orientación parcial de los grupos carboxílicos libres de moléculas de α-TOS hacía la corona rica en VP de las partículas autoensambladas.

La actividad biológica de las partículas vacías (NP-0) y cargadas se cuantificó mediante la realización de ensayos MTT utilizando cultivos de células tumorales FaDu y células no patológicas HMEpC. Los resultados de estos experimentos evidenciaron que la citoxicidad de estas partículas en células tumorales aumentaba significativamente con el incremento de la concentración de NPs, la capacidad de carga de α-TOS y el tiempo de incubación. En efecto, la formulación NP-0 sólo resultó citotóxica a la concentración más

alta de partículas utilizada y esta actividad prácticamente no aumentó con el tiempo de incubación (66% y 58 % viabilidad después de 24 y 48 h de tratamiento con NP-0 a 1 mg/mL, respectivamente). Sin embargo, las partículas cargadas presentaron mucha mayor actividad anticancerígena a concentraciones hasta de 0,250 mg/mL, incrementándose además a un tiempo de incubación mayor. Esta variación puede deberse a que las partículas se internalizan a las 24 h pero la liberación de la carga ocurre mayoritariamente a tiempos más prolongados. Además, estos estudios de viabilidad celular revelaron que las células no patológicas eran mucho menos sensibles a las NPs preparadas, existiendo intervalos de concentraciones de NPs con óptima selectividad hacía las células tumorales.

Una vez caracterizada la actividad biológica de las partículas preparadas, el siguiente paso era profundizar en su mecanismo de acción a nivel celular. Para ello, se realizaron diferentes ensayos bioquímicos utilizando la formulación NP-0 a 1 mg/mL por ser la única concentración que resulto citotóxica y NP-10 a una concentración de 0.25 mg/mL que era la concentración más alta y con mayor capacidad de carga que no afectaba a las células no patológicas.

La realización de ensayos Western Blot y ELISA permitió conocer que las partículas ensayadas disminuían significativamente los niveles del de los factores de crecimiento epidérmico (EGF, del inglés *epidermal growth factor*) y del endotelio vascular (VEGF, del inglés *vascular endothelial growth factor*) que están estrechamente relacionados con el crecimiento tumoral, la metástasis y los procesos de vascularización en la zona tumoral. Además, esta desregulación se favoreció con la carga adicional de α-TOS en los autoensamblados (la expresión VEGF fue reducida un 15 y 43 % tras el tratamiento con las formulaciones NP-0 y NP-10, respectivamente). Estos resultados indican que las partículas sintetizadas podrían regular la progresión tumoral y podrían formar parte de tratamientos duales anticancerígenos y antiangiogénicos.

Para evaluar el tipo de muerte celular que provoca el tratamiento de las partículas en cultivos de células FaDu, se cuantificó la enzima lactato deshidrogenasa (LDH) que se libera rápidamente cuando la membrana plasmática está dañada en un proceso de muerte por necrosis. En este caso, el tratamiento con partículas vacías y cargadas prácticamente no aumentó los niveles de esta enzima en comparación con el control. Así pues, las partículas sintetizadas ejercían su acción a través de una muerte celular programada o apoptosis lo que se confirmó mediante ensayos de inmunofluorescencia usando anexina V.

Cuando las células tumorales entran en apoptosis, se activan las proteínas que se denominan caspasas a través de dos posibles rutas: *vía extrínseca* a través de los "receptores de muerte" y regulada por la activación de la caspasa 9 o *vía intrínseca* mediada por las mitocondrias con la activación de la caspasa 8. Ambas vías convergen finalmente y tienen en común la activación de la caspasa 3. Así pues, los niveles de estos tres tipos de caspasas se cuantificaron con ensayos Western Blot de forma que sólo los niveles de caspasa 3 y 9 aumentaron significativamente tras el tratamiento con las partículas, confirmando un mecanismo de muerte por apoptosis vía mitoncondrial. Además, se comprobó que este mecanismo provoca además un aumento significativo del estrés celular, tanto oxidativo como nitrosativo. En efecto, la concentración de especies reactivas al oxígeno y al nitrógeno (ROS/RNS) aumentó un 71 y 177 % después del tratamiento con las formulaciones NP-0 y NP-10, respectivamente.

Finalmente y con el fin de indagar aún más en la acción apoptótica de las partículas a nivel mitocondrial, las células FaDu se pretrataron con MitoQ que es un antioxidante lipofílico que se une al complejo II de la cadena de transporte de electrones de las mitocondrias. Esta unión bloquea el punto de acción del α-TOS, evitando que se desencadene la cascada de eventos típicos de un proceso apoptótico por vía intrínseca. Así pues, este tratamiento previo de las células redujo la toxicidad de las partículas así como los niveles de caspasa 3 y estrés celular, evidenciando que las partículas tanto vacías como cargadas actúan a nivel mitocondrial vía complejo II de la cadena de transporte de electrones.

CAPÍTULO IV: RAFT polymer-drugs derived from α-tocopheryl succinate

- **Capítulo 4.1- α-TOS-based RAFT block copolymers and their NPs for the treatment of cancer.**

En este nuevo trabajo científico, el objetivo fue la preparación de una nueva generación de NPs poliméricas, portadoras de α-TOS en su estructura. Para ello, se introdujeron dos importantes modificaciones de diseño con respecto a los nanovehículos anteriormente descritos, basadas en un control exhaustivo de la arquitectura macromolecular de las cadenas poliméricas y en un cambio composicional mediante la sustitución de la VP por polietilenglicol (PEG) como polímero hidrofílico del sistema.

Para alcanzar con éxito el planteamiento inicial del trabajo, se decidió emplear la polimerización controlada vía RAFT ya que permite la obtención de polímeros de bloque con una organización microestructural precisa, en condiciones suaves de reacción y evitando el uso de catalizadores metálicos. Además, el PEG fue seleccionado por su excelente biocompatibilidad y su capacidad para formar una corona hidrofílica que favorece la acumulación de sistemas nanoparticulados en el tejido tumoral, evitan reconocimiento por el sistema retículo endotelial (RES, del inglés *reticuloendothelial system*).

Debido a que la polimerización vía RAFT requiere la participación de un agente de transferencia de cadena (CTA, del inglés *chain transfer agent*), el primer paso fue la incorporación del PEG al grupo carboxilo terminal del tritiocarbonato seleccionado para este fin. Así pues, se sintetizaron con éxito 5 diferentes PEG macro-CTAs (CTA-PEG) usando la 1-etil-3-(3-dimetilaminopropil)carbodiimida (EDC) como agente de acoplamiento y un peso molecular del PEG en el rango entre 4.6 y 20 kDa. La esterificación se confirmó por NMR, permitiendo además la obtención de distribuciones unimodales y estrechas de MW.

La polimerización del MTOS usando los diferentes PEG macro-CTAs sintetizados se llevó a cabo satisfactoriamente utilizando 1,4-dioxano anhidro como disolvente y 2,2´-azobiisobutironitrilo (AIBN) como iniciador. El tiempo de reacción, la concentración molar total (M) y la cantidad de AIBN fueron ajustados con el fin de mantener el control óptimo de la polimerización, evitando la aparición de reacciones secundarias. En efecto, el estudio de las cinéticas de polimerización por NMR y SEC confirmó la existencia en todos los casos de una cinética lineal con ausencia de reacciones de terminación significativas.

Adicionalmente, este estudio reveló que la velocidad de polimerización únicamente dependía de la concentración de radicales libres, sin existir una correlación directa con el MW del PEG utilizado. Además, el seguimiento de las reacciones de polimerización por SEC mostró el desplazamiento de las curvas de MW a tiempos de retención más bajos en función del tiempo de reacción. En todos los casos, se obtuvieron curvas bimodales que evidenciaron que la eficiencia de los agentes RAFT no fue completa.

La completa caracterización de los copolímeros PEG-*b*-poliMTOS sintetizados permitió conocer su composición de forma que la concentración molar de MTOS varió entre el 13 y 34 %, decreciendo con el aumento del MW del PEG utilizado. Además, su MW fue superior en todos los casos a 30 kDa con $Đ$ inferiores a 1.35 lo que confirma la obtención de polímeros anfifílicos de estructura en bloques bien definida. Finalmente, el análisis termogravimétrico determinó que los polímeros presentaban una temperatura máxima de descomposición que aumentaba con el contenido en PEG y que las curvas de la derivada de pérdida de peso presentaban un hombro a temperaturas más bajas que se hacía más acusado con el contenido en MTOS en los polímeros sintetizados.

El preciso control de la arquitectura macromolecular de los polímeros sintetizados así como su naturaleza anfifílica facilitó la preparación exitosa de NPs autoensambladas, para los copolímeros con una composición molar en PEG del 71, 76, 82 y 87 % que se designaron como NP-71, NP-76, y NP-82 y NP-87, respectivamente. Para ello, se añadió gota a gota una disolución de NaCl sobre las disoluciones de los copolímeros en dioxano, formándose partículas esféricas con una corona externa de PEG y un núcleo hidrofóbico de MTOS. Sin embargo, esto no fue posible con el copolímero menos rico en PEG (66 % molar, PEG-66), probablemente debido a la existencia de un balance hidrofóbico / hidrofílico no apropiado.

La caracterización de las NPs sintetizadas reveló cómo su D_h varía entre 88 y 135 nm, disminuyendo con el incremento de la composición molar en PEG de los copolímeros. Este fenómeno puede explicarse porque la presencia de cadenas de PEG en la corona de las partículas produce un efecto de estabilización debido a interacciones inter- e intramoleculares. Además, todas las NPs presentaron una carga superficial neutra, debido a la ausencia de grupos cargados en su superficie, y que se evidenció con valores de potencial zeta ligeramente negativos. En todos los casos, las distribuciones de tamaños de las autoensamblados fueron unimodales con PDI inferiores a los que se obtuvieron en la

primera generación de NPs, preparadas por polimerización radical convencional (**tabla 1**). En efecto, la polimerización RAFT no sólo permite obtener NPs con mejores propiedades sino que también con un control más exhaustivo de los parámetros que afectan a la organización de las cadenas poliméricas en medio acuoso, como son su composición química, MW y microestructura.

El núcleo hidrofóbico de las NPs sirvió para encapsular eficazmente c6 (EE superior al 90% en todos los casos) de forma que su fluorescencia fue usada para monitorizar la entrada de las NPs dentro de células de adenocarcinoma de mama MDA-MB-453. La acumulación de c6 en el citoplasma de las células aumentó gradualmente con el tiempo de incubación a lo largo de las 8 h de tratamiento. Sin embargo, la intensidad de fluorescencia decreció con el aumento en la composición molar en PEG de las partículas, de forma que la presencia de cadenas largas de este polímero interfieren en su internalización por endocitosis. Este fenómeno es conocido como el "dilema del PEG" y se basa en que el PEG no sólo impide la opsonización de las superficies, sino que la presencia de PEG de alto MW reduce las interacciones entre las partículas poliméricas y la superficie de la membrana celular.

Los estudios de Alamar Blue realizados en cultivos de células MDA-MB-453 mostraron cómo las NPs poliméricas disminuyen la viabilidad celular de forma dosis dependiente. Sin embargo, sólo las NPs con mayor contenido en MTOS (formulaciones NP-71 y NP-76 con un composición molar en MTOS del 29 y 24 %, respectivamente) fueron citotóxicas a la concentración de partículas más elevada de 2,5 mg/mL. En cambio, las formulaciones NP-82 y NP-87 presentaron una viabilidad celular superior al 80% en todo el rango de concentraciones utilizadas, a pesar de su menor D_h. Estos resultados ponen de manifiesto que la actividad anticancerígena de estas partículas depende del contenido en MTOS y también del MW o longitud del bloque hidrofílico de PEG. Así pues, la utilización de cadenas demasiado largas de este polímero favorecen el camuflaje de las partículas evitando su reconocimiento por el RES pero a su vez dificultan la interacción con las membranas celulares, impidiendo su endocitosis de forma efectiva.

- **Capítulo 4.2- Enhanced bioactivity of α-tocopheryl succinate based block copolymer nanoparticles by reduced hydrophobicity.**

En el anterior trabajo, se demuestra cómo la preparación de vehículos poliméricos a partir de copolímeros de bloque PEG-*b*-poliMTOS vía polimerización RAFT permite la obtención de autoensamblados bioactivos contra el cáncer, con un alto control sobre las variables que influyen en su proceso de preparación y con una microestructura de las cadenas poliméricas muy precisa.

A pesar de estas mejoras en su diseño, la actividad anticancerígena de las NPs basadas en los copolímeros PEG-*b*-poliMTOS fue sólo reseñable a una concentración elevada de partículas en aquellas formulaciones más ricas en MTOS (composición molar superior al 24 % a una concentración de NPs de 2,5 mg/mL). Sin embargo, la primera generación de NPs presentaba mayor bioactividad para un menor contenido en MTOS (una composición molar en MTOS del 11 % producía la mayor reducción de viabilidad a una concentración de NPs de 1 mg/mL) (**tabla 1**). Estas diferencias evidencian que las características microestructurales de las cadenas poliméricas influyen estrechamente en su actividad anticancerígena, cambiando la accesibilidad al núcleo hidrofóbico bioactivo o incluso mejorando la liberación de fármacos encapsulados dentro del mismo.

Por estas razones, el objetivo de este nuevo trabajo científico fue estudiar el efecto de la introducción de defectos hidrofílicos en el proceso de formación de NPs y también en su acción terapéutica mediante la copolimerización al azar del 2-hidroxietil metacrilato (HEMA) con el MTOS utilizando el PEG-CTA_8 (MW 8 kDa) como agente RAFT. El HEMA fue seleccionado por su excelente biocompatibilidad una vez polimerizado, óptima hidrofilia así como por su similitud estructural con el MTOS ya que ambos presentan la misma estructura química en la proximidad del doble enlace reactivo durante la polimerización. Estas características son una garantía de que ambos monómeros presentan una reactividad similar, favoreciendo la distribución al azar de las unidades de HEMA en el bloque hidrofóbico del MTOS.

Específicamente, terpolímeros PEG-*b*-[poli(MTOS-*co*-HEMA)] con un 10 y un 20 % mol de HEMA fueron obtenidos con éxito y designados como PEG-10H y PEG-20H, respectivamente. En ambos casos, la polimerización se llevó a cabo durante 5 h, a 70 ºC y empleando 1,4-dioxano anhidro como disolvente. La completa reacción del HEMA fue

confirmada por NMR y la determinación del número de unidades incorporadas durante la polimerización sólo fue posible por espectroscopía de infrarrojo (ATR-FTIR) gracias a la aparición de la banda de vibración del grupo O-H del HEMA a 3500 cm^{-1}.

Los terpolímeros sintetizados presentaron una distribución de peso moleculares estrecha con *Đ* inferior a 1,26 y cinéticas de polimerización lineales que confirman el buen control durante la polimerización que transcurre con una concentración constante de radicales libres y en ausencia de significativas reacciones de terminación. A pesar de que las curvas de MWs eran estrechas, su distribución fue bimodal lo que denota la presencia de una parte del agente RAFT sin reaccionar que, en gran parte, se eliminó mediante la purificación de los terpolímeros por diálisis.

La introducción de unidades al azar de HEMA en el bloque hidrofóbico de MTOS afectó estrechamente a los procesos de autoensamblado que regulan la formación de NPs. En este sentido, se obtuvieron NPs esféricas de 104 y 144 nm a partir de los terpolímeros PEG-10 H y PEG-20H, respectivamente. El D_h de estas formulaciones varió significativamente en función de la concentración de grupos hidroxilo presentes en su estructura. En ambos casos, las distribuciones de tamaño de las NPs fueron estrechas e unimodales, en conformidad con valores de PDI inferiores a 0,06.

Tanto los copolímeros de bloque PEG-*b*-poliMTOS como los terpolímeros PEG-*b*-[poli(MTOS-*co*-HEMA)] permitieron encapsular α-TOS en su núcleo hidrofóbico con una EE superior al 75 % en todos los casos. En concreto, este proceso fue más eficaz en las NPs con mayor contenido en PEG, fruto probablemente del efecto de protección y estabilización de la corona hidrofílica rica en cadenas de este polímero. En todos los casos, se obtuvieron D_h inferiores a 155 nm. Sin embargo, la presencia de la carga aumentó ligeramente el tamaño de los autoensamblados en comparación con las partículas vacías.

Las partículas obtenidas a partir de los terpolímeros PEG-*b*-[poli(MTOS-*co*-HEMA)] incorporaron con éxito c6 y su fluorescencia fue empleada para comprobar que son endocitadas por células tumorales MDA-MB-453. De hecho, estas partículas fueron capaces de atravesar la membrana de estas células en sólo 30 min y este proceso se prolongó durante las 6 h de incubación, aumentando progresivamente la intensidad de fluorescencia. En concreto, las NPs se acumulaban en el citoplasma de las células, alrededor del núcleo siendo capaces de penetrar dentro de sus mitocondrias.

La actividad anticancerígena de todas las NPs preparadas fue evaluada mediante ensayos Alamar Blue en células tumorales MCF-7 y MDA-MB-453. Los resultados de estos experimentos revelaron que la incorporación del HEMA significativamente mejoró el potencial terapéutico de los autoensamblados. La viabilidad de células MCF-7 disminuyó a un 49 y 68 % después de 24 h de tratamiento con las partículas obtenidas a partir de los terpolímeros PEG-10 H y PEG-20H. Este fenómeno puede explicarse porque las unidades de HEMA actúan como "defectos hidrofílicos" dentro del núcleo de MTOS de forma que se reduce su hidrofobicidad y se mejora la difusión de agua en su interior. Sin embargo, es necesario llegar a un balance óptimo que no suponga un reducción excesiva del contenido en MTOS en las partículas, tal y como ocurre con la formulación PEG-20H menos bioactiva. Adicionalmente, la carga de las partículas con α-TOS también mejoró significativamente su potencial terapéutico de forma que la presencia de las unidades de HEMA podría favorecer su liberación debido a la desestabilización que producen dentro del núcleo hidrofóbico de MTOS (**tabla 1**).

La incorporación del HEMA y la carga de α-TOS en el núcleo hidrofóbico de las NPs obtenidas a partir de la formulación poliméricas PEG-10H permitió una mejora sustancial de su actividad anticancerígena, manteniendo además una selectividad apropiada hacía células no patológicas HMEpiC que fueron en todos las casos menos sensibles al tratamiento con las NPs sintetizadas.

CAPÍTULO V: Phototherapeutic nanoparticles

- **Capítulo 5.1- Phototherapeutic effect of polymeric nanoparticles based on α-TOS-RAFT block copolymers conjugated to IR-780.**

Los copolímeros de bloque PEG-*b*-poliMTOS anteriormente descritos son excelentes candidatos para la incorporación de agentes terapéuticos que doten de nuevas propiedades a estos sistemas poliméricos, facilitando el desarrollo de tratamientos más avanzados contra el cáncer. En este sentido, una de las alternativas más novedosas es el uso de agentes de imagen que facilitan el tratamiento y diagnóstico simultáneo de la enfermedad, además de mejorar su eficacia y selectividad. Por ello, el objetivo de este capítulo fue optimizar la conjugación de la sonda de fluorescencia IR-780 a las cadenas de PEG que forman parte de copolímeros de bloque con MTOS como parte hidrofóbica. Además, la capacidad de este conjugado para formar NPs fue exhaustivamente estudiada, caracterizando sus propiedades ópticas así como su toxicidad intrínseca y su capacidad fototerapéutica *in vitro*.

Para obtener el conjugado polimérico deseado, se utilizó la funcionalidad terminal de las cadenas de PEG debido a que permiten llevar a cabo la reacción de conjugación de forma sencilla y eficaz. Para ello, era necesario sustituir los grupos hidroxilos terminales del PEG por grupos carboxilo de forma que la modificación se llevó a cabo previamente en el agente de transferencia PEG-CTA_8. Así pues, se obtuvo con éxito el agente RAFT COOH-PEG-CTA_8 mediante reacción con anhídrido succínico. A continuación, se llevó a cabo la polimerización vía RAFT del MTOS utilizando este agente de transferencia, 1,4-dioxano anhidro como disolvente y AIBN como iniciador. Después de su purificación por diálisis, el copolímero COOH-PEG-*b*-poliMTOS fue caracterizado de forma que se determinó su composición con un concentración molar de MTOS del 30 %. Además, este sistema polimérico presentó un alto peso molecular, 68 kDa, y una relativamente baja polidispersidad, fruto del óptimo control durante la reacción de polimerización.

La conjugación de la sonda al copolímero de bloque COOH-PEG-*b*-poliMTOS se realizó satisfactoriamente mediante la reacción de amidación entre el grupo amino previamente incorporado a la estructura de la sonda (IR-780-NH) y los grupo carboxilo terminales de las cadenas de PEG. Para ello, se empleó la DMTMM como agente de acoplamiento de forma que la estructura del conjugado obtenido, IR-780-PEG-*b*-poliMTOS se confirmó por ^{1}H-NMR.

La formación de NPs esféricas utilizando el conjugado polimérico IR-780-PEG-*b*-poliMTOS fue posible mediante la adición gota a gota de una disolución de NaCl sobre una disolución del polímero en una mezcla THF:EtOH (50:50 v:v). Siguiendo esta metodología, se obtuvieron partículas, denominadas IR-NP, de 88 nm y una PDI de 0.06. Además, partículas cargadas con un 3, 5 y 10 % w/w de sonda IR-780 adicional con respecto al polímero fueron sintetizadas exitosamente y designadas como IR-NP-eIR3, IR-NP-eIR5 y IR-NP-eIR10, respectivamente. La caracterización de estas partículas cargadas reveló que su D_h se incrementó significativamente con el porcentaje de sonda encapsulada, variando entre 110 y 170 nm. En todos los casos, el potencial zeta de las NPs preparadas presentó valores positivos, indicando la presencia de la sonda en la corona externa de las mismas.

El proceso de autoensamblado del sistema polimérico afectó significativamente a las propiedades ópticas de la sonda IR-780 conjugada. La intensidad máxima del pico de emisión a 810 nm de la sonda disminuyó de forma acusada a lo largo del proceso de formación de los autoensamblados debido a la incorporación de la fase acuosa que apantalla su fluorescencia. De la misma forma, las partículas cargadas IR-NP-eIR5 presentaron una mayor intensidad del pico característico de absorción a 780 nm que las partículas vacías IR-NP; sin embargo, la intensidad de emisión fue considerablemente menor, probable debido al apantallamiento de la sonda encapsulada por apilamiento π-π.

Las partículas IR-NP sintetizadas fueron endocitadas por células tumorales de mama MDA-MB-453, acumulándose en su citoplasma. La citotoxicidad de partículas vacías y cargadas IR-NP-eIR5 fue evaluada mediante ensayos Alamar Blue en un rango de concentraciones entre 1,5 y 0,094 mg/mL. La toxicidad de estos nanovehículos se incrementó significativamente tanto por la conjugación química la sonda como por su encapsulación física en el núcleo hidrofóbico de las partículas. En particular, la viabilidad de las células MDA-MB-453 disminuyó a un 50 y 14 % después de 24 h de tratamiento con las formulaciones IR-NP y IR-NP-eIR5 a la más alta concentración, respectivamente (**tabla 1**). Sin embargo, esta toxicidad también afectó de forma acusada a células no patológicas en el mismo rango de concentraciones, perdiendo la selectividad demostrada en las partículas no modificadas.

La capacidad fototérmica de las formulaciones IR-NP y IR-NP-eIR5 a tres concentraciones diferentes de partículas (0,375, 0,188 y 0,094 mg/mL) fue estudiada en disolución mediante la irradiación de un láser a 808 nm durante 5 min durante los cuales IR-780 absorbe la luz y pasa a un estado excitado singlete. Esta energía puede liberarse de tres maneras diferentes: (1) disipándola en forma de luz de mayor longitud de onda (fluorescencia); (2) liberando calor por relajación vibracional al pasar a estadíos de menor energía (efecto fototérmico); (3) evolucionando del estado excitado singlete a un estado excitado triplete de menor energía. En este estado IR-780 puede inducir la generación de especies reactivas letales para los tejidos orgánicos por oxidación de las biomoléculas que los forman (efecto fotodinámico). Los resultados obtenidos confirmaron que las partículas en ausencia de sonda no producían un calentamiento efectivo. Por el contrario, las partículas con la sonda conjugada a la más alta concentración mostraron un incremento de temperatura hasta alcanzar los 42 ºC. Sin embargo, esta temperatura se encuentra en el límite de la hipertermia efectiva para conseguir la muerte celular. Además, se comprobó como las partículas cargadas IR-NP-eIR5 permitían mejorar estos resultados, consiguiendo elevar la temperatura en disolución hasta las 55 ºC ya que, en este caso, la velocidad de liberación de calor era mucho mayor que la liberación de disipación de calor por el medio.

Por último, la fototoxicidad de las partículas IR-NP y IR-NP-eIR5 *in vitro* fue evaluada mediante la irradiación de las células cancerígenas tras permanecer 24 h en contacto con las partículas. De esta forma, se comprobó que la irradiación de las células tratadas con las partículas no modificadas no producía muerte celular. Sin embargo, la irradiación de las células en contacto con las formulaciones IR-NP y IR-NP-eIR5 causaba un descenso acusado de la viabilidad celular. Este efecto no puede explicarse en las partículas vacías únicamente por un calentamiento del medio durante la irradiación. Por ello, es probable la existencia de un efecto fotodinámico dependiente exclusivamente de la presencia de la sonda IR-780, sin que se produzca una modificación permanente de la estructura polimérica de las partículas y que requiere de la irradiación NIR en un contexto donde el nanomaterial haya entrado en contacto previamente con las células. Futuros ensayos son necesarios para profundizar en las reacciones fotodinámicas que justifican la toxicidad de las partículas IR-NP y que también permitan elucidar si la fototoxicidad de las partículas cargadas IR-NP-eIR5 se debe a su comportamiento fototérmico, a su actividad fotodinámica o a una combinación sinérgica de ambas.

Tabla 1: Resumen de las características más relevantes de los diferentes sistemas poliméricos más activos sintetizados en la presente tesis doctoral.

Tipo polimerización o modificación	Sistema polimérico	Caracterización polimeros			Caracterización NPs				Actividad anticancerigena			
		Nomenclatura	MW·10^{-3}	Composición molar	Carga (%)	EE (%)	D_h (nm)	PDI	Línea celular	[NPs] mg/mL	Viabilidad (%)
Radical convencional	poli(VP-*co*-MVE)	MVE-22	30	MVE-22%	---	---	138	0,14	MCF-7	1	~30
	poli(VP-*co*-MPHY)	MPHY-20	30	MPHY-20%	---	---	113	0,16	MCF-7	1	No tóxicas
	poli(VP-*co*-SPHY)	SPHY-13	82	SPHY-13%	---	---	131	0,16	MCF-7	1	No tóxicas
	poli(VP-*co*-MTOS)	MTOS-11	82	MTOS-11%	---	---	134	0,13	MCF-7, FaDu	1	~30 , ~60
					10 % α-TOS	72	164	0,18	FaDu	1	< 20
Radical controlada vía RAFT	PEG-*b*-poli(MTOS)	PEG-71	54	MTOS-29%	---	---	135	0,08	MDA	2,5	~60
					10 % α-TOS	89	154	0,12	MDA	2,5	~40
	PEG-*b*-[poli(MTOS-*co*-HEMA)]	PEG-10H	52	MTOS-24%	---	---	104	0,06	MDA	2,5	~50
					10 % α-TOS	75	124	0,11	MDA	2,5	~20
Post-modificación con DMTMM	IR780-PEG-*b*-poli(MTOS)	COOH-PEG-71	68	MTOS-30%	---		89	0.06	MDA	1,5	~50
					5 % IR780	---	135	0.15	MDA	1,5	~1%

Capítulo VII: Conclusiones

VII. Conclusiones

Tras la realización de la presente tesis doctoral, las conclusiones más relevantes son:

1- El succinato de la vitamina E (α-TOS) es un fármaco anticancerígeno y antiangiogénico con una limitada aplicación en el tratamiento contra el cáncer debido a su baja solubilidad en medio fisiológico. Por ello, este principio activo es un excelente candidato para el desarrollo de vehículos poliméricos selectivos contra el cáncer que eliminen los actuales problemas derivados de su administración.

2- Se copolimerizaron con éxito derivados metacrílicos del α-TOS (MTOS), de la vitamina E (MVE) y del dihidrofitol (SPHY y MPHY) con la *N*-vinil-pirrolidona (VP) por polimerización radical convencional. Debido a su naturaleza anfifílica y la mayor reactividad de los derivados metacrílicos frente a la VP, los copolímeros sintetizados se autoensamblaron en medio acuoso formando nanopartículas (NPs) esféricas con tamaños y propiedades óptimas para su aplicación en el tratamiento del cáncer.

3- Las NPs obtenidas a partir de los copolímeros poli(VP-*co*-MVE) y poli(VP-*co*-MTOS) resultaron bioactivas, con una actividad intrínseca anticancerígena y antiangiogénica dependiente del contenido en monómero hidrofóbico (MVE y MTOS). Adicionalmente, la actividad antitumoral de estas NPs poliméricas resultó estrechamente dependiente de la línea celular ensayada, siendo más activas frente a células de adenocarcinoma de mama MCF-7 debido, probablemente, a diferencias en su metabolismo energético y disfunción mitocondrial. Finalmente, la actividad anticancerígena y antiangiogénica de las partículas resultó altamente selectiva, afectando en menor medida a células no patológicas y quiescentes. Estos resultados mejoraron en gran medida los obtenidos con el único derivado soluble del α-TOS disponible en el mercado (TPGS).

4- Las NPs basadas en los copolímeros poli(VP-*co*-MTOS) se comportaron como excelentes nanovehículos, encapsulando eficazmente α-TOS en su núcleo hidrofóbico y mejorando significativamente su actividad anticancerígena *per se* frente a células de carcinoma de hipofaringe FaDu. Además, los estudios bioquímicos realizados demostraron que tanto las partículas vacías como las cargadas

producían la muerte celular por apoptosis intrínseca, vía complejo II de la cadena de transporte de electrones de las mitocondrias.

5- La preparación de vehículos poliméricos, portadores del α-TOS y con una arquitectura macromolecular controlada, se realizó satisfactoriamente mediante la polimerización radical controlada vía RAFT del MTOS con polietilenglicol (PEG) de diferente peso molecular. De esta forma, se obtuvieron copolímeros anfifílicos PEG-*b*-poliMTOS con una estructura de bloques bien definida que permitió la preparación de nanopartículas esféricas con un núcleo hidrofóbico de MTOS y una corona externa de PEG que les confería una óptima estabilidad.

6- Los estudios realizados en cultivos de células tumorales de mama de las NPs preparadas a partir de los copolímeros PEG-*b*-poliMTOS pusieron de manifiesto su óptima citotoxicidad y capacidad de internalizarse en el citoplasma de células tumorales. Asimismo, la actividad anticancerígena de estos autoensamblados mejoró significativamente con el contenido en MTOS y la presencia de cadenas relativamente cortas de PEG.

7- La copolimerización del 2-hidroxietil metacrilato (HEMA) con el MTOS vía RAFT permitió sintetizar con éxito terpolímeros PEG-*b*-[poli(MTOS-*co*-HEMA)] donde las unidades de HEMA se distribuyeron al azar en el bloque hidrofóbico del MTOS. Adicionalmente, estos terpolímeros formaron NPs esféricas que fueron capaces de internalizarse en las mitocondrias de células tumorales de mama, donde ejercían además su actividad anticancerígena. La encapsulación efectiva del α-TOS y la presencia de un número óptimo de unidades de HEMA permitió maximizar la bioactividad de estos autoensamblados. De hecho, los estudios celulares realizados evidenciaron que las unidades de HEMA actuaban como "defectos hidrofílicos" dentro del núcleo de MTOS reduciendo su hidrofobicidad, mejorando su accesibilidad y favoreciendo la liberación de la carga.

8- La conjugación de la sonda fluorescente IR-780 a las cadenas de PEG de los copolímeros de bloque PEG-*b*-poliMTOS permitió obtener NPs capaces de encapsular más sonda libre en su núcleo hidrofóbico. La conjugación o la encapsulación física de la sonda fluorescente aumentó la citotoxicidad *in vitro* del nanomaterial, dotándolo además de excelentes propiedades ópticas. Adicionalmente,

la irradiación de las partículas confirmó su capacidad fototérmica en disolución, especialmente atractiva por alcanzar altas temperaturas en el caso de los nanovehículos con más sonda encapsulada en su núcleo hidrofóbico. Finalmente, las partículas fluorescentes presentaron una atractiva fototoxicidad *in vitro* con la mediación de un efecto fotodinámico que demuestra el alto potencial de estos nanomateriales para el desarrollo de tratamientos más eficaces y avanzados contra el cáncer.

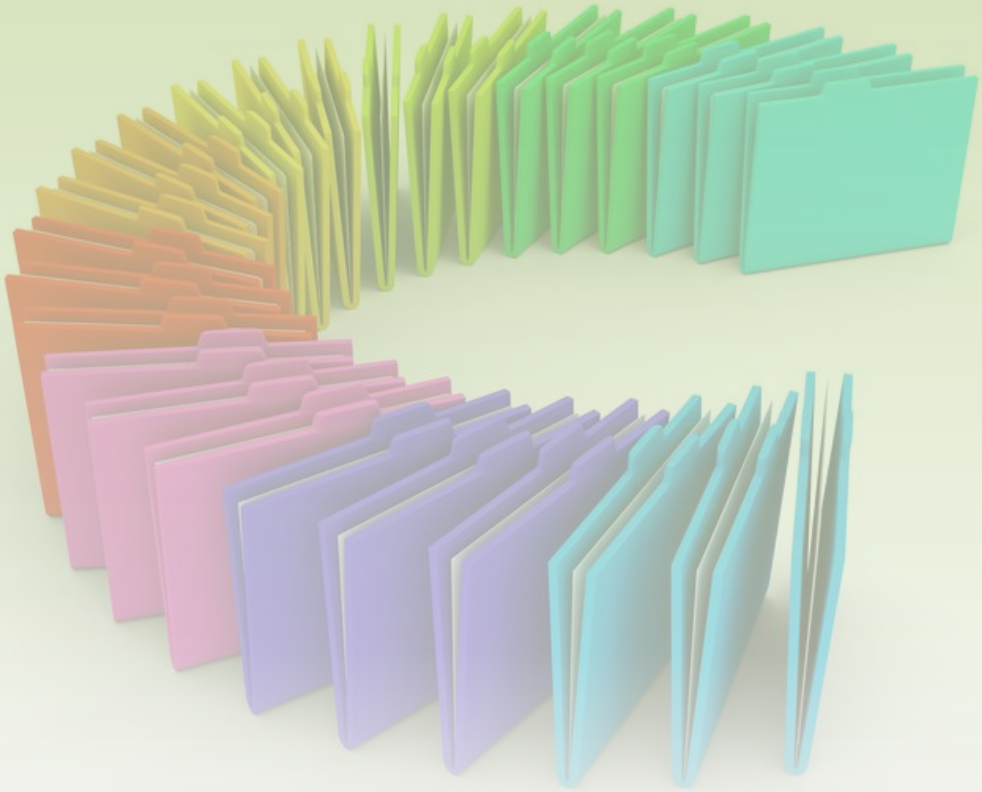

Anexo I: Publicaciones

ANEXO I. Publicaciones

Parte de los resultados obtenidos durante la realización de esta tesis doctoral han dado lugar a las siguientes publicaciones:

1- **Raquel Palao-Suay**, María Rosa Aguilar, Francisco J. Parra-Ruiz, Mar Fernández-Gutiérrez, Juan Parra, Julio San Román. **Copolímeros anfifílicos portadores de alfa-tocoferol con propiedades antitumorales**. *Patente Española* ES1641.864, **2012**.

2- **Raquel Palao-Suay**, María Rosa Aguilar, Francisco J. Parra-Ruiz, Mar Fernández-Gutiérrez, Juan Parra, Julio San Román. **New polymeric nanovehicles that selectively induce apoptosis of cancer cells and present anti-angiogenic activity**. *Fundación Eugenio Rodríguez Pascual*, **2015**, tomo II, 1011-1029.

3- **Raquel Palao-Suay**, María Rosa Aguilar, Francisco J. Parra-Ruiz, Mar Fernández-Gutiérrez, Juan Parra, Carolina Sánchez-Rodríguez, Ricardo Sanz-Fernández, Laura Rodrigáñez, Julio San Román. **Anticancer and Antiangiogenic Activity of Surfactant-Free Nanoparticles Based on Self-Assembled Polymeric Derivatives of Vitamin E: Structure – Activity Relationship**. *Biomacromolecules*, **2015**, 16, 1566-1581.

4- **Raquel Palao-Suay**, Laura Rodrigáñez, María Rosa Aguilar, Carolina Sánchez-Rodríguez, Francisco J. Parra-Ruiz, Mar Fernández, Juan Parra, Juan Riestra Ayora, Ricardo Sanz-Fernández, Julio San Román. **Mitochondrially Targeted Nanoparticles Based on α-TOS for the Selective Cancer Treatment**. *Macromolecular Bioscience*, **2015,** DOI: 10.1002/mabi.201500265.

5- **Raquel Palao-Suay,** Maria Rosa Aguilar, Francisco J. Parra-Ruiz, Samarendra Maji, Richard Hoogenboom, N. A. Rohner, Susan N. Thomas, Julio San Román. **α-TOS-based RAFT block copolymers and their NPs for the treatment of cancer**. *Polymer Chemistry*, **2016**, 7, 838-850.

6- **Raquel Palao-Suay,** Maria Rosa Aguilar, Francisco J. Parra-Ruiz, Samarendra Maji, Richard Hoogenboom, N. A. Rohner, Susan N. Thomas, Julio San Román. **Enchanced bioactivity of α-tocopheryl succinate based on block copolymer**

nanoparticles by reduced hydrophobicity. *Macromolecular Bioscience*, **2016,** submitted**.**

7- **Raquel Palao-Suay**, L.G. Gómez-Mascaraque, María Rosa Aguilar, Blanca Vázquez-Lasa, Julio San Román. **Self-assembling polymer systems for advanced treatment of cancer and inflammation**. *Progress in Polymer Science*, **2016**, 53, 207-248.

Otras publicaciones relacionadas con los nanomateriales descritos en esta tesis son:

8- Sergio Martín-Saldaña, **Raquel Palao-Suay**, Almudena Trinidad, María Rosa Aguilar, Rafael Ramírez-Camacho, Julio San Román. **Otoprotective properties of 6α-methylprednisolone-loaded nanoparticles against cisplatin: In vitro and in vivo correlation.** *Nanomedicine: Nanotechnology, Biology and Medicine*, **2016**, 12, 965-976.

9- Sergio Martín-Saldaña, **Raquel Palao-Suay**, María Rosa Aguilar, Rafael Ramírez-Camacho, Julio San Román**. Polymeric nanoparticles loaded with dexamethasone or α-tocopheryl succinate to ameliorate cisplatin-induced ototoxicity: study of caspase and proinflammatory dependent pathways**. *Journal of Controlled Release*, **2016**, submitted.

Article

pubs.acs.org/Biomac

Anticancer and Antiangiogenic Activity of Surfactant-Free Nanoparticles Based on Self-Assembled Polymeric Derivatives of Vitamin E: Structure−Activity Relationship

Raquel Palao-Suay,[†,‡] María Rosa Aguilar,[*,†,‡] Francisco J. Parra-Ruiz,[†] Mar Fernández-Gutiérrez,[†,‡] Juan Parra,[‡,§] Carolina Sánchez-Rodríguez,[∥,#] Ricardo Sanz-Fernández,[∥,#] Laura Rodrigáñez,[∥] and Julio San Román[†,‡]

[†]Group of Biomaterials, Department of Polymeric Nanomaterials and Biomaterials, Institute of Polymer Science and Technology, CSIC, C/Juan de la Cierva, 3, 28006 Madrid, Spain

[‡]Networking Biomedical Research Centre in Bioengineering, Biomaterials and Nanomedicine, CIBER-BBN, Zaragoza, Spain

[§]Clinical Research and Experimental Biopathology Unit, Healthcare Complex of Ávila, SACYL, C/Jesús del Gran Poder 42, 05003 Ávila, Spain

[∥]Foundation for Biomedical Research, University Hospital of Getafe, Carretera de Toledo, km 12,500, 28905, Getafe, Madrid, Spain

[#]European University of Madrid, C/ Tajo s/n. 28670, Villaviciosa de Odón (Madrid), Spain

Supporting Information

ABSTRACT: α-Tocopheryl succinate (α-TOS) is a well-known mitochondrially targeted anticancer compound, however, it is highly hydrophobic and toxic. In order to improve its activity and reduce its toxicity, new surfactant-free biologically active nanoparticles (NP) were synthesized. A methacrylic derivative of α-TOS (MTOS) was prepared and incorporated in amphiphilic pseudoblock copolymers when copolymerized with *N*-vinylpyrrolidone (VP) by free radical polymerization (poly(VP-*co*-MTOS)). The selected poly(VP-*co*-MTOS) copolymers formed surfactant-free NP by nanoprecipitation with sizes between 96 and 220 nm and narrow size distribution, and the in vitro biological activity was tested. In order to understand the structure−activity relationship three other methacrylic monomers were synthesized and characterized: MVE did not have the succinate group, SPHY did not have the chromanol ring, and MPHY did not have both the succinate group and the chromanol ring. The corresponding families of copolymers (poly(VP-*co*-MVE), poly(VP-*co*-SPHY), and poly(VP-*co*-MPHY)) were synthesized and characterized, and their biological activity was compared to poly(VP-*co*-MTOS). Both poly(VP-*co*-MTOS) and poly(VP-*co*-MVE) presented triple action: reduced cell viability of cancer cells with little or no harm to normal cells (anticancer), reduced viability of proliferating endothelial cells with little or no harm to quiescent endothelial cells (antiangiogenic), and efficiently encapsulated hydrophobic molecules (nanocarrier). The anticancer and antiangiogenic activity of the synthesized copolymers is demonstrated as the active compound (vitamin E or α-tocopheryl succinate) do not need to be cleaved to trigger the biological action targeting ubiquinone binding sites of complex II. Poly(VP-*co*-SPHY) and poly(VP-*co*-MPHY) also formed surfactant-free NP that were also endocyted by the assayed cells; however, these NP did not selectively reduce cell viability of cancer cells. Therefore, the chromanol ring of the vitamin E analogues has an important role in the biological activity of the copolymers. Moreover, when succinate moiety is substituted and vitamin E is directly linked to the macromolecular chain through an ester bond, the biological activity is maintained.

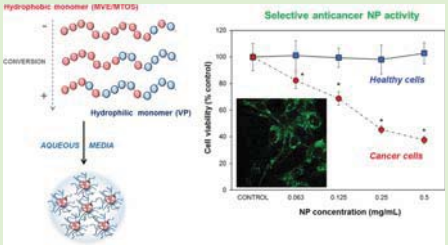

INTRODUCTION

α-Tocopheryl succinate (α-TOS) selectively induces apoptosis of cancer cells and acts as an angiogenesis regulator because it also induces apoptosis of proliferating endothelial cells with little or no harm to the quiescent endothelial cells. α-TOS presents mitochondrially targeted anticancer activity because it is a BH3 protein mimetic that blocks Bcl-2 or Bcl-xL antiapoptotic proteins (mitocan type II), and because it interferes with the electron transport chain, specifically α-TOS displaces ubiquinone from binding to complex II inhibiting succinate deshydrogenase activity of complex II in the mitochondrial transport chain (mitocan type V).[1,2] As a result, the generated electrons recombine with molecular oxygen to produce high levels of reactive oxygen species (ROS) that activate the proteins that regulate

Received: January 29, 2015
Revised: March 18, 2015
Published: April 7, 2015

DOI: 10.1021/acs.biomac.5b00130
Biomacromolecules 2015, 16, 1566−1581

Mitochondrially Targeted Nanoparticles Based on α-TOS for the Selective Cancer Treatment

Raquel Palao-Suay, Laura Rodrigáñez, María Rosa Aguilar,*
Carolina Sánchez-Rodríguez, Francisco Parra, Mar Fernández, Juan Parra,
Juan Riestra-Ayora, Ricardo Sanz-Fernández, Julio San Román

The aim of this work is the preparation of an active nanovehicle for the effective administration of α-tocopheryl succinate (α-TOS). α-TOS is loaded in the core of nanoparticles (NPs) based on amphiphilic pseudo-block copolymers of *N*-vinyl pyrrolidone and a methacrylic derivative of α-TOS. These well-defined spherical NPs have sizes below 165 nm and high encapsulation efficiencies. In vitro activity of NPs is tested in hypopharynx squamous carcinoma (FaDu) cells and nonmalignant epithelial cells, demonstrating that the presence of additional α-TOS significantly enhances its antiproliferative activity; however, a range of selective concentrations is observed. These NPs induce apoptosis of FaDu cells by activating the mitochondria death pathway (via caspase-9). Both loaded and unloaded NPs act via complex II and produce high levels of reactive oxygen species that trigger apoptosis. Additionally, these NPs effectively suppress the vascular endothelial growth factor (VEGF) expression of human umbilical vein endothelial cells (HUVECs). These results open the possibility to use this promising nanoformulation as an α-TOS delivery system for the effective cancer treatment, effectively resolving the current limitations of free α-TOS administration.

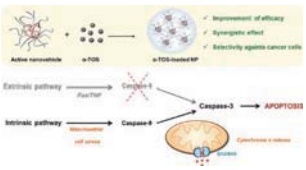

1. Introduction

Head and neck squamous cell carcinoma (HNSCC) is the sixth highest incidence worldwide cancer,[1] constituting the 6.5% of all tumors,[2] with more than 600 000 new cases each year.[3,4] Currently, the therapeutic approach of these tumors is the surgery when the tumor is resectable that is followed or combined with radiotherapy or chemoradiotherapy.[5,6] However, the adverse effects of these therapies are multiple, including mucositis, dermatitis, and dysphagia among others.[6,7]

R. Palao-Suay,† Dr. M. R. Aguilar, F. Parra,
M. Fernández, J. S. Román
Group of Biomaterials
Department of Polymeric Nanomaterials and Biomaterials
Institute of Polymer Science and Technology
CSIC, C/Juan de la Cierva, 3, 28006 Madrid, Spain
E-mail: mraguilar@ictp.csic.es
R. Palao-Suay, Dr. M. R. Aguilar, M. Fernández,
J. Parra, J. S. Román
Networking Biomedical Research Centre in Bioengineering
Biomaterials, and Nanomedicine
CIBER-BBN, Spain
†These authors contributed equally to this article.

L. Rodrigáñez,† C. Sánchez-Rodríguez, J. Riestra-Ayora,
R. Sanz-Fernández
Foundation for Biomedical Research
University Hospital of Getafe
Carretera de Toledo, km 12, 500, 28905 Getafe, Madrid, Spain
C. Sánchez-Rodríguez, R. Sanz-Fernández
European University of Madrid
C/Tajo s/n. 28670, Villaviciosa de Odón, Madrid, Spain
J. Parra
Clinical Research and Experimental Biopathology Unit
Healthcare Complex of Ávila
SACYL. C/Jesús del Gran Poder 42, 05003 Ávila, Spain

Macromol. Biosci. **2015**, DOI: 10.1002/mabi.201500265

Polymer Chemistry

PAPER

α-TOS-based RAFT block copolymers and their NPs for the treatment of cancer†

Cite this: *Polym. Chem.*, 2016, **7**, 838

Raquel Palao-Suay,[a,b] María Rosa Aguilar,*[a,b] Francisco J. Parra-Ruiz,[a] Samarendra Maji,[c] Richard Hoogenboom,[c] N. A. Rohner,[d] Susan N. Thomas[d] and Julio San Román[a,b]

Received 12th November 2015,
Accepted 25th November 2015

DOI: 10.1039/c5py01811k

www.rsc.org/polymers

α-Tocopheryl succinate (α-TOS) is a well-known mitochondrially targeted anticancer compound. However, a major factor limiting the use of α-TOS is its low solubility in physiological media. To overcome this problem, the aim of this work is the preparation of new polymeric and active α-TOS-based nanovehicle with a precise control over its macromolecular architecture. Reversible addition–fragmentation chain transfer polymerization (RAFT) is used to synthesize an α-TOS amphiphilic block copolymer with highly homogeneous molecular weight and relatively narrow dispersity. Macro-chain transfer agents (macro-CTA) based on poly(ethylene glycol) (PEG) of different molecular weights (MW, ranging from 4.6 to 20 kDa) are used to obtain block copolymers with different hydrophilic/hydrophobic ratios with PEG being the hydrophilic block and a methacrylic derivative of α-tocopheryl succinate (MTOS) being the monomer that formed the hydrophobic block. PEG-*b*-poly (MTOS) form spherical nanoparticles (NPs) by self-organized precipitation (SORP) or solvent exchange in aqueous media enabling to encapsulate and deliver hydrophobic molecules in their core. The resulting NPs are rapidly endocytosed by cancer cells. The biological activity of the synthesized NPs are found to depend on the MW of PEG, with the NP comprised of the higher MW copolymer resulting in a lower bioactivity due to PEG shielding, inhibiting cellular uptake by endocytosis. Moreover, the biological activity also depends on the MTOS content, as the biological activity increases as a function of MTOS concentration.

Introduction

The rapid growth of nanomedicine has opened the possibility to create sophisticated strategies against cancer and other diseases at a nanoscale where the properties of materials often differ from those of the corresponding bulk materials.[1,2] As such, a wide range of materials based on natural or synthetic polymers are available to design self-assembled nanostructures.[3–5] Macromolecular self-assembly represents a spontaneous process that involves the organization of amphiphilic macromolecules in an aqueous environment, forming different supramolecular structures.[6,7] One interesting example of this variety of supramolecular assemblies is nanoparticles (NPs) that exhibit a core–shell morphology based on the use of amphiphilic polymers with hydrophobic and hydrophilic domains.[8–10]

The preparation of advanced nano-assemblies using amphiphilic copolymeric systems requires optimal control over the chemical composition and distribution of monomeric units into the macromolecular chains. In this sense, amphiphilic polymers can be obtained by different synthetic methodologies, such as free radical or controlled radical polymerization (CRP). Both techniques proceed *via* the analogous radical mechanism. However, conventional free radical polymerization does not allow the complete control of the molecular weights (MW) and therefore, heterogeneous mixtures of macromolecular chains are obtained. Thus, CRP methods have emerged as potent tools for the synthesis of macromolecular architectures that exhibit a narrow dispersity

[a]*Group of Biomaterials, Department of Polymeric Nanomaterials and Biomaterials, Institute of Polymer Science and Technology, CSIC, Juan de la Cierva, 3, 28006 Madrid, Spain*
[b]*Networking Biomedical Research Centre in Bioengineering, Biomaterials and Nanomedicine, CIBER-BBN, Spain. E-mail: mraguilar@ictp.csic.es; Fax: +34 91564 48 53; Tel: +34 91561 88 06 (ext.212)*
[c]*Supramolecular Chemistry Group, Department of Organic and Macromolecular Chemistry, Ghent University. Krijgslaan 281-S4, 9000 Ghent, Belgium*
[d]*George W. Woodruff School of Mechanical Engineering and Parker H. Petit Institute of Bioengineering and Bioscience, Georgia Institute of Technology, 315 Ferst Dr NW, Atlanta, 30332 Georgia, USA*
†Electronic supplementary information (ESI) available. See DOI: 10.1039/c5py01811k

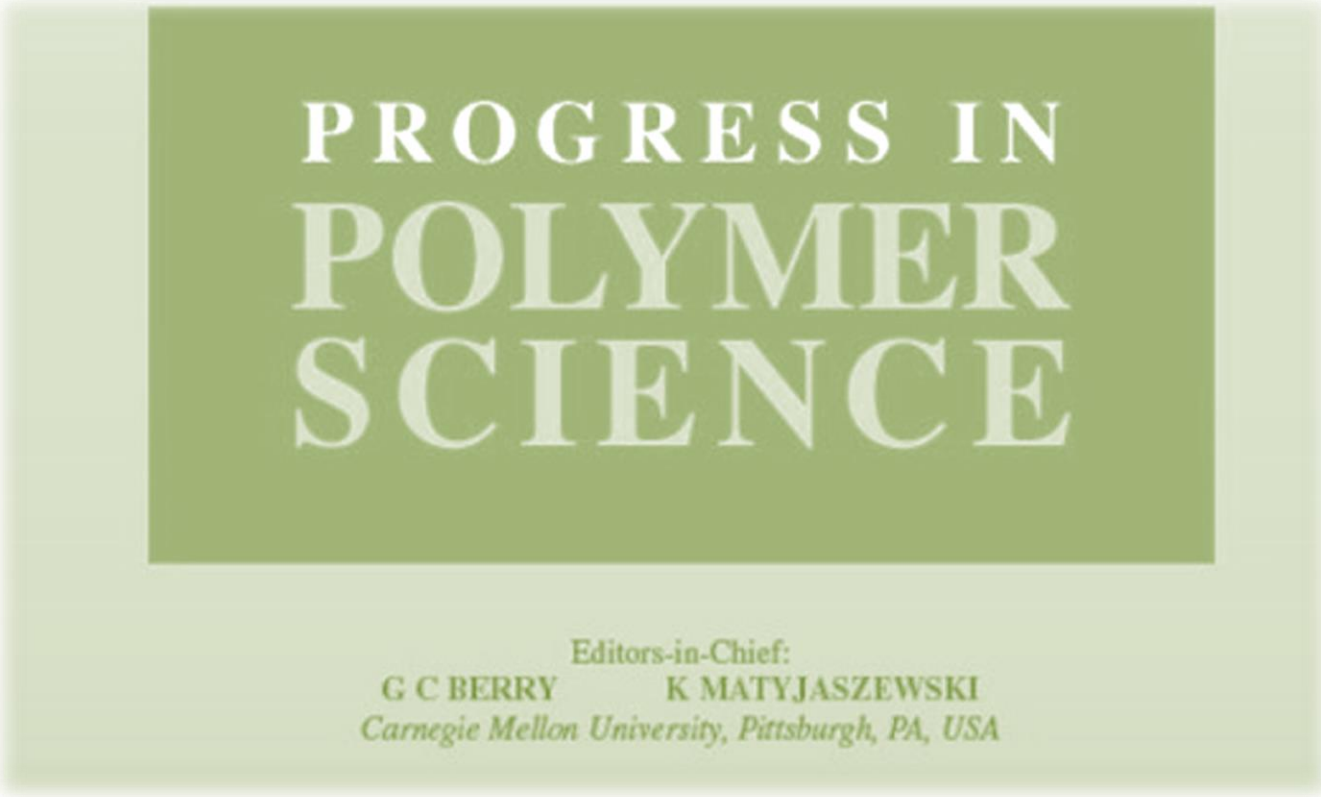

Anexo II: Self-assembling polymer systems for advanced treatment of cancer and inflammation

Progress in Polymer Science 53 (2016) 207–248

Contents lists available at ScienceDirect

Progress in Polymer Science

journal homepage: www.elsevier.com/locate/ppolysci

Self-assembling polymer systems for advanced treatment of cancer and inflammation

R. Palao-Suay[a,b], L.G. Gómez-Mascaraque[a,b], M.R. Aguilar[a,b], B. Vázquez-Lasa[a,b], J. San Román[a,b,*]

[a] Institute of Polymer Science and Technology, CSIC, C/Juan de la Cierva 3, 28006 Madrid, Spain
[b] Networking Biomedical Research Center in Bioengineering, Biomaterials and Nanomedicine (CIBER-BBN), Zaragoza, Spain

ARTICLE INFO

Article history:
Received 28 October 2014
Received in revised form 25 May 2015
Accepted 9 July 2015
Available online 26 July 2015

Keywords:
Self-assembling polymers
Nanoparticles
Micelles
Amphiphilic polymers
Cancer
Anti-inflammatory agents

ABSTRACT

Self-assembled nanoparticles have reached a growing interest for the improvement of cancer diseases and associated inflammation processes. This article describes the most representative types of self-assembling nanosystems, including a detailed review of different methodologies for their preparation. Nanoparticles are commonly formed by self-assembling of amphiphilic polymers in aqueous environment. For that reason, the main strategies for the design of amphiphilic polymeric systems are also reviewed, with an emphasis on the different polymerization techniques of synthetic monomers and several strategies of chemical modification of polysaccharides and proteins. Additionally, most advanced applications of self-assembled nanocarriers for the improvement of treatment of cancer and inflammation diseases are also discussed, focusing on the description of drug-loaded and drug-conjugated systems, active targeted strategies and most recently possibilities for the multimodality treatment of cancer diseases.

Contents

* Corresponding author at: Institute of Polymer Science and Technology, CSIC, C/Juan de la Cierva 3, 28006 Madrid, Spain. Tel.: +34 915618806; fax: +34 915644853.
E-mail address: jsroman@ictp.csic.es (J.S. Román).

http://dx.doi.org/10.1016/j.progpolymsci.2015.07.005
0079-6700/

1. Introduction

Nanomedicine is growing in directions of diagnostic, treatment and theranostics (diagnostic, drug delivery and therapeutics), and the participation of systems based on a macromolecular concept is well recognized [1–3]. In fact, we have to learn from nature that most of the activities in the living organism, including the human body, are based on the design and application of bioactive systems and drugs developed in a macromolecular or polymeric concept. Nature shows a lot of examples that we have the opportunity to apply; *i.e.* bioactive systems and macromolecular drugs. Systems such as heparin, chondroitin sulfate, heparan sulfate (polysaccharides), or insulin, growth hormone, fibroblast growth factor, morphogenetic proteins, fibronectin, albumin, fibrinogen (proteins) and other well-known bioactive compounds are designed and fabricated in our organism within a macromolecular architecture.

High molecular weight (MW) polymers with specific molecular architectures present the ability of association and distribution in specific nanodomains, with morphologies and properties depending on the nature of the molecules [4]. The design, composition and morphological assembly of the cells and the extracellular matrix in the human organism are developed on the basis of the interactions and arrangements of long molecules with specific properties. On this way, the cytoplasmic membrane is composed of a bilayer assembled organization of lipid molecules containing a hydrophilic head. These individual and isolated structures develop their activity in a medium of controlled viscosity constituted by a macromolecular hydrogel of unique characteristics (collagen), which allows the development of the cellular activity and at the end, the proliferation of cells and fabrication of tissues and organs.

Macromolecular self-assembly is a spontaneous process based on the ensemble of molecules into 3D supramolecular structures with different morphologies such as polymeric micelles (PM), nanoparticles (NP), polymerosomes, *etc.* [5,6]. This process is possible due to the amphiphilic nature of these structures, containing both hydrophobic and hydrophilic domains. Particularly, in the core–shell organization, the inner core is composed of the hydrophobic part of the amphiphilic polymer and serves as a nanocontainer of poor soluble drugs. This core is surrounded by an outer shell based on hydrophilic polymers [7–9]. The characteristics of self-assembling systems depend on several important factors:

- Design, molecular composition and structure, considering macromolecular size and size distribution.
- Monomeric or co-monomeric sequences arrangement and distribution along the macromolecular chains.
- Functionality and its distribution in the structure of the macromolecular systems.
- Structural and morphological distribution in nanodomains.
- Macromolecular associations of natural and synthetic polymers, and stability in physiological conditions.

The structural characteristics of self-assembling systems have several advantages to improve the effectiveness and safety of cancer and anti-inflammation therapies for clinical use [10–13]. For example, the encapsulation of chemotherapeutic and anti-inflammatory drugs in the core of these assemblies improves their aqueous diffusion and transport, as well as bioavailability, decreasing their toxic side effects [14,15]. Moreover, their hydrophilic surfaces decrease clearance by the reticuloendothelial system (RES),

Nomenclature

α-TOS	α-tocopheryl succinate
5-FU	5-fluorouracil
A549	human lung adenocarcinoma epithelial cells
AA	amino acids
ADR	adriamycin
ALG	alginates
ATRA	all *trans* retinoic acid
ATRP	atom transfer radical polymerization
CD44	cluster determinant 44
CDDP	hydrophilic derivative of cisplatin
CL	ε-caprolactone
CPT	camptothecin
CSO	chitosan oligosaccharide
DCC	*N*,*N*′-dicyclohexylcarbodiimide
DCT	docetaxel
DD	deacetylation degree
DEX	dextran
DMAP	*N*,*N*-dimethyl amino pyridine
DMT	dexamethasone
DOCA	deoxycholic acid
DOX	doxorubicin
DS	degree of substitution
DSPE	distearoylphosphatidylethanolamine
EDC	1-ethyl-3-(3-dimethylaminopropyl) carbodiimide
EGCG	epigallocatechin-3-gallate
EPR	enhanced permeability and retention
FA	folic acid
FDA	Food and Drug Administration
Fol	folate
GRA	glycyrrhetinic acid
HA	hyaluronic acid
HARE	hyaluronan receptor for endocytosis
Hases	hyaluronidases
HCPT	hydroxycamptothecin
HeLa	human cervical cancer cells
HER2	human epidermal growth factor receptor 2
HES	Hydroxyethyl starch
His	histidine
HPMA	poly(*N*-(2-hydroxypropyl)methacrylamide)
IMC	indomethacin
IR	inhibition rate
KB	human nasopharyngeal epidermoid cancer cells
LA	lactic acid
LCST	lower critical solution temperature
LMWC	low molecular weight chitosan
MAA	methacrylic acid
MDR	multidrug resistance
mPEG	methoxypoly(ethylene glycol)
MTO	mitoxantrone
MTX	methotrexate
MW	molecular weight
NC	nanocapsules
NCA	*N*-carboxyanhydride
NHS	*N*-hydroxysuccinimide
NMP	nitroxide-mediated polymerization
NP	nanoparticles
NSCL	non-small cell lung cancer
o/w	oil-in-water emulsion
OX	2-oxazoline monomer
PA	peptide amphiphiles
PAA	poly(amino acids)
PAsp	poly(aspartic acid)
Pba	pheophorbide
PBS	phosphate buffered saline
PCL	poly(ε-caprolactone)
pDNA	plasmid DNA
PDT	photodynamic therapy
PE	phosphatidylethanolamine
PEG	poly(ethylene glycol)
PEGMA	poly(ethylene glycol methacrylate)
PEI	polyethyleneimine
PEO	polyethylenoxide
PEtOx	poly(2-ethyl-2-oxazoline)
PGlu	poly(glutamic acid)
PLA	poly(lactic acid)
PLGA	poly(lactic-*co*-glycolic acid)
PLL	poly(L-lysine)
PM	polymeric micelles
PMAA	poly(methacrylic acid)
PMDETA	*N*,*N*,*N*′,*N*″,*N*″-pentamethyldiethylenetriamine
PNIPAm	poly(*N*-isopropylacrylamide)
Poly(L-His)	poly(L-histidine)
POX	poly(2-oxazolines)
PPhe	polyphenylalanine
PPO	poly(propylene oxide)
PS80	polysorbate 80
PTX	paclitaxel
RAFT	reversible addition and fragmentation transfer chain polymerization
RES	reticuloendothelial system
RGD	Arg-Gly-Asp
ROP	ring opening polymerization
SCF	supercritical fluid technology
SF	silk fibroin
SPIONs	superparamagnetic iron oxide nanoparticles
TEA	triethylamine
THP	tumor-homing peptides
TPGS	tocopheryl polyethylene glycol 1000 succinate
VEGF	vascular endothelial growth factor
w/o/w	water-in-oil-in-water emulsion

presumably preventing opsonization by reducing the protein interaction. This strategy also allows the protection of drugs from degradation and produces their controlled release to the tumor site due to the enhanced permeability and retention (EPR) effect [16–18]. On the other hand, advances in engineering of block copolymers offer a wide range of possibilities to control the most influential properties of the polymeric assemblies, such as the particle size, stability or loading capacity of drugs, and to achieve an optimal active targeting to tumor site by modification

of the shell of the macromolecular structures with specific ligands to promote cell targeting [7,19]. In fact the structure and morphology of self-assembled systems in a biomimetic scenario, including the decoration of the NP by ligands with high affinity to receptors overexpressed in cancer cells, are the most important parameters to control and to enhance the most frequent mechanism of the incorporation of the bioactive NP systems that is the endocytosis or pinocytosis. The application of NP systems brings novel and advanced possibilities including the lowering of the toxicity of the applied systems, without a noticeable decrease of the drug activity. The specific decoration of NP offers an additional contribution to new and advanced perspectives for the treatment of cancer and the application of anti-inflammatory therapies.

"Polymer therapeutics" can be considered the first generation nanomedicine. It includes polymers with inherent biological activity, polymer–proteins and polymer–drug hybrid conjugates, PM, supramolecular assemblies that form multicomponent polyplexes designed for intracellular delivery of genes and proteins [20,21]. According to the properties of the macromolecular systems, they can be designed in different ways and morphologies. Fig. 1 shows schematically the design and configuration of a sensitive system that can be considered a good nanocarrier for drugs with anti-tumor activity and anti-inflammatory effects. The self-assembled NP contains the drug (normally a non-polar compound with a limited solubility in water or in physiological fluid) in the core and a sensitizer (in this case a photosensitizer), and in the shell layer a targeting ligand for interaction and selective linking to the cytoplasmatic membrane [22]. The design of this micellar system protects the drug from the external medium (the physiological medium) until the cytoplasmatic membrane is reached, where the adequate interaction between the targeting ligand and the receptor of the membrane favors the endocytosis process. The release of the active compounds and the direct activity of the anti-tumor or anti-inflammatory drug, with high efficacy and low toxicity, are produced in the cytoplasm of the cells. If the carrier or NP is designed with a biodegradable or resorbable polymer component, the system is cleared from the cell and from the body without accumulation [23,24].

This review describes the possibilities of design and formulation of advanced pharmacologically active systems and polymer drugs to obtain self-assembled NP for anticancer and/or anti-inflammatory applications, considering the origin and nature of the polymeric materials that can be used as support matrices of nanocarriers.

2. Methodologies for self-assembling systems

2.1. Types of self-assembling nanosystems

Synthetic or natural-derived amphiphilic polymers can self-associate in aqueous media due to intra- and/or intermolecular hydrophobic interactions [25] giving rise to a variety of nanosized structures with potential application in advanced cancer therapies. These delivery systems can be classified according to their different supramolecular organization into micelles and diverse types of NP.

PM are among the first polymeric self-aggregates which were described in the literature as nanoscale drug delivery systems [26,27]. It is generally accepted that micelles are built from individual polymeric molecules [28] which are thermodynamically driven to self-assemble due to their amphiphilic nature. PM can be obtained from block or random copolymers, or either from hydrophobically modified hydrophilic polymers where the hydrophobic residues can be attached to one end of the polymer or randomly distributed within the polymeric structure, giving rise to different supramolecular structures (see Fig. 2).

The cores of the micelles can act as reservoirs for anticancer agents, which are usually hydrophobic, and their hydrophilic shells facilitate their solubility in aqueous media [29]. The small size of PM, commonly between 10 and 100 nm, has several advantages such as the possibility of extravasation of the nanocarriers along with the minimization of the risks of embolism in capillaries [30]. Furthermore, their unique small size facilitates longer blood circulation times and thus leads to enhanced accumulation at tissue sites with vascular abnormalities such as tumor tissues [7].

NP can be prepared by spontaneous self-organization due to the same thermodynamic principles previously described for micelles, which are generally based on the amphiphilic nature of the polymers or the association of oppositely charged polyions. Two different types of self-assembling NP can be obtained depending on the preparation procedure: nanospheres or nanocapsules (NC) (see Fig. 2). Nanospheres consist of packed polymeric matrices while NC are vesicular systems with an inner cavity surrounded by a polymeric membrane [31]. When nanospheres are loaded with anticancer agents, these are dispersed throughout the NP. However, these agents are confined in the cavity when loaded into NC, which acts as a reservoir systems.

Nanospheres can in turn be divided into micellar associations, formed by aggregation of individual micelles, and nanogels, consisting of nanosized polymeric matrices which are physically cross-linked by the interaction between the hydrophobic chains or residues of amphiphilic polymers. In addition, hydrogen bond or electrostatic interactions can also support the cross-linking of nanogels to form water-swollen NP [32].

NC can be classified according to the nature of their cavities, which can contain active substances in liquid or solid form, or as molecular dispersions, being this reservoir either lipophilic or hydrophobic [33]. A particular nanocapsular structure are polymersomes, which are similar to liposomes but are composed of amphiphilic polymers instead of amphiphilic lipids [5].

Conventional dendrimers lack self-assembling behavior. However, amphiphilic dendrimers are able to form micelle-like NP by self-assembly, usually exhibiting hydrophilic groups on their surface [5,34]. Moreover, dendronized polymers-based NP, which can combine both the characteristics of self-assembled nanostructures and dendrimers have been prepared by covalently linking hydrophobic dendrons to hydrophilic polymer backbones so that the resulting conjugates have an amphiphilic nature capable of self-organizing into core–shell structures [35].

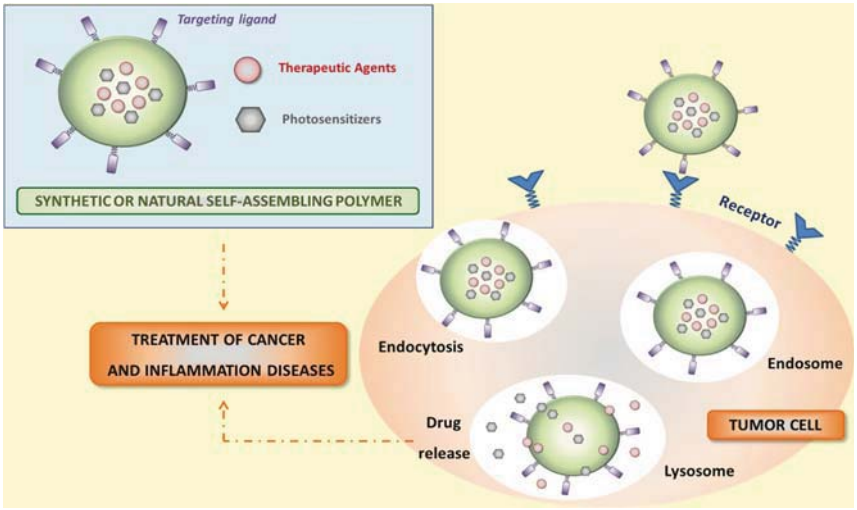

Fig. 1. Active targeting of advanced self-assembled nanoparticles. Design of components and mechanism of bioactivity.

Alternatively, monomers already carrying dendrons can be subjected to polymerization giving rise to dendronized polymers [36,37].

2.2. Methodologies for the obtaining of self-assembling nanosystems

Self-assembling polymer nanosystems (*i.e.* micelles, nanospheres or NC) are normally obtained from preformed polymers with an appropriate hydrophobic/hydrophilic balance using the following techniques:

Solvent evaporation: this is a widely used method for the preparation of NP for drug delivery formulations. The polymer is dissolved in a volatile solvent and an emulsion is formulated with or without surfactant using high-speed homogeneization or ultrasonication. The solvent diffuses through the continuous phase and evaporates by continuous magnetic stirring or under reduced pressure, giving rise to a nanoparticle suspension. The process can be carried out in single emulsions, *e.g.* oil-in-water (o/w) or double emulsions, *e.g.* water-in-oil-in-water emulsion (w/o/w).

Saeed et al. [38] prepared well-defined smart NP by (w/o)/w double emulsion to encapsulate DNA with high efficiency. NP were based on poly(lactic-*co*-glycolic acid)-S-S-poly(lactic-*co*-glycolic acid) (PLGA-S-S-PLGA) and PLGA-S-S-Poly(ethylene glycol methacrylate)-folate (PLGA-S-S-PEGMA-Fol) block polymers synthesized using a combination of ring opening polymerization (ROP) and atom transfer radical polymerization (ATRP). The terminal functionality of the ATRP-obtained polymer was modified in order to incorporate an azide moiety to be reactive with propargyl folate *via* Huisgen [1,3] dipolar cycloaddition. Block polymers self-assembled using the following conditions: PLGA-S-S-PLGA and PLGA-S-S-PEGMA-Fol were dissolved in dichloromethane and mixed with an aqueous solution with or without plasmid DNA using vortex agitation. The emulsion was poured in ethanol. The organic solvent was evaporated under reduced pressure yielding the final NP.

Nanoprecipitation (or solvent displacement method): the polymer is dissolved in a semipolar solvent (miscible in water) and is added dropwise in water (non-solvent of the polymer). A rapid diffusion of the semipolar solvent takes place and a decrease of interfacial tension between the two phases occurs, giving rise to the formation of small droplets of precipitated polymer. This method has been widely used in the preparation of self-assembled NP for the synthesis of anti-cancer drug delivery systems. For example, Sanna et al. [39] prepared resveratrol loaded NP by dissolving poly(ε-caprolactone) (PCL) and PLGA–poly(ethylene glycol)–COOH (PLGA–PEG–COOH) (1.5:1), and resveratrol (2, 3, and 4% w/w) in acetonitrile and added into water under magnetic stirring. The colloidal suspension was stirred at room temperature to remove the organic solvent and NP were isolated by centrifugation and washed with water to eliminate the non-encapsulated drug.

Li et al. [40] used a modified nanoprecipitation method to prepared doxorubicin (DOX) loaded NP based on dextran-*b*-PCL (DEX-*b*-PCL). Briefly, DEX-*b*-PCL was dissolved in DMSO and DOX·HCl was neutralized with triethylamine (TEA) in DMSO. Both solutions were mixed and stirred at 60 °C and added dropwise to water. The resulting suspension was dialyzed against water (MW cut-off 12,000) to remove unloaded DOX and the product was filtered through a 0.45 μm syringe filter before used.

Salting-out: In this method the polymer is dissolved in a solvent that is miscible with water (*i.e.* acetone, ethanol, ethyl acetate, *etc.*) and an emulsion is obtained dissolving high concentrations of salt (*e.g.* magnesium chloride, calcium chloride or magnesium acetate) or sucrose in the

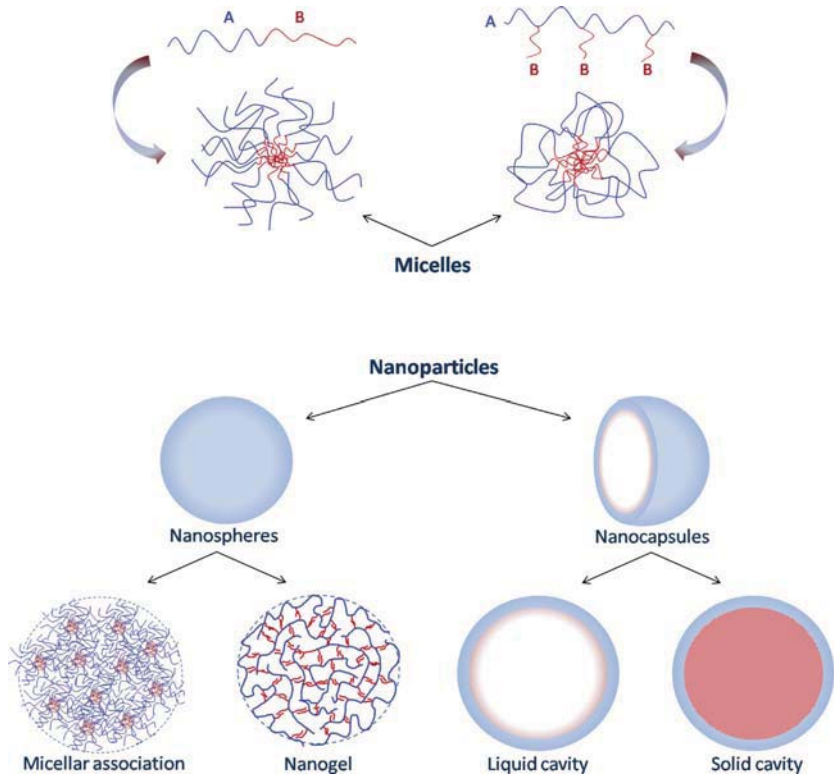

Fig. 2. Morphology of self-assembling polymeric nanocarriers.

aqueous medium. A strong salting-out effect is produced changing the miscibility of the used solvent. However, dilution of the emulsion by the addition of water produces the precipitation of the polymer dissolved in the droplets of the emulsion by a reverse salting-out effect. For example Cirstoiu-Hapca et al. [41] prepared paclitaxel (PTX) loaded NP using acetone, poly(lactic acid) (PLA) and PTX as organic phase and a solution of 15% poly(vinyl alcohol) (PVA) and 60% w/w of magnesium chloride in water. The surface of these NP was decorated with monoclonal human epidermal growth factor receptor 2 (HER2) antibody (trastuzumab, Herceptin®) in order to target HER2 membrane receptors of certain primary and metastatic tumors.

Dialysis: the polymer is dissolved in an organic solvent and placed in a dialysis membrane with a cut-off low enough to avoid the polymer diffusion. The dialysis is performed against a non-solvent miscible with the organic solvent and the displacement of the solvent in the membrane produces the formation of narrow-distribution of small NP. This simple method has been widely used in the preparation of hydrotropic oligomer-conjugated glycol chitosan NP for tumor-targeted PTX delivery [42].

Supercritical fluid technology (SCF): is an environmentally friendly technology as it avoids the use of organic solvents in the synthetic process providing a residuum-free and effective alternative to traditional methods used in the synthesis of NP. Carbon dioxide (CO_2) in supercritical conditions (72.9 atm or 7.39 MPa and 304.25 K) behaves midway between a gas and a liquid, *i.e.* expanding to fill the container like a gas, but with a density proper of liquid state. SCF has been used to obtain NP and more specifically to prepare self-assembled NP of amphiphilic polymers. Zhang et al. [43] prepared 5-fluorouracil-loaded-poly(L-lactic)-polyethylene glycol/polyethylene glycol (5-FU-loaded-PLLA–PEG/PEG) NP using a novel supercritical CO_2 technique.

Spray-drying: This method is commonly used in the pharmaceutical industry to obtain a dry powder from a liquid or slurry by the fast drying of a hot gas (air or nitrogen depending on the sensitivity of the compounds). It is not commonly used to obtain NP from amphiphilic copolymers

but Meenach et al. [44] have recently used this technique in the preparation of an aerosol of advanced spray-dried chemotherapeutic PEGylated phospholipid particles for dry powder inhalation delivery in lung cancer.

Dispersion polymerization: Shalviri et al. [45,46] designed a novel one-pot method to simultaneously obtain grafting onto starch and NP formation. Briefly, methacrylic acid (MAA) and polysorbate 80 (PS80) were grafted onto starch (PMAA-PS80-*g*-starch) being the obtained amphiphilic polymer sensitive to acidic pH in order to overcome multidrug resistance (MDR).

2.3. Preparation of amphiphilic polymers

Amphiphilic polymers present at least a combination of hydrophilic and hydrophobic segments. They form self-assembled structures when placed in aqueous environments with a hydrophobic inner core and a hydrophilic shell. Chemical composition of the repeating units and the monomer distribution in the macromolecular chains will define the physico-chemical properties of the polymers that will drive the self-assembled process, stability and drug encapsulation efficiency and release profiles. Therefore, the choice of appropriate monomers, macromolecular architecture and hydrophobic/hydrophilic balance will be crucial in the design of drug delivery systems for anticancer and anti-inflammatory applications.

2.3.1. Synthetic polymers

Synthetic polymers have been broadly explored for the design of nanocarriers in the field of biomedical applications and, particularly, for their application in cancer diseases and anti-inflammatory therapies due to their high versatility and optimal balance of physicochemical and biological properties. The most widely used components for the preparation of amphiphilic polymers are typically PEG, Pluronics®, poly(*N*-(2-hydroxypropyl)methacrylamide) (HPMA), poly(glutamic acid) (PGlu) and different poly(amino acids) (PAA) and poly(esters). Additionally, peptide amphiphiles (PA) and poly(2-oxazolines) (POX) have also been used because of their advanced properties and interesting potentials in this field (see Fig. 3).

Amphiphilic polymers have been obtained by different synthetic methods including ROP, free radical copolymerization, controlled/living radical polymerization, or click chemistry reactions. ROP is the most straightforward and practical approach for large-scale production of high MW polyethers, polyesters, polypeptides and POX. Bae et al. [47] reviewed the designed efforts to obtain smart PM from functional PEG-*b*-PAA block copolymers. PAA have been obtained by traditional solid-phase peptide synthesis methods, such as the condensation of monomers protected at one carboxyl and activated for polymerization at the other, followed by protecting group removal (protection/conjugation/deprotection). Activated amino acid monomers, *e.g.* activated esters or *N*-carboxyanhydride (NCA), have been used to obtain sequences longer than 10 repeating units. Fuchs–Farthing method has been used to obtain pure NCA with high yields, and good control of microstructure and MW [48].

Ding et al. [49,50] combined ROP with ATRP to obtain a cationic PAA vesicle for drug and gene-codelivery. ROP was used in the synthesis of poly(γ-2-chloroethyl-L-glutamate) (PCELG) using γ-2-chloroethyl-L-glutamate NCA as starting material and *n*-hexylamine as initiator. A "grafting from" approach was used to attach oligo(2-aminoethyl methacrylate hydrochloride) (OAMA) to the PCELG yielding amphiphilic poly(L-glutamate)-*g*-OAMA that formed vesicles in phosphate buffered saline (PBS). Authors not only encapsulated and released DOX·HCl but also, the cationic nature of the vesicles allowed the incorporation of DNA, which makes these vesicles promising carriers for codelivery of anti-cancer drugs and genes.

Free radical polymerization is a well-known and cheap synthetic route that can be used to obtain amphiphilic pseudo-block copolymers with an appropriate monomer distribution to allow self-assembling in suitable conditions. This occurs by the copolymerization of a hydrophilic monomer and a hydrophobic monomer of very different reactivity ratios. Lopez-Donaire et al. [51] synthesized copolymers based on oleyl 2-acetamido-2-deoxy-α-D-glucopyranoside (OAG) due to the potent anti-mitotic activity that OAG presents against glioma cells (U-373). For this purpose a methacrylic group was covalently linked through a carboxylic ester function at position C-6 on the pyranosidic ring, and the obtained methacrylic derivative was copolymerized with *N*-vinyl pyrrolidone. The big difference between the monomers reactivity ratios ($r_{OAGMA} = 5.94$ and $r_{VP} = 0.01$) gave rise to pseudo-blocks, with long sequences of the hydrophilic or the hydrophobic monomer. The monomer distribution and the hydrophilic/hydrophobic balance allowed the formation of NP in aqueous media [52]. Cell culture assays demonstrated a selective effect of the obtained NP that reduced significantly cell viability of human glioblastoma cell line (A-172) compared to normal human fibroblasts.

García-Fernández et al. also prepared antiangiogenic copolymers by free radical copolymerization of a methacrylic derivative of 5-amino-2-naphthalene sulfonic acid (MANSA) [53] and butyl acrylate (BA) by free radical polymerization. The copolymers poly(BA-*co*-MANSA) formed spontaneously stable NP in aqueous media. The antiangiogenic activity of the heparin-like system was related to the direct interaction of the sulfonic acid groups of MANSA with specific growth factors involved in endothelial cell migration and proliferation, and depended not only on the chemical composition but also on their supramolecular organization [54,55].

Nitroxide-mediated polymerization (NMP) [56], ATRP [57–60] and reversible addition and fragmentation transfer chain polymerization (RAFT) [61,62] are the main approaches used in the development of amphiphilic polymers, however due to its versatility and the lack of metal catalyzers, RAFT has gained importance in the development of polymeric NP for cancer and anti-inflammatory applications [63,64].

Blunden et al. [65] prepared block copolymers by ring-opening polymerization of D,L-lactide using a RAFT agent with an additional hydroxyl group, followed by the RAFT copolymerization of 2-hydroxyethyl methacrylate and 2-chloroethyl methacrylate. The well-structured polymers

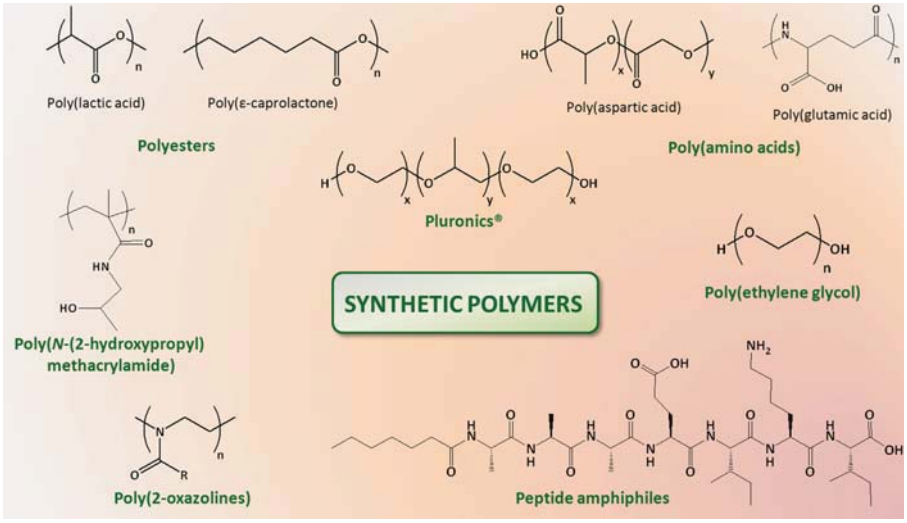

Fig. 3. Chemical structures of the most widely used synthetic polymers.

were modified to incorporate the ruthenium metallodrug RAPTA-C [$RuCl_2$(*p*-cymene)-(PTA)] in their structure using the Filkestein reaction. RAPTA-C inhibits cell growth by triggering G2/M phase arrest and apoptosis in cancer cells, and slowing cell division resulting selective and efficient on metastases *in vivo*. Zhao et al. have recently developed a pH sensitive acid degradable amphiphilic graft copolymer using two sequential controlled/living radical polymerization processes: RAFT and ATRP. First, 2,4,6-trimethoxybenzylidene-1,1,1-tris(hydroxymethyl) ethane methacrylate (TTMA) was polymerized by RAFT and then 2-hydroxyethyl methacrylate was polymerized by ATRP. The well-structured copolymer formed NP by solvent exchange methods at pH 7.4 that presented low critical micelle concentration (CMC), high loading efficiency, excellent biocompatibility and rapid disassembly in acidic conditions [66].

Click chemistry offers a powerful toolbox for material scientists to design amphiphilic block copolymers for their application in biomedicine as click reactions present high efficiency under mild conditions, minimal and limited side reactions.

Xu et al. [67] reported the synthesis of dendron-like poly(ε-benzyloxycarbonyl-L-lysine)/linear polyethylenoxide (PEO) block copolymers by the combination of ROP of ε-benzyloxycarbonyl-L-lysine NCA and click chemistry. The encapsulation and controlled release of anticancer drug DOX highlight the potential of these systems in cancer therapy.

Click chemistry has been used not only in the synthesis of amphiphilic block copolymers of defined structure and architecture, but also in the functionalization of systems to provide them with complex functionalities [68]. In this sense Schoichet et al. [69] performed a Diels–Alder [4+2] cycloaddition and a Huisgen 1,3-dipolar cycloaddition azide-alkyne click reactions for surface modification of polymeric NP. The authors prepared poly(lactide-*co*-2-methyl-2-carboxytrimethylene carbonate)-*g*-polyethylene glycol-furan/azide NP that exhibit furan and azide dual functionality in the PEG corona. These moieties enabled orthogonal click reactions to sequentially conjugate trastuzumab-maleimide antibodies and alkyne-functionalized antisense oligonucleotide for gene silencing to the PEG corona. The modified NP were tested using the human ovary cancer line SKOV-3luc that express HER2 and firefly luciferase. The results obtained when cells were treated with dual functionalized NP (having both small interfering RNA (siRNA), and trastuzumab) in terms of gene knockdown were as good as lipofectamine LTX® transfection.

The thiol–ene reaction has also been used in the surface modification of NP. Van der Ende et al. [70] linked targeting peptides to polyester-based 3D-nanonetworks. The particles (53 nm) were formulated based on poly(valerolactone-epoxyvalerolactone-allylvalerolactone-oxepanedione) containing 11% epoxy and crosslinked with 2 equivalents of diamines per epoxide. Targeting peptides (HVGGSSV and Arg-Gly-Asp (RGD)) were conjugated to the free allyl groups on the surface of the particles by a thiol–ene reaction carried out in DMSO.

Table 1 summarizes the main methods used in the preparation of amphiphilic synthetic polymers for application in cancer therapy.

2.3.2. Natural polymers

A variety of amphiphilic derivatives of polysaccharides and proteins for application in chemotherapy and anti-inflammatory therapies have been reported in recent years

Table 1
Representative methods used in the preparation of amphyphilic synthetic copolymers.

Method		Polymeric formulation	Synthesis of NP	Type of drug	Reference
Free radical polymerization	Amphiphilic poly(OAG-*co*-VP)	Nanoprecipitation in water using dioxane as solvent	OAG (antimitotic activity)		[51]
	Amphiphilic poly(BA-*co*-MANSA)	Spontaneous self-assembling in aqueous media	ANSA (antiangiogenic agent)		[53]
Controlled radical polymerization	RAFT	PNIPAm-*b*-PDMAm	Nanoprecipitation in THF	Dipyridamole (DIP)	[61]
		PHPMA-*b*-PPDSM	Crosslinking *via* hydrazone bonds and reducible disulfide bonds in methanol	DOX conjugation *via* acid-sensitive bonds	[223]
		Thermo-sensitive PNAS-*b*-PNIPAm-*b*-PCL	Spontaneous self-assembling in aqueous media into micellar aggregates	DOX encapsulation	[64]
		Amphiphilic triblock HPMA copolymer with enzyme-sensitive peptide GFLGKGLFG in its main chain	Self-assembling in aqueous media mediated by polymer–DOX block	DOX conjugation *via* enzyme-sensitive peptide	[218]
	ATRP	PEO-*b*-PG2MA	Micellization induced by slow addition of water over a solution of polymer in THF.	Indomethacin (anti-inflammatory drug) encapsulation	[59]
		(alkynyl-POEGMA-*b*-PDMA-*b*-PDEA)	Micellization by self-assembling in aqueous media induced by adjusting the solution pH to 9 with 0.1 M NaOH solution	–	[60]
Ring opening polymerization	mPEG-*b*-PGlu	self-assembled NP in aqueous media *via* electrostatic interactions	DOX·HCl encapsulation		[133]
	PEG-*b*-PLA	Oil/water (o/w) emulsion	PTX encapsulation		[144]
	PLGA-*b*-PEG-*b*-PLGA	Dialysis	Curcumin encapsulation		[170]
	PCL-modified Pluronic P105	Dialysis	PTX encapsulation		[164]
Post-modification reactions	Thiol–ene	HVGGSSV and RGD conjugated on the surface of NP based on poly(valerolactone-epoxyvalerolactone-allylvalerolactone-oxepanedione)	Emulsification process	PTX encapsulation	[70]
	Click chemistry	poly(lactide-*co*-2-methyl-2-carboxytrimethylene carbonate)-*g*-polyethylene glycol-furan/azide NP	Co-self-assembly by membrane dialysis	Trastuzuma*b*-maleimide antibodies and oligonucleotide conjugation	[69]
		KGRGDS conjugated on NP based onpoly(TMCC-*co*-LA)	Dialysis	–	[68]

[71]. Among polysaccharides, it can be said that hyaluronic acid (HA) and chitosan have been the most extensively studied but other polymers such as heparine, chondroitin sulfate, DEX, starch and its derivatives, pullulans, and alginates (ALG) have also been investigated (see Fig. 4). Some proteins are amphiphilic by nature or can be modified easily with amphiphiles to form micelles under different conditions, and can be applied as nanocarriers.

Given the significant importance of a homogeneous and anhydrous environment to achieve high yields in coupling reactions [72], and avoid the limitations of conjugation in mixed water/organic solvents (such as the necessity of multiple activation steps) [73], it is critical to find an organic solvent in which both the natural polymer and the hydrophobic moiety are soluble. Some polysaccharides such as pullulans [72,74,75] or heparins [76,77]

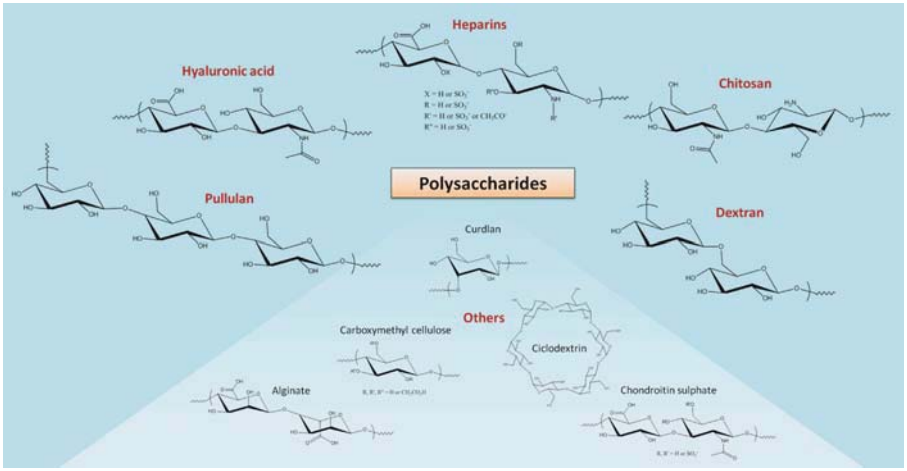

Fig. 4. Chemical structures of polysaccharides applied in targeting and drug delivery.

can be readily dissolved in organic solvents upon mild heating. For the solubilisation of other polysaccharides in organic solvents, inventive strategies have been designed. For instance, HA was solubilized in anhydrous DMSO by complexing with dimethoxy poly(ethyleneglycol) to generate HA–PTX bioconjugates with high yield without using any salts and blocking agents [73]. HA and heparins can be chemically modified mainly through their carboxylic acid or hydroxyl groups. It is noteworthy that carbonyl compounds preferably bind to their hydroxyl groups at C_6 [75]. Since polysaccharides have one reductive end, they can also be modified through this functional site. Functional amino groups may also be recovered from HA by deacetylation of the *N*-acetyl group [78], and from heparins by *N*-desulfonation [79]. Analysis of the chemical modifications on HA and heparin have been reviewed by Schanté et al. [80] and Fernández et al. [81], respectively. Concerning self-assembling systems for the treatment of cancer HA and heparins have been conjugated to a variety of hydrophobic moieties, from molecules as simple as acetyl groups linked by a thermally activated reaction (40 °C) between acetic anhydride and the hydroxyl groups on the polysaccharide [82], to biomimetic hydrophobic polymers such as poly(γ-benzyl L-glutamate) coupled using more sophisticated Click chemistry (Huisgen 1,3-dipolar cycloaddition using CuBr as the catalyst and *N,N,N′,N″,N″*-pentamethyldiethylenetriamine (PMDETA) as a ligand) [83].

Amphiphilic HA has been obtained *via* esterification of its carboxylic acids by conjugation of with hydrophobic molecules such as monostearin [84] or octadecyl moieties [85] through 1-ethyl-3-(3-dimethylaminopropyl) carbodiimide/*N*-hydroxysuccinimide (EDC/NHS)-mediated reactions. EDC/NHS activation was also used for the amidation of HA *via* its carboxylic acids using histidine (His) [86], a number of different fatty amines and polyamines [87], as well as amine-functionalized 5β-cholanic acid [88] and deoxycholic acid (DOCA) [89], Amine-terminated hydrotropic oligomers have also been reacted with the carboxylic acid of HA in the presence of EDC and HOBt [90]. Heparin derivatives have also been obtained *via* amidation of its carboxylic acids. Heparin–DOCA conjugates were prepared by linker-mediated coupling of *N*-(2-aminoethyl)-deoxycholylamide with the carboxylic groups of heparin in the presence of EDC [77]. Similar approaches were used to conjugate heparin with amine-terminated poly(β-benzyl-L-aspartate) using EDC [76] and aminated folate using EDC [76,91,92] or *N,N′*-dicyclohexylcarbodiimide (DCC)/NHS [93]. Aminoacids have been used as spacers for the conjugation of HA with PTX, where HA tetrabutylammonium salt was conjugated with 2′-aminoacyl-PTX using EDC/NHS activation [94]. Similar approaches consisting of previous amination of PTX or (docetaxel) DCT for subsequent reaction with the carboxylic acids of heparin in the presence of EDC/NHS were exploited to obtain heparin-PTX [95] and heparin-DCT conjugates [96], respectively. Curcumin and DOX have also been conjugated to HA, either by direct conjugation *via* DDC/*N,N*-dimethyl amino pyridine (DMAP)-mediated esterification [97], or by linker-mediated coupling using spacers such as adipic dihydrazide [98,99]. Retinoic acid has been conjugated with heparins in a number of works, either by amidation of their carboxylic groups with previously aminated retinoic acid using EDC [91,92,100,101] or *via* reaction of DCC/NHS-activated all-*trans* retinoic acid (ATRA) with hydroxyl groups of heparin [93]. Several strategies for the preparation of amphiphilic ALG with potential application in cancer therapy as nanocarriers exist in the literature. A library of amphiphilic ALG esters with different degree

of substitution (DS) and hydrophobic alkyl length were synthesized by the reaction between partially protonated sodium ALG and aliphatic alcohols (octanol, dodecanol or hexadecanol) [102,103]. NP of alginic acid (ALG-H) and poly[(2-(diethylamino)ethyl methacrylate)] (PDEMA) were successfully prepared in aqueous medium using a polymer–monomer pair reaction system consisting of the anionic ALG and the cationic monomer DEA in presence of potassium peroxydisulfate ($K_2S_2O_8$) as a radical initiator. Ca^{2+} was introduced to gel the ALG moieties at the outer shell of NP that encapsulated hydroxycamptothecin (HCPT) [104]. Chitosan has been chemically modified by linking hydrophobic groups on hydroxyl [105] or amino groups. Due to the higher reactivity of amino groups, the majority of the modifications have used this group mainly through *N*-acylation reactions [106,107].

N-octyl-*N*,*O*-carboxymethyl–low molecular weight chitosan (LMWC) was synthesized by two-step modification of LMWC to prepare self-assembled PM for encapsulation of PTX. Alkyl chains were conjugated to the firstly prepared carboxymethylchitosan using octanal and sodium borohydride ($NaBH_4$) as a reducing agent [108]. Conjugates of chitosan oligosaccharide with linoleic acid have been synthesized using EDC to obtain micelles as a carrier for DOX [109]. Stearic acid grafted chitosan oligosaccharide with different DS was also synthesized by EDC mediated coupling reaction. PTX was incorporated into the micelles and the surfaces of the micelles were further cross-linked with glutaraldehyde to form drug loaded and shell cross-linked NP with improved *in vivo* stability [110]. Micelles of this type presented excellent internalization into cancer cells and accumulation in cytoplasm, either for PTX-loaded [111] or DOX-loaded [112]. Self-assembled amphiphilic *N*-(2,3-dihydroxypropyl)–chitosan–cholic acid was synthesized by linking small molecules of cholic acid and glycidol onto primary amine group of chitosan, respectively [113]. Hydrophobically modified glycol chitosan (HGC) NP conjugated with interleukin-4 receptor binding peptides were prepared to enhance cellular uptake of NP in tumor tissues [114]. Some polysaccharides can only be modified through their hydroxyl groups or reductive ends, because of these are the only available functional groups. This is the case of pullulans, starch and its derivatives, DEX, cellulose or curdlan.

Various amphiphilic pullulans have been prepared for cancer treatment applications. Cholesteryl pullulan has been prepared by reacting pullulan with cholesterol succinate as a carrier for mitoxantrone (MTO) [115]. Further modification of cholesteryl pullulan with biotin was achieved by direct esterification of its hydroxyl groups with EDC/DMAP [116]. Folated pullulan was likewise prepared as a carrier for DOX by direct conjugation using DDC/DMAP in a simple, one-step reaction obtaining very high substitution yields [75]. Following the same method, folated pullulan was further coupled with the photosensitizer pheophorbide (Pba) [72]. Alternatively, DOX was chemically linked to pullulan by first functionalizating the polysaccharide with carboxylic acid groups *via* reaction with maleic anhydride, using TEA as a catalyst, and subsequent amidation with DOX in the presence of EDC/NHS and TEA [117]. This conjugate was further folated using the same catalytic system [117]. Folated pullulan–DOX conjugates were also obtained using a different strategy: oxidized pullulan was first conjugated to cysteamine and diamino-PEG, followed by conjugation of DOX to the cysteamine thiol groups and coupling of folic acid (FA) to the pending amino groups of diamino-PEG [118].

Akiyoshi et al. [119] have prepared very interesting amphiphilic systems through the conjugation of cholesterol to pulullans of different MW. The addition of only 5 mol% of cholesterol to the polysaccharide chains was enough to give self-assembled NP which offer excellent opportunities to be applied as nanocarriers for specific drugs with good stability and very low toxicity for healthy cells.

Amphiphilic starch derivatives have been prepared for cancer therapy using different routes. Hydroxyethyl starch (HES) was esterified with lauric, palmitic, and stearic acids under mild reaction conditions using DCC/DMAP. The amphiphilic derivatives gave rise to the formation micelles and polymeric vesicles [120]. Other researchers synthetized amphiphilic PLA grafted HES for the preparation of DCT-loaded micelles by graft polymerization of D,L-lactide with HES under partial protection of the hydroxyl groups with trimethyl chlorosilane (TMSCl) [121]. The preparation of starch–drug conjugates with 5-FU-1-acetic acid (FUAC) through ester bonds has been recently reported [122] *via* the coupling reaction with DCC/NHS.

Carboxymethylated curdlan was substituted with *N*-[4-[2-[(4-carboxyphenyl (amino) ethyl)] phenyl] sulfonyl]-N9-cyclohexylurea as a hydrophobic moiety by DCC/DMAP-mediated ester formation for the encapsulation of ATRA. This derivative was further conjugated to lactobionic acid using ethylenediamine linkers in the presence of DCC [123].

Amphiphilic protein derivatives with self-assembling properties to entrap anti-tumor drugs have been prepared by reaction of the amino groups of the protein. Li et al. [124] reported the reaction of gelatine with different amounts of hexanoyl anhydride in alkaline conditions. Conjugates of gelatine and oleic acid were synthesized by a novel aqueous solvent-based method that overcame the opposite solubility between gelatin and oleic acid [125]. Gelatin was conjugated with high contents of cholesterol using *N*,*N*′-disuccinimidyl carbonate. The gelatine–cholesterol conjugates formed micelles that entrapped curcumin for cancer research [126]. Hydrophobically modified casein, casein-*g*-poly(*N*-isopropylacrylamide) (PNIPAm), was prepared as a novel dual stimuli responsive. The amphiphilic casein was synthesized by free radical graft copolymerization of NIPAm in presence of the protein, using *t*-butyl hydroperoxide (TBHP) as an initiator [127]. A different strategy was reported for SF that basically consisted of silk based ionomers obtained *via* carbodiimide coupling of fibroin with poly(L-lysine) (PLL) hydrobromide and PGlu sodium salts, respectively. The assembly of the ionomers *via* electrostatic interactions led to particles where the PAA chains formed the core and the protein backbone the surface. DOX was encapsulated in the core of the ionomeric NP and it was released in a pH-dependent manner [128].

3. Role of synthetic biostable and biodegradable systems

A wide range of synthetic polymers have been extensively studied for the preparation of self-nanoassemblies. Focusing on the hydrophilic part of amphiphilic polymers that typically form the shell of nanocarries, commonly used synthetic polymers are: PEG, Pluronics®, HPMA and PGlu. Furthermore, hydrophobic polyesters such as PLA and PCL have been successfully used to prepare self-assembled nanocarriers. Other advanced polymers based on PA and POX are new promising platforms to create self-assembling nanostructures [4,129–131]. Advanced applications of these synthetic polymers for cancer therapies and anti-inflammatory therapies are described below.

3.1. Self-assemblies based on PEG

Among all hydrophilic polymers, PEG hydrophilic block is the most used for the preparation of self-assembling polymers due to several reasons. Mainly, PEG is a water soluble polymer, nonionic, nonvolatile, biocompatible and a poorly immunogenic polymer approved by the Food and Drug Administration (FDA) for its use in drugs products and pharmaceutical applications. PEG with a MW less than 30 kDa can be cleared from the body through renal filtration.

Additionally, the PEGylation is an essential strategy to improve the stealth properties of polymeric NP, and therefore, to reduce the adhesion of opsonins that are present in the blood serum. This methodology avoids the NP recognition by the RES, being camouflaged or invisible to phagocytic cells. Several theories have been proposed to explain this behavior. However, the most widely accepted is based on the extended conformation PEG chains on the NP surface which can create repulsive forces that effectively block the interactions of opsonins. The MW, the surface chain density and the conformation of PEG are critical factors to improve the blood circulation half-life of polymeric NP and therefore to favor their preferential accumulation in tumor tissues.

Table 2 relates the main nanocarriers developed using PEG for delivery of anticancer drugs in chemotherapy.

3.1.1. Drug-loaded self-assembled systems based on PEG

Self-assembled PM with hydrophilic shell of PEG can be composed of a wide range of hydrophobic polymers to form the inner core of different self-assembling structures that have been successfully used to encapsulate several drugs. The most frequently investigated block copolymers to design these drug-loaded self-assembled systems are PEG-*b*-PAA, PEG-*b*-polyesters and PEG-*b*- PLGA, as are described below in detail.

3.1.1.1. PEG-b-PAA block copolymers. Self-assembling block copolymers of PEG-*b*-PAA are probably one of the most promising vehicles to improve anti-tumor drug delivery. Self-assembled NP are formed by a hydrophilic PEG shell and a PAA core that can encapsulate different anti-tumor and anti-inflammatory drugs with significantly low toxicity compared with free drugs. PAAs provide interesting properties such as an excellent biocompatibility, biodegradability and nontoxicity. Moreover, PAAs have high versatility with a wide range of functional groups such as hydroxyl, carboxyl, amino and thiol groups that can be used for the modification of the chemical structure of the nanoassembled systems in order to improve the drug loading and other physico-chemical properties. Several self-assembling polymer systems based on PEG-*b*-PAA have been widely studied for advanced cancer and inflammation therapies. The most typical PAA used for these systems are poly(aspartic acid) (PAsp) and PGlu [47,132–134].

Micelles based on PEG-*b*-PAsp block copolymers have been extensively investigated to encapsulate other hydrophobic drugs. Hamaguchi et al. incorporated PTX by physical entrapment into the inner core of micelles based on PEG-*b*-PAsp copolymers modified with 4-phenyl-1-butanol by esterification reaction (designated as NK105). After freeze drying, the drug loading was about 25%. These micelles were stable and significantly small in size (approximately 85 nm) that allowed a uniform distribution and great accumulation in tumor tissues. Particularly, NK105 was evaluated *in vitro* on 12 human tumor cell lines, obtaining a similar cytotoxicity to PTX. *In vivo* results showed substantial tumor suppression in a dose dependent manner [135–137]. Currently, Phase III clinical trials are ongoing with promising results. In fact, NK105 showed a reduced toxicity with few adverse reactions in patients at the early stage (Phase I/II clinical trials) of clinical development [7,138–140].

Eckman et al. [141] investigated the importance of interactions between drugs and polymers by the preparation of DOX-loaded micelles based on PEG-*b*-PAsp block copolymers in three different core environments. Basically, the carboxyl groups of PEG-*b*-PAsp were protected by benzyl esters (hydrophobic interactions) and ionized by sodium salt or remained as free acids, in order to encapsulate DOX through hydrophobic or ionic interactions, respectively. The ionic interactions between DOX and inner core of micelles favored the stability, the prolonged release of the drug in a pH-dependent manner and the effective cytotoxicity against prostate and lung cancer cell lines. The increase of the hydrophobic character of NP could be an interesting route to improve their anti-cancer activity. In this way, Lv et al. [132] investigated the incorporation of polyphenylalanine (PPhe) in order to increase the stability of these micelles through hydrophobic and aromatic interactions. Particularly, they synthesized methoxypoly(ethylene glycol) mPEG-*b*-poly(glutamic acid-*co*-L-PPhe) triblock copolymers that self-assembled into NP where DOX·HCl was successfully loaded by simple mixing in the aqueous phase. The appropriate combination of electrostatic interactions between PGlu domains and the cationic drug and the stabilizing effect of PPhe domains allowed to optimize the therapeutic efficacy of these micelles that exhibited higher cell proliferation inhibition and toxicity compared with free DOX·HCl against human pulmonary carcinoma cells (see Fig. 5).

Desale et al. [142] reported the synthesis of triblock copolymers formed by PEG, PGlu and PPhe

Table 2
A selection of main nanocarriers prepared with PEG and applied in cancer therapy.

Type of copolymer	Nanocarrier type	Drug/Bonding type	Cancer cell type	Biological/Clinical status	Reference	
PEG-*b*-PAA	PASA	PEG-*b*-PASA micelles protected by benzyl esters	DOX encapsulation	Human prostate and lung cancer	*In vitro*	[141]
		PEG-*b*-PASA NP	PTX encapsulation	12 human tumor cell lines	Phase III clinical trials (NK105)	[135]
		PEG-*b*-PASA NP (pH-sensitive)	DOX Conjugation (hydrazide linker)	–	–	[192]
	PGlu	Hybrid micelles (PPhe hydrophobic core, cross-linked PGlu shell layer and PEG external shell)	CDDP, PTX encapsulation	Human ovarian cancer cells	*In vitro* and *in vivo*	[142]
		PEG-*b*-PGlu NP with FA conjugated on the surface	DOX, SPIONs encapsulation	Human hepatic carcinoma cells	*In vitro*	[134]
		Polymer–metal complex formation between PEG-*b*-PGlu block copolymers	CDDP conjugation	12 human tumor cell lines	Phase II (NC6004)	[195]
PEG-*b*-polyester	PLA	mPEG-*b*-PDLLA micelles	PTX encapsulation	Lung, ovarian, breast and gastric cancer	Commercial market Genexol®-PM	[147]
		PEG-*b*-PLA polymersomes	DOX encapsulation	Breast adenocarcinoma cells	*In vitro*	[148]
		c(RGDyK)-PEG-*b*-PLA micelles	PTX encapsulation	Glioblastoma cells	*In vitro* and *in vivo*	[159]
		PEG-*b*-PLA NP	Cisplatin, PTX conjugation	SKOV-3 human ovarian carcinoma cells, U14 xenograft model of cervical carcinoma	*In vitro* and *in vivo*	[207]
	PCL	mPEG-*b*-PCL micelles	Luteolin encapsulation	4T1 breast and C26 colon adenocarcinoma cells	*In vitro* and *in vivo*	[163]
		PEG-*b*-PCL micelles	PTX, cyclopamine, gossypol encapsulation	ES-2 and SKOV3 human ovarian cancer cells	*In vitro* and *in vivo*	[164]
		CGKRK-PEG-*b*-PCL micelles	PTX encapsulation	HUVEC and Human U87MG cells	*In vitro* and *in vivo*	[166]
PEG-*b*-PLGA		PEG-*b*-PLGA micelles	THPP encapsulation	HN5 head and neck and H2009 lung cancer cells	*In vitro*	[169]
		Folate-targeted PLGA-*b*-PEG NP	17-AAG encapsulation	MCF7 human breast adenocarcinoma cells	*In vitro*	[175]
		APRPG peptide-modified PEG-*b*-PLGA NP	TNP-470 encapsulation	HUVECs and SKOV3 ovarian cancer cells	*In vitro* and *in vivo*	[176]
Others		PEG-*b*-poly(methacrylic acid) cross-linked micelles	Cisplatin, encapsulation and metal complex formation	A2780 human ovarian carcinoma cells	*In vivo*	[183]
		PEG-*b*-DSPE and TPGS NP	PTX, parthenolide, encapsulation	A549 and A549-T24 human lung adenocarcinoma cell lines	*In vitro*	[185]

(PEG-*b*-$PGlu_{90}$-*b*-$PPhe_{25}$) with the aim to prepare hybrid micelles for the loading of drugs with different physico-chemical properties. In particular, a hydrophilic derivative of cisplatin (CDDP) and hydrophobic PTX. Specifically, hybrid micelles were designed with multi-compartment morphology, characterized by PPhe hydrophobic core, cross-linked PGlu intermediate shell layer and PEG external shell. In addition, micelles exhibited higher anti-cancer

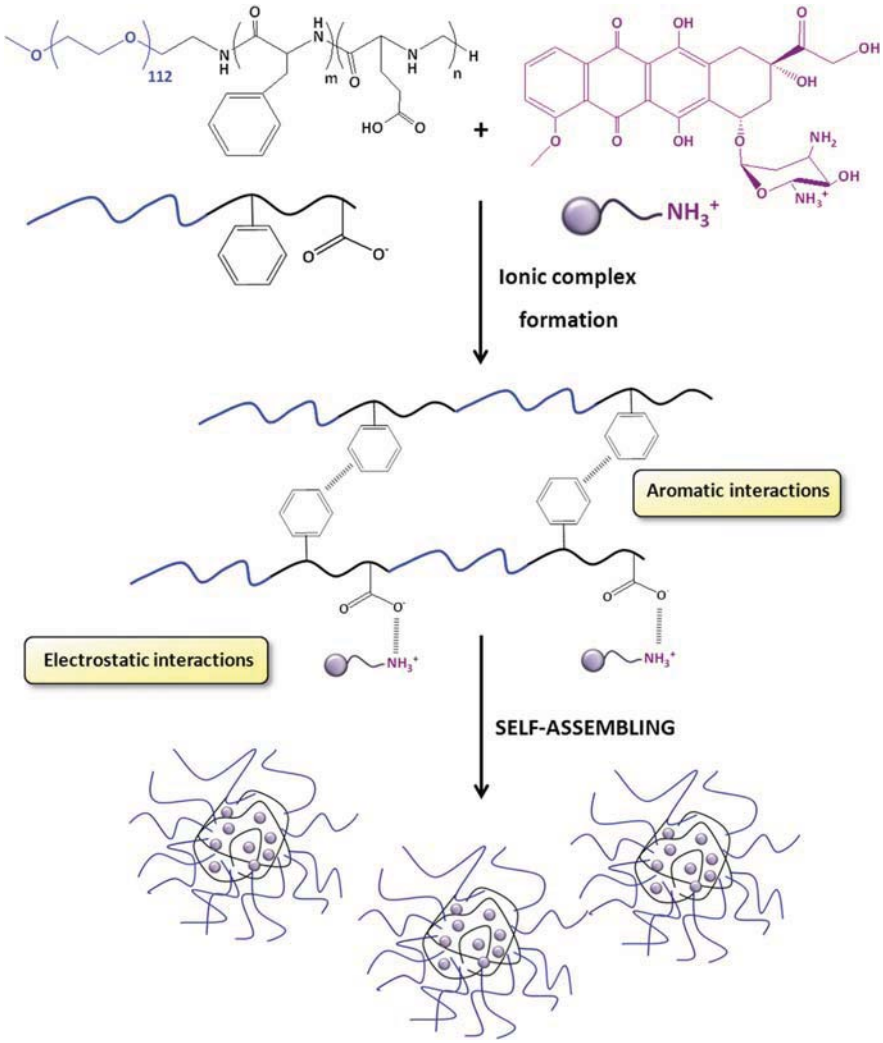

Fig. 5. Aromatic and electrostatic interactions involved in the formation of DOX-loaded NP.

activity compared to individual drug-loaded micelles. These results suggested the promising potential of these carriers for chemotherapeutic drug combination delivery with attractive advantages such as the synergistic therapeutic effects of the drugs and spatial–temporal synchronization of drug exposure. Other route to enhance the intracellular delivery of low MW drugs is the use of disulfide bearing carriers. In this way, Thambi et al. [143] prepared amphiphilic PEG-*b*-poly(γ-benzyl L-glutamate) (PEG-*b*-PBLG) block copolymers that were synthesized by ring-opening polymerization of benzyl glutamate in the presence of a PEG macro-initiator bearing disulfide bond (PEG-SS-NH_2). These amphiphilic copolymers self-assembled in aqueous medium, encapsulating effectively camptothecin (CPT) with a drug loading of about 12%. These biodegradable micelles released the drug in the presence of glutathione (GSH) that is an abundant cytoplasmic peptide capable to reduce disulfide bonds.

3.1.1.2. PEG-b-polyester block copolymers. PEG-*b*-polyester copolymers have received considerable attention for the preparation of self-assembled nanostructures. Particularly, nanoassemblies composed of PLA inner core have demonstrated a great potential for the delivery of different agents [144]. In fact, Genexol®-PM is a polymeric micelle-based formulation of PTX encapsulated in mPEG-*b*-poly(D,L-lactide) (mPEG-*b*-PDLLA) micelles that is commercially available for treatment of non-small cell lung cancer (NSCL), ovarian cancer, breast cancer and gastric cancer. This polymeric formulation was synthesized by a ring-opening polymerization and PTX was loaded using a solid dispersion technique with a drug loading of about 17%. *In vitro* and *in vivo* studies demonstrated that mPEG-*b*-PDLLA micelles were biocompatible with remarkable anti-tumor efficacy against various human cancer cell lines. Moreover, a rapid release of PTX from micelles was observed, probably due to their decomposition in the presence of α- and β-globulins in the blood [7,137]. Particularly, Genexol®-PM showed superior efficacy and less adverse reactions compared with free PTX. Due to the encouraging anti-tumor activity and the safety profile, different Phases of clinical trials have been developed in patients with excellent results, reaching the commercial market [145–147].

In a study by Garkhal et al. [148], DOX-loaded polymersomes were prepared by nanoprecipitation method using amphiphilic PEG-*b*-PLA copolymers. These polymersomes showed a favored profile release at acidic pH, exhibited enhanced cellular uptake of DOX and improved cytotoxicity compared to free DOX using breast adenocarcinoma cancer cells. Currently, polymersomes represent an excellent alternative platform to NP or micelles for the encapsulation of different drugs in the treatment of cancer and inflammation diseases [149,150].

Blanco et al. encapsulated β-lapachone (β-lap) that is a novel poor water soluble anti-cancer drug. Particularly, PEG-*b*-PLA micelles were prepared using a film sonication technique, obtaining particles with core–shell architecture and optimal size (approximately 30 nm). In two types of subcutaneous lung carcinoma models, these micelles showed prolonged blood circulation times, significant accumulation in tumor tissues *via* EPR effect and interesting anti-cancer efficacy [151,152]. On the other hand, Siddiqui et al. [153] demonstrated that the load of an extract of green tea, epigallocatechin-3-gallate (EGCG), into biodegradable micelles based on PLA-*b*-PEG block copolymers allowed retaining its biological effectiveness and enhancing its tumor growth suppressive properties. Moreover, the use of over 10-fold dose advantage of EGCG was possible to exert its proapoptotic and angiogenesis inhibitory effects in both *in vitro* and *in vivo* models for the treatment of prostate cancer [153,154].

Mu et al. [155] prepared mixed micelles of PEG-*b*-PLA and Pluronic® copolymers in order to encapsulate DCT and improve significantly its therapeutic effectiveness compared to Taxotere®. The appropriate ratio of PEG-*b*-PLA and Pluronic® copolymers enabled to obtain stable micelles with more potent anti-tumor activity than the commercial DCT formulation, probable due to the inhibitory activity of Pluronic® copolymer against *P*-glycoprotein (*P*-gp) [152,155].

On the other hand, different authors have explored the preparation of Fol targeting NP with pH-sensitivity [152,156]. In this direction, Gao et al. synthesized different pH-sensitive mixed micelles formed by two types of copolymers: mixture of FA-conjugated to PEG-*b*-PLA and PEG-*b*-poly(L-histidine) (poly(L-His)) copolymers as well as PEG-*b*-poly(L-His-*co*-PPhe) (PEG-poly(L-His-*co*-PPhe)) copolymers (designed as first and second generation of micelles, respectively). In both cases, these micelles were successfully used to encapsulate DOX. The incorporation of poly(L-His) allowed to endowing of pH sensitivity to the particles. The combination of Fol targeting and pH sensitivity considerably improved the anti-cancer activity of DOX [157,158].

Zhang et al. studied other class of tumor targeting ligands based on the use of different sequences of peptides that recognize integrins, overexpressed in a wide range of solid tumors [152]. Specifically, they prepared PTX-loaded PEG-*b*-PLA micelles. Moreover, cyclic RGD peptide, cyclic Arg–Gly–Asp-d-Tyr-Lys, c(RGDyK), was effectively conjugated in order to enhance the treatment of integrin αvβ3 overexpressed glioblastoma. Biological experiments confirmed the efficacy and great potential of the incorporation of RGD-containing peptides into these micelles, improving the anti-glioblastoma cell cytotoxic efficacy by 2.5-folds and exhibiting a potent tumor growth inhibition [159].

PCL is another biodegradable polyester that has been extensively investigated as hydrophobic block to prepare micelles based on PEG copolymers for advanced treatments of cancer and inflammation diseases. The optimal combination of hydrophilicity, biodegradability and mechanical properties of these assemblies has enabled their use as delivery systems for a wide range of poor soluble drugs [160]. For the treatment of inflammation, Wang et al. [161] synthesized tacrolimus-loaded micelles by self-assembly of PCL-*b*-PEG-*b*-PCL triblock copolymers. Tacrolimus-loaded assemblies were prepared by a solid disperse method with a high drug loading and encapsulation efficiency (maximum values of 22.5 and 95.5%, respectively). *In vitro* results of these micelles showed a sustained drug release and suitable cytotoxicity for their use for immunosuppressive therapy.

Combination of two complementary drugs is an attractive approach. Gong et al. developed curcumin-loaded biodegradable self-assembled polymeric PEG-*b*-PCL micelles with a size lower than 30 nm. These micelles were also used to encapsulate luteolin. *In vitro* and *in vivo* studies for curcumin and luteolin loaded micelles confirmed their potential for the treatment of breast and colon cancers [162,163]. Additionally, PEG-*b*-PCL micelles have been investigated as vehicles for combined cytotoxic agents delivery in the treatment of tumors with a high rate of chemoresistance. Lai et al. [164] loaded 3 types of drugs in the core of PEG-*b*-PCL micelles: PTX (cytotoxic agent), cyclopamine (hedgehog inhibitor) and gossypol (Bcl-2 inhibitor). They investigated exhaustively the most optimal combination of these drugs to achieve their solubilization, obtaining a maximum load efficiency of each drug of about 2%. After intravenous injection of these multidrug loaded micelles, a significant tumor growth inhibition and prolonged survival was demonstrated against metastatic

ovarian cancer. Furthermore, Peng et al. [165] studied the growing interest of drug and photodynamic combination therapies in order to improve cancer treatments. Particularly, a derivative of campthothecin (7-ethyl-10-HCPT (SN-38)) was loaded into chlorine-core star-shaped micelles that were prepared by conjugation of chlorine derivative to mPEG-*b*-PCL block copolymer.

Different authors have also decorated the surface of PEG-*b*-PCL micelles with small molecules with the aim to enhance the delivery of poor soluble drugs *via* EPR effect and achieve active targeting. Antibodies, herceptin, FA and peptides are representative examples of molecules that target specific receptors, overexpressed in inflammation processes and involved in the most aggressive cancers. Hu et al. [166] decorated the surfaced of PEG-*b*-PCL micelles with a specific peptide sequence (CGKRK) to obtain angiogenic blood vessels and tumor cells dual targeting effect. Moreover, PTX was successfully loaded in order to evaluate the enhancement of its cytotoxicity using human umbilical vein endothelial cells (HUVEC) and tumor cancer (U87MG) cells. In fact, peptide decoration improved the apoptosis induction and anti-proliferative activity of PTX.

Finally, PLGA is one of the most successfully biodegradable and biocompatible polyesters used for the development of nanomedicines, because its hydrolysis leads to lactic acid (LA) and glycolic acid that are endogenous and easily metabolized by the body. In fact, PLGA is approved by the FDA and European Medicine Agency (EMA) for its use as a drug delivery system in humans. PLGA NP have been used as carriers for chemotherapeutic and anti-inflammatory drugs, photosensitizers and imaging agents for the diagnosis and treatment of cancer and inflammation diseases. The PEG conjugation to PLGA enables the preparation of self-assembling micelles with a hydrophilic shell based on PEG and a hydrophobic core of PLGA [23,167–169]. Song et al. [170] loaded curcumin into the inner core of NP based on PLGA-*b*-PEG-*b*-PLGA copolymers. A dialysis method was used to form self-assembled micelles with an average size of 26 nm and entrapment efficiency of 70%. *In vivo* studies demonstrated an improved biodistribution of curcumin. The conjugation of different target moieties is an effective method for improving the targeted ability of these NP by the ligand-receptor recognition. Different peptides, antibodies and small molecules as FA have been successfully linked to PLGA-*b*-PEG NP [171–174]. Saxena et al. [175] conjugated FA to PLGA-*b*-PEG NP and their inner core was used to load of 17-allylamino-17-demethoxy geldanamycin (17-AAG), that is a hydrophobic inhibitor of heat shock protein 90 (HSP90). Fol-targeted NP were selectively uptaken by breast cancer cells. Moreover, the anti-cancer activity of these micelles was 2-fold higher than that of non-targeted NP. Additionally, Wang et al. [176] modified PLGA-*b*-PEG NP with the aim to incorporate Ala-Pro-Arg-Pro-Gly (APRPG) peptide.

3.1.1.3. Other drug-loaded self-assembled systems based on PEG. One of the most important drawbacks of the use of PEG nanocarriers for cancer treatment is their poor stability. This disadvantage has an appreciable impact for the appropriate control of circulation times of assemblies in blood and the drug delivery efficiency. Different strategies have been proposed in order to improve the stability of polymeric systems that include PEG in their structure.

Lai et al. reported the use of new lipophilic moieties based on cinnamic acid and 7-carboxyl methoxycoumarin that are conjugated using the terminal groups of mPEG. These small molecules have π–π conjugated structures that enhance the load of poor water soluble drugs into the nanoassemblies as well as their stability. Particularly, micelles were used to encapsulate different anti-cancer drugs, such as DOX or an active derivative of CPT (9-nitro-20(S)-CPT). In all cases, the results showed that both hydrophobic and π–π conjugated interactions contributed to the self-assembly. Furthermore, these assemblies had promising anti-cancer activities and could represent a promising strategy to produce stable nanocarriers for cancer diseases [177–179].

Other attractive alternative to improve the stability of nanoassemblies is the use of cross-linked micelles. The characteristic morphology and structural properties of these nanoassemblies allow achieving an exceptional stability, a prolonged circulation time in blood and an appropriate regulation of the drug release. Cross-linked micelles have been investigated to load anti-cancer drugs, like DOX and cisplatin [180–182]. Particularly, Oberoi et al. [183] prepared core cross-linked micelles composed of PEG-*b*-poly(methacrylic acid) (PEG-*b*-PMAA) where cisplatin was successfully loaded. The average size of these micelles was 110 nm with a loading capacity of about 30%. *In vitro* and *in vivo* studies demonstrated the efficacy of these assemblies for the treatment of ovarian cancer with an improved safety profile, tumor accumulation and anti-cancer activity relative to the use of free cisplatin. On the other hand, Talelli et al. [184] synthesized core cross-linked micelles based on block copolymers of PEG-*b*-poly[*N*-(2-hydroxypropyl) methacrylamide-lactate]. After the formation of micelles by rapid heating, DOX was encapsulated and then copolymerized through the methacryltate groups. For this purpose, DOX was previously functionalized with a methacrylamide group using hydrazone bond in order to obtain core-crosslinked micelles with pH-sensitivity. In these specific conditions, the cellular uptake by endocytosis and intracellular release of DOX were significantly favored due to the slightly acidic pH of the intratumoral environment. Moreover, these assemblies had excellent anti-tumoral behavior against human ovarian carcinoma cells.

Effective strategies to improve the solubility of poor water soluble drugs have been proposed combined with advanced clinical trials and final commercialization. In this sense, PEG-*b*-lipid micelles formed by hydrophilic PEG blocks and hydrophobic distearoyl phosphatidylethanolamine (DSPE) segments have been extensively investigated. These vehicles have interesting properties for delivery of hydrophobic drugs with appropriate control of their release and high stability due to the presence of long fatty acyl chains [185]. Tong et al. [186] prepared docetaxel-loaded micelles based on mPEG-*b*-DSPE. DCT-loaded micelles showed anti-tumor efficacy and retarded tumor growth in mice bearing breast cancer.

Finally, the introduction of an “intelligent” stimulus to improve the drug release from micelles has been

extensively applied in last years. Zhu et al. [187] evaluated the anti-tumor activity of acid-sensitive micelles that were obtained by directly conjugating PEG to a hydrophobic derivative of stearic acid through hydrazone bond. These assemblies served as vehicles of an analogue of gemcitabine (4-(*N*)-stearoyl gemcitabine). *In vivo* assays demonstrated a higher anti-cancer activity of pH-sensitive micelles than that of non-sensitive assemblies using murine B16–F10 tumors.

3.1.2. Drug-conjugated self-assembled systems based on PEG

All above reported nanoassemblies incorporated different drugs into their hydrophobic segments through physical entrapment. However, a wide range of active molecules has been covalently attached to amphiphilic copolymers that include PEG in their structure. The preparation of polymer–drug conjugates was proposed by Ringsdorf in the mid-1970s. Since then, the covalently attaching of chemotherapeutic and active agents to polymer chains has greatly developed due to improvement of their physico-chemical, biopharmaceutical and pharmacokinetic properties [188–191]. These systems now are called 'polymeric drugs' and its application 'polymer therapeutics'.

Liu et al. used PEG with the aim to conjugate DCT through an ester linkage and to form amphiphilic micelles in aqueous medium. The efficiency of these micelles was improved by encapsulation of free DCT into their inner core. The *in vitro* anti-cancer activity of this formulation was demonstrated using three different human cancer cell lines [192].

Conjugates based on PEG-*b*-PAA copolymers, including PAsp and PGlu as hydrophobic blocks, have reached various stages of clinical trials for the treatment of cancer diseases [137,139,189,191,193]. NC-6004 is a hydrophilic derivative of cisplatin (CDDP) formulation based on polymer–metal complex forming chain. Particularly, the coordinate complex of PGlu and CDDP forms the inner core of micelles with outer shell of PEG. These micelles were exhaustively characterized by Uchino et al. [137,194]. This formulation was evaluated on 12 human tumor cell lines, preserving the anti-tumor activity of CDDP and reducing its nephrotoxicity. For those reasons, Phase I/II clinical trials with NC6004 have been recently developed with advanced pancreatic cancer [139,195].

Additionally, Cabral et al. prepared analogous micelles (designed as NC-4016), containing dichloro(1,2-diaminocyclohexane)platinum(II) (DACHPt) that is an oxalilplatin parent complex [196,197]. The safety and anti-tumor activity of NC-4016 was evaluated by Nanocarrier ® in Japan. In fact, Phase I clinical trials started in 2009 [137].

Koizumi et al. developed PEG-*b*-PGlu PM (named as NK012) to encapsulate an active metabolite derivative of CPT (SN38). In particular, this drug was conjugated to PGlu segment of block copolymer [198,199]. Micelles exhibited a controlled size of 20 nm and approximately 20% of drug loading. Furthermore, these PM showed excellent *in vitro* and *in vivo* anti-tumor activities, especially in highly vascular endothelial growth factor (VEGF) secreting tumors [139,200]. Different clinical trials are currently undergoing with the aim to evaluate the real efficiency of this formulation in patients [201,202]. Up to date, the anti-tumor activity of this conjugate has been evaluated in several orthotopic tumor models including glioma, renal cancer, stomach cancer, and pancreatic cancer with promising results. They demonstrated enhanced distribution and prolonged SN-38 release as well as partial responses and several occurrences of prolonged stable diseases in patients [203].

PEG-*b*-PAsp copolymers have also served to attach poor soluble water drugs. The micelle carrier NK911 was formed by the block copolymer of PEG (MW of about 5000) and PAsp (about 30 unit) was chemical conjugated with DOX. Moreover, free DOX was encapsulated in the inner core of these micelles. This combination allowed the formation of self-assembling micelles with particle size of about 40 nm that could be accumulated in tumor tissues [137,204,205] and possessed higher anti-cancer activity than the free DOX. Phase I/II clinical trials were performed at National Cancer Center Hospital in Japan with promising results. Among the 23 patients, a partial response was obtained in one patient with metastatic pancreatic cancer and 8 had stable disease [7,206].

Recently, Ponta and Bae [192] have applied PEG-*b*-PAsp block copolymers to conjugate DOX through different hydrazide bonds as spacers. NP were prepared by a dialysis method with hydrodynamic sizes lower than 50 nm. *In vitro* studies demonstrated that the drug release from micelles was pH-dependent and it was tuned as a function of the chain length of the blocks and the type of spacer used.

Other researchers have also prepared conjugates based on PEG and polyesters, such as PEG-*b*-PLA block copolymers. Xiao and Song [207] prepared micelles by co-assembling the 2 different conjugates containing cisplatin and PTX. Both hydrophobic drugs were conjugated to PEG-*b*-PLA copolymers that self-assembled into micelles with an inner core composed of PLA block and PEG hydrophilic shell (see Fig. 6). These nanoassemblies showed an effective anti-tumor activity and inhibiting the tumor growth using a U14 xenograft model of cervical cancer with superior efficacy compared to free drugs solutions.

3.2. Self-assemblies based on Pluronics®

Pluronic® block copolymers have been exhaustively investigated as an excellent alternative for the preparation of self-assembling systems and the solubilization of hydrophobic drugs. These amphiphilic polymers are composed of hydrophilic PEO and hydrophobic poly(propylene oxide) (PPO) segments, organized in triblock structures (PEOx-*b*-PPOy-*b*-PEOx) with a wide range of molecular weights and PEO/PPO ratios. Pluronic® copolymers have important advantages for their use in nanoassemblies for cancer treatments because they can be modified by reactions through the terminal hydroxyl groups in order to achieve the optimal targeting in tumor site [208].

Different binary mixing Pluronic® micelles have been developed to form stable self-assembling carriers for anti-cancer drugs. Particularly, Fang et al. [209] prepared Pluronic® P105 and F127 block copolymers that self-assembled into micelles in order to encapsulate

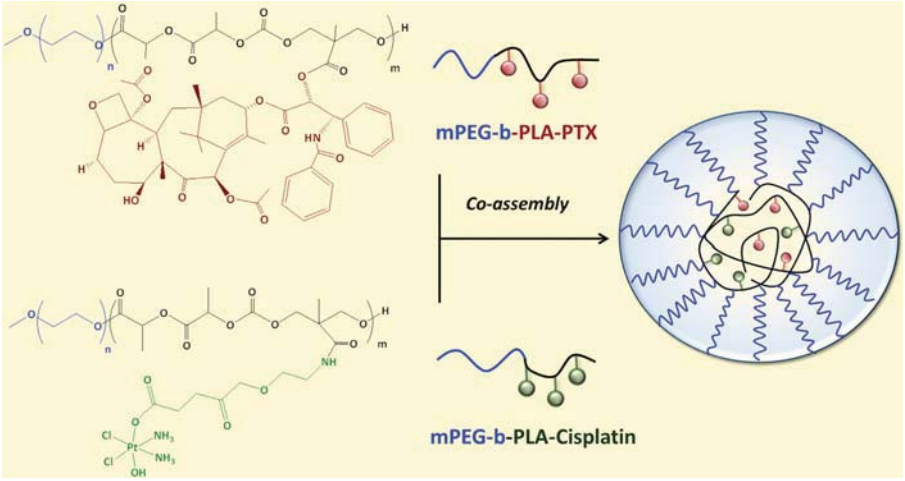

Fig. 6. Chemical structures of cisplatin and paclitaxel conjugated to PEG-*b*-PLA copolymers and representative mechanism of their co-assembly in aqueous enviroment.

methotrexate (MTX) as anti-tumor compound. MTX-loaded mixed micelles exhibited *in vitro* and *in vivo* anti-tumor activities and optimal pharmacokinetic parameters. Wang et al. [210] prepared a PTX-loaded Pluronic® P105 micellar system by a thin-film method, obtaining micelles with small particle size, spherical shape and excellent stability. *In vitro* and *in vivo* activities, pharmacokinetics and biodistribution parameters were evaluated with promising results that suggested that P105 PM could be a useful drug carrier for intravenous administration of PTX.

Other mixed Pluronics® micelles have been studied to encapsulate DOX. In fact, Pluronics® can interact with MDR cancer cells obtaining a significant sensitization of resistant tumors with respect to DOX. For instance, DOX-loaded micelles composed of Pluronic® L61 and F127 (formulation designed as SP1049C) have already achieved Phase III of clinical trials. In this formulation, the most effective regulator of DOX activity against a wide range of tumor cell lines was Pluronic® L61. Promising results indicated that out of 19 patients evaluated, 9 patients had a partial response without a complete response and 8 patients had a stable disease. Moreover, the median overall survival was longer than for formulation based on free DOX [211–213].

Currently, active targeted delivery therapy using Pluronic® block copolymer micelles is being investigated. Song et al. [214] developed PTX-loaded Pluronic® P123 micelles that were used to chemically conjugate anti-HIF-1a antibody with the aim to selectively target cancer cells with overexpression of HIF-1a. In the same way, FA-functionalized Pluronic® P123/F127 mixed micelles were evaluated *in vitro* and *in vivo* by Zhang et al. [208]. The biological assays demonstrated the selective and active targeting of these self-assembled micelles.

3.3. Self-assemblies based on 2-hydroxypropyl methacrylamide (HPMA)

HPMA is a hydrophilic, non-immunogenic and biocompatible polymer that is very attractive to form the shell of polymeric nanoassemblies. Moreover, HPMA has an interesting multifunctionality based on the presence of secondary groups in its structure that facilitates the conjugation with different poor water soluble drugs and targeted moieties. In fact, the conjugation of hydrophobic drugs to hydrophilic HPMA polymer facilitates the formation of nanoassemblies that could be attractive drug delivery systems for the treatment of inflammation and cancer diseases [215–218]. Chytil et al. [219] conjugated DOX to a HPMA copolymer using different contents of various hydrophobic substituents, particularly, dodecyl, oleoyl and cholesterol moieties. These conjugates self-assembled in aqueous solutions forming supramolecular structures with an optimal stability and a range of hydrodynamic sizes between 13 and 37 nm as a function of the type and content of hydrophobic substituents. Moreover, these assemblies released DOX at acidic pH (approximately 70% DOX released after 24 h at pH 5.0), that is, the conditions in endosomes and lysosomes of tumor cells. *In vivo* experiments showed that theses micelles exhibited significant anti-tumor activity against EL-4 T lymphoma cells and enhanced tumor accumulation due to the EPR effect.

In a study by Miller et al., a conjugate of HPMA copolymer with anti-angiogenic and cytotoxic drugs, aminobisphosphonate alendronate (ALN) and PTX, was successfully prepared. Particularly, PTX was conjugated through specific peptide linker that can be cleaved by lysosomal enzymes in order to release both drugs. This conjugate self-assembled in aqueous environment into

particles with sizes of approximately 100 nm. These nanoassemblies demonstrated significant anti-angiogenic activity, inhibiting the proliferation of prostate carcinoma cells. These nanoconjugates have potential for the treatment of prostate cancer bone metastases and osteosarcomas [220–222].

Jia et al. [223] synthesized new amphiphilic block copolymers of HPMA with 2-(2-pyridyldisulfide) ethylmethacrylate (PDSM) *via* RAFT polymerization. The high versatility of PDS groups was used to covalently conjugate maleimide-modified DOX *via* acid-sensitive bonds with the aim to obtain assemblies with pH-sensitivity (see Fig. 7). In aqueous environment, this block copolymer self-assembled through acid-cleavable hydrazone and cross-linked *via* reducible disulfide bonds. *In vitro* studies showed that cross-linked micelles released preferentially DOX at pH 5.0.

On the other hand, different authors have been investigated the use of nanoassemblies based on polymer conjugates in order to improve the selectivity and tumor-imaging capacity of small molecular photosensitizers that are usually used for photodynamic therapy (PDT) [224,225]. In this way, Nakamura et al. [226] conjugated zinc protoporphyrin (ZnPP) to HPMA polymer for its application for diagnosis and cancer treatment by imaging and light exposure, respectively. NP based on this conjugate exhibited a hydrodynamic diameter of 82 nm with excellent stability in aqueous medium. These assemblies accumulated preferentially in tumors and inhibited tumor growth after light-irradiation. ZnnPP-conjugated NP represent a promising method for cancer detection due to their easily visualization by fluorescence after intravenous injection.

3.4. Self-assemblies based on polyesters

PLA has been used as an excellent matrix to form self-assembling NP to encapsulate different chemotherapeutic drugs. This polymer can be also combined with peptides to create polymer–peptide hybrids with the aim to enhance cell uptake without changing their functionality. Jabbari et al. [227] prepared self-assembled polymer–peptide NP formed by a VVVVVVKK peptide (V6K2) conjugated to PLA matrix. These NP with spherical shape and average size of 100 nm were used to encapsulate DOX or PTX and their cell uptake and cytotoxicity was tested against murine breast carcinoma and marrow stromal cells. *In vitro* and *in vivo* studies demonstrated that PLA-V6K2 NP exhibited a high tumor cell uptake due to interactions between the lysine groups of peptide and negatively charged moieties at the cell surface.

Also, peptides can be incorporated at the surface of NP. Xu et al. [228] prepared PLA NP to load oridonin that is an anti-cancer drug successfully used for the treatment of liver cancer and esophageal carcinoma. The surface of these NP was modified by incorporating the peptide RGD *via* cross-linking. The results of *in vivo* studies showed the anti-cancer efficiency of these NP, a decrease in the tumor growth, improving the survival time of mice bearing H22 tumors.

PCL is other polyester extensively studied to prepare nanocarriers for medical applications. Ortiz et al. [229] studied the therapeutic efficacy of the combination of chemotherapeutic agents with gene therapy using 5-FU loaded PCL NP, prepared by an interfacial polymer disposition method. These NP exhibited 40 times superior anti-cancer activity than the free drug. Moreover, the utility of gene therapy based of the cytotoxic suicide gene E was demonstrated against colon cancer cells and it was attributed to the synergistic effect with the 5-FU loaded NP.

Huang et al. [230] synthesized complex amphiphilic NP composed of PCL-*b*-poly-(propargyl methacrylate-click-mercaptosuccinic acid-*co*-PEG methyl ether methacrylate) (PCL-*b*-*p*(PMA-click-MSA-*co*-PEGMA)). In this case, superparamagnetic iron oxide NP (SPIONs) were loaded into the inner PCL core. Moreover, cisplatin was coordinated with pendant dicarboxylic groups in the hydrophilic shell. These multifunctional NP revealed great anti-cancer activity against UMUC3 bladder cancer cells. Moreover, the anti-cancer efficacy of these NP by cisplatin delivery can be combined with SPIONs-induced hyperthermia.

On the other hand, PLA-*b*-tocopheryl polyethylene glycol 1000 succinate (TPGS) NP could be successfully applied for the multimodality treatment of cancer [231]. For instance, Mi et al. [232] loaded DCT and SPIONs in the inner core of NP formed by PLA-*b*-TPGS copolymers. Moreover, carboxyl group-terminated TPGS was added to conjugate Herceptin® (see Fig. 8). The combination of these different active molecules could allow the treatment of cancer diseases with chemotherapy, hyperthermia and an appropriate active targeting to HER2-overexpressing cancer cells. In fact, the results demonstrated that the treatment with these NP using an *in vitro* model of the HER2-positive breast cancer was 2130-fold more efficient than the corresponding single modality treatments.

3.5. Self-assembled systems of peptide–amphiphiles

Currently, peptides represent an emerging platform to create self-assembling nanostructures for the cancer treatment and inflammation diseases [233]. These small molecules have attracted much attention due to their inherent biocompatibility, biodegradability, weak immunogenicity and high versatility based on the combination of a wide range of chemical compositions and bioconjugation strategies and their ability to adopt different supramolecular structures [234–236].

Typically, PA are formed by a hyprophobic peptide block, in most cases a long alkyl chain, attached to a short peptide sequence, capable of forming intermolecular hydrogen bonding, usually β-sheet formation. PA include charged amino acids (AA) following the hydrophobic peptide sequence to enhance their solubility in water and to design intelligent materials with, for example, pH sensitivity. Finally, different peptide epitopes as bioactive signals can be incorporated with several purposes, for instance, the improvement of cell adhesion [235].

The appropriate combination of different regions of PA allows the self-assembly into a variety of different structures, such as micelles, vesicles, or nanofibers, through

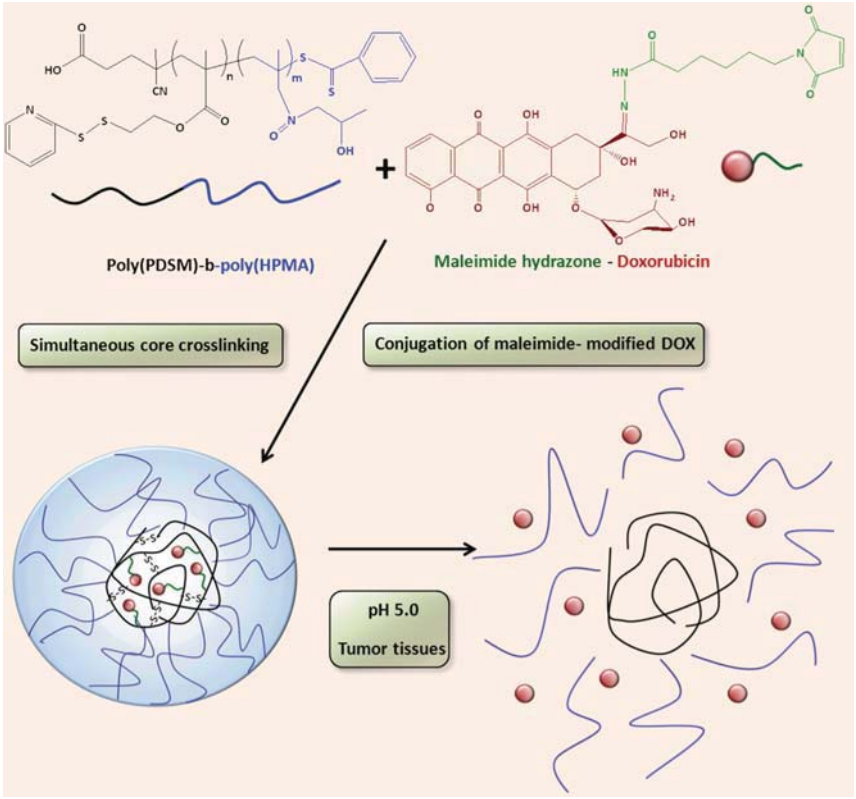

Fig. 7. Preparation of advanced HPMA nanoparticles by simultaneous conjugation of DOX and core-crosslinking *via* reducible disulfide bonds.

hydrophobic collapse of the aliphatic tails and the formation of intermolecular hydrogen bonding. This spontaneous organization allows to minimizing unfavorable interactions with hydrophobic tails in the core and bioactive residue on the surface of the nanoassemblies. The structural characteristics and physico-chemical properties of these assemblies can be modified by changing the segments of amphiphilic molecules. The hydrophobicity can be tuned with the use of different alkyl chain lengths and the solubility or responsive behavior of these materials can be controlled with the appropriate number of charged AA [235,237].

Over the last decade, Stupp and co-workers have exhaustively investigated self-assembling peptide-based materials for different applications, including cancer therapy and inflammation treatment [238]. For these applications, peptides provide a wide range of biological specific interactions, environmental responsive phase behaviors that can be properly controlled, different alternatives to direct self-assembly and a unique source of functional units into a single polymer that can target different tissues [239].

Stupp et al. [240] integrated a cationic α-helical (KLAKLAK)2 peptide into a PA that self-assembled into cylindrical and bioactive nanofibers by stabilization of its bioactive α-helical conformation. The biological activity of this PA was evaluated using human breast cancer cells. The results of these studies demonstrated that (KLAKLAK)2—nanostructures selectively reduced the viability of cancer cells by induction of apoptosis. Additionally, PA incorporating specific cancer biomarkers in their structure have also been investigated. One interesting example is the incorporation of a consensus substrate sequence specific to protein kinase A (PKA) to form filamentous nanostructures with enzyme-responsive behavior. In fact, these nanostructures disassembled as a result of enzymatic phosphorylation, upon treatment with PKA. However, the treatment with an enzyme to cleave the phosphate group allowed to reconstructing the filamentous nanostructures. Furthermore, these nanostructures were used to encapsulate DOX, exhibiting significant cytotoxicity against a cancer cell line that secretes high levels of PKA. This strategy could be considered for the preparation of

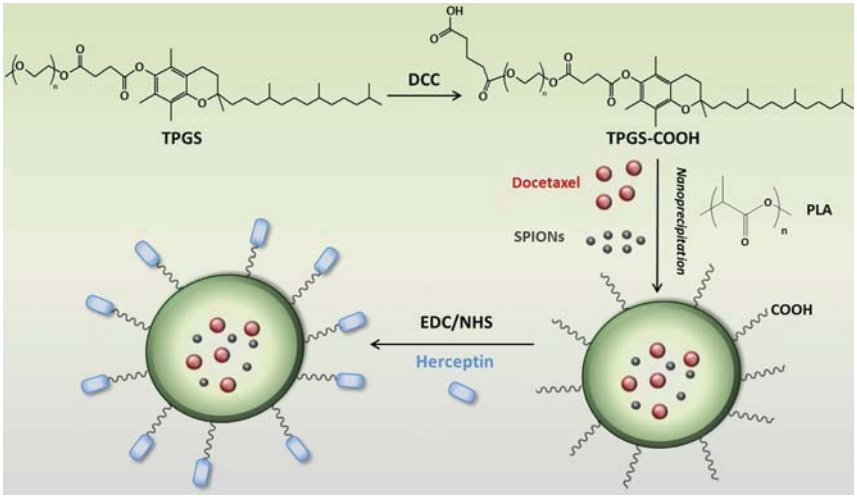

Fig. 8. Preparation of herceptin-conjugated NP loaded with DCT and SPIONs by nanoprecipiattion and surface modification.

biodegradable dynamic assemblies with a wide range of biological stimuli-sensing capabilities [241].

Different authors have investigated the use of PA to encapsulate a wide range of poor water-soluble drugs. Stupp et al. [242] encapsulated CPT into self-assembling PA nanofibers. This strategy allowed to improve significantly the solubility of this drug. Moreover, the anti-cancer activity of these nanofibers was superior to that of the free drug using human breast cancer cells. Chilkoti et al. [243] developed biodegradable chimeric polypeptides that were attached to a short cysteine-rich segment and self-assembled into sub-100-nm-sized NP. The modification of polypeptides with cysteine residues allowed their conjugation to DOX. *In vivo* experiments showed that these assemblies inhibited completely the tumor growth using a murine cancer model. This advanced strategy offers the possibility to design diverse multifunctional nanoassemblies due to their capability to incorporate drugs, targeting molecules and imaging agents. On the other hand, Wiradharma et al. [244] prepared an oligopeptide amphiphile as a delivery system of DOX. Cationic core–shell nanostructures of approximately 100 nm were obtained with load efficiency up to 22%. The biological behavior of these nanostructures was tested using HepG2 cells. The results showed the significant anti-proliferative activity of DOX loaded assemblies.

The control of drug release in PA can be achieved covalently attaching a drug to a hydrolytically labile bond. Particularly, the incorporation of hydrazone bonds represents an excellent alternative to control the drug release as a function of the pH of the surrounding media [245]. Recently, Stupp et al. [246] developed a PA covalently conjugated to dexamethasone (DMT) through a labile hydrazone bond. This conjugate self-assembled spontaneously in water into long supramolecular nanofibers. *In vitro* and *in vivo* experiments demonstrated the anti-inflammatory response of these assemblies with an optimal control of drug release and without systemic immune suppression.

3.6. Self-assemblies based on poly(2-oxazolines) (POX)

Recently, the use of POX for biomedical applications has reached growing interest due to their biocompatibility as well as their stealth behavior. The living cationic ring-opening polymerization of 2-oxazoline monomer (OX) that was discovered in the middle of the 1960s allows the preparation of a wide variety of well-defined polymers. Additionally, the properties of POX can be easily modified by varying the side chain of OX. This strategy enables the easy access to hydrophilic and hydrophobic polymers for the synthesis of a wide range of self-assembled amphiphilic copolymer structures. For all these reasons, drug loaded micellar carriers formed from POX block copolymers have been developed for the treatment of cancer diseases [247–249].

The most commonly POX investigated to prepare nanoassemblies is poly(2-ethyl-2-oxazoline) (PEtOx). This polymer exhibits a lower critical solution temperature (LCST) in water that facilitates the development of thermoresponsive micelles. Cheon et al. [250] prepared micelles composed of PEtOx-*b*-PCL amphiphilic block copolymers for the loading of PTX. PTX-loaded micelles exhibited an *in vitro* anti-proliferation activity against human nasopharyngeal epidermoid cancer cells (KB) comparable to that observed with the current clinical formulations. However, this micellar formulation reduced side effects such as hypersensitivity and neurotoxicity [250].

Wang et al. [251] encapsulated DOX in the inner core of micelles formed by PEtOx-*b*-PLA block copolymers. These micelles exhibited pH-sensitivity in aqueous solution. This behavior allowed the targeted release of DOX in endosomes and lysosomes of cancer cells. In addition, DOX-loaded NP showed significant cytotoxicity against non-small-cell lung carcinoma CL3 cells and preferentially accumulated in the acidic compartments of the cells.

Recently, Luxenhofer et al. [252] synthesized well-defined amphiphilic block copolymers composed of PEtOx, poly(2-methyl-2-oxazoline) (MeOx) and poly(2-butyl-2-oxazoline) (BuOx) with different compositions ($MeOx_a$-*b*-$BuOx_b$-*b*-$MeOx_a$ and $EtOx_a$-*b*-$BuOx_b$). These copolymers self-assembled in aqueous environment because BuOx exhibited limited water solubility. For this reason, BuOx formed the inner core of self-assembled micelles that were an excellent platform for the solubilization of diferent hydrophobic drugs such as PTX, cyclosporine A, etopiside and amphotericin B. In fact, loading capacities up to 45% were obtained using these novel formulations. *In vitro* studies demonstrated that PTX-loaded micelles exhibited more efficient anti-cancer activity in comparison with the commercial formulation of this chemotherapeutic drug.

On the other hand, micelles based on POX have also been used to incorporate other different agents such as photosensitizers and to be conjugated with small molecules in order to achieve an optimal targeted drug release mechanism and an improvement of cellular uptake [253,254]. Syu et al. [255] conjugated FA to micelles based on PEtOx-*b*-PLA block copolymers for the loading of meta tetra(hydroxyphenyl)chlorin (THPC) (see Fig. 9). TPHC-loaded NP were selectively internalized into cancer cells with more potent anti-cancer activity in KB s.c. xenograft-bearing mice compared to free THPC and non-targeted micelles.

4. Application of natural functionalized polymers

4.1. Hyaluronic acid derivatives

Among all naturally occurring polysaccharides, HA is of particular interest in the development of advanced cancer therapies. HA is an anionic, linear glycosaminoglycan made of alternating disaccharide units of D-glucuronic acid and *N*-acetyl-D-glucosamine with β(1,4) and β(1,3) glycosidic linkages [256]. As a biocompatible, non-immunogenic and biodegradable polysaccharide with a number of biological roles and attractive physicochemical characteristics [257] it has been extensively investigated for a wide range of biomedical applications [80], including drug delivery for cancer therapies. In fact, increased levels of HA in tissues and body fluids have been observed in many cancers [258], suggesting its use as prognostic marker of various types of tumors [259,260]. This accumulation has been related to the overexpression of HA-binding receptors such as the cluster determinant 44 (CD44), which is implicated in the regulation of tumor growth and metastasis [261], the receptor for HA-mediated motility (RAHMM) or the lymphatic vessel endothelial receptor-1 (LYVE-1) in cancer cells [82]. Indeed, Choi et al. [262] demonstrated that NP obtained by self-assembling of HA–5β-cholanic acid conjugates were efficiently uptake by SCC7 cancer cells overexpressing CD44 while no significant uptake was observed by normal fibroblasts. Hence, the preparation of HA-based drug delivery systems can simultaneously exploit active targeting of HA-binding receptors on cancer cells along with the passive targeting of tumors based on the EPR effect, without the need of further modification with targeting ligands [188]. Furthermore, HA can be readily degraded by hyaluronidases (Hases), which are present in abundance in the cytosol of tumor cells, facilitating a rapid release of loaded anti-cancer drugs [263]. Besides, HA also acts as a signaling molecule in inflammation processes [264–266] which are greatly related with cancer progression [267,268]. Table 3 shows a list of the main amphiphilic nanocarriers based on hyaluronic acid for cancer treatment developed in recent years.

4.1.1. Drug-loaded self-assembled systems based on HA

Park et al. [269] reported the self-assembling of DOX-loaded nanogels based on HA with cancer cell selectivity by simple acetylation of HA with acetic anhydride. They confirmed that an increase in the DS of acetyl groups produced a reduction of the critical aggregation concentration values and the size of the nanogels due to the increase in hydrophobicity, which in turn increased the drug-loading efficiency and capacity, and prolonged the half-maximal DOX release time [82]. Similar tendencies were observed for other systems described below [84,90].

Several other hydrophobic moieties have been used to modify HA in order to give rise to drug-loaded, self-assembled nanostructures for cancer therapies. Saravanakumar et al. [90] conjugated an amine-terminated 2-(4-(vinylbenzyloxy)-*N*,*N*-diethylnicotinamide) (VBODENA) oligomer to HA for the encapsulation of PTX upon self-assembling into NP, achieving drug loadings up to 20.7% for an optimal DS of 3.17. The proposed system exhibited selective cytotoxicity to cancer cells overexpressing CD44. Interestingly, the PTX release rate was lower for NP containing the larger drug loadings, as observed also in other core–shell structured systems [270]. Kong et al. [84,270] esterified HA with monostearin to develop self-assembled HA-based noisomes as transdermal drug delivery systems for cancer therapy and loaded them with α-tocopherol. The noisomes underwent transdermal permeation both *in vitro* (in a stratum corneum model) and *in vivo* (in male Kunming mouse), and exhibited higher endocytosis by mouse breast tumor cell (4T1) than the control (Ch NP). Ray et al. [271] developed self-assembled 6-*O*-(3-hexadecyloxy-2-hydroxypropyl)–HA (HDHA) NP and loaded them with DOX (4%) for intravenous infusion with simultaneous oral administration of EGCG, a green tea polyphenol. This system significantly enhanced the toxicity against Ehrlich's ascites carcinoma (EAC) cells as compared to free DOX. One of the drawbacks of some self-assembled polymeric systems is their usual sustained drug release over long time periods, which may decrease the efficacy of anti-cancer drugs. Recently, Li et al. [89] designed HA-based redox-sensitive micelles for targeted, rapid intracellular release of encapsulated PTX. The nano-sized micelles self-assembled from amphiphiles prepared by conjugation of DOCA to a cystamine-modified

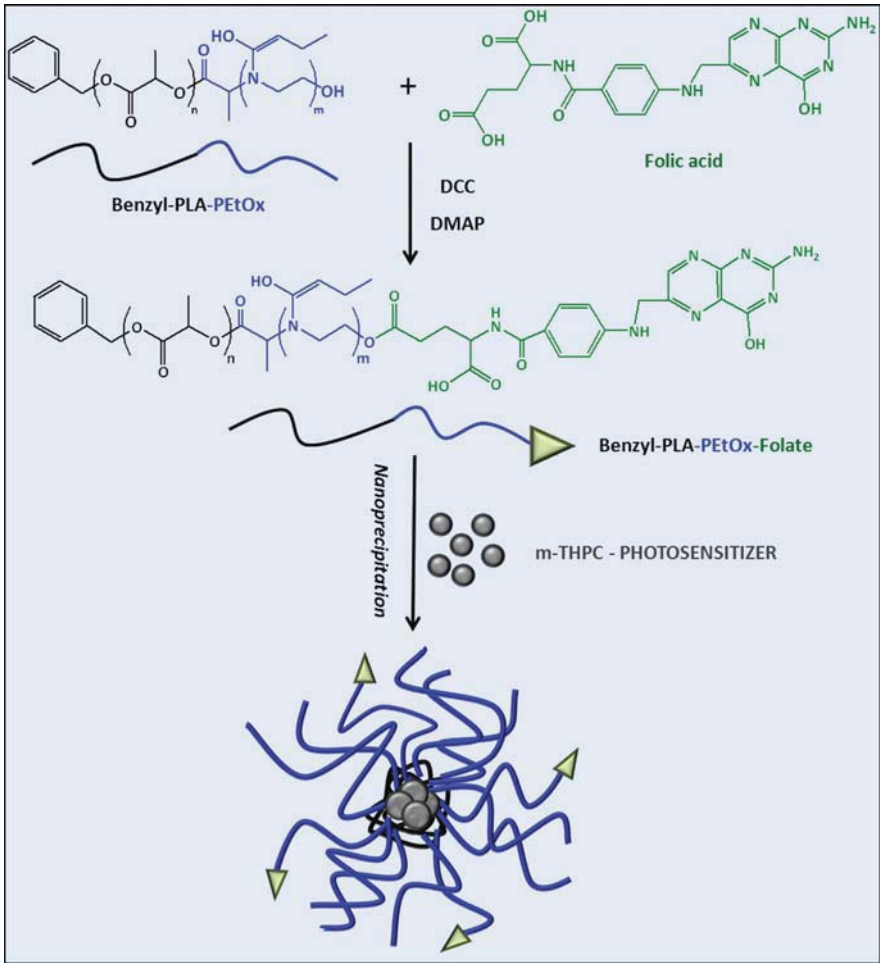

Fig. 9. Preparation of PEtOx-*b*-PLA block copolymers and schematic illustration of TPHC-loaded NP for PDT.

HA, efficiently encapsulating PTX (up to 34.1% wt load). Under reducing conditions, which mimic the reducing environment of tumor cells, the micelles disassembled due to the cleavage of the disulfide linkage triggering a fast drug release. As a consequence, the redox-sensitive micelles exhibited an enhanced cytotoxicity for human breast adenocarcinoma cells (MDA-MB-231) as compared with an insensitive control prepared by using adipic dihydrazide instead of cystamine as a linker for the conjugation of HA–DOCA. Wu et al. [86] also exploited stimuli responsiveness of HA derivatives for the targeted delivery of anti-cancer drugs to tumor cells. In their work they used His as a hydrophobic residue to induce the self-assembling of His-modified HA and encapsulate DOX. Under weakly acidic pH, such as the slightly acidic extracellular pH of solid tumors, the His residues in the His-HA NP became hydrophilic as a consequence of the protonation of their imidazole group, resulting in a higher DOX release at acidic pH than at neutral pH. The prepared DOX-loaded His-HA NP showed similar dose and time-dependent cytotoxicity against MCF-7 cells than free DOX and could exploit both pH-sensitivity and selective receptor-mediated endocytosis to target solid tumors.

Regardless of the selective intracellular uptake of HA-based systems by receptor-mediated endocytosis in tumor cells, successful efforts have been made in order to further improve tumor targetability of self-assembled HA derivatives by reducing their accumulation in the liver

Table 3
A summary of amphiphilic nanodelivery systems of cancer drugs based on hyaluronic acid.

Polymer backbone	Type of modification	Nanocarrier type	Drug/Bonding type	Cancer cell type	Biological/Clinical status	Reference
HA	Acetylation	Nanogels	DOX encapsulation	HeLa cells	*In vitro*	[82]
	Conjugation of 2-(4-(vinylbenzyloxy)-*N*,*N*-diethylnicotinamide)	NP	PTX encapsulation	SCC7, squamous cells carcinoma	*In vitro*	[90]
	Esterification with monostearin	Noisomes	α-tocopherol encapsulation	4T1 mouse breast tumor cells	*In vitro* and *in vivo*	[84]
	Conjugation of 6-*O*-(3-hexadecyloxy-2-hydroxypropyl)	NP	DOX encapsulation	EAC, Ehrlich's ascites carcinoma	*In vitro*	[271]
	Conjugation of histidine residues	NP	DOX encapsulation	MCF-7 human breast adeno-carcinoma cells	*In vitro*	[86]
	Conjugation to drug (PTX)	Micelles	PTX conjugation	MCF-7 breast and HCT-116 colon adeno-carcinoma cells	*In vitro*	[73]
	Conjugation to drug (PTX)	-	PTX conjugation	Human bladder cancer	*In vitro* and *in vivo*	[279]
	Conjugation to drug (PTX)	NP	PTX amino acids Linkers	MCF-7	*In vitro*	[94]
Cystamine-modified HA	Conjugation of DOCA	Micelles	PTX encapsulation	MDA-MB-231 human breast adenocarci-noma cells	*In vitro*	[89]
Adipic dihydrazide-modified HA	Conjugation to drug (PTX)	-	PTX linker mediated coupling	Ovarian carcinoma xenografts	*In vitro*	[279]
PEGylated HA	Conjugation of 5β-cholanic acid plus black hole quencher3	NP	Chlorin e6 (photosensi-tizer) encapsulation	HT29 human colorectal ade-nocarcinoma cells	*In vitro* and *in vivo*	[280]

after systemic administration, which had been observed in other works [262,272,273] and is attributed to the presence of another HA receptor in the liver sinusoidal endothelial cells, namely the hyaluronan receptor for endocytosis (HARE) [274]. Because of the relevant role of HA in inflammation processes, this polysaccharide is also especially interesting for the development of polymer-based anti-inflammatory therapies. For instance, DMT was recently loaded in self-assembled NP of Flt1 peptide–HA conjugates showing efficient internalization into lung epithelial cells by HA-receptor mediated endocytosis, exhibiting long-term retention in deep lung tissues attributed to the mucoadhesive property of HA, and decreasing cytokine levels of lipopolysaccharide-stimulated cells more efficiently than free DMT [275].

4.1.2. Anti-cancer agent-conjugated self-assembled systems based on HA

Instead of physically loading the anti-cancer agent into the nanocarriers, some authors suggest its chemical conjugation with HA, serving both as active anti-cancer agent and as the hydrophobic residue required to obtain an amphiphilic self-assembling construct. Lee et al. prepared round-shaped self-assembled micelles (~200 nm) by direct conjugation of PTX to HA, achieving up to 12% PTX loadings. The generated ester linkage was cleavable in acidic conditions, potentially favoring the differential PTX delivery to acidic tumor tissues as shown in the drug release assays performed *in vitro* at different pHs. In addition, these micelles showed enhanced cytotoxicity in CD44-overexpressing MCF-7 and HCT-116 cells as compared to Taxol®, but lower cytotoxic effects than the commercial formulation for NIH-3T3 (no CD44-overexpression), suggesting a HA-receptor mediated internalization process for PTX uptake [73]. Previous works had already reported the development of HA–PTX conjugates by linker mediated coupling [276–278], their selective uptake by malignant cells *via* receptor-mediated internalization [276,277] and the anti-tumor activity of HA–PTX derivatives against human ovarian carcinoma xenografts [279] or superficial bladder cancer.

Despite the predominant role of self-organizing HA-based systems as vehicles for the delivery of anti-cancer drugs, they have also been exploited for other strategies to combat cancer, such as photodynamic imaging and therapy. Yoon et al. [280] used PEGylated HA–5β-cholanic acid conjugates and further coupled them to black hole quencher3 (BHQ3), obtaining self-assembled NP in which

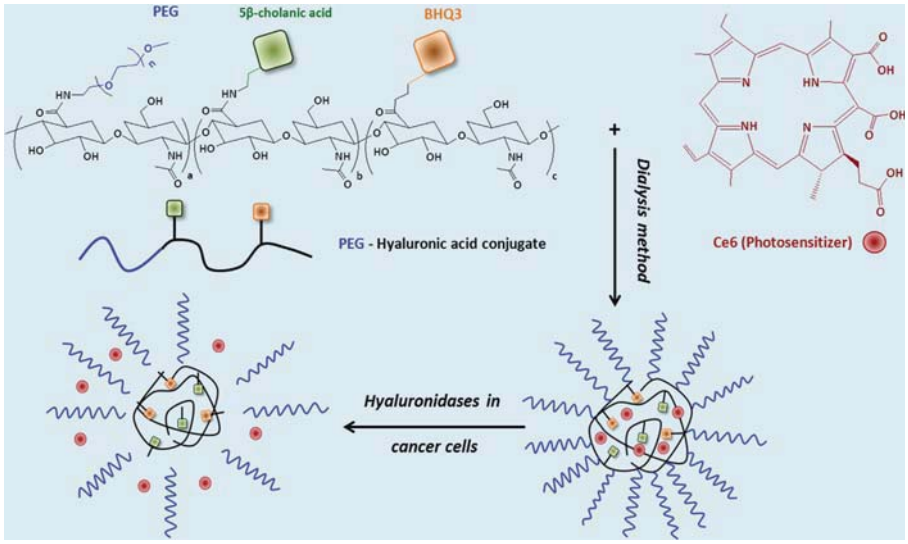

Fig. 10. Representative preparation and enzimatic release mechanism of a HA based system for photodynamic imaging and cancer therapy.

they incorporated chlorin e6 (Ce6), a hydrophobic photosensitizer capable of generating fluorescence and singlet oxygen upon irradiation for combined cancer diagnosis and therapy (see Fig. 10). Being smaller than 300 nm, these NP were selectively uptaken by HT29 human colon cancer cells *via* CD44-binding interactions, as compared to normal NIH3T3 mouse embryo fibroblasts, and they effectively accumulated in the tumor tissue of HT29 tumor-bearing miceCovalent attachment of steroidal and nonsteroidal anti-inflammatory drugs to functionalized HA has also been accomplished [281]. However, scarce literature can be found regarding self-assembling properties of these conjugates into nanoparticulate systems for cancer or inflammation therapies.

4.2. Heparin derivatives

As negatively charged polysaccharides, heparins have the ability to bind to a variety of proteins and other biomolecules altering their activity. Hence, apart from their known anticoagulant effects, heparins can play a role in a number of biological activities including interference with malignant processes [282]. Although the exact mechanism of action is still unknown, several works suggest that heparins can efficiently inhibit the proliferation and induce apoptosis on different cancer cell lines [101,283], thus constraining tumor growth and metastasis. In recent studies has been proposed that the mechanism is related to the ability of heparin to interact with tumor related factors such as selectins, heparanases and growth factors [35]. Furthermore, specific binding properties to certain receptors in metastatic cells, such as peptides in B16F10 cells, have been attributed to heparin [101,284], potentially facilitating binding and internalization into those cells *via* targeted endocytosis. For this reasons, heparin-derived self-assembled systems have also been extensively investigated for their use in advanced cancer therapies.

4.2.1. Drug-loaded self-assembled systems based on heparin

Over the last decade, a number of anti-cancer drug-loaded self-assembled systems based on heparin have been developed. Park et al. [77] prepared self-organizing heparin–DOCA conjugates and efficiently loaded them with DOX up to 12%. They observed that bare heparin-DOCA NP inhibited tumor and endothelial cell proliferation in tumor tissues by their own, and were more active than free heparin *in vitro*. When loaded with DOX, these NP where more effective reducing tumor growth and had better anti-tumor activity than free DOX, reducing its side effects. Li et al. [76] did attempt the design of targeted delivery systems for antineoplastic drugs by investigating the role of chemically linked Fol residues in the selectivity of self-assembled heparin-*b*-poly(benzyl-L-aspartate) (PBLA) block copolymers encapsulating PTX toward cancer cells. They found that Fol-conjugated NP were more efficiently uptaken by KB cells (positive for Fol-receptor) than the ones which did not incorporate targeting ligands. Further, they showed that when a PEG fragment was inserted as spacer between Fol and heparin the cellular uptake was improved to a greater extent. In addition, Fol-conjugated PTX-loaded NP exhibited enhanced selective cytotoxicity toward KB cells as compared with Fol-receptor-negative human lung adenocarcinoma epithelial (A549) cells, especially when PEG was used as spacer.

4.2.2. Drug-conjugated self-assembled systems based on heparin

Heparin based anti-cancer prodrugs have also been developed by chemical conjugation of the free drug with heparin. Park et al. [95] conjugated PTX with heparin obtaining spherical NP with diameters in the range of 200–400 nm which exhibited enhanced cytotoxicity against KB cancer cells compared to free PTX. These NP also showed inferior anticoagulant activity than free heparin, another clue feature to take into account in order to reduce hemorrhagic side effects when using heparin-based prodrugs. By chemically modifying heparins, critical functional groups or units on their antithrombin-binding sequence may be inactivated, thus reducing their anticoagulant effect [283]. Park et al. [93] also modified heparin by chemical conjugation of retinoic acid and FA to the polysaccharide backbone and obtained self-assembled NP (150–300 nm). The presence of FA showed to improve the cellular uptake of the NP in Fol receptor-positive cells, and the cytotoxicity of retinoic acid against these cells was also enhanced using this system compared to the free drug. Again, the modification of heparin reduced its anticoagulant activity. Tran et al. [91] used folated heparin-retinoic acid self-assembling prodrugs to encapsulate the photosensitizer Pba for combined PDT and chemotherapy. Apart from the improved cytotoxicity of retinoic acid and the enhanced and selective cellular uptake in Fol receptor-positive human cervical cancer (HeLa) cells compared to Fol receptor-negative HT-29 cells, these complex NP selectively enhanced the phototoxicity of Pba in HeLa cells upon irradiation.

Hou et al. [285] also designed a dual cancer therapy based on heparin-retinoic acid conjugates. Their strategy consisted of combining the chemical conjugation of ATRA and the physical encapsulation of PTX in a single heparin-based delivery system for simultaneous delivery of both anti-cancer drugs. The obtained self-assemblies, with particle sizes ranging from 228 to 108 nm and PTX contents of up to 33%, extended the plasma circulation periods for PTX and ATRA and showed improved cytotoxicity to human hepatocellular carcinoma HepG2 cells compared to free PTX. Most Recently, an innovative approach which combines both the features of self-assembled nanostructures and the benefits of dendrimers for chemotherapeutic drug delivery was proposed by She et al. [35] In their work, they prepared "dendronized" heparin by covalently linking polypeptide dendrons to heparin, and subsequently conjugated DOX to these dendrons *via* acid-liable hydrazone bonds, obtaining 9% DOX contents. The dendronized heparin-DOX conjugates self-assembled in aqueous media to form compact NP displaying average hydrodynamic diameters around 90 nm, a suitable size to accumulate in tumor tissues by the EPR effect. Due to the liability of the hydrazone bonds, these NP exhibited pH sensitivity, with greater DOX release rates at acidic pH. The *in vitro* and *in vivo* assays showed considerable anti-tumor activity by anti-angiogenic and apoptotic effects against 4T1 breast cancer cells and in 4T1 tumor bearing-mice.

As oral drug delivery is the most convenient route of administration for the patients, some authors have focused on improving the oral absorption and targeting of chemotherapeutics. Khatun et al. [96] designed a strategy based on the conjugation of taurocholic acid (TCA), capable of interacting with the bile acid transporter of the small intestine, with heparin as a therapeutic polymer, and further modification of this conjugate by chemical linkage of DCT. These ternary bioconjugates self-assembled in water giving rise to NP (115–124 nm) which showed positive results in MDA-MB231 and KB tumor bearing mice, indeed enhancing oral absorption compared to bare heparin, efficiently accumulating in tumors and improving tumor growth inhibition compared to free DCT.

4.3. Chitosan derivatives

Chitosan, the *N*-deacetylated derivative of chitin (poly-β-(1 → 4)-*N*-acetyl-D-glucosamine), has drawn rising interest in the development of nanocarriers due to its unique and versatile physico-chemical properties and biodegradability. In particular, development of colloidal amphiphilically modified chitosan nanocarriers has increasing attention for chemotherapy applications [286] due to the fact that chitosan and its oligosaccharides were reported to be potent angioinhibitory and anti-tumor compounds, as confirmed by inhibition of angiogenesis and inducing apoptosis as a function of DNA fragmentation [287]. Thus, together with HA, chitosan has a relevant role in the development of nanocarriers for cancer therapy [288].

4.3.1. Drug-loaded self-assembled systems based on chitosan

Zhang et al. [289] prepared micellar systems of amphiphilic chitosan derivatives based on alkyl chains ($n = 8$, 10, 12) and sulfated groups of which the *N*-octyl-*O*-sulfate chitosan system was selected to encapsulate PTX in amounts up to 25%. The PTX-loaded micelles showed slow *in vitro* released of PTX (up to 220 h) from micellar solution [290]. This chitosan amphiphile showed no intravenous stimulation, injection anaphylaxis, hemolysis and cytotoxicity [291]. Chitosan derivatives with hydrophobic moieties of *N*-octyl and hydrophilic moieties of sulfate and mPEG groups were reported by Qu et al. [292]. These amphiphiles formed micelles that were charged with PTX. The tissue distribution studies in mice indicated that PEG conjugated micelles were phagocytized less than unconjugated micelles by RES. Furthermore, the higher targeting efficiency of PEGylated micelles to uterus (including ovary) suggested that this carrier could be promising for the chemotherapy of ovarian cancer.

Dufes et al. [293] prepared targeted carrier systems for DOX by covalent linking of transferrin (TfR) to DOX-loaded palmitoylated glycol chitosan vesicles using dimethylsuberimidate (DMSI). For comparison purposes, glucose targeted niosomes were prepared using *N*-palmitoyl glucosamine. *In vivo* experiments with a mouse xenograft model showed that all vesicle formulations had a superior *in vivo* safety profile compared to that of the free drug. And also, all vesicles reduced tumor size on day 2 but were overall less active than the free drug.

Micelles with high *in vivo* stability based on stearic acid grafted chitosan oligosaccharide amphiphiles (CSO-SA)

were developed by Hu et al. [110]. To obtain an active-targeting carrier to cancer cells, Fol-conjugated CSO–SA amphiphiles were synthesized. The targeting ability of these micelles was investigated against two kinds of cell lines, A549 and HeLa, which have different amounts of Fol receptors on their surfaces. The results revealed good internalization of the micelles into both types of cells. Then, PTX was encapsulated into the micelles, and the anti-tumor efficacy was investigated *in vitro*. The cytotoxicity of PTX-loaded micelles was improved sharply for both strains of cells compared with that of Taxol®, what was attributed to the increased intracellular delivery of the drug [294]. Curcumin-loaded CSO–SA micelles were effective for inhibiting subpopulations of CD44+/CD24+ cells (putative colorectal cancer stem cell markers) both *in vitro* and *in vivo* [295]. Amphiphilic micelles of stearyl chitosan (SC) and sulfated stearyl chitosan (S-SC) were developed for the controlled delivery of atorvastatin (ATV) in cancer cells. Micelles encapsulating ATV exhibited a sustained release and more cytotoxic activity against MCF 7 and HCT 116 cell lines than ATV alone [296].

An effective and safe vehicle for systemic administration of hydrophobic drugs based on novel chitosan derivatives carrying linoleic acid and poly(β-malic acid) was synthesized by Zhao et al. [297]. This double grafted chitosan self-assembled into NP which could encapsulate PTX. The PTX-loaded NP demonstrated to have a potent tumor inhibition efficacy relative to that of Taxol® in sarcoma-180 bearing mice. Self-assembled NP of 5β-cholanic acid–glycol chitosan conjugates were efficiently loaded with PTX up to 10% content using a dialysis method (400 nm, average diameter). Injection of PTX-loaded NP into the tail vein of tumor-bearing mice prevented increases in tumor volume for 8 days. PTX was less toxic to the tumor-bearing mice when formulated in NP than when formulated with Cremophor® EL [108,298]. pH-sensitive self-aggregated NP (ranging from 87 to 174 nm) based on DOCA modified carboxymethyl chitosan (DCMC), were developed by Jin et al. [299] for delivery of DOX. The unloaded NP showed an acidic pH-induced aggregation and deformation behavior. The DOX-loaded NP exhibited a sustained drug release profile, dependent on pH and DS of the hydrophobic chitosan. DOX-loaded NP effectively suppressed both sensitive and resistant MCF-7 cells in a dose- and time-dependent manner.

Yang et al. [300] proposed a novel thermal sensitive amphiphilic chitosan containing hydroxybutyl groups and DOCA moieties as a drug carrier in combined hyperthermia and chemotherapy. By tuning the hydrophobic/hydrophilic balance of DOCA decorated hydroxybutyl chitosan (DAHBC), LCST of this novel polymer was adjusted to 38.2 °C for hyperthermia therapy. These NP delivered the encapsulated DOX at a temperature above the LCST. DOX-loaded nanocarriers exhibited an improved drug uptake by mouse embryo fibroblasts MCF-7 cells with the incubation temperature rising from 37 to 43 °C.

N-acetyl histidine-conjugated glycol chitosan (NAcHis-GC) self-assembled NP are a promising system for intracytoplasmic delivery of PTX. At neutral pH, the conjugates formed self-assembled NP with mean diameters ranging between 150 and 250 nm. In slightly acidic environments, such as those in endosomes, the NP were disassembled due to breakdown of the hydrophilic/hydrophobic balance by the protonation of the imidazole group of NAcHis and could release the encapsulated PTX into the cytosol (see Fig. 11) [301].

A CSO–arachidic acid (CSOAA) amphiphilic derivative of chitosan was successfully synthesized as a self-assembled nanocarrier of DOX by Termsarasab et al. [302]. *In vitro* release of DOX was sustained and pH-dependent. Cellular uptake of DOX in FaDu cells was higher in the NP-treated group compared to the free DOX group. The anti-tumor efficacy of DOX-loaded NP was also verified in FaDu tumor xenografted mouse model. The amphiphilic grafted copolymer *N*-phthaloylchitosan-g-mPEG was proposed as a carrier for ATRA by Bouterfa et al. [303]. It was found that deacetylation degree (DD) of chitosan, which corresponded to the *N*-phthaloyl groups in the inner core of the micelles, was a key factor in controlling the loading efficiency, stability of the drug-loaded micelles and drug release behavior. As the % DD increased, the loading efficiency and ATRA-loaded micelles stability increased. The sustained release profiles were also obtained at high % DD (90 and 95%) [99]. Similar results were reported for the encapsulation of CPT in this carrier [304].

NP based on graft copolymers of PNIPAm onto chitosan were developed as a pH-sensitive carrier of CPT for targeting tumors. The cumulative release rate of CPT was optimal at pH 6.8 and decreased rapidly either below pH 6.5 or above pH 6.9 in 37 °C. Based on 3-(4,5-dimethylthiazol-2-yl)-2,5-diphenyltetrazolium bromide (MTT) tests performed with SW480 cells at pH values of 6.8 and 7.4, CPT-loaded NP showed enhanced cytotoxicity at pH 6.8 but minimal cytotoxicity at pH 7.4 what was attributed to pH-sensitivity release of the drug. Particularly, for a PNIPAm:chitosan mass ratio of 4:1 the CPT-loaded NP were more sensitive to tumor pH [305].

Non-steroidal anti-inflammatory drugs (NSAIDS) are emerging as a particularly valuable class of drugs due to their recently recognized anti-tumor activity in colorectal cancer. Micellar nanocarriers (108–252 nm) composed of amphiphilic chitosan with encapsulated ibuprofen were readily internalized by tumor cells and deliver the drug in the intracellular compartment provoking a remarkable reduction in cancer cell viability (<13%), at a relatively low drug dosage, what illustrated the anti-tumor activity of ibuprofen when delivered to breast cancer cells [306].

4.3.2. Conjugated self-assembled systems based on chitosan

A variety of polymer drug conjugates of chitosan have been reported in recent years. Adriamycin (ADR) glycol chitosan conjugates *via* an acid-labile cis-aconityl linkage [307] were capable of forming spherical nano-sized self-aggregates in an aqueous medium, when the ADR content in the conjugate was in the range of 2–5%. The release of ADR was significantly dependent on the pH of the medium due to the cis-aconityl linkage. The cell viability results demonstrated that free ADR showed more potent cytotoxicity than the conjugates, primarily attributed to the sustained release of ADR from the self-aggregates.

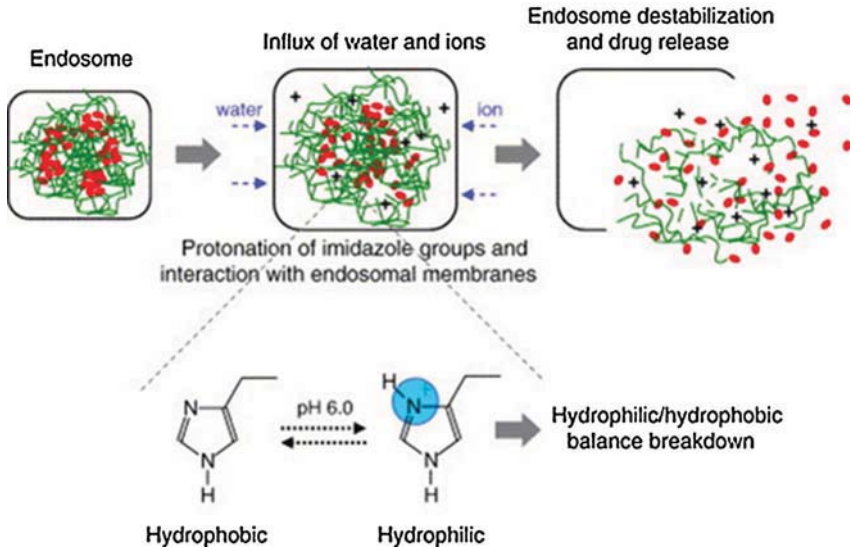

Fig. 11. Schematic representation of endosomal escape and drug release of histidylated polymer nanoparticles. The pH-dependent endosomal-membrane destabilization by histidine correlated with the protonation of its imidazole groups. The p*K*a of the imidazole group is around 6.5. In a slightly acidic milieu, such as in endosomes, the imidazole group is protonated, interacts with negatively charged lipid bilayers and induces the influx of water and ions into endosomes, thus causing endosome destabilization and drug release into the cytosol. [301], Copyright 2006. Reproduced with permission from Elsevier Ltd.

PTX-loaded tocopheryl succinate (α-TOS) conjugated CSO (CSO-α-TOS) NP were proposed for synergistic chemotherapy by Tao et al. [308]. PTX-loaded CSO-α-TOS NP had excellent cellular uptake ability by human glioma U87 cells. *In vitro* cytotoxicity studies revealed that the PTX-loaded NP system was more potent than free PTX, and a synergistic effect between α-TOS and PTX was observed. *In vivo* pharmacokinetic results indicated that the PTX-loaded CSO-α-TOS NP had a longer systemic circulation time and slower plasma elimination rate than those of Taxol®.

Selective targeting of drugs to kidneys may improve renal effectiveness and reduce extrarenal toxicity. For that purpose Yuan et al. [309] developed and evaluated a novel renal drug carrier randomly based on 50% *N*-acetylated LMWC and prednisolone covalently coupled with chitosan *via* a succinic acid spacer. The mean residence time in plasma of prednisolone conjugates increased as the MW of the chitosan increased. The conjugate with MW of 19 kDa displayed the highest accumulation rate in the kidneys. The total amount of this conjugate in the kidneys was 13-fold higher than that of prednisolone.

pH Sensitive NP based on polyethylenglycol tethered carboxylated chitosan modified with FA/DNA nanocomplexes containing a high mobility group box1 (HMGB1) have been developed recently as an efficient non-viral gene delivery system (see Fig. 12). This kind of complex bioactive NP gives very good transfection and expression efficiency in most folate receptor (FR-α)-positive cancer cells [310].

4.4. Pullulan derivatives

Pullulan is a linear homopolysaccharide of glucose consisting of α-(1 → 6) linked maltotriose units, which is secreted mainly by *Aureobasidium pullulans*. Its distinctive and regular linkage pattern gives rise to unique properties such as structural flexibility and superior water solubility as compared to other polysaccharides [311]. This polysaccharide is a good candidate for chemical modification with hydrophobic residues leading to self-organizing systems with potential application in cancer treatment since it can be readily dissolved in organic solvents such as DMSO upon mild heating, [72,74,75] facilitating its chemical derivatization. Besides, it can be easily modified to include active targeting ligands like biotin or folate in its structure to confer specificity to cancer cells.

4.4.1. Drug-loaded self-assembled systems based on pullulan

Yang et al. [116] proposed the use of biotin as a targeting ligand to develop pullulan-based self-aggregated NP for the encapsulation and targeted delivery of MTO to cancer cells, as biotin specific receptors are generally overexpressed on numerous tumor cells [312]. Previously, they had developed cholesterol-modified pullulan NP as carrier for MTO [115], however, these self-aggregates lacked active targeting to tumor tissues. To overcome these limitation, in their latter work they suggested the conjugation of biotin to cholesteryl pullulan and the obtaining of MTO-loaded NP by self-organization in aqueous media. The prepared NP

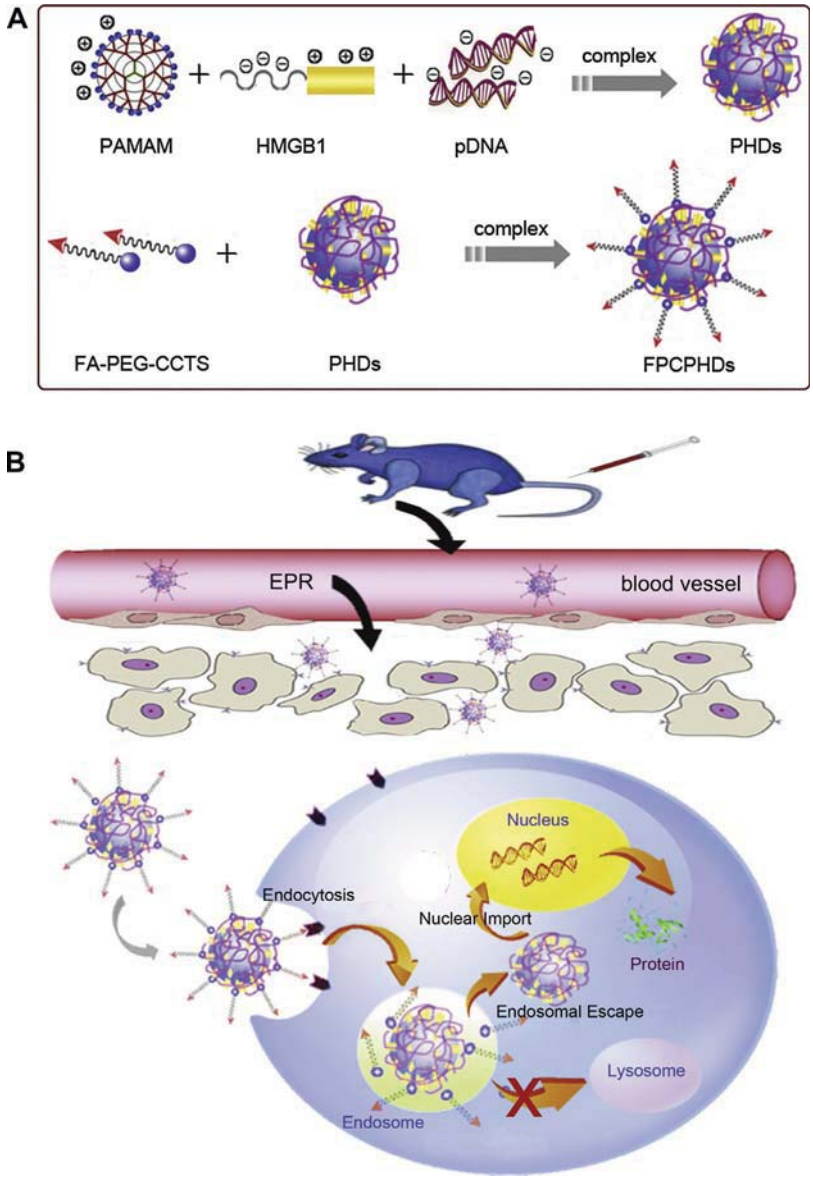

Fig. 12. A schematic diagram showing (A) the formation of FPCPHDs nanocomplexes and (B) the extracellular and intracellular trafficking for the systemic delivery of plasmid DNA to a tumor. FPCPHDs accumulates in the tumor via the EPR effect and is associated with the tumor cell surface, followed by cellular uptake by folate receptor-mediated endocytosis. FAPEG–CCTS dissociates from PHDs ternary complexes in the acidic endosomes and then PHDs escapes from endosomes through the proton sponge effect. Finally, the plasmid DNA is delivered to the nucleus with the help of HMGB1 due to its nuclear locating ability. [310], Copyright 2013. Reproduced with permission from Elsevier Ltd. Abbreviations: FPCPHDs, FAPEG-CCTS/PAMAM/HMGB1/pDNA nanocomplexes; FAPEG-CCTS, folate-modified polyethylene glycol tethered carboxylated chitosan; PAMAM, polyamidoamine dendrimer; EPR, enhanced permeability and retention effect; PHDs, PAMAM/HMGB1/pDNA nanocomplexes.

were able to encapsulate MTO with loading capacities up to 14% and showed pH-dependent drug release behavior. However, their efficacy and selectivity toward tumor cells has not been reported [116].

4.4.2. Conjugated self-assembled systems based on pullulan

Zhang et al. [117] preferred conjugation of DOX onto the pullulan backbone instead of physically loading it and they prepared pullulan–DOX conjugates with maleic acid as spacer, followed by further modification of this prodrug to incorporate Fol the residues by direct conjugation. Although the effectiveness of this system against ovarian carcinoma A2780 cells was improved with respect to the parent drug, its self-assembling properties were not reported. Pullulan self-assembling derivatives have also been exploited in the field of PDT. Bae and Na [72] used Fol–pullulan conjugates previously described by Kim et al. and further coupled them to Pba, obtaining self-assembling and self-quenching nanogels with the aim of both reducing the phototoxicity of Pba in normal tissue and improving the efficacy of the PDT using this photosensitizer. Indeed, owing to a self-quenching effect between photosensitizer moieties, the photoactivity of Pba was not detected when the nanogels were suspended in PBS. However, upon digestion by the enzymes present in the lysosome, the photoactivity of Pba could be restored. Moreover, their results suggested that these nanogels could be uptaken by HeLa cancer cells by Fol receptor-mediated endocytosis (see Fig. 13).

4.5. Dextran derivatives

DEX is a polysaccharide containing glucose units linked by α-(1 → 6) glycosidic linkages in the main chains and α-(1 → 3) linkages in the branches. DEX has been also widely used in the development of drug delivery systems for anticancer therapy. Several anti-tumor drugs such as DOX, CPT, MTX and mitomycin have been conjugated to DEX either directly or using spacers to form anti-cancer prodrugs [313]. Oxidized DEX-DOX conjugates and carboxymethyl DEX CPT derivative conjugates have entered clinical trials [314]. A review of this was reported by Goodarzi et at. [257] In recent years, DEX nanocarriers for cancer therapy have been developed based on the modification of DEX to obtain amphiphilic derivatives that self-assemble into micellar or nanoparticulate systems.

Varshosaz et al. [315] prepared DEX stearate PM as carriers of etoposide. The composition was tuned by changing MW of DEX and molar ratio of stearate. Both parameters demonstrated to have a dominant role on particle size of etoposide-loaded micelles and also on cytotoxicity and cellular uptake of etoposide-loaded PM using CT-26 colorectal carcinoma cell line.

Jeong et al. [316] reported the preparation of DEX amphiphilic derivatives by linking DOCA to DEX. These amphiphiles showed self-aggregation behavior at aqueous environment and gave rise to DOX-incorporated NP with sizes lower than 200 nm. These NP had higher anti-tumor activity compared to free DOX on DOX-resistant CT26 colon carcinoma cells. In addition, DOX-loaded NP were properly entered into tumor cells and maintained longer compared to DOX by itself.

Stimuli responsive DEX based nanocarriers have also been developed. DEX-*b*-polyHis block copolymers were synthesized by Hwang et al. [317] to prepare pH-responsive NP for DOX targeting. The viability of DOX-loaded NP using HuCC-T1 cholangiocarcinoma cells was decreased at acidic pH in cells treated with active NP, whereas cell viability did not vary according to changes of pH for free DOX. Sun et al. [318] reported the preparation of reduction-responsive biodegradable micelles from block copolymers of disulfide-linked DEX-SS-PCL and used them as a targeting delivery system of DOX. *In vitro* studies revealed that DOX-loaded micelles released DOX quantitatively in 10 h under a reductive environment, mimicking that of the intracellular compartments such as cytosol and the cell nucleus, however, only about 20% DOX released was measured in 20 h under the non-reductive conditions. In cellular experiments using mouse leukemic monocyte macrophage cell line (RAW 264.7), it was observed that DOX was rapidly released to the cytoplasm as well as to the cell nucleus. Cytotoxicity studies revealed an enhanced drug efficacy of DOX-loaded micelles compared to DOX-loaded reduction-insensitive micelles.

Prabu et al. [319,320] proposed a self-assembled core–shell micellar vehicle for PTX based on PCL-grafted DEX. PTX-loaded NP were prepared by a modified oil/water emulsion method. PTX-loaded NP so-obtained presented significant drug encapsulation efficiency, cellular uptake, and cancer cell mortality using the human gastric cancer cell line (SNU-638).

Graft copolymers of DEX-*b*-poly(ethyleneimine) (DEX-*b*-PEI) were synthesized by Liu et al. [321] for developing redox-responsive DOX prodrug micelles (100–140 nm average size) to overcome MDR. DOX was conjugated to the graft copolymer through redox-responsive cleavable disulfide linkers. DOX-conjugating micelles enhanced the cellular accumulation of DOX and achieved endosomal escape in human breast carcinoma multidrug resistant (MCF-7/ADR) cells. The therapeutic efficacy of DOX prodrug micelles against MCF-7/ADR cells was remarkably enhanced compared with free DOX.

Thermosensitive NP as carriers of indomethacin (IMC) have been prepared from a graft copolymer of DEX and PNIPAm by Tan et al. [322] In absence of drug, compact NP were formed at a temperature above the LCST, however, in presence of IMC uniform IMC-loaded NP were formed even below the LCST that was attributed to hydrogen bonding between IMC and the PNIPAm side chains. The IMC release rate was accelerated at a higher temperature because of the dissociation of the hydrogen bonds.

4.6. Derivatives of other polysaccharides

Alginates (ALG) are (1 → 4) linked linear copolysaccharides composed of β-D-mannuronic acid (M) and its C-5 epimer, α-L-guluronic acid (G). ALG also can play a role in cancer therapy [323]. It has been demonstrated that ALG obtained from *Sargassum* sp. (Phaeophyta) showed a considerable anti-tumor activity against various murine tumors, such as Sarcoma 180 (solid and ascitic types),

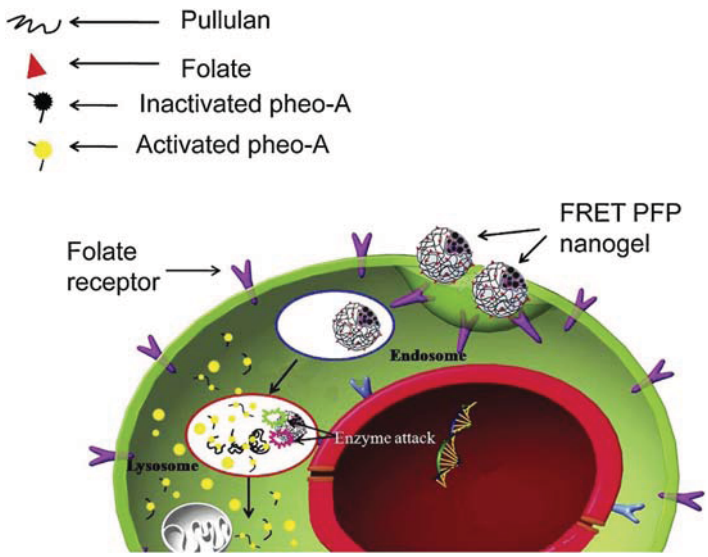

Fig. 13. Conceptual image of the change in photoactivity of PFP nanogels in cells. PFP nanogels do not show photoactivity during blood circulation due to self-quenching of photosensitizers (FRET effect). When the nanogels are internalized in cancer cells, photoactivity is restored due to loss of the FRET effect by enzymatic attack within cellular compartments such as lysosomes. [72], Copyright 2010. Reproduced with permission from Elsevier Ltd. Abbreviations: PFP, pullulan/folate–pheophorbide–conjugates; FRET, fluorescence resonance energy transfer.

Ehrlich ascites carcinoma and IMC carcinoma [324]. For that reason, self-assembled nanocarriers of amphiphilic ALG were developed recently.

Zhang et al. [325] have proposed DOX-loaded amphiphilic NP consisted of glycyrrhetinic acid-modified alginate (GRA-ALG) for targeting therapy of liver cancer. After intravenous administration of DOX-loaded GRA-ALG NP in Kunming mice, the biodistribution study showed that the concentration of DOX in the liver was higher compared with non-GRA-modified NP and DOX·HCl, respectively. The liver tumor growth inhibition rate (IR) *in situ* was 76.6% and no mice died in the DOX-loaded GRA-ALG NP group. Histological examination showed that the heart and liver cells surrounding the tumor were not affected by administration of DOX loaded GRA-ALG NP, whereas myocardial necrosis and apparent liver cell swelling were observed after DOX·HCl administration.

Recently, Du et al. [326] used a reactive template method to fabricate alginate-based hydrogel microcapsules with a high drug loading capacity for application in cancer therapy. The capsules coated by a Fol-linked lipid mixture on the surface possessed higher cell uptake efficiency due to the molecule recognition between Fol and the Fol-receptor overexpressed by the cancer cells. Moreover, in this bioconjugate, the lipid could also encapsulate the hydrophobic photosensitizer hypocrellin B, giving drug carriers for combined treatment of cancer using chemotherapy and photodynamic. This strategy may be extended to fabricate other multidrug carriers for combined anti-cancer treatment.

Shalviri et al. [46] synthesized new pH-responsive NP to overcome MDR [45] based on graft copolymers of PMA and PS80 onto starch (PMA-PS80-*g*-starch) by using a one-pot method that achieved simultaneous grafting and NP formation in an aqueous medium. The relatively spherical NP exhibited pH-dependent swelling in a physiological pH with magnitude of phase transition dependent on polymer composition and formulation parameters. The NP were able to load up to 50% of DOX maintaining good colloidal stability. DOX-loaded NP released the drug at a higher rate at acidic pH attributable to weaker DOX-polymer molecular interactions. The DOX-loaded NP were taken up by MDR1 cells *in vitro* and significantly enhanced cytotoxicity of these cells with respect to that of free DOX, showing a 20-fold decrease in the IC_{50} values [327]. In further studies the activity of the self-assembled DOX-loaded NP was evaluated *in vivo* using a murine orthotopic breast cancer model and compared with the activity of preformed NP prepared by cross-linking graft polymerization reaction. Blood circulation, tumor uptake, penetration and tumor growth inhibition of self-assembled DOX-loaded NP was superior to those of preformed NP, what was attributed to a denser structure of the self-assemblies, suggesting the usefulness of these bi-functional NP as nanotheranostics [327].

A number of other polysaccharides have been used for the preparation of self-assembling drug conjugates. CPT was covalently conjugated to a linear cyclodextrin-PEG copolymer, and the obtained conjugates self-assembled into NP. Preclinical studies showed that these self-aggregates exhibited enhanced pharmacokinetics

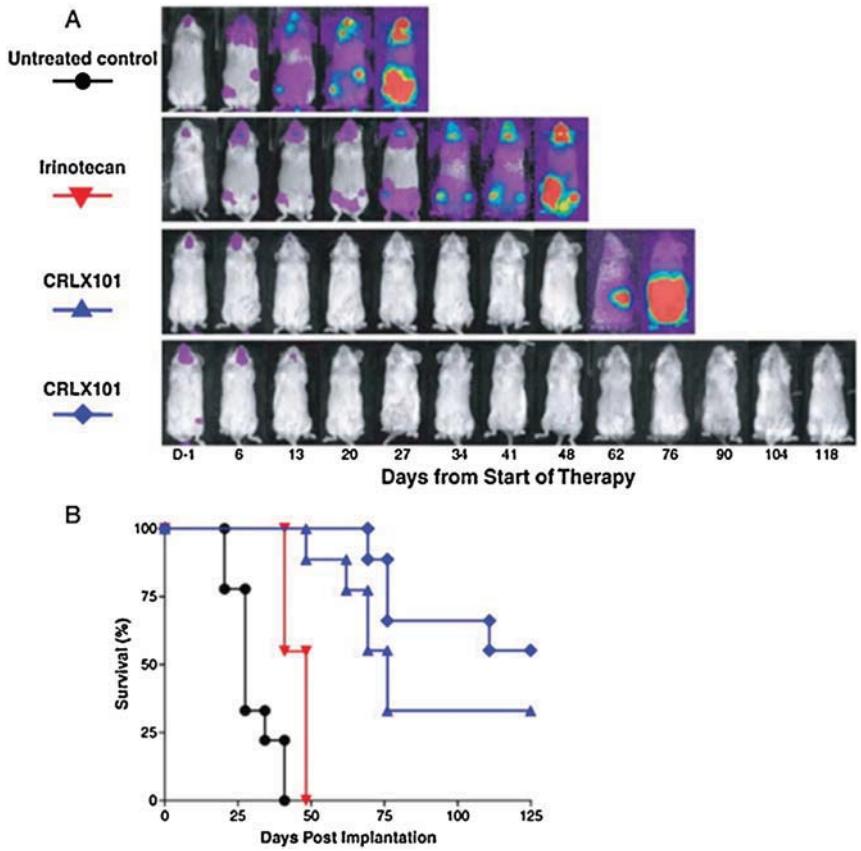

Fig. 14. Efficacy study of CRLX101 compared to irinotecan using a disseminated Daudi B-cell lymphoma xenograft in mice. Above: bioluminescence study using Daudi B-cell line expressing luciferase activity. Weekly dosing × 3 at 100 mg/kg (irinotecan), 5 mg/kg (CRLX101, triangles), and 10 mg/kg (CRLX101, diamonds). Below: corresponding survival graphs. CRLX101 achieved 55.6% complete tumor response at Day 125 post-treatment at the 10 mg/kg dose, while no complete tumor responses were observed in irinotecan-treated mice. [328], Copyright 2011. Reproduced with permission from Elsevier Ltd. Abbreviations: CRLX101, Cyclodextrin-poly(ethylene glycol) copolymer (CDP) conjugated to CPT.

compared to the parent drug, and their anti-tumor activity was superior compared to FDA-approved Irinotecan® in a number of xenograft models (see Fig. 14) [328,329]. This novel nanopharmaceutical, named CRLX101®, is currently in Phase 2 clinical studies and evidence has been provided that its behavior in animals is translatable to humans [330].

4.7. Proteins and proteins derivatives

Proteins also played an important role in the development of nanocarriers for chemotherapy and inflammation diseases. Some protein anti-tumor drug conjugates have been approved by FDA in treatment of cancer, such is the case of PTX albumin conjugate (Abraxane®, ABI-008, nab-PTX) approved for treatment of metastatic breast cancer. This formulation does not use solvents as vehicles but instead, it is based on the natural properties of albumin to reversibly bind PTX and transport it through the endothelial cell to tumor site [331]. This was confirmed in preclinical studies that in fact showed that the concentration of PTX-albumin conjugate in endothelial cells and in the extravascular space was significantly increased (3–10 fold) [332]. These data suggest that albumin may have intrinsic targeting ability to tumors, although the EPR effect may also contribute to their in tumor accumulation. Overall, the albumin-bound PTX formulation allowed higher dosages than the Taxol® one and demonstrated improved efficacy and safety [333]. In addition, albumin was tested as a platform for delivery of other molecules that have anti-proliferative activity, such as rapamycin (~2.5 mg/ml). Albumin-bound rapamycin (ABI-009) has been in a clinical phase trial for the treatment of non-hematologic

malignancies since January 2008 [334]. These recent advances as well as multiple clinical trials currently in progress for other types of cancer, opened the development of protein based NP for delivery of therapeutic agents [5].

Taking advantage of the high affinity that PTX showed for strong binding to human serum albumin (HAS), Lee et al. obtained shell crosslinked NC employing HAS and amine reactive multi-arm PEG. The NC were prepared by emulsifying the branched PEG in dichloromethane into aqueous solution of HAS, followed by cross-linking at the organic/aqueous interface [335]. PTX-loaded NC were spherical with an average diameter of about 280 nm. Surface modification was conducted using a flexible PEG linker with a cell-penetrating peptide, Hph1. *In vitro* cellular studies using different cell lines, human breast adenocarcinoma (MCF-7), human ovarian carcinoma (OVCAR-3), human nasopharyngeal epidermal carcinoma (KB) and human coronary artery and smooth muscle cells (hCASMCs), it was observed that the peptide facilitated cellular uptake and apoptosis effects of PTX. The targeted anti-tumor activity of the PTX-loaded NC tested in a mouse tumor model indicated minimal clearance of the NC in the liver, and hence targeting to the tumor tissue. Tumor growth was significantly reduced in mice after intravenous administration of the system compared to control group.

With respect to the use of other proteins in the preparation of NP, Lu et al. [336,337] prepared PTX loaded gelatin NP which showed good perspectives for intravesical therapy of superficial bladder cancer. PTX-loaded NP were obtained using a desolvation method with sizes from 600 to 1000 nm and they resulted active against human RT4 bladder transitional cancer cells. Results of *in vivo* experiments performed in dogs giving an intravesical dose of PTX-loaded NP, showed PTX concentration in the urothelium and lamina propria tissue layers 2.6 times the concentrations reported for dogs treated with the commercial Cremophor formulation.

For the treatment of lung cancer, one of the most malignant cancers today, gelatin NP were grafted with NeutrAvidin® FITC on the particle's surface, and afterward, biotinylated EGF (bEGF) was conjugated with NeutrAvidin® FITC to improve targeting efficiency, forming a core–shell-like structure (bEGF-Av-NP of 220 nm average size). *In vitro* studies on adenocarcinoma A549 cells showed that entrance efficiency of bEGF-Av-NP and lysosomal entrapment was higher than that on normal lung cells (HFL1), and the uptake of bEGF-Av-NP by A549 cells was time and dose dependent [338]. Specific accumulation of the nanosystem in cancerous lung was confirmed after *in vivo* aerosol administration to cancerous lung of the SCID mice model [339].

Thiolated gelatin NP were modified with PEG chains giving NP of 300–350 nm average diameter, to improve circulation and *in vivo* tumor-targeting of breast cancer. The *in vivo* behavior of the system was evaluated by injecting indium-111 (^{111}In)-labeled NP into breast tumor (MDA-MB-435) bearing nude mice. *In vivo* circulation times were found to be longer in PEG modified NP, showing plasma and tumor half-lives of 15.3 and 37.8 h, respectively, and preferential localization of thiolated NO in the tumor mass was detected [340]. These PEG modified thiolated gelatin NP were proposed as nanovectors for systemic delivery of therapeutic genes to human solid tumors. Thus, plasmid DNA (pDNA) encoding for the soluble form of the extracellular domain of VEG factor receptor-1 (VEGF-R1 or sFlt-1) was encapsulated in these NP. pDNA delivery produced the highest levels of sFlt-1 expression in the MDA-MB-435 human breast adenocarcinoma cell line. After intravenous administration in female Nu/Nu mice bearing orthotopic MDA-MB-435 breast adenocarcinoma xenografts, efficient *in vivo* expression of sFlt-1 pDNA was confirmed qualitatively and quantitatively. The expressed sFlt-1 was therapeutically active as shown by suppression of tumor growth and microvessel density measurements [341].

Tran et al. [342] synthetized amphiphilic gelatin with oleoyl moieties that successfully formed NP with versatile potential in drug delivery and tumor targeting. The amphiphilic NP entrapped PTX and they were further conjugated with FA for targeting HeLa cells. All NP were stable in human blood serum and their average size was below 300 nm, suitable for passive targeting. The release of PTX from both plain PTX- and FA conjugated PTX-loaded NP was controlled for a long time. The cytotoxicity results demonstrated great advantages of PTX-loaded NP either conjugated or not with FA, over the conventional dosage form of PTX (Taxol®) [125]. Wareechuensook et al. [126] modified gelatin into an amphiphilic molecule *via* conjugation with cholesterol. These amphiphiles aggregated in micelles in water at pH 5, and subsequently fabricated with entrapment of curcumin for a cancer research.

Silk fibroin (SF) is a protein that possesses inherent amphiphilicity because the repetition of the hexapeptide -Gly-Ser-Gly-Ala-Gly-Ala- gives rise to hydrophobic and hydrophilic blocks which self-assemble into micelles. In addition, the fibroin chains adopt the β-sheet conformation that acts as a stabilizing element of the nanostructures [343]. Another advantage of fibroin is that it possesses reactive carboxylic end groups that can be used for preparation of fibroin derivatives. Based on all these features, numerous silk SF micellar and nanoparticulate systems have been developed for cancer and inflammation treatment.

Chiang et al. [344] prepared silk fibroin NP with controllable size by a simple method in which the encapsulation of PTX was successfully achieved, leading to PTX-loaded NP with average size from 270 to 520 nm. PTX release was controlled over 9 days, and the release could be prolonged for 2 weeks varying the drug charge, what improved the potential of this system for chemotherapy in clinical applications. Other SF nanocarriers were prepared by Zhao et al. [345] using a novel solution-enhanced dispersion method using supercritical CO_2. The anti-inflammatory drug IMC was charged. Treatment with ethanol did not affect the biocompatibility of the system. *In vitro* IMC release from the IMC-loaded NP after ethanol treatment was significantly sustained over 2 days. These studies indicated the suitability of the supercritical CO_2 process to achieve the co-precipitation of drug and protein to form active NP with potential in the treatment of inflammatory processes.

SF has been chemically modified for tumor specific gene delivery by Numata et al. [346]. In this work, block copolymers of SF with PLL domains were prepared to

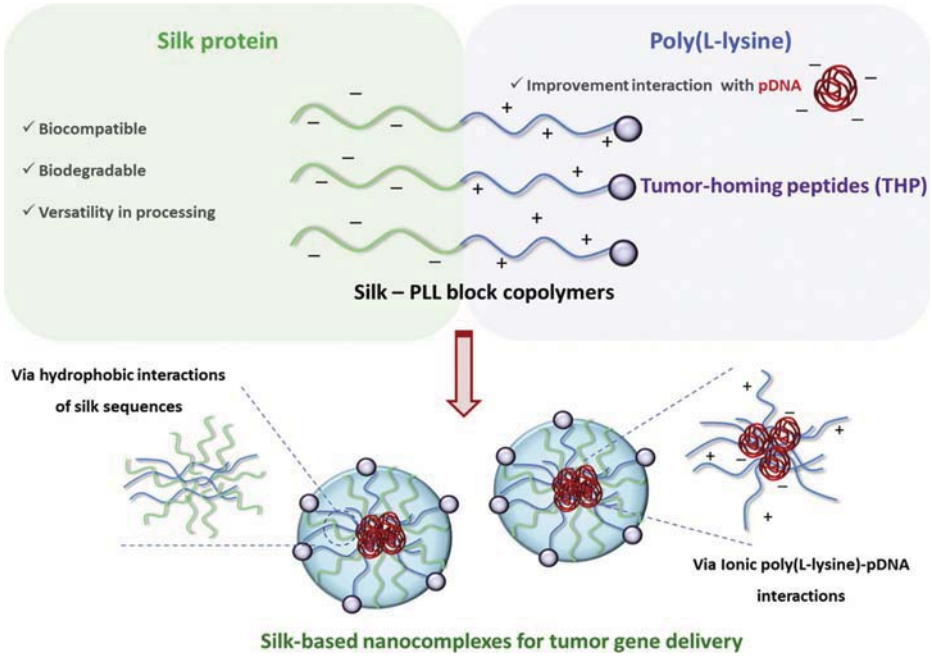

Fig. 15. Schematic representation of the formation of pDNA nanocomplexes based on block copolymers of silk fibroin with poly(L-lysine) domains for tumor cell-specific delivery.

interact with pDNA and the tumor-homing peptides (THP), to bind specific tumor cells and achieve pDNA delivery. Globular nanocomplexes of average diameter in the range 150–250 nm were obtained. After *in vitro* transfection experiments into MDA-MB-435 melanoma cells and MDA-MB-231 metastatic human breast tumor cells, using non-tumorigenic MCF-10A breast epithelial cells as a control, this system was proposed as a new platform for nonviral gene delivery in tumor cells. Further studies focused on the optimization of the content of THP to enhance specificity and efficiency to tumor cells. The silk-*b*-PLL block copolymer containing Lyp1 (ML-Lyp1) showed significant differences in cytotoxicity to MCF10A cells from the block copolymer containing F3 (ML-F3), indicating that ML-F3 was the best candidate for target delivery into tumorigenic cells (see Fig. 15) [347].

5. Conclusions and perspectives for the future

The challenge of the application of drugs for cancer and anti-inflammatory therapies is the preparation and application of selective drugs and drug delivery systems with high efficacy and selectivity for the tumor cells. The design of polymer systems with the specific functionality and equilibrated balance of hydrophobic and hydrophilic components offers exceptional possibilities for the preparation of bioactive formulations of high efficacy and low toxicity. In addition, the incorporation of signaling functions and targeting ligands to the macromolecular matrices offers very interesting approaches for the specific targeting of the bioactive systems with the guarantee of very low toxicity while are moving to the target site.

The application of resorbable or biodegradable polymers and composites, as well as bioactive "polymer drugs", should involve the development of novel and advanced methodologies for treatments of high efficacy, selectivity and low toxicity, which would offer new alternatives to those traditionally used in cancer therapies. It is probably more necessary to find the best, more active and less toxic way to apply bioactive compounds and specific drugs, than the discovery of new drugs.

From a biomimetic point of view, there is a challenge for the design, preparation and application of polymer therapeutics with the design and morphology offered by self-assembling bioactive polymer systems, which can offer the appropriate conditions of low toxicity, targeting and selectivity by the incorporation of specific compounds such as cell signaling (ligands) and a core–shell morphology that guarantees the circulation and accumulation in the site of action. In addition, the combination of diagnostic and treatment (theranostic) is of great importance in new developments. The application of well-known polymer systems with the appropriate balance of hydrophobic/hydrophilic components in a biomimetic

scenario, together with the incorporation of effective drugs applied in the clinics, offers a very interesting alternative to classical treatments, and facilitates the development of cheap and effective treatments for cancer therapies and anti-inflammatory strategies.

Acknowledgements

Financial support from CIBER-BBN/ECO (NANOVIT) is appreciated.

References

[1] Nazir S, Hussain T, Ayub A, Rashid U, MacRobert AJ. Nanomaterials in combating cancer: therapeutic applications and developments. Nanomedicine 2014;10:19–34.
[2] Uchegbu IF, Siew A. Nanomedicines and nanodiagnostics come of age. J Pharm Sci 2013;102:305–10.
[3] MacKay JA, Almutairi A, Hennink W, Hoffman AS. NanoDDS 2013: the 11th International Nano Drug Delivery Symposium. J Controlled Release 2014;191:1–3.
[4] Branco MC, Schneider JP. Self-assembling materials for therapeutic delivery. Acta Biomater 2009;5:817–31.
[5] Alexis F, Pridgen EM, Langer R, Farokhzad OC. Nanoparticle technologies for cancer therapy. In: Schäfer-Korting M, editor. Drug delivery. Berlin Heidelberg: Springer; 2010. p. 55–86.
[6] Mei L, Zhang Z, Zhao L, Huang L, Yang XL, Tang J, Feng SS. Pharmaceutical nanotechnology for oral delivery of anticancer drugs. Adv Drug Deliv Rev 2013;65:880–90.
[7] Lu Y, Park K. Polymeric micelles and alternative nanonized delivery vehicles for poorly soluble drugs. Int J Pharm 2013;453:198–214.
[8] Nishiyama N, Kataoka K. Current state, achievements, and future prospects of polymeric micelles as nanocarriers for drug and gene delivery. Pharmacol Ther 2006;112:630–48.
[9] Oerlemans C, Bult W, Bos M, Storm G, Nijsen JFW, Hennink WE. Polymeric micelles in anticancer therapy: targeting, imaging and triggered release. Pharm Res 2010;27:2569–89.
[10] Wang R, Billone PS, Mullett WM. Nanomedicine in action: an overview of cancer nanomedicine on the market and in clinical trials. J Nanomater 2013;1:1–12.
[11] Shaji J, Lal M. Nanocarriers for targeting in inflammation. Asian J Pharm Clin Res 2013;6:3–12.
[12] Wang AZ, Langer R, Farokhzad OC. Nanoparticle delivery of cancer drugs. Annu Rev Med 2012;63:185–98.
[13] Egusquiaguirre SP, Igartua M, Hernández RM, Pedraz JL. Nanoparticle delivery systems for cancer therapy: advances in clinical and preclinical research. Clin Transl Oncol 2012;14:83–93.
[14] Davis ME. Nanoparticle therapeutics: an emerging treatment modality for cancer. Nat Rev Drug Discov 2008;7:771–82.
[15] Misra R, Upadhyay M, Mohanty S. Nanoparticles as carriers for chemotherapeutic drugs: a review. J Nanopharm Drug Deliv 2013;1:103–37.
[16] Park JH, Lee S, Kim JH, Park K, Kim K, Kwon IC. Polymeric nanomedicine for cancer therapy. Prog Polym Sci 2008;33:113–37.
[17] Parveen S, Misra R, Sahoo SK. Nanoparticles: a boon to drug delivery, therapeutics, diagnostics and imaging. Nanomedicine 2012;8:147–66.
[18] Kedar U, Phutane P, Shidhaye S, Kadam V. Advances in polymeric micelles for drug delivery and tumor targeting. Nanomedicine 2010;6:714–29.
[19] Rösler A, Vandermeulen GWM, Klok HA. Advanced drug delivery devices via self-assembly of amphiphilic block copolymers. Adv Drug Deliv Rev 2012;64(Suppl.):270–9.
[20] Duncan R. Polymer therapeutics as nanomedicines: new perspectives. Curr Opin Biotechnol 2011;22:492–501.
[21] Duncan R, Vicent MJ. Polymer therapeutics-prospects for 21st century: the end of the beginning. Adv Drug Deliv Rev 2013;65:60–70.
[22] Mousa SA, Bharali DJ. Nanotechnology-based detection and targeted therapy in cancer: nano-bio paradigms and applications. Cancers 2011;3:2888–903.
[23] Kumari A, Yadav SK, Yadav SC. Biodegradable polymeric nanoparticles based drug delivery systems. Colloids Surf, B: Biointerfaces 2010;75:1–18.
[24] Deng C, Jiang Y, Cheng R, Meng F, Zhong Z. Biodegradable polymeric micelles for targeted and controlled anticancer drug delivery: promises, progress and prospects. Nano Today 2012;7:467–80.
[25] Hassani LN, Hendra F, Bouchemal K. Auto-associative amphiphilic polysaccharides as drug delivery systems. Drug Discov Today 2012;17:608–14.
[26] Miyata K, Christie RJ, Kataoka K. Polymeric micelles for nano-scale drug delivery. React Funct Polym 2011;71:227–34.
[27] Gombotz WR, Hoffman AS. B.6—polymeric micelles. In: Ratmer BD, Hoffman AS, Schonene FJ, Lemons JE, editors. Biomaterials science. 3rd ed. Madison, WI: Academic Press; 2013. p. 1041–5.
[28] Ding H, Wang XJ, Zhang S, Liu X. Applications of polymeric micelles with tumor targeted in chemotherapy. J Nanopart Res 2012;14(1254):1–13.
[29] Rapoport N. Physical stimuli-responsive polymeric micelles for anti-cancer drug delivery. Prog Polym Sci 2007;32:962–90.
[30] Jones MC, Leroux JC. Polymeric micelles—a new generation of colloidal drug carriers. Eur J Pharm Biopharm 1999;48:101–11.
[31] Brigger I, Dubernet C, Couvreur P. Nanoparticles in cancer therapy and diagnosis. Adv Drug Deliv Rev 2012;64(Supplement):24–36.
[32] Choi JH, Jang JY, Joung YK, Kwon MH, Park KD. Intracellular delivery and anti-cancer effect of self-assembled heparin–Pluronic nanogels with RNase A. J Controlled Release 2010;147:420–7.
[33] Mora-Huertas C, Fessi H, Elaissari A. Polymer-based nanocapsules for drug delivery. Int J Pharm 2010;385:113–42.
[34] Percec V, Wilson DA, Leowanawat P, Wilson CJ, Hughes AD, Kaucher MS, Hammer DA, Levine DH, Kim AJ, Bates FS, Davis KP, Lodge TP, Klein ML, DeVane RH, Aqad E, Rosen BM, Argintaru AO, Sienkowska MJ, Rissanen K, Nummelin S, Ropponen J. Self-assembly of Janus dendrimers into uniform dendrimersomes and other complex architectures. Science 2010;328:1009–14.
[35] She W, Li N, Luo K, Guo C, Wang G, Geng Y, Gu Z. Dendronized heparin–doxorubicin conjugate based nanoparticle as pH-responsive drug delivery system for cancer therapy. Biomaterials 2013;34:2252–64.
[36] Schlüter AD, Rabe JP. Dendronized polymers: synthesis, characterization, assembly at interfaces, and manipulation. Angew Chem Int Ed 2000;39:864–83.
[37] Frauenrath H. Dendronized polymers—building a new bridge from molecules to nanoscopic objects. Prog Polym Sci 2005;30:325–84.
[38] Saeed AO, Magnusson JP, Moradi E, Soliman M, Wang W, Stolnik S, Thurecht KJ, Howdle SM, Alexander C. Modular construction of multifunctional bioresponsive cell-targeted nanoparticles for gene delivery. Bioconj Chem 2011;22:156–68.
[39] Sanna V, Siddiqui IA, Sechi M, Mukhtar H. Resveratrol-loaded nanoparticles based on poly(epsiloncaprolactone) and poly(D,L-lactic-*co*-glycolic acid)-poly(ethylene glycol) blend for prostate cancer treatment. Mol Pharm 2013;10:3871–81.
[40] Li B, Wang Q, Wang X, Wang C, Jiang X. Preparation, drug release and cellular uptake of doxorubicin-loaded dextran-*b*-poly(ε-caprolactone) nanoparticles. Carbohydr Polym 2013;93:430–7.
[41] Cirstoiu-Hapca A, Buchegger F, Bossy L, Kosinski M, Gurny R, Delie F. Nanomedicines for active targeting: physico-chemical characterization of paclitaxel-loaded anti-HER2 immunonanoparticles and in vitro functional studies on target cells. Eur J Pharm Sci 2009;38:230–7.
[42] Koo H, Min KH, Lee SC, Park JH, Park K, Jeong SY, Choi K, Kwon IC, Kim K. Enhanced drug-loading and therapeutic efficacy of hydrotropic oligomer-conjugated glycol chitosan nanoparticles for tumor-targeted paclitaxel delivery. J Controlled Release 2013;172:823–31.
[43] Zhang C, Li G, Wang Y, Cui F, Zhang J, Huang Q. Preparation and characterization of 5-fluorouracil-loaded PLLA-PEG/PEG nanoparticles by a novel supercritical CO_2 technique. Int J Pharm 2012;436:272–81.
[44] Meenach SA, Anderson KW, Zach Hilt J, McGarry RC, Mansour HM. Characterization and aerosol dispersion performance of advanced spray-dried chemotherapeutic PEGylated phospholipid particles for dry powder inhalation delivery in lung cancer. Eur J Pharm Sci 2013;49:699–711.
[45] Shalviri A, Chan HK, Raval G, Abdekhodaie MJ, Liu Q, Heerklotz H, Wu XY. Design of pH-responsive nanoparticles of terpolymer of poly(methacrylic acid), polysorbate 80 and starch for delivery of doxorubicin. Colloids Surf, B: Biointerfaces 2013;101:405–13.
[46] Shalviri A, Raval G, Prasad P, Chan C, Liu Q, Heerklotz H, Rauth AM, Wu XY. PH-Dependent doxorubicin release from terpolymer of starch, polymethacrylic acid and polysorbate 80 nanoparticles for overcoming multi-drug resistance in human breast cancer cells. Eur J Pharm Biopharm 2012;82:587–97.

[47] Bae Y, Kataoka K. Intelligent polymeric micelles from functional poly(ethylene glycol)-poly(amino acid) block copolymers. Adv Drug Deliv Rev 2009;61:768–84.
[48] Rettig H, Krause E, Börner HG. Atom transfer radical polymerization with polypeptide initiators: a general approach to block copolymers of sequence-defined polypeptides and synthetic polymers. Macromol Rapid Commun 2004;25:1251–6.
[49] Ding J, Xiao C, He C, Li M, Li D, Zhuang X, Chen X. Facile preparation of a cationic poly(amino acid) vesicle for potential drug and gene co-delivery. Nanotechnology 2011;22:1–9.
[50] Ding J, Xiao C, Tang Z, Zhuang X, Chen X. Highly efficient "grafting from" an α-helical polypeptide backbone by atom transfer radical polymerization. Macromol Biosci 2011;11:192–8.
[51] Lopez-Donaire ML, Parra-Caceres J, Vazquez-Lasa B, Garcia-Alvarez I, Fernandez-Mayoralas A, Lopez-Bravo A, San Roman J. Polymeric drugs based on bioactive glycosides for the treatment of brain tumours. Biomaterials 2009;30:1613–26.
[52] Lopez-Donaire ML, Sussman EM, Fernandez-Gutierrez M, Mendez-Vilas A, Ratner BD, Vazquez-Lasa B, San Roman J. Amphiphilic self-assembled "polymeric drugs": morphology, properties, and biological behavior of nanoparticles. Biomacromolecules 2012;13:624–35.
[53] García-Fernández L, Aguilar MR, Fernandez MM, Lozano RM, Gimenez G, Valverde S, San Roman J. Structure, morphology, and bioactivity of biocompatible systems derived from functionalized acrylic polymers based on 5-amino-2-naphthalene sulfonic acid. Biomacromolecules 2010;11:1763–72.
[54] García-Fernández L, Aguilar MR, Ochoa-Callejero L, Abradelo C, Martinez A, San Roman J. BFGF interaction and in vivo angiogenesis inhibition by self-assembling sulfonic acid-based copolymers. J Mater Sci Mater Med 2012;23:129–35.
[55] Garcia-Fernandez L, Halstenberg S, Unger RE, Aguilar MR, Kirkpatrick CJ, San Roman J. Anti-angiogenic activity of heparin-like polysulfonated polymeric drugs in 3D human cell culture. Biomaterials 2010;31:7863–72.
[56] Nicolas J, Guillaneuf Y, Lefay C, Bertin D, Gigmes D, Charleux B. Nitroxide-mediated polymerization. Prog Polym Sci 2013;38:63–235.
[57] Siegwart DJ, Oh JK, Matyjaszewski K. ATRP in the design of functional materials for biomedical applications. Prog Polym Sci 2012;37:18–37.
[58] Coessens VMC, Matyjaszewski K. Fundamentals of atom transfer radical polymerization. J Chem Educ 2010;87:916–9.
[59] Giacomelli C, Schmidt V, Borsali R. Nanocontainers formed by self-assembly of poly(ethylene oxide)-*b*-poly(glycerol monomethacrylate)–drug conjugates. Macromolecules 2007;40:2148–57.
[60] Jiang X, Zhang G, Narain R, Liu S. Covalently stabilized temperature and pH responsive four-layer nanoparticles fabricated from surface 'clickable' shell cross-linked micelles. Soft Matter 2009;5:1530–8.
[61] Gregory A, Stenzel MH. Complex polymer architectures via RAFT polymerization: from fundamental process to extending the scope using click chemistry and nature's building blocks. Prog Polym Sci 2012;37:38–105.
[62] Sun JT, Hong CY, Pan CY. Recent advances in RAFT dispersion polymerization for preparation of block copolymer aggregates. Polym Chem 2013;4:873–81.
[63] De P, Gondi SR, Sumerlin BS. Folate-conjugated thermoresponsive block copolymers: highly efficient conjugation and solution self-assembly. Biomacromolecules 2008;9:1064–70.
[64] Quan CY, Wu DQ, Chang C, Zhang GB, Cheng SX, Zhang XZ, Zhuo RX. Synthesis of thermo-sensitive micellar aggregates self-assembled from biotinylated PNAS-*b*-PNIPAAm-*b*-PCL triblock copolymers for tumor targeting. J Phys Chem C 2009;113:11262–7.
[65] Blunden BM, Lu H, Stenzel MH. Enhanced delivery of the RAPTA-C macromolecular chemotherapeutic by conjugation to degradable polymeric micelles. Biomacromolecules 2013;14:4177–88.
[66] Zhao J, Liu J, Han S, Deng H, Deng L, Liu J, Meng A, Dong A, Zhang J. Acid-induced disassemblable nanoparticles based on cyclic benzylidene acetal-functionalized graft copolymer via sequential RAFT and ATRP polymerization. Polym Chem 2014;5:1852–6.
[67] Xu YC, Dong CM. Dendron-like poly(e-benzyloxycarbonyl-L-lysine)/linear PEO block copolymers: synthesis, physical characterization, self-assembly, and drug-release behavior. J Polym Sci, A: Polym Chem 2012;50:1216–25.
[68] Lu J, Shi M, Shoichet MS. Click chemistry functionalized polymeric nanoparticles target corneal epithelial cells through RGD-cell surface receptors. Bioconj Chem 2008;20:87–94.
[69] Chan DPY, Deleavey GF, Owen SC, Damha MJ, Shoichet MS. Click conjugated polymeric immuno-nanoparticles for targeted siRNA and antisense oligonucleotide delivery. Biomaterials 2013;34:8408–15.
[70] Van der Ende AE, Sathiyakumar V, Diaz R, Hallahan DE, Harth E. Linear release nanoparticle devices for advanced targeted cancer therapies with increased efficacy. Polym Chem 2010;1:93–6.
[71] Shukla RK, Tiwari A. Carbohydrate molecules: an expanding horizon in drug delivery and biomedicine. Crit Rev Ther Drug Carrier Syst 2011;28:255–92.
[72] Bae Bc, Na K. Self-quenching polysaccharide-based nanogels of pullulan/folate–photosensitizer conjugates for photodynamic therapy. Biomaterials 2010;31:6325–35.
[73] Lee H, Lee K, Park TG. Hyaluronic acid–paclitaxel conjugate micelles: synthesis, characterization, and antitumor activity. Bioconj Chem 2008;19:1319–25.
[74] Kim S, Chae SY, Na K, Kim SW, Bae YH. Insulinotropic activity of sulfonylurea/pullulan conjugate in rat islet microcapsule. Biomaterials 2003;24:4843–51.
[75] Kim S, Park KM, Ko JY, Kwon IC, Cho HG, Kang D, Yu IT, Kim K, Na K. Minimalism in fabrication of self-organized nanogels holding both anti-cancer drug and targeting moiety. Colloids Surf, B: Biointerfaces 2008;63:55–63.
[76] Li L, Kim JK, Huh KM, Lee Yk, Kim SY. Targeted delivery of paclitaxel using folate-conjugated heparin-poly(β-benzyl-L-aspartate) self-assembled nanoparticles. Carbohydr Polym 2012;87:2120–8.
[77] Park K, Lee GY, Kim YS, Yu M, Park RW, Kim IS, Kim SY, Byun Y. Heparin–deoxycholic acid chemical conjugate as an anticancer drug carrier and its antitumor activity. J Controlled Release 2006;114:300–6.
[78] Bellini D, Topai A. Amides of hyaluronic acid and the derivatives thereof and a process for their preparation. In: US PCT Int Appl Wo. Abano, Terme (Italy): Fidia Farmaceutici SPA; 2013.
[79] Huang L, Kerns RJ. Diversity-oriented chemical modification of heparin: identification of charge-reduced *N*-acyl heparin derivatives having increased selectivity for heparin-binding proteins. Biorg Med Chem 2006;14:2300–13.
[80] Schanté CE, Zuber G, Herlin C, Vandamme TF. Chemical modifications of hyaluronic acid for the synthesis of derivatives for a broad range of biomedical applications. Carbohydr Polym 2011;85:469–89.
[81] Fernández C, Hattan CM, Kerns RJ. Semi-synthetic heparin derivatives: chemical modifications of heparin beyond chain length, sulfate substitution pattern and *N*-sulfo/*N*-acetyl groups. Carbohydr Res 2006;341:1253–65.
[82] Park W, Kim Ks, Bae Bc, Kim YH, Na K. Cancer cell specific targeting of nanogels from acetylated hyaluronic acid with low molecular weight. Eur J Pharm Sci 2010;40:367–75.
[83] Upadhyay KK, Meins JFL, Misra A, Voisin P, Bouchaud V, Ibarboure E, Schatz C, Lecommandoux S. Biomimetic doxorubicin loaded polymersomes from hyaluronan-block-poly((-benzyl glutamate) copolymers. Biomacromolecules 2009;10:2802–8.
[84] Kong M, Park H, Feng C, Hou L, Cheng X, Chen X. Construction of hyaluronic acid noisome as functional transdermal nanocarrier for tumor therapy. Carbohydr Polym 2013;94:634–41.
[85] Liu Y, Sun J, Cao W, Yang J, Lian H, Li X, Sun Y, Wang Y, Wang S, He Z. Dual targeting folate-conjugated hyaluronic acid polymeric micelles for paclitaxel delivery. Int J Pharm 2011;421:160–9.
[86] Wu JL, Liu CG, Wang XL, Huang ZH. Preparation and characterization of nanoparticles based on histidine–hyaluronic acid conjugates as doxorubicin carriers. J Mater Sci Mater Med 2012;23:1921–9.
[87] Ganesh S, Iyer AK, Morrissey DV, Amiji MM. Hyaluronic acid based self-assembling nanosystems for CD44 target mediated siRNA delivery to solid tumors. Biomaterials 2013;34:3489–502.
[88] Han HS, Lee J, Kim HR, Chae SY, Kim M, Saravanakumar G, Yoon HY, You DG, Ko H, Kim K, Kwon IC, Park JC, Park JH. Robust PEGylated hyaluronic acid nanoparticles as the carrier of doxorubicin: mineralization and its effect on tumor targetability in vivo. J Controlled Release 2013;168:105–14.
[89] Li J, Huo M, Wang J, Zhou J, Mohammad JM, Zhang Y, Zhu Q, Waddad AY, Zhang Q. Redox-sensitive micelles self-assembled from amphiphilic hyaluronic acid-deoxycholic acid conjugates for targeted intracellular delivery of paclitaxel. Biomaterials 2012;33:2310–20.
[90] Saravanakumar G, Choi KY, Yoon HY, Kim K, Park JH, Kwon IC, Park K. Hydrotropic hyaluronic acid conjugates: synthesis, characterization, and implications as a carrier of paclitaxel. Int J Pharm 2010;394:154–61.

[91] Tran TH, Bae Bc, Lee Yk, Na K, Huh KM. Heparin–folate–retinoic acid bioconjugates for targeted delivery of hydrophobic photosensitizers. Carbohydr Polym 2013;92:1615–24.
[92] Oh Ih, Cho K, Tran T, Huh K, Lee Yk. Biofuntional nanoparticle formation and folate-targeted antitumor effect of heparin–retinoic acid conjugates. Macromol Res 2012;20:520–7.
[93] Park IK, Tran TH, Oh IH, Kim YJ, Cho KJ, Huh KM, Lee YK. Ternary biomolecular nanoparticles for targeting of cancer cells and anti-angiogenesis. Eur J Pharm Sci 2010;41:148–55.
[94] Xin D, Wang Y, Xiang J. The use of amino acid linkers in the conjugation of paclitaxel with hyaluronic acid as drug delivery system: synthesis, self-assembled property, drug release, and in vitro efficiency. Pharm Res 2010;27:380–9.
[95] Park IK, Kim YJ, Tran TH, Huh KM, Lee Yk. Water-soluble heparin–PTX conjugates for cancer targeting. Polymer 2010;51:3387–93.
[96] Khatun Z, Nurunnabi M, Reeck GR, Cho KJ, Lee YK. Oral delivery of taurocholic acid linked heparin–docetaxel conjugates for cancer therapy. J Controlled Release 2013;170:74–82.
[97] Manju S, Sreenivasan K. Conjugation of curcumin onto hyaluronic acid enhances its aqueous solubility and stability. J Colloid Interface Sci 2011;359:318–25.
[98] Basu S, Das A. Curcumin-Hyaluronan Compounds. US 11/966,398 Wo, Kent State University; 2009.
[99] Opanasopit P, Ngawhirunpat T, Rojanarata T, Choochottiros C, Chirachanchai S. *N*-Phthaloylchitosan-g-mPEG design for all-trans retinoic acid-loaded polymeric micelles. Eur J Pharm Sci 2007;30:424–31.
[100] Du YZ, Weng Q, Yuan H, Hu FQ. Synthesis and antitumor activity of stearate-g-dextran micelles for intracellular doxorubicin delivery. ACS Nano 2010;4:6894–902.
[101] Hou L, Yao J, Zhou J, Zhang Q. Pharmacokinetics of a paclitaxel-loaded low molecular weight heparin-all-*trans*-retinoid acid conjugate ternary nanoparticulate drug delivery system. Biomaterials 2012;33:5431–40.
[102] Yang JS, Zhou QQ, He W. Amphipathicity and self-assembly behavior of amphiphilic alginate esters. Carbohydr Polym 2013;92:223–7.
[103] Zhang C, Wang W, Wang C, Tian Q, Huang W, Yuan Z, Chen X. Cytotoxicity of liver targeted drug-loaded alginate nanoparticles. Sci China Ser B 2009;52:1382–7.
[104] Guo R, Zhang L, Jiang Z, Cao Y, Ding Y, Jiang X. Synthesis of alginic acid-poly[2-(diethylamino)ethyl methacrylate] monodispersed nanoparticles by a polymer–monomer pair reaction system. Biomacromolecules 2007;8:843–50.
[105] Chen M, Liu Y, Yang W, Li X, Liu L, Zhou Z, Wang Y, Li R, Zhang Q. Preparation and characterization of self-assembled nanoparticles of 6-*O*-cholesterol-modified chitosan for drug delivery. Carbohydr Polym 2011;84:1244–51.
[106] Kurita K. Controlled functionalization of the polysaccharide chitin. Prog Polym Sci 2001;26:1921–71.
[107] Sashiwa H, Aiba SI. Chemically modified chitin and chitosan as biomaterials. Prog Polym Sci 2004;29:887–908.
[108] Zhang Y, Huo M, Zhou J, Yu D, Wu Y. Potential of amphiphilically modified low molecular weight chitosan as a novel carrier for hydrophobic anticancer drug: synthesis, characterization, micellization and cytotoxicity evaluation. Carbohydr Polym 2009;77:231–8.
[109] Du YZ, Wang L, Yuan H, Wei XH, Hu FQ. Preparation and characteristics of linoleic acid-grafted chitosan oligosaccharide micelles as a carrier for doxorubicin. Colloids Surf, B: Biointerfaces 2009;69:257–63.
[110] Hu FQ, Ren GF, Yuan H, Du YZ, Zeng S. Shell cross-linked stearic acid grafted chitosan oligosaccharide self-aggregated micelles for controlled release of paclitaxel. Colloids Surf, B: Biointerfaces 2006;50:97–103.
[111] You J, Hu FQ, Du YZ, Yuan H. Polymeric micelles with glycolipid-like structure and multiple hydrophobic domains for mediating molecular target delivery of paclitaxel. Biomacromolecules 2007;8:2450–6.
[112] Hu FQ, Wu XI, Du YZ, You J, Yuan H. Cellular uptake and cytotoxicity of shell crosslinked stearic acid-grafted chitosan oligosaccharide micelles encapsulating doxorubicin. Eur J Pharm Biopharm 2008;69:117–25.
[113] Pan Z, Gao Y, Heng L, Liu Y, Yao G, Wang Y, Liu Y. Amphiphilic *N*-(2,3-dihydroxypropyl)-chitosan–cholic acid micelles for paclitaxel delivery. Carbohydr Polym 2013;94:394–9.
[114] Kim JH, Bae SM, Na MH, Shin H, Yang YJ, Min KH, Choi KY, Kim K, Park RW, Kwon IC. Facilitated intracellular delivery of peptide-guided nanoparticles in tumor tissues. J Controlled Release 2012;157:493–9.
[115] Yang Wz, Chen Hl, Gao Fp, Chen Mm, Li Xm, Zhang Mm, Zhang Qq, Liu Lr, Jiang Q, Wang Ys. Self-aggregated nanoparticles of cholesterol-modified pullulan conjugate as a novel carrier of mitoxantronep. Curr Nanosci 2010;6:298–306.
[116] Yang W, Wang M, Ma L, Li H, Huang L. Synthesis and characterization of biotin modified cholesteryl pullulan as a novel anticancer drug carrier. Carbohydr Polym 2014;99:720–7.
[117] Zhang H, Li F, Yi J, Gu C, Fan L, Qiao Y, Tao Y, Cheng C, Wu H. Folate-decorated maleilated pullulan–doxorubicin conjugate for active tumor-targeted drug delivery. Eur J Pharm Sci 2011;42:517–26.
[118] Scomparin A, Salmaso S, Bersani S, Satchi-Fainaro R, Caliceti P. Novel folated and non-folated pullulan bioconjugates for anticancer drug delivery. Eur J Pharm Sci 2011;42:547–58.
[119] Sasaki Y, Asayama W, Niwa T, Sawada SI, Ueda T, Taguchi H, Akiyoshi K. Amphiphilic polysaccharide nanogels as artificial chaperones in cell-free protein synthesis. Macromol Biosci 2011;11:814–20.
[120] Besheer A, Hause G, Kressler J, Mäder K. Hydrophobically modified hydroxyethyl starch: synthesis, characterization, and aqueous self-assembly into nano-sized polymeric micelles and vesicles. Biomacromolecules 2007;8:359–67.
[121] Liu Q, Yang X, Xu H, Pan K, Yang Y. Novel nanomicelles originating from hydroxyethyl starch-g-polylactide and their release behavior of docetaxel modulated by the PLA chain length. Eur Polym J 2013;49:3522–9.
[122] Luo Q, Wang P, Miao Y, He H, Tang X. A novel 5-fluorouracil prodrug using hydroxyethyl starch as a macromolecular carrier for sustained release. Carbohydr Polym 2012;87:2642–7.
[123] Na K, Park KH, Kim SW, Bae YH. Self-assembled hydrogel nanoparticles from curdlan derivatives: characterization, anti-cancer drug release and interaction with a hepatoma cell line (HepG2). J Controlled Release 2000;69:225–36.
[124] Li WM, Liu DM, Chen SY. Amphiphilically-modified gelatin nanoparticles: self-assembly behavior, controlled biodegradability, and rapid cellular uptake for intracellular drug delivery. J Mater Chem 2011;21:12381–8.
[125] Tran PHL, Tran TTD, Vo TV, Vo CLN, Lee BJ. Novel multifunctional biocompatible gelatin–oleic acid conjugate: self-assembled nanoparticles for drug delivery. J Biomed Nanotechnol 2013;9:1416–31.
[126] Wareechuensook M, Tabata Y, Kanokpanont S. Characteristics of cholesterol-grafted gelatin micelles. Adv Mater Res 2010;93–94:595–8.
[127] Cao Z, Jin Y, Zhang B, Miao Q, Ma C. A novel temperature- and pH-responsive polymer-biomolecule conjugate composed of casein and poly(*N*-isopropylacrylamide). Iran Polym J 2010;19:689–98.
[128] Serban MA, Kaplan DL. PH-sensitive ionomeric particles obtained via chemical conjugation of silk with poly(amino acid)s. Biomacromolecules 2010;11:3406–12.
[129] Drbohlavova J, Chomoucka J, Adam V, Ryvolova M, Eckschlager T, Hubalek J, Kizek R. Nanocarriers for anticancer drugs—new trends in nanomedicine. Curr Drug Metab 2013;14:547–64.
[130] Webster DM, Sundaram P, Byrne ME. Injectable nanomaterials for drug delivery: carriers, targeting moieties, and therapeutics. Eur J Pharm Biopharm 2013;84:1–20.
[131] Stephanopoulos N, Ortony JH, Stupp SI. Self-assembly for the synthesis of functional biomaterials. Acta Mater 2013;61:912–30.
[132] Lv S, Li M, Tang Z, Song W, Sun H, Liu H, Chen X. Doxorubicin-loaded amphiphilic polypeptide-based nanoparticles as an efficient drug delivery system for cancer therapy. Acta Biomater 2013;9:9330–42.
[133] Li M, Song W, Tang Z, Lv S, Lin L, Sun H, Li Q, Yang Y, Hong H, Chen X. Nanoscaled poly(L-glutamic acid)/doxorubicin–amphiphile complex as pH-responsive drug delivery system for effective treatment of nonsmall cell lung cancer. ACS Appl Mater Interfaces 2013;5:1781–92.
[134] Li X, Li H, Yi W, Chen J, Liang B. Acid-triggered core cross-linked nanomicelles for targeted drug delivery and magnetic resonance imaging in liver cancer cells. Int J Nanomed 2013;8:3019–31.
[135] Hamaguchi T, Matsumura Y, Suzuki M, Shimizu K, Goda R, Nakamura I, Nakatomi I, Yokoyama M, Kataoka K, Kakizoe T. NK105, a paclitaxel-incorporating micellar nanoparticle formulation, can extend in vivo antitumour activity and reduce the neurotoxicity of paclitaxel. Br J Cancer 2005;92:1240–6.
[136] Matsumura Y. Poly(amino acid) micelle nanocarriers in preclinical and clinical studies. Adv Drug Deliv Rev 2008;60:899–914.

[137] Gong J, Chen M, Zheng Y, Wang S, Wang Y. Polymeric micelles drug delivery system in oncology. J Controlled Release 2012;159:312–23.
[138] Hamaguchi T, Kato K, Yasui H, Morizane C, Ikeda M, Ueno H, Muro K, Yamada Y, Okusaka T, Shirao K. A phase I and pharmacokinetic study of NK105, a paclitaxel-incorporating micellar nanoparticle formulation. Br J Cancer 2007;97:170–6.
[139] Matsumura Y, Kataoka K. Preclinical and clinical studies of anticancer agent-incorporating polymer micelles. Cancer Sci 2009;100:572–9.
[140] Kato K, Hamaguchi T, Yasui H, Okusaka T, Ueno H, Ikeda M, Shirao K, Shimada Y, Nakahama H, Muro K. Phase I study of NK105, a paclitaxel-incorporating micellar nanoparticle, in patients with advanced cancer. J Clin Oncol 2006;24:2018.
[141] Eckman AM, Tsakalozou E, Kang NY, Ponta A, Bae Y. Drug release patterns and cytotoxicity of PEG–poly(aspartate) block copolymer micelles in cancer cells. Pharm Res 2012;29:1755–67.
[142] Desale SS, Cohen SM, Zhao Y, Kabanov AV, Bronich TK. Biodegradable hybrid polymer micelles for combination drug therapy in ovarian cancer. J Controlled Release 2013;171:339–48.
[143] Thambi T, Yoon HY, Kim K, Kwon IC, Yoo CK, Park JH. Bioreducible block copolymers based on poly(ethylene glycol) and poly(γ-benzyl L-glutamate) for intracellular delivery of camptothecin. Bioconj Chem 2011;22:1924–31.
[144] Araki T, Kono Y, Ogawara KI, Watanabe T, Ono T, Kimura T, Higaki K. Formulation and evaluation of paclitaxel-loaded polymeric nanoparticles composed of polyethylene glycol and polylactic acid block copolymer. Biol Pharm Bull 2012;35:1306–13.
[145] Kim D, Kim S, Kim H, Kim S, Shin S, Kim J, Park K, Lee M, Heo D. Multicenter phase II trial of Genexol-PM, a novel Cremophor-free, polymeric micelle formulation of paclitaxel, with cisplatin in patients with advanced non-small-cell lung cancer. Ann Oncol 2007;18:2009–14.
[146] Lee KS, Chung HC, Im SA, Park YH, Kim CS, Kim SB, Rha SY, Lee MY, Ro J. Multicenter phase II trial of Genexol-PM, a Cremophor-free, polymeric micelle formulation of paclitaxel, in patients with metastatic breast cancer. Breast Cancer Res Treat 2008;108:241–50.
[147] Lim W, Tan E, Toh C, Hee S, Leong S, Ang P, Wong N, Chowbay B. Phase I pharmacokinetic study of a weekly liposomal paclitaxel formulation (Genexol®-PM) in patients with solid tumors. Ann Oncol 2010;21:382–8.
[148] Ayen WY, Garkhal K, Kumar N. Doxorubicin-loaded (PEG) 3-PLA nanopolymersomes: effect of solvents and process parameters on formulation development and in vitro study. Mol Pharm 2011;8:466–78.
[149] Jain JP, Ayen WY, Kumar N. Self assembling polymers as polymersomes for drug delivery. Curr Pharm Des 2011;17:65–79.
[150] Levine DH, Ghoroghchian PP, Freudenberg J, Zhang G, Therien MJ, Greene MI, Hammer DA, Murali R. Polymersomes: a new multi-functional tool for cancer diagnosis and therapy. Methods 2008;46:25–32.
[151] Blanco E, Bey EA, Khemtong C, Yang SG, Setti-Guthi J, Chen H, Kessinger CW, Carnevale KA, Bornmann WG, Boothman DA. β-Lapachone micellar nanotherapeutics for non-small cell lung cancer therapy. Cancer Res 2010;70:3896–904.
[152] Tan C, Wang Y, Fan W. Exploring polymeric micelles for improved delivery of anticancer agents: recent developments in preclinical studies. Pharmaceutics 2013;5:201–19.
[153] Siddiqui IA, Adhami VM, Bharali DJ, Hafeez BB, Asim M, Khwaja SI, Ahmad N, Cui H, Mousa SA, Mukhtar H. Introducing nanochemoprevention as a novel approach for cancer control: proof of principle with green tea polyphenol epigallocatechin-3-gallate. Cancer Res 2009;69:1712–6.
[154] Bharali DJ, Mousa SA. Emerging nanomedicines for early cancer detection and improved treatment: current perspective and future promise. Pharmacol Ther 2010;128:324–35.
[155] Mu CF, Balakrishnan P, Cui FD, Yin YM, Lee YB, Choi HG, Yong CS, Chung SJ, Shim CK, Kim DD. The effects of mixed MPEG–PLA/Pluronic copolymer micelles on the bioavailability and multidrug resistance of docetaxel. Biomaterials 2010;31:2371–9.
[156] Tsai HC, Chang WH, Lo CL, Tsai CH, Chang CH, Ou TW, Yen TC, Hsiue GH. Graft and diblock copolymer multifunctional micelles for cancer chemotherapy and imaging. Biomaterials 2010;31:2293–301.
[157] Gao ZG, Tian L, Hu J, Park IS, Bae YH. Prevention of metastasis in a 4T1 murine breast cancer model by doxorubicin carried by folate conjugated pH sensitive polymeric micelles. J Controlled Release 2011;152:84–9.
[158] Kim D, Gao ZG, Lee ES, Bae YH. In vivo evaluation of doxorubicin-loaded polymeric micelles targeting folate receptors and early endosomal pH in drug-resistant ovarian cancer. Mol Pharm 2009;6:1353–62.
[159] Zhan C, Gu B, Xie C, Li J, Liu Y, Lu W, Cyclic RGD. conjugated poly(ethylene glycol)-*co*-poly(lactic acid) micelle enhances paclitaxel anti-glioblastoma effect. J Controlled Release 2010;143:136–42.
[160] Wei X, Gong C, Gou M, Fu S, Guo Q, Shi S, Luo F, Guo G, Qiu L, Qian Z. Biodegradable poly(ε-caprolactone)–poly(ethylene glycol) copolymers as drug delivery system. Int J Pharm 2009;381:1–18.
[161] Wang Y, Wang C, Fu S, Liu Q, Dou D, Lv H, Fan M, Guo G, Luo F, Qian Z. Preparation of tacrolimus loaded micelles based on poly(ε-caprolactone)–poly(ethylene glycol)–poly(ε-caprolactone). Int J Pharm 2011;407:184–9.
[162] Liu L, Sun L, Wu Q, Guo W, Li L, Chen Y, Li Y, Gong C, Qian Z, Wei Y. Curcumin loaded polymeric micelles inhibit breast tumor growth and spontaneous pulmonary metastasis. Int J Pharm 2013;443:175–82.
[163] Gao X, Wang BL, Wei XW, Gou ML, Men K, Liu XY, Guo G, Qian ZY, Huang MJ. Preparation and characterization of monomethoxy poly(ethylene glycol)–poly(ε-caprolactone) micelles for the solubilization and in vivo delivery of luteolin. Int J Nanomed 2013;8:3061–9.
[164] Cho H, Lai TC, Kwon GS. Poly(ethylene glycol)-block-poly(ε-caprolactone) micelles for combination drug delivery: evaluation of paclitaxel, cyclopamine and gossypol in intraperitoneal xenograft models of ovarian cancer. J Controlled Release 2013;166:1–9.
[165] Peng CL, Lai PS, Lin FH, Yueh Hsiu Wu S, Shieh MJ. Dual chemotherapy and photodynamic therapy in an HT-29 human colon cancer xenograft model using SN-38-loaded chlorin-core star block copolymer micelles. Biomaterials 2009;30:3614–25.
[166] Hu Q, Gao X, Kang T, Feng X, Jiang D, Tu Y, Song Q, Yao L, Jiang X, Chen H. CGKRK-modified nanoparticles for dual-targeting drug delivery to tumor cells and angiogenic blood vessels. Biomaterials 2013;34:9496–508.
[167] Danhier F, Ansorena E, Silva JM, Coco R, Le Breton A, Préat V. PLGA-based nanoparticles: an overview of biomedical applications. J Controlled Release 2012;161:505–22.
[168] Sah H, Thoma LA, Desu HR, Sah E, Wood GC. Concepts and practices used to develop functional PLGA-based nanoparticulate systems. Int J Nanomed 2013;8:747–65.
[169] Ding H, Mora R, Gao J, Sumer BD. Characterization and optimization of mTHPP nanoparticles for photodynamic therapy of head and neck cancer. Otolaryngol Head Neck Surg 2011;145:612–7.
[170] Song Z, Feng R, Sun M, Guo C, Gao Y, Li L, Zhai G. Curcumin-loaded PLGA–PEG–PLGA triblock copolymeric micelles: preparation, pharmacokinetics and distribution in vivo. J Colloid Interface Sci 2011;354:116–23.
[171] Graf N, Bielenberg DR, Kolishetti N, Muus C, Banyard J, Farokhzad OC, Lippard SJ. αVβ3 integrin-targeted PLGA–PEG nanoparticles for enhanced anti-tumor efficacy of a Pt(IV) prodrug. ACS Nano 2012;6:4530–9.
[172] Chen J, Li S, Shen Q. Folic acid and cell-penetrating peptide conjugated PLGA–PEG bifunctional nanoparticles for vincristine sulfate delivery. Eur J Pharm Sci 2012;47:430–43.
[173] Chen J, Li S, Shen Q, He H, Zhang Y. Enhanced cellular uptake of folic acid-conjugated PLGA–PEG nanoparticles loaded with vincristine sulfate in human breast cancer. Drug Dev Ind Pharm 2011;37:1339–46.
[174] Liu P, Wang H, Wang Q, Sun Y, Shen M, Zhu M, Wan Z, Duan Y. cRGD conjugated mPEG–PLGA–PLL nanoparticles for SGC-7901 gastric cancer cells-targeted delivery of fluorouracil. J Nanosci Nanotechnol 2012;12:4467–71.
[175] Saxena V, Naguib Y, Hussain MD. Folate receptor targeted 17-allylamino-17-demethoxygeldanamycin (17-AAG) loaded polymeric nanoparticles for breast cancer. Colloids Surf, B: Biointerfaces 2012;94:274–80.
[176] Wang Y, Liu P, Duan Y, Yin X, Wang Q, Liu X, Wang X, Zhou J, Wang W, Qiu L, Di W. Specific cell targeting with APRPG conjugated PEG–PLGA nanoparticles for treating ovarian cancer. Biomaterials 2014;35:983–92.
[177] Lei Y, Lai Y, Li Y, Li S, Cheng G, Li D, Li H, He B, Gu Z. Anticancer drug delivery of PEG based micelles with small lipophilic moieties. Int J Pharm 2013;453:579–86.
[178] Liang Y, Lai Y, Li D, He B, Gu Z. Novel polymeric micelles with cinnamic acid as lipophilic moiety for 9-Nitro-20 (S)-camptothecin delivery. Mater Lett 2013;97:4–7.
[179] Lai Y, Long Y, Lei Y, Deng X, He B, Sheng M, Li M, Gu Z. A novel micelle of coumarin derivative monoend-functionalized PEG for

anti-tumor drug delivery: in vitro and in vivo study. J Drug Target 2012;20:246–54.
[180] Oberoi HS, Laquer FC, Marky LA, Kabanov AV, Bronich TK. Core cross-linked block ionomer micelles as pH-responsive carriers for cis-diamminedichloroplatinum(II). J Controlled Release 2011;153:64–72.
[181] Kim JO, Sahay G, Kabanov AV, Bronich TK. Polymeric micelles with ionic cores containing biodegradable cross-links for delivery of chemotherapeutic agents. Biomacromolecules 2010;11:919–26.
[182] Nukolova NV, Oberoi HS, Cohen SM, Kabanov AV, Bronich TK. Folate-decorated nanogels for targeted therapy of ovarian cancer. Biomaterials 2011;32:5417–26.
[183] Oberoi HS, Nukolova NV, Laquer FC, Poluektova LY, Huang J, Alnouti Y, Yokohira M, Arnold LL, Kabanov AV, Cohen SM. Cisplatin-loaded core cross-linked micelles: comparative pharmacokinetics, antitumor activity, and toxicity in mice. Int J Nanomed 2012;7:2557.
[184] Talelli M, Iman M, Varkouhi AK, Rijcken CJ, Schiffelers RM, Etrych T, Ulbrich K, van Nostrum CF, Lammers T, Storm G. Core-crosslinked polymeric micelles with controlled release of covalently entrapped doxorubicin. Biomaterials 2010;31:7797–804.
[185] Gill KK, Kaddoumi A, Nazzal S. Mixed micelles of PEG2000-DSPE and vitamin-E TPGS for concurrent delivery of paclitaxel and parthenolide: enhanced chemosenstization and antitumor efficacy against non-small cell lung cancer (NSCLC) cell lines. Eur J Pharm Sci 2012;46:64–71.
[186] Tong SW, Xiang B, Dong DW, Qi XR. Enhanced antitumor efficacy and decreased toxicity by self-associated docetaxel in phospholipid-based micelles. Int J Pharm 2012;434:413–9.
[187] Zhu S, Lansakara PDS, Li X, Cui Z. Lysosomal delivery of a lipophilic gemcitabine prodrug using novel acid-sensitive micelles improved its antitumor activity. Bioconj Chem 2012;23:966–80.
[188] Bildstein L, Dubernet C, Couvreur P. Prodrug-based intracellular delivery of anticancer agents. Adv Drug Deliv Rev 2011;63:3–23.
[189] Kopeček J. Polymer–drug conjugates: origins, progress to date and future directions. Adv Drug Deliv Rev 2012;65:49–59.
[190] Canal F, Sanchis J, Vicent MJ. Polymer–drug conjugates as nano-sized medicines. Curr Opin Biotechnol 2011;22:894–900.
[191] Li C, Wallace S. Polymer–drug conjugates: recent development in clinical oncology. Adv Drug Deliv Rev 2008;60:886–98.
[192] Ponta A, Bae Y. PEG–poly(amino acid) block copolymer micelles for tunable drug release. Pharm Res 2010;27:2330–42.
[193] Svenson S. Clinical translation of nanomedicines. Curr Opin Solid State Mater Sci 2012;16:287–94.
[194] Uchino H, Matsumura Y, Negishi T, Koizumi F, Hayashi T, Honda T, Nishiyama N, Kataoka K, Naito S, Kakizoe T. Cisplatin-incorporating polymeric micelles (NC-6004) can reduce nephrotoxicity and neurotoxicity of cisplatin in rats. Br J Cancer 2005;93:678–87.
[195] Plummer R, Wilson R, Calvert H, Boddy A, Griffin M, Sludden J, Tilby M, Eatock M, Pearson D, Ottley C. A Phase I clinical study of cisplatin-incorporated polymeric micelles (NC-6004) in patients with solid tumours. Br J Cancer 2011;104:593–8.
[196] Cabral H, Nishiyama N, Okazaki S, Koyama H, Kataoka K. Preparation and biological properties of dichloro(1,2-diaminocyclohexane)platinum(II) (DACHPt)-loaded polymeric micelles. J Controlled Release 2005;101:223–32.
[197] Cabral H, Nishiyama N, Kataoka K. Optimization of (1,2-diaminocyclohexane)platinum(II)-loaded polymeric micelles directed to improved tumor targeting and enhanced antitumor activity. J Controlled Release 2007;121:146–55.
[198] Pasut G, Veronese FM. PEG conjugates in clinical development or use as anticancer agents: an overview. Adv Drug Deliv Rev 2009;61:1177–88.
[199] Bala V, Rao S, Boyd BJ, Prestidge CA. Prodrug and nanomedicine approaches for the delivery of the camptothecin analogue SN38. J Controlled Release 2013;172:48–61.
[200] Koizumi F, Kitagawa M, Negishi T, Onda T, Matsumoto Si, Hamaguchi T, Matsumura Y. Novel SN-38-incorporating polymeric micelles, NK012, eradicate vascular endothelial growth factor-secreting bulky tumors. Cancer Res 2006;66:10048–56.
[201] Nagano T, Yasunaga M, Goto K, Kenmotsu H, Koga Y, Kuroda Ji, Nishimura Y, Sugino T, Nishiwaki Y, Matsumura Y. Synergistic antitumor activity of the SN-38-incorporating polymeric micelles NK012 with S-1 in a mouse model of non-small cell lung cancer. Int J Cancer 2010;127:2699–706.
[202] Hamaguchi T, Doi T, Eguchi-Nakajima T, Kato K, Yamada Y, Shimada Y, Fuse N, Ohtsu A, Matsumoto Si, Takanashi M. Phase I study of NK012, a Novel SN-38-incorporating micellar nanoparticle, in adult patients with solid tumors. Clin Cancer Res 2010;16:5058–66.
[203] Matsumura Y. Preclinical and clinical studies of NK012, an SN-38-incorporating polymeric micelles, which is designed based on EPR effect. Adv Drug Deliv Rev 2011;63:184–92.
[204] Nakanishi T, Fukushima S, Okamoto K, Suzuki M, Matsumura Y, Yokoyama M, Okano T, Sakurai Y, Kataoka K. Development of the polymer micelle carrier system for doxorubicin. J Controlled Release 2001;74:295–302.
[205] Tsukioka Y, Matsumura Y, Hamaguchi T, Koike H, Moriyasu F, Kakizoe T. Pharmaceutical and biomedical differences between micellar doxorubicin (NK911) and liposomal doxorubicin (Doxil). Cancer Sci 2002;93:1145–53.
[206] Matsumura Y, Hamaguchi T, Ura T, Muro K, Yamada Y, Shimada Y, Shirao K, Okusaka T, Ueno H, Ikeda M. Phase I clinical trial and pharmacokinetic evaluation of NK911, a micelle-encapsulated doxorubicin. Br J Cancer 2004;91:1775–81.
[207] Xiao H, Song H, Yang Q, Cai H, Qi R, Yan L, Liu S, Zheng Y, Huang Y, Liu T, Jing X. A prodrug strategy to deliver cisplatin(IV) and paclitaxel in nanomicelles to improve efficacy and tolerance. Biomaterials 2012;33:6507–19.
[208] Zhang W, Shi Y, Chen Y, Ye J, Sha X, Fang X. Multifunctional Pluronic P123/F127 mixed polymeric micelles loaded with paclitaxel for the treatment of multidrug resistant tumors. Biomaterials 2011;32:2894–906.
[209] Chen Y, Sha X, Zhang W, Zhong W, Fan Z, Ren Q, Chen L, Fang X. Pluronic mixed micelles overcoming methotrexate multidrug resistance: in vitro and in vivo evaluation. Int J Nanomed 2013;8:1463–76.
[210] Wang Y, Li Y, Zhang L, Fang X. Pharmacokinetics and biodistribution of paclitaxel-loaded pluronic P105 polymeric micelles. Arch Pharm Res 2008;31:530–8.
[211] Danson S, Ferry D, Alakhov V, Margison J, Kerr D, Jowle D, Brampton M, Halbert G, Ranson M. Phase I dose escalation and pharmacokinetic study of pluronic polymer-bound doxorubicin (SP1049C) in patients with advanced cancer. Br J Cancer 2004;90:2085–91.
[212] Valle JW, Armstrong A, Newman C, Alakhov V, Pietrzynski G, Brewer J, Campbell S, Corrie P, Rowinsky EK, Ranson M. A phase 2 study of SP1049C, doxorubicin in *P*-glycoprotein-targeting pluronics, in patients with advanced adenocarcinoma of the esophagus and gastroesophageal junction. Invest New Drugs 2011;29:1029–37.
[213] Alakhova DY, Zhao Y, Li S, Kabanov AV. Effect of Doxorubicin/Pluronic SP1049C on tumorigenicity, aggressiveness, DNA methylation and stem cell markers in murine leukemia. PLoS ONE 2013;8:1–14.
[214] Song H, He R, Wang K, Ruan J, Bao C, Li N, Ji J, Cui D. Anti-HIF-1α antibody-conjugated pluronic triblock copolymers encapsulated with Paclitaxel for tumor targeting therapy. Biomaterials 2010;31:2302–12.
[215] Talelli M, Rijcken C, Van Nostrum C, Storm G, Hennink W. Micelles based on HPMA copolymers. Adv Drug Deliv Rev 2010;62:231–9.
[216] Segal E, Satchi-Fainaro R. Design and development of polymer conjugates as anti-angiogenic agents. Adv Drug Deliv Rev 2009;61:1159–76.
[217] Kopecek J, Kopecková P. HPMA copolymers: origins, early developments, present, and future. Adv Drug Deliv Rev 2010;62:122–49.
[218] Yang Y, Pan D, Luo K, Li L, Gu Z. Biodegradable and amphiphilic block copolymer–doxorubicin conjugate as polymeric nanoscale drug delivery vehicle for breast cancer therapy. Biomaterials 2013;34:8430–43.
[219] Chytil P, Etrych T, Konák C, Sírová M, Mrkvan T, Boucek J, Říhová B, Ulbrich K. New HPMA copolymer-based drug carriers with covalently bound hydrophobic substituents for solid tumour targeting. J Controlled Release 2008;127:121–30.
[220] Miller K, Erez R, Segal E, Shabat D, Satchi-Fainaro R. Targeting bone metastases with a bispecific anticancer and antiangiogenic polymer–alendronate–taxane conjugate. Angew Chem Int Ed 2009;48:2949–54.
[221] Miller K, Eldar-Boock A, Polyak D, Segal E, Benayoun L, Shaked Y, Satchi-Fainaro R. Antiangiogenic antitumor activity of HPMA copolymer–paclitaxel–alendronate conjugate on breast cancer bone metastasis mouse model. Mol Pharm 2011;8:1052–62.
[222] Segal E, Pan H, Benayoun L, Kopečková P, Shaked Y, Kopeček J, Satchi-Fainaro R. Enhanced anti-tumor activity and safety profile of targeted nano-scaled HPMA copolymer–alendronate–TNP-470 conjugate in the treatment of bone malignances. Biomaterials 2011;32:4450–63.
[223] Jia Z, Wong L, Davis TP, Bulmus V. One-pot conversion of RAFT-generated multifunctional block copolymers of HPMA to doxorubicin conjugated acid- and reductant-sensitive crosslinked micelles. Biomacromolecules 2008;9:3106–13.

[224] Regehly M, Greish K, Rancan F, Maeda H, Böhm F, Röder B. Water-soluble polymer conjugates of ZnPP for photodynamic tumor therapy. Bioconj Chem 2007;18:494–9.
[225] Iyer AK, Greish K, Seki T, Okazaki S, Fang J, Takeshita K, Maeda H. Polymeric micelles of zinc protoporphyrin for tumor targeted delivery based on EPR effect and singlet oxygen generation. J Drug Target 2007;15:496–506.
[226] Nakamura H, Liao L, Hitaka Y, Tsukigawa K, Subr V, Fang J, Ulbrich K, Maeda H. Micelles of zinc protoporphyrin conjugated to *N*-(2-hydroxypropyl)methacrylamide (HPMA) copolymer for imaging and light-induced antitumor effects in vivo. J Controlled Release 2013;165:191–8.
[227] Jabbari E, Yang X, Moeinzadeh S, He X. Drug release kinetics, cell uptake, and tumor toxicity of hybrid VVVVVVKK peptide-assembled polylactide nanoparticles. Eur J Pharm Biopharm 2013;84:49–62.
[228] Xu J, Zhao JH, Liu Y, Feng NP, Zhang YT. RGD-modifed poly(D,L-lactic acid) nanoparticles enhance tumor targeting of oridonin. Int J Nanomed 2012;7:211–9.
[229] Ortiz R, Prados J, Melguizo C, Arias JL, Ruiz MA, Álvarez PJ, Caba O, Luque R, Segura A, Aránega A. 5-Fluorouracil-loaded poly(ε-caprolactone) nanoparticles combined with phage E gene therapy as a new strategy against colon cancer. Int J Nanomed 2012;7:95–107.
[230] Huang C, Neoh KG, Xu L, Kang ET, Chiong E. Polymeric nanoparticles with encapsulated superparamagnetic iron oxide and conjugated cisplatin for potential bladder cancer therapy. Biomacromolecules 2012;13:2513–20.
[231] Tan YF, Chandrasekharan P, Maity D, Yong CX, Chuang KH, Zhao Y, Wang S, Ding J, Feng SS. Multimodal tumor imaging by iron oxides and quantum dots formulated in poly(lactic acid)–D-alpha-tocopheryl polyethylene glycol 1000 succinate nanoparticles. Biomaterials 2011;32:2969–78.
[232] Mi Y, Liu X, Zhao J, Ding J, Feng SS. Multimodality treatment of cancer with herceptin conjugated, thermomagnetic iron oxides and docetaxel loaded nanoparticles of biodegradable polymers. Biomaterials 2012;33:7519–29.
[233] McDaniel JR, Bhattacharyya J, Vargo KB, Hassouneh W, Hammer DA, Chilkoti A. Self-assembly of thermally responsive nanoparticles of a genetically encoded peptide polymer by drug conjugation. Angew Chem Int Ed 2013;52:1683–7.
[234] Branco MC, Sigano DM, Schneider JP. Materials from peptide assembly: towards the treatment of cancer and transmittable disease. Curr Opin Chem Biol 2011;15:427–34.
[235] Cui H, Webber MJ, Stupp SI. Self-assembly of peptide amphiphiles: from molecules to nanostructures to biomaterials. Pept Sci 2010;94:1–18.
[236] Mart RJ, Osborne RD, Stevens MM, Ulijn RV. Peptide-based stimuli-responsive biomaterials. Soft Matter 2006;2:822–35.
[237] Kokkoli E, Mardilovich A, Wedekind A, Rexeisen EL, Garg A, Craig JA. Self-assembly and applications of biomimetic and bioactive peptide–amphiphiles. Soft Matter 2006;2:1015–24.
[238] Toft DJ, Moyer TJ, Standley SM, Ruff Y, Ugolkov A, Stupp SI, Cryns VL. Coassembled cytotoxic and pegylated peptide amphiphiles form filamentous nanostructures with potent antitumor activity in models of breast cancer. ACS Nano 2012;6:7956–65.
[239] Aluri S, Janib SM, Mackay JA. Environmentally responsive peptides as anticancer drug carriers. Adv Drug Deliv Rev 2009;61:940–52.
[240] Standley SM, Toft DJ, Cheng H, Soukasene S, Chen J, Raja SM, Band V, Band H, Cryns VL, Stupp SI. Induction of cancer cell death by self-assembling nanostructures incorporating a cytotoxic peptide. Cancer Res 2010;70:3020–6.
[241] Webber MJ, Newcomb CJ, Bitton R, Stupp SI. Switching of self-assembly in a peptide nanostructure with a specific enzyme. Soft Matter 2011;7:9665–72.
[242] Soukasene S, Toft DJ, Moyer TJ, Lu H, Lee HK, Standley SM, Cryns VL, Stupp SI. Antitumor activity of peptide amphiphile nanofiber-encapsulated camptothecin. ACS Nano 2011;5:9113–21.
[243] MacKay JA, Chen M, McDaniel JR, Liu W, Simnick AJ, Chilkoti A. Self-assembling chimeric polypeptide–doxorubicin conjugate nanoparticles that abolish tumours after a single injection. Nat Mater 2009;8:993–9.
[244] Wiradharma N, Tong YW, Yang YY. Self-assembled oligopeptide nanostructures for co-delivery of drug and gene with synergistic therapeutic effect. Biomaterials 2009;30:3100–9.
[245] Matson JB, Stupp SI. Drug release from hydrazone-containing peptide amphiphiles. Chem Commun 2011;47:7962–4.
[246] Webber MJ, Matson JB, Tamboli VK, Stupp SI. Controlled release of dexamethasone from peptide nanofiber gels to modulate inflammatory response. Biomaterials 2012;33:6823–32.
[247] Hoogenboom R. Poly (2-oxazoline)s: a polymer class with numerous potential applications. Angew Chem Int Ed 2009;48:7978–94.
[248] Schlaad H, Diehl C, Gress A, Meyer M, Demirel AL, Nur Y, Bertin A. Poly(2-oxazoline)s as smart bioinspired polymers. Macromol Rapid Commun 2010;31:511–25.
[249] Hoogenboom R, Schlaad H. Bioinspired poly(2-oxazoline)s. Polymers 2011;3:467–88.
[250] Lee SC, Kim C, Kwon IC, Chung H, Jeong SY. Polymeric micelles of poly (2-ethyl-2-oxazoline)-block-poly (ε-caprolactone) copolymer as a carrier for paclitaxel. J Controlled Release 2003;89:437–46.
[251] Hsiue GH, Wang CH, Lo CL, Wang CH, Li JP, Yang JL. Environmental-sensitive micelles based on poly (2-ethyl-2-oxazoline)-*b*-poly (L-lactide) diblock copolymer for application in drug delivery. Int J Pharm 2006;317:69–75.
[252] Luxenhofer R, Schulz A, Roques C, Li S, Bronich TK, Batrakova EV, Jordan R, Kabanov AV. Doubly amphiphilic poly(2-oxazoline)s as high-capacity delivery systems for hydrophobic drugs. Biomaterials 2010;31:4972–9.
[253] Tong J, Luxenhofer R, Yi X, Jordan R, Kabanov AV. Protein modification with amphiphilic block copoly (2-oxazoline) s as a new platform for enhanced cellular delivery. Mol Pharm 2010;7:984–92.
[254] Shieh MJ, Peng CL, Chiang WL, Wang CH, Hsu CY, Wang SJJ, Lai PS. Reduced skin photosensitivity with meta-tetra (hydroxyphenyl) chlorin-loaded micelles based on a poly(2-ethyl-2-oxazoline)-*b*-poly(D,L-lactide) diblock copolymer in vivo. Mol Pharm 2010;7:1244–53.
[255] Syu WJ, Yu HP, Hsu CY, Rajan YC, Hsu YH, Chang YC, Hsieh WY, Wang CH, Lai PS. Improved photodynamic cancer treatment by folate-conjugated polymeric micelles in a KB xenografted animal model. Small 2012;8:2060–9.
[256] Huang SJ, Sun SL, Chiu CC, Wang LF. Retinol-encapsulated water-soluble succinated chitosan nanoparticles for antioxidant applications. J Biomater Sci Polym Ed 2013;24:315–29.
[257] Goodarzi N, Varshochian R, Kamalinia G, Atyabi F, Dinarvand R. A review of polysaccharide cytotoxic drug conjugates for cancer therapy. Carbohydr Polym 2013;92:1280–93.
[258] Luo Y, Bernshaw NJ, Lu ZR, Kopecek J, Prestwich GD. Targeted delivery of doxorubicin by HPMA copolymer–hyaluronan bioconjugates. Pharm Res 2002;19:396–402.
[259] Patel S, Page MJ. The role of hyaluronan in cancer. In: Hari GG, Hales CA, editors. Chemistry and biology of hyaluronan. Oxford: Elsevier Science Ltd; 2004. p. 285–305.
[260] Götte M, Yip GW. Heparanase, hyaluronan, and CD44 in cancers: a breast carcinoma perspective. Cancer Res 2006;66:10233–7.
[261] Bartolazzi A, Peach R, Aruffo A, Stamenkovic I. Interaction between CD44 and hyaluronate is directly implicated in the regulation of tumor development. J Exp Med 1994;180:53–66.
[262] Choi KY, Chung H, Min KH, Yoon HY, Kim K, Park JH, Kwon IC, Jeong SY. Self-assembled hyaluronic acid nanoparticles for active tumor targeting. Biomaterials 2010;31:106–14.
[263] Szarpak A, Cui D, Dubreuil Fdr, De Geest BG, De Cock LJ, Picart C, Auzély-Velty R. Designing hyaluronic acid-based layer-by-layer capsules as a carrier for intracellular drug delivery. Biomacromolecules 2010;11:713–20.
[264] Campo GM, Avenoso A, Campo S, D'Ascola A, Nastasi G, Calatroni A. Molecular size hyaluronan differently modulates toll-like receptor-4 in LPS-induced inflammation in mouse chondrocytes. Biochimie 2010;92:204–15.
[265] Cheng G, Swaidani S, Sharma M, Lauer ME, Hascall VC, Aronica MA. Hyaluronan deposition and correlation with inflammation in a murine ovalbumin model of asthma. Matrix Biol 2011;30:126–34.
[266] Campo GM, Avenoso A, D'Ascola A, Scuruchi M, Prestipino V, Calatroni A, Campo S. Hyaluronan in part mediates IL-1beta-induced inflammation in mouse chondrocytes by up-regulating CD44 receptors. Gene 2012;494:24–35.
[267] Jiang X, Shapiro DJ. The immune system and inflammation in breast cancer. Mol Cell Endocrinol 2014;382:673–82.
[268] August EM, Nguyen T, Malinowski NM, Cysyk RL. Non-steroidal anti-inflammatory drugs and tumor progression: inhibition of fibroblast hyaluronic acid production by indomethacin and mefenamic acid. Cancer Lett 1994;82:49–54.
[269] Ossipov DA. Nanostructured hyaluronic acid-based materials for active delivery to cancer. Expert Opin Drug Deliv 2010;7:681–703.
[270] Jeong YI, Kim DH, Chung CW, Yoo JJ, Choi KH, Kim CH, Ha SH, Kang DH. Self-assembled nanoparticles of hyaluronic

acid/poly(D,L-lactide-*co*-glycolide) block copolymer. Colloids Surf, B: Biointerfaces 2012;90:28–35.
[271] Ray L, Kumar P, Gupta KC. The activity against Ehrlich's ascites tumors of doxorubicin contained in self assembled, cell receptor targeted nanoparticle with simultaneous oral delivery of the green tea polyphenol epigallocatechin-3-gallate. Biomaterials 2013;34:3064–76.
[272] Choi KY, Min KH, Na JH, Choi K, Kim K, Park JH, Kwon IC, Jeong SY. Self-assembled hyaluronic acid nanoparticles as a potential drug carrier for cancer therapy: synthesis, characterization, and in vivo biodistribution. J Mater Chem 2009;19:4102–7.
[273] Huang J, Zhang H, Yu Y, Chen Y, Wang D, Zhang G, Zhou G, Liu J, Sun Z, Sun D, Lu Y, Zhong Y. Biodegradable self-assembled nanoparticles of poly(D,L-lactide-*co*-glycolide)/hyaluronic acid block copolymers for target delivery of docetaxel to breast cancer. Biomaterials 2014;35:550–66.
[274] Zhou B, Weigel JA, Fauss L, Weigel PH. Identification of the hyaluronan receptor for endocytosis (HARE). J Biol Chem 2000;275:37733–41.
[275] Kim H, Park HT, Tae YM, Kong WH, Sung DK, Hwang BW, Kim KS, Kim YK, Hahn SK. Bioimaging and pulmonary applications of self-assembled Flt1 peptide–hyaluronic acid conjugate nanoparticles. Biomaterials 2013;34:8478–90.
[276] Luo Y, Prestwich GD. Synthesis and selective cytotoxicity of a hyaluronic acid–antitumor bioconjugate. Bioconj Chem 1999;10:755–63.
[277] Luo Y, Ziebell MR, Prestwich GD. A hyaluronic acid–taxol antitumor bioconjugate targeted to cancer cells. Biomacromolecules 2000;1:208–18.
[278] Rosato A, Banzato A, De Luca G, Renier D, Bettella F, Pagano C, Esposito G, Zanovello P, Bassi P. HYTAD1-p20: a new paclitaxel–hyaluronic acid hydrosoluble bioconjugate for treatment of superficial bladder cancer. Urol Oncol 2006;24:207–15.
[279] Auzenne E. Hyaluronic acid-paclitaxel: antitumor efficacy against CD44 (+) human ovarian carcinoma xenografts. Neoplasia 2007;9:479–86.
[280] Yoon HY, Koo H, Choi KY, Lee SJ, Kim K, Kwon IC, Leary JF, Park K, Yuk SH, Park JH, Choi K. Tumor-targeting hyaluronic acid nanoparticles for photodynamic imaging and therapy. Biomaterials 2012;33:3980–9.
[281] Ito T, Fraser IP, Yeo Y, Highley CB, Bellas E, Kohane DS. Anti-inflammatory function of an in situ cross-linkable conjugate hydrogel of hyaluronic acid and dexamethasone. Biomaterials 2007;28:1778–86.
[282] Smorenburg SM, Van Noorden CJ. The complex effects of heparins on cancer progression and metastasis in experimental studies. Pharmacol Rev 2001;53:93–106.
[283] Casu B, Vlodavsky I, Sanderson RD. Non-anticoagulant heparins and inhibition of cancer. Pathophysiol Haemost Thromb 2009;36:195–203.
[284] Han HD, Lee A, Song CK, Hwang T, Seong H, Lee CO, Shin BC. In vivo distribution and antitumor activity of heparin-stabilized doxorubicin-loaded liposomes. Int J Pharm 2006;313:181–8.
[285] Hou L, Fan Y, Yao J, Zhou J, Li C, Fang Z, Zhang Q. Low molecular weight heparin-all-*trans*-retinoid acid conjugate as a drug carrier for combination cancer chemotherapy of paclitaxel and all-*trans*-retinoid acid. Carbohydr Polym 2011;86:1157–66.
[286] Larsson M, Huang WC, Hsiao MH, Wang YJ, Nydén M, Chiou SH, Liu DM. Biomedical applications and colloidal properties of amphiphilically modified chitosan hybrids. Prog Polym Sci 2013;38:1307–28.
[287] Harish Prashanth KV, Tharanathan RN. Depolymerized products of chitosan as potent inhibitors of tumor-induced angiogenesis. Biochim Biophys Acta Gen Subj 2005;1722:22–9.
[288] Park JH, Saravanakumar G, Kim K, Kwon IC. Targeted delivery of low molecular drugs using chitosan and its derivatives. Adv Drug Deliv Rev 2010;62:28–41.
[289] Zhang C, Ping Q, Zhang H, Shen J. Preparation of *N*-alkyl-*O*-sulfate chitosan derivatives and micellar solubilization of taxol. Carbohydr Polym 2003;54:137–41.
[290] Zhang C, Qineng P, Zhang H. Self-assembly and characterization of paclitaxel-loaded *N*-octyl-*O*-sulfate chitosan micellar system. Colloids Surf, B: Biointerfaces 2004;39:69–75.
[291] Zhang C, Qu G, Sun Y, Yang T, Yao Z, Shen W, Shen Z, Ding Q, Zhou H, Ping Q. Biological evaluation of *N*-octyl-*O*-sulfate chitosan as a new nano-carrier of intravenous drugs. Eur J Pharm Sci 2008;33:415–23.
[292] Qu G, Yao Z, Zhang C, Wu X, Ping Q. PEG conjugated *N*-octyl-*O*-sulfate chitosan micelles for delivery of paclitaxel: in vitro characterization and in vivo evaluation. Eur J Pharm Sci 2009;37:98–105.
[293] Dufes C, Muller JM, Couet W, Olivier JC, Uchegbu IF, Schätzlein AG. Anticancer drug delivery with transferrin targeted polymeric chitosan vesicles. Pharm Res 2004;21:101–7.
[294] You J, Li X, De Cui F, Du YZ, Yuan H, Hu FQ. Folate-conjugated polymer micelles for active targeting to cancer cells: preparation, in vitro evaluation of targeting ability and cytotoxicity. Nanotechnology 2008;19:1–9.
[295] Wang K, Zhang T, Liu L, Wang X, Wu P, Chen Z, Ni C, Zhang J, Hu F, Huang J. Novel micelle formulation of curcumin for enhancing antitumor activity and inhibiting colorectal cancer stem cells. Int J Nanomed 2012;7:4487–97.
[296] Mekhail GM, Kamel AO, Awad GAS, Mortada ND. Anticancer effect of atorvastatin nanostructured polymeric micelles based on stearyl-grafted chitosan. Int J Biol Macromol 2012;51:351–63.
[297] Zhao Z, He M, Yin L, Bao J, Shi L, Wang B, Tang C, Yin C. Biodegradable nanoparticles based on linoleic acid and poly(β′-malic acid) double grafted chitosan derivatives as carriers of anticancer drugs. Biomacromolecules 2009;10:565–72.
[298] Kim JH, Kim YS, Kim S, Park JH, Kim K, Choi K, Chung H, Jeong SY, Park RW, Kim IS, Kwon IC. Hydrophobically modified glycol chitosan nanoparticles as carriers for paclitaxel. J Controlled Release 2006;111:228–34.
[299] Jin YH, Hu HY, Qiao MX, Zhu J, Qi JW, Hu CJ, Zhang Q, Chen DW. PH-sensitive chitosan-derived nanoparticles as doxorubicin carriers for effective anti-tumor activity: preparation and in vitro evaluation. Colloids Surf, B: Biointerfaces 2012;94:184–91.
[300] Yang K, Gao T, Bao Z, Su J, Chen X. Preparation and characterization of a novel thermosensitive nanoparticle for drug delivery in combined hyperthermia and chemotherapy. J Mater Chem B 2013;1:6442–8.
[301] Park JS, Han TH, Lee KY, Han SS, Hwang JJ, Moon DH, Kim SY, Cho YW. *N*-acetyl histidine-conjugated glycol chitosan self-assembled nanoparticles for intracytoplasmic delivery of drugs: endocytosis, exocytosis and drug release. J Controlled Release 2006;115:37–45.
[302] Termsarasab U, Cho HJ, Kim DH, Chong S, Chung SJ, Shim CK, Moon HT, Kim DD. Chitosan oligosaccharide–arachidic acid-based nanoparticles for anti-cancer drug delivery. Int J Pharm 2013;441:373–80.
[303] Bouterfa H, Picht T, Keß D, Herbold C, Noll E, Black PM, Roosen K, Tonn JC. Retinoids inhibit human glioma cell proliferation and migration in primary cell cultures but not in established cell lines. Neurosurgery 2000;46:419–30.
[304] Opanasopit P, Ngawhirunpat T, Rojanarata T, Choochottiros C, Chirachanchai S. Camptothecin-incorporating *N*-phthaloylchitosan-g-mPEG self-assembly micellar system: effect of degree of deacetylation. Colloids Surf, B: Biointerfaces 2007;60:117–24.
[305] Fan L, Wu H, Zhang H, Li F, Yang Th, Gu Ch, Yang Q. Novel super pH-sensitive nanoparticles responsive to tumor extracellular pH. Carbohydr Polym 2008;73:390–400.
[306] Marques JG, Gaspar VM, Costa E, Paquete CM, Correia IJ. Synthesis and characterization of micelles as carriers of non-steroidal anti-inflammatory drugs (NSAID) for application in breast cancer therapy. Colloids Surf, B: Biointerfaces 2014;113:375–83.
[307] Park JH, Cho YW, Son YJ, Kim K, Chung H, Jeong SY, Choi K, Park CR, Park RW, Kim IS, Kwon IC. Preparation and characterization of self-assembled nanoparticles based on glycol chitosan bearing adriamycin. Colloid Polym Sci 2006;284:763–70.
[308] Tao Y, Han J, Dou H. Paclitaxel-loaded tocopheryl succinate-conjugated chitosan oligosaccharide nanoparticles for synergistic chemotherapy. J Mater Chem 2012;22:8930–7.
[309] Yuan ZX, Sun X, Gong T, Ding H, Fu Y, Zhang ZR. Randomly 50% *N*-acetylated low molecular weight chitosan as a novel renal targeting carrier. J Drug Target 2007;15:269–78.
[310] Wang M, Hu H, Sun Y, Qiu L, Zhang J, Guan G, Zhao X, Qiao M, Cheng L, Cheng L. A pH-sensitive gene delivery system based on folic acid-PEG-chitosan–PAMAM-plasmid DNA complexes for cancer cell targeting. Biomaterials 2013;34:10120–32.
[311] Leathers TD. Biotechnological production and applications of pullulan. Appl Microbiol Biotechnol 2003;62:468–73.
[312] Li M, Lam JW, Mahtab F, Chen S, Zhang W, Hong Y, Xiong J, Zheng Q, Tang BZ. Biotin-decorated fluorescent silica nanoparticles with aggregation-induced emission characteristics: fabrication, cytotoxicity and biological applications. J Mater Chem B 2013;1:676–84.
[313] Ochi Y, Shiose Y, Kuga H, Kumazawa E. A possible mechanism for the long-lasting antitumor effect of the macromolecular conjugate DE-310: mediation by cellular uptake and drug release of its

active camptothecin analog DX-8951. Cancer Chemother Pharmacol 2005;55:323–32.
[314] Veltkamp SA, Witteveen EO, Capriati A, Crea A, Animati F, Voogel-Fuchs M, Van Den Heuvel IJGM, Beijnen JH, Voest EE, Schellens JHM. Clinical and pharmacologic study of the novel prodrug delimotecan (MEN 4901/T-0128) in patients with solid tumors. Clin Cancer Res 2008;14:7535–44.
[315] Varshosaz J, Hassanzadeh F, Sadeghi H, Firozian F, Mirian M. Effect of molecular weight and molar ratio of dextran on self-assembly of dextran stearate polymeric micelles as nanocarriers for etoposide. J Nanomater 2012;2012:1–10.
[316] Jeong YI, Chung KD, Choi KC. Doxorubicin release from self-assembled nanoparticles of deoxycholic acid-conjugated dextran. Arch Pharm Res 2011;34:159–67.
[317] Hwang JH, Choi CW, Kim HW, Kim DH, Kwak TW, Lee HM, Kim CH, Chung CW, Jeong YI, Kang DH. Dextran-*b*-poly(L-histidine) copolymer nanoparticles for pH-responsive drug delivery to tumor cells. Int J Nanomed 2013;8:3197–207.
[318] Sun H, Guo B, Li X, Cheng R, Meng F, Liu H, Zhong Z. Shell-sheddable micelles based on dextran-SS-poly(ε-caprolactone) diblock copolymer for efficient intracellular release of doxorubicin. Biomacromolecules 2010;11:848–54.
[319] Prabu P, Chaudhari AA, Aryal S, Dharmaraj N, Park SY, Kim WD, Kim HY. In vitro evaluation of poly(caporlactone) grafted dextran (PGD) nanoparticles with cancer cell. J Mater Sci Mater Med 2008;19:2157–63.
[320] Prabu P, Chaudhari AA, Ko JA, Dharmaraj N, Park SY, Kim HY, Khil MS. Cellular uptake and in vitro drug release studies on paclitaxel-loaded poly(caprolactone)-grafted dextran copolymeric nanoparticles. Nanobiotechnology 2009;5:42–9.
[321] Liu P, Shi B, Yue C, Gao G, Li P, Yi H, Li M, Wang B, Ma Y, Cai L. Dextran-based redox-responsive doxorubicin prodrug micelles for overcoming multidrug resistance. Polym Chem 2013;4:5793–9.
[322] Tan S, Zhao D, Yuan D, Wang H, Tu K, Wang LQ. Influence of indomethacin-loading on the micellization and drug release of thermosensitive dextran-graft-poly(*N*-isopropylacrylamide). React Funct Polym 2011;71:820–7.
[323] Roberts K, Spychal R, Brookes MJ, Strugala V, Dettmar PW, Johnstone LM, Jolliffe IG, Tselepis C. M2016 potential therapeutic role of alginates in the management of oesophageal adenocarcinoma. Gastroenterology 2008;134(Suppl 1):A-451.
[324] de Sousa APA, Torres MR, Pessoa C, Moraes MOd, Filho FDR, Alves APNN, Costa-Lotufo LV. In vivo growth-inhibition of Sarcoma 180 tumor by alginates from brown seaweed Sargassum vulgare. Carbohydr Polym 2007;69:7–13.
[325] Zhang C, Wang W, Liu T, Wu Y, Guo H, Wang P, Tian Q, Wang Y, Yuan Z. Doxorubicin-loaded glycyrrhetinic acid-modified alginate nanoparticles for liver tumor chemotherapy. Biomaterials 2012;33:2187–96.
[326] Du C, Zhao J, Fei J, Gao L, Cui W, Yang Y, Li J. Alginate-based microcapsules with a molecule recognition linker and photosensitizer for the combined cancer treatment. Chem Asian J 2013;8:736–42.
[327] Shalviri A, Cai P, Rauth AM, Henderson JT, Wu XY. Evaluation of new bi-functional terpolymeric nanoparticles for simultaneous in vivo optical imaging and chemotherapy of breast cancer. Drug Deliv Transl Res 2012;2:437–53.
[328] Svenson S, Wolfgang M, Hwang J, Ryan J, Eliasof S. Preclinical to clinical development of the novel camptothecin nanopharmaceutical CRLX101. J Controlled Release 2011;153:49–55.
[329] Young C, Schluep T, Hwang J, Eliasof S. CRLX101 (formerly IT-101)—A Novel nanopharmaceutical of camptothecin in clinical development. Curr Bioact Compd 2011;7:8–14.
[330] Eliasof S, Lazarus D, Peters CG, Case RI, Cole RO, Hwang J, Schluep T, Chao J, Lin J, Yen Y. Correlating preclinical animal studies and human clinical trials of a multifunctional, polymeric nanoparticle. Proc Natl Acad Sci USA 2013;110:15127–32.
[331] Gradishar WJ. Albumin-bound paclitaxel: a next-generation taxane. Expert Opin Pharmacother 2006;7:1041–53.
[332] Desai N, Trieu V, Yao Z, Louie L, Ci S, Yang A, Tao C, De T, Beals B, Dykes D, Noker P, Yao R, Labao E, Hawkins M, Soon-Shiong P. Increased antitumor activity, intratumor paclitaxel concentrations, and endothelial cell transport of cremophor-free, albumin-bound paclitaxel, ABI-007, compared with cremophor-based paclitaxel. Clin Cancer Res 2006;12:1317–24.
[333] Nyman DW, Campbell KJ, Hersh E, Long K, Richardson K, Trieu V, Desai N, Hawkins MJ, Von Hoff DD, Phase I. and pharmacokinetics trial of ABI-007, a novel nanoparticle formulation of paclitaxel in patients with advanced nonhematologic malignancies. J Clin Oncol 2005;23:7785–93.
[334] Cirstea D, Hideshima T, Rodig S, Santo L, Pozzi S, Vallet S, Ikeda H, Perrone G, Gorgun G, Patel K, Desai N, Sportelli P, Kapoor S, Vali S, Mukherjee S, Munshi NC, Anderson KC, Raje N. Dual inhibition of akt/mammalian target of rapamycin pathway by nanoparticle Albumin-Bound—rapamycin and perifosine induces antitumor activity in multiple myeloma. Mol Cancer Ther 2010;9:963–75.
[335] Lee JY, Bae KH, Kim JS, Nam YS, Park TG. Intracellular delivery of paclitaxel using oil-free, shell cross-linked HSA—multi-armed PEG nanocapsules. Biomaterials 2011;32:8635–44.
[336] Lu Z, Yeh TK, Tsai M, Au JLS, Wientjes MG. Paclitaxel-loaded gelatin nanoparticles for intravesical bladder cancer therapy. Clin Cancer Res 2004;10:7677–84.
[337] Ge J, Neofytou E, Lei J, Beygui RE, Zare RN. Protein–polymer hybrid nanoparticles for drug delivery. Small 2012;8:3573–8.
[338] Tseng CL, Wang TW, Dong GC, Yueh-Hsiu Wu S, Young TH, Shieh MJ, Lou PJ, Lin FH. Development of gelatin nanoparticles with biotinylated EGF conjugation for lung cancer targeting. Biomaterials 2007;28:3996–4005.
[339] Tseng CL, Wu SYH, Wang WH, Peng CL, Lin FH, Lin CC, Young TH, Shieh MJ. Targeting efficiency and biodistribution of biotinylated-EGF-conjugated gelatin nanoparticles administered via aerosol delivery in nude mice with lung cancer. Biomaterials 2008;29:3014–22.
[340] Kommareddy S, Amiji M. Biodistribution and pharmacokinetic analysis of long-circulating thiolated gelatin nanoparticles following systemic administration in breast cancer-bearing mice. J Pharm Sci 2007;96:397–407.
[341] Kommareddy S, Amiji M. Antiangiogenic gene therapy with systemically administered sFlt-1 plasmid DNA in engineered gelatin-based nanovectors. Cancer Gene Ther 2007;14:488–98.
[342] Tran PHL, Tran TTD, Lee BJ. Enhanced solubility and modified release of poorly water-soluble drugs via self-assembled gelatin–oleic acid nanoparticles. Int J Pharm 2013;455:235–40.
[343] Boulet-Audet M, Terry AE, Vollrath F, Holland C. Silk protein aggregation kinetics revealed by Rheo-IR. Acta Biomater 2013:776–84.
[344] Chiang WH, Lan YJ, Huang YC, Chen YW, Huang YF, Lin SC, Chern CS, Chiu HC. Multi-scaled polymersomes from self-assembly of octadecanol-modified dextrans. Polymer 2012;53:2233–44.
[345] Zhao Z, Chen A, Li Y, Hu J, Liu X, Li J, Zhang Y, Li G, Zheng Z. Fabrication of silk fibroin nanoparticles for controlled drug delivery. J Nanopart Res 2012;14:736/1–736.
[346] Numata K, Reagan MR, Goldstein RH, Rosenblatt M, Kaplan DL. Spider silk-based gene carriers for tumor cell-specific delivery. Bioconj Chem 2011;22:1605–10.
[347] Numata K, Mieszawska-Czajkowska AJ, Kvenvold LA, Kaplan DL. Silk-based nanocomplexes with tumor-homing peptides for tumor-specific gene delivery. Macromol Biosci 2012;12:75–82.